HEREDITARY SPASTIC PARAPLEGIAS: AT THE CROSSROADS OF MOLECULAR PATHWAYS AND CLINICAL OPTIONS

EDITED BY: Andrea Martinuzzi, Giovanni Stevanin, Craig Blackstone and Cahir Joseph O'Kane

PUBLISHED IN: Frontiers in Neuroscience

frontiers Research Topics

frontiers

ISSN 1664-8714
ISBN 978-2-88971-217-5
DOI 10.3389/978-2-88971-217-5

About Frontiers

Frontiers is more than just an open-access publisher of scholarly articles: it is a pioneering approach to the world of academia, radically improving the way scholarly research is managed. The grand vision of Frontiers is a world where all people have an equal opportunity to seek, share and generate knowledge. Frontiers provides immediate and permanent online open access to all its publications, but this alone is not enough to realize our grand goals.

Frontiers Journal Series

The Frontiers Journal Series is a multi-tier and interdisciplinary set of open-access, online journals, promising a paradigm shift from the current review, selection and dissemination processes in academic publishing. All Frontiers journals are driven by researchers for researchers; therefore, they constitute a service to the scholarly community. At the same time, the Frontiers Journal Series operates on a revolutionary invention, the tiered publishing system, initially addressing specific communities of scholars, and gradually climbing up to broader public understanding, thus serving the interests of the lay society, too.

Dedication to Quality

Each Frontiers article is a landmark of the highest quality, thanks to genuinely collaborative interactions between authors and review editors, who include some of the world's best academicians. Research must be certified by peers before entering a stream of knowledge that may eventually reach the public - and shape society; therefore, Frontiers only applies the most rigorous and unbiased reviews.
Frontiers revolutionizes research publishing by freely delivering the most outstanding research, evaluated with no bias from both the academic and social point of view. By applying the most advanced information technologies, Frontiers is catapulting scholarly publishing into a new generation.

What are Frontiers Research Topics?

Frontiers Research Topics are very popular trademarks of the Frontiers Journals Series: they are collections of at least ten articles, all centered on a particular subject. With their unique mix of varied contributions from Original Research to Review Articles, Frontiers Research Topics unify the most influential researchers, the latest key findings and historical advances in a hot research area! Find out more on how to host your own Frontiers Research Topic or contribute to one as an author by contacting the Frontiers Editorial Office: frontiersin.org/about/contact

HEREDITARY SPASTIC PARAPLEGIAS: AT THE CROSSROADS OF MOLECULAR PATHWAYS AND CLINICAL OPTIONS

Topic Editors:
Andrea Martinuzzi, Eugenio Medea (IRCCS), Italy
Giovanni Stevanin, INSERM U1127 Institut du Cerveau et de la Moelle épinière (ICM), France
Craig Blackstone, National Institute of Neurological Disorders and Stroke (NINDS), United States
Cahir Joseph O'Kane, University of Cambridge, United Kingdom

Citation: Martinuzzi, A., Stevanin, G., Blackstone, C., O'Kane, C. J., eds. (2021). Hereditary Spastic Paraplegias: at the Crossroads of Molecular Pathways and Clinical Options Lausanne: Frontiers Media SA. doi: 10.3389/978-2-88971-217-5

Table of Contents

frontiers in Neuroscience

EDITORIAL
published: 22 June 2021
doi: 10.3389/fnins.2021.708642

Editorial: Hereditary Spastic Paraplegias: At the Crossroads of Molecular Pathways and Clinical Options

Andrea Martinuzzi[1]*, *Craig Blackstone*[2], *Cahir J. O'Kane*[3]* and *Giovanni Stevanin*[4]

[1] Department of Conegliano, Istituto di Ricovero e Cura a Carattere Scientifico "E. Medea" Scientific Institute, Pieve di Soligo, Italy, [2] Department of Neurology, Massachusetts General Hospital, Boston, MA, United States, [3] Department of Genetics, University of Cambridge, Cambridge, United Kingdom, [4] Paris Sciences Lettres Research University, EPHE, Institut du Cerveau — Paris Brain Institute, Sorbonne Université, INSERM, CNRS, APHP, Paris, France

Keywords: hereditary spastic paraplegia, models, assessment, treatment, pathophysiology

Editorial on the Research Topic

Hereditary Spastic Paraplegias: Intersecting Molecular Pathways and Clinical Syndromes

Hereditary spastic paraplegias (HSPs) are a large group of rare neurologic conditions primarily affecting the longest corticospinal axons, with the pathognomonic triad of lower limb spasticity, weakness, and mild deep sensation impairment. Additional signs and symptoms are found in patients with complex (or complicated) forms. In spite of its low incidence and prevalence, the condition has attracted rapidly growing interest from the scientific community.

Why is a rare disorder initially described in the late nineteenth century by the German neurologist Adolph Strümpell and barely covered by the scientific literature throughout most of the twentieth century now exploding in terms of clinical, physiological, molecular and genetic interest? Certainly, the advent of next generation sequencing and the rapid identification of new disease genes play key roles. Indeed, the number of HSP disease loci is fast approaching one hundred. The paradox of extreme genetic heterogeneity, still growing (∼40% of clinically diagnosed patients still escape molecular characterization) in the face of a mostly stereotypical clinical presentation, garners broad interest. Added to this is the conundrum of reconciling the multiple diverse cellular pathogenic themes proposed, which has piqued the interest of both basic and clinical scientists. It is thus not surprising that HSPs are among the conditions to which the large European initiative "Solve rare diseases" (http://solve-rd.eu/) has directed its attention, and there are also global efforts to gather data from dispersed clinical studies into structured, shared databases to facilitate investigations. In this issue of *Frontiers in Neuroscience*, 11 leading research groups from throughout the world discuss a diverse range of HSP topics, ranging from cellular and animal models to clinical investigations, emphasizing links of different cellular pathogenic themes to observable phenotypic and clinical manifestations.

The underlying physiopathologies of HSP dovetail with mechanisms currently in the spotlight for other, more common, neurologic disorders. These include the dysregulation of lipid metabolism, reviewed by Darios et al. in this issue and illustrated in detail by Sunderhaus et al. for PNPLA6 (SPG39). Lipid homeostasis is important for membrane maintenance and trafficking as well as synaptic and organelle functions, and alterations in the synthesis or degradation of various classes of lipids can led to CNS pathologies, which is not surprising for a tissue so highly enriched in lipids. Alterations of mitochondrial function, oxidative stress or impairment of axonal transport can occur in some HSP forms directly due to lipid metabolism impairment. On the other hand, lipid alterations can be observed in HSP forms associated to mutations in genes apparently unrelated to lipid metabolism, and the link between alterations of lipid metabolism and neurodegeneration remains unclear for many forms of HSP.

OPEN ACCESS

Edited and reviewed by:
Mark P. Burns,
Georgetown University, United States

***Correspondence:**
Andrea Martinuzzi
andrea.martinuzzi@lanostrafamiglia.it
Cahir J. O'Kane
cahiro@gmail.com

Specialty section:
This article was submitted to Neurodegeneration, a section of the journal Frontiers in Neuroscience

Received: *12 May 2021*
Accepted: *27 May 2021*
Published: *22 June 2021*

Citation:
Martinuzzi A, Blackstone C, O'Kane CJ and Stevanin G (2021) Editorial: Hereditary Spastic Paraplegias: At the Crossroads of Molecular Pathways and Clinical Options. Front. Neurosci. 15:708642. doi: 10.3389/fnins.2021.708642

Endolysosomal functions are also commonly implicated in HSP; and Allison et al. show here that some variants in the MIT domain of the spastin protein do not directly affect its microtubule severing activity, as demonstrated for most other mutations, but rather alter endosomal tubule fission, molecule sorting via the tubular-vesicular pathway and lysosomal morphology, prefiguring future personalized "mutation-oriented" therapies. In addition, most neurodegenerative diseases have been considered for decades as resulting from cell autonomous mechanisms, meaning that single pathological events in neurons suffice to produce the disease. This has been reconsidered in many neurodegenerative conditions with the "neighborhood matters" concept, and HSP is no exception. Ozdowski et al. demonstrate here the important contributions of glial dysfunction to the synaptic defects in SPG4. They showed that the synaptic anomalies due to spastin knock-out can be reverted through Pak3 loss of function in glial cells; Pak3 is a kinase crucial for actin distribution and cell mobility, particularly important for glial projections at the neuromuscular junction.

While identification of human HSP causative genes has opened new routes to understanding the pathogenic mechanisms underlying these diseases, model organisms have proved invaluable in understanding how these genes, and mutations affecting them, affect neuronal function in whole organisms, from both genetic and physiological perspectives. Genetically, both Sunderhaus et al. and Montagna et al. use *Drosophila* to assay effects of disease-associated mutations in human HSP genes. Sunderhaus et al. show that HSP-causative alleles of human *PNPLA6* (*SPG39*) retain some biological functions in transgenic flies, and Montagna et al. provide evidence for loss-of-function effects of disease-causing mutations in *atlastin-1* (*SPG3A*). Transgenic targeted-expression tools were used by Ozdowski et al. to show the potential for glial cells to contribute to the phenotypes resulting from loss of spastin. Many HSP proteins are structural or enzymatic components of endoplasmic reticulum (ER) membrane, suggesting that axonal ER dysfunction might be a key mechanism for HSP. Thus, Oliva et al. and Napoli et al. characterize effects of HSP-related mutant genotypes on ER Ca^{2+} handling (Oliva et al.) and ER stress (Napoli et al.), and the latter study also shows pharmacological effects on the phenotypes. While not yet translatable to patients, the Napoli et al. study shows the potential of such models to assess pharmacological target proteins and processes. Finally, this collection contains two review articles that draw on genetic and physiological work on model organisms. Naef et al. review the genetic and cellular insights into complicated HSPs derived from zebrafish studies, while Fowler et al. review how interactions between organelles may be sites for some of the cellular defects that contribute to HSP pathology.

The clinical perspective is addressed from two important points of view: the search for clinically useful and efficient biomarkers (Montanaro et al.) and the evaluation of the efficacy of currently available interventions (Paparella et al.). The work on the multimodal MRI is particularly intriguing. Besides confirming the ability of so-called "advanced MRI" to capture widespread structural alterations in the brains of HSP patients, it provides the problematic finding of a paradoxical increase in Fractional Anisotropy (reflecting in certain ways the degree of order and organization of the axons within the central nervous tissue) in the longitudinal assessment of these patients. The interpretation of this finding is challenging. Some hypotheses are given in the paper, but certainly this is an area where information coming from studies on animal and cellular models might offer insight. The paper on the efficacy and safety of the approach combining chemodenervation with botulinum toxin and intensive physiotherapy highlights the importance of individualizing treatment solutions to the specific pattern of spasticity and motor impairment presented by each patient. In a condition characterized by wide heterogeneity of genes involved and pathways deranged in the setting of a shared principal phenotype (lower limb spasticity and weakness), this is a much needed reminder that the unifying feature of spastic paraplegia can mask subtle but clinically very relevant nuances that need to be taken into consideration when planning interventional trials. Again, a systematic appraisal of phenotypic patterns across the different SPG types might reveal patterns coherent with data emerging from the pathophysiology studies.

In summary, the goal of this scientific topic issue was to provide an arena for encounters between basic science advancements and clinical aspects in HSP. The topic has been addressed from various perspectives, but it is noteworthy that in addition to two papers overtly dedicated to the clinical approach, at least four other papers approaching the topic from a basic science perspective specifically mention the possible uses of these insights toward the development of much needed new therapies. This Research Topic issue in just a few months has attracted well over 30,000 views, confirming the fervent interest across the scientific and medical community for the HSPs. Indeed, the crossroads that the issue sought to portray between molecular pathways and clinical investigations looks more like a bridge, linking the two worlds.

AUTHOR CONTRIBUTIONS

All authors listed have made a substantial, direct and intellectual contribution to the work, and approved it for publication.

ACKNOWLEDGMENTS

The financial support of the Italian Ministry of health is gratefully acknowledged (RC2021).

Conflict of Interest: The authors declare that the research was conducted in the absence of any commercial or financial relationships that could be construed as a potential conflict of interest.

frontiers in Neuroscience

REVIEW
published: 11 October 2019
doi: 10.3389/fnins.2019.01051

NeurodegenERation: The Central Role for ER Contacts in Neuronal Function and Axonopathy, Lessons From Hereditary Spastic Paraplegias and Related Diseases

*Philippa C. Fowler[1], M. Elena Garcia-Pardo[1], Jeremy C. Simpson[2] and Niamh C. O'Sullivan[1]**

[1] UCD School of Biomolecular and Biomedical Science, UCD Conway Institute, University College Dublin, Dublin, Ireland,
[2] UCD School of Biology and Environmental Science, UCD Conway Institute, University College Dublin, Dublin, Ireland

OPEN ACCESS

Edited by:
Giovanni Stevanin, INSERM U1127 Institut du Cerveau et de la Moelle Épinière (ICM), France

Reviewed by:
Yang Hu, Stanford University, United States
Soledad Matus, Fundación Ciencia and Vida, Chile

***Correspondence:**
Niamh C. O'Sullivan
niamh.osullivan@ucd.ie

Specialty section:
This article was submitted to Neurodegeneration, a section of the journal Frontiers in Neuroscience

Received: *26 July 2019*
Accepted: *19 September 2019*
Published: *11 October 2019*

Citation:
Fowler PC, Garcia-Pardo ME, Simpson JC and O'Sullivan NC (2019) NeurodegenERation: The Central Role for ER Contacts in Neuronal Function and Axonopathy, Lessons From Hereditary Spastic Paraplegias and Related Diseases. Front. Neurosci. 13:1051. doi: 10.3389/fnins.2019.01051

The hereditary spastic paraplegias (HSPs) are a group of inherited neurodegenerative conditions whose characteristic feature is degeneration of the longest axons within the corticospinal tract which leads to progressive spasticity and weakness of the lower limbs. Though highly genetically heterogeneous, the majority of HSP cases are caused by mutations in genes encoding proteins that are responsible for generating and organizing the tubular endoplasmic reticulum (ER). Despite this, the role of the ER within neurons, particularly the long axons affected in HSP, is not well understood. Throughout axons, ER tubules make extensive contacts with other organelles, the cytoskeleton and the plasma membrane. At these ER contacts, protein complexes work in concert to perform specialized functions including organelle shaping, calcium homeostasis and lipid biogenesis, all of which are vital for neuronal survival and may be disrupted by HSP-causing mutations. In this article we summarize the proteins which mediate ER contacts, review the functions these contacts are known to carry out within neurons, and discuss the potential contribution of disruption of ER contacts to axonopathy in HSP.

Keywords: endoplasmic reticulum, axon, mitochondria, lipid droplet, endolysosome, plasma membrane, microtubule

INTRODUCTION

Hereditary spastic paraplegias (HSPs) are a genetically complex group of neurodegenerative disorders characterized by degeneration of the longest axons within the corticospinal tract leading to progressive lower limb spasticity and weakness. To date, mutations in over 80 spastic paraplegia genes (SPGs) and 60 gene products have been identified to give rise to HSP (Blackstone, 2018). Proteins encoded by these SPGs have roles in an apparently diverse range of cellular functions including: organelle shaping, axonal transport, lipid metabolism, mitochondrial function and endosomal trafficking. Despite this genetic and functional diversity, it has become clear over the last decade that the most prevalent SPGs, accounting for over half of all cases of autosomal dominant

HSP, encode proteins that are involved in the shaping and organization of the tubular endoplasmic reticulum (ER) (Boutry et al., 2019).

The ER-shaping proteins are integral membrane proteins which localize to the outer layer of the ER bilayer and regulate the organization of the tubular ER network. These proteins generally share little sequence homology, however, they all possess a reticulon homology domain (RHD) (**Figure 1**). This conserved domain consists of two hydrophobic sequences separated by a hydrophilic linker that forms a wedge by which the proteins insert into the lipid bilayer (Voeltz et al., 2006; Hu et al., 2008). By forming homomeric and heteromeric oligomers the ER-shaping proteins shape and stabilize the highly curved ER tubules (Shibata et al., 2009). Many different ER-shaping proteins are known including: Spastin (Park et al., 2010), Atlastin (Hu et al., 2009), REEP (Shibata et al., 2008) and Reticulon (Voeltz et al., 2006). Mutations in any one of these genes causes axonopathy and gives rise to HSP (Hazan et al., 1999; Zhao et al., 2001; Züchner et al., 2006b; Montenegro et al., 2012; Esteves et al., 2014). It is therefore evident that the tubular ER has a vital role in the maintenance of long axons. However, the axonal functions of tubular ER are not well understood and mechanism(s) by which disruption of this organelle by HSP-causing mutations leads to neurodegeneration is not known.

The ER network is morphologically and functionally compartmentalized within different areas of cells, none more so than in highly polarized neurons (**Figure 2**). Within the neuronal cell body, ribosome-studded rough-ER (RER) predominates, the primary function of which is likely protein synthesis (Broadwell and Cataldo, 1983; Rolls, 2002; Wu et al., 2017). ER-shaping proteins are localized only at the curved edges of RER nanoholes and sheets (Shibata et al., 2010; Schroeder et al., 2019). In contrast to the cell body, ribosome-studded RER is not observed within the long axonal projections of neurons. Instead, tubules of smooth ER (SER) can be seen to extend the entire length of the axon into the presynaptic boutons (Wu et al., 2017; Yalçın et al., 2017). Throughout the axon these ER tubules make extensive contacts with other organelles and the cytoskeleton. At these contact sites, organelle membranes remain closely tethered but do not fuse. ER contacts are highly dynamic yet are not merely fleeting glances and can be maintained during organelle movement or trafficking (Friedman et al., 2010). Through these interactions, the tubular ER can regulate an array of cellular functions. Moreover, mutations in the genes encoding the protein tethers that mediate these contacts cause axonopathy in HSP and other neurodegenerative diseases including amyotrophic lateral sclerosis (ALS) and Charcot-Marie-Tooth disease (CMT) (**Table 1**). It is therefore important that we further our understanding of ER contacts to understand the role of tubular ER in axons and axonopathy.

The aim of this article is to review the current studies examining the functions of tubular ER in neurons and to highlight the areas where more work is urgently needed to further our understanding of the mechanism(s) by which disruption of this organelle may cause pathogenicity in HSP. We focus on discussing ER contacts with organelles and cytoskeletal elements for which there is the strongest evidence of a role in neurons.

ER-MITOCHONDRIAL CONTACTS IN NEURONS

Contact sites between the ER and mitochondria have been observed in electron micrographs since the 1950s, with those early experiments revealing a number of electron dense structures that localize to specialized domains between the ER and mitochondria (Copeland, 1959). These mitochondria-associated ER membranes (MAMs) are maintained at ∼10–30 nm, depending on cell type and the level of stress to which the cells are exposed, and it is estimated that ∼5–12% of the outer mitochondrial surface remains connected to the ER (Csordás et al., 2006; Stoica et al., 2014; Wu et al., 2017). This tight association suggests that maintenance of ER-mitochondrial contacts are vital for the function of both organelles and the cell more generally, and many studies have focused on elucidating the molecular complexes that are involved in ER-mitochondrial tethering.

How Are ER-Mitochondrial Contacts Regulated?

In yeast, the ER-mitochondria encounter surface (ERMES) and the ER membrane protein complex (EMC) proteins that mediate tethering of ER and mitochondria are well established (Kornmann et al., 2009; Lahiri et al., 2014). The identity of ER-mitochondrial tethers in eukaryotic cells however, has been much more complicated. In part, this is due to the large number of proteins that localize to ER-mitochondrial contacts (transporters, enzymes, receptors etc.) most of which are not in fact tethers. Distinguishing between these and *bona fide* tethers required to mediate the contact of these two organelles has proved challenging. Here we will discuss the most recent findings on the best studied of the proposed ER-mitochondrial tethers Mfn2, VAPB-PTPIP5 and PDZD8 (**Figure 3A**).

Mitofusins 1 and 2 (Mfn1 and Mfn2) are GTPases which regulate fusion of the outer mitochondrial membrane (OMM) during mitochondrial fusion. More recently, it has been shown that ER-resident Mfn2 also plays an important role in regulating ER-mitochondrial tethering. The first study identifying this novel role of Mfn2 outside the mitochondria used confocal microscopy to detect a disruption in ER morphology and a decrease in the distance between the ER and mitochondria in Mfn2 knockout cells (De Brito and Scorrano, 2008). The same group has more recently used electron microscopy (EM) and fluorescence-based proximity probes to further support their assertion that Mfn2 acts as an ER-mitochondrial tether via homodimers or heterodimers with Mfn1 (Naon et al., 2016). However, the exact nature of Mfn2's role in ER-mitochondrial contacts remains debated as several independent studies have found that loss of Mfn2 results in an increase in ER-mitochondrial association (Cosson et al., 2012; Filadi et al., 2015; Leal et al., 2016). These conflicting findings have not yet been fully explained, however, it is worth considering that under different conditions and with localized variations in protein concentrations, Mfn2 may contribute differently to the maintenance of ER-mitochondrial contacts.

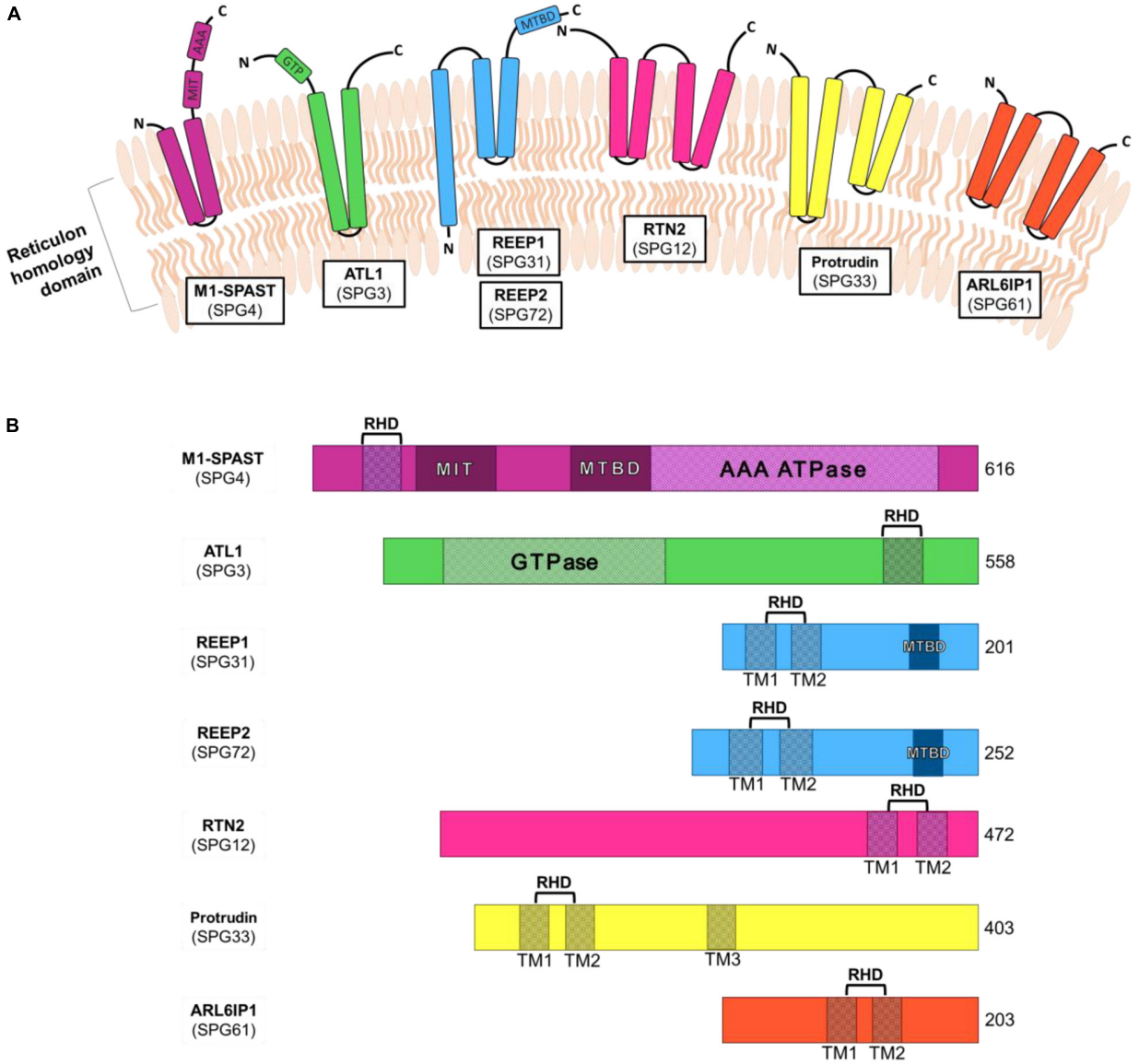

FIGURE 1 | Schematic diagrams of the structural domains of HSP-causing ER-associated genes. **(A)** ER-shaping proteins insert into the ER membrane via the reticulon homology domain. **(B)** ER-shaping protein domains include reticulon homology domain (RHD), made up of one or more transmembrane regions (TM), as well as microtubule interacting domain (MIT), microtubule binding domain (MTBD) and ATPase associated with various cellular activities (AAA). Shown are the amino acid number for the full-length longest isoforms of each protein.

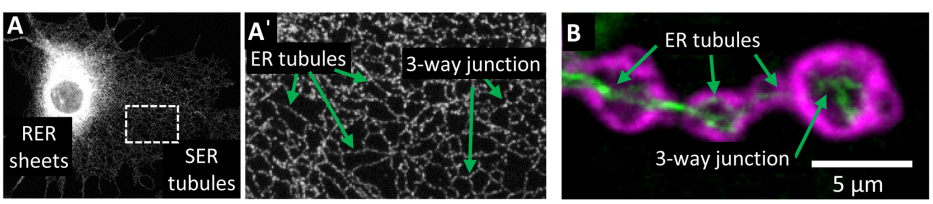

FIGURE 2 | Organization of the tubular ER network. **(A)** Visualization of ER compartments in Cos7 cells stained with REEP5 antibody. Rough ER (RER) sheets radiate from the nuclear envelope and are densely packed in the perinuclear region. Smooth ER (SER) tubules form a highly interconnecting network that extends to the periphery of the cell **(A')**. **(B)** Visualization of ER tubules within terminal boutons of *Drosophila melanogaster* motor neurons expressing Rtnl1:YFP (green) and stained with post-synaptic density protein DLG antibody (magenta). Within neurons, ER tubules extend the length of the axon and into the terminal boutons.

TABLE 1 | Overview of the proteins mediating tubular ER contacts and their involvement in neurodegenerative disease.

Protein	Subcellular localization	Function at ER contact	Causative link to neurological disease (if known)	References
ER-mitochondrial contacts				
VAPB	ER	VAPB and PTPIP51 interact forming tethers between the ER and mitochondria	Mutations in VAPB cause ALS type-8	Nishimura et al., 2004
PTPIP51	Mitochondria			
MFN2	ER, mitochondria	MFN2 contributes to the maintenance of ER-mitochondrial contacts through homo- or hetero-meric interactions with MFN1	Mutations in MFN2 cause CMT type 2A and hereditary motor and sensory neuropathy type 2A (HMSN2A)	Züchner et al., 2004; Züchner et al., 2006a
MFN1	Mitochondria			
PDZD8	ER	PDZD8 mediates ER-mitochondrial contacts by a mechanism that is yet to be determined and regulates Ca^{2+} transfer		
ER-lipid droplet (LD) contacts				
Seipin	ER/LD	Seipin dodecamers mediate ER-LD contacts and function to transfer lipids from the ER into bound LDs	Mutations in Seipin cause SPG17	Windpassinger et al., 2004
Snxl4	ER/LD	Snxl4 forms a tether between ER and LDs	Mutations in Snxl4 cause spinocerebellar ataxia autosomal recessive 20	Thomas et al., 2014
Rabl8	ER/LD	Rabl8-DFCP1 complexes form tethers between ER and LDs	Mutations in Rabl8 cause Warburg Micro syndrome	Bem et al., 2011
DFCP1	ER/LD			
ER-endolysosome contacts				
VAPA/B Mospd2	ER	Interactions between ER proteins VAPA/B or MOSPD2 and FFAT domain proteins (ORP1L, StARD3, StARD3NL) mediate	Mutations in VAPB cause ALS type-8	Nishimura et al., 2004
F FAT domain proteins	Late endosome	ER-eondosomal contacts which contribute to endosomal fission, endosomal trafficking and sterol transfer		
Protrudin	ER	Protrudin interacts with Rab7 and PI3P to promote ER- endome contacts which regulates endosomal trafficking along neurites	A mutation in Protrudin is associated with SPG33, however, the pathogenicity of the mutation is debated; Mutations in Rab7 cause CMT type 2B	Verhoeven et al., 2003; Mannan et al., 2006; Martignoni et al., 2008
Rab7	Endosome			
PTP1B	ER	PTP1B promotes ER-endosomal contacts by interacting with endosomal proteins such as EGFR		
EGFR	Endosome			
ER-plasma membrane (PM) contacts				
E-Sytl-3	ER	E-Syts mediate ER-PM contact and may function to regulate Ca^{2+} and lipid transfer		
VAPA/B	ER	VAPA/VAPB interactions with Kv2.1/2.2 form ER-PM contacts which act as traffickin hubs for intracellular signaling	Mutations in VAPB cause ALS type-8	Nishimura et al., 2004
Kv2.1/2.2	PM			
TMEM24	ER	TMEM24 mediates ER-PM contacts by electrostatic interaction and may regulate lipid transfer		
ER-microtubule (MT) contacts				
CLIMP-63	ER	CLIMP-63 binds MTs forming ER-MT contacts which function to regulate ER distribution in axons		
p180	ER	p180 binds MTs forming ER-MT contacts which function to stabilize MTs		
Sec61β	ER	Sec61β binds MTs forming ER-MT contacts which function to organize ER tubules along MTs		
REEP1	ER	REEP1 binds MTs forming ER-MT contacts which function to organize ER tubules along MTs	Mutations in REEP1 cause SPG31	Züchner et al., 2006b
MI-Spastin	ER	MI-Spastin binds and severs MTs regulating MT organization and regrowth	Mutations in Spastin cause SPG4	Hazan et al., 1999
STIM1/2	ER	STIM1/2-EB1 interactions for ER-MT contacts which regulate the transport of ER tubules along growing MTs		
EB1	MT			

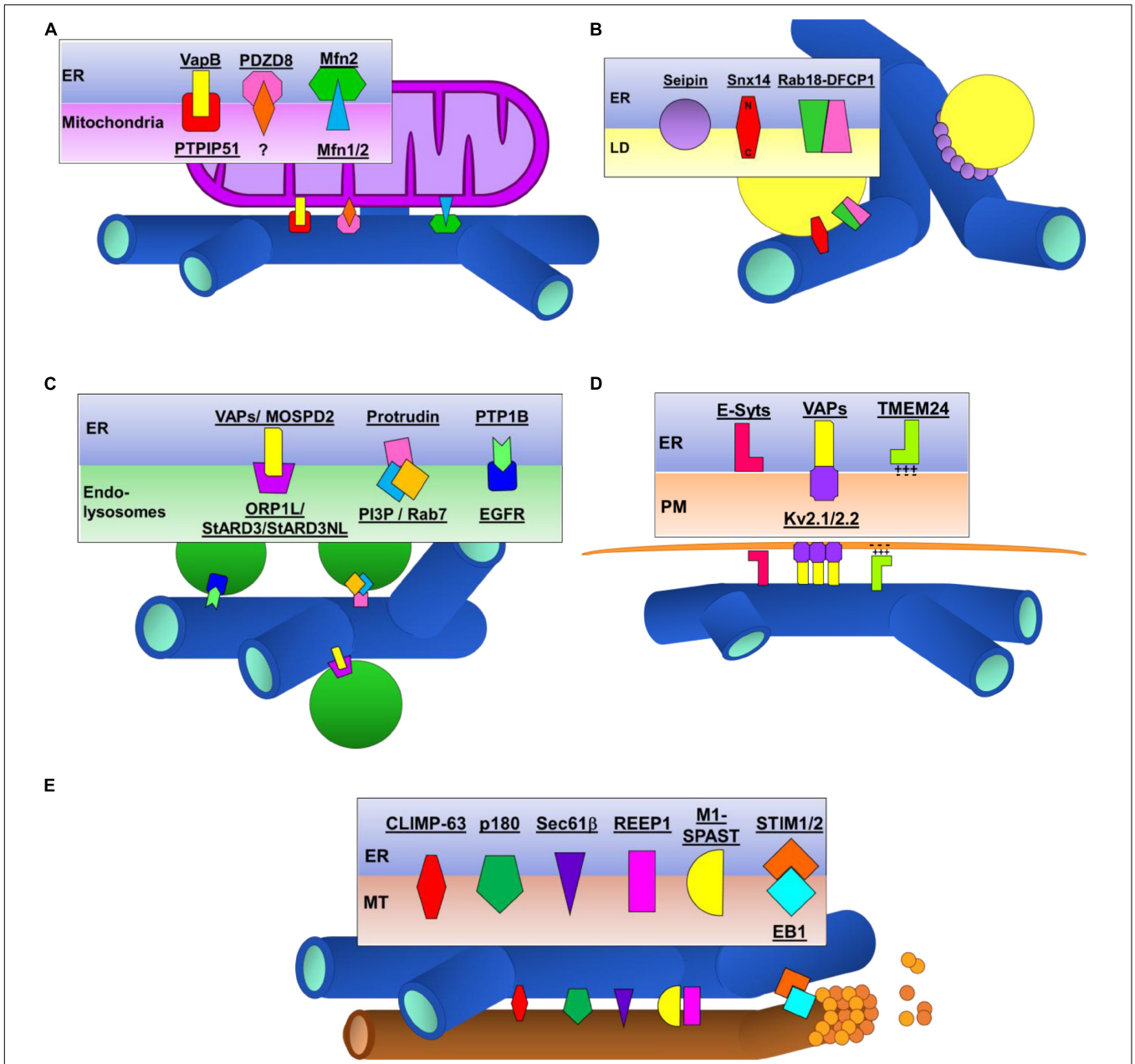

FIGURE 3 | Schematic illustrations of proteins tethers that contact the ER to other organelles and the cytoskeleton. **(A)** ER-mitochondrial contacts. **(B)** ER-lipid droplet (LD) contacts. **(C)** ER-endolysosomal contacts. **(D)** ER-plasma membrane (PM) contacts. **(E)** ER-microtubule (MT) contacts.

Probably the best studied ER-mitochondrial tether is VAPB-PTPIP51. It was through a yeast two-hybrid screen looking for interactors of the ALS-associated vesicle-associated membrane protein B (VAPB) that the interaction between VAPB and protein tyrosine phosphatase-interacting protein 51 (PTPIP51) was first identified (De vos et al., 2012). VAPB is an ER-resident protein whose cytoplasmic domain binds to the cytoplasmic domain of the OMM-resident PTPIP51. Knockdown of either VAPB or PTPIP51 reduces, and overexpression of either protein increases, ER-mitochondrial contacts detectable by EM or confocal microscopy (Stoica et al., 2014; Gómez-Suaga et al., 2019), providing evidence that these proteins form structural tethers between these organelles.

Recently, PDZD8, a paralog of the yeast ERMES protein Mmm1, has been found to be an important player in regulating ER-mitochondrial contacts in mammalian cells. Similar to Mmm1, PDZD8 localizes to ER and ER-mitochondrial contact sites (Hirabayashi et al., 2017). Focus ion beam–scanning EM of control and PDZD8 knockout HeLa cells reveals an ∼80% reduction in ER-mitochondrial contacts, with no detectable effect

on the organization of ER or mitochondrial networks. More studies are now required to identify the mitochondrial protein to which PDZD8 binds to mediate ER-mitochondrial contacts.

Where Are ER-Mitochondrial Contacts Within Neurons?

Whilst ER-mitochondrial contacts have been observed for 60+ years, it is only very recently that MAM structure within neurons has begun to be investigated. Initially, EM analysis of developing and adult hippocampal neurons revealed ER contacts covering ∼10% of the mitochondrial perimeter (Hedskog et al., 2013). Most recently, focused ion beam scanning electron microscopy of mouse brain tissue has revealed that MAMs are abundant throughout neurons, covering 4–5% of the mitochondrial surface (Wu et al., 2017). In fact, ER contacts with mitochondria are the most abundant ER contacts within axons and dendrites where the ER can be seen to wrap around mitochondria.

Known proteins involved in ER-mitochondrial tethering, Mfn2, VAPB-PTPIP51 and PDZD8, are all highly expressed in neurons throughout the brain of developing and adult mice (Eura et al., 2003; Stoica et al., 2014; Hirabayashi et al., 2017). Indeed, MAM-associated proteins have been observed within the ER-mitochondrial interface within synaptic regions, where interactions between VAPB and PTPIP51 have been shown to modulate dendritic spine morphology and synaptic activity in rat hippocampal neurons (Hedskog et al., 2013; Gómez-Suaga et al., 2019). The prevalence of axonal ER-mitochondrial interactions, together with the axonopathies which occur when ER-mitochondrial proteins are mutated, indicates that these contacts mediate functions which are critical to maintain intracellular homeostasis.

What Are the Functions of ER-Mitochondrial Contacts in Neurons?

Endoplasmic reticulum-mitochondrial contacts are functionally active sites at which several cellular processes occur including: calcium transfer from ER stores to mitochondria; mitochondrial fission; autophagosome formation; lipid biosynthesis; inflammation; apoptosis; ER stress. We will focus here on those functions that have are currently known to be physiologically relevant in neurons.

The most extensively studied function of MAMs within neurons is the regulation of Ca^{2+} signaling which has a fundamental role in the regulation of synaptic transmission and plasticity. Neurons have developed an intricate signaling pathway to couple Ca^{2+} signaling between the ER and mitochondria through specialized domains, permitting mitochondria to take advantage of localized Ca^{2+} release from the ER. Ca^{2+} released from ER stores can be imported into mitochondria via VDAC channels situated on the OMM, however, this requires localized high concentrations of Ca^{2+} (Giacomello et al., 2007). Mitochondria use this Ca^{2+} to generate ATP via the tricarboxylic cycle (Clapham, 2007). ER-mitochondrial contacts are vital for this Ca^{2+} transfer as expression of synthetic linker proteins, which increase the proportion of mitochondria in contact with the ER, increase ER-mitochondrial Ca^{2+} transfer (Csordás et al., 2010). Conversely, loss of PDZD8 or VAPB-PTPIP51 in cultured neurons, which decreases ER-mitochondrial contacts, inhibits ER-mitochondrial Ca^{2+} transfer (Hirabayashi et al., 2017; Gómez-Suaga et al., 2019). This Ca^{2+} shuttling at ER-mitochondrial contacts is vital for the function of neurons. Loss of VAPB-PTPIP51 decreases synaptic activity and number of active spines in cultured hippocampal neurons (Gómez-Suaga et al., 2019). Interestingly, this same study has found that synaptic activity increases ER-mitochondrial contacts pointing to an important role for ER-mitochondrial contacts in regulating synaptic function.

The first direct evidence that mitochondrial fission is regulated at sites where ER and mitochondria interact came from a seminal study by the Voeltz laboratory. Using 3D-EM, ER tubules were observed to wrap around mitochondria constricting the mitochondrial membrane (Friedman et al., 2011). Time-lapse imaging of these constriction sites in mammalian cells show that ER-mitochondrial contacts precede the recruitment of mitochondrial fission factors Drp1 and Mff and that following fission, both daughter mitochondria retain their contacts with the ER (Friedman et al., 2011; Elgass et al., 2015). Due to the exceptionally long nature of axons, mitochondrial processes need to be tightly regulated in order to maintain neuronal health, which need a healthy supply of mitochondria to meet the high energy demands required to maintain synaptic function. Mitochondria in axons are relatively short, ∼1 μm long compared to ∼4 μm long in dendrites, with fission tightly controlled. Impaired mitochondrial fission by knocking down Mff causes reduced neurotransmitter release and disrupts terminal axon branching (Lewis et al., 2018). Indeed, the importance of mitochondrial fission within neurons is highlighted by the fact that loss of Drp1 depletes mitochondria from synapses which causes impaired mitochondrial function and a failure to maintain proper synaptic transmission (Verstreken et al., 2005; Sandoval et al., 2014; Oettinghaus et al., 2016). Disruption of axonal ER by knocking down the ER-shaping proteins Arl6IP1 or Reticulon-like 1 (Rtnl1) also leads to impaired mitochondrial fission and neurodegenerative phenotypes which can be partially restored by increased Drp1 expression (Fowler and O'Sullivan, 2016). Together, these studies point to an important mechanism by which ER-mitochondrial contacts regulate axonal function.

Another function of MAMs that is particularly relevant to axonal physiology is the regulation of autophagy. Autophagy is the degradative pathway responsible for removing dysfunctional intracellular components and damaged organelles by sequestering them in double-membraned vesicles called autophagosomes. In the final step of autophagy, autophagosomes fuse with lysosomes, forming autolysosomes, the contents of which are degraded and their components recycled (He and Klionsky, 2009). The efficient initiation and completion of autophagy is essential for neuronal health which is reflected by the fact that a growing number of neurodegenerative diseases are characterized by autophagic dysfunction (Menzies et al., 2017). The formation of the isolation membrane is the first step in autophagy and the ER-mitochondrial interface has been proposed to serve as a nucleation site during the

formation of the isolation membrane. The autophagosomal marker Atg14 localizes to MAMs and the isolation membrane can be observed to form at ER-mitochondrial contact sites upon starvation induced-autophagy (Hamasaki et al., 2013). Altering ER-mitochondrial contacts disrupts autophagy such that increasing ER-mitochondrial contacts by expression of synthetic tethers impairs autophagic flux while knockdown of the ER-mitochondrial tethers VAPB-PTPIP51 activates the autophagy-initiating factor beclin 1 and increases autophagosome formation in a neuroblastoma cell line (Gomez-Suaga et al., 2017; Wu et al., 2018). More research is still required to uncover the mechanisms by which ER-mitochondrial contacts regulate autophagy in neurons.

Evidence That Links ER-Mitochondrial Contacts to HSP

Several lines of evidence have linked ER-shaping proteins REEP1, Reticulon 2 (RTN2), Atlastin and ARL6IP1, mutations in which cause HSP subtypes SPG31, SPG12, SPG3A and SPG61, respectively, to ER-mitochondrial contacts. Many ER-shaping proteins are found to localize to MAMs and expression of REEP1 or RTN2, but not HSP-causing mutant proteins, increases ER-mitochondrial contacts in split luciferase assays (Lim et al., 2015; Cho et al., 2017). Mutations in animal models of SPG3A and SPG61 reduce mitochondrial fission events indicative of defective ER-mitochondrial contacts (Fowler and O'Sullivan, 2016; Liu et al., 2019). Notably, highly elongated and hyperfused mitochondria and impaired mitochondrial fission have also been reported in fibroblasts of SPG31 patients indicating that that disrupted ER-mitochondrial contacts are a feature of this disease (Goizet et al., 2011; Lavie et al., 2017).

Defects pointing to impaired ER-mitochondrial contacts are also a fairly common feature of non-ER-shaping protein models of HSP. iPSCs from patients with SPG15 and SPG48, caused by mutations in spastizin and AP5Z1, respectively, have altered mitochondrial organization and mitochondrial fission (Denton et al., 2018). Furthermore, mitochondrial defects are evident in lympoblasts from patients with SPG28 and SPG56, caused by mutations in fatty acid metabolism proteins DDHD1 and CYP2U1 (Tesson et al., 2012). Taken together, whilst further studies are required to determine the exact consequences of HSP-causing mutations on MAM organization or function, it is becoming apparent that downstream processes dependant on the ER-mitochondrial axis are affected across many forms of HSP.

ER-LIPID DROPLET CONTACTS IN NEURONS

Lipid droplets (LDs) are densely packed neutral lipids, predominantly triacylglycerol (TG) and steryl esters (SE), surrounded by a phospholipid monolayer. LDs are used by many cells as fatty acid reservoirs for use in energy production or membrane biogenesis, but also act as a sink for fatty acids that could otherwise be toxic for cells. The lipids themselves are synthesized within the ER, in which the enzymes required to catalyze the biosynthesis of TG and SE reside. The LDs can either remain in contact with the ER or bud off from it to travel into the cytoplasm (Kassan et al., 2013; Wilfling et al., 2013).

How Are ER-LD Contacts Regulated?

Several proteins have been identified to play a role in initiating and regulating ER-LD contacts. Here we summarize recent findings on the best studied of these: Seipin, Rab18 and Snx14 (**Figure 3B**).

Numerous studies have shown that Seipin localizes to ER–LD contacts in yeast, insect, and mammalian cells (Szymanski et al., 2007; Salo et al., 2016; Wang et al., 2016). Recent structural analysis of the *Drosophila* Seipin protein revealed that Seipin forms a ring-shaped complex comprised of 12 Seipin monomers (Sui et al., 2018). This Seipin dodecamer consists of 3 distinct regions: short N- and C-terminal segments which orientate toward the cytoplasm; hydrophobic helices which imbed Seipin into the ER membrane; and a large β-sandwich domain, with similarity to lipid-binding proteins, which projects into the ER lumen. Seipin is required for the proper maturation of LDs and loss of Seipin leads aberrant LD morphology, specifically a general marked reduction in LD size with some very large LDs which are deficient in phospholipids (Szymanski et al., 2007; Fei et al., 2008; Salo et al., 2016; Wang et al., 2016). The current model suggests that Seipin complexes within the ER may localize to areas of high neutral lipid concentration where they can anchor the developing LD to the ER (via the N- and C-terminal segments). It is proposed that the ER luminal β-sandwich domain could function to transfer lipids from the ER into bound LDs, however, the mechanism by which this might occur is not yet known (Sui et al., 2018).

Rab18 was originally described as a lipid-droplet localized protein that induced contacts between ER and LDs (Ozeki et al., 2005). More recently, super-resolution live-cell imaging has revealed that activated Rab18 is normally distributed throughout the ER but upon induction of LD formation Rab18, along with another ER-resident protein DFCP1, localizes to discreet sites on the ER (Li et al., 2019). These discreet sites are likely early LD structures within the ER as treatment with TG synthesis inhibitors blocks formation of these sites. The Rab18-DFCP1 complex interacts with ZW10 and ER-resident SNAREs which maintain the ER-LD contact for these developing LDs (Xu et al., 2018; Li et al., 2019). Rab18 and DFCP1 are required for the formation of ER-LD contacts such that loss of Rab18 or DFCP1 reduces ER-LD contacts while overexpression of either protein increases ER-LD contacts (Xu et al., 2018; Li et al., 2019).

Sorting nexin protein 14 (Snx14) resides within the ER via transmembrane domains and characterization of Snx14 mutants revealed neutral lipid metabolism and LD defects (Bryant et al., 2018). During LD maturation upon treatment with fatty acids, Snx14 specifically localizes to ER-LD contacts (Datta et al., 2019). At these contacts, Snx14 remains embedded in the ER via its N-terminal transmembrane domains and binds to the LD surface via a C-terminal amphipathic helix domain (Datta et al., 2019). Loss of Snx14 reduces ER-LD contacts while over-expression of Snx14 increases ER-LD contacts indicating that Snx14 is acting as a protein tether for these contacts.

Current findings suggest that while there is crosstalk between some ER-LD tethers, others seem to function independently of each other. For example, Seipin regulates the growth of DFCP1-Rab18-labelled developing LDs, though it is not known if this control occurs by a direct interaction between these complexes or by an indirect mechanism (Li et al., 2019). In contrast, Seipin and Snx14 seem to function independently of each other to regulate LD morphology as overexpression of Seipin cannot rescue LD defects in Snx14 cells and vice versa (Datta et al., 2019). It will be important to determine whether distinct ER-LD tethers function in discreet regions of the cytoplasm or in response to different stimuli.

Where Are ER-LD Contacts Within Neurons?

Endoplasmic reticulum-LD contacts have been visualized extensively in yeast, insect and mammalian cell cultures by both electron and confocal microscopy (Novikoff et al., 1980; Wilfling et al., 2013). More recently, the stability of ER-LD contacts has been measured in real time using sub-diffraction limited confocal microscopy revealing that a large proportion of ER-LD contacts are stable with LD remaining associated with the ER as it moves throughout the cytoplasm of mammalian cell cultures (Salo et al., 2016).

In contrast, ER-LD contacts have been reliably visualized in neurons. In fact, while various studies have reported LDs in *Drosophila* axons (Papadopoulos et al., 2015), rodent cortical neurons (Renvoisé et al., 2016) and primary cultures of cortical neurons (Branchu et al., 2017), many other studies do not see LDs within neurons under normal conditions. While LDs are not readily found within neurons, they are clearly present in the glia adjacent to neurons within central and peripheral neuronal structures. Within *Drosophila*, LDs can be seen within epithelial glia surrounding photoreceptors (Liu et al., 2015) and within cortical glia within the ventral nerve cord (Bailey et al., 2015). Moreover, LDs have been found to accumulate within neurons and glia in response to stressors such as nutrient deprivation, hypoxia, increased reactive oxygen species (ROS), or expression of mutations in proteins involved in lipid production (Inloes et al., 2014; Bailey et al., 2015; Liu et al., 2015).

Given the elusive nature of neuronal LDs, it is unsurprising that ER-LD contacts have not so far been studied in neurons. However, ER-LD protein tethers are present in neurons. Seipin (Wang et al., 2018), Rab18 (Wu et al., 2016) and Snx14 (Huang et al., 2014) are all highly expressed in the mouse brain, localizing within neurites in cultured neurons (Huang et al., 2014; Nian et al., 2019). It is therefore likely that ER-LD contacts can be generated and maintained within neurons and may be dysregulated during neurodegeneration.

What Are the Functions of ER-LD Contacts in Neurons?

As a result of the paucity of information on LDs and ER-LD contacts within neurons, there are no studies validating their functions within neurons generally or axons specifically. Given the clear overlap between ER-LD organization and neurodegeneration in HSP, it seems crucial that future studies aim to determine the mechanisms by which disrupted ER-LD contacts contribute to pathological dysfunction in motor neurons. A recent paper puts forward several hypotheses as to the potential functions of LDs which may be disrupted during neurodegeneration (Pennetta and Welte, 2018). These include that neuronal LD might act to: prevent neuronal lipotoxicity by sequestering fatty acids and transferring them to glia; traffic proteins and lipids required for synapse assembly along the axon; and sequester mutated or aggregated proteins for degradation. While some evidence exists which could support each of these hypotheses, a significant amount of work is now required to determine whether any of these mechanisms are relevant to neurodegenerative disease.

Evidence That Links ER-LD Contacts to HSP

Mutations in the ER-LD tether Seipin causes autosomal dominant (AD) HSP subtype SPG17, also known as Silver syndrome, a complicated form of HSP which is characterized by amyotrophy in the hands and sometimes lower limbs (Windpassinger et al., 2004). Expression of disease-causing Seipin mutants *in vitro* and *in vivo* triggers ER stress responses with increased production of ER chaperones (Ito et al., 2008; Yagi et al., 2011) which was proposed to be the mechanism by which motor neurons degenerate in disease. As discussed above, it is now clear that Seipin has a crucial role in LD biogenesis at ER-LD contacts (Salo et al., 2016; Wang et al., 2016). To understand the pathophysiological significance of this in HSP, we need to uncover how HSP-causing mutations affect LD biogenesis *in vivo*.

In addition to Seipin, mutations in several genes encoding enzymes which regulate lipid metabolism cause HSP. DDHD1 and DDHD2 are lipid metabolizing enzymes mutations in which give rise to autosomal recessive (AR) HSP subtypes SPG28 (Bouslam et al., 2005) and SPG54 (Schuurs-Hoeijmakers et al., 2012), respectively. Brain tissue from DDHD1$^{-/-}$ or DDHD2$^{-/-}$ knockout mice has disrupted lipid content (Inloes et al., 2014, 2018). Perturbed lipid processing appears to be an important contributor to neuronal dysfunction with large LD accumulations accompanying marked motor impairments in DDHD2$^{-/-}$ mice (Inloes et al., 2014) and evidence of lipid accumulation in the brains of SPG54 patients (Schuurs-Hoeijmakers et al., 2012). Furthermore, mutations in fatty acid 2-hydroxylase (FA2H) and patatin like phospholipase domain containing 6 (PNPLA6) cause complicated AR-HSP subtypes SPG35 and SPG39, respectively (Rainier et al., 2008; Dick et al., 2010) and mutations in carnitine palmitoyl-transferase (CPT1C) cause pure AD-HSP subtype SPG73 (Rinaldi et al., 2015). Animal models of these disorders frequently display LD defects and motor neuron defects (Song et al., 2013; Rinaldi et al., 2015; Li et al., 2019), highlighting the conserved link between LD organization and neuronal function.

Finally, LD defects are frequently detected in models of HSP which are not directly known to function in lipid metabolism or LD biogenesis. Mutations in the ER-shaping proteins REEP1, Atlastin and Spastin have all been shown to disrupt LD formation

in vivo (Klemm et al., 2013; Papadopoulos et al., 2015; Renvoisé et al., 2016). This likely occurs largely as a result of the defective tubular ER network organization that loss of these proteins causes though specific roles for these proteins in LD organization cannot be ruled out. To that end, HSP-causing M1 Spastin has recently been shown to disrupt LD content by impaired LD-peroxisome contact formation (Chang et al., 2019). Loss of SPG20 (Spartin) or SPG11 (Spatacsin) causes altered LD regulation in mouse embryonic fibroblasts and primary cortical neurons, possibly by impaired LD turnover (Renvoisé et al., 2012; Branchu et al., 2017). Taken together, it is clear that disruption of lipid metabolism and/or storage at the ER-LD interface is a common feature of HSP.

ER-ENDOLYSOSOMAL CONTACTS IN NEURONS

The endolysosomal system is a dynamic network of intracellular membranous compartments that continuously interconvert and play essential roles in nutrient uptake, metabolic control, macromolecular degradation and signaling (Klumperman and Raposo, 2014). According to their functions, several different types of compartments have been identified, which include early endosomes, late endosomes, recycling endosomes and lysosomes. The maturation of early endosomes into late endosomes is characterized by a series of defined stages, including endosome growth and acidification, which creates a unique environment within the cell to allow for the breakdown of products into smaller polypeptides to help maintain amino acid pools and energy balance. The ER makes dynamic contacts with endosomal compartments which increase as endosomes mature (Friedman et al., 2010, 2013).

How Are ER-Endolysosomal Contacts Regulated?

Multiple protein tethers regulating contacts between the ER and endosomes/lysosomes have been identified. The best studied of these involve VAPs localized to the ER and FFAT domain-containing proteins ORP1L, StARD3 and StARD3NL localized on endosomes (Loewen et al., 2003). Several other proteins have more recently been shown to contribute to ER-endolysosomal contacts including MOSPD2, protrudin-PI(3)B and PTP1B-EGFR (**Figure 3C**).

The first ER-endoslysosomal contact site to be characterized in mammalian cells were contacts between the integral ER protein VAPA and the late endosomal cholesterol binding protein ORP1L. ORP1L encodes a member of the oxysterol-binding protein (OSBP) family, a group of intracellular lipid receptors which are characterized by a C-terminal sterol binding and FFAT domains (Loewen et al., 2003). ORP1L is recruited to late endosomes via its interaction with Rab7 where it modulates ER-late endosome interactions. Under conditions of low cholesterol, the cholesterol-binding domain of ORP1L is unoccupied favoring a conformation that promotes interactions between the FFAT domain of ORP1L and VAPA forming ER-late endosomal contacts (Rocha et al., 2009). In addition to ORP1L, two other FFAT domain containing late endosomal proteins StARD3 (steroidogenic acute regulatory domain-3) and StARD3NL (StARD3 N-terminal like) have been shown to modulate ER-late endosomal contacts by directly interacting with VAPA and VAPB proteins (Alpy et al., 2013). Overexpression of ORP1L, StARD3 or StARD3NL increases both the size and number of ER-late endosome interactions, pointing to a crucial role of these proteins in the formation of contacts between these two organelles (Rocha et al., 2009; Alpy et al., 2013). However, whilst the number of contacts increases upon overexpression of these proteins, no studies have reported a reduction in contact site formation upon depletion of ORP1L, StARD3 or StARD3NL. Therefore, whilst is remains unclear whether these proteins function to stabilize or promote ER-endosomal contacts, it is likely that other tethering systems exist to compensate for the absence of VAP proteins. In line with this, a study using a proteomic approach has recently identified MOSPD2 (motile sperm domain containing 2) as a novel ER-anchored protein which binds FFAT motifs and consequently allows membrane tethering *in vitro*, where silencing of MOSPD2 leads to a reduction in the surface contact between ER and endosomes (Di Mattia et al., 2018).

The integral ER protein protrudin, which promotes cellular protrusions and neurite outgrowth in cultured cells (Shirane and Nakayama, 2006; Hashimoto et al., 2014), interacts with PI3P and Rab7 at the endosome to promote ER-endosomal interactions. Overexpression of protrudin causes increased stabilization of tubular SER and the formation of multiple and extended endosomal contacts (Hashimoto et al., 2014; Raiborg et al., 2015). Conversely, reduced protrudin expression disrupts ER organization with an expansion of RER into the periphery of cultured cells (Chang et al., 2013).

Two other proteins reported to promote ER-endolysosomal contacts includes interactions with the endosomal epidermal growth factor receptor (EGFR) and the ER-localized PTP1B (protein tyrosine phosphatase) (Eden et al., 2010). Specifically, the ER has been shown to form direct contact sites with multivesicular bodies (MVBs) where it regulates the trafficking and signaling of the EGFR. These contacts form in both the presence and absence of EGF. Depletion of PTP1B decreases the number of contacts between EGFR-containing MVBs and the ER while overexpression of PTP1B slightly enhanced these contacts suggesting that this protein acts in the formation of the contacts between these two organelles (Eden et al., 2010).

Several additional tethers have been proposed to play a role in regulating contacts between the ER and endosomes, however, it remains unclear whether these serve as functional rather than structural tethers. This includes the endosomal-localized TMCC1 which localizes to discrete sites in the peripheral ER that are spatially and temporally linked to endosomal fission (Hoyer et al., 2018). Additionally, regions in which lysosomes remain closely associated with the ER have been shown to be densely populated by clusters of IP3Rs, however, it is thought that these do not contribute to the assembly of ER-lysosome contacts but rather serve as a functional tether to facilitate Ca^{2+} delivery from the ER to lysosomes (Atakpa et al., 2018).

Where Are ER-Endolysosomal Contacts Within Neurons?

Contacts between the ER membrane and endosomes, lysosomes and MVBs within yeast and mammalian cells have been visualized by high-resolution electron microscopy (Rocha et al., 2009; Eden et al., 2010; Di Mattia et al., 2018). Within mammalian cells, associations between the ER and endosomes typically cover ∼5% of the endosomal surface, which remain bound to the ER as they traffic (Friedman et al., 2010, 2013). This is achieved through the dynamic nature of ER tubules, which have been shown to rearrange their tubules in order to ensure maintained contact with dynamic endosomes (Friedman et al., 2010). Interestingly, contacts between the ER and endosomes become more tightly associated as they transition through the maturation steps, where endosomes that acquire Rab7, a marker of late endosomes, have been shown to be almost completely bound to the ER membrane (Friedman et al., 2013).

Most known ER-endolysosomal protein tethers have been shown to be expressed in neurons with high levels of expression of VAPA/B (Teuling et al., 2007), FFAT proteins (Johansson, 2003), protrudin (Shirane and Nakayama, 2006) and PTP1B (Song et al., 2016) found in rodent and human brain tissues. Despite this, it is only recently that ER-endolysosomal contacts have been examined within neurons. Focused ion beam scanning electron microscopy of mouse brain tissue reveals extensive contacts between the ER and endosomes, lysosomes and MVBs throughout neurons (Wu et al., 2017). Within neuronal cell bodies the ER was found to contact ∼2% of endosomal and lysosomal membranes while in dendrites and axons the extent of ER-endosomal contacts were somewhat less (1–2%) but were still clearly evident (Wu et al., 2017).

What Are the Functions of ER-Endolysosomal Contacts in Neurons?

Several different cellular functions have been attributed to ER-endolysosomal contacts including the regulation of endosomal tubule fission and endosome transport as well as lipid and Ca^{2+} transfer between these two organelles. The functions of these contacts have mostly been studied in non-neuronal cells, but recent studies have confirmed some of these functions in neurons.

The endolysosomal system is highly dynamic and ER-endolysosomal contacts play an important role in the regulation of endomembrane fission and vesicle budding. This function was first uncovered in Cos7 cells where contacts between the ER and early and late endosomes were found to mark sites of endosomal constriction and fission (Rowland et al., 2014). Disruption of the SER network by dysregulated expression of the ER-shaping proteins RTN4a or Spastin impairs endosome fission (Rowland et al., 2014; Allison et al., 2017). The mechanism for how ER-endolysosomal contacts regulate endosomal fission is not fully understood but it requires the action of the ESCRT protein IST1 (increased sodium tolerance 1) which forms a helical complex with CHMP1B (charged MVB protein 1B) to modulate endosomal constriction by promoting positive membrane curvature (McCullough et al., 2015; Allison et al., 2017). Additionally, the WASH complex, an actin-regulating complex that is recruited to endosomes by interactions with the retromer complex, has recently been shown to regulate endosomal fission through via interactions with VAP-proteins which act directly at the ER-endosome interface (Derivery et al., 2009; Dong et al., 2016). ER-endolysosomal contacts similarly regulate endolysosomal fission in neurons as disruption of the SER network in mouse primary cortical neurons results in elongated lysosomes, indicative of impaired fission (Allison et al., 2017).

Endoplasmic reticulum-endolysosome contacts are also important in controlling the association of endosomes with the cytoskeleton (Nielsen et al., 1999). Endosomes destined for lysosomal fusion and degradation are trafficked along the cytoskeleton as they undergo many sorting, fusion and fission events. The ER-endosomal tethering complex VAPA-ORP1L modulates the positioning and transport of late-endosomes by forming a complex with Rab7 and its effector RILP (Rab7-interacting lysosomal protein) (Tong et al., 2019). RILP in turn binds the $p150^{Glued}$ subunit of the dynactin protein complex, and under low cholesterol in the endocytic pathway, VAPA-ORP1L interactions at ER-endosome contacts result in VAPA-mediated dissociation of RILP from $p150^{Glued}$ and its associated motors (Rocha et al., 2009; Tong et al., 2019). Additionally, VAPA-ORP1L contacts have been shown to modulate the positioning and transport of autophagosomes by forming ER-autophagosome contacts that prevent transport by the Rab7-RILP-dynein complex (Wijdeven et al., 2016). Given the unique morphology of neurons, the directed traffic of cargo along axons poses a significant challenge which must be tightly regulated in order to maintain neuronal homeostasis. However, to date the role of ER-endolysosome contacts in endosomal trafficking has not been extensively investigated within neurons. The one exception would be protrudin-Rab7-PI(3)B-mediated ER-endolysosome contacts which are required to load the motor protein kinesin-1 on another Rab7 effector FYCO1, allowing for the plus-end transport of late endosomes (Pankiv et al., 2010). Knockdown of protrudin in the neural crest-derived PC12 cell line impairs trafficking of synaptic vesicles from the cell body along neurites providing evidence that ER-endolysosomal contacts do contribute to endosomal trafficking in this neuronal model (Shirane and Nakayama, 2006).

Given that most interactions between the ER and late endosomes involve cholesterol-binding proteins, it is not surprising that an emerging function attributed to ER-late endosomal contacts involves the transfer of sterols between these two organelles. This originally came from the observation of ER-endolysosomal contact sites that were linked with the flow of cholesterol between these two organelles, and most recently, a more directed manner of cholesterol transport has now been shown to occur through these contact sites (Du et al., 2011; Olkkonen and Li, 2013). These include the tethering complexes VAP-ORP1L and VAP-StARD3, where loss of either of these have been shown to impair cholesterol transfer from endosomes to the ER (Wilhelm et al., 2017; Zhao and Ridgway, 2017). However,

whilst the functions of these have been extensively studied within non-neuronal cells, whether or how these tethering complexes mediate cholesterol transfer from endosomes to the ER within neurons remain undetermined. Similarly, whilst the bidirectional amplification of ER and lysosome Ca^{2+} signals has been shown to occur at ER-lysosomal contact sites within non-neuronal cells, it remains unclear whether or how ER-lysosomal Ca^{2+} signaling within neurons is mediated. Given that Ca^{2+} signaling between the ER and lysosomes are widely believed to promote endosome–lysosome fusion, endolysosomal trafficking and endosome refilling (Calcraft et al., 2009; Galione et al., 2010; Cao et al., 2017; Feng and Yang, 2017), further studies are required in order to determine whether any of these mechanisms are relevant to maintaining neuronal homeostasis.

Evidence That Links ER-Endolysosomal Contacts to HSP

Disruption in the organization and/or function of the endolysosomal network is a hallmark of *in vivo* and *in vitro* models of several forms of HSP. Loss spatacsin or spastizin, associated with AR-HSP subtypes SPG11 and SPG15, respectively, results in depletion of the number of lysosomes available for fusion with autophagosomes (Chang et al., 2013; Varga et al., 2015). Loss of the WASH complex protein strumpellin, mutations in which give rise to AD-HSP subtype SPG8, similarly results in a reduction in lysosomal number and a significant enlargement of lysosomes (Allison et al., 2017; Song et al., 2018). Moreover, fibroblasts from SPG48 patients, caused by mutations in the AP-5 subunit AP5Z1, exhibit an accumulation of endolysosomes containing aberrant storage material (Hirst et al., 2015).

There is also mounting evidence for a conserved role for HSP-causing ER-shaping proteins in endolysosomal organization. *In vivo* models of HSP caused by loss of the ER-shaping proteins Spastin, Atlastin and REEP1 give rise to endosomal or lysosomal abnormalities. Time-lapse imaging of tagged endosomes in Arabidopsis *rhd3* mutants, the plant homolog of mammalian Atlastins, reveals that loss of rhd3 significantly disrupts endosomal streaming (Stefano et al., 2015). Primary cortical neurons derived from knockout Spastin or REEP1 mice develop significantly enlarged lysosomes containing membranous material and similar lysosomal abnormalities have been observed in iPSC-derived neurons from a SPG4 patient (Allison et al., 2017). It is interesting to speculate that these phenotypes may arise because of impaired endosomal budding or trafficking but to date there is no direct evidence to support this hypothesis. It is clear however, that impaired autolysosomal clearance results in the accumulation of undegraded material which may be of relevance to disease pathogenesis.

Finally, the ER-endolysosomal protein tether Protrudin has been linked directly to AD-HSP subtype SPG33 (Mannan et al., 2006). It should be noted, however, that the role of Protrudin in HSP is debated as the missense mutation associated with SPG33 has been identified in a SNP in several population and does not lead to loss of function of Protrudin (Martignoni et al., 2008).

ER-PLASMA MEMBRANE CONTACTS IN NEURONS

Contacts between the ER and plasma membrane (PM) are ubiquitous in neuronal and non-neuronal cells. These contacts appear to be highly heterogeneous, being made up of various structural and functional proteins and performing a variety of roles depending on both the type and state of the cell.

How Are ER-PM Contacts Regulated?

Quite a large number of proteins have been shown to localize to ER-PM contacts where they contribute to the maintenance of cellular Ca^{2+} and lipid homeostasis, adequate response to extracellular stimuli or organelle dynamics. Here, we will summarize the proteins known to act as ER-PM structural tethers but not the purely functional, regulator or sorting proteins which also localize to these contacts (**Figure 3D**).

The integral ER proteins VAPA and VAPB have been mentioned in previous sections functioning as ER-mitochondrial and ER-endolysosomal tethers. The VAPs also mediate ER-PM contacts via interaction with non-conducting Kv2 channels in neurons. Kv2 channels (Kv2.1 and Kv2.2) are voltage-gated potassium channels, abundantly expressed in the mammalian brain, that contain a proximal restriction and clustering (PRC) motif, phosphorylation of which dynamically modulates clustering of Kv2-channels in the PM (Lim et al., 2000). While freely diffusing Kv2 channels regulate neuronal electrical activity, clustered Kv2 channels are non-conducting and seem to act as trafficking hubs (Fox et al., 2013). The PRC motif also functions as a non-canonical FFAT motif by which Kv2 channels bind to VAPs at ER-PM contacts (Johnson et al., 2018; Kirmiz et al., 2018). Overexpression of GFP-tagged Kv2.1 causes a nearly 10-fold increase in the proportion of PM in contact with the ER in HEK cells demonstrating a clear role for Kv2 channel clusters in ER-PM contact formation (Fox et al., 2015).

The extended-synaptotagmins (E-Syts1-3 in mammals) are highly conserved ER-anchored proteins that mediate ER-PM contacts. These contacts are formed by the E-Syt phospholipid-binding C2 domain interacting with the PM phospholipid phosphatidylinositol-4,5-bisphosphate (PI(4,5)P2) (Giordano et al., 2013). E-Syt's interaction with the PM is regulated by Ca^{2+} such that Ca^{2+} binding to E-Syt releases the C2 domain from an inhibitory binding or conformation so that it can interact with PI(4,5)P2 at the PM (Bian et al., 2018). E-Syts clearly have an important role in ER-PM formation as overexpression of the E-Syts increases, and knockdown decreases, the extent of ER-PM contacts (Giordano et al., 2013). Moreover, the distance between the ER and PM at ER-PM contacts can be regulated by localization of different E-Syts and by $[Ca^{2+}]$ (Fernández-Busnadiego et al., 2015).

Transmembrane protein 24 (TMEM24) is an ER-resident protein which forms contacts with the PM. It consists of an N-terminal transmembrane domain, by which it anchors to the ER, and a C-terminal region by which if forms electrostatic interactions with the PM (Lees et al., 2017). Overexpression of TMEM24 increases the proportion of PM in contact with the ER

in both HeLa cells and primary neurons (Lees et al., 2017; Sun et al., 2019). This protein tether mediates ER-PM contacts in an activity-dependent manner.

Several proteins are also known to localize to and carry out important functions at ER-PM contacts but have not yet been shown be required to form these contacts. The ER resident stromal interacting molecules STIM1 and STIM2 translocate to the PM upon Ca^{2+} depletion from the ER to bind and activate the PM Orai protein (ORAI1 and ORAI2). STIM-ORAI binding opens the calcium release-activated channels thereby triggering Ca^{2+} entry into the cell, a process known as store-operated Ca^{2+} entry (SOCE) (Park et al., 2009). While Ca^{2+} depletion causes STIM to move toward the PM to interact with ORAI, it is the action of E-Syt1 that seems to mediate the extended ER-PM contacts that occur during Ca^{2+} store replenishment (Poteser et al., 2016; Kang et al., 2019). In addition, several members of the oxysterol-binding protein–related protein (ORP) family localize to ER-PM contacts. Of these, ORP5 an ORP8 possess a transmembrane domain enabling them to directly insert into the ER membrane, while ORP3 and ORP6 lack this transmembrane domain and interact with VAPs within the ER to mediate the ER-PM contacts (Chung et al., 2015; Mochizuki et al., 2018). ORP proteins bind PM phosphatidylinositol lipids through a pleckstrin homology domain and act as lipid transporters, but, no direct evidence exists that these proteins contribute to the structure of ER-PM contacts. Finally, Sec22b is an ER protein which interacts with synataxin 1 (Stx1) at ER-PM contacts without triggering fusion of the two membranes. Artificially elongating Sec22b increases the distance between ER and PM at contacts, but again there is not definitive evidence that Sec22b-Stx1 are required for ER-PM contact formation (Petkovic et al., 2014).

Where Are ER-PM Contacts Within Neurons?

Endoplasmic reticulum-PM contacts are abundant within neurons having first been reported by electron microscopy studies in the 1960s (Rosenbluth, 1962). This is most clearly evident in the neuronal cell body where ∼12% of the PM surface appears in contact with the ER (Wu et al., 2017). These contacts are not static and are reversibly decreased following neuronal activity (Tao-Cheng, 2018). Within axons and dendrites ER-PM contacts are much less prevalent, perhaps reflecting a much greater PM-to-cytoplasmic ratio in these neuronal compartments (Wu et al., 2017). Nonetheless, ER-PM contacts are present along the length of axons in mammalian neurons.

The Kv2 channel proteins Kv2.1 and Kv2.2 are highly expressed in neuronal tissue and they colocalize with VAP proteins at ER-PM contacts in the cell bodies and axon initial segments of cultured and *in vivo* neurons (Kirmiz et al., 2018; Lebowitz et al., 2019). The interaction between Kv2 channels and VAPs seems to be an important determinant in the localization of these proteins in neurons with overexpression of Kv2.1 causing VAPs to redistribute to large ER-PM clusters while loss of VAPs reduce Kv2 clustering in the PM (Johnson et al., 2018; Kirmiz et al., 2018). Kv2 clusters in motor neurons can also be seen to be dynamic, redistributing into smaller clusters following neuronal activity (Romer et al., 2019).

In non-neuronal cells, E-Syt1 localizes throughout the ER but rapidly translocates to the ER-PM upon increase in cytosolic $[Ca^{2+}]$ (Saheki et al., 2016). Within neurons, the E-Syts are expressed in the adult mammalian brain, though only at modest levels (Min et al., 2007; Herdman et al., 2014). However, high levels of E-Syt expression has been reported in the motor neurons of mice and *Drosophila* (Meyer, 2014; Kikuma et al., 2017). The subcellular distribution of E-Syts in neurons has not yet been elucidated.

TMEM24 is highly expressed in neurons and its expression is increased in mature rather than developing neurons (Sun et al., 2019). In both neuronal and non-neuronal cells, TMEM24 localizes throughout the ER but is enriched at ER-PM contacts (Lees et al., 2017; Sun et al., 2019). TMEM24 staining is particularly evident in cell bodies but is faintly detectable in the axons of primary cultured neurons. Synaptic activity triggers the transient removal of TMEM24 from ER-PM contacts and dispersal through the ER (Sun et al., 2019), which corresponds with the observed activity-dependent reduction in the area of ER-PM contacts (Tao-Cheng, 2018).

What Are the Functions of ER-PM Contacts in Neurons?

Several functions have been ascribed to ER-PM contacts, the best studied of which are their roles in Ca^{2+} regulation, lipid transfer and as trafficking hubs.

The ER acts as a Ca^{2+} sink, providing the internal stores of Ca^{2+} required to propagate Ca^{2+} waves along axons and to stimulate the release of synaptic vesicles from presynaptic terminals. An important role of ER-PM contacts is replenishment of these ER Ca^{2+} stores by SOCE. In *Drosophila*, loss of E-Syt impairs presynaptic neurotransmitter release, despite a comparable number of synaptic vesicles, suggesting that E-Syt-mediated ER-PM contacts function to regulate Ca^{2+}-driven synaptic vesicle release (Kikuma et al., 2017). However, a similar function has not been confirmed in mammalian studies. In fact, E-Syt1-3 triple knockout mice do not have any reported brain abnormalities (Sclip et al., 2016), though disruption of SOCE has been linked with several neurodegenerative disorders as reviewed recently (Secondo et al., 2018).

As discussed previously, the ER produces lipids which are then transported throughout the cell either in packaged LDs or by direct transfer which can occur at ER-PM contacts. Furthermore, lipid metabolites are returned from the PM to the ER for recycling. The ORPs, which localize to ER-PM contacts regulate lipid levels by transporting phosphatidylinositol (PI) from the PM to the ER and phosphatidylserine (PS) from the ER to the PM. Altered expression of ORP5 or ORP6 disrupts PI and PS levels at the PM in neurons and non-neuronal cells (Chung et al., 2015; Mochizuki et al., 2018). TMEM24 has also been shown to transport PI from the ER to the PM *in vitro*, though this function has yet to be validated in neurons (Lees et al., 2017). E-Syts may act to link the ER-PM contact functions in Ca^{2+} and lipid transfer as they have been found to transfer various lipids between

membranes but only when Ca^{2+} is bound to the C2 of the E-Syt (Yu et al., 2016; Bian et al., 2018). However, this function has also not yet been validated in neurons.

Endoplasmic reticulum-PM contacts mediated by VAP-Kv2.1 interactions form micro-domains within the PM which serve as important trafficking hubs for intracellular signaling. Monitoring sites of single channel insertion into the PM reveals that the majority of endocytosis and exocytosis of ion channels occurs at the perimeter of Kv2.1-labelled ER-PM contacts in cultured neurons (Deutsch et al., 2012). Furthermore, increased expression of Kv2.1, known to drastically increase ER-PM contacts (Fox et al., 2015), decreases the PM mobility and internalization of the dopamine transporter DAT (Lebowitz et al., 2019). Given that Ca^{2+} channels including STIM1-ORAI and CaV1.2 also localize to Kv2.1 clusters, ER-PM contacts may function regulate to activity-dependent trafficking within neurons (Fox et al., 2015).

Evidence That Links ER-PM Contacts to HSP

To date there is no direct evidence that ER-PM contacts are disrupted in HSP. No known HSP-causing gene product acts as an ER-PM tether, nor have ER-PM contact defects been reported in HSP models. This may reflect the fact that disruption of this contact is not a common feature of disease or maybe that this contact site has not yet been studied in HSP. Several HSP-causing proteins have been found to localize to the PM, in addition to other membrane structures. Both Spartin and NIPA1, mutations in which cause SPG20 and SPG6, respectively, can localize to the PM where they function to regulate the internalization and degradation of receptor proteins (Bakowska et al., 2007; Zhao et al., 2008). Furthermore, Protrudin (linked with SPG33) associates with both ER and PM proteins in neurons, however, the role of these interacts has not been investigated (Hashimoto et al., 2014). Further studies will ascertain whether ER-PM contacts play a role in pathogenicity in HSP.

ER-MICROTUBULE CONTACTS IN NEURONS

Microtubules (MTs), like the ER, form an extensive network that extends the length of neurons from the cell body to the synapse. The ER contacts this MT network via cross-bridging proteins to regulate MT remodeling via MT severing and regrowth (Cui-Wang et al., 2012; Kuo et al., 2019). Furthermore, treatment with the MT-depolymerizing drug nocodazole alters the ratio of ER sheets and tubules indicating that ER-MT contacts also contribute to modulation of ER organization in neurons (Lu et al., 2009; Farías et al., 2019; Schroeder et al., 2019).

How Are ER-Microtubule Contacts Regulated?

Several integral ER proteins mediate direct (CLIMP-63, p180, REEP1, Sec61β and Spastin) and indirect (STIM1) binding to MTs (**Figure 3E**).

CLIMP-63 (cytoskeleton-linking membrane protein 63) was the first ER-resident protein to be identified as a MT-binding protein. CLIMP-63 binds MTs via a microtubule binding domain (MTBD) which is regulated by post-translational modification of the C-terminal coiled-coil domains such that phosphorylation leads to release of the MT contacts (Klopfenstein et al., 1998; Vedrenne et al., 2005). Overexpression of CLIMP-63 results in thickening of the ER tubules which align along bundled MTs (Klopfenstein et al., 1998). Several other proteins including syntaxin 5, microtubule-binding protein MAP2 and valosin-containing protein/p97-interacting membrane protein (VIMP) can all interact with CLIMP-63 to modulate ER-MT interactions as reviewed elsewhere (Sandoz and van der Goot, 2015). Packed MT bundles also occur when the ER protein p180 is overexpressed. p180 was originally identified as a ribosome-binding protein but was subsequently identified to contain a MTBD. Knockdown of p180 conversely results in a decrease in MT extensions and collapsed ER (Ogawa-Goto et al., 2007). The ER-shaping proteins REEP1-4, but not REEP5 or REEP6, possess a C-terminal MTBD which is sufficient for MT binding. Increased expression of REEP1 enhances SER alignment with MTs (Park et al., 2010). A very similar phenotype of ER tubules aligning with MTs was recently identified in cells over-expressing the ER protein Sec61β. Sec61β contains a cytoplasmic MTBD, loss of which disrupts ER contacts with MT (Zhu et al., 2018). Together these studies indicate that ER-MT contacts mediated by CLIMP-63, p180, REEP1 or Sec61β contribute to the organization of ER tubules along the MT network.

The M1 isoform of the ER-shaping protein Spastin comprises a RHD, by which it embeds into the outer leaflet of the ER lipid bilayer, in addition to a MTBD and an AAA ATPase domain which catalyzes MT severing. The MTBD of Spastin binds directly to the C-terminal tail of tubulin in an ATP-independent manner (White et al., 2007). Once bound to MTs, Spastin can sever tubulin-tubulin interactions generating internal breaks in the MT network (Evans et al., 2005; Roll-Mecak and Vale, 2008). In addition to its severing activity, Spastin has recently been shown to promote MT regrowth. Spastin stabilizes the new minus-end MTs created by its own severing activity, which serve as templates to support new MT growth and allowing for expansion of the MT network (Kuo et al., 2019).

The Ca^{2+} sensor proteins STIM1 and STIM2 localize to the ER and regulate SOCE. Several years ago, STIM1 was shown to bind to the end-binding (EB) proteins that decorate the dynamic plus-end of MTs (Grigoriev et al., 2008). These STIM1-EB1 interactions are dynamic but can be maintained during MT growth or contraction. STIM1-EB1 contacts stimulate the elongation of ER tubules along the growing MTs and provide a mechanism by which ER-MT contacts couple MT organization and ER-derived calcium signals (Grigoriev et al., 2008; Pavez et al., 2019).

Where Are ER-Microtubule Contacts Within Neurons?

All ER proteins that mediate ER-MT contacts are highly expressed in neurons, however, many of these proteins have

different subcellular distributions in neuronal and non-neuronal cells. In non-neuronal cells, CLIMP-63 (Chang et al., 2013), p180 (Ogawa-Goto et al., 2007) and Sec61β (Shibata et al., 2010) expression is concentrated on perinuclear RER sheets. In neurons, CLIMP-63 expression is similarly predominantly in the RER sheets in the cell body and in elongated tubular structures throughout dendrites mediating the contacts between tubular SER and MTs (Cui-Wang et al., 2012; Farías et al., 2019). p180 localizes to neuronal cell bodies and SER tubules in the proximal regions of axons but not dendrites (Farías et al., 2019). GFP-labeled Sec61β is a commonly used SER marker in neuronal axons in vertebrates and invertebrates, however, this may not reflect endogenous localization as GFP tags are known to disrupt translocon association and localization *in vitro* (Shibata et al., 2010).

The ER-shaping proteins REEP1 (Park et al., 2010) and Spastin (Allison et al., 2017) are expressed throughout the ER network of non-neuronal cells, though M1 Spastin is expressed at low levels and localizes to discrete puncta. In neurons, both REEP1 and M1 Spastin are highly expressed in axonal SER tubules where they colocalize with each other and other ER-shaping proteins including Atlastin (Park et al., 2010).

There are 2 homologs of STIM (STIM1 and STIM2) and 3 homologs of EB (EB1, EB2 and EB3) all of which are highly expressed in neurons. Immunohistochemical analysis reveals that STIM1, STIM2 and EB3 localize to the cell body and along the length of cultured hippocampal neurites (Klejman et al., 2009; Pchitskaya et al., 2017). Furthermore, both STIM1 and STIM2 are required for normal neuronal growth and morphology in primary cultured neurons (Pchitskaya et al., 2017; Pavez et al., 2019).

What Are the Functions of ER-Microtubule Contacts in Neurons?

Several different lines of evidence have shown that ER-MT contacts play an important role in MT remodeling within neurons. This can occur by either directly by MT severing or indirectly by MT stabilization via post-translational modification of MTs. We will focus on ER-MT contacts in axons.

Spastin functions to sever MTs and it is therefore not a surprise that overexpression of Spastin causes increased MT severing leading to complete MT disassembly. Overexpression of Spastin results in loss of the MT network in cultured neurons (Yu et al., 2008; Riano et al., 2009) and in motor neuron axons *in vivo* (Trotta et al., 2004). Contrary to what might be expected, loss of Spastin actually decreases the MT axonal network *in vitro* and *in vivo* (Sherwood et al., 2004; Roll-Mecak and Vale, 2005; Wood et al., 2006). Recently, mathematical modeling of results from purified proteins identified that in addition to MT severing, Spastin functions to promote MT regrowth (Kuo et al., 2019). While this mechanism would explain *in vivo* loss of Spastin results, it will be important to validate whether Spastin carries out this function in axons. Dynamic instability of MTs can be regulated by post-translational modification of tubulin molecules. Loss of p180 reduces tubulin acetylation, a marker of stable MTs, in axons of cultured neurons resulting in more dynamic MTs (Farías et al., 2019). This confirms previous findings in non-neuronal cells that p180 ER-MT contacts function to stabilize MTs (Ogawa-Goto et al., 2007). Regulation of MT remodeling by ER-MT contacts, whether via severing or altered stability, can have important impacts on neuronal function. Defects in the MT network caused by mutations in Spastin gives rise to impaired axonal trafficking of mitochondria and syanptic vescles as well as causing axonal swellings (Kasher et al., 2009; Denton et al., 2014; Plaud et al., 2018) which are likely pathogenic to neurons.

While many studies have focused on the role of ER-MT contacts on MT remodeling, recent work has pointed to an important role for ER-MT contacts in regulating the distribution and organization of tubular ER in axons. Overexpression of CLIMP-63 or treatment with the MT depolymerizing agent nocodazole drastically increases RER within the cell body and reduces the proportion of axonal SER tubules. Conversely, knockdown of CLIMP-63 increases localization of Sec61β in axons suggestive of increased axonal SER tubules (Farías et al., 2019). This provides strong evidence that ER-MT contacts mediated by CLIMP-63 contribute to regulation of the distribution of ER in axons. Within neuronal axons, ER tubules are transported along stable MTs by MT motor proteins kinesin and dynein. Knockdown of family members of either of these motor protein familes disrupts the anterograde and retrograde transport of ER tubules in the axon. In contrast, knockdown of EB1 or EB3 reduces dedritic SER distribution but does not affect SER transport in axons (Farías et al., 2019). Within neuronal dendrites therefore, STIM-EB interactions regulate SER transport by forming ER-MT contacts at the growing plus ends of dynamic MTs. Together, this study has identified that ER-MT contacts contribute to SER localization within axons which may be vital for establishing neuronal polarity.

Evidence That Links ER-Microtubule Contacts to HSP

Mutations in the ER-MT contact proteins Spastin and REEP1 cause 2 of the most common forms of AD-HSP, SPG4 and SPG31, respectively. This has led to a lot of work to identify the mechanisms by which disease-causing mutations in these genes cause pathogenicity.

The mutation spectrum of Spastin comprises over 300 pathological mutations which include missense, frameshift, splice site, nonsense and deletions. Many of these mutations cause a reduction in the levels of Spastin protein produced or disrupt Spastin's ability to bind to or sever MTs (Roll-Mecak and Vale, 2008; Denton et al., 2014). Accordingly, some Spastin mutations appear to mediate disease via a haploinsufficiency mechanism (Roll-Mecak and Vale, 2008; Fassier et al., 2013; Denton et al., 2014), while others function through gain-of-function mechanisms (Solowska et al., 2014; Qiang et al., 2019). *Drosophila*, zebrafish and mouse models of SPG4 display mobility defects, disrupted MT network within motor neurons and axonal swellings (Sherwood et al., 2004; Wood et al., 2006; Qiang et al., 2019). Similarly, patient-derived cells exhibit altered MT stability, trafficking defects and axonal swellings (Denton et al., 2014).

SPG31 is predominantly caused by nonsense mutations in REEP1, resulting in truncated or loss of function proteins. Mice models of HSP generated by knockout of REEP1 develop motor dysfunction and axon length is decreased in primary neurons derived from these mice (Beetz et al., 2013; Renvoisé et al., 2016). It is unclear whether these neurodegenerative phenotypes can be attributed to REEP1s role in ER-MT contacts, however, REEP1 has been shown to modulate the neurotoxicity associated with increased MT stabilization. Neurotoxicity caused by overexpression of the MT-binding protein Tau, which functions to stabilize MTs, can be quantified in the *Drosophila* eye. Overexpressing REEP1 rescues, while knockdown of REEP1 exacerbates, Tau-induced neurotoxicity (Appocher et al., 2014). REEP1 interacts with M1 Spastin in axons mediating ER-MT contacts. Given that HSP-causing mutations in REEP1 fail to interact with M1 Spastin, one hypothesis could be that reduced REEP1 disrupts MT severing, which occurs at ER-MT contacts, and the resulting increase in MT stability contributes the axonal degeneration.

CONCLUSION

Within neurons, the ER forms an unbroken network of tubules which extends the entire length of the axon, up to 1 m in the longest axons within the corticospinal tract, making extensive contacts with other organelles, the cytoskeleton and the plasma membrane. The continuous nature of the ER allows it to regulate neuron-wide as well as localized functions. As we have discussed here, many of the functions of neuronal tubular ER occur at ER contacts sites including: ion exchange and homeostasis, lipid synthesis and organelle shaping and organization. However, a significant amount of work is still required to elucidate the exact functions of ER contacts within axons. Furthermore the functional repertoire of ER contacts are likely to expand as novel tethers are identified or known tethers are better characterized within neurons. It has become evident that mutations in ER-shaping proteins, the most common cause of HSP, disrupt ER contacts. Therefore to better understand the pathogenic mechanisms underpinning axonopathy in HSP, it is vital that continued research uncovers the function of the ER and ER contacts in neurons.

AUTHOR CONTRIBUTIONS

PF, MG-P, and NO'S wrote and edited the manuscript and prepared the figures. JS commented on and reviewed the manuscript prior to submission. All authors contributed to manuscript revision, read and approved the submitted version.

FUNDING

This work was supported by the SFI-HRB-Wellcome Trust Biomedical Research Partnership and the Irish Research Council (IRC). NO'S and PF were supported by Seed Award in Science (Grant Number 202020/Z/16/Z) awarded to NO'S. MG-P was supported by an IRC-Government of Ireland Ph.D. studentship (Grant Number GOIPG/2018/3011). Work in the JCS laboratory was supported by a research grant from SFI co-funded under the European Regional Development Fund (Grant Number 13/RC/2073).

REFERENCES

Allison, R., Edgar, J. R., Pearson, G., Rizo, T., Newton, T., Günther, S., et al. (2017). Defects in ER-endosome contacts impact lysosome function in hereditary spastic paraplegia. *J. Cell Biol.* 216, 1337–1355. doi: 10.1083/jcb.201609033

Alpy, F., Rousseau, A., Schwab, Y., Legueux, F., Stoll, I., Wendling, C., et al. (2013). STARD3 or STARD3NL and VAP form a novel molecular tether between late endosomes and the ER. *J. Cell Sci.* 126(Pt 23), 5500–5512. doi: 10.1242/jcs.139295

Appocher, C., Klima, R., and Feiguin, F. (2014). Functional screening in *Drosophila* reveals the conserved role of REEP1 in promoting stress resistance and preventing the formation of Tau aggregates. *Hum. Mol. Genet.* 23, 6762–6772. doi: 10.1093/hmg/ddu393

Atakpa, P., Thillaiappan, N. B., Mataragka, S., Prole, D. L., and Taylor, C. W. (2018). IP3 receptors preferentially associate with ER-lysosome contact sites and selectively deliver Ca2+ to lysosomes. *Cell Rep* 25, 3180.e7–3193.e7. doi: 10.1016/j.celrep.2018.11.064

Bailey, A. P., Koster, G., Guillermier, C., Hirst, E. M. A., MacRae, J. I., Lechene, C. P., et al. (2015). Antioxidant role for lipid droplets in a stem cell niche of *Drosophila*. *Cell* 163, 340–353. doi: 10.1016/j.cell.2015.09.020

Bakowska, J. C., Jupille, H., Fatheddin, P., Puertollano, R., and Blackstone, C. (2007). Troyer syndrome protein spartin is mono-ubiquitinated and functions in EGF receptor trafficking. *Mol. Biol. Cell.* 18, 1683–1692. doi: 10.1091/mbc.e06-09-0833

Beetz, C., Koch, N., Khundadze, M., Zimmer, G., Nietzsche, S., Hertel, N., et al. (2013). A spastic paraplegia mouse model reveals REEP1-dependent ER shaping. *J. Clin. Invest.* 123, 4273–4282. doi: 10.1172/JCI65665

Bem, D., Yoshimura, S., Nunes-Bastos, R., Bond, F. C., Kurian, M. A., Rahman, F., et al. (2011). Loss-of-function mutations in RAB18 cause Warburg micro syndrome. *Am J Hum Genet.* 88, 499–507. doi: 10.1016/j.ajhg.2011.03.012

Bian, X., Saheki, Y., and De Camilli, P. (2018). Ca 2+ releases E-Syt1 autoinhibition to couple ER-plasma membrane tethering with lipid transport. *EMBO J.* 37, 219–234. doi: 10.15252/embj.201797359

Blackstone, C. (2018). Converging cellular themes for the hereditary spastic paraplegias. *Curr. Opin. Neurobiol.* 51, 139–146. doi: 10.1016/j.conb.2018.04.025

Bouslam, N., Benomar, A., Azzedine, H., Bouhouche, A., Namekawa, M., Klebe, S., et al. (2005). Mapping of a new form of pure autosomal recessive spastic paraplegia (SPG28). *Ann. Neurol.* 57, 567–571. doi: 10.1002/ana.20416

Boutry, M., Morais, S., and Stevanin, G. (2019). Update on the genetics of spastic paraplegias. *Curr. Neurol. Neurosci. Rep.* 19:18. doi: 10.1007/s11910-019-0930-2

Branchu, J., Boutry, M., Sourd, L., Depp, M., Leone, C., Corriger, A., et al. (2017). Loss of spatacsin function alters lysosomal lipid clearance leading to upper and lower motor neuron degeneration. *Neurobiol. Dis.* 102, 21–37. doi: 10.1016/j.nbd.2017.02.007

Broadwell, R. D., and Cataldo, A. M. (1983). The neuronal endoplasmic reticulum: its cytochemistry and contribution to the endomembrane system. *I. Cell bodies and dendrites. J. Histochem. Cytochem.* 230, 231–248. doi: 10.1177/31.9.6309951

Bryant, D., Liu, Y., Datta, S., Hariri, H., Seda, M., Anderson, G., et al. (2018). SNX14 mutations affect endoplasmic reticulumassociated neutral lipid metabolism in autosomal recessive spinocerebellar ataxia 20. *Hum. Mol. Genet.* 27, 1927–1940. doi: 10.1093/hmg/ddy101

Calcraft, P. J., Ruas, M., Pan, Z., Cheng, X., Arredouani, A., Hao, X., et al. (2009). NAADP mobilizes calcium from acidic organelles through two-pore channels. *Nature.* 459, 596–600. doi: 10.1038/nature08030

Cao, Q., Yang, Y., Zhong, X. Z., and Dong, X. P. (2017). The lysosomal Ca2+ release channel TRPML1 regulates lysosome size by activating calmodulin. *J. Biol. Chem.* 292, 8424–8435. doi: 10.1074/jbc.M116.772160

Chang, C.-L., Weigel, A. V., Ioannou, M. S., Pasolli, H. A., Xu, C. S., Peale, D. R., et al. (2019). Spastin tethers lipid droplets to peroxisomes and directs fatty acid trafficking through ESCRT-III. *J. Cell Biol.* 218, 2583–2599. doi: 10.1083/jcb.201902061

Chang, J., Lee, S., and Blackstone, C. (2013). Protrudin binds atlastins and endoplasmic reticulum-shaping proteins and regulates network formation. *Proc. Natl. Acad. Sci. U.S.A.* 110, 14954–14959. doi: 10.1073/pnas.1307391110

Cho, I. T., Adelmant, G., Lim, Y., Marto, J. A., Cho, G., and Golden, J. A. (2017). Ascorbate peroxidase proximity labeling coupled with biochemical fractionation identifies promoters of endoplasmic reticulum–mitochondrial contacts. *J. Biol. Chem.* 292:16393. doi: 10.1074/jbc.M117.795286

Chung, J., Torta, F., Masai, K., Lucast, L., Czapla, H., Tanner, L. B., et al. (2015). PI4P/phosphatidylserine countertransport at ORP5- and ORP8-mediated ER - Plasma membrane contacts. *Science* 349, 428–432. doi: 10.1126/science.aab1370

Clapham, D. E. (2007). Calcium signaling. *Cell* 131, 1047–1058. doi: 10.1201/9781420038231

Copeland, D. E. (1959). An association between mitochondria and the endoplasmic reticulum in cells of the pseudobranch gland of a teleost. *J. Cell Biol.* 5, 393–396. doi: 10.1083/jcb.5.3.393

Cosson, P., Marchetti, A., Ravazzola, M., and Orci, L. (2012). Mitofusin-2 independent juxtaposition of endoplasmic reticulum and mitochondria: an ultrastructural study. *PLoS One.* 7:e46293. doi: 10.1371/journal.pone.0046293

Csordás, G., Renken, C., Várnai, P., Walter, L., Weaver, D., Buttle, K. F., et al. (2006). Structural and functional features and significance of the physical linkage between ER and mitochondria. *J. Cell Biol.* 174, 915–921. doi: 10.1083/jcb.200604016

Csordás, G., Várnai, P., Golenár, T., Roy, S., Purkins, G., Schneider, T. G., et al. (2010). Imaging interorganelle contacts and local calcium dynamics at the ER-Mitochondrial interface. *Mol. Cell.* 39, 121–132. doi: 10.1016/j.molcel.2010.06.029

Cui-Wang, T., Hanus, C., Cui, T., Helton, T., Bourne, J., Watson, D., et al. (2012). Local zones of endoplasmic reticulum complexity confine cargo in neuronal dendrites. *Cell* 148, 309–321. doi: 10.1016/j.cell.2011.11.056

Datta, S., Liu, Y., Hariri, H., Bowerman, J., and Henne, W. M. (2019). Cerebellar ataxia disease-associated Snx14 promotes lipid droplet growth at ER-droplet contacts. *J. Cell Biol.* 218, 1335–1351. doi: 10.1083/jcb.201808133

De Brito, O. M., and Scorrano, L. (2008). Mitofusin 2 tethers endoplasmic reticulum to mitochondria. *Nature* 456, 605–610. doi: 10.1038/nature07534

De vos, K. J., Mórotz, G. M., Stoica, R., Tudor, E. L., Lau, K. F., Ackerley, S., et al. (2012). VAPB interacts with the mitochondrial protein PTPIP51 to regulate calcium homeostasis. *Hum. Mol. Genet.* 21, 1299–1311. doi: 10.1093/hmg/ddr559

Denton, K., Mou, Y., Xu, C. C., Shah, D., Chang, J., Blackstone, C., et al. (2018). Impaired mitochondrial dynamics underlie axonal defects in hereditary spastic paraplegias. *Hum. Mol. Genet.* 27, 2517–2530. doi: 10.1093/hmg/ddy156

Denton, K. R., Lei, L., Grenier, J., Rodionov, V., Blackstone, C., and Li, X. J. (2014). Loss of spastin function results in disease-specific axonal defects in human pluripotent stem cell-based models of hereditary spastic paraplegia. *Stem Cell.* 32, 414–423. doi: 10.1002/stem.1569

Derivery, E., Sousa, C., Gautier, J. J., Lombard, B., Loew, D., and Gautreau, A. (2009). The Arp2/3 Activator WASH controls the fission of endosomes through a large multiprotein complex. *Dev. Cell.* 17, 712–723. doi: 10.1016/j.devcel.2009.09.010

Deutsch, E., Weigel, A. V., Akin, E. J., Fox, P., Hansen, G., Haberkorn, C. J., et al. (2012). Kv2.1 cell surface clusters are insertion platforms for ion channel delivery to the plasma membrane. *Mol. Biol. Cell.* 23, 2917–2929. doi: 10.1091/mbc.e12-01-0047

Di Mattia, T., Wilhelm, L. P., Ikhlef, S., Wendling, C., Spehner, D., Nominé, Y., et al. (2018). Identification of MOSPD2, a novel scaffold for endoplasmic reticulum membrane contact sites. *EMBO Rep.* 19:e45453. doi: 10.15252/embr.201745453

Dick, K. J., Eckhardt, M., Paisán-Ruiz, C., Alshehhi, A. A., Proukakis, C., Sibtain, N. A., et al. (2010). Mutation of FA2H underlies a complicated form of hereditary spastic paraplegia (SPG35). *Hum. Mutat.* 31, E1251–E1260. doi: 10.1002/humu.21205

Dong, R., Saheki, Y., Swarup, S., Lucast, L., Harper, J. W., and De Camilli, P. (2016). Endosome-ER contacts control actin nucleation and retromer function through VAP-Dependent regulation of PI4P. *Cell.* 166, 408–423. doi: 10.1016/j.cell.2016.06.037

Du, X., Kumar, J., Ferguson, C., Schulz, T. A., Ong, Y. S., Hong, W., et al. (2011). A role for oxysterol-binding protein-related protein 5 in endosomal cholesterol trafficking. *J. Cell Biol.* 192, 121–135. doi: 10.1083/jcb.201004142

Eden, E. R., White, I. J., Tsapara, A., and Futter, C. E. (2010). Membrane contacts between endosomes and ER provide sites for PTP1B-epidermal growth factor receptor interaction. *Nat. Cell Biol.* 12, 267–272. doi: 10.1038/ncb2026

Elgass, K. D., Smith, E. A., LeGros, M. A., Larabell, C. A., and Ryan, M. T. (2015). Analysis of ER-mitochondria contacts using correlative fluorescence microscopy and soft X-ray tomography of mammalian cells. *J. Cell Sci.* 128, 2795–2804. doi: 10.1242/jcs.169136

Esteves, T., Durr, A., Mundwiller, E., Loureiro, J. L., Boutry, M., Gonzalez, M. A., et al. (2014). Loss of association of REEP2 with membranes leads to hereditary spastic paraplegia. *Am J Hum Genet* 94, 268–277. doi: 10.1016/j.ajhg.2013.12.005

Eura, Y., Ishihara, N., Yokota, S., and Mihara, K. (2003). Two mitofusin proteins, mammalian homologues of FZO, with distinct functions are both required for mitochondrial fusion. *J. Biochem.* 134, 333–344. doi: 10.1093/jb/mvg150

Evans, K. J., Gomes, E. R., Reisenweber, S. M., Gundersen, G. G., and Lauring, B. P. (2005). Linking axonal degeneration to microtubule remodeling by Spastin-mediated microtubule severing. *J. Cell Biol.* 168, 599–606. doi: 10.1083/jcb.200409058

Farías, G. G., Fréal, A., Tortosa, E., Stucchi, R., Pan, X., Portegies, S., et al. (2019). Feedback-driven mechanisms between microtubules and the endoplasmic reticulum instruct neuronal polarity. *Neuron* 102, 184.e8–201.e8. doi: 10.1016/j.neuron.2019.01.030

Fassier, C., Tarrade, A., Peris, L., Courageot, S., Mailly, P., Dalard, C., et al. (2013). Microtubule-targeting drugs rescue axonal swellings in cortical neurons from spastin knockout mice. *Dis. Model. Mech.* 6, 72–83. doi: 10.1242/DMM.008946

Fei, W., Shui, G., Gaeta, B., Du, X., Kuerschner, L., Li, P., et al. (2008). Fld1p, a functional homologue of human seipin, regulates the size of lipid droplets in yeast. *J. Cell Biol.* 180, 473–482. doi: 10.1083/jcb.200711136

Feng, X., and Yang, J. (2017). Lysosomal calcium in neurodegeneration. *Messenger* 51, 56–66. doi: 10.1166/msr.2016.1055

Fernández-Busnadiego, R., Saheki, Y., and De Camilli, P. (2015). Three-dimensional architecture of extended synaptotagmin-mediated endoplasmic reticulum–plasma membrane contact sites. *Proc. Natl. Acad. Sci.* 112, E2004–E2013. doi: 10.1073/pnas.1503191112

Filadi, R., Greotti, E., Turacchio, G., Luini, A., Pozzan, T., and Pizzo, P. (2015). Mitofusin 2 ablation increases endoplasmic reticulum–mitochondria coupling. *Proc. Natl. Acad. Sci. U.S.A.* 112, E2174–E2181. doi: 10.1073/pnas.1504880112

Fowler, P. C., and O'Sullivan, N. C. (2016). ER-shaping proteins are required for ER and mitochondrial network organization in motor neurons. *Hum. Mol. Genet.* 25, 2827–2837. doi: 10.1093/hmg/ddw139

Fox, P. D., Haberkorn, C. J., Akin, E. J., Seel, P. J., Krapf, D., and Tamkun, M. M. (2015). Induction of stable ER-plasma-membrane junctions by Kv2.1 potassium channels. *J. Cell Sci.* 128, 2096–2105. doi: 10.1242/jcs.166009

Fox, P. D., Loftus, R. J., and Tamkun, M. M. (2013). Regulation of Kv2.1 K+ Conductance by Cell Surface Channel Density. *J. Neurosci.* 33, 1259–1270. doi: 10.1523/jneurosci.3008-12.2013

Friedman, J. R., Dibenedetto, J. R., West, M., Rowland, A. A., and Voeltz, G. K. (2013). Endoplasmic reticulum-endosome contact increases as endosomes traffic and mature. *Mol. Biol. Cell* 24, 1030–1040. doi: 10.1091/mbc.E12-10-0733

Friedman, J. R., Lackner, L. L., West, M., DiBenedetto, J. R., Nunnari, J., and Voeltz, G. K. (2011). ER tubules mark sites of mitochondrial division. *Science* 334, 358–362. doi: 10.1126/science.1207385

Friedman, J. R., Webster, B. M., Mastronarde, D. N., Verhey, K. J., and Voeltz, G. K. (2010). ER sliding dynamics and ER-mitochondrial contacts occur on acetylated microtubules. *J. Cell Biol.* 190, 363–375. doi: 10.1083/jcb.200911024

Galione, A., Morgan, A. J., Arredouani, A., Davis, L. C., Rietdorf, K., Ruas, M., et al. (2010). NAADP as an intracellular messenger regulating lysosomal calcium-release channels. *Biochem. Soc. Trans.* 38, 1424–1431. doi: 10.1042/bst0381424

Giacomello, M., Drago, I., Pizzo, P., and Pozzan, T. (2007). Mitochondrial Ca2+ as a key regulator of cell life and death. *Cell Death Differ.* 14, 1267–1274. doi: 10.1038/sj.cdd.4402147

Giordano, F., Saheki, Y., Idevall-Hagren, O., Colombo, S. F., Pirruccello, M., Milosevic, I., et al. (2013). PI(4,5)P2-dependent and Ca2+-regulated ER-PM interactions mediated by the extended synaptotagmins. *Cell* 153, 1494–1509. doi: 10.1016/j.cell.2013.05.026

Goizet, C., Depienne, C., Benard, G., Boukhris, A., Mundwiller, E., Solé, G., et al. (2011). REEP1 mutations in SPG31: frequency, mutational spectrum, and potential association with mitochondrial morpho-functional dysfunction. *Hum. Mutat.* 32, 1118–1127. doi: 10.1002/humu.21542

Gómez-Suaga, P., Pérez-Nievas, B. G., Glennon, E. B., Lau, D. H. W., Paillusson, S., Mórotz, G. M., et al. (2019). The VAPB-PTPIP51 endoplasmic reticulum-mitochondria tethering proteins are present in neuronal synapses and regulate synaptic activity. *Acta Neuropathol. Commun.* 7:35 doi: 10.1186/s40478-019-0688-4

Gomez-Suaga, P., Paillusson, S., Stoica, R., Noble, W., Hanger, D. P., and Miller, C. C. J. (2017). The ER-mitochondria tethering complex VAPB-PTPIP51 regulates autophagy. *Curr. Biol.* 27, 371–385. doi: 10.1016/j.cub.2016.12.038

Grigoriev, I., Gouveia, S. M., van der Vaart, B., Demmers, J., Smyth, J. T., Honnappa, S., et al. (2008). STIM1 is a MT-plus-end-tracking protein involved in remodeling of the ER. *Curr. Biol.* 18, 177–182. doi: 10.1016/j.cub.2007.12.050

Hamasaki, M., Furuta, N., Matsuda, A., Nezu, A., Yamamoto, A., Fujita, N., et al. (2013). Autophagosomes form at ER-mitochondria contact sites. *Nature* 495, 389–393. doi: 10.1038/nature11910

Hashimoto, Y., Shirane, M., Matsuzaki, F., Saita, S., Ohnishi, T., and Nakayama, K. I. (2014). Protrudin regulates endoplasmic reticulum morphology and function associated with the pathogenesis of hereditary spastic paraplegia. *J. Biol. Chem.* 289, 12946–12961. doi: 10.1074/jbc.M113.528687

Hazan, J., Fonknechten, N., Mavel, D., Paternotte, C., Samson, D., Artiguenave, F., et al. (1999). Spastin, a new AAA protein, is altered in the most frequent form of autosomal dominant spastic paraplegia. *Nat. Genet.* 23, 296–303. doi: 10.1038/15472

He, C., and Klionsky, D. J. (2009). Regulation mechanisms and signaling pathways of autophagy. *Annu. Rev. Genet.* 43, 67–93. doi: 10.1146/annurev-genet-102808-114910

Hedskog, L., Pinho, C. M., Filadi, R., Ronnback, A., Hertwig, L., Wiehager, B., et al. (2013). Modulation of the endoplasmic reticulum-mitochondria interface in Alzheimer's disease and related models. *Proc. Natl. Acad. Sci. U.S.A.* 110, 7916–7921. doi: 10.1073/pnas.1300677110

Herdman, C., Tremblay, M. G., Mishra, P. K., and Moss, T. (2014). Loss of extended synaptotagmins ESyt2 and ESyt3 does not affect mouse development or viability, but in vitro cell migration and survival under stress are affected. *Cell Cycle* 13, 2616–2625. doi: 10.4161/15384101.2014.943573

Hirabayashi, Y., Kwon, S. K., Paek, H., Pernice, W. M., Paul, M. A., Lee, J., et al. (2017). ER-mitochondria tethering by PDZD8 regulates Ca2+ dynamics in mammalian neurons. *Science* 358, 623–630. doi: 10.1126/science.aan6009

Hirst, J., Edgar, J. R., Esteves, T., Darios, F., Madeo, M., Chang, J., et al. (2015). Loss of AP-5 results in accumulation of aberrant endolysosomes: defining a new type of lysosomal storage disease. *Hum. Mol. Genet.* 24, 4984–4996. doi: 10.1093/hmg/ddv220

Hoyer, M. J., Chitwood, P. J., Ebmeier, C. C., Striepen, J. F., Qi, R. Z., Old, W. M., et al. (2018). A novel class of ER membrane Proteins regulates ER-associated endosome fission. *Cell* 175, 254.e14–265.e14. doi: 10.1016/j.cell.2018.08.030

Hu, J., Shibata, Y., Voss, C., Shemesh, T., Li, Z., Coughlin, M., et al. (2008). Membrane proteins of the endoplasmic reticulum induce high-curvature tubules. *Science* 319, 1247–1250. doi: 10.1126/science.1153634

Hu, J., Shibata, Y., Zhu, P. P., Voss, C., Rismanchi, N., Prinz, W. A., et al. (2009). A class of dynamin-like GTPases involved in the generation of the tubular er network. *Cell* 138, 549–561. doi: 10.1016/j.cell.2009.05.025

Huang, H. S., Yoon, B. J., Brooks, S., Bakal, R., Berrios, J., Larsen, R. S., et al. (2014). Snx14 regulates neuronal excitability, promotes synaptic transmission, and is imprinted in the brain of mice. *PLoS One* 9:e98383. doi: 10.1371/journal.pone.0098383

Inloes, J. M., Hsu, K.-L., Dix, M. M., Viader, A., Masuda, K., Takei, T., et al. (2014). The hereditary spastic paraplegia-related enzyme DDHD2 is a principal brain triglyceride lipase. *Proc. Natl. Acad. Sci. U.S.A.* 111, 14924–14929. doi: 10.1073/pnas.1413706111

Inloes, J. M., Kiosses, W. B., Wang, H., Walther, T. C., Farese, R. V. Jr., and Cravatt, B. F. (2018). Functional contribution of the spastic paraplegia-related triglyceride hydrolase DDHD2 to the formation and content of lipid droplets. *Biochemistry* 57, 827–838. doi: 10.1021/acs.biochem.7b01028

Ito, D., Fujisawa, T., Iida, H., and Suzuki, N. (2008). Characterization of seipin/BSCL2, a protein associated with spastic paraplegia 17. *Neurobiol. Dis.* 31, 266–277. doi: 10.1016/j.nbd.2008.05.004

Johansson, M. (2003). The two variants of oxysterol binding protein-related protein-1 display different tissue expression patterns, have different intracellular localization, and are functionally distinct. *Mol. Biol. Cell.* 14, 903–915. doi: 10.1091/mbc.e02-08-0459

Johnson, B., Leek, A. N., Solé, L., Maverick, E. E., Levine, T. P., and Tamkun, M. M. (2018). Kv2 potassium channels form endoplasmic reticulum/plasma membrane junctions via interaction with VAPA and VAPB. *Proc. Natl. Acad. Sci. U.S.A.* 115, E7331–E7340. doi: 10.1073/pnas.1805757115

Kang, F., Zhou, M., Huang, X., Fan, J., Wei, L., Boulanger, J., et al. (2019). E-syt1 Re-arranges STIM1 clusters to stabilize ring-shaped ER-PM contact sites and accelerate Ca 2+ store replenishment. *Sci. Rep.* 9:3975. doi: 10.1038/s41598-019-40331-0

Kasher, P. R., De Vos, K. J., Wharton, S. B., Manser, C., Bennett, E. J., Bingley, M., et al. (2009). Direct evidence for axonal transport defects in a novel mouse model of mutant spastin-induced hereditary spastic paraplegia (HSP) and human HSP patients. *J. Neurochem.* 110, 34–44. doi: 10.1111/j.1471-4159.2009.06104.x

Kassan, A., Herms, A., Fernández-Vidal, A., Bosch, M., Schieber, N. L., Reddy, B. J. N., et al. (2013). Acyl-CoA synthetase 3 promotes lipid droplet biogenesis in ER microdomains. *J. Cell Biol.* 203:985. doi: 10.1083/jcb.201305142

Kikuma, K., Li, X., Kim, D., Sutter, D., and Dickman, D. K. (2017). Extended synaptotagmin localizes to presynaptic ER and promotes neurotransmission and synaptic growth in *Drosophila*. *Genetics* 207, 993–1006. doi: 10.1534/genetics.117.300261

Kirmiz, M., Vierra, N. C., Palacio, S., and Trimmer, J. S. (2018). Identification of VAPA and VAPB as Kv2 channel-interacting proteins defining endoplasmic reticulum–plasma membrane junctions in mammalian brain neurons. *J. Neurosci.* 38, 7562–7584. doi: 10.1523/JNEUROSCI.0893-18.2018

Klejman, M. E., Gruszczynska-Biegala, J., Skibinska-Kijek, A., Wisniewska, M. B., Misztal, K., Blazejczyk, M., et al. (2009). Expression of STIM1 in brain and puncta-like co-localization of STIM1 and ORAI1 upon depletion of Ca2+ store in neurons. *Neurochem. Int.* 54, 49–55. doi: 10.1016/j.neuint.2008.10.005

Klemm, R. W., Norton, J. P., Cole, R. A., Li, C. S., Park, S. H., Crane, M. M., et al. (2013). A conserved role for atlastin GTPases in regulating lipid droplet size. *Cell Rep.* 3, 1465–1475. doi: 10.1016/j.celrep.2013.04.015

Klopfenstein, D. R. C., Kappeler, F., and Hauri, H. P. (1998). A novel direct interaction of endoplasmic reticulum with microtubules. *EMBO J.* 17, 6168–6177. doi: 10.1093/emboj/17.21.6168

Klumperman, J., and Raposo, G. (2014). The complex ultrastructure of the endolysosomal system. *Cold Spring Harb. Perspect. Biol.* 6, a016857. doi: 10.1101/cshperspect.a016857

Kornmann, B., Currie, E., Collins, S. R., Schuldiner, M., Nunnari, J., Weissman, J. S., et al. (2009). An ER-mitochondria tethering complex revealed by a synthetic biology screen. *Science* 325, 477–481. doi: 10.1126/science.1175088

Kuo, Y.-W., Trottier, O., Mahamdeh, M., and Howard, J. (2019). Spastin is a dual-function enzyme that severs microtubules and promotes their regrowth to increase the number and mass of microtubules. *Proc. Natl. Acad. Sci. U.S.A.* 116, 5533–5541. doi: 10.1073/pnas.1818824116

Lahiri, S., Chao, J. T., Tavassoli, S., Wong, A. K. O., Choudhary, V., Young, B. P., et al. (2014). A conserved endoplasmic reticulum membrane protein complex (EMC) facilitates phospholipid transfer from the ER to mitochondria. *PLoS Biol.* 12:e1001969. doi: 10.1371/journal.pbio.1001969

Lavie, J., Serrat, R., Bellance, N., Courtand, G., Dupuy, J. W., Tesson, C., et al. (2017). Mitochondrial morphology and cellular distribution are altered in SPG31 patients and are linked to DRP1 hyperphosphorylation. *Hum. Mol. Genet.* 26, 674–685. doi: 10.1093/hmg/ddw425

Leal, N. S., Schreiner, B., Pinho, C. M., Filadi, R., Wiehager, B., Karlström, H., et al. (2016). Mitofusin-2 knockdown increases ER–mitochondria contact and decreases amyloid β-peptide production. *J. Cell. Mol. Med.* 20, 1686–1695. doi: 10.1111/jcmm.12863

Lebowitz, J. J., Pino, J. A., Mackie, P. M., Lin, M., Hurst, C., Divita, K., et al. (2019). Clustered Kv2.1 decreases dopamine transporter activity and internalization. *J. Biol. Chem.* 294, 6957–6971. doi: 10.1074/jbc.RA119.007441

Lees, J. A., Messa, M., Sun, E. W., Wheeler, H., Torta, F., Wenk, M. R., et al. (2017). Lipid transport by TMEM24 at ER-plasma membrane contacts regulates pulsatile insulin secretion. *Science* 355:eaah6171. doi: 10.1126/science.aah6171

Lewis, T. L., Kwon, S.-K., Lee, A., Shaw, R., and Polleux, F. (2018). MFF-dependent mitochondrial fission regulates presynaptic release and axon branching by limiting axonal mitochondria size. *Nat. Commun.* 9:5008. doi: 10.1038/s41467-018-07416-2

Li, D., Zhao, Y. G., Li, D., Zhao, H., Huang, J., Miao, G., et al. (2019). The ER-Localized Protein DFCP1 modulates ER-Lipid droplet contact formation. *Cell Rep.* 27, 343.e5–358.e5. doi: 10.1016/j.celrep.2019.03.025

Lim, S. T., Antonucci, D. E., Scannevin, R. H., and Trimmer, J. S. (2000). A novel targeting signal for proximal clustering of the Kv2.1 K + channel in hippocampal neurons. *Neuron* 25, 385–397. doi: 10.1016/S0896-6273(00)80902-2

Lim, Y., Cho, I.-T., Schoel, L. J., Cho, G., and Golden, J. A. (2015). Hereditary spastic paraplegia-linked REEP1 modulates endoplasmic reticulum/mitochondria contacts. *Ann. Neurol.* 78, 679–696. doi: 10.1002/ana.24488

Liu, L., Zhang, K., Sandoval, H., Yamamoto, S., Jaiswal, M., Sanz, E., et al. (2015). Glial lipid droplets and ROS induced by mitochondrial defects promote neurodegeneration. *Cell* 160, 177–190. doi: 10.1016/j.cell.2014.12.019

Liu, X., Guo, X., Niu, L., Li, X., Sun, F., Hu, J., et al. (2019). Atlastin-1 regulates morphology and function of endoplasmic reticulum in dendrites. *Nat. Commun.* 10:568. doi: 10.1038/s41467-019-08478-6

Loewen, C. J. R., Roy, A., and Levine, T. P. (2003). A conserved ER targeting motif in three families of lipid binding proteins and in Opi1p binds VAP. *EMBO J.* 22, 2025–2035. doi: 10.1093/emboj/cdg201

Lu, L., Ladinsky, M. S., and Kirchhausen, T. (2009). Cisternal organization of the endoplasmic reticulum during mitosis. *Mol. Biol. Cell* 20, 3471–3480. doi: 10.1091/mbc.e09-04-0327

Mannan, A. U., Krawen, P., Sauter, S. M., Boehm, J., Chronowska, A., Paulus, W., et al. (2006). ZFYVE27 (SPG33), a novel spastin-binding protein, is mutated in hereditary spastic paraplegia. *Am J Hum Genet.* 79, 351–357. doi: 10.1086/504927

Martignoni, M., Riano, E., and Rugarli, E. I. (2008). The role of ZFYVE27/protrudin in hereditary spastic paraplegia. *Am J Hum Genet.* 83, 127–128. doi: 10.1016/j.ajhg.2008.05.014

McCullough, J., Clippinger, A. K., Talledge, N., Skowyra, M. L., Saunders, M. G., Naismith, T. V., et al. (2015). Structure and membrane remodeling activity of ESCRT-III helical polymers. *Science* 350, 1548–1551. doi: 10.1126/science.aad8305

Menzies, F. M., Fleming, A., Caricasole, A., Bento, C. F., Andrews, S. P., Ashkenazi, A., et al. (2017). Autophagy and neurodegeneration: pathogenic mechanisms and therapeutic opportunities. *Neuron* 93, 1015–1034. doi: 10.1016/j.neuron.2017.01.022

Meyer, M. A. (2014). Identification of 17 highly expressed genes within mouse lumbar spinal cord anterior horn region from an in-situ hybridization atlas of 3430 genes: implications for motor neuron disease. *Neurol. Int.* 6:5367. doi: 10.4081/ni.2014.5367

Min, S.-W., Chang, W.-P., and Sudhof, T. C. (2007). E-Syts, a family of membranous Ca2+-sensor proteins with multiple C2 domains. *Proc. Natl. Acad. Sci. U.S.A.* 104, 3823–3828. doi: 10.1073/pnas.0611725104

Mochizuki, S., Miki, H., Zhou, R., Kido, Y., Nishimura, W., Kikuchi, M., et al. (2018). Oxysterol-binding protein-related protein (ORP) 6 localizes to the ER and ER-plasma membrane contact sites and is involved in the turnover of PI4P in cerebellar granule neurons. *Exp. Cell Res.* 370, 601–612. doi: 10.1016/j.yexcr.2018.07.025

Montenegro, G., Rebelo, A. P., Connell, J., Allison, R., Babalini, C., D'Aloia, M., et al. (2012). Mutations in the ER-shaping protein reticulon 2 cause the axon-degenerative disorder hereditary spastic paraplegia type 12. *J. Clin. Invest.* 122, 538–544. doi: 10.1172/JCI60560

Naon, D., Zaninello, M., Giacomello, M., Varanita, T., Grespi, F., Lakshminaranayan, S., et al. (2016). Critical reappraisal confirms that Mitofusin 2 is an endoplasmic reticulum–mitochondria tether. *Proc. Natl. Acad. Sci. U.S.A.* 13, 11249–11254. doi: 10.1073/pnas.1606786113

Nian, F. S., Li, L. L., Cheng, C. Y., Wu, P. C., Lin, Y. T., Tang, C. Y., et al. (2019). Rab18 collaborates with Rab7 to modulate lysosomal and autophagy activities in the nervous system: an overlapping mechanism for warburg micro syndrome and charcot-marie-tooth neuropathy type 2B. *Mol. Neurobiol.* 56, 6095–6105. doi: 10.1007/s12035-019-1471-z

Nielsen, E., Severin, F., Backer, J. M., Hyman, A. A., and Zerial, M. (1999). Rab5 regulates motility of early endosomes on microtubules. *Nat. Cell Biol.* 1, 376–382. doi: 10.1038/14075

Nishimura, A. L., Mitne-Neto, M., Silva, H. C., Richieri-Costa, A., Middleton, S., Cascio, D., et al. (2004). A mutation in the vesicle-trafficking protein VAPB causes late-onset spinal muscular atrophy and amyotrophic lateral sclerosis. *Am. J. Hum. Genet.* 75, 822–831. doi: 10.1086/425287

Novikoff, A. B., Novikoff, P. M., Rosen, O. M., and Rubin, C. S. (1980). Organelle relationships in cultured 3T3-L1 preadipocytes. *J. Cell Biol.* 87, 180–196. doi: 10.1083/jcb.87.1.180

Oettinghaus, B., Schulz, J. M., Restelli, L. M., Licci, M., Savoia, C., Schmidt, A., et al. (2016). Synaptic dysfunction, memory deficits and hippocampal atrophy due to ablation of mitochondrial fission in adult forebrain neurons. *Cell Death Differ.* 23, 18–28. doi: 10.1038/cdd.2015.39

Ogawa-Goto, K., Tanaka, K., Ueno, T., Tanaka, K., Kurata, T., Sata, T., et al. (2007). p180 is involved in the interaction between the endoplasmic reticulum and microtubules through a novel microtubule-binding and bundling domain. *Mol. Biol. Cell.* 18, 3741–3751. doi: 10.1091/mbc.e06-12-1125

Olkkonen, V. M., and Li, S. (2013). Oxysterol-binding proteins: sterol and phosphoinositide sensors coordinating transport, signaling and metabolism. *Prog. Lipid Res.* 52, 529–538. doi: 10.1016/j.plipres.2013.06.004

Ozeki, S., Cheng, J., Tauchi-Sato, K., Hatano, N., Taniguchi, H., and Fujimoto, T. (2005). Rab18 localizes to lipid droplets and induces their close apposition to the endoplasmic reticulum-derived membrane. *J. Cell Sci.* 118(Pt 12), 2601–2611. doi: 10.1242/jcs.02401

Pankiv, S., Alemu, E. A., Brech, A., Bruun, J. A., Lamark, T., Øvervatn, A., et al. (2010). FYCO1 is a rab7 effector that binds to LC3 and PI3P to mediate microtubule plus end - directed vesicle transport. *J. Cell Biol.* 188:253. doi: 10.1083/jcb.200907015

Papadopoulos, C., Orso, G., Mancuso, G., Herholz, M., Gumeni, S., Tadepalle, N., et al. (2015). Spastin binds to lipid droplets and affects lipid metabolism. *PLoS Genet.* 11:e1005149. doi: 10.1371/journal.pgen.1005149

Park, C. Y., Hoover, P. J., Mullins, F. M., Bachhawat, P., Covington, E. D., Raunser, S., et al. (2009). STIM1 clusters and activates CRAC channels via direct binding of a cytosolic domain to orai1. *Cell* 136, 876–890. doi: 10.1016/j.cell.2009.02.014

Park, S. H., Zhu, P. P., Parker, R. L., and Blackstone, C. (2010). Hereditary spastic paraplegia proteins REEP1, spastin, and atlastin-1 coordinate microtubule interactions with the tubular ER network. *J. Clin. Invest.* 120, 1097–1110. doi: 10.1172/JCI40979

Pavez, M., Thompson, A. C., Arnott, H. J., Mitchell, C. B., D'Atri, I., Don, E. K., et al. (2019). STIM1 is required for remodelling of the endoplasmic reticulum and microtubule cytoskeleton in steering growth cones. *J. Neurosci.* 39, 5095–5114. doi: 10.1523/JNEUROSCI.2496-18.2019

Pchitskaya, E., Kraskovskaya, N., Chernyuk, D., Popugaeva, E., Zhang, H., Vlasova, O., et al. (2017). Stim2-Eb3 association and morphology of dendritic spines in hippocampal neurons. *Sci. Rep.* 7:17625. doi: 10.1038/s41598-017-17762-8

Pennetta, G., and Welte, M. A. (2018). Emerging links between lipid droplets and motor neuron diseases. *Dev. Cell.* 45, 427–432. doi: 10.1016/j.devcel.2018.05.002

Petkovic, M., Jemaiel, A., Daste, F., Specht, C. G., Izeddin, I., Vorkel, D., et al. (2014). The SNARE Sec22b has a non-fusogenic function in plasma membrane expansion. *Nat. Cell Biol.* 16, 434–444. doi: 10.1038/ncb2937

Plaud, C., Joshi, V., Kajevu, N., Poüs, C., Curmi, P. A., and Burgo, A. (2018). Functional differences of short and long isoforms of spastin harboring missense mutation. *Dis. Model. Mech.* 11:dmm033704. doi: 10.1242/dmm.033704

Poteser, M., Leitinger, G., Pritz, E., Platzer, D., Frischauf, I., Romanin, C., et al. (2016). Live-cell imaging of ER-PM contact architecture by a novel TIRFM approach reveals extension of junctions in response to store-operated Ca2+-entry. *Sci. Rep.* 6:35656. doi: 10.1038/srep35656

Qiang, L., Piermarini, E., Muralidharan, H., Yu, W., Leo, L., Hennessy, L. E., et al. (2019). Hereditary spastic paraplegia: gain-of-function mechanisms revealed by new transgenic mouse. *Hum. Mol. Genet.* 28, 1136–1152. doi: 10.1093/hmg/ddy419

Raiborg, C., Wenzel, E. M., Pedersen, N. M., Olsvik, H., Schink, K. O., Schultz, S. W., et al. (2015). Repeated ER-endosome contacts promote endosome translocation and neurite outgrowth. *Nature* 520, 234–238. doi: 10.1038/nature14359

Rainier, S., Bui, M., Mark, E., Thomas, D., Tokarz, D., Ming, L., et al. (2008). Neuropathy target esterase gene mutations cause motor neuron disease. *Am. J. Hum. Genet.* 82, 780–785. doi: 10.1016/j.ajhg.2007.12.018

Renvoisé, B., Malone, B., Falgairolle, M., Munasinghe, J., Stadler, J., Sibilla, C., et al. (2016). Reep1 null mice reveal a converging role for hereditary spastic paraplegia proteins in lipid droplet regulation. *Hum. Mol. Genet.* 25, 5111–5125. doi: 10.1093/hmg/ddw315

Renvoisé, B., Stadler, J., Singh, R., Bakowska, J. C., and Blackstone, C. (2012). Spg20-/- mice reveal multimodal functions for Troyer syndrome protein spartin in lipid droplet maintenance, cytokinesis and BMP signaling. *Hum. Mol. Genet.* 21, 3604–3618. doi: 10.1093/hmg/dds191

Riano, E., Martignoni, M., Mancuso, G., Cartelli, D., Crippa, F., Toldo, I., et al. (2009). Pleiotropic effects of spastin on neurite growth depending on expression levels. *J. Neurochem.* 108, 1277–1288. doi: 10.1111/j.1471-4159.2009.05875.x

Rinaldi, C., Schmidt, T., Situ, A. J., Johnson, J. O., Lee, P. R., Chen, K. L., et al. (2015). Mutation in CPT1C associated with pure autosomal dominant spastic paraplegia. *JAMA Neurol.* 72, 561–570. doi: 10.1001/jamaneurol.2014.4769

Rocha, N., Kuijl, C., Van Der Kant, R., Janssen, L., Houben, D., Janssen, H., et al. (2009). Cholesterol sensor ORP1L contacts the ER protein VAP to control Rab7-RILP-p150Glued and late endosome positioning. *J. Cell Biol.* 185, 1209–1225. doi: 10.1083/jcb.200811005

Roll-Mecak, A., and Vale, R. D. (2005). The *Drosophila* homologue of the hereditary spastic paraplegia protein, spastin, severs and disassembles microtubules. *Curr. Biol.* 15, 650–655. doi: 10.1016/j.cub.2005.02.029

Roll-Mecak, A., and Vale, R. D. (2008). Structural basis of microtubule severing by the hereditary spastic paraplegia protein spastin. *Nature* 451, 363–367. doi: 10.1038/nature06482

Rolls, M. M. (2002). Targeting of rough endoplasmic reticulum membrane proteins and ribosomes in invertebrate neurons. *Mol. Biol. Cell.* 13, 1778–1791. doi: 10.1091/mbc.01-10-0514

Romer, S. H., Deardorff, A. S., and Fyffe, R. E. W. (2019). A molecular rheostat: Kv2.1 currents maintain or suppress repetitive firing in motoneurons. *J. Physiol.* 597, 3769–3786. doi: 10.1113/JP277833

Rosenbluth, J. (1962). Subsurface cisterns and their relationship to the neuronal plasma membrane. *J. Cell Biol.* 13, 405–421. doi: 10.1083/jcb.13.3.405

Rowland, A. A., Chitwood, P. J., Phillips, M. J., and Voeltz, G. K. (2014). ER contact sites define the position and timing of endosome fission. *Cell* 159, 1027–1041. doi: 10.1016/j.cell.2014.10.023

Saheki, Y., Bian, X., Schauder, C. M., Sawaki, Y., Surma, M. A., Klose, C., et al. (2016). Control of plasma membrane lipid homeostasis by the extended synaptotagmins. *Nat. Cell Biol.* 18, 504–515. doi: 10.1038/ncb3339

Salo, V. T., Belevich, I., Li, S., Karhinen, L., Vihinen, H., Vigouroux, C., et al. (2016). Seipin regulates ER–lipid droplet contacts and cargo delivery. *EMBO J.* 35, 2699–2716. doi: 10.15252/embj.201695170

Sandoval, H., Yao, C.-K., Chen, K., Jaiswal, M., Donti, T., Lin, Y. Q., et al. (2014). Mitochondrial fusion but not fission regulates larval growth and synaptic development through steroid hormone production. *Elife* 14:3. doi: 10.7554/elife.03558

Sandoz, P. A., and van der Goot, F. G. (2015). How many lives does CLIMP-63 have? *Biochem. Soc. Trans.* 43, 222–228. doi: 10.1042/bst20140272

Schroeder, L. K., Barentine, A. E. S., Merta, H., Schweighofer, S., Zhang, Y., Baddeley, D., et al. (2019). Dynamic nanoscale morphology of the ER surveyed by STED microscopy. *J. Cell Biol.* 218:83. doi: 10.1083/jcb.201809107

Schuurs-Hoeijmakers, J. H. M., Geraghty, M. T., Kamsteeg, E. J., Ben-Salem, S., De Bot, S. T., Nijhof, B., et al. (2012). Mutations in DDHD2, encoding an intracellular phospholipase A 1, cause a recessive form of complex hereditary spastic paraplegia. *Am. J. Hum. Genet.* 91, 1073–1081. doi: 10.1016/j.ajhg.2012.10.017

Sclip, A., Bacaj, T., Giam, L. R., and Südhof, T. C. (2016). Extended synaptotagmin (ESyt) triple knock-out mice are viable and fertile without obvious endoplasmic reticulum dysfunction. *PLoS One* 11:e0158295. doi: 10.1371/journal.pone.0158295

Secondo, A., Bagetta, G., and Amantea, D. (2018). On the role of store-operated calcium entry in acute and chronic neurodegenerative diseases. *Front. Mol. Neurosci.* 11:87. doi: 10.3389/fnmol.2018.00087

Sherwood, N. T., Sun, Q., Xue, M., Zhang, B., and Zinn, K. (2004). *Drosophila* spastin regulates synaptic microtubule networks and is required for normal motor function. *PLoS Biol.* 2:e429. doi: 10.1371/journal.pbio.0020429

Shibata, Y., Hu, J., Kozlov, M. M., and Rapoport, T. A. (2009). Mechanisms shaping the membranes of cellular organelles. *Annu. Rev. Cell Dev. Biol.* 25, 329–354. doi: 10.1146/annurev.cellbio.042308.113324

Shibata, Y., Shemesh, T., Prinz, W. A., Palazzo, A. F., Kozlov, M. M., and Rapoport, T. A. (2010). Mechanisms determining the morphology of the peripheral ER. *Cell* 143, 774–788. doi: 10.1016/j.cell.2010.11.007

Shibata, Y., Voss, C., Rist, J. M., Hu, J., Rapoport, T. A., Prinz, W. A., et al. (2008). The reticulon and Dp1/Yop1p proteins form immobile oligomers in the tubular endoplasmic reticulum. *J. Biol. Chem.* 283, 18892–18904. doi: 10.1074/jbc.M800986200

Shirane, M., and Nakayama, K. I. (2006). Protrudin induces neurite formation by directional membrane trafficking. *Science* 314, 818–821. doi: 10.1126/science.1134027

Solowska, J. M., D'Rozario, M., Jean, D. C., Davidson, M. W., Marenda, D. R., and Baas, P. W. (2014). Pathogenic mutation of spastin has Gain-of-Function effects on microtubule dynamics. *J. Neurosci.* 34, 1856–1867. doi: 10.1523/jneurosci.3309-13.2014

Song, G. J., Jung, M., Kim, J. H., Park, H., Rahman, M. H., Zhang, S., et al. (2016). A novel role for protein tyrosine phosphatase 1B as a positive regulator of neuroinflammation. *J. Neuroinflammation.* 13:86. doi: 10.1186/s12974-016-0545-3

Song, L., Rijal, R., Karow, M., Stumpf, M., Hahn, O., Park, L., et al. (2018). Expression of N471D strumpellin leads to defects in the endolysosomal system. *Dis. Model. Mech.* 11:dmm033449. doi: 10.1242/dmm.033449

Song, Y., Wang, M., Mao, F., Shao, M., Zhao, B., Song, Z., et al. (2013). Knockdown of Pnpla6 protein results in motor neuron defects in zebrafish. *Dis. Model. Mech.* 6, 404–413. doi: 10.1242/dmm.009688

Stefano, G., Renna, L., Lai, Y., Slabaugh, E., Mannino, N., Buono, R. A., et al. (2015). ER network homeostasis is critical for plant endosome streaming and endocytosis. *Cell Discov.* 1:15033. doi: 10.1038/celldisc.2015.33

Stoica, R., De Vos, K. J., Paillusson, S., Mueller, S., Sancho, R. M., Lau, K. F., et al. (2014). ER-mitochondria associations are regulated by the VAPB-PTPIP51 interaction and are disrupted by ALS/FTD-associated TDP-43. *Nat. Commun.* 5:3996. doi: 10.1038/ncomms4996

Sui, X., Arlt, H., Brock, K. P., Lai, Z. W., DiMaio, F., Marks, D. S., et al. (2018). Cryo–electron microscopy structure of the lipid droplet–formation protein seipin. *J. Cell Biol.* 217, 4080–4091. doi: 10.1083/jcb.201809067

Sun, E. W., Guillén-Samander, A., Bian, X., Wu, Y., Cai, Y., Messa, M., et al. (2019). Lipid transporter TMEM24/C2CD2L is a Ca 2+ -regulated component of ER–plasma membrane contacts in mammalian neurons. *Proc. Natl. Acad. Sci. U.S.A.* 116, 5775–5784. doi: 10.1073/pnas.1820156116

Szymanski, K. M., Binns, D., Bartz, R., Grishin, N. V., Li, W.-P., Agarwal, A. K., et al. (2007). The lipodystrophy protein seipin is found at endoplasmic reticulum lipid droplet junctions and is important for droplet morphology. *Proc. Natl. Acad. Sci. U.S.A.* 104, 20890–20895. doi: 10.1073/pnas.0704154104

Tao-Cheng, J. H. (2018). Activity-dependent decrease in contact areas between subsurface cisterns and plasma membrane of hippocampal neurons. *Mol. Brain.* 11:23. doi: 10.1186/s13041-018-0366-7

Tesson, C., Nawara, M., Salih, M. A. M., Rossignol, R., Zaki, M. S., Al Balwi, M., et al. (2012). Alteration of fatty-acid-metabolizing enzymes affects mitochondrial form and function in hereditary spastic paraplegia. *Am. J. Hum. Genet.* 91, 1051–1064. doi: 10.1016/j.ajhg.2012.11.001

Teuling, E., Ahmed, S., Haasdijk, E., Demmers, J., Steinmetz, M. O., Akhmanova, A., et al. (2007). Motor neuron disease-associated mutant vesicle-associated membrane protein-associated PROTEIN (VAP) B recruits wild-type VAPs into endoplasmic reticulum-derived tubular aggregates. *J. Neurosci.* 27, 9801–9815. doi: 10.1523/jneurosci.2661-07.2007

Thomas, A. C., Williams, H., Setó-Salvia, N., Bacchelli, C., Jenkins, D., O'Sullivan, M., et al. (2014). Mutations in SNX14 cause a distinctive autosomal-recessive cerebellar ataxia and intellectual disability syndrome. *Am J Hum Genet.* 95, 611–621. doi: 10.1016/j.ajhg.2014.10.007

Tong, J., Tan, L., Chun, C. J., and Im, Y. J. (2019). Structural basis of human ORP1-Rab7 interaction for the late-endosome and lysosome targeting. *PLoS One* 14:e0211724. doi: 10.1371/journal.pone.0211724

Trotta, N., Orso, G., Rossetto, M. G., Daga, A., and Broadie, K. (2004). The hereditary spastic paraplegia gene, spastin, regulates microtubule stability to modulate synaptic structure and function. *Curr. Biol.* 14, 1135–1147. doi: 10.1016/j.cub.2004.06.058

Varga, R. E., Khundadze, M., Damme, M., Nietzsche, S., Hoffmann, B., Stauber, T., et al. (2015). In vivo evidence for lysosome depletion and impaired autophagic clearance in hereditary spastic paraplegia type SPG11. *PLoS Genet.* 11:e1005454. doi: 10.1371/journal.pgen.1005454

Vedrenne, C., Klopfenstein, D. R., and Hauri, H.-P. (2005). Phosphorylation controls CLIMP-63–mediated anchoring of the endoplasmic reticulum to microtubules. *Mol. Biol. Cell.* 16, 1928–1937. doi: 10.1091/mbc.e04-07-0554

Verhoeven, K., De Jonghe, P., Coen, K., Verpoorten, N., Auer-Grumbach, M., Kwon, J. M., et al. (2003). Mutations in the small GTP-ase late endosomal protein RAB7 cause Charcot-Marie-Tooth type 2B neuropathy. *Am J Hum Genet.* 72, 722–727. doi: 10.1086/367847

Verstreken, P., Ly, C. V., Venken, K. J. T., Koh, T. W., Zhou, Y., and Bellen, H. J. (2005). Synaptic mitochondria are critical for mobilization of reserve pool vesicles at *Drosophila* neuromuscular junctions. *Neuron* 47, 365–378. doi: 10.1016/j.neuron.2005.06.018

Voeltz, G. K., Prinz, W. A., Shibata, Y., Rist, J. M., and Rapoport, T. A. (2006). A class of membrane proteins shaping the tubular endoplasmic reticulum. *Cell* 124, 573–586. doi: 10.1016/j.cell.2005.11.047

Wang, H., Becuwe, M., Housden, B. E., Chitraju, C., Porras, A. J., Graham, M. M., et al. (2016). Seipin is required for converting nascent to mature lipid droplets. *Elife* 5:e16582. doi: 10.7554/eLife.16582

Wang, S., Idrissi, F. Z., Hermansson, M., Grippa, A., Ejsing, C. S., and Carvalho, P. (2018). Seipin and the membrane-shaping protein Pex30 cooperate in organelle budding from the endoplasmic reticulum. *Nat. Commun.* 9:2939. doi: 10.1038/s41467-018-05278-2

White, S. R., Evans, K. J., Lary, J., Cole, J. L., and Lauring, B. (2007). Recognition of C-terminal amino acids in tubulin by pore loops in Spastin is important for microtubule severing. *J. Cell Biol.* 176, 995–1005. doi: 10.1083/jcb.200610072

Wijdeven, R. H., Janssen, H., Nahidiazar, L., Janssen, L., Jalink, K., Berlin, I., et al. (2016). Cholesterol and ORP1L-mediated ER contact sites control autophagosome transport and fusion with the endocytic pathway. *Nat. Commun.* 7:11808. doi: 10.1038/ncomms11808

Wilfling, F., Wang, H., Haas, J. T., Krahmer, N., Gould, T. J., Uchida, A., et al. (2013). Triacylglycerol synthesis enzymes mediate lipid droplet growth by relocalizing from the ER to lipid droplets. *Dev. Cell.* 24, 384–399. doi: 10.1016/j.devcel.2013.01.013

Wilhelm, L. P., Wendling, C., Védie, B., Kobayashi, T., Chenard, M., Tomasetto, C., et al. (2017). STARD3 mediates endoplasmic reticulum-to-endosome cholesterol transport at membrane contact sites. *EMBO J.* 36, 1412–1433. doi: 10.15252/embj.201695917

Windpassinger, C., Auer-Grumbach, M., Irobi, J., Patel, H., Petek, E., Hörl, G., et al. (2004). Heterozygous missense mutations in BSCL2 are associated with distal hereditary motor neuropathy and Silver syndrome. *Nat. Genet.* 36, 271–276. doi: 10.1038/ng1313

Wood, J. D., Landers, J. A., Bingley, M., McDermott, C. J., Thomas-McArthur, V., Gleadall, L. J., et al. (2006). The microtubule-severing protein spastin is essential for axon outgrowth in the zebrafish embryo. *Hum. Mol. Genet.* 15, 2763–2771. doi: 10.1093/hmg/ddl212

Wu, D., Hao, Z., Ren, H., and Wang, G. (2018). Loss of VAPB regulates autophagy in a beclin 1-dependent manner. *Neurosci. Bull.* 34, 1037–1046. doi: 10.1007/s12264-018-0276-9

Wu, Q., Sun, X., Yue, W., Lu, T., Ruan, Y., Chen, T., et al. (2016). RAB18, a protein associated with warburg micro syndrome, controls neuronal migration in the developing cerebral cortex. *Mol. Brain.* 9:19. doi: 10.1186/s13041-016-0198-2

Wu, Y., Whiteus, C., Xu, C. S., Hayworth, K. J., Weinberg, R. J., Hess, H. F., et al. (2017). Contacts between the endoplasmic reticulum and other membranes in neurons. *Proc. Natl. Acad. Sci. U.S.A.* 114, E4859–E4867. doi: 10.1073/pnas.1701078114

Xu, D., Li, Y., Wu, L., Li, Y., Zhao, D., Yu, J., et al. (2018). Rab18 promotes lipid droplet (LD) growth by tethering the ER to LDs through SNARE and NRZ interactions. *J. Cell Biol.* 217, 975–995. doi: 10.1083/jcb.201704184

Yagi, T., Ito, D., Nihei, Y., Ishihara, T., and Suzuki, N. (2011). N88S seipin mutant transgenic mice develop features of seipinopathy/BSCL2-related motor neuron disease via endoplasmic reticulum stress. *Hum. Mol. Genet.* 20, 3831–3840. doi: 10.1093/hmg/ddr304

Yalçın, B., Zhao, L., Stofanko, M., O'Sullivan, N. C., Kang, Z. H., Roost, A., et al. (2017). Modeling of axonal endoplasmic reticulum network by spastic paraplegia proteins. *Elife* 6:e23882. doi: 10.7554/eLife.23882

Yu, H., Liu, Y., Gulbranson, D. R., Paine, A., Rathore, S. S., and Shen, J. (2016). Extended synaptotagmins are Ca 2+ -dependent lipid transfer proteins at membrane contact sites. *Proc. Natl. Acad. Sci. U.S.A.* 34, 2291–2305. doi: 10.1073/pnas.1517259113

Yu, W., Qiang, L., Solowska, J. M., Karabay, A., Korulu, S., and Baas, P. W. (2008). The microtubule-severing proteins spastin and katanin participate differently in the formation of axonal branches. *Mol. Biol. Cell* 19, 1485–1498. doi: 10.1091/mbc.e07-09-0878

Zhao, J., Matthies, D. S., Botzolakis, E. J., Macdonald, R. L., Blakely, R. D., and Hedera, P. (2008). Hereditary spastic paraplegia-associated mutations in the NIPA1 Gene and its caenorhabditis elegans homolog trigger neural degeneration in vitro and in vivo through a gain-of-function mechanism. *J. Neurosci.* 28, 13938–13951. doi: 10.1523/jneurosci.4668-08.2008

Zhao, K., and Ridgway, N. D. (2017). Oxysterol-binding protein-related protein 1L regulates cholesterol egress from the endo-lysosomal system. *Cell Rep.* 19, 1807–1818. doi: 10.1016/j.celrep.2017.05.028

Zhao, X., Alvarado, D., Rainier, S., Lemons, R., Hedera, P., Weber, C. H., et al. (2001). Mutations in a newly identified GTPase gene cause autosomal dominant hereditary spastic paraplegia. *Nat. Genet.* 29, 326–331. doi: 10.1038/ng758

Zhu, Y., Zhang, G., Lin, S., Shi, J., Zhang, H., and Hu, J. (2018). Sec61β facilitates the maintenance of endoplasmic reticulum homeostasis by associating microtubules. *Protein Cell* 9, 616–628. doi: 10.1007/s13238-017-0492-5

Züchner, S., Mersiyanova, I. V., Muglia, M., Bissar-Tadmouri, N., Rochelle, J., Dadali, E. L., et al. (2004). Mutations in the mitochondrial GTPase mitofusin 2 cause Charcot-Marie-Tooth neuropathy type 2A. *Nat Genet.* 36, 449–451. doi: 10.1038/ng1341

Züchner, S., De Jonghe, P., Jordanova, A., Claeys, K. G., Guergueltcheva, V., Cherninkova, S., et al. (2006a). Axonal neuropathy with optic atrophy is caused by mutations in mitofusin 2. *Ann. Neurol.* 59, 276–281. doi: 10.1002/ana.20797

Züchner, S., Wang, G., Tran-Viet, K.-N., Nance, M. A., Gaskell, P. C., Vance, J. M., et al. (2006b). Mutations in the novel mitochondrial protein REEP1 cause hereditary spastic paraplegia type 31. *Am. J. Hum. Genet.* 79, 365–369. doi: 10.1086/505361

Conflict of Interest: The authors declare that the research was conducted in the absence of any commercial or financial relationships that could be construed as a potential conflict of interest.

frontiers in Neuroscience

BRIEF RESEARCH REPORT
published: 06 November 2019
doi: 10.3389/fnins.2019.01207

Disease-Associated PNPLA6 Mutations Maintain Partial Functions When Analyzed in *Drosophila*

*Elizabeth R. Sunderhaus†, Alexander D. Law and Doris Kretzschmar**

Oregon Institute of Occupational Health Sciences, Oregon Health & Science University, Portland, OR, United States

Mutations in patatin-like phospholipase domain-containing protein 6 (PNPLA6) have been linked with a number of inherited diseases with clinical symptoms that include spastic paraplegia, ataxia, and chorioretinal dystrophy. PNPLA6 is an evolutionary conserved protein whose ortholog in *Drosophila* is Swiss-Cheese (SWS). Both proteins are phospholipases hydrolyzing lysophosphatidylcholine (LPC) and phosphatidylcholine (PC). Consequently, loss of SWS/PNPLA6 in flies and mice increases both lipids and leads to locomotion deficits and neurodegeneration. PNPLA6 knock-out mice are embryonic lethal, and a mutation creating an early stop codon in human PNPLA6 has only been identified in compound heterozygote patients. In contrast, disease-causing point mutations are found in homozygous patients, with some localized in the phospholipase domain while others are in a region that contains several cNMP binding sites. To investigate how different mutations affect the function of PNPLA6 in an *in vivo* model, we expressed them in the *Drosophila sws*^{1} null mutant. Expressing wild-type PNPLA6 suppressed the locomotion and degenerative phenotypes in *sws*^{1} and restored lipid levels, confirming that the human protein can replace fly SWS. In contrast, none of the mutant proteins restored lipid levels, although they suppressed the behavioral and degenerative phenotypes, at least in early stages. These results show that these mutant forms of PNPLA6 retain some biological function, indicating that disruption of lipid homeostasis is only part of the pathogenic mechanism. Furthermore, our finding that mutations in the cNMP binding sites prevented the restoration of normal lipid levels supports previous evidence that cNMP regulates the phospholipase activity of PNPLA6.

Keywords: neuropathy target esterase, lipid homeostasis, spastic paraplegia/ataxia, hypogonadism, chorioretinal dystrophy, organophosphate-induced delayed neuropathy

OPEN ACCESS

Edited by:
Cahir Joseph O'Kane, University of Cambridge, United Kingdom

Reviewed by:
Anthea Letsou, The University of Utah, United States
Yong Qing Zhang, Chinese Academy of Sciences, China

***Correspondence:**
Doris Kretzschmar
kretzsch@ohsu.edu

†Present address:
Elizabeth R. Sunderhaus, School of Medicine, University of Colorado Denver, Aurora, CO, United States

Specialty section:
This article was submitted to Neurodegeneration, a section of the journal Frontiers in Neuroscience

Received: *29 July 2019*
Accepted: *25 October 2019*
Published: *06 November 2019*

Citation:
Sunderhaus ER, Law AD and Kretzschmar D (2019) Disease-Associated PNPLA6 Mutations Maintain Partial Functions When Analyzed in Drosophila. Front. Neurosci. 13:1207. doi: 10.3389/fnins.2019.01207

INTRODUCTION

Hereditary spastic paraplegias (HSPs) are inherited degenerative disorders that mainly affect motor neurons, leading to progressive spasticity and weakness of the lower extremities (Fink, 2013; de Souza et al., 2017; Parodi et al., 2017; Blackstone, 2018). Mutations in several genes have been shown to cause HSP, including patatin-like phospholipase domain-containing protein 6 (PNPLA6) (de Souza et al., 2017; Synofzik and Schule, 2017). The first mutations identified in PNPLA6, which is also called neuropathy target esterase (NTE), were shown to cause Spastic Paraplegia Type 39 in two affected families (Rainier et al., 2008). Subsequently, mutations in PNPLA6 have also been

linked with Boucher–Neuhäuser, Gordon–Holmes, Laurence–Moon, and Oliver–McFarlane Syndrome, complex diseases with varying clinical symptoms that include hypogonadism, chorioretinal dystrophy, ataxia, spasticity, and, although less frequently, peripheral neuropathy and impaired cognitive functions (Deik et al., 2014; Synofzik et al., 2014; Topaloglu et al., 2014; Kmoch et al., 2015). PNPLA6 belongs to a family of hydrolases with at least eight members in mammals that react with different substrates such as phospholipids, triacylglycerols, and retinol esters (Kienesberger et al., 2009). PNPLA6 preferably hydrolyzes phosphatidylcholine (PC) and lysophosphatidylcholine (LPC) (Lush et al., 1998; van Tienhoven et al., 2002; Quistad et al., 2003). PC is primarily synthesized in the endoplasmic reticulum (ER), which also contains substantial amounts of PC in its membranous network (Kienesberger et al., 2009; Lagace and Ridgway, 2013). In contrast, the levels of LPC in membranes are normally quite low and it can readily leave membranes and act as a messenger by signaling through membrane receptors (van Meer et al., 2008). Elevated levels of LPC, as described in a variety of diseases, may therefore have pathogenic effects by disrupting signaling pathways (Wang and Dennis, 1999; Fuchs and Schiller, 2009; Drzazga et al., 2014; Velasco et al., 2017).

Mutations in proteins that affect lipid homeostasis have been identified as the cause of over a hundred human diseases, many of them affecting the central and peripheral nervous system, confirming the importance of lipid homeostasis in neuronal health (Garcia-Cazorla et al., 2015). However, in most cases, only a few patients have been described for each disease, and the underlying mechanisms for how these mutations lead to the clinical symptoms are still mostly unknown. In the case of PNPLA6, several animal models have been used to analyze phenotypes caused by the loss of this protein. In mice, the complete loss of PNPLA6 leads to lethality during embryogenesis around day 9 postcoitum (Moser et al., 2004). Mutant embryos show growth retardation due to failed placental development and impaired vasculogenesis in the yolk sac. Brain-specific knock-out mice initially develop normally, but they exhibit defects in motor coordination and neuronal degeneration when aged (Akassoglou et al., 2004). Knocking out PNPLA6 specifically in glia resulted in incomplete ensheathment of Remak fibers by non-myelinating Schwann cells in adult sciatic nerves (McFerrin et al., 2017). In agreement with these phenotypes, PNPLA6 is expressed in Schwann cells in the peripheral nervous system starting around post-natal day 5 (McFerrin et al., 2017). PNPLA6 is also expressed in the nervous system during development, first being detectable in spinal ganglia around day 13 postcoitum (Moser et al., 2000). Postnatally, PNPLA6 is expressed in all or most neurons; however, its distribution becomes more restricted during aging, with strong expression levels persisting in large neurons within the cortex, olfactory bulb, thalamus, hypothalamus, pons, and medulla oblongata (Glynn et al., 1998; Moser et al., 2000).

PNPLA6 is an evolutionary conserved protein, and its *Drosophila* ortholog is encoded by the *swiss-cheese* (*sws*) gene (Lush et al., 1998; Moser et al., 2000). Similar to PNPLA6, SWS is expressed in most neurons when the flies are young, but as PNPLA6, it becomes primarily restricted to large neurons with age (Muhlig-Versen et al., 2005). In addition, SWS is expressed by ensheathing glia that form processes around axons, analogous to the expression of PNPLA6 in Schwann cells (Dutta et al., 2016). SWS is also enriched in the ER, and its loss causes structural alterations in the ER (Muhlig-Versen et al., 2005). Mutant *sws* flies show locomotion deficits and neuronal degeneration, both of which progress with age (Kretzschmar et al., 1997; Dutta et al., 2016). Furthermore, SWS exhibits phospholipase activity, and *sws* mutants have increased levels of PC and LPC (Muhlig-Versen et al., 2005; Kmoch et al., 2015). In addition to the phospholipase domain, both *Drosophila* SWS and mammalian PNPLA6 contain domains that are predicted to bind cAMP or cGMP and a domain that binds to catalytic subunits of protein kinase A (PKA). For SWS, it has been shown that the latter is indeed required for binding to the C3 catalytic domain of PKA (PKA-C3), whereby SWS inhibits the activity of PKA-C3 (Bettencourt da Cruz et al., 2008). These similarities indicate that SWS and PNPLA6 are both structurally and functionally conserved, which we confirmed by demonstrating that expression of either mouse or human PNPLA6 restored SWS function in *Drosophila* (Muhlig-Versen et al., 2005; Topaloglu et al., 2014). We therefore have now used the fly SWS model to investigate the consequences that different disease-associated PNPLA6 mutations have on the functions of this protein.

MATERIALS AND METHODS

Drosophila Stocks

The sws^1 allele has been described in Kretzschmar et al. (1997). *Appl*-GAL4 was kindly provided by L. Torroja (Universidad Autonoma de Madrid, Spain) and *loco*-GAL4 by C. Klämbt (Universitat Muenster, Muenster, Germany). The $sws^{JF03428}$ RNAi line was obtained from the Bloomington Stock Center. To obtain the transgenic lines expressing human PNPLA6, a human cDNA encoding transcript variant 2 (NM_006702.2) was used and the mutations introduced by site-directed mutagenesis using the Quikchange Lightning site-directed mutagenesis kit according to the instructions of the manufacturer (Stratagene, La Jolla, CA, United States). The location of the substituted amino acids is referring to the PNPLA6 protein annotated as Q8IY17, as listed in UniProtKB. The PNPLA6 cDNAs were cloned into pUASTattB and integrated into the genome at the 68E attP site using the PhiC31 integrase-mediated transgenesis system (Bischof et al., 2007) and the BestGene transformation service. The lines expressing wild-type PNPLA6 and $PNPLA6^{D376GfsX18}$ are described in Topaloglu et al. (2014). Flies were maintained on standard fly food under a 12:12 h light:dark cycle. Stocks were maintained at 18°C while crosses and aging flies were maintained at 25°C.

Western Blots

Adult fly heads were dissected on an ice-cold plate, homogenized in RIPA lysis buffer [150 mM NaCl, 1% DOC, 1% SDS, 50 mM Tris, 5 mM ethylenediaminetetraacetic acid (EDTA), 5 mM ethylene glycol-bis(β-aminoethyl ether)-N,N,N′,N′-tetraacetic acid (EGTA), 1% triton X-100, and protease

inhibitors (Cell Signaling Technology 5872S)] at 5 μl per head, and centrifuged at 25,000 × *g* for 20 min at 4°C. The supernatant was kept, mixed with NuPAGE LDS Sample Buffer (ThermoFisher B0008) and beta-mercaptoethanol to a final concentration of 1.25× and 2.5%, respectively, and denatured at 85°C for 10 min. Samples containing the equivalent of one to two heads were electrophoresed through 8% bis–tris gels (ThermoFisher NW00082) and transferred onto PVDF membranes (ThermoFisher T2234). To detect PNPLA6, we used a biotinylated secondary antibody and Streptavidin-conjugated HRP (Vector Labs PK-6200) following the manufacturer protocol with the exception that all antibodies were diluted in 1× casein blocking buffer (Sigma C7594) and all washing steps were carried out with 1× TBST (Tris-buffered saline + 0.05% TWEEN-20). To detect GAPDH, the primary antibody was diluted in 1× casein and subsequent washing and secondary antibody steps were carried out in 1× TBST. Enhanced chemiluminescent substrate (Michigan Diagnostics FWPD02) was used to visualize bands. The antisera/antibodies were used at the following dilution: rabbit anti-PNPLA6/NTE (Chen et al., 2007) (1:100; provided by Y.-J. Wu, Chinese Academy of Sciences), mouse anti-GAPDH G-9 (1:1000; Santa Cruz sc-365062), Biotinylated Goat Anti-Rabbit (1:200; Vector Labs BA-1000), and goat anti-mouse peroxidase conjugate (1:10,000; Jackson ImmunoResearch 115-035-166). For the quantification of protein levels, the intensity of the PNPLA6 bands was measured and normalized to GAPDH using Fiji (Schindelin et al., 2012). The levels of the mutant PNPLA6 proteins were then compared to the mean level of wild-type PNPLA6. Statistical analysis was done using measurements from five independent Western blots and GraphPad Prism with one-way ANOVA and a Dunnett's *post hoc* test.

Fast Phototaxis

Fast phototaxis assays were conducted in the dark using the countercurrent apparatus described by Benzer (1967) and a single light source. A detailed description of the experimental conditions can be found in Strauss and Heisenberg (1993). Flies were starved overnight, but had access to water and were tested the following morning. Five consecutive tests were performed in each experiment with a time allowance of 6 s to make a transition toward the light and into the next vial. Flies were obtained from four to five independent crosses from which the progeny with the correct genotype was collected every day and pooled into one vial for aging. Vials were exchanged with fresh ones every 4–5 days. Flies were then tested in groups of five to nine flies and a value determined for each fly based on which vial it reached; flies that reached the last of the six vials were scored as 100% performance, reaching the fifth vial 80%, the fourth vial 60%, the third vial 40%, the second vial 20%, and flies not leaving the first vial were scored at 0%. Progeny collected from at least four different days were tested. Statistical analysis was done using GraphPad Prism and one-way ANOVA with Dunnett's *post hoc* tests.

Tissue Sections and Measurement of Vacuolar Pathology

Flies were obtained and aged as described for the phototaxis experiments. Paraffin sections for light microscopy were prepared and analyzed for vacuole formation as described in Botella et al. (2003) and Sunderhaus and Kretzschmar (2016). Briefly, whole flies were fixed in Carnoy's solution and dehydrated in an ethanol series followed by incubation in methyl benzoate before embedding in paraffin. Sections were cut at 7 μm and analyzed with a Zeiss Axioskope 2 microscope using the autofluorescence caused by the dispersed eye pigment. To quantify the vacuolization, we photographed sections at the level of the great commissure and numbered the pictures for a double-blind analysis. The area of the vacuoles in the deutocerebral neuropil was then calculated in ImageJ as total pixel number, converted into μm^2, and the genotype determined. Statistical analysis was done using GraphPad Prism and one-way ANOVA with Dunnett's *post hoc* tests.

Lipid Analysis

Forty *Drosophila* heads were collected and pulverized in cold methyl *tert*-butyl ether:methanol:water using a ceramic bead blaster, centrifuged, and the top layer was collected for UPLC-HDMS and UPLC-SWATH analyses. Five microliters of Lipidomix™ was added as an internal standard to each sample. Samples were analyzed in duplicates in positive and negative ion modes. Acquired data were searched by Peakview's™ XIC Manager and LPC, PC and PE XIC (extracted ion chromatograms) lists were searched based on formula, accurate mass, isotope ratio, and msms fragmentation. Lipid measurements were conducted at the Mass Spectrometry Facility of the Oregon State University. LPC, PC, and PE were determined and compared to one of the two sws^1 samples added to each measurement. Two independently prepared sets, containing extracts from all genotypes, were used and two independent measurements obtained from each set. PC and LPC levels were normalized to PE, which we previously showed to be unchanged in sws^1 (Muhlig-Versen et al., 2005). Statistical analysis was done using GraphPad Prism and one-way ANOVA with Dunnett's *post hoc* tests or Student's *t*-tests.

RESULTS AND DISCUSSION

As mentioned above, SWS and PNPLA6 contain a phospholipase domain, plus a domain similar to regulatory PKA subunits that includes three cNMP binding sites, whereby the second and the third are located next to each other. Disease-associated mutations have been identified in both domains (at this time 23 pathogenic mutations are listed at https://varsome.com/gene/PNPLA6); however, there is no clear correlation between clinical features and location of the mutations. To determine the functional consequences of these mutations, we created transgenic lines expressing different PNPLA6 variants and tested their ability to restore SWS function in the sws^1 mutant line. The sws^1 mutation is caused by a stop codon at the position of $serine^{375}$, shortening the protein to about a quarter of its normal length, lacking two of its three cNMP binding sites and the entire phospholipase domain (Kretzschmar et al., 1997). Furthermore, this shortened protein could not be detected by Western blots or immunohistochemistry, suggesting that

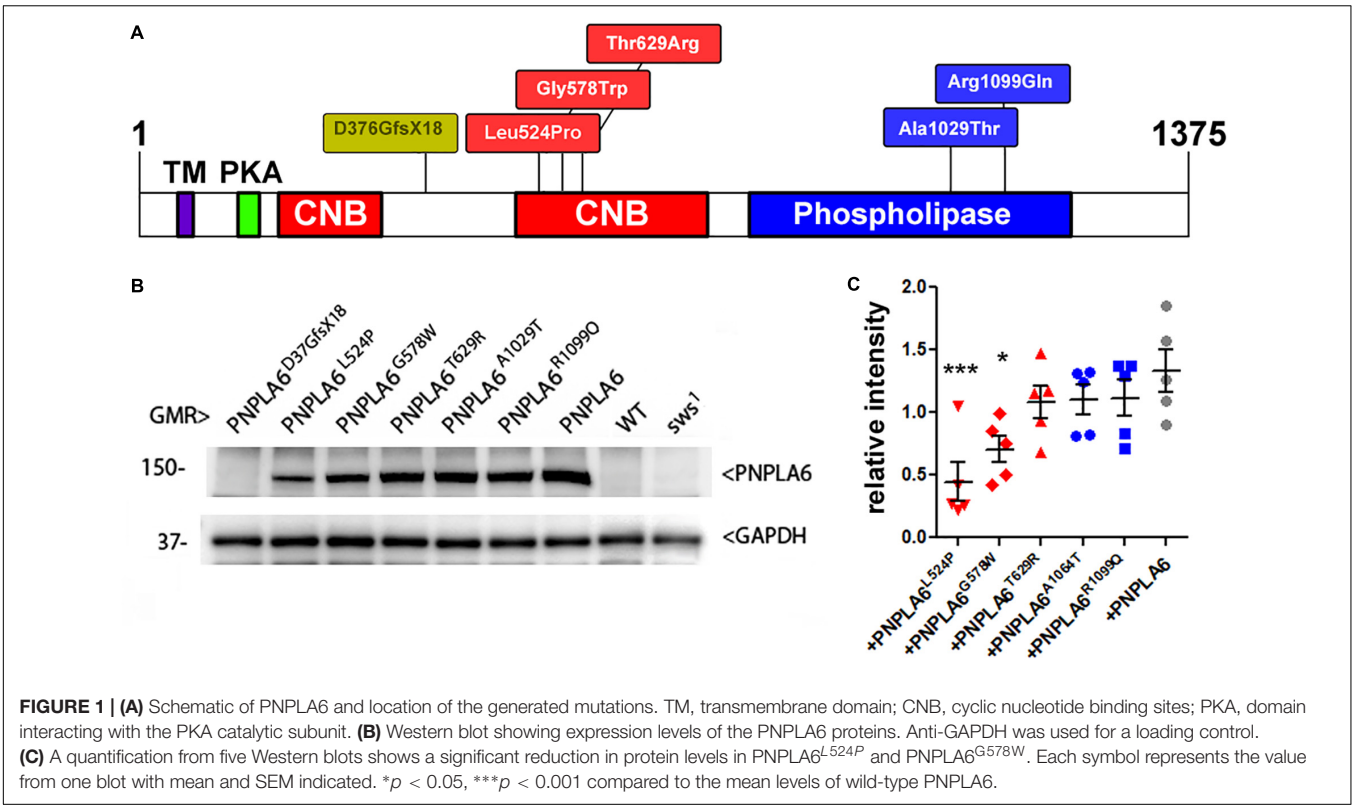

FIGURE 1 | (A) Schematic of PNPLA6 and location of the generated mutations. TM, transmembrane domain; CNB, cyclic nucleotide binding sites; PKA, domain interacting with the PKA catalytic subunit. **(B)** Western blot showing expression levels of the PNPLA6 proteins. Anti-GAPDH was used for a loading control. **(C)** A quantification from five Western blots shows a significant reduction in protein levels in PNPLA6^{L524P} and PNPLA6^{G578W}. Each symbol represents the value from one blot with mean and SEM indicated. *$p < 0.05$, ***$p < 0.001$ compared to the mean levels of wild-type PNPLA6.

sws^{1} is a null mutation (Dutta et al., 2016). We previously generated flies that express either wild-type human PNPLA6 or a mutant form (PNPLA6^{D376GfsX18}) and whereas wild-type PNPLA6 did rescue the neurodegenerative phenotype of the *sws*^{1} mutant, PNPLA6^{D376GfsX18} did not (Topaloglu et al., 2014). PNPLA6^{D376GfsX18} also shortens the protein to about a quarter of its length (Topaloglu et al., 2014), deleting the entire phospholipase domain and two of the three cyclic nucleotide binding domains (**Figure 1A**), providing a "negative control" for our experiments. The PNPLA6^{D376GfsX18} mutation is only found in compound heterozygous patients together with the pathogenic PNPLA6^{R1099C} mutation, which also failed to rescue the degenerative phenotype of *sws*^{1} (Topaloglu et al., 2014). In addition to these two constructs, we subsequently generated five new lines carrying different PNPLA6 mutations identified in patients. All of these constructs were placed under control of the Upstream Activation Sequence (UAS) that can be activated by the yeast GAL4 transcription factor (Brand and Perrimon, 1993). Three of these new constructs contained mutations in the cNMP binding sites: PNPLA6^{L524P}, PNPLA6^{G578W}, and PNPLA6^{T629R}, while PNPLA6^{A1029T} and PNPLA6^{R1099Q} carried mutations in the phospholipase domain (**Figure 1A**). PNPLA6^{L524P} and PNPLA6^{R1099Q} were identified in patients diagnosed with Oliver McFarlane Syndrome, and while they showed chorioretinopathy and hypothyroidism, they did not show signs of hypogonadism or ataxia (Hufnagel et al., 2015; Kmoch et al., 2015). PNPLA6^{G578W} is a mutation causing Boucher-Neuhäuser Syndrome, and the patients expressing this mutation exhibited cerebellar atrophy, ataxia, hypogonadism, and chorioretinal dystrophy (Synofzik et al., 2014). Patients with the PNPLA6^{A1029T} and PNPLA6^{T629R} mutations exhibit hypogonadism with absent or delayed pubertal development, characteristic for Gordon–Holmes syndrome (Kotan et al., 2016). Individuals with the PNPLA6^{T629R} mutation (PNPLA6^{T581R} in the original paper due to referring to another protein isoform) showed digenic inheritance, being heterozygote for this PNPLA6 mutation and a mutation in the steroid receptor RNA activator 1 (Kotan et al., 2016). We chose these mutations to represent different syndromes as well as to include mutations in the two identified functional domains of PNPLA6. To obtain similar expression levels in our different transgenic lines, all of the PNPLA6 constructs were inserted into the same chromosomal site using the PhiC31 integrase-mediated transgenesis system (Bischof et al., 2007). To confirm this, we performed Western blots (**Figure 1B**) with flies expressing the PNPLA6 constructs with GMR-GAL4 (a relatively strong promoter). As expected PNPLA6^{T629R}, PNPLA6^{A1029T}, and PNPLA6^{R1099Q} were expressed at similar levels as wild-type PNPLA6 (**Figure 1C**). However, the levels of PNPLA6^{L524P} and PNPLA6^{G578W} were significantly reduced, suggesting that the mutations affect the stability of the protein. Both mutations are localized within the cyclic nucleotide binding region while the two mutations in the phospholipase domain have no significant effect on protein levels. This indicates that cyclic nucleotide binding may play a role in stabilizing the protein. However, it should be noted that the T629R mutation, which also localizes to the cyclic nucleotide binding domain, did not reduce protein levels but it is not known

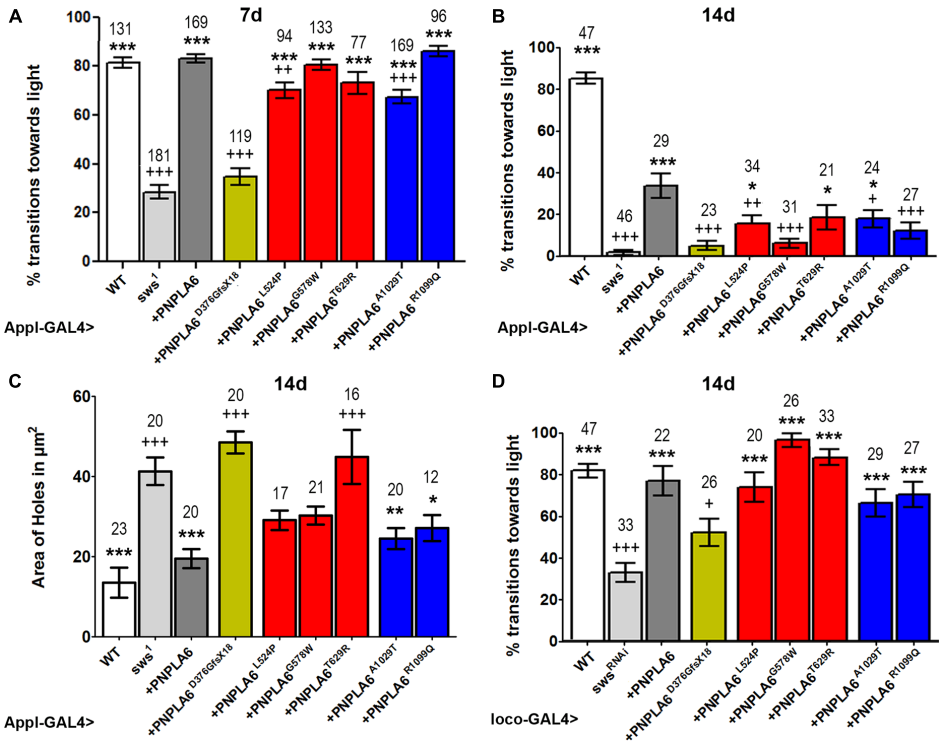

FIGURE 2 | Effects of PNPLA6 expression on *sws*^{1}-associated phenotypes. **(A)** Fast phototaxis assays of 7-day-old flies expressing the PNPLA6 proteins pan-neuronally with *Appl*-GAL4. Wild-type PNPLA6 and all point mutations rescue the reduced performance of *sws*^{1} while the shortened PNPLA6^{D376GfsX18} protein does not. **(B)** When the fast phototaxis assays were performed with 14-day-old flies, wild-type PNPLA6, PNPLA6^{L524P}, PNPLA6^{T629R}, and PNPLA6^{R1099Q} partially improved the performance. With the exception of PNPLA6^{T629R}, all mutant constructs were significantly less efficient than wild-type PNPLA6 at this age. **(C)** Measuring the area of vacuoles in the deutocerebral neuropil of 14-day-old *sws*^{1} flies expressing wild-type PNPLA6 with *Appl*-GAL4 showed a suppression of the degeneration. Two of the point mutations in the phospholipase domain also suppressed the degeneration observed in *sws*^{1}. **(D)** Fast phototaxis assays of 14-day-old flies co-expressing the PNPLA6 proteins and the sws^{RNAi} construct in all glia using *loco*-GAL4. All PNPLA6 construct besides PNPLA6^{D376GfsX18} suppressed the locomotion deficits of the *sws* knockdown flies. Means and SEMs are indicated. The number of analyzed individuals is given above each bar. For the phototaxis experiments in panels **A**, **B**, and **D**, the flies were tested in groups of five to nine flies. $^*p < 0.05$, $^{**}p < 0.01$, $^{***}p < 0.001$ compared to *sws*^{1} **(A–C)**, the sws^{RNAi} **(D)**. $^+p < 0.05$, $^{++}p < 0.01$, $^{+++}p < 0.001$ compared to wild-type PNPLA6. One-way ANOVA with Dunnett's *post hoc* test was used for statistical analyses.

yet how the different mutations affect cyclic nucleotide binding.

Mutant PNPLA6 Proteins Are Partially Functional

To assess the impact of each mutation on the *in vivo* function of PNPLA6, we expressed them pan-neuronally in *sws*^{1} mutants via *Appl*-GAL4. As shown in **Figure 2A**, *sws*^{1} flies show a severe reduction in locomotion in the fast phototaxis assay by as early as 7 day old. Expressing wild-type PNPLA6 restored locomotory behavior to wild-type levels, demonstrating that the human protein can replace fly SWS. As expected, the PNPLA6^{D376GfsX18} mutant, which we previously showed does not rescue degenerative phenotypes in *sws*^{1} flies, failed to rescue the locomotion phenotype. In contrast, all of the other PNPLA6-mutant forms did improve locomotion (significances to *sws*^{1} indicated by *). Whereas *sws*^{1} flies expressing PNPLA6^{G578W}, PNPLA6^{T629R}, and PNPLA6^{R1099Q} were not significantly different from flies expressing wild-type PNPLA6, flies expressing either PNPLA6^{L524P} or PNPLA6^{A1029T} only partially restored normal locomotion (significances to wild-type PNPLA6 indicated by +). Due to the locomotor deficits in *sws*^{1} flies becoming progressively worse with age, 14-day-old *sws*^{1} flies barely move (**Figure 2B**). Again, this deficit was significantly improved by the induction of wild-type PNPLA6 with *Appl*-GAL4, although it did not fully restore normal locomotor behavior. This partial effect is consistent with our previous results showing that the loss of SWS in glia also causes locomotor deficits that cannot be rescued by expression of SWS in neurons (Muhlig-Versen et al., 2005; Dutta et al., 2016). PNPLA6^{L524P}, PNPLA6^{T629R}, and PNPLA6^{A1029T} also still partially rescued although not as efficiently as wild-type PNPLA6. With the exception of PNPLA6^{T629R}, all mutant lines were significantly worse than wild-type PNPLA6, suggesting that even constructs like PNPLA6^{G578W} and PNPLA6^{R1099Q} that could prevent deleterious effects on the locomotion as efficiently as wild-type PNPLA6 in young flies cannot significantly delay the progression.

Next, we tested whether expressing the PNPLA6 constructs in neurons could ameliorate the neurodegeneration observed in

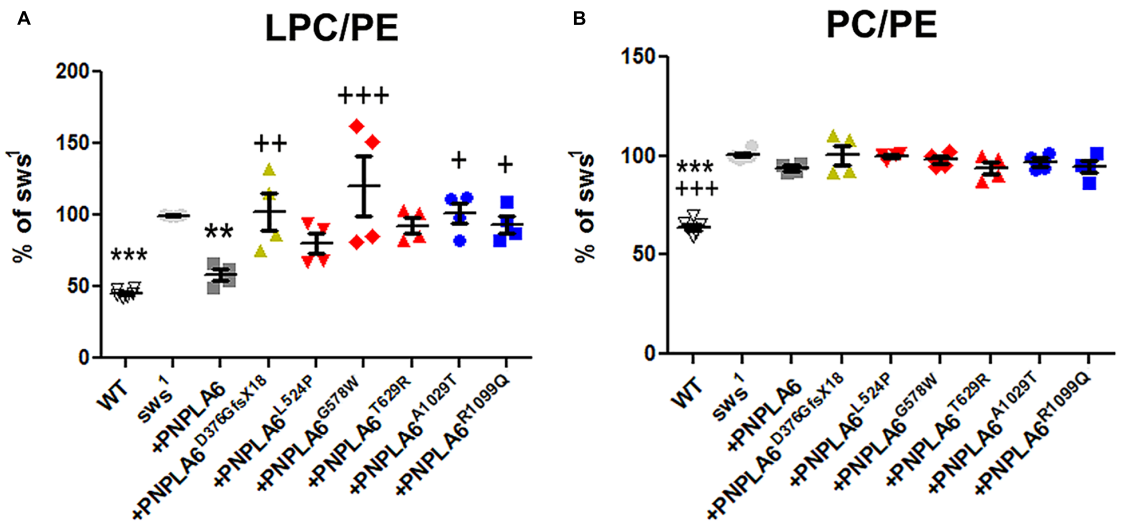

FIGURE 3 | (A) Pan-neuronal expression of wild-type PNPLA6 reduces the LPC/PE ratio in *sws*^{1} but none of the mutations does. **(B)** None of the PNPLA6 proteins significantly reduces the PC/PE ratio in *sws*^{1}. Mean from four measurements and SEM shown. Flies were 3–5 days old. Each symbol represent the value form one measurement. $^{**}p < 0.01$, $^{***}p < 0.001$ compared to *sws*^{1}. $^{+}p < 0.05$, $^{++}p < 0.01$, $^{+++}p < 0.001$ compared to wild-type PNPLA6. One-way ANOVA with Dunnett's *post hoc* test was used for statistical analyses.

sws^1. For this analysis, we measured the area of vacuoles that form in 14-day-old *sws*^{1} flies (**Figure 2C**). As expected, expressing wild-type PNPLA6 prevented neurodegeneration, as did both PNPLA6 proteins with mutations in the phospholipase domain. In contrast, none of the constructs with mutations in the cNMP-binding region had a significant beneficial effect. Although the suppression was not significant compared to *sws*^{1}, PNPLA6^{L524P} and PNPLA6^{G578W} did show some improvement and they were not significantly different from wild-type PNPLA6.

As mentioned above, SWS also has a cell-autonomous function in glia, and knocking down SWS specifically in glia results in locomotor deficits (Dutta et al., 2016). We therefore tested how each of our PNPL6 mutations affected glial function in SWS knockdown flies by expressing them in all glia using *loco*-GAL4. Testing 14-day-old flies in the fast phototaxis assay revealed that all PNPLA6 forms could suppress the locomotion defects seen in the knock-down flies, with the exception of PNPLA6^{D376GfsX18} (**Figure 2D**). Together our results show that human PNPLA6 can functionally replace SWS in neurons and glia, confirming previous results with either human or mouse PNPLA6 (Muhlig-Versen et al., 2005; Topaloglu et al., 2014). They also confirm that the PNPLA6^{D376GfsX18} mutation, which results in a shortened protein that has lost the phospholipase domain as well as two of the cAMP binding sites, is not functional. As mentioned above, this mutation is only found in compound heterozygous patients (Topaloglu et al., 2014) and together with our findings that the loss of PNPLA6 in mice causes lethality during embryonic development, these results support the conclusion that the complete loss of functional PNPLA6 in humans is lethal. In contrast, none of the point mutations induces a complete loss of function. Although all of these mutations do impair aspects of PNPLA6 function (see below), they are still capable of partially rescuing the degenerative phenotypes and locomotion deficits observed in the *sws*^{1} null mutant. Furthermore, we did not detect significant differences in the rescue ability of mutations associated with a specific disease, suggesting that the different phenotypic presentation may be due to genetic background effects or other individual differences rather than different effects on PNPLA6 function. It should also be noted that a specific syndrome can be caused by mutations in either the phospholipase domain or the cyclic nucleotide binding domain; like the L524P and R1099Q mutations which are both described to cause Oliver–McFarlane syndrome, or the T629R and A1029T mutations associated with Gordon–Holmes syndrome, also supporting that these syndromes are not due to effects on specific PNPLA6 functions.

Mutations in Both Domains Interfere With the Phospholipase Function

Loss of PNPLA6 or SWS results in a rise in PC and LPC levels in flies and mice (Muhlig-Versen et al., 2005; Read et al., 2009; Kmoch et al., 2015), whereby LPC has been suggested to be the preferred substrate of SWS/NTE (van Tienhoven et al., 2002; Quistad et al., 2003). To determine how the different PNPLA6 mutations affect its phospholipase function, we measured LPC and PC levels in *sws*^{1} flies expressing these constructs pan-neuronally with *Appl*-GAL4. PC and LPC levels were normalized to phosphatidylethanolamine (PE), which we previously showed not to be altered in *sws*^{1} (Muhlig-Versen et al., 2005). Consistent with our previous results, we detected an increase in LPC and PC levels in 3–5-day-old *sws*^{1} flies (**Figures 3A,B**). Expressing wild-type PNPLA6 reduced LPC levels in *sws*^{1} flies, but the PC levels were not significantly decreased compared to *sws*^{1} when using multiple comparison tests. However in a direct comparison, *sws*^{1} flies expressing

PNPLA6 did show a significant reduction ($P = 0.002$, Student's *t*-test). In contrast, none of the mutant constructs had an effect on PC levels in sws^1 flies either in direct or in multiple comparison tests (**Figure 3B**), nor did they improve LPC levels. Moreover, PNPLA6^{D376GfsX18}, PNPLA6^{G578W}, PNPLA6^{A1029T}, and PNPLA6^{R1099Q} were significantly worse than PNPLA6 (**Figure 3A**). This shows that all mutations interfere with the phospholipase activity of PNPLA6.

Although none of the mutants could suppress the phospholipid defects, all the point mutations reduced the locomotion deficits at 7th day and the two mutations in the phospholipase domain also ameliorated neuronal degeneration when tested at 14 days. These results suggest that changes in phospholipid levels are not the only factor in the pathogenicity of PNPLA6 mutant forms, and that the mutant constructs still can fulfill other PNPLA6-dependent functions. That effects on the phospholipase activity are not sufficient to cause disease has also been suggested by measuring PNPLA6 activity in human fibroblasts. While some carriers of mutations that cause spastic paraplegia revealed even less PNPLA6 activity than the patients, they were nevertheless symptom-free (Hein et al., 2010). In addition, we found that the constructs containing mutations in the cNMP-binding sites (but with an intact phospholipase domain) were equally deficient in reducing LPC or PC, supporting previous findings that cNMP can regulate the phospholipase activity of PNPLA6 (Chen et al., 2010). Lastly, whereas expressing wild-type PNPLA6 could reduce the levels of LPC to near-control levels it had a much weaker effect on PC. Nevertheless, PNPLA6 did suppress the locomotion and degenerative phenotypes of sws^1. We previously obtained similar results by activating ER stress responses in sws^1, which also reduced LPC levels but not PC levels, as well as suppressing behavioral and degenerative phenotypes (Sunderhaus et al., 2019). Together, these results suggest that the rise in LPC is more toxic than the increased PC. Whereas PC is a major component of all cell membranes, the concentration of LPC is normally quite low (Kienesberger et al., 2009; Lagace and Ridgway, 2013). Moreover, increased levels of LPC have been linked with a variety of diseases, including demyelination and neuropathic pain (Wang and Dennis, 1999; Fuchs and Schiller, 2009; Drzazga et al., 2014; Velasco et al., 2017). Although we did not detect significant changes in myelin in a glial-specific knock-out of PNPLA6 in mice, it did cause an incomplete ensheathment of Remak bundles by non-myelinating Schwann cells in the sciatic nerve (McFerrin et al., 2017). However, lipid composition also regulates vesicle fusion and therefore synaptic transmission (Lauwers et al., 2016). Furthermore, LPC can promote apoptosis by increasing the pro-apoptotic proteins Bax and cleaved caspase-3 (Lin and Ye, 2003; Kakisaka et al., 2012; Wang et al., 2016; Chang et al., 2017). Therefore, reducing only LPC levels may be sufficient to suppress the behavioral and degenerative phenotype of sws^1.

DATA AVAILABILITY STATEMENT

The datasets generated for this study are available on request to the corresponding author.

AUTHOR CONTRIBUTIONS

ES performed the behavioral and anatomical experiments, and provided the samples for the lipid measurements. AL performed the Western blot experiments. ES and DK designed and analyzed the experiments. DK wrote the manuscript.

FUNDING

This work was supported by a grant from the National Institute of Health (NS047663) to DK and a fellowship to ES from a training grant from the National Institute of Health (5T32AG023477).

ACKNOWLEDGMENTS

We thank Drs. Torroja and Klämbt for providing fly stocks, Dr. Topaloglu for providing the PNPLA6 cDNA and the PNPLA6^{A1029T} mutation, and Dr. Wu for providing the anti-PNPLA6 antiserum.

REFERENCES

Akassoglou, K., Malester, B., Xu, J., Tessarollo, L., Rosenbluth, J., and Chao, M. V. (2004). Brain-specific deletion of neuropathy target esterase/*swisscheese* results in neurodegeneration. *Proc. Natl. Acad. Sci. U.S.A.* 101, 5075–5080. doi: 10.1073/pnas.0401030101

Benzer, S. (1967). Behavioral mutants of drosophila isolated by countercurrent distribution. *Proc. Natl. Acad. Sci. U.S.A.* 58, 1112–1119. doi: 10.1073/pnas.58.3.1112

Bettencourt da Cruz, A., Wentzell, J., and Kretzschmar, D. (2008). Swiss cheese, a protein involved in progressive neurodegeneration, acts as a noncanonical regulatory subunit for PKA-C3. *J. Neurosci.* 28, 10885–10892. doi: 10.1523/JNEUROSCI.3015-08.2008

Bischof, J., Maeda, R. K., Hediger, M., Karch, F., and Basler, K. (2007). An optimized transgenesis system for drosophila using germ-line-specific phiC31 integrases. *Proc. Natl. Acad. Sci. U. S. A.* 104, 3312–3317. doi: 10.1073/pnas.0611511104

Blackstone, C. (2018). Hereditary spastic paraplegia. *Handb. Clin. Neurol.* 148, 633–652. doi: 10.1016/b978-0-444-64076-5.00041-7

Botella, J. A., Kretzschmar, D., Kiermayer, C., Feldmann, P., Hughes, D. A., and Schneuwly, S. (2003). Deregulation of the Egfr/Ras signaling pathway induces age-related brain degeneration in the Drosophila mutant vap. *Mol. Biol. Cell.* 14, 241–250. doi: 10.1091/mbc.E02-05-0297

Brand, A. H., and Perrimon, N. (1993). Targeted gene expression as a means of altering cell fates and generating dominant phenotypes. *Development* 118, 401–415.

Chang, M.-C., Lee, J.-J., Chen, Y.-J., Lin, S.-I., Lin, L.-D., Jein-Wen Liou, E., et al. (2017). Lysophosphatidylcholine induces cytotoxicity/apoptosis and IL-8 production of human endothelial cells: related mechanisms. *Oncotarget* 8, 106177–106189. doi: 10.18632/oncotarget.22425

Chen, J. X., Long, D. X., Hou, W. Y., Li, W., and Wu, Y. J. (2010). Regulation of neuropathy target esterase by the cAMP/protein kinase A signal. *Pharmacol. Res.* 62, 259–264. doi: 10.1016/j.phrs.2010.03.006

Chen, R., Chang, P. A., Long, D. X., Yang, L., and Wu, Y. J. (2007). Down-regulation of neuropathy target esterase by protein kinase C activation with PMA stimulation. *Mol. Cell Biochem.* 302, 179–185. doi: 10.1007/s11010-007-9439-0

de Souza, P. V. S., de Rezende Pinto, W. B. V., de Rezende Batistella, G. N., Bortholin, T., and Oliveira, A. S. B. (2017). Hereditary spastic paraplegia: clinical and genetic hallmarks. *Cerebellum* 16, 525–551. doi: 10.1007/s12311-016-0803-z

Deik, A., Johannes, B., Rucker, J. C., Sánchez, E., Brodie, S. E., Deegan, E., et al. (2014). Compound heterozygous *PNPLA6* mutations cause Boucher–Neuhäuser syndrome with late-onset ataxia. *J. Neurol.* 261, 2411–2423. doi: 10.1007/s00415-014-7516-3

Drzazga, A., Sowinska, A., and Koziolkiewicz, M. (2014). Lysophosphatidylcholine and lysophosphatidylinosiol–novel promissing signaling molecules and their possible therapeutic activity. *Acta Pol. Pharm.* 71, 887–899.

Dutta, S., Rieche, F., Eckl, N., Duch, C., and Kretzschmar, D. (2016). Glial expression of Swiss cheese (SWS), the drosophila orthologue of neuropathy target esterase (NTE), is required for neuronal ensheathment and function. *Dis. Model Mech.* 9, 283–294. doi: 10.1242/dmm.022236

Fink, J. K. (2013). Hereditary spastic paraplegia: clinico-pathologic features and emerging molecular mechanisms. *Acta Neuropathol.* 126, 307–328. doi: 10.1007/s00401-013-1115-8

Fuchs, B., and Schiller, J. (2009). Lysophospholipids: their generation, physiological role and detection. are they important disease markers? *Mini. Rev. Med. Chem.* 9, 368–378. doi: 10.2174/1389557510909030368

Garcia-Cazorla, A., Mochel, F., Lamari, F., and Saudubray, J. M. (2015). The clinical spectrum of inherited diseases involved in the synthesis and remodeling of complex lipids. a tentative overview. *J. Inherit. Metab. Dis.* 38, 19–40. doi: 10.1007/s10545-014-9776-6

Glynn, P., Holton, J. L., Nolan, C. C., Read, D. J., Brown, L., Hubbard, A., et al. (1998). Neuropathy target esterase: immunolocalization to neuronal cell bodies and axons. *Neuroscience* 83, 295–302. doi: 10.1016/s0306-4522(97)00388-6

Hein, N. D., Rainier, S. R., Richardson, R. J., and Fink, J. K. (2010). Motor neuron disease due to neuropathy target esterase mutation: enzyme analysis of fibroblasts from human subjects yields insights into pathogenesis. *Toxicol. Lett.* 199, 1–5. doi: 10.1016/j.toxlet.2010.06.020

Hufnagel, R. B., Arno, G., Hein, N. D., Hersheson, J., Prasad, M., Anderson, Y., et al. (2015). Neuropathy target esterase impairments cause oliver–mcfarlane and laurence–moon syndromes. *J. Med. Genet.* 52:85. doi: 10.1136/jmedgenet-2014-102856

Kakisaka, K., Cazanave, S. C., Fingas, C. D., Guicciardi, M. E., Bronk, S. F., Werneburg, N. W., et al. (2012). Mechanisms of lysophosphatidylcholine-induced hepatocyte lipoapoptosis. *Am. J. Physiol. Gastrointest. Liver Physiol.* 302, G77–G84. doi: 10.1152/ajpgi.00301.2011

Kienesberger, P. C., Oberer, M., Lass, A., and Zechner, R. (2009). Mammalian patatin domain containing proteins: a family with diverse lipolytic activities involved in multiple biological functions. *J. Lipid. Res.* 50(Suppl.), S63–S68. doi: 10.1194/jlr.R800082-JLR200

Kmoch, S., Majewski, J., Ramamurthy, V., Cao, S., Fahiminiya, S., Ren, H., et al. (2015). Mutations in PNPLA6 are linked to photoreceptor degeneration and various forms of childhood blindness. *Nat. Commun.* 6:5614. doi: 10.1038/ncomms6614

Kotan, L. D., Cooper, C., Darcan, Ş, Carr, I. M., Özen, S., Yan, Y., et al. (2016). Idiopathic hypogonadotropic hypogonadism caused by inactivating mutations in SRA1. *J. Clin. Res. Pediatr. Endocrinol.* 8, 125–134. doi: 10.4274/jcrpe.3248

Kretzschmar, D., Hasan, G., Sharma, S., Heisenberg, M., and Benzer, S. (1997). The swiss cheese mutant causes glial hyperwrapping and brain degeneration in drosophila. *J. Neurosci.* 17, 7425–7432. doi: 10.1523/jneurosci.17-19-07425.1997

Lagace, T. A., and Ridgway, N. D. (2013). The role of phospholipids in the biological activity and structure of the endoplasmic reticulum. *Biochim. Biophys. Acta* 1833, 2499–2510. doi: 10.1016/j.bbamcr.2013.05.018

Lauwers, E., Goodchild, R., and Verstreken, P. (2016). Membrane lipids in presynaptic function and disease. *Neuron* 90, 11–25. doi: 10.1016/j.neuron.2016.02.033

Lin, P., and Ye, R. D. (2003). The lysophospholipid receptor G2A activates a specific combination of G proteins and promotes apoptosis. *J. Biol. Chem.* 278, 14379–14386. doi: 10.1074/jbc.M209101200

Lush, M. J., Li, Y., Read, D. J., Willis, A. C., and Glynn, P. (1998). Neuropathy target esterase and a homologous Drosophila neurodegeneration-associated mutant protein contain a novel domain conserved from bacteria to man. *Biochem. J.* 332(Pt 1), 1–4. doi: 10.1042/bj3320001

McFerrin, J., Patton, B. L., Sunderhaus, E. R., and Kretzschmar, D. (2017). NTE/PNPLA6 is expressed in mature schwann cells and is required for glial ensheathment of remak fibers. *Glia* 65, 804–816. doi: 10.1002/glia.23127

Moser, M., Li, Y., Vaupel, K., Kretzschmar, D., Kluge, R., Glynn, P., et al. (2004). Placental failure and impaired vasculogenesis result in embryonic lethality for neuropathy target esterase-deficient mice. *Mol. Cell. Biol.* 24, 1667–1679. doi: 10.1128/mcb.24.4.1667-1679.2004

Moser, M., Stempfl, T., Li, Y., Glynn, P., Buttner, R., and Kretzschmar, D. (2000). Cloning and expression of the murine sws/NTE gene. *Mech. Dev.* 90, 279–282. doi: 10.1016/s0925-4773(99)00239-7

Muhlig-Versen, M., da Cruz, A. B., Tschape, J. A., Moser, M., Buttner, R., Athenstaedt, K., et al. (2005). Loss of Swiss cheese/neuropathy target esterase activity causes disruption of phosphatidylcholine homeostasis and neuronal and glial death in adult drosophila. *J. Neurosci.* 25, 2865–2873. doi: 10.1523/JNEUROSCI.5097-04.2005

Parodi, L., Fenu, S., Stevanin, G., and Durr, A. (2017). Hereditary spastic paraplegia: more than an upper motor neuron disease. *Rev. Neurol.* 173, 352–360. doi: 10.1016/j.neurol.2017.03.034

Quistad, G. B., Barlow, C., Winrow, C. J., Sparks, S. E., and Casida, J. E. (2003). Evidence that mouse brain neuropathy target esterase is a lysophospholipase. *Proc. Natl. Acad. Sci. U.S.A.* 100, 7983–7987. doi: 10.1073/pnas.1232473100

Rainier, S., Bui, M., Mark, E., Thomas, D., Tokarz, D., Ming, L., et al. (2008). Neuropathy target esterase gene mutations cause motor neuron disease. *Am. J. Hum. Genet.* 82, 780–785. doi: 10.1016/j.ajhg.2007.12.018

Read, D. J., Li, Y., Chao, M. V., Cavanagh, J. B., and Glynn, P. (2009). Neuropathy target esterase is required for adult vertebrate axon maintenance. *J. Neurosci.* 29, 11594–11600. doi: 10.1523/JNEUROSCI.3007-09.2009

Schindelin, J., Arganda-Carreras, I., Frise, E., Kaynig, V., Longair, M., Pietzsch, T., et al. (2012). Fiji: an open-source platform for biological-image analysis. *Nat. Methods* 9, 676–682. doi: 10.1038/nmeth.2019

Strauss, R., and Heisenberg, M. (1993). A higher control center of locomotor behavior in the drosophila brain. *J. Neurosci.* 13, 1852–1861. doi: 10.1523/jneurosci.13-05-01852.1993

Sunderhaus, E. R., and Kretzschmar, D. (2016). Mass histology to quantify neurodegeneration in drosophila. *J. Vis. Exp.* 118. doi: 10.3791/54809

Sunderhaus, E. R., Law, A. D., and Kretzschmar, D. (2019). ER responses play a key role in swiss-cheese/neuropathy target esterase-associated neurodegeneration. *Neurobiol. Dis.* 130:104520. doi: 10.1016/j.nbd.2019.104520

Synofzik, M., Gonzalez, M. A., Lourenco, C. M., Coutelier, M., Haack, T. B., Rebelo, A., et al. (2014). PNPLA6 mutations cause Boucher-Neuhäuser and Gordon Holmes syndromes as part of a broad neurodegenerative spectrum. *Brain* 137, 69–77. doi: 10.1093/brain/awt326

Synofzik, M., and Schule, R. (2017). Overcoming the divide between ataxias and spastic paraplegias: shared phenotypes, genes, and pathways. *Mov. Disord.* 32, 332–345. doi: 10.1002/mds.26944

Topaloglu, A. K., Lomniczi, A., Kretzschmar, D., Dissen, G. A., Kotan, L. D., McArdle, C. A., et al. (2014). Loss-of-function mutations in PNPLA6 encoding neuropathy target esterase underlie pubertal failure and neurological deficits in gordon holmes syndrome. *J. Clin. Endocrinol. Metab.* 99, E2067–E2075. doi: 10.1210/jc.2014-1836

van Meer, G., Voelker, D. R., and Feigenson, G. W. (2008). Membrane lipids: where they are and how they behave. *Nat. Rev. Mol. Cell Biol.* 9, 112–124. doi: 10.1038/nrm2330

van Tienhoven, M., Atkins, J., Li, Y., and Glynn, P. (2002). Human neuropathy target esterase catalyzes hydrolysis of membrane lipids. *J. Biol. Chem.* 277, 20942–20948. doi: 10.1074/jbc.M200330200

Velasco, M., O'Sullivan, C., and Sheridan, G. K. (2017). Lysophosphatidic acid receptors (LPARs): potential targets for the treatment of neuropathic pain. *Neuropharmacology* 113, 608–617. doi: 10.1016/j.neuropharm.2016.04.002

Wang, A., and Dennis, E. A. (1999). Mammalian lysophospholipases. *Biochim. Biophys. Acta* 1439, 1–16. doi: 10.1016/s1388-1981(99)00063-3

Wang, Y., Wang, Y., and Li, G.-R. (2016). TRPC1/TRPC3 channels mediate lysophosphatidylcholine-induced apoptosis in cultured human coronary artery smooth muscles cells. *Oncotarget* 7, 50937–50951. doi: 10.18632/oncotarget.10853

Conflict of Interest: The authors declare that the research was conducted in the absence of any commercial or financial relationships that could be construed as a potential conflict of interest.

frontiers in Neuroscience

ORIGINAL RESEARCH
published: 08 November 2019
doi: 10.3389/fnins.2019.01179

Spastin MIT Domain Disease-Associated Mutations Disrupt Lysosomal Function

Rachel Allison[1], *James R. Edgar*[2] *and Evan Reid*[1]*

[1] Department of Medical Genetics, Cambridge Institute for Medical Research, University of Cambridge, Cambridge, United Kingdom, [2] Department of Pathology, University of Cambridge, Cambridge, United Kingdom

The hereditary spastic paraplegias (HSPs) are genetic motor neuron diseases characterized by progressive degeneration of corticospinal tract axons. Mutations in SPAST, encoding the microtubule-severing ATPase spastin, are the most common causes of HSP. The broad SPAST mutational spectrum indicates a haploinsufficiency pathogenic mechanism in most cases. Most missense mutations cluster in the ATPase domain, where they disrupt the protein's ability to sever microtubules. However, several putative missense mutations in the protein's microtubule interacting and trafficking (MIT) domain have also been described, but the pathogenicity of these mutations has not been verified with functional studies. Spastin promotes endosomal tubule fission, and defects in this lead to lysosomal enzyme mistrafficking and downstream lysosomal abnormalities. We investigated the function of three disease-associated spastin MIT mutants and found that none was able to promote normal endosomal tubule fission, lysosomal enzyme receptor trafficking, or lysosomal morphology. One of the mutations affected recruitment of spastin to endosomes, a property that requires the canonical function of the MIT domain in binding endosomal sorting complex required for transport (ESCRT)-III proteins. However, the other mutants did not affect spastin's endosomal recruitment, raising the possibility of pathologically important non-canonical roles for the MIT domain. In conclusion, we demonstrate that spastin MIT mutants cause functional abnormalities related to the pathogenesis of HSP. These mutations do not directly affect spastin's microtubule-severing capacity, and so we identify a new molecular pathological mechanism by which spastin mutations may cause disease.

Keywords: ESCRT, endosome tubule fission, IST1, CHMP1B, hereditary spastic paraplegia

OPEN ACCESS

Edited by:
Craig Blackstone, National Institute of Neurological Disorders and Stroke (NINDS), United States

Reviewed by:
Jennifer Fifita, Macquarie University, Australia
Mattia Volta, Eurac Research, Italy

***Correspondence:**
Evan Reid
ealr4@cam.ac.uk

Specialty section:
This article was submitted to Neurodegeneration, a section of the journal Frontiers in Neuroscience

Received: *19 July 2019*
Accepted: *18 October 2019*
Published: *08 November 2019*

Citation:
Allison R, Edgar JR and Reid E (2019) Spastin MIT Domain Disease-Associated Mutations Disrupt Lysosomal Function. Front. Neurosci. 13:1179. doi: 10.3389/fnins.2019.01179

INTRODUCTION

The hereditary spastic paraplegias (HSPs) are a group of inherited neurodegenerative disorders characterized by spastic paralysis of the legs. This is caused by progressive degeneration of the longest axons of the corticospinal tract, the main motor pathway that connects the brain to the spinal cord (Harding, 1993; Reid, 1999; Fink, 2006). To date, more than 70 genes linked to HSP have been identified (Hensiek et al., 2015). Mutations in the gene encoding spastin (SPAST/SPG4; MIM:604277) are the most common cause of autosomal dominant uncomplicated "pure" HSP (MIM:182601) in North America and northern Europe, accounting for ∼40% of cases (Hazan et al., 1999; Blackstone et al., 2011). The wide spectrum of SPG4 mutations, including non-sense,

frameshift, splice site, and missense mutations, as well as whole exon and whole gene deletions, has led to a general consensus that the disease has a haploinsufficiency pathological mechanism in most cases, and this is supported by findings of reduced expression of spastin protein in stem cell-derived neurons or olfactory neurospheres from patients with a variety of spastin mutational classes (Abrahamsen et al., 2013; Denton et al., 2014; Havlicek et al., 2014; Rehbach et al., 2019). However, the potential for dominant negative effects or even a gain of function mechanism for some missense mutations has also been raised (Hazan et al., 1999; Fonknechten et al., 2000; Errico et al., 2002; Solowska et al., 2010, 2017).

Spastin is a microtubule-severing ATPase that uses energy from ATP hydrolysis to sever microtubules. In microtubule severing, spastin's ATPase domains associate to form a hexameric ring structure with a central pore, within which basic residues interact with the C-terminal acidic tail of tubulin (Errico et al., 2002; White et al., 2007; Roll-Mecak and Vale, 2008). ATP hydrolysis is then coupled to microtubule severing by a process that is still not fully understood, but which by analogy with structures of the related enzyme katanin may involve cycling of the hexameric complex between an open spiral and closed ring, so providing the power stroke for microtubule breakage (Roll-Mecak and Vale, 2008; Zehr et al., 2017).

There are two major isoforms of the spastin protein, which are both ubiquitously expressed; a full-length M1 isoform and a shorter M87 isoform, generated by mechanisms involving a combination of alternative translation start sites in the full-length transcript and an alternative transcript encoding only the M87 form (**Figure 1A**) (Claudiani et al., 2005). At steady state, M87 spastin is mainly cytosolic, while M1-spastin predominantly localizes to the endoplasmic reticulum (ER), where it interacts with a number of other HSP proteins that are involved in ER shaping, such as REEP1 and Atlastin-1 (Sanderson et al., 2006; Connell et al., 2009; Park et al., 2010; Montenegro et al., 2012). These two isoforms of spastin appear to act in concert to drive efficient fission of tubules from the early sorting endosome, specifically at sites of contact between the endosomal tubules and the ER (Connell et al., 2009; Allison et al., 2013, 2017).

Defective endosomal tubule fission following depletion of spastin results in the missorting of receptors that traffic via this tubular-vesicular pathway, including the mannose 6-phosphate receptors (M6PRs) (Allison et al., 2013, 2017). As these receptors are not properly sorted away from early endosomes in cells lacking spastin, they remain in the endosomal compartment and traffic through to the LAMP1-positive endolysosomal degradative compartment. M6PRs normally cycle between the endosome and Golgi; upon reaching the trans-Golgi network (TGN), they capture M6P-tagged lysosomal enzymes and mediate their traffic to the endoso-lysosomal degradative compartment (Carlton et al., 2004). Thus, in cells lacking spastin, deficiency of M6PRs at the TGN causes mistrafficking of lysosomal enzymes that should be delivered from the TGN to the endolysosomal compartment (Allison et al., 2017). In turn, this causes abnormal lysosome morphology and function, characterized by increased lysosomal size, the accumulation of dense membranous material within the lysosomes, increased lysosomal acidity, and a slight reduction in lysosome numbers (Allison et al., 2017; Newton et al., 2018). The morphological abnormalities are found in lysosomes in the cell bodies and axons of human neurons derived from spastin-HSP patients via induced pluripotent stem cells (iPSCs) and in mouse primary cortical neurons from a spastin-HSP mouse model (Allison et al., 2017). The abnormal lysosomes accumulate in axonal swellings and so are compelling candidates to be involved in the pathogenesis of spastin-HSP. Similar abnormal lysosomal morphologies have also been observed in several other genetic subtypes of HSP, and we have proposed that lysosomal dysfunction is a final common disease pathway for many subtypes of HSP (Renvoise et al., 2014; Hirst et al., 2015; Allison et al., 2017).

Spastin's recruitment to endosomal membranes relies upon the interaction of its microtubule interacting and trafficking (MIT) domain with two non-canonical members of the endosomal sorting complex required for transport (ESCRT)-III, CHMP1B and IST1 (Reid et al., 2005; Agromayor et al., 2009; Yang et al., 2009; Renvoise et al., 2010). The MIT domain of spastin binds to MIT-interaction motifs (MIMs) in the C-terminal ends of CHMP1B and IST1. A functional MIT domain that is able to interact with ESCRT-III is critical for the correct regulation of endosomal tubule fission and downstream trafficking pathways by spastin, as introduction of the artificial F124D mutation into the MIT domain, which abrogates ESCRT binding and endosomal recruitment, leads to defective endosomal tubule fission, perturbed endosome-to-Golgi M6PR traffic, and abnormal lysosomal morphology (Yang et al., 2009; Allison et al., 2013, 2017).

Most missense mutations associated with spastin-HSP are in the ATPase domain and affect spastin's microtubule severing ability in a number of different ways; for example, they may block ATP binding or hydrolysis, preventing hexamerization, or disrupt the interaction between the ATPase domain and tubulin, thereby rendering the ATPase domain non-functional (White et al., 2007; Roll-Mecak and Vale, 2008). However, several families with sequence changes in the region encoding the MIT domain have also been described, although the pathogenicity or mechanism of action of such putative mutations has not been verified (Patrono et al., 2002; Crippa et al., 2006; Rudenskaia et al., 2010). In this study, we investigate the effects of several MIT domain mutants upon functions of spastin. We show that these mutations are unable to correctly regulate endosomal tubule fission, M6PR traffic, or lysosomal morphology. One of the mutations studied affected the canonical function of the MIT domain in recruitment of spastin to endosomes. However, two other mutations did not affect endosomal recruitment of spastin, indicating that non-canonical functions of the MIT domain are also important in driving endosomal tubule fission. Thus, we demonstrate that MIT mutants cause cellular abnormalities related to the pathogenesis of HSP via a novel mechanism that does not directly involve disruption of the protein's microtubule-severing activity.

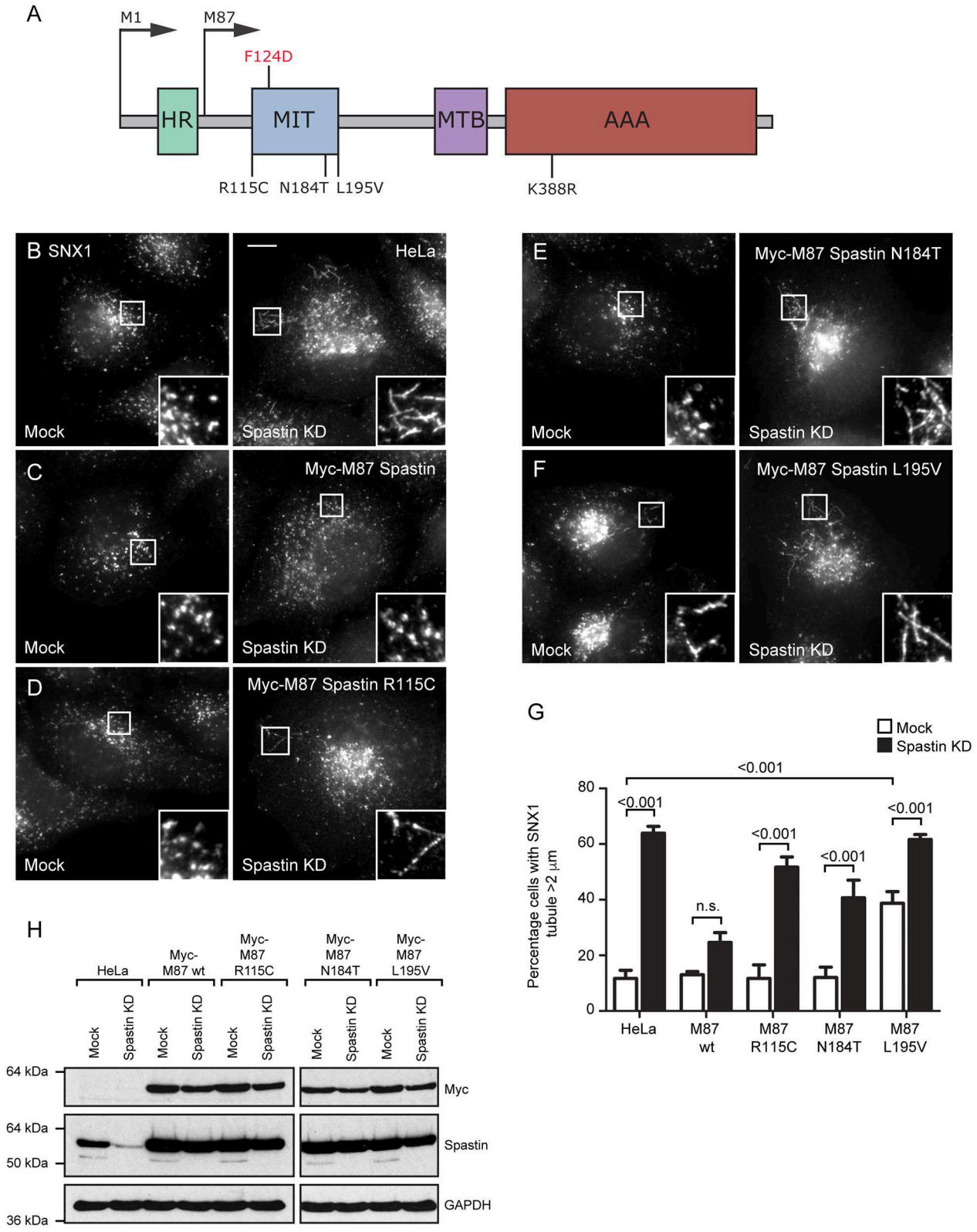

FIGURE 1 | Disease-associated spastin MIT mutants cannot support normal endosomal tubule fission. **(A)** Schematic diagram of spastin's domain structure, annotated with the position of artificial (above) and disease-associated (below) mutants used in this study. HR, hydrophobic region; MIT, MIT domain; MTB, microtubule binding domain; AAA, ATPase domain. **(B–F)** Wild-type HeLa cells or cells expressing the siRNA-resistant spastin constructs indicated were subjected to

(Continued)

FIGURE 1 | mock transfection or siRNA knockdown (KD) of endogenous spastin, then fixed and labeled for endogenous SNX1. Insets show higher magnification views of the boxed areas. Scale bar = 10 μm. **(G)** The percentage of cells with the longest SNX1 tubule >2 μm was counted ($n = 100$ cells per condition). Mean and SEM are shown for three biological repeats. *P*-values were calculated using one-way ANOVA with Bonferroni's *post hoc* multiple comparison test. In addition to the *p*-values shown, the M87-wild-type KD value was significantly different from all other KD values, with a significance of at least $p < 0.05$. **(H)** Depletion of spastin and expression of siRNA resistant constructs was confirmed by Western blotting with the antibodies indicated. GAPDH labeling is shown to verify equal sample loading.

METHODS

Patient

Informed written consent was obtained to publish anonymized clinical and molecular genetic details from a patient with HSP who attended the East Anglian Regional Genetics Service. The participant also gave written informed consent to participate in the Molecular Pathology of Human Genetic Disease study, for which ethical approval was granted by the South Birmingham and East of England Cambridgeshire research ethics committees.

Antibodies

Rabbit polyclonal anti-spastin (86–340) (raised against a glutathione S-transferase fusion protein that incorporated residues 86–340 of M1-spastin) antibodies were produced as previously described (Connell et al., 2009). Mouse monoclonal α-tubulin (DM1A) and peroxidase-conjugated secondary antibodies for Western blotting were obtained from Sigma-Aldrich; mouse monoclonal anti-myc (4A6) from EMD Millipore; mouse monoclonal anti-SNX1 (611482) from BD transduction laboratories; rabbit polyclonal anti-GFP (ab6556) and mouse monoclonal anti-M6PR (ab2733) from Abcam; mouse monoclonal anti-LAMP1 (H4A3) from Santa Cruz Biotechnology, Inc.; rabbit polyclonal anti-GAPDH (2118) from Cell Signaling Technology; and Alexa Fluor 488– and 568–labeled secondary antibodies for immunofluorescence from Molecular Probes.

Constructs

pLXIN-myc-Spastin constructs were generated as previously described (Allison et al., 2013). In brief, M87- or M1-spastin was cloned into the pIRESneo2 vector (NheI–BamHI; Takara Bio Inc.) followed by insertion of a myc tag (EcoRV–NheI), and then myc-spastin was further cloned into the pLXIN vector (SalI–BamHI; Takara Bio Inc.). Constructs were made resistant to spastin siRNA1 and three by introducing two mutations into each of the relevant sequences by site-directed mutagenesis. Mutant versions of pLXIN-myc-M87-spastin were then generated by site-directed mutagenesis. The GFP-VPS4-E235Q construct was a gift from P. Whitley (University of Bath, Bath, England, UK).

Generation of Stable Cell Lines

Stable cell lines were generated by retroviral transduction of HeLa cells using the spastin pLXIN constructs described above, according to previous methods (Allison et al., 2013).

Cell Culture and Transfection

HeLa cells were maintained as previously described (Connell et al., 2009). HeLa cells stably expressing spastin constructs were additionally cultured in the presence of 500 μg/ml Geneticin/G418 (Invitrogen). This selected for cells expressing the constructs that contain a gentamycin resistance cassette. In DNA transfections, cells were transfected using Effectene Transfection Reagent (Qiagen) following the manufacturer's protocol and typically incubated with transfection reagents for 24 h. For siRNA transfection, cells were transfected with the relevant siRNAs, using Oligofectamine transfection reagent (Invitrogen), according to a protocol modified from Motley et al. (2003). In brief, cells were plated into one well of a six-well plate and transfected after 24 h. Cells were harvested 48–96 h later. The efficiency of siRNA knockdown was verified by immunoblotting cell lysates or by immunofluorescent microscopy of fixed cells, with an antibody against the relevant protein. The following siRNA sequences and concentrations were used: spastin (10 nM): siRNA1, 5′-GAACUUCAACCUUCUAUAA-3′ (Dharmacon D-014070-01); siRNA3, 5′-UAUAAGUGCUGCAAGUUUA-3′ (Dharmacon D-014070-03).

Immunofluorescence Microscopy

Cells were fixed at room temperature (RT) in 3.8% (vol/vol) formaldehyde in phosphate buffered saline (PBS) and permeabilized in PBS containing 0.1% (vol/vol) saponin (Sigma-Aldrich) or 0.1% (vol/vol) Triton X-100 (Sigma-Aldrich). Coverslips were labeled with primary and secondary antibodies as previously described (Connell et al., 2009). Slides were analyzed with an LSM880 confocal microscope (100× NA 1.40 oil immersion objective, 37°C), LSM780 confocal microscope (63× NA 1.40 oil immersion objective, 37°C), or AxioImager Z2 Motorized Upright Microscope (63× NA 1.40 oil immersion objective, RT, Axiocam 506; ZEISS), all with ZEN analysis software (ZEISS). Images were subsequently processed using ImageJ, Adobe Photoshop, Adobe Illustrator, and ZEN analysis software. Co-localization of proteins was quantified using Volocity (PerkinElmer).

Endosomal Tubule Counts on Fixed Cells

Cells were processed for immunofluorescence microscopy and imaged with an AxioImager Motorized Upright Microscope under a 63×/1.4-NA oil immersion objective as described earlier. Tubulation was quantified as described previously (Allison et al., 2017). Briefly, images of typically 100 cells per experimental condition were randomized and scored blind for the presence of tubules longer than 2 μm. The percentage of cells with such tubules was then calculated.

Lysosome Quantification

The percentage of cells with large lysosomes was determined as described previously (Allison et al., 2017); fixed cells labeled with LAMP1 were processed for immunofluorescence microscopy and imaged with an AxioImager Motorized Upright Microscope. At least 100 cells were recorded per experimental condition. Images

were randomized, and the largest lysosome per cell was measured using ZEN analysis software.

Electron Microscopy

HeLa cells were grown on plastic dishes and fixed with 2% PFA, 2.5% glutaraldehyde, and 0.1 M cacodylate buffer, pH 7.2, before being scraped and spun into a pellet. All samples were postfixed with 1% osmium tetroxide:1.5% potassium ferricyanide before being incubated with 1% tannic acid to enhance contrast. Cells were dehydrated using increasing percentages of ethanol before being embedded onto EPON stubs or beam capsules. Resin was cured overnight at 65°C, and coverslips were removed using a heat-block (plastic) or repetitive freeze-thaw cycles with liquid nitrogen (glass). Ultrathin (50–70-nm) conventional sections were cut using a diamond knife mounted to a Reichart ultracut S ultramicrotome. Sections were collected onto copper grids stained using lead citrate. Sections were viewed on a FEI Tecnai transmission electron microscope at a working voltage of 80 kV.

Yeast Two Hybrid Assay

Yeast two hybrid (Y2H) assays were carried out using the Clontech Matchmaker system as previously described (Harbour et al., 2010). Residues 110–199 of the spastin MIT domain (WT, F124D, E112K, R115C, V162I, N184T, or L195V), full-length IST1 or CHMP1B, were cloned into both pGBT9 (bait) and pGAD424 (prey), generating fusions with the GAL4 binding protein and GAL4 activation protein, respectively. The HF7c strain was used as the reporter strain with growth on plates lacking histidine (–His) as the readout, indicating that an interaction has occurred. Yeast transformations were carried out as described in Reddy and Seaman (2001).

GST Pull-Down Assay

Residues 110–199 of the spastin MIT domain (WT, F124D, E112K, R115C, V162I, N184T, or L195V) were cloned into the BamHI-XhoI sites of pGEX-4T2 (GE Healthcare Life Sciences). The MIM domains of IST1, residues 319–364, and the single MIM of CHMP1B, residues 174–199, with the addition of a myc and a 6His tag were cloned into the BamHI-NotI sites of pGEX-6P-1 (GE Healthcare Life Sciences).

Protein was expressed in BL21(DE3)pLysS *Escherichia coli* and subsequently purified on GST sepharose as described in Collins et al. (2002). Spastin MIT domain proteins were eluted in buffer containing 10 mM glutathione (Collins et al., 2002), whereas the GST tag was removed from IST1 and CHMP1B MIMs by overnight cleavage at 4°C with Prescission protease (GE Healthcare Life Sciences) as described in the manufacturer's protocol.

GST pull-down assays were carried out as follows: 2 nmole of both bait (MIT domain) and prey (MIM) protein were bound to 20 μl packed volume of glutathione sepharose beads in 1 ml pull-down buffer (PBS + 0.1% NP-40 + 1 mM DTT) overnight at 4°C with rotation. Pull-downs were then washed three times in ice-cold pull-down buffer and resuspended in 30 μl of 3x protein sample buffer. Samples were then separated on an 18% Tris-Tricine gel at 120 V for 3 h in duplicate, half of each pull-down Coomassie stained to assess total protein, and the other half subject to Western blotting and subsequent detection of prey protein bands with anti-myc antibody (Millipore).

TABLE 1 | Results of pathogenicity prediction programs for MIT domain sequence changes identified in HSP patients.

Mutation	SIFT prediction (score)	PolyPhen prediction (score)
E112K	Tolerated (0.74)	Benign (0.017)
R115C	Deleterious (0.02)	Benign (0.251)
N184T	Deleterious (0)	Probably damaging (1)
L195V	Deleterious (0)	Possibly damaging (0.823)

Statistical Analysis

Statistical analyses were performed by paired two-tailed *t*-tests or one-way ANOVA with Bonferroni's (when multiple treatments were compared against each other) or Dunnett's (when multiple treatments were compared to a single control value) *post hoc* tests for multiple comparisons tests, using GraphPad Prism version 5.01 for Windows, GraphPad Software, La Jolla California, USA (www.graphpad.com).

RESULTS

Disease-Associated MIT Domain Mutants Cannot Regulate Endosomal Tubulation

Three putative mutations in the MIT domain of spastin were identified from the existing literature, E112K, N184T, and L195V (Patrono et al., 2002; Crippa et al., 2006; Rudenskaia et al., 2010). All were found in patients with pure HSP. A novel MIT domain mutation was also identified in a patient attending the East Anglian Medical Genetics Service, with a phenotype consistent with pure HSP and no family history of spastic paraplegia, R115C (SPAST c.343C>T). In each case, limited segregation data were available, but the sequence changes each affect moderately to highly evolutionarily conserved amino acids and are not present, or in the case of R115C only present once, in the gnomAD database of several hundred thousand alleles (Lek et al., 2016). SIFT and Polyphen pathogenicity predictions for each variant, generated via the Ensemble Variant Effect Predictor, are shown in **Table 1** (McLaren et al., 2016).

The MIT domain consists of three α helices that form an anti-parallel up and down helix bundle fold, forming a MIM binding region in between helices α1 and α3 (Yang et al., 2009). R115C and E112K lie at the N-terminus of the MIT domain, in the linker region adjoining helix α1, and L195V is at the very C-terminus of helix α3. N184T lies within the MIM binding region on α3 and is one of the residues involved in MIT-CHMP1B MIM interaction (**Figure 1A**) (Yang et al., 2009). We generated constructs encoding forms of spastin containing each mutant. We began by confirming that each retained the ability to sever microtubules, which we tested by transiently expressing in HeLa cells and then assessing the microtubule architecture by immunofluorescence microscopy (**Supplementary Figures 1A–F**). Each of the mutants exhibited a similar degree of microtubule depletion, which was comparable

to that of wild-type spastin and distinct from the microtubule bundling phenotype that has been observed in some missense mutations that block ATP binding or hydrolysis (e.g., K388R; **Figure 1A**; **Supplementary Figure 1C**) (Errico et al., 2002).

We next examined whether the patient MIT mutants affected spastin's role in endosomal tubule fission. Spastin requires the ability to bind ESCRT-III and to hydrolyze ATP for this function, as previous siRNA rescue experiments showed that forms of spastin containing either the artificial F124D MIT mutation (which blocks ESCRT-III interaction) or the disease-associated K388R mutation (which blocks ATP hydrolysis), failed to rescue the increased tubulation of sorting nexin 1 (SNX1; marker of a subset of endosomal tubules) seen in cells lacking endogenous spastin (Allison et al., 2013). We investigated the ability of the disease-associated MIT mutants to promote endosomal tubule fission using siRNA-rescue experiments with cells stably expressing siRNA-resistant forms of M87-spastin harboring each of the mutants (except the E112K mutant, as repeated attempts to generate a stable cell line failed). Stable expression of the patient mutants did not affect the cellular microtubule architecture (**Supplementary Figures 1G–K**). The increased SNX1 tubulation phenotype seen in cells lacking endogenous spastin was rescued by wild-type siRNA-resistant spastin but not by any of the patient MIT mutant forms (**Figures 1B–H**). As the spastin-depleted cells lack both endogenous M1- and M87-spastin, this effect of the mutants cannot be via a dominant negative effect on wild-type M1-spastin, as has been proposed as a mechanism for some mutations that lie outside of the ATPase domain (Solowska et al., 2010). We concluded that the amino acids affected by the patient mutations are essential for spastin's role in promoting endosomal tubule fission.

Mutations in Spastin's MIT Domain Disrupt Endosome-To-Golgi Traffic

In cells depleted of spastin, defective endosomal tubule fission causes failure of M6PR to sort away from the endosome, resulting in its accumulation in a LAMP1-positive endolysosomal compartment (Allison et al., 2017). This phenotype can be rescued by wild-type spastin but not by forms unable to bind ESCRT-III or hydrolye ATP (Allison et al., 2017). We examined whether the disease-associated MIT mutants were able to rescue this mislocalization of M6PR. Following siRNA-mediated spastin depletion in wild-type HeLa cells, we observed a significant increase in the co-localization of LAMP1 and M6PR, which as expected was rescued by expression of wild-type myc-M87 spastin (**Figures 2A–D,K**). However, none of the MIT mutant forms rescued this phenotype (**Figures 2E–K**). Disease-associated mutations in spastin's MIT domain are therefore unable to support normal sorting of M6PR from the endosome to the Golgi, consistent with their inability to drive efficient endosomal tubule fission.

Mutations in Spastin's MIT Domain Lead to Abnormal Lysosome Morphology

The abnormal M6PR traffic seen in HeLa cells lacking spastin causes abnormal lysosomal enzyme delivery, resulting in the development of enlarged lysosomes (Allison et al., 2017), associated with increased cellular abundance and altered migration of LAMP1 on immunoblotting (**Supplementary Figure 2**). We interrogated the ability of the MIT mutants to rescue the lysosomal enlargement phenotype with siRNA-rescue experiments and found that lysosomal enlargement was rescued by wild-type M87-spastin but not by any of the MIT mutant forms (**Figures 3A–F**). Two of the mutants, R115C and L195V, also had a significant dominant negative effect on lysosomal size in cells not depleted for endogenous spastin (**Figures 3C,E,F**).

Lysosomes in spastin-HSP cellular models have a characteristic ultrastructure, including the development of thick membrane whorls and dense honeycomb networks of membrane. We investigated the effects of the MIT mutants on lysosome ultrastructure. As expected, upon spastin depletion, we observed lysosomes with the characteristic abnormal appearances (Allison et al., 2017). This phenotype was rescued by wild-type M87 spastin but not by any of the MIT mutants (**Figure 3G**). The residues affected by the patient mutations are therefore required for spastin's role in maintaining correct lysosome morphology.

Spastin MIT Domain Mutants Show Differential Recruitment to Endosomes

We next sought to understand the mechanism by which the MIT mutants might affect spastin's function in endosomal tubule fission. At steady state, M87-spastin is mostly cytosolic and shows minimal association with endosomal markers. The canonical role of the MIT domain is to recruit spastin to endosomes via interactions with ESCRT-III, and this can be reported by expression of a dominant negative form of VPS4 (VPS4-E235Q). VPS4 normally acts to remove ESCRT-III proteins from endosomes, while the dominant negative form traps ESCRT-III proteins and associated proteins, including spastin, on the endosomal membrane, so revealing transient endosomal localizations (Stuchell-Brereton et al., 2007; Connell et al., 2009; Allison et al., 2013). Interestingly, the patient MIT mutants showed differential recruitment to GFP-VPS4-E235Q endosomes. Spastin-R115C and spastin-L195V showed no significant reduction in recruitment when compared to wild-type M87 spastin, while spastin-N184T had significantly reduced co-localization with GFP-VPS4-E235Q. As expected, endosomal recruitment of the ATPase mutant K388R was not reduced, while recruitment of the artificial F124D MIT domain mutant was almost completely abolished (**Figures 4A–G**). These experiments suggest that, at least for the N184T mutant, altered endosomal recruitment may account for the inability to rescue the tubulation phenotype. However, these data also indicate that the L195V and R115C mutants likely affect tubule fission by a mechanism independent of spastin's ability to recruit to endosomes.

Finally, we tested directly whether the MIT mutants affect binding of the spastin MIT domain to IST1 or CHMP1B. We first examined this by yeast two-hybrid, where as expected the artificial F124D MIT mutant showed no interaction

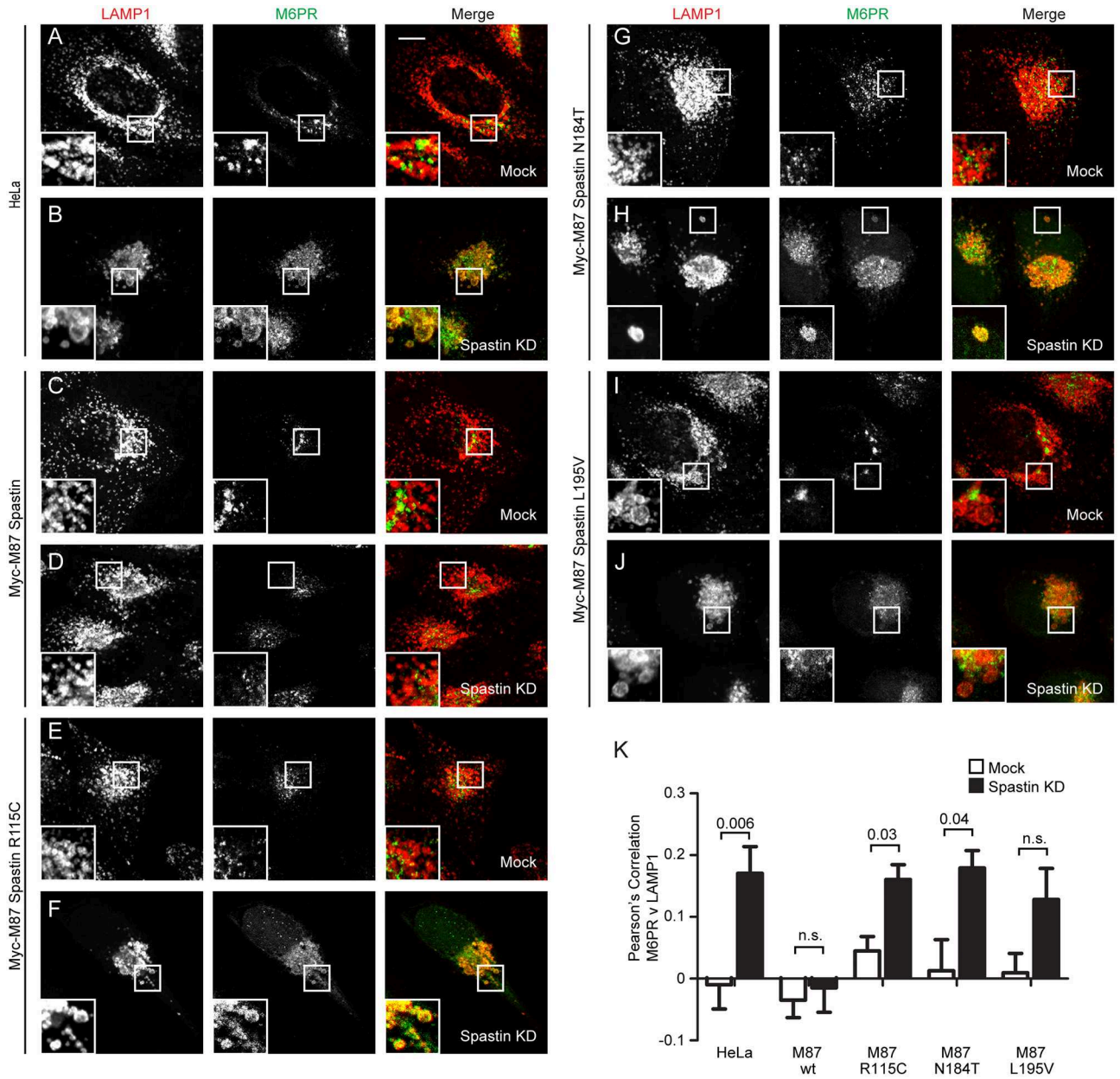

FIGURE 2 | Endosome to Golgi M6PR traffic is disrupted by MIT domain mutations in spastin. **(A–J)** Wild-type HeLa cells or cells expressing the siRNA-resistant spastin constructs indicated were subjected to mock transfection or siRNA-mediated KD of endogenous spastin, then processed for immunofluorescence microscopy and labeled with antibodies to M6PR and the lysosomal marker LAMP1. Insets show higher magnification views of the boxed areas. Scale bar = 10 μm. **(K)** Co-localization between M6PR and LAMP1 was quantified by calculating the Pearson's correlation coefficient for red and green pixels in each cell using Volocity software (20 cells per condition quantified in each experiment). Mean and SEM are shown for $n = 4$ experiments. *P*-values were calculated using paired two-tailed *t*-tests.

with CHMP1B or IST1 (**Figures 5A–D**). Unfortunately, autoactivation of the N184T mutant in this assay meant that its binding to the ESCRT proteins could not be assessed. However, there was no clear reduction in binding of any of the other patient MIT mutants, which exhibited interactions comparable to the wild-type MIT domain and to a known benign spastin polymorphism, V162I, which has an allele frequency of 2.22 $\times 10^{-3}$ in the general population (Lek et al., 2016). We next examined binding using GST pull-downs, testing the ability of purified wild-type and mutant spastin MIT domains to interact with regions containing the MIMs of CHMP1B (amino acids 174–199) and IST1 (amino acids 319–364) (Agromayor et al., 2009; Bajorek et al., 2009; Yang et al., 2009). As expected, there was no binding between the MIT domain harboring the

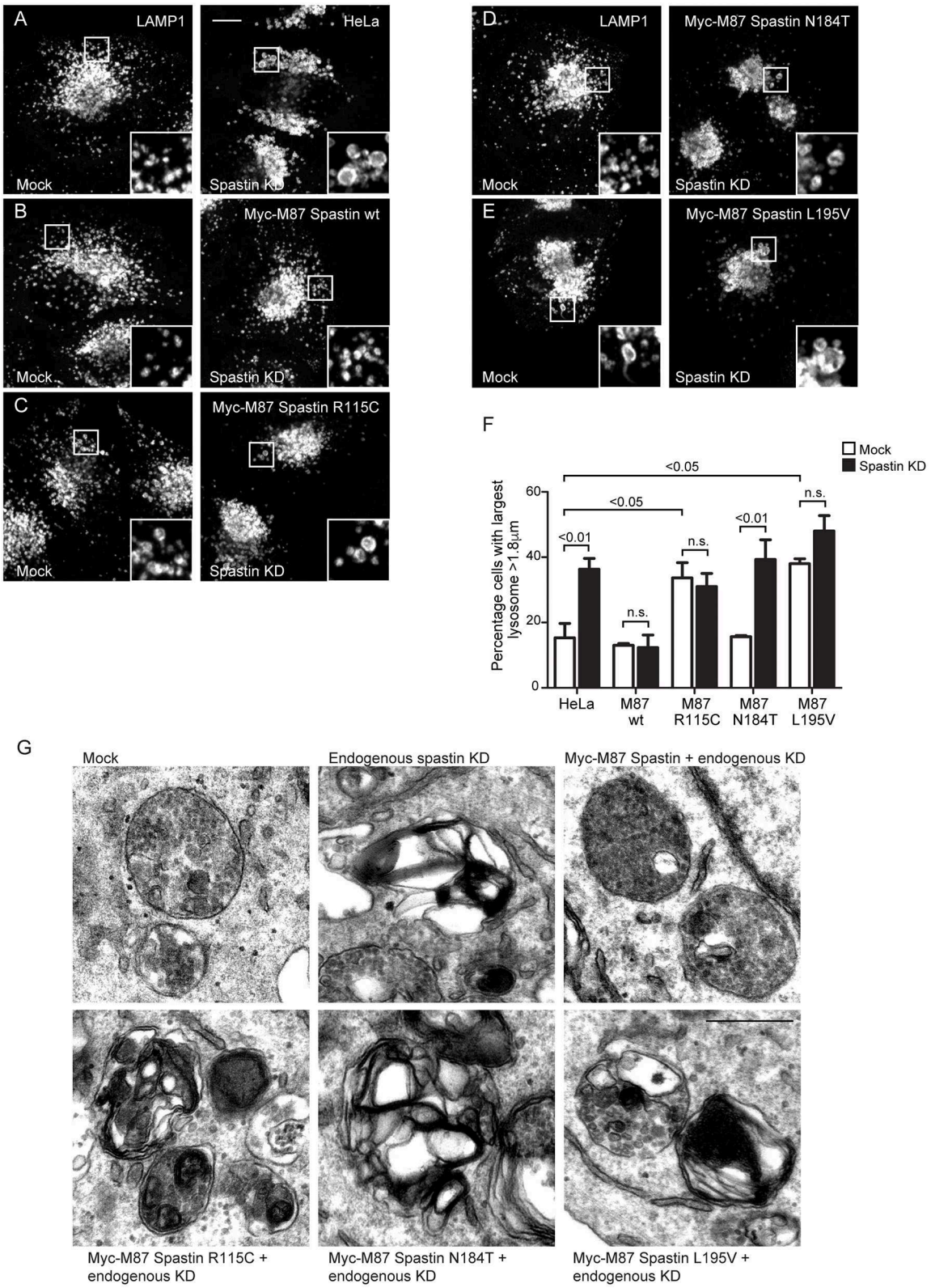

FIGURE 3 | Spastin MIT domain mutants cannot support normal lysosomal morphology. **(A–E)** Wild-type HeLa cells or cells expressing the siRNA-resistant spastin constructs indicated were subjected to mock transfection or siRNA-mediated KD of endogenous spastin, then processed for immunofluorescence microscopy and labeled for LAMP1. Insets show higher magnification views of the boxed areas. Scale bar = 10 μm. **(F)** The diameter of the largest lysosome was measured in 100

(Continued)

FIGURE 3 | cells per condition. The mean and SEM of the percentage of cells with largest lysosome >1.8 μm is shown ($n = 4$ biological repeats). *P*-values were calculated by one-way ANOVA with Bonferroni's *post hoc* multiple comparison test. In addition to the *p*-values shown, the M87 wild-type KD value was significantly different from all other KD values with a significance of at least $p < 0.01$. **(G)** Wild-type HeLa cells or HeLa cells expressing the siRNA-resistant spastin constructs indicated were subjected to mock transfection or siRNA-mediated KD of endogenous spastin. Electron micrographs of representative endolysosomal structures are shown. Note the presence of highly abnormal structures in each of the cells expressing mutant spastin. Scale bar = 500 nm.

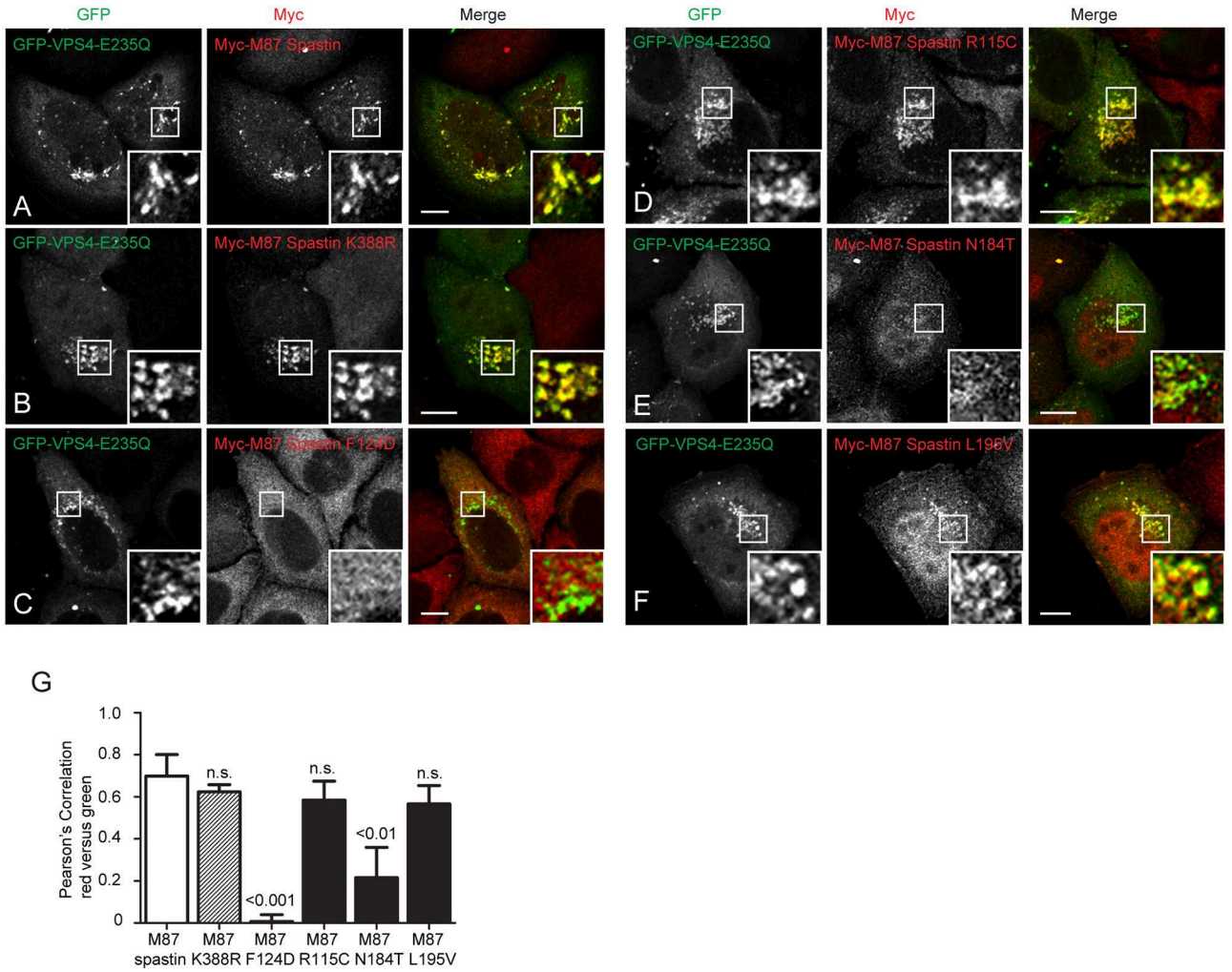

FIGURE 4 | MIT mutant forms of spastin show differential recruitment to VPS4-E235Q endosomes. GFP-VPS4-E235Q was transiently transfected into cell lines stably expressing myc-tagged wild-type spastin **(A)** or spastin mutants **(B–F)**, and then cells were fixed and labeled with an anti-myc antibody. Insets show higher magnification views of the boxed areas. **(G)** Co-localization between GFP-VPS4-E235Q and spastin proteins was estimated by calculating the Pearson's correlation coefficient for red and green pixels in each cell, using Volocity software ($n = 4$ experiments, 15 cells per condition quantified in each experiment). Mean and SEM are shown, *p*-values vs. M87 wild-type spastin were calculated using one-way ANOVA with Dunnett's multiple comparison posttest. Scale bar = 10 μm.

F124D artificial mutant and the ESCRT MIMs (data not shown). Furthermore, in this system interaction was abolished (in the case of CHMP1B) or reduced (in the case of IST1) by introduction of another artificial MIT mutant (F124A) that is known to significantly diminish, but not completely inhibit, binding of spastin's MIT domain to CHMP1B (data not shown) (Yang et al., 2009). In contrast, there was no appreciable difference between the MIM-binding capacity of the wild-type spastin MIT, an MIT containing the benign polymorphism V162I, or any of the spastin MIT mutants, including N184T (**Figures 6A,B**). Thus, the abnormal functional effects of the mutants do not appear to be related to their capacity to bind CHMP1B or IST1.

DISCUSSION

In this study, we have shown that three patient-associated missense changes in the MIT domain affect the function of

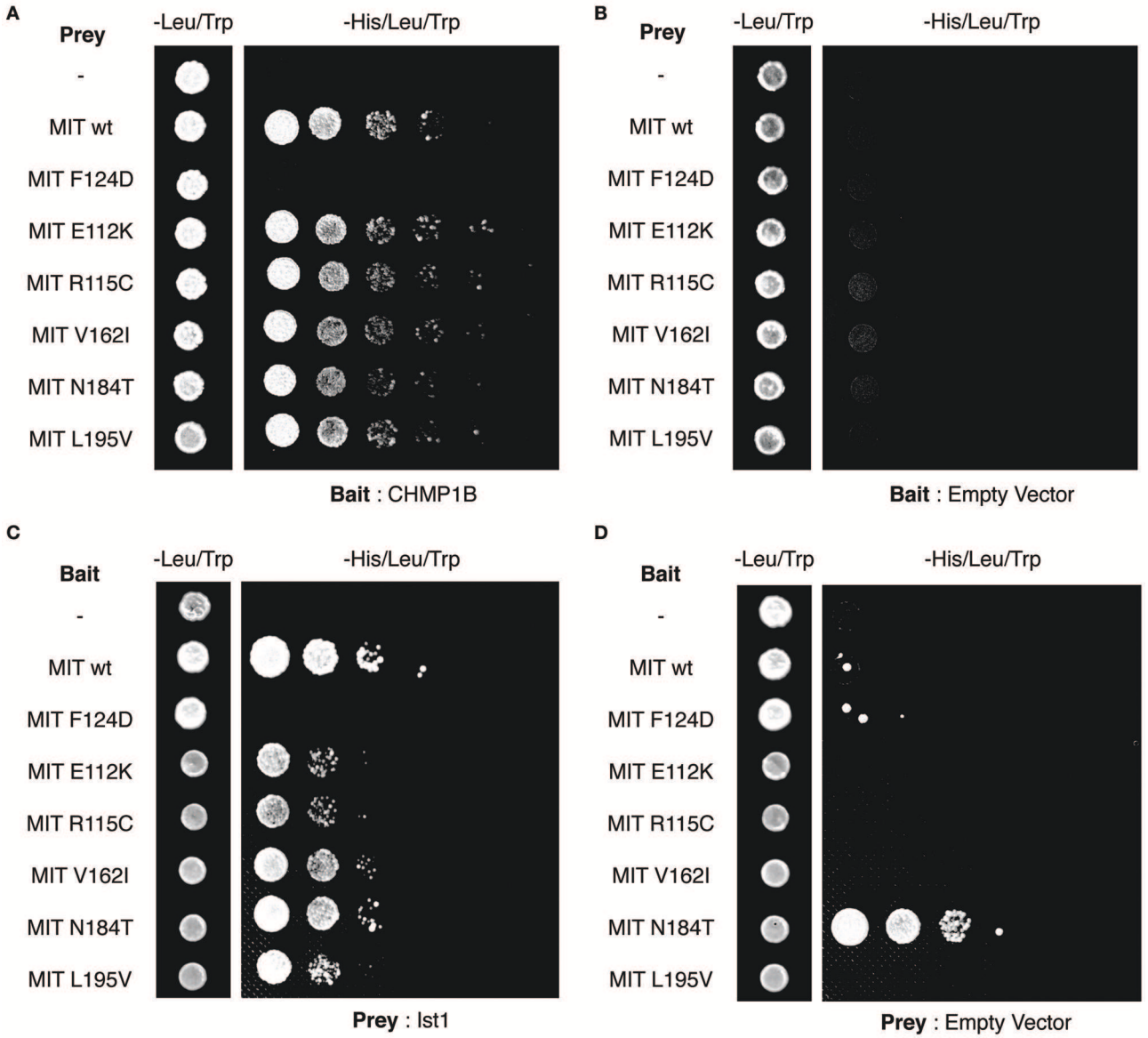

FIGURE 5 | Yeast two-hybrid analysis of spastin MIT domain binding to CHMP1B and IST1. **(A–D)** Interactions between the combinations of MIT domain, CHMP1B, and IST1 bait and prey vectors indicated in each panel. In each case, the first column shows the growth of diploid colonies on media lacking leucine and tryptophan, to select for the presence of both bait and prey vectors, while columns 2–6 show the growth of serial dilutions of diploid colonies on media lacking leucine, tryptophan, and histidine, which also require the activation of the His reporter gene that occurs on interaction of bait and prey proteins. In **(B,D)**, empty vector controls test for auto-activation of by the MIT mutant proteins under investigation. Note that the N184T mutant causes auto-activation, and so binding results for this mutant were uninterpretable.

spastin, rendering it unable to correctly regulate endosomal tubule fission, with consequent effects on endosome-to-Golgi trafficking of M6PRs and lysosomal morphology. The lysosomal abnormalities are likely to be pathologically relevant as very similar lysosomal morphologies are observed in neurons from a spastin-HSP mouse model and from patient-derived neurons, including in concentrations within pathological axonal swellings (Allison et al., 2017). Considered together with the absence, or in the case of R115C very low frequency, of these mutations from general population databases, we conclude that these missense changes are likely to be pathogenic. As these mutations do not directly affect spastin's microtubule-severing capacity, coupling of these MIT mutations to lysosomal dysfunction represents a new molecular pathological mechanism by which spastin mutations may cause disease. A key challenge now is to understand how lysosomal abnormality causes axonopathy—numerous possibilities require exploration. Functional lysosomes are required for autophagy and mitophagy,

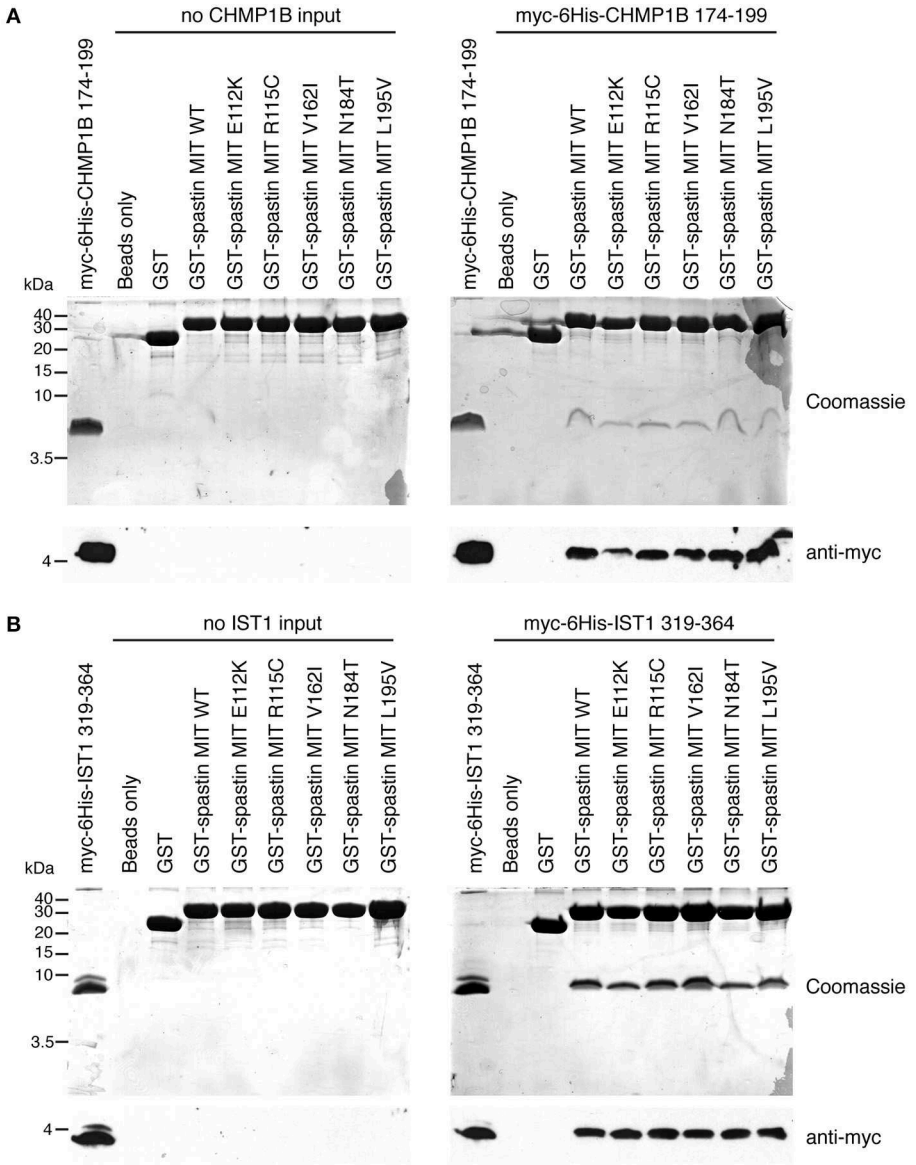

FIGURE 6 | Assessment of interactions between spastin MIT domains and MIM-regions of CHMP1B and IST1 by GST pull-down. Purified proteins consisting of GST alone, GST fused to the wild-type spastin MIT domain, or to spastin MIT domains harboring the sequence changes indicated were used in *in vitro* GST pull-down experiments vs. myc- and 6His-tagged fragments of CHMP1B **(A)** or IST1 **(B)** that incorporate the spastin-binding MIM regions. In each set of experiments, the upper panels show Coomassie-stained gels, while the bottom panel shows corresponding anti-myc immunoblotting.

with defects in these processes linked to axonopathy (Ashrafi et al., 2014; Gowrishankar et al., 2015; Xie et al., 2015). They are also required for lipid metabolism, and altered lipid metabolism appears sufficient to cause HSP (Boutry et al., 2019). Finally, lysosomes are key sites of receptor degradation, and upregulated bone morphogenetic protein signaling caused by defective receptor degradation is implicated in HSP pathogenesis (Wang et al., 2007; Tsang et al., 2009; Blackstone et al., 2011).

Of the mutations that we investigated in this study, only the N184T change caused a large reduction (>50%) in the endosomal recruitment of spastin, as compared to the wild-type protein. Thus, in the case of this mutation, defects in endosomal tubule fission, with consequent downstream defects on lysosome function, are probably caused by insufficient endosomal spastin. However, although structural studies of the binding of the MIT domain to CHMP1B show that this mutation lies within the MIM binding site and directly participates in MIM binding, surprisingly, it did not appear to affect MIT-MIM binding when assayed by GST pull-down (Yang et al., 2009). Spastin's recruitment to endosomes requires its MIT domain, but it is not known whether CHMP1B and IST1 are the only endosomal proteins involved in this recruitment. The simplest interpretation

of our data is that another, perhaps novel, ESCRT-like protein in addition to IST1 and CHMP1B participates in spastin's recruitment to endosomes, and that it is this binding that is affected by the N184T alteration.

The other two mutants studied caused no reduction in endosomal recruitment, consistent with their location outside of the MIM-binding region of the spastin MIT domain. This suggests that they are affecting a non-canonical function of the MIT domain that is independent of ESCRT-III interaction and invites the possibility that non-canonical functions of the MIT domain are important for the correct function of spastin in endosomal tubule fission. Although non-canonical functions of the spastin MIT domain have not been elucidated, other MIT domains have been proposed to have Ca^{2+} or phospholipid binding properties (Iwaya et al., 2013). Interestingly, both of these mutations showed dominant negative effects on lysosomal size when stably expressed in HeLa cells. We suggest that in the physiological situation in HSP patients, when these alleles are expressed together with a wild-type allele, the mutant proteins are likely incorporated into, and negatively affect the function of, the spastin hexamer at the endosome.

In summary, by showing that MIT domain mutants do not directly affect microtubule severing, but still have pathologically relevant functional effects, we have identified a novel molecular pathological mechanism by which alteration of spastin may cause HSP. Our work hints at the existence of novel factors that may determine recruitment of spastin to endosomes, as well as indicating that interference with non-canonical functions of the MIT domain may cause the disease.

DATA AVAILABILITY STATEMENT

The raw data supporting the conclusions of this manuscript will be made available by the authors, without undue reservation, to any qualified researcher.

ETHICS STATEMENT

The studies involving human participants were reviewed and approved by East of England Cambridgeshire research ethics committee. The patients/participants provided their written informed consent to participate in this study. Written informed consent was obtained from the individual(s) for the publication of any potentially identifiable images or data included in this article.

AUTHOR'S NOTE

An additional description of a family with an N184T spastin mutation was recently published (Kadnikova et al., 2019).

AUTHOR CONTRIBUTIONS

RA performed experiments, analyzed the data, helped direct the research, and helped write the article. JE performed experiments, analyzed the data, and helped write the article. ER directed the research, analyzed the data, and wrote the article.

FUNDING

This work was supported by grants to ER: UK Medical Research Council Project Grants [MR/M00046X/1] and [MR/R026440/1], Project grant from National Institute of Health Research Biomedical Research Center at Addenbrooke's Hospital, Wellcome Trust Senior Research Fellowship in Clinical Science [082381]. JE was supported by a Wellcome Trust Principal Research Fellowship Grant to Margaret S. Robinson [086598]. CIMR was supported by a Wellcome Trust Strategic Award [100140] and Equipment Grant [093026]. We are grateful to Hazel and Keith Satchell for their generous charitable support for our work on HSP.

ACKNOWLEDGMENTS

We thank the patients whose DNA changes we studied, Beth Latimer-Bowman for technical assistance, and Wes Sundquist for helpful information on the spastin MIT domain.

SUPPLEMENTARY MATERIAL

The Supplementary Material for this article can be found online at: https://www.frontiersin.org/articles/10.3389/fnins.2019.01179/full#supplementary-material

Supplementary Figure 1 | Spastin's microtubule severing activity is unaffected by MIT mutants. **(A–F)** Wild-type Hela cells were transiently transfected with the myc-tagged M87-spastin constructs indicated. Cells were fixed and then processed for immunofluorescence microscopy and labeled with antibodies to myc and α-tubulin. Representative images showing the appearance of the microtubule architecture following spastin overexpression are shown. Scale bar = 10 μm. **(G–K)** Wild-type Hela cells or cells stably expressing the myc-tagged M87-spastin constructs indicated were fixed, then processed for immunofluorescence microscopy and labeled with **(G)** spastin and α-tubulin or **(H–K)** myc and α-tubulin. Representative images showing the appearance of microtubule cytoskeleton in each cell line, with and without endogenous spastin depletion, are shown. Scale bars = 10 μm.

Supplementary Figure 2 | Cells lacking spastin exhibit upregulation and altered migration of LAMP1. **(A)** HeLa cells were mock-transfected or subjected to spastin depletion by siRNA transfection, then immunoblotted with the antibodies shown. Note increased abundance and altered LAMP1 migration in the immunoblot from cells lacking spastin. Quantification of LAMP1 immunoblot band intensity is shown in **(B)**, $n = 4$, p-values generated by paired t-tests.

REFERENCES

Abrahamsen, G., Fan, Y., Matigian, N., Wali, G., Bellette, B., Sutharsan, R., et al. (2013). A patient-derived stem cell model of hereditary spastic paraplegia with SPAST mutations. *Dis. Model. Mech.* 6, 489–502. doi: 10.1242/dmm.010884

Agromayor, M., Carlton, J. G., Phelan, J. P., Matthews, D. R., Carlin, L. M., Ameer-Beg, S., et al. (2009). Essential role of hIST1 in cytokinesis. *Mol. Biol. Cell.* 20, 1374–1387. doi: 10.1091/mbc.e08-05-0474

Allison, R., Edgar, J. R., Pearson, G., Rizo, T., Newton, T., Günther, S., et al. (2017). Defects in ER–endosome contacts impact lysosome function in hereditary spastic paraplegia. *J. Cell Biol.* 216, 1337–1355. doi: 10.1083/jcb.201609033

Allison, R., Lumb, J. H., Fassier, C., Connell, J. W., Ten Martin, D., Seaman, M. N., et al. (2013). An ESCRT-spastin interaction promotes fission of recycling tubules from the endosome. *J. Cell Biol.* 202, 527–543. doi: 10.1083/jcb.201211045

Ashrafi, G., Schlehe, J. S., LaVoie, M. J., and Schwarz, T. L. (2014). Mitophagy of damaged mitochondria occurs locally in distal neuronal axons and requires PINK1 and Parkin. *J. Cell Biol.* 206, 655–670. doi: 10.1083/jcb.201401070

Bajorek, M., Morita, E., Skalicky, J. J., Morham, S. G., Babst, M., and Sundquist, W. I. (2009). Biochemical analyses of human IST1 and its function in cytokinesis. *Mol. Biol. Cell*. 20, 1360–1373. doi: 10.1091/mbc.e08-05-0475

Blackstone, C., O'Kane, C. J., and Reid, E. (2011). Hereditary spastic paraplegias: membrane traffic and the motor pathway. *Nat. Rev. Neurosci.* 12, 31–42. doi: 10.1038/nrn2946

Boutry, M., Morais, S., and Stevanin, G. (2019). Update on the genetics of spastic paraplegias. *Curr. Neurol. Neurosci. Rep.* 19:18. doi: 10.1007/s11910-019-0930-2

Carlton, J., Bujny, M., Peter, B. J., Oorschot, V. M., Rutherford, A., Mellor, H., et al. (2004). Sorting nexin-1 mediates tubular endosome-to-TGN transport through coincidence sensing of high- curvature membranes and 3-phosphoinositides. *Curr. Biol.* 14, 1791–1800. doi: 10.1016/j.cub.2004.09.077

Claudiani, P., Riano, E., Errico, A., Andolfi, G., and Rugarli, E. I. (2005). Spastin subcellular localization is regulated through usage of different translation start sites and active export from the nucleus. *Exp. Cell Res.* 309, 358–369. doi: 10.1016/j.yexcr.2005.06.009

Collins, B. M., McCoy, A. J., Kent, H. M., Evans, P. R., and Owen, D. J. (2002). Molecular architecture and functional model of the endocytic AP2 complex. *Cell*. 109, 523–535. doi: 10.1016/S0092-8674(02)00735-3

Connell, J. W., Lindon, C., Luzio, J. P., and Reid, E. (2009). Spastin couples microtubule severing to membrane traffic in completion of cytokinesis and secretion. *Traffic*. 10, 42–56. doi: 10.1111/j.1600-0854.2008.00847.x

Crippa, F., Panzeri, C., Martinuzzi, A., Arnoldi, A., Redaelli, F., Tonelli, A., et al. (2006). Eight novel mutations in SPG4 in a large sample of patients with hereditary spastic paraplegia. *Arch. Neurol.* 63, 750–755. doi: 10.1001/archneur.63.5.750

Denton, K. R., Lei, L., Grenier, J., Rodionov, V., Blackstone, C., and Li, X. J. (2014). Loss of spastin function results in disease-specific axonal defects in human pluripotent stem cell-based models of hereditary spastic paraplegia. *Stem Cells*. 32, 414–423. doi: 10.1002/stem.1569

Errico, A., Ballabio, A., and Rugarli, E. I. (2002). Spastin, the protein mutated in autosomal dominant hereditary spastic paraplegia, is involved in microtubule dynamics. *Hum. Mol. Genet.* 11, 153–163. doi: 10.1093/hmg/11.2.153

Fink, J. K. (2006). Hereditary spastic paraplegia. *Curr. Neurol. Neurosci. Rep.* 6, 65–76. doi: 10.1007/s11910-996-0011-1

Fonknechten, N., Mavel, D., Byrne, P., Davoine, C. S., Cruaud, C., Bonsch, D., et al. (2000). Spectrum of SPG4 mutations in autosomal dominant spastic paraplegia. *Hum. Mol. Genet.* 9, 637–644. doi: 10.1093/hmg/9.4.637

Gowrishankar, S., Yuan, P., Wu, Y., Schrag, M., Paradise, S., Grutzendler, J., et al. (2015). Massive accumulation of luminal protease-deficient axonal lysosomes at Alzheimer's disease amyloid plaques. *Proc. Natl. Acad. Sci. U.S.A.* 112, E3699–E708. doi: 10.1073/pnas.1510329112

Harbour, M. E., Breusegem, S. Y., Antrobus, R., Freeman, C., Reid, E., and Seaman, M. N. (2010). The cargo-selective retromer complex is a recruiting hub for protein complexes that regulate endosomal tubule dynamics. *J. Cell Sci.* 123(Pt 21), 3703–3717. doi: 10.1242/jcs.071472

Harding, A. E. (1993). Hereditary spastic paraplegias. *Semin. Neurol.* 13, 333–336. doi: 10.1055/s-2008-1041143

Havlicek, S., Kohl, Z., Mishra, H. K., Prots, I., Eberhardt, E., Denguir, N., et al. (2014). Gene dosage-dependent rescue of HSP neurite defects in SPG4 patients' neurons. *Hum. Mol. Genet.* 23, 2527–2541. doi: 10.1093/hmg/ddt644

Hazan, J., Fonknechten, N., Mavel, D., Paternotte, C., Samson, D., Artiguenave, F., et al. (1999). Spastin, a new AAA protein, is altered in the most frequent form of autosomal dominant spastic paraplegia. *Nat. Genet.* 23, 296–303. doi: 10.1038/15472

Hensiek, A., Kirker, S., and Reid, E. (2015). Diagnosis, investigation and management of hereditary spastic paraplegias in the era of next-generation sequencing. *J. Neurol.* 272, 1601–1612. doi: 10.1007/s00415-014-7598-y

Hirst, J., Edgar, J. R., Esteves, T., Darios, F., Madeo, M., Chang, J., et al. (2015). Loss of AP-5 results in accumulation of aberrant endolysosomes: defining a new type of lysosomal storage disease. *Hum. Mol. Genet.* 24, 4984–4996. doi: 10.1093/hmg/ddv220

Iwaya, N., Takasu, H., Goda, N., Shirakawa, M., Tanaka, T., Hamada, D., et al. (2013). MIT domain of Vps4 is a Ca2+-dependent phosphoinositide-binding domain. *J. Biochem.* 153, 473–481. doi: 10.1093/jb/mvt012

Kadnikova, V. A., Rudenskaya, G. E., Stepanova, A. A., Sermyagina, I. G., and Ryzhkova, O. P. (2019). Mutational spectrum of Spast (Spg4) and Atl1 (Spg3a) genes in Russian patients with hereditary spastic paraplegia. *Sci. Rep.* 9:14412. doi: 10.1038/s41598-019-50911-9

Lek, M., Karczewski, K. J., Minikel, E. V., Samocha, K. E., Banks, E., Fennell, T., et al. (2016). Analysis of protein-coding genetic variation in 60,706 humans. *Nature*. 536:285–91. doi: 10.1038/nature19057

McLaren, W., Gil, L., Hunt, S. E., Riat, H. S., Ritchie, G. R. S., Thormann, A., et al. (2016). The ensembl variant effect predictor. *Genome Biol.* 17:122. doi: 10.1186/s13059-016-0974-4

Montenegro, G., Rebelo, A. P., Connell, J., Allison, R., Babalini, C., D'Aloia, M., et al. (2012). Mutations in the ER-shaping protein reticulon 2 cause the axon-degenerative disorder hereditary spastic paraplegia type 12. *J. Clin. Invest.* 122, 538–544. doi: 10.1172/JCI60560

Motley, A., Bright, N. A., Seaman, M. N., and Robinson, M. S. (2003). Clathrin-mediated endocytosis in AP-2-depleted cells. *J. Cell Biol.* 162, 909–918. doi: 10.1083/jcb.200305145

Newton, T., Allison, R., Edgar, J. R., Lumb, J. H., Rodger, C. E., Manna, P. T., et al. (2018). Mechanistic basis of an epistatic interaction reducing age at onset in hereditary spastic paraplegia. *Brain*. 141, 1286–1299. doi: 10.1093/brain/awy034

Park, S. H., Zhu, P. P., Parker, R. L., and Blackstone, C. (2010). Hereditary spastic paraplegia proteins REEP1, spastin, and atlastin-1 coordinate microtubule interactions with the tubular ER network. *J. Clin. Invest.* 120, 1097–1110. doi: 10.1172/JCI40979

Patrono, C., Casali, C., Tessa, A., Cricchi, F., Fortini, D., Carrozzo, R., et al. (2002). Missense and splice site mutations in SPG4 suggest loss-of-function in dominant spastic paraplegia. *J. Neurol.* 249, 200–205. doi: 10.1007/PL00007865

Reddy, J. V., and Seaman, M. N. (2001). Vps26p, a component of retromer, directs the interactions of Vps35p in endosome-to-Golgi retrieval. *Mol. Biol. Cell*. 12, 3242–3256. doi: 10.1091/mbc.12.10.3242

Rehbach, K., Kesavan, J., Hauser, S., Ritzenhofen, S., Jungverdorben, J., Schüle, R., et al. (2019). Multiparametric rapid screening of neuronal process pathology for drug target identification in HSP patient-specific neurons. *Sci. Rep.* 9:9615. doi: 10.1038/s41598-019-45246-4

Reid, E. (1999). The hereditary spastic paraplegias. *J. Neurol.* 246, 995–1003. doi: 10.1007/s004150050503

Reid, E., Connell, J., Edwards, T. L., Duley, S., Brown, S. E., and Sanderson, C. M. (2005). The hereditary spastic paraplegia protein spastin interacts with the ESCRT-III complex-associated endosomal protein CHMP1B. *Hum. Mol. Genet.* 14, 19–38. doi: 10.1093/hmg/ddi003

Renvoise, B., Chang, J., Singh, R., Yonekawa, S., FitzGibbon, E. J., Mankodi, A., et al. (2014). Lysosomal abnormalities in hereditary spastic paraplegia types SPG15 and SPG11. *Ann. Clin. Transl. Neurol.* 1, 379–389. doi: 10.1002/acn3.64

Renvoise, B., Parker, R. L., Yang, D., Bakowska, J. C., Hurley, J. H., and Blackstone, C. (2010). SPG20 protein spartin is recruited to midbodies by ESCRT-III protein Ist1 and participates in cytokinesis. *Mol. Biol. Cell*. 21, 3293–3303. doi: 10.1091/mbc.e09-10-0879

Roll-Mecak, A., and Vale, R. D. (2008). Structural basis of microtubule severing by the hereditary spastic paraplegia protein spastin. *Nature* 451, 363–367. doi: 10.1038/nature06482

Rudenskaia, G. E., Sermiagina, I. G., Illarioshkin, S. N., Sidorova, O. P., Fedotov, V. P., and Poliakov, A. V. (2010). [Hereditary spastic paraplegia type 4 (SPG4): clinical and molecular-genetic characteristics]. *Zh. Nevrol. Psikhiatr. Im. S S Korsakova*. 110, 12–19.

Sanderson, C. M., Connell, J. W., Edwards, T. L., Bright, N. A., Duley, S., Thompson, A., et al. (2006). Spastin and atlastin, two proteins mutated in autosomal-dominant hereditary spastic paraplegia, are binding partners. *Hum. Mol. Genet.* 15, 307–318. doi: 10.1093/hmg/ddi447

Solowska, J. M., Garbern, J. Y., and Baas, P. W. (2010). Evaluation of loss of function as an explanation for SPG4-based hereditary spastic paraplegia. *Hum. Mol. Genet.* 19, 2767–2779. doi: 10.1093/hmg/ddq177

Solowska, J. M., Rao, A. N., and Baas, P. W. (2017). Truncating mutations of SPAST associated with hereditary spastic paraplegia indicate greater accumulation and toxicity of the M1 isoform of spastin. *Mol. Biol. Cell*. 28, 1728–1737. doi: 10.1091/mbc.e17-01-0047

Stuchell-Brereton, M. D., Skalicky, J. J., Kieffer, C., Karren, M. A., Ghaffarian, S., and Sundquist, W. I. (2007). ESCRT-III recognition by VPS4 ATPases. *Nature* 449, 740–744. doi: 10.1038/nature 06172

Tsang, H. T., Edwards, T. L., Wang, X., Connell, J. W., Davies, R. J., Durrington, H. J., et al. (2009). The hereditary spastic paraplegia proteins NIPA1, spastin and spartin are inhibitors of mammalian BMP signalling. *Hum. Mol. Genet.* 18, 3805–3821. doi: 10.1093/hmg/ddp324

Wang, X., Shaw, W. R., Tsang, H. T., Reid, E., and O'Kane, C. J. (2007). Drosophila spichthyin inhibits BMP signaling and regulates synaptic growth and axonal microtubules. *Nat. Neurosci.* 10, 177–185. doi: 10.1038/nn1841

White, S. R., Evans, K. J., Lary, J., Cole, J. L., and Lauring, B. (2007). Recognition of C-terminal amino acids in tubulin by pore loops in Spastin is important for microtubule severing. *J. Cell Biol.* 176, 995–1005. doi: 10.1083/jcb.200610072

Xie, Y., Zhou, B., Lin, M.-Y., Wang, S., Foust Kevin, D., and Sheng, Z.-H. (2015). Endolysosomal deficits augment mitochondria pathology in spinal motor neurons of asymptomatic fALS mice. *Neuron* 87, 355–370. doi: 10.1016/j.neuron.2015.06.026

Yang, D., Rismanchi, N., Renvoise, B., Lippincott-Schwartz, J., Blackstone, C., and Hurley, J. H. (2009). Structural basis for midbody targeting of spastin by the ESCRT-III protein CHMP1B. *Nat. Struct. Mol. Biol.* (2008) 15, 1278–1286. doi: 10.1038/nsmb.1512

Zehr, E., Szyk, A., Piszczek, G., Szczesna, E., Zuo, X., and Roll-Mecak, A. (2017). Katanin spiral and ring structures shed light on power stroke for microtubule severing. *Nat. Struct. Mol. Biol.* 24:717. doi: 10.1038/nsmb.3448

Conflict of Interest: The authors declare that the research was conducted in the absence of any commercial or financial relationships that could be construed as a potential conflict of interest.

frontiers in Neuroscience

ORIGINAL RESEARCH
published: 19 November 2019
doi: 10.3389/fnins.2019.01202

Naringenin Ameliorates *Drosophila* ReepA Hereditary Spastic Paraplegia-Linked Phenotypes

Barbara Napoli[1†], Sentiljana Gumeni[2†], Alessia Forgiarini[3], Marianna Fantin[1], Concetta De Filippis[4], Elena Panzeri[1], Chiara Vantaggiato[1] and Genny Orso[3]*

[1] Scientific Institute, IRCCS Eugenio Medea, Laboratory of Molecular Biology, Bosisio Parini, Lecco, Italy, [2] Department of Cell Biology and Biophysics, Faculty of Biology, National and Kapodistrian University of Athens, Athens, Greece, [3] Department of Pharmaceutical and Pharmacological Sciences, University of Padova, Padova, Italy, [4] Foundation Institute of Pediatric Research, "Città della Speranza", Padova, Italy

OPEN ACCESS

Edited by:
Craig Blackstone,
National Institute of Neurological Disorders and Stroke (NINDS), United States

Reviewed by:
Filippo M. Santorelli,
Fondazione Stella Maris (IRCCS), Italy
Cahir Joseph O'Kane,
University of Cambridge, United Kingdom
Evan Reid,
University of Cambridge, United Kingdom

***Correspondence:**
Genny Orso
genny.orso@unipd.it;
genny7575@gmail.com

[†] These authors have contributed equally to this work

Specialty section:
This article was submitted to Neurodegeneration, a section of the journal Frontiers in Neuroscience

Received: 31 July 2019
Accepted: 23 October 2019
Published: 19 November 2019

Citation:
Napoli B, Gumeni S, Forgiarini A, Fantin M, De Filippis C, Panzeri E, Vantaggiato C and Orso G (2019) Naringenin Ameliorates Drosophila ReepA Hereditary Spastic Paraplegia-Linked Phenotypes. Front. Neurosci. 13:1202. doi: 10.3389/fnins.2019.01202

Defects in the endoplasmic reticulum (ER) membrane shaping and interaction with other organelles seem to be a crucial mechanism underlying Hereditary Spastic Paraplegia (HSP) neurodegeneration. REEP1, a transmembrane protein belonging to TB2/HVA22 family, is implicated in SPG31, an autosomal dominant form of HSP, and its interaction with Atlastin/SPG3A and Spastin/SPG4, the other two major HSP linked proteins, has been demonstrated to play a crucial role in modifying ER architecture. In addition, the *Drosophila* ortholog of REEP1, named ReepA, has been found to regulate the response to ER neuronal stress. Herein we investigated the role of ReepA in ER morphology and stress response. ReepA is upregulated under stress conditions and aging. Our data show that ReepA triggers a selective activation of Ire1 and Atf6 branches of Unfolded Protein Response (UPR) and modifies ER morphology. *Drosophila* lacking ReepA showed Atf6 and Ire1 activation, expansion of ER sheet-like structures, locomotor dysfunction and shortened lifespan. Furthermore, we found that naringenin, a flavonoid that possesses strong antioxidant and neuroprotective activity, can rescue the cellular phenotypes, the lifespan and locomotor disability associated with ReepA loss of function. Our data highlight the importance of ER homeostasis in nervous system functionality and HSP neurodegenerative mechanisms, opening new opportunities for HSP treatment.

Keywords: endoplasmic reticulum, hereditary spastic paraplegia, naringenin, REEP1, ReepA, UPR

INTRODUCTION

Receptor expression-enhancing protein 1 (REEP1) is an endoplasmic reticulum (ER) resident protein involved in the SPG31 form of Hereditary Spastic Paraplegia (HSP), a neurodegenerative disorder affecting motoneurons. *In vitro* and *in vivo* studies confer to REEP1 a role in different ER related pathways. REEP1 modifies ER architecture, is implicated in ER stress response and finally has a role in Lipid Droplet (LD) biogenesis (Park et al., 2010; Beetz et al., 2013; Björk et al., 2013; Appocher et al., 2014; Falk et al., 2014; Lim et al., 2015; Renvoisé et al., 2016). The ER is a dynamic organelle characterized by a complex interconnected system of endomembranes, tubules, and sheets. ER sheets are cisternal structures with two closely apposed membranes localized in the

perinuclear region, while ER tubules form a reticular network in both perinuclear and peripheral regions (Chen et al., 2013; Goyal and Blackstone, 2013). ER architecture is created and maintained thanks to a continuous process of membrane remodeling, governed by homotypic fusion events, tubulation, and curvature rearrangements. Different families of membrane-shaping proteins are part of this complex regulation (De Craene et al., 2006; Hu et al., 2008; Orso et al., 2009). Some of the major players of ER-shaping are also involved in HSP disease. REEP1 and Reticulon 2 are two of the main ER-shaping proteins involved in HSP (in SPG31 and SPG12 respectively), and due to their particular topology, are supposed to induce high membrane curvature of the ER, a process facilitated by cytoskeleton changes (Park et al., 2010; Beetz et al., 2013; Wang and Rapoport, 2019). On the other hand, Spastin, an ATPase protein mutated in 40% of HSP patients, is involved in the disassembly and remodeling of neuronal microtubules and participates in the maintenance of ER integrity together with REEP1, Atlastin1 and Reticulon 2 (Evans et al., 2006; Sanderson et al., 2006).

ER homeostasis is another important cellular mechanism that participates in ER remodeling. REEP1 is also required in the activation of cellular response in *Drosophila* neuronal ER stress, but the molecular mechanism has not been investigated yet. ER stress is activated by various stimuli, including those of cellular redox regulation or by the accumulation of unfolded proteins in the ER, triggering an evolutionarily conserved pathway, known as unfolded protein response (UPR) (Gumeni et al., 2017). UPR is regulated by three major ER proteins (or ER stress sensors): inositol-requiring protein 1 (IRE1), pancreatic eukaryotic translation initiation factor 2α (eIF-2α) kinase (PERK) and activating transcription factor 6 (ATF6) (Inagi et al., 2014; Gumeni et al., 2017). In physiological conditions, all three effectors bind to the 78 kDa ER chaperone glucose-regulated protein/binding immunoglobulin protein (GRP78/BIP) on their luminal domains (Moreno and Tiffany-Castiglioni, 2015). During ER stress, ATF6 is activated after being cleaved, whereas PERK and IRE1 are activated by self-transphosphorylation (Scheper and Hoozemans, 2015). ATF6 is imported into the nucleus to induce the expression of protein quality control genes, while PERK activates the ubiquitous translation initiation factor eIF2α to upregulate genes involved in redox control, metabolism and folding, and mediates transient inhibition of most protein through ATF4 (Scheper and Hoozemans, 2015). The third UPR sensor, IRE1, alternatively splices inactive X box-binding protein 1 (XBP1) mRNA, producing active spliced XBP1 (sp-XBP1) (Tsaytler et al., 2011), which also controls the expression of several genes encoding for chaperons or involved in endoplasmic reticulum associated protein degradation (ERAD) (Yoshida et al., 2001; Calfon et al., 2002; Credle et al., 2005). UPR is highly conserved among species, also in *Drosophila melanogaster* (Hetz, 2012). Increased protein synthesis requires the expansion of the ER membrane network, thus associating UPR and ER membrane extension (Mandl et al., 2013). However, another study indicates that ER membrane expansion and generation of new ER sheets could act as a stress alleviating response independently of UPR activation, suggesting that ER expansion is an integral part of an effective UPR (Schuck et al., 2009).

Dysregulation of ER homeostasis is also involved in metabolic processes, like gluconeogenesis and lipid synthesis. Lipids, such as fatty acids, are essential components of the cellular membranes and act as signaling molecules. UPR activation results in increased expression of lipogenic markers and promotes LD formation, whereas the loss of LD formation up-regulates UPR response. Also, LDs are believed to work as a temporary depot for proteins destined for degradation (Shyu et al., 2018), thus suggesting a strong correlation between UPR and LD formation. REEP1 has been shown to localize or affect LD turnover in cells and murine models with lipodystrophy (Belzil and Rouleau, 2012; Tan et al., 2014).

In the last years, flavonoids have gained growing interest as therapeutic targets, mostly due to their health-promoting properties, and have been largely investigated on cell survival and stress response pathways. Specifically, several studies highlight the role of flavonoids in the oxidative stress responses and particularly on ER stress (Zhang and Tsao, 2016; Yu et al., 2019; Zeng et al., 2019). Among the different flavonoids, naringenin, a flavanone with estrogenic and anti-estrogenic activities, which is mainly extracted from citrus fruits, displays several biological properties such as antioxidant, antitumoral, antiviral, antibacterial, anti-inflammatory, anti-adipogenic, cardio-protective and neuro-protective activity (Gao et al., 2006; Salehi et al., 2019). In the last 3 years, several works focused on the beneficial effects of naringenin on neuronal development, maintenance and functionality (Hegazy et al., 2016; Wang et al., 2017, 2019). In this study, we used *Drosophila melanogaster* to study REEP1-related HSP disease effects on ER homeostasis. Our data show that the *Drosophila* ortholog ReepA plays an evolutionary conserved function in ER remodeling and the absence of ReepA in flies leads to the activation of two specific branches of UPR pathway, Ire1 and Atf6, and finally induces aging phenotypes. Moreover, naringenin administration restores ER homeostasis, climbing capacity and lifespan defects of ReepA mutant.

MATERIALS AND METHODS

Fly Strains and Materials

Fly stocks were raised on standard medium (yeast 27 g/l, agar 10 g/l, cornmeal 22 g/l, molasses 66 ml/l, nipagin 2.5 g/l, 12.5 ml/l ethanol 96%) and in standard conditions at 25°C and 12:12 h light:dark cycle. The *Drosophila* strains used are shown in **Table 1**. ReepA^{+C591} was used as a genetic background control. ReepA^{-541} mutant and ReepA^{+C591} flies were maintained on standard food at 25°C and Gal4/UAS crossings were performed at 28°C. All reagents, antibodies and compounds are listed in **Table 2**.

Generation of Constructs/Transgenic Flies

Full-length H-REEP1 cDNA (606 bp) was previously obtained from HeLa cells RNA extract followed by PCR reaction and cloned in the pUAST plasmid. The ReepA^{E} cDNA (867 bp) was obtained from *Drosophila*

TABLE 1 | List of fly stocks used.

Genotype	Source	References	RRID
ReepA^{-541}/*ReepA*$^{-541}$	O'Kane CJ (Department of Genetics, University of Cambridge, Cambridge, United Kingdom)	Yalçın et al., 2017	RRID:DGGR_123207
ReepA^{+C591}/*ReepA*$^{+C591}$	O'Kane CJ (Department of Genetics, University of Cambridge, Cambridge, United Kingdom)	Yalçın et al., 2017	
UAS ReepA^{E} *myc*	Generated in our laboratory	See section Materials and Methods	
UAS H-Reep1	Generated in our laboratory	See section Materials and Methods	
UAS HNEU-GFP	Generated in our laboratory	Kassan et al., 2013 See section Materials and Methods	
Tubulin-Gal4	Bloomington		RRID:BDSC_5138

TABLE 2 | List of reagents and compounds used.

Reagent	Source	RRID	Catalog number	Batch number
Tunicamycin	Sigma-Aldrich		T7765	078M4017V
Ethanol	Carlo Erba Reagents		308640	V9A122089B
Naringenin	Sigma-Aldrich		W530098	MKBW8466
Hydroxylpropyl-β-cyclodextrin	Sigma-Aldrich		H107	WXBC6699
Sucrose	Applichem		A 1125	R14248
Trizol	Euroclone		EMR507100	062117
Direct-Zol TM RNA MiniPrep kit	Zymo Research, Tustin, CA, United States		R2052	ZRC202785
One Step SYBR Prime Script TM RT-PCR Kit II	Takara-Clontech		RR066A	AIG1932A
GRS FullSample purification kit	Grisp Research Solutions		GK26.0050	7E30114A
Bradford proteins quantification kit	Sigma-Aldrich		B6916	SLBP3810V
Laemmli buffer	Sigma-Aldrich		S3401	SLBC5254V
Tween 20	Sigma-Aldrich		P1379	044K0139
Rabbit anti-phospho eIF2aS1	Abcam	RRID:AB_732117		
Mouse anti-α-tubulin	Sigma-Aldrich	RRID:AB_477593		
Goat anti-rabbit immunoglobulins HRP	DakoCytomation	RRID:AB_2617138		
Rabbit anti-mouse immunoglobulins HRP	DakoCytomation	RRID:AB_2687969		
Triton X-100	Sigma-Aldrich		X100	SLBC2688V

RNA extract and cloned in the pUAST plasmid. UAS-HNEU-GFP fly line was generated by cloning HNEU-GFP (Kassan et al., 2013) in pUASTattB, and transgenic lines were generated by BestGene Inc service (Chino Hills, CA, United States).

Drosophila Drug Treatments

Tunicamycin (Sigma-Aldrich, MO, United States), previously dissolved in ethanol (Carlo Erba Reagents, Milan, Italy), and naringenin complexed with hydroxypropyl-β-cyclodextrin (Sigma-Aldrich, MO, United States) in a mole ratio of 1:1, were added to standard *Drosophila* food at the final concentration of 0.024 mM and 0.5 mM respectively.

Starvation Assay

For the starvation assay, third instar larvae were individually selected and placed in Petri plates containing a solution of 20% sucrose (Applichem, Ottoweg, D, Germany) in PBS for 4 h.

RNA Extraction and Real-Time PCR

The relative expression levels of *Bip, Xbp1 total, Xbp1 spliced, Ldh, Atf4, Gp93, Hrd3, Herp, ReepA* were determined using quantitative real-time PCR. Total RNA was isolated from 5 third instar larvae and was extracted by Trizol reagent (Euroclone, Pero, MI, Italy), and purified using Direct-Zol TM RNA MiniPrep kit according to the manufacturer's instructions (Zymo Research, Tustin, CA, United States). The concentration and purity of RNA samples were determined using a NanoDrop 2000c spectrophotometer (Thermo Fisher Scientific, Waltham, MA, United States). Real-time PCR (qPCR) was performed on Eco Real-Time PCR System (Illumina Inc, San Diego, CA, United States), using One-Step SYBR® Prime Script TM RT-PCR Kit II (Takara-Clontech, Kusatsu, Japan) as in Castellani et al. (2016). The real-time PCR cycling conditions were: reverse transcription 50°C for 15 min, polymerase activation 95°C for 2 min, followed by 40 cycles of 95°C for 15 s, 60°C for a 1 min; melting curve 95°C for 15 s, 55°C for 15 s and 95°C for 15 s for all target genes. The housekeeping *Rp49* gene was used as an internal control to normalize the data. Relative mRNA expression levels were calculated by the threshold cycle (Ct) value of each PCR product and normalized using a comparative $2^{-\Delta\Delta Ct}$ method (Fantin et al., 2019). Data represented are the result of five independent biological replicates. Each biological sample was loaded in triplicate. The gene-specific primers used are shown in **Table 3**.

TABLE 3 | List of primer sequences used in Real Time PCR experiments.

Gene	Primer sequence
Bip(Hsc3)	Fw: 5′-GATTTGGGCACCACGTATTCC-3′ Rv: 5′-GGAGTGATGCGGTTACCCTG-3′
Xbp1 total	Fw: 5′-TCTAACCTGGGAGGAGAAAG-3′ Rv: 5′-GTCCAGCTTGTGGTTCTTG-3′
Xbp1 spliced	Fw: 5′-CCGAACTGAAGCAGCAACAGC-3′ Rv: 5′-GTATACCCTGCGGCAGATCC-3′
Atf4	Fw: 5′-TGCGAGTCTCAGGCG TCTTCATCTT-3′ Rv: 5′-CTGCTCGATGGTTGTAGGAGCTGG-3′
Ldh	Fw: 5′-GTGTGACATCCGTGGTCAAG-3′ Rv: 5′-CTACGATCCGTGGCATCTTT-3′
Gp93	Fw: 5′-TACCTGAGCTTCATTCGTGGCGTCG-3′ Rv: 5′-GCGGACCAGCTTCTTCTTGATCACC-3′
Hrd3	Fw: 5′-GCTGTGAGAAGGCGCTGATCCACTA-3′ Rv: 5′-CCAGCAGTCTTACCCGATGCACAAC-3′
Herp	Fw: 5′-CTTACGCGCAGTACATGCAGCAGTT-3′ Rv: 5′-CAGCTGCTCCTGCCACTTGTTGTAC-3′
ReepA (s,p,j,h,g,e)	Fw: 5′-ATGATCAGCAGCCTGTTTTC-3′ Rv: 5′-CAGTACATCATTCATTTAACATATTC-3′
Rp49	Fw: 5′-AGGCCCAAGATCGTGAAG AA-3′ Rv: 5′-TCGATACCCTTGGGCTTGC-3′

Lifespan Assay

For lifespan assay, control ReepA^{+C591} and ReepA^{-541} mutant flies were collected after hatching and raised on standard medium or 0.5 mM naringenin enriched food at 25°C in a 12:12 h light-dark cycle. Flies were kept in groups of 20 individuals and were maintained in a *Drosophila* vial. Flies were transferred to a fresh medium every 3 days and death events were scored daily. The experiment was repeated ten times for each genotype.

Climbing Assay

For climbing assays, 30 flies for each genotype were collected after hatching and were transferred twice a week to tubes containing fresh standard or 0.5 mM naringenin enriched food. Climbing capability was tested six times along the life of these flies (5, 10, 15, 20, 25 and 30 days).

Drosophilae were placed in an empty plastic vial with a line drawn 2 cm from the bottom of the tube and allowed to recover from anesthesia for 1 h. Flies were gently tapped to the bottom of the tube and the number of flies above the 2 cm mark at 20 s was recorded as a percentage of flies able to climb the vial. Ten separate and consecutive trials were performed and the results were averaged. The experiment was repeated 10 times for each genotype.

Western Blotting

For western blots, total proteins were obtained from 10 adult flies using GRS FullSample purification kit (Grisp, Research solutions, Porto, Portugal). The protein levels were quantified using the Bradford proteins quantification kit (Sigma-Aldrich, MO, United States). Each sample was diluted 1:2 with standard 2X Laemmli buffer (Sigma-Aldrich, MO, United States), boiled for 5 min a 95°C and 20–25 mg of proteins were separated on 5% stacking-10% separating SDS polyacrylamide gels. The resolved proteins were transferred electrophoretically to polyvinylidene difluoride (PVDF) membrane as described before (Di Francesco et al., 2015). Membranes were blocked in 10% non-fat dried milk in Tris-Buffer Saline and 0.1% Tween 20 (Sigma-Aldrich, MO, United States) (TBST) as in Floreani et al. (2012) and were incubated using primary antibody rabbit anti-phospho eIF2aS1 (1:1000, ab32157, Abcam, Cambridge, United Kingdom) overnight at 4°C. Mouse anti-α-tubulin (1:2000, T9026, Sigma-Aldrich, St. Louis, MO, United States) was used as loading control. Secondary polyclonal goat anti-rabbit and anti-mouse immunoglobulins HRP (1:2000, DakoCytomation, Glostrup, DK) were used in all cases. The protein bands were detected using the C400 Azure chemiluminescence biosystem (Aurogene, Rome, Italy) and band densities were quantified with ImageJ Fiji 1.52 software. The ratio of the target protein to α-Tubulin was recorded and analyzed. At least three independent biological replicates were used for each genotype and condition.

Immunohistochemistry

Third instar larvae raised at 25°C or 28°C were harvested, dissected in HL3, fixed in 4% paraformaldehyde for 10 min, washed in PBS containing 0.3% Triton X-100 (Sigma-Aldrich, MO, United States) and mounted on glass slides using Mowiol 4-88 as reported in Mushtaq et al. (2016). For live imaging, larvae were dissected in HL3 and acquired as described previously (D'Amore et al., 2016). All confocal images were acquired using a confocal microscope (Nikon D-ECLIPSE C1) equipped with a Nikon 60x/1.40 oil Plan Apochromat objective using the Nikon EZ-C1 acquisition software as described in Caputi et al. (2017).

Measure of ER Morphology

For ER morphological analysis, muscles of ten third instar larvae were quantified and analyzed with ImageJ Fiji 1.52 software. All quantitative analyses were performed on muscle 6/7 of abdominal segment A3. Fluorescence intensities were measured on maximum projections of confocal stacks (step size 0.55 μm) taken with a Nikon 60x/1.40 oil Plan Apochromat objective using the Nikon EZ-C1 acquisition software. For each sample, three Region of Interest (ROI) with a range of 800–1000 μm^2 were analyzed.

To quantify cisterna-like structures, an 8-bit ER image was requested. The image was processed with a manual threshold. Threshold values were 80–255 to eliminate the intensity distortion and 40–255 to preserve the continuity of tubules. Then a binary and open image was created and processed by erosion (subtract pixels) and dilation (add pixels) commands of ImageJ software. In the binary and opened image, tubules were eliminated and cisterna-like structures were isolated. The sheet-like structures were analyzed with Analyze Particle tool and their number and size were quantified (Griffing, 2018).

Statistical Analysis

Statistical analysis was performed with Microsoft Office Excel 2013 software and Prism version 6.00 for Windows (GraphPad Software, La Jolla, CA, United States). Survival data were analyzed using the log-rank test (Mantel-Cox method).

Significance was calculated using one-way analysis of variance (ANOVA) followed by Dunnett's or Tukey's multiple comparison test. Student's *t*-test for unpaired variables (two-tailed) was used for real-time PCR in young and old flies (**Figure 2B**) and in climbing assay in **Figure 2D**. Differences were considered statistically significant at $p < 0.05$(*) and $p < 0.01$(**) and $p < 0.001$(***). Data are presented as means and bars are s.e.m. (standard error of the mean).

RESULTS

ReepA Regulates ER Morphology

REEP1 homologs are ER-resident proteins implicated in ER remodeling (Beetz et al., 2013; Zheng et al., 2018). To evaluate the function of *Drosophila* ReepA (firstly named DREEP1 in Appocher et al., 2014) in ER membrane shaping, we analyzed ER structure in *Drosophilae* overexpressing ReepA isoform E (here reported as ReepA^{E}), which shows the highest homology with human REEP1. REEP1 humanized flies obtained by overexpressing *REEP1* human gene, were also analyzed to identify possible conservation of the REEP1 function (**Supplementary Figure 1**). Besides the gain-of-function lines, we analyzed the ReepA^{-541} *Drosophila* null mutant (Yalçın et al., 2017) for loss-of-function phenotypes. Two of the most used ER markers in *Drosophila* are Lys-GFP-KDEL (Frescas et al., 2006) and BiP–sfGFP–HDEL (Summerville et al., 2016). Lys-GFP fails to recognize the complexity of ER and discriminate tubules and cisternae (**Supplementary Figure 2**). On the other hand, BiP–sfGFP–HDEL, defines better the ER structures but

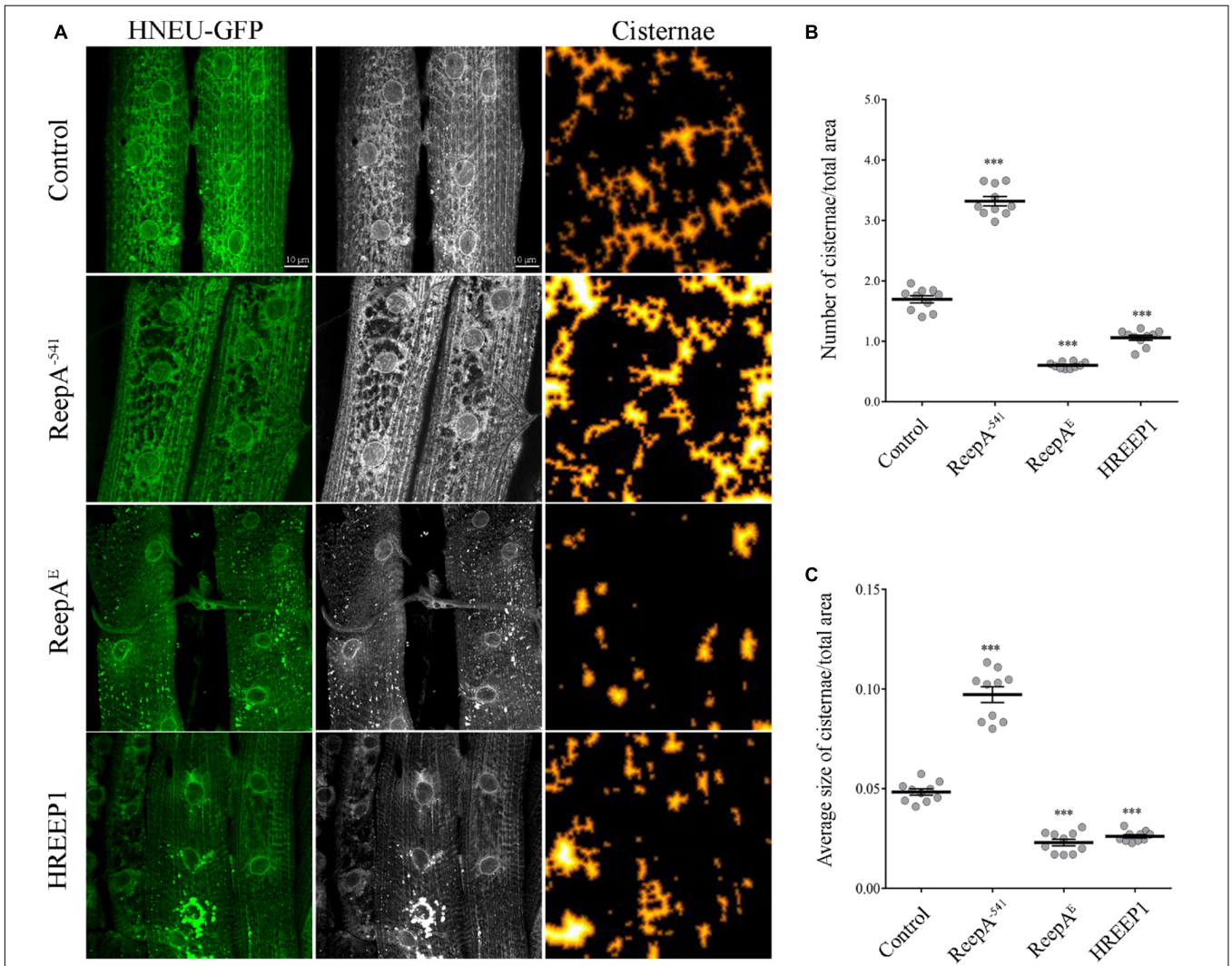

FIGURE 1 | *In vivo* ubiquitous expression of ER-marker HNEU-GFP in *Drosophila melanogaster* ReepA model. **(A)** Representative confocal images of larval muscle 6/7 of abdominal segment A3 of control (*ReepA*$^{+C591}$/*ReepA*$^{+C591}$*; Tubulin-Gal4/UAS HNEU-GFP*), ReepA^{-541} mutant (*ReepA*$^{-541}$/*ReepA*$^{-541}$*; Tubulin-Gal4/UAS HNEU-GFP*), ReepA^{E} (*UAS ReepA*^{E} *myc/+; UAS HNEU-GFP, Tubulin-Gal4/+*) and HREEP1 (*UAS HREEP1/UAS HNEU-GFP, Tubulin-Gal4*) larvae, expressing ubiquitously UAS HNEU-GFP. Scale bar = 10 μm. Quantification of cisterna-like structures number **(B)** and size **(C)** of ER-marker HNEU-GFP. Significance was calculated using one-way ANOVA followed by Dunnett's multiple comparison test. Significance vs. ctr. (***$P < 0.001$). The bars indicate s.e.m., $n = 10$ larvae.

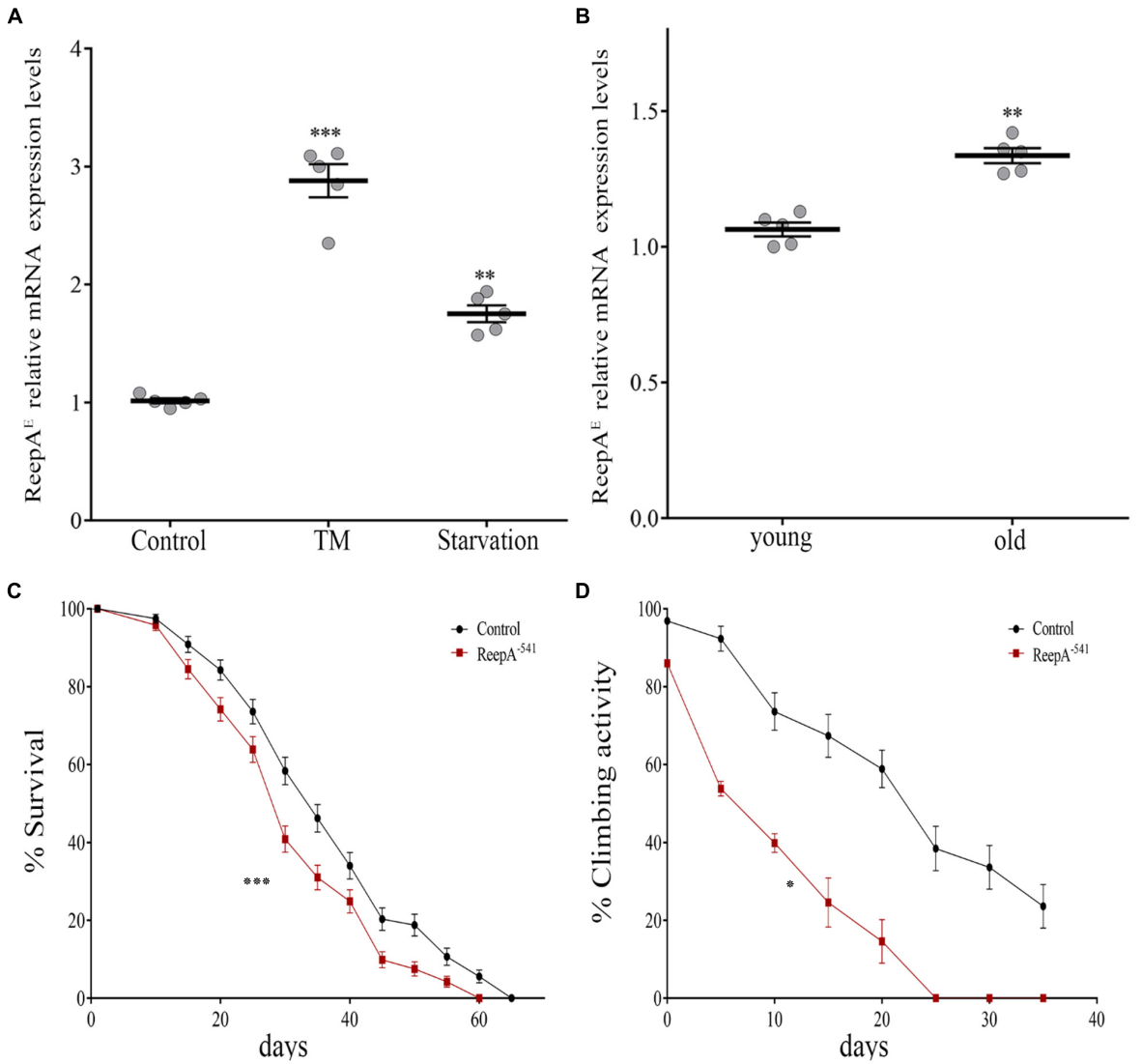

FIGURE 2 | Loss of *ReepA* reduces *Drosophila* longevity and flies' climbing activity. **(A)** *ReepA*^{E} relative gene expression in control (*ReepA*$^{+C591}$/*ReepA*$^{+C591}$) larvae raised on standard, TM 0.024 mM enriched food, or on starvation conditions. Significance was calculated using one-way ANOVA followed by Dunnett's multiple comparison test. Significance vs. ctr. (**$P < 0.01$; ***$P < 0.001$). The bars indicate s.e.m., $n = 5$. **(B)** *ReepA*^{E} relative gene expression in young (1 day) and old (30 days) control (*ReepA*$^{+C591}$/*ReepA*$^{+C591}$) flies raised on standard food. Significance was calculated by using two-tailed T-test, **$P < 0.01$. The bars indicate s.e.m., $n = 5$. **(C)** Lifespan in control (*ReepA*$^{+C591}$/*ReepA*$^{+C591}$) and ReepA^{-541} mutant (*ReepA*$^{-541}$/*ReepA*$^{-541}$) raised on standard food. Significance was calculated by using the log-rank Mantel-Cox test, *P*-value: ***$P < 0.001$. The bars indicate s.e.m., $n = 10$ (30 flies for each vial). **(D)** Climbing activity in control (*ReepA*$^{+C591}$/*ReepA*$^{+C591}$) and ReepA^{-541} mutant (*ReepA*$^{-541}$/*ReepA*$^{-541}$) raised on standard food and tested at 0, 5, 10, 15, 20, 25, 30, and 35 days. Significance was calculated by using two tailed *T*-test, *P*-value: *$P < 0.05$. The bars indicate s.e.m., $n = 10$ (20 flies for each vial).

it resulted lethal at the pupal stage when expressed with drivers as Elav-Gal4 and Mef2-Gal4 and at the larval stage if expressed with Tubulin-Gal4 driver (**Supplementary Figure 3**). Therefore, we used a recently published ER marker (HNEU-GFP) to visualize ER structure complexity (Forgiarini et al., 2019). The expression of HNEU-GFP transgene is not lethal, also with strong drivers and at relatively high temperatures (28–29°C), allowing us to distinguish the tubule and sheet-like structure of *Drosophila* muscles in both living and fixed samples (**Supplementary Figure 4**).

To quantify the ER defects we ubiquitously expressed UAS HNEU-GFP with Tubulin-Gal4 driver and we followed the protocol described by Griffing (2018). The total area of the ER cisternae was measured along the muscle stacks and quantified as specified in methods section. Both the ubiquitous overexpression of ReepA and HREEP1 and its absence in ReepA^{-541} induced evident morphological alteration of ER architecture, as shown by the HNEU-GFP marker profile (**Figures 1A–C**). In ReepA^{-541} mutant, the cisterna-like structures were increased and peripheral tubular ER tended to lose its complexity (**Figure 1A**). On

the contrary, the ubiquitous expression of ReepA^{E} induced a reduction of cisternae (**Figures 1A–C**), thus implying a direct role of ReepA on *Drosophila* ER structure modulation. Interestingly, the overexpression of human REEP1 led to a reduction of cisternal structures, a phenotype similar to that of ReepA^{E} overexpression, suggesting high conservation of Reep1 function in ER remodeling. Therefore, our data confirmed that *Drosophila* ReepA, similarly to its ortholog REEP1, mediates ER membrane shaping.

ReepA Is Required During Aging and Stress

A functional screening performed in *Drosophila melanogaster* demonstrated that ReepA promotes neuronal resistance to ER stress and prevents Tau toxicity (Appocher et al., 2014). Neuronal resistance was tested in adult flies against heat-shock stress and tunicamycin (TM) treatment, identifying ReepA as a new modulator of cellular response to stress. In spite of this, the molecular mechanism remains still unclear. To better understand the role of ReepA under stressors stimuli we first evaluated the transcript expression levels of ReepA^{E} after TM chronic treatment or starvation (Appocher et al., 2014; Lindström et al., 2016). Therefore, we compared ReepA^{E} transcription levels of stressed wild type larvae versus untreated flies. Our analysis showed that ReepA^{E} was upregulated during starvation similarly (but less effective) to TM chronic feeding treatment (**Figure 2A**). We thus deeply investigated the role of ReepA during aging. We tested the expression level of ReepA^{E} in young versus old wild-type adult flies. Adult-aged flies (30 days) expressed higher levels of ReepA^{E} compared to 1-day flies (**Figure 2B**), suggesting an upregulation of ReepA during the adult lifespan. Furthermore, we found that ReepA^{-541} null mutant flies displayed a significant reduction of lifespan (**Figure 2C**) and climbing ability (**Figure 2D**), reinforcing the hypothesis that ReepA is required during aging processes.

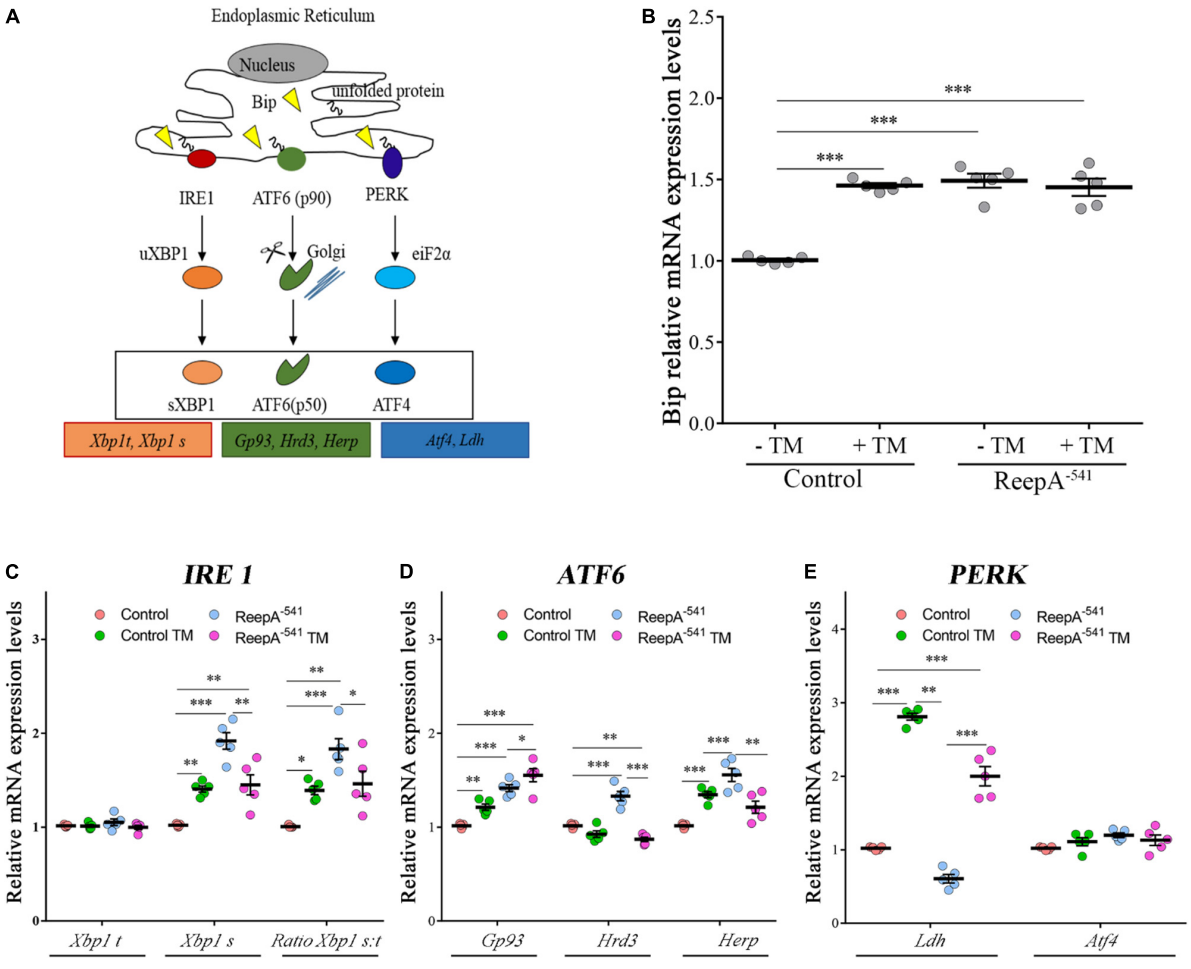

FIGURE 3 | *ReepA* alters the expression levels of genes involved in Ire1/Xbp1, Atf6 and Perk-Atf4 pathways. **(A)** Schematic representation of the three branches of UPR: PERK, IRE1α, and ATF6. Boxes show the genes considered in our analyses. Relative mRNA expression levels of *Bip* **(B)**, *Xbp1 t* and *Xbp1 s* **(C)**; *Gp93, Hrd3* and *Herp* **(D)**; *Ldh* and *Atf4* **(E)** in control (*ReepA*$^{+C591}$/*ReepA*$^{+C591}$) and ReepA^{-541} mutant (*ReepA*$^{-541}$/*ReepA*$^{-541}$) larvae raised on standard food or TM 0.024 mM enriched medium. Significance was calculated by using one-way ANOVA with Tukey's *post hoc* test. *$P < 0.05$; **$P < 0.01$; ***$P < 0.001$. The bars indicate s.e.m., $n = 5$.

Our data confirmed a crucial role of ReepA in aging and stress conditions.

ReepA Mutant Flies Triggered a Selective Activation of Atf6 and Ire1 Branches

To elucidate the molecular mechanism underlying ReepA function in cellular stress we tested the effects of the loss of ReepA on UPR response, one of the main cellular signaling activated in case of ER stress (**Figure 3A**) (Rutkowski and Kaufman, 2007; Mandl et al., 2013). We thus measured the activation of the three main branches of UPR signaling (Perk, Ire1 and Atf6) in *Drosophila* under normal or stress conditions induced by TM administration.

A qRT-PCR analysis on control and ReepA^{-541} third instar larvae, grown on standard or TM enriched food, was performed. Our data showed that the expression of *Hsc3,* the homolog of Bip/GPR94 chaperon, was significantly increased in control larvae treated with TM (**Figure 3B**), in agreement with previous *in vitro* studies (Lindström et al., 2016). Intriguingly, untreated ReepA^{-541} mutant larvae showed an increase of 1.5 fold in *Bip* transcript levels that remained high even after TM treatment (**Figure 3B**). The activation of the IRE1 pathway was quantified by measuring the levels of the unspliced [*Xbp1 total (Xbp1 t)*] and IRE1-dependent spliced forms of *Xbp1* [*Xbp1 spliced* (*Xbp1 s*)]. Our analysis showed that the levels of spliced *Xbp1* mRNA were significantly increased in ReepA^{-541} mutant and in control larvae exposed to chronic TM feeding (**Figure 3C**), supporting the activation of the IRE1 pathway in absence of ReepA. Similar data were obtained by analyzing the Atf6 pathway. Specifically, we found that the Atf6 targets genes *Gp93*, *Herp* and *Hrd3* were upregulated in ReepA^{-541} mutant, mimicking again the response of control larvae treated with TM (**Figure 3D**). Finally, we evaluated the activation of the Perk pathway by quantifying the expression levels of *Atf4*, but no statistically significant changes were observed in ReepA^{-541} mutant nor in TM treated larvae (**Figure 3E**). We then considered the expression levels of *Lactate Dehydrogenase* (*Ldh*), a marker of ER stress activation in *Drosophila*, mediated by Atf4 (Lee et al., 2015). Our results showed that *Ldh* expression was strongly increased in control and ReepA^{-541} mutant larvae fed with TM (3 and 2.5 folds as compared to untreated control, respectively), but was decreased in ReepA^{-541} mutant untreated larvae (**Figure 3E**), suggesting that loss of ReepA does not trigger Perk activation. We further confirmed our findings by measuring the phosphorylated eIF2α protein levels, which were upregulated in TM chronic feeding flies but not in the ReepA loss–of-function background (**Figures 4A,B**). Thus, our results demonstrate a selective role of ReepA in both Atf6 and Ire1 pathway regulation.

Defects of ReepA^{-541} Mutant Are Rescued by Naringenin Administration

Naringenin (4′,5,7-trihydroxy flavanone) is a flavonoid that exerts antioxidant activity, triggering the antioxidant system, and it is demonstrated to protect cells from ER stress (Panche et al., 2016; Tang et al., 2017; Salehi et al., 2019). Moreover, like other natural compounds, naringenin has gained attention in the last year as a phytochemical with neuroprotective effects. Several studies described its effects and its ability to inhibit

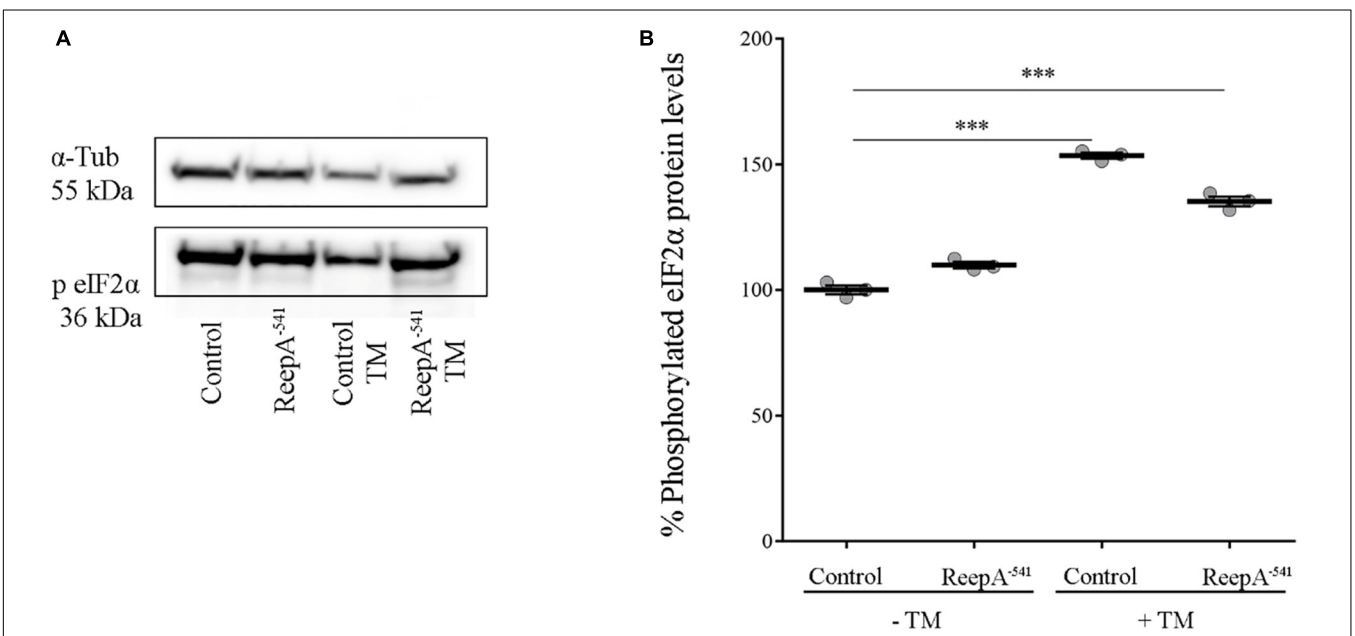

FIGURE 4 | Phosphorylated eIF2α protein expression in ReepA^{-541} mutant and control adults. **(A)** Western blots showing the phosphorylated eIF2α and α-Tubulin (used as the loading control) protein levels in control (*ReepA*$^{+C591}$/*ReepA*$^{+C591}$) and ReepA^{-541} mutant (*ReepA*$^{-541}$/*ReepA*$^{-541}$) raised on standard and TM 0.024 mM enriched food. **(B)** eIF2α western blot band quantification. Phosphorylated eIF2α levels were quantified, normalized on α-Tubulin levels and expressed as percent increase versus control. Significance was calculated by using one way ANOVA test with Tukey's *post hoc* test ***$P < 0.001$. The bars indicate s.e.m., $n = 3$.

neuro-apoptosis, ameliorate cognitive impairment in different rodent models of neurodegenerative disorders, reduce oxidative stress improving mitochondrial dysfunction in neurons, support dopaminergic neurons and protect from neuroinflammation (Khan et al., 2012; Hsu et al., 2014; Manchope et al., 2017; Wang et al., 2017, 2019; Akang et al., 2019).

One of the stumbling blocks when naringenin or other flavonoids were administrated, is the relatively low bioavailability that could be ameliorated by the complexation with hydroxylpropyl-β-cyclodextrin as described by different groups (Shulman et al., 2011).

Therefore, we focused our experiments on testing the effects of naringenin on ReepA^{-541} mutant-associated phenotypes, administrating the flavonoid at the concentration of 0.5 mM after its complexation with hydroxylpropyl-β-cyclodextrin. This concentration was chosen based on a previous report that claims a beneficial effect of naringenin in the range between 0.2 and 0.6 mM in *Drosophila* (Chattopadhyay et al., 2016). We conducted a pilot test using different concentrations of naringenin, on ReepA^{-541} mutant and quantified the expression levels of *Bip* transcript (**Supplementary Figure 5**). The minimum concentration with rescue effect, 0.5 mM, was used to analyze the effects of the flavonoid on ReepA-linked phenotypes. Larvae were grown in naringenin and the expression levels of the genes involved in UPR response were analyzed. Administration of naringenin completely rescued *Bip, Xbp1 s, Gp93, Hrd3, Herp,* and *Ldh* expression levels in ReepA^{-541} mutant (**Figure 5**). Of note, as shown in

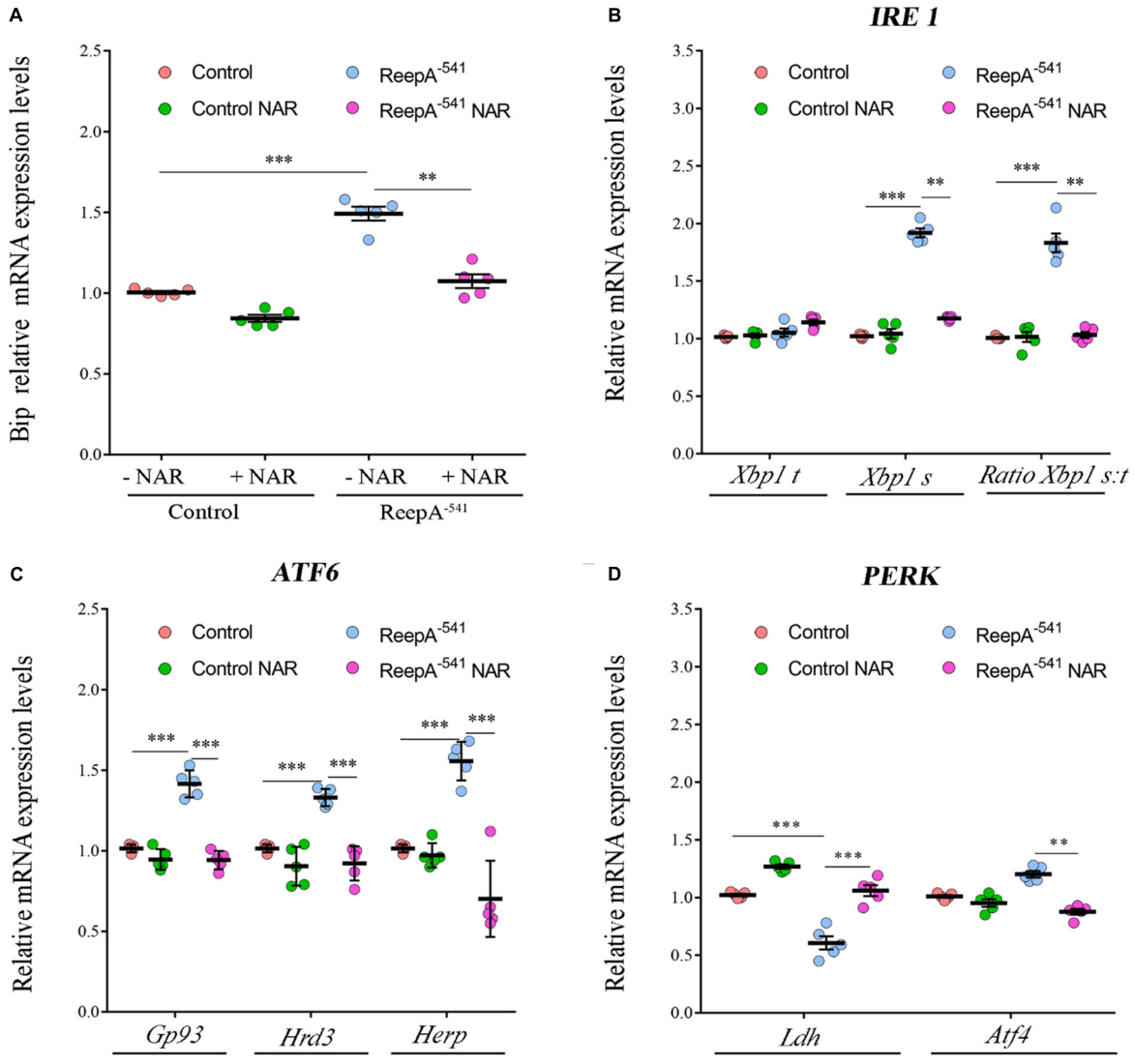

FIGURE 5 | Naringenin restores the expression levels of the genes involved in Ire1/Xbp1, Atf6 and Perk-Atf4 pathways in ReepA^{-541} mutant. Relative mRNA levels of *Bip* **(A)**, *Xbp1 t* and *Xbp1 s* **(B),** *Gp93, Hrd3,* and *Herp* **(C),** *Ldh* and *Atf4* **(D)** in control (*ReepA*$^{+C591}$/*ReepA*$^{+C591}$) and ReepA^{-541} mutant (*ReepA*$^{-541}$/*ReepA*$^{-541}$) larvae raised on NAR 0.5 mM enriched or standard food. Significance was calculated by using one-way ANOVA with Tukey's *post hoc* test. $^{**}P < 0.01$; $^{***}P < 0.001$. The bars indicate s.e.m., $n = 5$.

Figure 5, control larvae treated with the flavonoid displayed a transcription profile of UPR genes similar to that of the untreated control. We also analyzed the effect of naringenin on ER morphology and we found that the treatment was able to significantly restore the increased cisterna-like structures phenotype caused by the loss of ReepA (**Figure 6**). Analogously to what observed for UPR genes, naringenin did not affect ER morphology of control animals. We finally evaluated if the flavonoid was able to restore the ReepA^{-541} mutant related age and climbing phenotypes (**Figure 7**). The analysis of the average lifespan revealed a significant positive effect (but not total) of naringenin on ReepA mutant flies (**Figure 7A**, and **Supplementary Figure 6**). In this case, naringenin also affects the longevity of control flies. We then investigated the flavonoid effect on the climbing activity. Our data showed that, after naringenin administration, ReepA^{-541} flies almost totally recovered their moving deficits (**Figure 7B**). Thus, naringenin reverted the cellular (ER morphology and UPR activation), age and locomotor associated phenotypes induced by ReepA loss of function.

Overall, our *in vivo* findings further confirm that ER structure and function are crucial in HSP neurodegeneration. Additionally, our results suggest that naringenin exerts beneficial effects in *Drosophila* ReepA HSP disease model and enlists a new compound to the future pharmacological therapy implementation in HSP disorders.

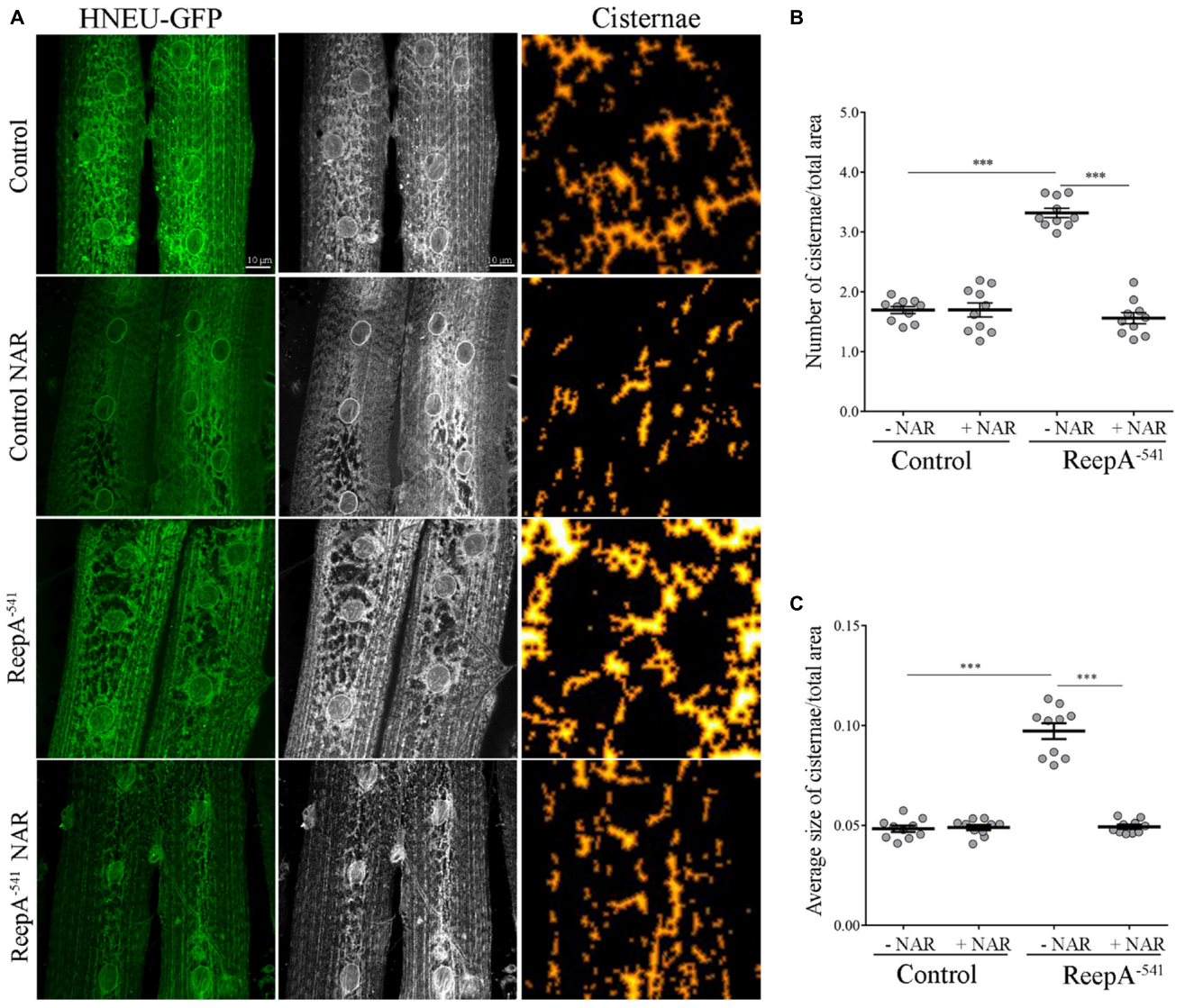

FIGURE 6 | Naringenin rescues ReepA^{-541} mutant ER morphology defects. **(A)** Representative confocal images of muscle 6/7 of abdominal segment A3 of control (*ReepA*$^{+C591}$*/ReepA*$^{+C591}$*; Tubulin-Gal4/UAS HNEU-GFP*) and ReepA^{-541} mutant (*ReepA*$^{-541}$*/ReepA*$^{-541}$*; Tubulin-Gal4/UAS HNEU-GFP*) third instar larvae expressing ubiquitously UAS HNEU-GFP raised on standard or NAR 0.5 mM enriched food. Scale bar = 10 µm. Quantification of cisterna-like structures number **(B)** and size **(C)** of ER- marker HNEU-GFP. Significance was calculated by using one-way ANOVA with Tukey's *post hoc* test. ***$P < 0.001$. The bars indicate s.e.m., $n = 10$ larvae.

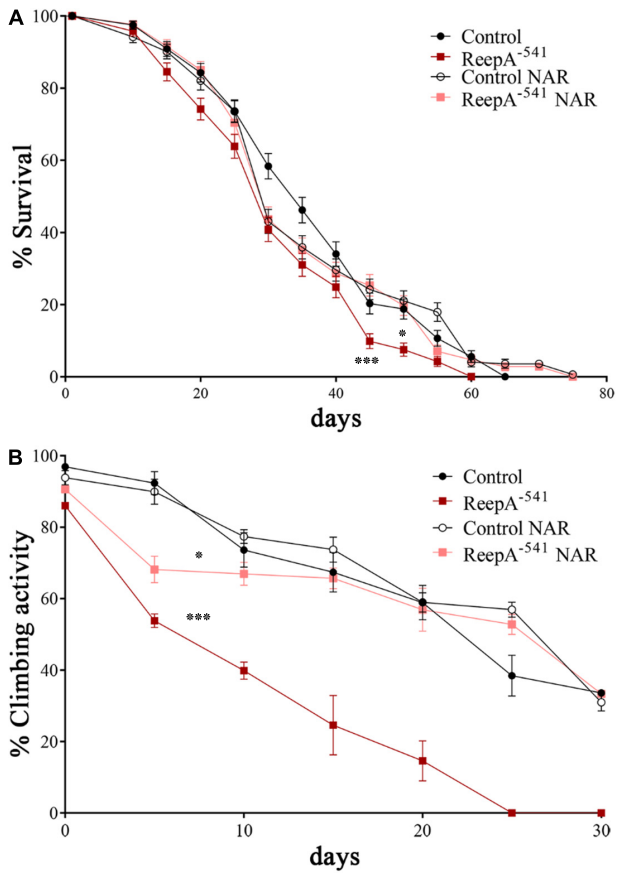

FIGURE 7 | Naringenin ameliorates ReepA^{-541} flies' lifespan and climbing activity. **(A)** Lifespan in control (*ReepA*$^{+C591}$/*ReepA*$^{+C591}$) and ReepA^{-541} mutant (*ReepA*$^{-541}$/*ReepA*$^{-541}$) raised on NAR 0.5 mM enriched or standard food. Significance was calculated using log-rank Mantel–Cox test. *P*-value: $^{*}P < 0.05$ (ReepA^{-541} mutant NAR vs. ReepA^{-541} mutant), *P*-value: $^{***}P < 0.001$ (ReepA^{-541} mutant vs. control), $n = 10$ (30 flies for each vial). **(B)** Climbing activity in control (*ReepA*$^{+C591}$/*ReepA*$^{+C591}$) and ReepA^{-541} mutant (*ReepA*$^{-541}$/*ReepA*$^{-541}$) raised on NAR 0.5 mM enriched or standard food and tested at 0, 5, 10, 15, 20, 25, 30, and 35 days. Significance was calculated using one-way ANOVA with Tukey's *post hoc* test. *P*-value: $^{*}P < 0.05$ (ReepA^{-541} mutant NAR vs. ReepA^{-541} mutant), $^{*}P < 0.05$ (ReepA^{-541} mutant vs. control). The bars indicate s.e.m., $n = 10$ (20 flies for each vial).

DISCUSSION

To date, 56 disease-causing variants in REEP1, have been reported. HSP-associated REEP1 mutations are predominantly truncating mutations that have been proposed to act by a haploinsufficiency loss-of-function mechanism (Züchner et al., 2006; Beetz et al., 2008; Schlang et al., 2008; Goizet et al., 2011; Richard et al., 2017). In this study, we explored the role of ReepA in ER homeostasis by investigating the consequences of its loss. Our data showed a functional link between the absence of ReepA and the corresponding activation of two specific branches of the UPR pathway: Ire1 and Atf6. Moreover, we found a morphological adaptation of ER in loss-of-function ReepA animals characterized by the increase of ER membrane sheet-like structures. In parallel to these intracellular alterations, we reported reduced lifespan and deficits of locomotor activity of the mutant flies. The function of REEP homologs in cellular stress has been previously investigated by different groups: HVA22, the plant homolog gene of REEP1, is required to counteract stressful situations by inhibiting the activation of programed cell death in plants (Chen et al., 2002); *Drosophila* ReepA downregulation enhances Tau aggregates, whereas its overexpression results protective, suggesting that ReepA is required to confer stress resistance against the accumulation of unfolded proteins induced by TM (Appocher et al., 2014); DNA damage in human cells triggers tubular ER extension via the p53-mediated expression of REEP1/2 and EI24, and this facilitates contacts between ER and mitochondria (Zheng et al., 2018). All these reports support the role of REEPs in response to stressors, but the molecular mechanism remains still to be elucidated. In our work, we analyzed the activation of the three main pathways involved in UPR response and showed a peculiar selective induction of Atf6 and Ire1 in the absence of ReepA. Moreover, it has been demonstrated that the activation of Atf6 and Ire1, but not of Perk signaling, increases the synthesis of phosphatidylcholine, a key ER lipid, and induces ER expansion (Chiang et al., 2012; McQuiston and Diehl, 2017). When a constitutively active form of ATF6α or Xbp1 is expressed in cultured cells, the ER appears enlarged and distended. On the contrary, PERK pathway has not been implicated in ER biogenesis. The selective activation of Atf6 and Ire1, but not of Perk, in ReepA^{-541} mutant and the concomitant morphological ER aberrations suggest a specific role of ReepA in controlling ER homeostasis. Modulation of UPR after the disruption of optimal membrane rearrangements has already been reported: in *Drosophila*, downregulation of the ER-shaping protein Rtln1, causes partial loss of tubular ER and a significant increase of the ER stress response in epidermal cells and neurons (O'Sullivan et al., 2012); the expression of *RTN3*, a specific receptor for the degradation of ER tubules, is upregulated by ER stress and its loss is associated to attenuated basal ER stress (Chen et al., 2011; Grumati et al., 2017); the *Arabidopsis* mutants of *RHD3*, an ER-shaping GTPase, which have long unbranched ER tubular structures, lack the ability to invoke UPR interfering with IRE1 function (Lai et al., 2014). Although the mechanism by which these ER-shaping proteins regulate UPR is not clear, a link between tubular ER structure and ER stress exists. Indeed, recent findings indicate that the UPR can be directly activated by altering ER lipid composition (Hapala et al., 2011; Volmer et al., 2013; Halbleib et al., 2017). UPR activation is observed in yeast lacking the enzymes required for the biosynthesis of triacylglycerol and sterol esters, and is thus devoid of LDs. *Reep1*$^{-/-}$ mice that present ER sheet expansion showed an impairment of LDs and lipoatrophy, with significantly decreased visceral fat (Park et al., 2010; Beetz et al., 2013; Falk et al., 2014; Lim et al., 2015; Renvoisé et al., 2016).

Furthermore, we found that loss of ReepA resulted in a decline in motor ability and a reduction of the lifespan. A previous report, in which another ReepA mutant was described, showed no aging phenotypes in absence of stress, but a drastic reduction of lifespan was seen under stress conditions (Appocher et al., 2014). The

discrepancy in this finding could be due to the different fly models used; however, we were not able to obtain the same mutant line to repeat the experiments and compare the data. In our work, climbing test and lifespan analysis were carried out in parallel in a Spastin *Drosophila* model as indicated (Orso et al., 2005; Julien et al., 2016) to compare the results and the methodology (not shown). Based on the outcome, we feel confident that the experimental conditions and methodology were performed correctly.

Finally, we explored the pharmacological effects of naringenin on ReepA *Drosophila* model. Besides the efficacy of naringenin in pathological models of liver diseases, obesity, and diabetes, an interesting role of naringenin is emerged in the last years relating to neurological disorders. The protective effects of naringenin in cellular and animal Parkinson's models are demonstrated by its ability to restore dopaminergic function, neuro-inflammation and locomotor deficit (Khan et al., 2012; Hegazy et al., 2016; Wang et al., 2019). Naringenin protects motor neuron against methylglyoxal-induced neurotoxicity *in vitro* (Lo et al., 2017). The relatively recent interest in the molecule, the reduced data on pharmacokinetic and metabolic aspects, as well as the chemical instability of this compound have prevented the development of clinical trials activity, at least for now. The increasing attention to naringenin, in fact, has stimulated the researchers to work on delivering systems (Joshi et al., 2018). In this study, we tested the effects of naringenin after the complexation with β-cyclodextrin, an FDA approved excipient that enhances its solubility and increases the absorption rate, as previously reported (Sangpheak et al., 2015; Salehi et al., 2019).

The phenotypes of ReepA loss-of-function model reported in this work were greatly ameliorated by administration of naringenin that rescues not only the phenotypes at molecular and cellular levels, but also restores the climbing behavior as well as ameliorates flies' lifespan. Overall, our *in vivo* data strongly support the beneficial effects of the natural compound naringenin and open the way for future studies devoted to pharmacotherapy in HSP. We propose a possible protective role of naringenin in HSP neurodegeneration and, therefore, the testing of this compound in additional HSP models. Naringenin inhibits the ER stress in several pathological models. The mechanism by which naringenin acts is poorly understood but most of the studies support the notion that naringenin influences the cellular antioxidant balance through its own chemical structure and by inducing the cell antioxidant system: activating nuclear factor-erythroid 2-related factor 2 (Nrf2) pathway, upregulating superoxide dismutase, catalase, glutathione peroxidase and glutathione transferase and decreasing the expression of *miR-17-3* (Song et al., 2016; Curti et al., 2017; de Oliveira et al., 2017; Tang et al., 2017; Wang et al., 2017, 2019). Naringenin has also the capacity to accumulate in the membrane hydrophobic core, decreasing membrane fluidity in a concentration-dependent manner, and therefore to reduce the interaction between free radical and lipids, blocking lipid peroxidation (Arora et al., 2000).

In this light, future studies of naringenin targets, mechanisms, dosage, and delivering routes could be beneficial also for other disorders that share metabolic and oxidative stress activation, such as amyotrophic lateral sclerosis, myoclonic epilepsy, ataxia, and muscular dystrophy, for which pharmacological treatments are still not available (Fischer et al., 2007; Crimella et al., 2011; Joardar et al., 2015; Wang, 2016).

DATA AVAILABILITY STATEMENT

The datasets generated for this study are available on request to the corresponding author.

AUTHOR CONTRIBUTIONS

BN, SG, and GO conceived and designed the experiments. BN, SG, AF, MF, CD, EP, and CV performed the experiments. BN, SG, AF, CD, EP, CV, and GO analyzed the data. GO contributed to reagents, materials, and analysis tools. BN, SG, and GO wrote the manuscript.

FUNDING

This work has been supported by grants from the Italian Ministry of Health (Ricerca Corrente 2018 - 2019) and PRIDJ 18_01 (University of Padova). The funders had no role in study design, data collection and analysis, decision to publish, or preparation of the manuscript.

ACKNOWLEDGMENTS

The manuscript is part of the Ph.D. thesis of BN (Napoli, unpublished).

SUPPLEMENTARY MATERIAL

The Supplementary Material for this article can be found online at: https://www.frontiersin.org/articles/10.3389/fnins.2019.01202/full#supplementary-material

REFERENCES

Akang, E. N., Dosumu, O. O., Afolayan, O. O., Fagoroye, A. M., Osiagwu, D. D., Usman, I. T., et al. (2019). Combination antiretroviral therapy (cART)-induced hippocampal disorders: highlights on therapeutic potential of Naringenin and Quercetin. *IBRO Rep.* 6, 137–146. doi: 10.1016/J.IBROR.2019.04.002

Appocher, C., Klima, R., and Feiguin, F. (2014). Functional screening in *Drosophila* reveals the conserved role of REEP1 in promoting stress resistance and preventing the formation of Tau aggregates. *Hum. Mol. Genet.* 23, 6762–6772. doi: 10.1093/hmg/ddu393

Arora, A., Byrem, T. M., Nair, M. G., and Strasburg, G. M. (2000). Modulation of liposomal membrane fluidity by flavonoids and isoflavonoids. *Arch. Biochem. Biophys.* 373, 102–109. doi: 10.1006/abbi.1999.1525

Beetz, C., Koch, N., Khundadze, M., Zimmer, G., Nietzsche, S., Hertel, N., et al. (2013). A spastic paraplegia mouse model reveals REEP1-dependent ER shaping. *J. Clin. Invest.* 124, 4273–4282. doi: 10.1172/JCI76634

Beetz, C., Schüle, R., Deconinck, T., Tran-Viet, K.-N., Zhu, H., Kremer, B. P. H., et al. (2008). REEP1 mutation spectrum and genotype/phenotype correlation in hereditary spastic paraplegia type 31. *Brain* 131, 1078. doi: 10.1093/BRAIN/AWN026

Belzil, V. V., and Rouleau, G. A. (2012). Endoplasmic reticulum lipid rafts and upper motor neuron degeneration. *Ann. Neurol.* 72, 479–480. doi: 10.1002/ana.23678

Björk, S., Hurt, C. M., Ho, V. K., and Angelotti, T. (2013). REEPs are membrane shaping adapter proteins that modulate specific g protein-coupled receptor trafficking by affecting ER cargo capacity. *PLoS One* 8:e76366. doi: 10.1371/journal.pone.0076366

Calfon, M., Zeng, H., Urano, F., Till, J. H., Hubbard, S. R., Harding, H. P., et al. (2002). IRE1 couples endoplasmic reticulum load to secretory capacity by processing the XBP-1 mRNA. *Nature* 415, 92–96. doi: 10.1038/415092a

Caputi, V., Marsilio, I., Cerantola, S., Roozfarakh, M., Lante, I., Galuppini, F., et al. (2017). Toll-like receptor 4 modulates small intestine neuromuscular function through nitrergic and purinergic pathways. *Front. Pharmacol.* 8:350. doi: 10.3389/fphar.2017.00350

Castellani, G., Paliuri, G., Orso, G., Paccagnella, N., D'Amore, C., Facci, L., et al. (2016). An intracellular adrenomedullin system reduces IL-6 release via a NF-kB-mediated, cAMP-independent transcriptional mechanism in rat thymic epithelial cells. *Cytokine* 88, 136–143. doi: 10.1016/j.cyto.2016.09.003

Chattopadhyay, D., Sen, S., Chatterjee, R., Roy, D., James, J., and Thirumurugan, K. (2016). Context- and dose-dependent modulatory effects of naringenin on survival and development of Drosophila melanogaster. *Biogerontology* 17, 383–393. doi: 10.1007/s10522-015-9624-6

Chen, C.-N., Chu, C.-C., Zentella, R., Pan, S.-M., and David Ho, T.-H. (2002). AtHVA22 gene family in *Arabidopsis*: phylogenetic relationship, ABA and stress regulation, and tissue-specific expression. *Plant Mol. Biol.* 49, 631–642. doi: 10.1023/A:1015593715144

Chen, R., Jin, R., Wu, L., Ye, X., Yang, Y., Luo, K., et al. (2011). Reticulon 3 attenuates the clearance of cytosolic prion aggregates via inhibiting autophagy. *Autophagy* 7, 205–216. doi: 10.4161/auto.7.2.14197

Chen, S., Novick, P., and Ferro-Novick, S. (2013). ER structure and function. *Curr. Opin. Cell Biol.* 25, 428–433. doi: 10.1016/j.ceb.2013.02.006

Chiang, W.-C., Hiramatsu, N., Messah, C., Kroeger, H., and Lin, J. H. (2012). Selective activation of ATF6 and PERK endoplasmic reticulum stress signaling pathways prevent mutant rhodopsin accumulation. *Invest. Opthalmol. Vis. Sci.* 53, 7159–7166. doi: 10.1167/iovs.12-10222

Credle, J. J., Finer-Moore, J. S., Papa, F. R., Stroud, R. M., and Walter, P. (2005). On the mechanism of sensing unfolded protein in the endoplasmic reticulum. *Proc. Natl. Acad. Sci. U.S.A.* 102, 18773–18784. doi: 10.1073/pnas.0509487102

Crimella, C., Cantoni, O., Guidarelli, A., Vantaggiato, C., Martinuzzi, A., Fiorani, M., et al. (2011). A novel nonsense mutation in the APTX gene associated with delayed DNA single-strand break removal fails to enhance sensitivity to different genotoxic agents. *Hum. Mutat.* 32, E2118–E2133. doi: 10.1002/humu.21464

Curti, V., Di Lorenzo, A., Rossi, D., Martino, E., Capelli, E., Collina, S., et al. (2017). Enantioselective modulatory effects of naringenin enantiomers on the expression levels of miR-17-3p involved in endogenous antioxidant defenses. *Nutrients* 9:215. doi: 10.3390/nu9030215

D'Amore, C., Orso, G., Fusi, F., Pagano, M. A., Miotto, G., Forgiarini, A., et al. (2016). An NBD derivative of the selective rat toxicant norbormide as a new probe for living cell imaging. *Front. Pharmacol.* 7:315. doi: 10.3389/fphar.2016.00315

De Craene, J.-O., Coleman, J., Estrada de Martin, P., Pypaert, M., Anderson, S., Yates, J. R., et al. (2006). Rtn1p is involved in structuring the cortical endoplasmic reticulum. *Mol. Biol. Cell* 17, 3009–3020. doi: 10.1091/mbc.E06-01-0080

de Oliveira, M. R., Brasil, F. B., and Andrade, C. M. B. (2017). Naringenin attenuates H_2O_2-induced mitochondrial dysfunction by an Nrf2-dependent mechanism in SH-SY5Y cells. *Neurochem. Res.* 42, 3341–3350. doi: 10.1007/s11064-017-2376-8

Di Francesco, L., Dovizio, M., Trenti, A., Marcantoni, E., Moore, A., O'Gaora, P., et al. (2015). Dysregulated post-transcriptional control of COX-2 gene expression in gestational diabetic endothelial cells. *Br. J. Pharmacol.* 172, 4575–4587. doi: 10.1111/bph.13241

Evans, K., Keller, C., Pavur, K., Glasgow, K., Conn, B., and Lauring, B. (2006). Interaction of two hereditary spastic paraplegia gene products, spastin and atlastin, suggests a common pathway for axonal maintenance. *Proc. Natl. Acad. Sci. U.S.A.* 103, 10666–10671. doi: 10.1073/pnas.0510863103

Falk, J., Rohde, M., Bekhite, M. M., Neugebauer, S., Hemmerich, P., Kiehntopf, M., et al. (2014). Functional mutation analysis provides evidence for a role of REEP1 in lipid droplet biology. *Hum. Mutat.* 35, 497–504. doi: 10.1002/humu.22521

Fantin, M., Garelli, F., Napoli, B., Forgiarini, A., Gumeni, S., De Martin, S., et al. (2019). Flavonoids regulate lipid droplets biogenesis in *Drosophila melanogaster*. *Nat. Prod. Commun.* 14:1934578X1985243. doi: 10.1177/1934578X19852430

Fischer, J., Lefèvre, C., Morava, E., Mussini, J.-M., Laforêt, P., Negre-Salvayre, A., et al. (2007). The gene encoding adipose triglyceride lipase (PNPLA2) is mutated in neutral lipid storage disease with myopathy. *Nat. Genet.* 39, 28–30. doi: 10.1038/ng1951

Floreani, M., Gabbia, D., Barbierato, M., De Martin, S., and Palatini, P. (2012). Differential inducing effect of benzo[a]pyrene on gene expression and enzyme activity of cytochromes P450 1A1 and 1A2 in Sprague-Dawley and Wistar rats. *Drug Metab. Pharmacokinet.* 27, 640–652. doi: 10.2133/dmpk.dmpk-12-rg-035

Forgiarini, A., Wang, Z., D'Amore, C., Jay-Smith, M., Li, F. F., Hopkins, B., et al. (2019). Live applications of norbormide-based fluorescent probes in *Drosophila melanogaster*. *PLoS One* 14:e0211169. doi: 10.1371/journal.pone.0211169

Frescas, D., Mavrakis, M., Lorenz, H., DeLotto, R., and Lippincott-Schwartz, J. (2006). The secretory membrane system in the *Drosophila* syncytial blastoderm embryo exists as functionally compartmentalized units around individual nuclei. *J. Cell Biol.* 173, 219–230. doi: 10.1083/jcb.200601156

Gao, K., Henning, S. M., Niu, Y., Youssefian, A. A., Seeram, N. P., Xu, A., et al. (2006). The citrus flavonoid naringenin stimulates DNA repair in prostate cancer cells. *J. Nutr. Biochem.* 17, 89–95. doi: 10.1016/j.jnutbio.2005.05.009

Goizet, C., Depienne, C., Benard, G., Boukhris, A., Mundwiller, E., Solé, G., et al. (2011). REEP1 mutations in SPG31: frequency, mutational spectrum, and potential association with mitochondrial morpho-functional dysfunction. *Hum. Mutat.* 32, 1118–1127. doi: 10.1002/humu.21542

Goyal, U., and Blackstone, C. (2013). Untangling the web: mechanisms underlying ER network formation. *Biochim. Biophys. Acta* 1833, 2492–2498. doi: 10.1016/j.bbamcr.2013.04.009

Griffing, L. R. (2018). "Dancing with the Stars: using image analysis to study the choreography of the endoplasmic reticulum and its partners and of movement within its tubules," in *The Plant Endoplasmic Reticulum. Methods in Molecular Biology*, Vol. 1691, eds C. Hawes, and V. Kriechbaumer, (New York, NY: Humana Press), 75–102. doi: 10.1007/978-1-4939-7389-7_7

Grumati, P., Morozzi, G., Hölper, S., Mari, M., Harwardt, M.-L. I., Yan, R., et al. (2017). Full length RTN3 regulates turnover of tubular endoplasmic reticulum via selective autophagy. *eLife* 6:e25555. doi: 10.7554/eLife.25555

Gumeni, S., Evangelakou, Z., Gorgoulis, V. G., and Trougakos, I. P. (2017). Proteome stability as a key factor of genome integrity. *Int. J. Mol. Sci.* 18:E2036. doi: 10.3390/ijms18102036

Halbleib, K., Pesek, K., Covino, R., Hofbauer, H. F., Wunnicke, D., Hänelt, I., et al. (2017). Activation of the unfolded protein response by lipid bilayer stress. *Mol. Cell* 67, 673–684.e8. doi: 10.1016/J.MOLCEL.2017.06.012

Hapala, I., Marza, E., and Ferreira, T. (2011). Is fat so bad? Modulation of endoplasmic reticulum stress by lipid droplet formation. *Biol. Cell* 103, 271–285. doi: 10.1042/BC20100144

Hegazy, H. G., Ali, E. H. A., and Sabry, H. A. (2016). The neuroprotective action of naringenin on oseltamivir (Tamiflu) treated male rats. *J. Basic Appl. Zool.* 77, 83–90. doi: 10.1016/j.jobaz.2016.12.006

Hetz, C. (2012). The unfolded protein response: controlling cell fate decisions under ER stress and beyond. *Nat. Rev. Mol. Cell Biol.* 13, 89–102. doi: 10.1038/nrm3270

Hsu, H.-T., Tseng, Y.-T., Lo, Y.-C., and Wu, S.-N. (2014). Ability of naringenin, a bioflavonoid, to activate M-type potassium current in motor neuron-like cells and to increase BKCa-channel activity in HEK293T cells transfected with α-hSlo subunit. *BMC Neurosci.* 15:135. doi: 10.1186/s12868-014-0135-1

Hu, J., Shibata, Y., Voss, C., Shemesh, T., Li, Z., Coughlin, M., et al. (2008). Membrane proteins of the endoplasmic reticulum induce high-curvature tubules. *Science* 319, 1247–1250. doi: 10.1126/science.1153634

Inagi, R., Ishimoto, Y., and Nangaku, M. (2014). Proteostasis in endoplasmic reticulum—new mechanisms in kidney disease. *Nat. Rev. Nephrol.* 10, 369–378. doi: 10.1038/nrneph.2014.67

Joardar, A., Menzl, J., Podolsky, T. C., Manzo, E., Estes, P. S., Ashford, S., et al. (2015). PPAR gamma activation is neuroprotective in a *Drosophila* model of ALS based on TDP-43. *Hum. Mol. Genet.* 24, 1741–1754. doi: 10.1093/hmg/ddu587

Joshi, R., Kulkarni, Y. A., and Wairkar, S. (2018). Pharmacokinetic, pharmacodynamic and formulations aspects of Naringenin: an update. *Life Sci.* 215, 43–56. doi: 10.1016/J.LFS.2018.10.066

Julien, C., Lissouba, A., Madabattula, S., Fardghassemi, Y., Rosenfelt, C., Androschuk, A., et al. (2016). Conserved pharmacological rescue of hereditary spastic paraplegia-related phenotypes across model organisms. *Hum. Mol. Genet.* 25, 1088–1099. doi: 10.1093/hmg/ddv632

Kassan, A., Herms, A., Fernández-Vidal, A., Bosch, M., Schieber, N. L., Reddy, B. J. N., et al. (2013). Acyl-CoA synthetase 3 promotes lipid droplet biogenesis in ER microdomains. *J. Cell Biol.* 203, 985–1001. doi: 10.1083/jcb.201305142

Khan, M. B., Khan, M. M., Khan, A., Ahmed, M. E., Ishrat, T., Tabassum, R., et al. (2012). Naringenin ameliorates Alzheimer's disease (AD)-type neurodegeneration with cognitive impairment (AD-TNDCI) caused by the intracerebroventricular-streptozotocin in rat model. *Neurochem. Int.* 61, 1081–1093. doi: 10.1016/j.neuint.2012.07.025

Lai, Y.-S., Stefano, G., and Brandizzi, F. (2014). ER stress signaling requires RHD3, a functionally conserved ER-shaping GTPase. *J. Cell Sci.* 127, 3227–3232. doi: 10.1242/jcs.147447

Lee, J. E., Oney, M., Frizzell, K., Phadnis, N., and Hollien, J. (2015). Drosophila melanogaster activating transcription factor 4 regulates glycolysis during endoplasmic reticulum stress. *G3* 5, 667–675. doi: 10.1534/g3.115.017269

Lim, Y., Cho, I.-T., Schoel, L. J., Cho, G., and Golden, J. A. (2015). Hereditary spastic paraplegia-linked REEP1 modulates endoplasmic reticulum/mitochondria contacts. *Ann. Neurol.* 78, 679–696. doi: 10.1002/ana.24488

Lindström, R., Lindholm, P., Kallijärvi, J., Palgi, M., Saarma, M., and Heino, T. I. (2016). Exploring the conserved role of MANF in the unfolded protein response in *Drosophila melanogaster*. *PLoS One* 11:e0151550. doi: 10.1371/journal.pone.0151550

Lo, Y. C., Tseng, Y. T., Hsu, H. T., Liu, C. M., and Wu, S. N. (2017). Naringenin protects motor neuron against methylglyoxal-induced neurotoxicity through activatinG IGF-1R-related neuroprotection. *J. Neurol. Sci.* 381, 616–617. doi: 10.1016/j.jns.2017.08.1737

Manchope, M. F., Casagrande, R., and Verri, W. A. Jr. (2017). Naringenin: an analgesic and anti-inflammatory citrus flavanone. *Oncotarget* 8, 3766–3767. doi: 10.18632/oncotarget.14084

Mandl, J., Mészáros, T., Bánhegyi, G., and Csala, M. (2013). Minireview: endoplasmic reticulum stress: control in protein, lipid, and signal homeostasis. *Mol. Endocrinol.* 27, 384–393. doi: 10.1210/me.2012-1317

McQuiston, A., and Diehl, J. A. (2017). Recent insights into PERK-dependent signaling from the stressed endoplasmic reticulum. *F1000Research* 6:1897. doi: 10.12688/f1000research.12138.1

Moreno, J. A., and Tiffany-Castiglioni, E. (2015). The chaperone Grp78 in protein folding disorders of the nervous system. *Neurochem. Res.* 40, 329–335. doi: 10.1007/s11064-014-1405-0

Mushtaq, Z., Choudhury, S. D., Gangwar, S. K., Orso, G., and Kumar, V. (2016). Human senataxin modulates structural plasticity of the neuromuscular junction in drosophila through a neuronally conserved TGFβ signalling pathway. *Neurodegener. Dis.* 16, 324–336. doi: 10.1159/000445435

Orso, G., Martinuzzi, A., Rossetto, M. G., Sartori, E., Feany, M., and Daga, A. (2005). Disease-related phenotypes in a *Drosophila* model of hereditary spastic paraplegia are ameliorated by treatment with vinblastine. *J. Clin. Invest.* 115, 3026–3034. doi: 10.1172/JCI24694

Orso, G., Pendin, D., Liu, S., Tosetto, J., Moss, T. J., Faust, J. E., et al. (2009). Homotypic fusion of ER membranes requires the dynamin-like GTPase atlastin. *Nature* 460, 978–983. doi: 10.1038/nature08280

O'Sullivan, N. C., Jahn, T. R., Reid, E., and O'Kane, C. J. (2012). Reticulon-like-1, the *Drosophila* orthologue of the Hereditary Spastic Paraplegia gene reticulon 2, is required for organization of endoplasmic reticulum and of distal motor axons. *Hum. Mol. Genet.* 21, 3356–3365. doi: 10.1093/hmg/dds167

Panche, A. N., Diwan, A. D., and Chandra, S. R. (2016). Flavonoids: an overview. *J. Nutr. Sci.* 5:e47. doi: 10.1017/jns.2016.41

Park, S. H., Zhu, P.-P., Parker, R. L., and Blackstone, C. (2010). Hereditary spastic paraplegia proteins REEP1, spastin, and atlastin-1 coordinate microtubule interactions with the tubular ER network. *J. Clin. Invest.* 120, 1097–1110. doi: 10.1172/JCI40979

Renvoisé, B., Malone, B., Falgairolle, M., Munasinghe, J., Stadler, J., Sibilla, C., et al. (2016). Reep1 null mice reveal a converging role for hereditary spastic paraplegia proteins in lipid droplet regulation. *Hum. Mol. Genet.* 25:ddw315. doi: 10.1093/hmg/ddw315

Richard, S., Lavie, J., Banneau, G., Voirand, N., Lavandier, K., and Debouverie, M. (2017). Hereditary spastic paraplegia due to a novel mutation of the REEP1 gene: case report and literature review. *Medicine* 96:e5911. doi: 10.1097/MD.0000000000005911

Rutkowski, D. T., and Kaufman, R. J. (2007). That which does not kill me makes me stronger: adapting to chronic ER stress. *Trends Biochem. Sci.* 32, 469–476. doi: 10.1016/J.TIBS.2007.09.003

Salehi, B., Fokou, P., Sharifi-Rad, M., Zucca, P., Pezzani, R., Martins, N., et al. (2019). The therapeutic potential of Naringenin: a review of clinical trials. *Pharmaceuticals* 12:11. doi: 10.3390/ph12010011

Sanderson, C. M., Connell, J. W., Edwards, T. L., Bright, N. A., Duley, S., Thompson, A., et al. (2006). Spastin and atlastin, two proteins mutated in autosomal-dominant hereditary spastic paraplegia, are binding partners. *Hum. Mol. Genet.* 15, 307–318. doi: 10.1093/hmg/ddi447

Sangpheak, W., Kicuntod, J., Schuster, R., Rungrotmongkol, T., Wolschann, P., Kungwan, N., et al. (2015). Physical properties and biological activities of hesperetin and naringenin in complex with methylated β-cyclodextrin. *Beilstein J. Org. Chem.* 11, 2763–2773. doi: 10.3762/bjoc.11.297

Scheper, W., and Hoozemans, J. J. M. (2015). The unfolded protein response in neurodegenerative diseases: a neuropathological perspective. *Acta Neuropathol.* 130, 315–331. doi: 10.1007/s00401-015-1462-8

Schlang, K. J., Arning, L., Epplen, J. T., and Stemmler, S. (2008). Autosomal dominant hereditary spastic paraplegia: novel mutations in the REEP1 gene (SPG31). *BMC Med. Genet.* 9:71. doi: 10.1186/1471-2350-9-71

Schuck, S., Prinz, W. A., Thorn, K. S., Voss, C., and Walter, P. (2009). Membrane expansion alleviates endoplasmic reticulum stress independently of the unfolded protein response. *J. Cell Biol.* 187, 525–536. doi: 10.1083/jcb.200907074

Shulman, M., Cohen, M., Soto-Gutierrez, A., Yagi, H., Wang, H., Goldwasser, J., et al. (2011). Enhancement of naringenin bioavailability by complexation with Hydroxypropoyl-β-Cyclodextrin. *PLoS One* 6:e18033. doi: 10.1371/journal.pone.0018033

Shyu, P. Jr., Wong, X. F. A., Crasta, K., and Thibault, G. (2018). Dropping in on lipid droplets: insights into cellular stress and cancer. *Biosci. Rep.* 38:BSR20180764. doi: 10.1042/BSR20180764

Song, H. M., Park, G. H., Eo, H. J., and Jeong, J. B. (2016). Naringenin-mediated ATF3 expression contributes to apoptosis in human colon cancer. *Biomol. Ther. (Seoul).* 24, 140–146. doi: 10.4062/biomolther.2015.109

Summerville, J. B., Faust, J. F., Fan, E., Pendin, D., Daga, A., Formella, J., et al. (2016). The effects of ER morphology on synaptic structure and function in *Drosophila melanogaster*. *J. Cell Sci.* 129, 1635–1648. doi: 10.1242/jcs.184929

Tan, J. S. Y., Seow, C. J. P., Goh, V. J., and Silver, D. L. (2014). Recent advances in understanding proteins involved in lipid droplet formation, growth and fusion. *J. Genet. Genomics* 41, 251–259. doi: 10.1016/j.jgg.2014.03.003

Tang, J.-Y., Jin, P., He, Q., Lu, L.-H., Ma, J.-P., Gao, W.-L., et al. (2017). Naringenin ameliorates hypoxia/reoxygenation-induced endoplasmic reticulum stress-mediated apoptosis in H9c2 myocardial cells: involvement in ATF6, IRE1α and PERK signaling activation. *Mol. Cell. Biochem.* 424, 111–122. doi: 10.1007/s11010-016-2848-1

Tsaytler, P., Harding, H. P., Ron, D., and Bertolotti, A. (2011). Selective inhibition of a regulatory subunit of protein phosphatase 1 restores proteostasis. *Science* 332, 91–94. doi: 10.1126/science.1201396

Volmer, R., van der Ploeg, K., and Ron, D. (2013). Membrane lipid saturation activates endoplasmic reticulum unfolded protein response transducers through their transmembrane domains. *Proc. Natl. Acad. Sci. U.S.A.* 110, 4628–4633. doi: 10.1073/pnas.1217611110

Wang, C.-W. (2016). Lipid droplets, lipophagy, and beyond. *Biochim. Biophys. Acta Mol. Cell Biol. Lipids* 1861, 793–805. doi: 10.1016/J.BBALIP.2015.12.010

Wang, G.-Q., Zhang, B., He, X.-M., Li, D.-D., Shi, J.-S., and Zhang, F. (2019). Naringenin targets on astroglial Nrf2 to support dopaminergic neurons. *Pharmacol. Res.* 139, 452–459. doi: 10.1016/j.phrs.2018.11.043

Wang, K., Chen, Z., Huang, L., Meng, B., Zhou, X., Wen, X., et al. (2017). Naringenin reduces oxidative stress and improves mitochondrial dysfunction via activation of the Nrf2/ARE signaling pathway in neurons. *Int. J. Mol. Med.* 40, 1582–1590. doi: 10.3892/ijmm.2017.3134

Wang, N., and Rapoport, T. A. (2019). Reconstituting the reticular ER network – mechanistic implications and open questions. *J. Cell Sci.* 132:jcs227611. doi: 10.1242/jcs.227611

Yalçın, B., Zhao, L., Stofanko, M., O'Sullivan, N. C., Kang, Z. H., Roost, A., et al. (2017). Modeling of axonal endoplasmic reticulum network by spastic paraplegia proteins. *eLife* 6:e23882. doi: 10.7554/eLife.23882

Yoshida, H., Matsui, T., Yamamoto, A., Okada, T., and Mori, K. (2001). XBP1 mRNA is induced by ATF6 and spliced by IRE1 in response to ER stress to produce a highly active transcription factor. *Cell* 107, 881–891. doi: 10.1016/S0092-8674(01)00611-0

Yu, Y., Li, Z., Cao, G., Huang, S., and Yang, H. (2019). Bamboo leaf flavonoids extracts alleviate oxidative stress in HepG2 cells via naturally modulating reactive oxygen species production and Nrf2-mediated antioxidant defense responses. *J. Food Sci.* 84, 1609–1620. doi: 10.1111/1750-3841.14609

Zeng, X., Xi, Y., and Jiang, W. (2019). Protective roles of flavonoids and flavonoid-rich plant extracts against urolithiasis: a review. *Crit. Rev. Food Sci. Nutr.* 59, 2125–2135. doi: 10.1080/10408398.2018.1439880

Zhang, H., and Tsao, R. (2016). Dietary polyphenols, oxidative stress and antioxidant and anti-inflammatory effects. *Curr. Opin. Food Sci.* 8, 33–42. doi: 10.1016/j.cofs.2016.02.002

Zheng, P., Chen, Q., Tian, X., Qian, N., Chai, P., Liu, B., et al. (2018). DNA damage triggers tubular endoplasmic reticulum extension to promote apoptosis by facilitating ER-mitochondria signaling. *Cell Res* 28, 833–854. doi: 10.1038/s41422-018-0065-z

Züchner, S., Wang, G., Tran-Viet, K.-N., Nance, M. A., Gaskell, P. C., Vance, J. M., et al. (2006). Mutations in the novel mitochondrial protein REEP1 cause hereditary spastic paraplegia type 31. *Am. J. Hum. Genet.* 79, 365–369. doi: 10.1086/505361

Conflict of Interest: The authors declare that the research was conducted in the absence of any commercial or financial relationships that could be construed as a potential conflict of interest.

frontiers in Neuroscience

SYSTEMATIC REVIEW
published: 10 December 2019
doi: 10.3389/fnins.2019.01311

Swimming in Deep Water: Zebrafish Modeling of Complicated Forms of Hereditary Spastic Paraplegia and Spastic Ataxia

Valentina Naef[1†], *Serena Mero*[1,2†], *Gianluca Fichi*[1,3†], *Angelica D'Amore*[1,2,4], *Asahi Ogi*[1,5], *Federica Gemignani*[2], *Filippo M. Santorelli*[1*] and *Maria Marchese*[1*]

[1] Neurobiology and Molecular Medicine, IRCCS Stella Maris, Pisa, Italy, [2] Department of Biology, University of Pisa, Pisa, Italy, [3] Struttura Complessa Toscana Sud (Sede Grosseto), Istituto Zooprofilattico Sperimentale del Lazio e Toscana M. Aleandri, Grosseto, Italy, [4] Department of Neurology, The F.M. Kirby Neurobiology Center, Boston Children's Hospital, Harvard Medical School, Boston, MA, United States, [5] Department of Veterinary Sciences, University of Pisa, Pisa, Italy

OPEN ACCESS

Edited by:
Andrea Martinuzzi,
Eugenio Medea (IRCCS), Italy

Reviewed by:
Genny Orso,
University of Padova, Italy
Chiara F. Valori,
German Center for Neurodegenerative Diseases (DZNE), Germany

***Correspondence:**
Filippo M. Santorelli
filippo3364@gmail.com
Maria Marchese
maria.marchese2086@gmail.com

[†] These authors have contributed equally to this work

Specialty section:
This article was submitted to Neurodegeneration, a section of the journal Frontiers in Neuroscience

Received: 03 September 2019
Accepted: 22 November 2019
Published: 10 December 2019

Citation:
Naef V, Mero S, Fichi G, D'Amore A, Ogi A, Gemignani F, Santorelli FM and Marchese M (2019) Swimming in Deep Water: Zebrafish Modeling of Complicated Forms of Hereditary Spastic Paraplegia and Spastic Ataxia. Front. Neurosci. 13:1311. doi: 10.3389/fnins.2019.01311

Hereditary spastic paraplegia (HSP) and hereditary ataxia (HA) are two groups of disorders characterized, respectively, by progressive dysfunction or degeneration of the pyramidal tracts (HSP) and of the Purkinje cells and spinocerebellar tracts (HA). Although HSP and HA are generally shown to have distinct clinical-genetic profiles, in several cases the clinical presentation, the causative genes, and the cellular pathways and mechanisms involved overlap between the two forms. Genetic analyses in humans in combination with *in vitro* and *in vivo* studies using model systems have greatly expanded our knowledge of spinocerebellar degenerative disorders. In this review, we focus on the zebrafish (*Danio rerio*), a vertebrate model widely used in biomedical research since its overall nervous system organization is similar to that of humans. A critical analysis of the literature suggests that zebrafish could serve as a powerful experimental tool for molecular and genetic dissection of both HA and HSP. The zebrafish, found to be very useful for demonstrating the causal relationship between defect and mutation, also offers a useful platform to exploit for the development of therapies.

Keywords: zebrafish, hereditary ataxia (HA), hereditary spastic paraplegia (HSP), neurodegenerative disorders, motor neuron disease

INTRODUCTION

The term hereditary spastic paraplegia (HSP) refers to a large group of clinically and genetically heterogeneous neurodegenerative diseases, essentially characterized by progressive spasticity and weakness, mainly affecting the lower limbs (Bellofatto et al., 2019; Boutry et al., 2019a; Peng et al., 2019). The clinical classification of HSP includes pure and complicated forms (Harding, 1983), the latter defined by the presence of additional extra-neurological and neurological symptoms, including minor sensory disturbances and hypertonic bladder, retinal changes, and gastroesophageal reflux with persistent vomiting. At times, however, the clinical manifestations can be relatively homogenous within single families (Hensiek et al., 2015; Boutry et al., 2019a; Elert-Dobkowska et al., 2019; Peng et al., 2019). Genetically, HSP can be inherited by any mode of inheritance: autosomal-dominant (AD-HSP), autosomal-recessive (AR-HSP), X-linked, and maternally inherited forms have been described, the latter mainly presenting with complicated

clinical phenotypes (Parodi et al., 2017). The prevalence of HSP has been estimated to range from 1.2 to 9.6 per 100,000 individuals (Ruano et al., 2014). Due to the vast genetic diversity of HSP, researchers have turned to the zebrafish, considered a potentially powerful experimental tool for uncovering genotype/phenotype correlations, on account of its having a nervous system organization very similar to that of humans. Pure HSP is characterized by slowly progressive lower extremity spasticity and weakness often associated with urinary disturbances and sensory abnormalities, and it usually shows autosomal dominant inheritance.

Pathologically, the neurodegeneration characterizing HSP is a progressive distal axonopathy of the corticospinal tract and posterior columns in the spinal cord (Salinas et al., 2008; Parodi et al., 2017; Synofzik and Schüle, 2017), in other words a dying-back degeneration that progresses from the distal end of the axons (Boutry et al., 2019b). The axons involved in this degeneration are commonly characterized by a unique, highly polarized architecture (Boutry et al., 2019b). This evidence, together with the discovery that genes involved in axonal transport, intracellular trafficking, and mitochondrial functions are implicated in HSP, suggests that abnormalities in these processes play a role in HSP. However, in complicated HSP, the fact that the neurodegeneration can also involve the cerebellum, cerebral cortex, corpus callosum, and basal ganglia (Hensiek et al., 2015) suggests the involvement of other pathological mechanisms (Boutry et al., 2019b). The identification of other HSP causative genes, together with the discovery of the function of the related proteins, has made it possible to hypothesize at least 10 functional "modes of action" that could play a role in HSP pathogenesis, and also appear to be involved in other neurological disorders: namely, dysfunction of axonal transport, abnormal membrane trafficking and organelle shaping, abnormal endosome membrane trafficking and vesicle formation, oxidative stress, abnormal lipid metabolism, abnormal DNA repair, dysregulation of myelination, autophagy, impairment of axonal development, and abnormal cellular signaling in protein morphogenesis (Lo Giudice et al., 2014; Boutry et al., 2019b). The various forms of HSP, as well as the groups of similar neurodegenerative diseases, such as hereditary ataxia (HA), spinocerebellar ataxia (SCA), autosomal-recessive spinocerebellar ataxia (SCAR), and spastic paraplegia, can be due to mutations in either the spastic paraplegia gene (SPG) or the spastic ataxia genes (SPAX). Clinically, they can present as pure or complicated phenotypes (Synofzik and Schüle, 2017). Formally, HSP and HA are characterized, respectively, by progressive dysfunction or degeneration of the pyramidal tracts (HSP) and of the Purkinje cells and spinocerebellar tracts (HA) (Synofzik and Schüle, 2017). In recent years, genes that cause both cerebellar and pyramidal phenotypes have been discovered, and some genes classified among the HA causative genes have been found to cause HSP phenotypes, too, and vice versa (Galatolo et al., 2018). Furthermore, it is possible that HSP and HA could also share certain pathological mechanisms and cellular pathways. For all these reasons, a new classification of ataxia-spasticity spectrum (ASS) genes has recently been proposed (Synofzik and Schüle, 2017). In the next generation-sequencing era, more than 80 known SPG causative genes and 85 different spastic gait disease loci have been identified as responsible for HSP, some of them very rare and found in few families. However, unusual phenotypes have been described and a larger than expected continuum between the different forms of HSP and other neurodegenerative diseases has been demonstrated (Novarino et al., 2014; Hensiek et al., 2015; Klebe et al., 2015; D'Amore et al., 2018; Galatolo et al., 2018).

In recent years, the zebrafish has emerged as an attractive model for studying human genetic disorders such as HSP, in spite of the existence of key differences between neuroanatomy of the human vs. the zebrafish motor system (Babin et al., 2014), for example, the absence of corticospinal and rubrospinal tracts in the zebrafish central nervous system (CNS). Although this model is limited by its capacity to reproduce only partially the spasticity and the key diagnostic clinical features of the human HSP disorders, the zebrafish remains an indispensable vertebrate model and a valuable tool for the molecular and genetic dissection of HSP mechanisms *in vivo* (Patten et al., 2014). Indeed, the zebrafish offers several key embryological and experimental advantages, including its small size and the optical transparency that allows visualization of cell- and system-level processes in early developmental stages; it also offers a range of quantifiable behavioral responses, which facilitates functional studies. However, the real power of the zebrafish lies in the availability of a very rich collection of mutants and transgenic lines in which is possible to observe the cellular and subcellular events leading to the pathology (Orger and de Polavieja, 2017; Basnet et al., 2019). In this way, the functional connection between a human pathological mutation and disease can be tested experimentally, provided an ortholog with a conserved function has been identified in the model organism (Dahlem et al., 2012; Hwang et al., 2013).

Using zebrafish, it is easy to induce gain or loss of function of the HSP-related genes. By exploiting strategies designed to obtain transient or stable genetic changes, it is possible to characterize and define *in vivo* the function and the role of genes found to be mutated in HSP patients (**Figure 1**). The majority of previous works reported a transient knockdown approach involving the use of antisense oligonucleotides (morpholinos, MOs) (e.g., Nasevicius and Ekker, 2000), in order to validate the effects of gene variants through morphant phenotype rescue experiments based on injection of the human, or zebrafish, wild-type transcript and the mutated version. On the contrary, few mutant genetic models of HSP have been generated. Generally, the lack of function of HSP-related genes leads to major motor neuron defects with greatly impaired locomotion. The morphant phenotype can be rescued through injection of the human, mouse, or zebrafish wild-type transcript. Use of the zebrafish model would seem to be essential in order to close the gap between *in vitro* studies and more costly (in terms of both money and animal distress) assays in mammals, and also in order to develop possible new therapeutic avenues.

With reference, mainly, to the mode of inheritance-based genetic classification of HSP, we here review the HSP genes studied in zebrafish, recalling the original contributions and

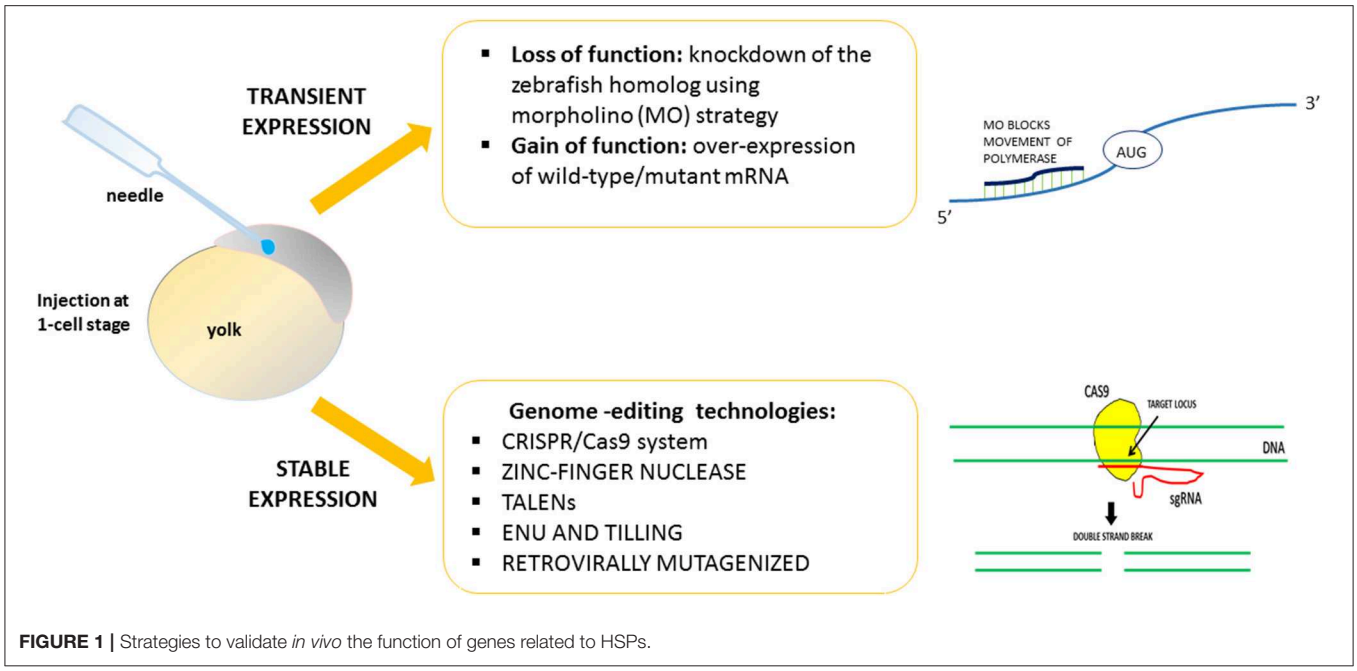

FIGURE 1 | Strategies to validate *in vivo* the function of genes related to HSPs.

highlighting the recent discoveries that might help to elucidate the functional effects of human HSP-related mutations. In addition, to further expand our review, we also consider genes classified as part of the ASS spectrum and not routinely included in the formal HSP classifications.

MATERIALS AND METHODS

The PubMed database was queried using the following three search strings: <<zebrafish [All Fields]>> AND <<hereditary spastic paraplegia [All Fields]>>, OR <<zebrafish [All Fields]>> AND <<spasticity [All Fields]>>, OR <<zebrafish>> AND <<paraplegia [All Fields]>>. Articles retrieved by the literature search had to be full-text articles written in English, and they had to have been published by May 31, 2019. Application of the three strings yielded 33, 14, and 39 publications, respectively. We then performed a manual search of the references listed in publications found to discuss HSP in relation to the use of zebrafish. After excluding all articles not reporting direct research on zebrafish and HSP, 42 articles remained for inclusion in the review (see **Figure 2** for a scheme of the methodology).

AUTOSOMAL DOMINANT COMPLICATED HSP GENES

To date, eight complicated HSP genes showing an autosomal dominant pattern of inheritance have been studied in zebrafish, namely: SPG3A, SPG4, SPG33, SPG10, SPG8, SPG17, SPG42, and SPG80.

SPG3A

Fassier et al. (2010) generated an *atlastin-1* (*atl1*) morphant zebrafish model (mutations in *ATL1*/SPG3A are the second most common cause of HSP in humans). Atlastin-1 is a protein implicated in the vesicle trafficking and neurite outgrowth (Zhu, 2006; Orso et al., 2009; Kadnikova et al., 2019).

ATL1 has been shown to be a major locus for early-onset autosomal dominant pure and complicated forms of HSP (Scarano et al., 2005; Fusco et al., 2010). More than 95% of individuals diagnosed with SPG3A have an affected parent, while the proportion of cases arising *de novo*, and is not fully known. The gene encodes a member of the dynamin superfamily of large GTPases (Zhao et al., 2001) and it is predominantly expressed in the mammalian brain, in particular at the level of hippocampus and pyramidal neurons (Zhu et al., 2003). Fassier et al. (2010) demonstrated expression of the gene at the level of motor neurons during early CNS development. Loss of *atl1* led to a dramatic reduction of larval motility in combination with increased branching of spinal motor axons (**Table 1**). This phenotype seemed to be specific to motor and cerebellar neurons and it was rescued by injection of human *ATL1* mRNA (Fassier et al., 2010). Therefore, overexpression of human *ATL1* or zebrafish *atl1* mRNA was shown to inhibit bone morphogenetic protein (BMP) signaling leading to complete loss of ventral structures. This idea was also supported by the co-localization of Alt1 and type I BMP receptor in endosomal structures along neurites. In addition, the phenotypes observed in *atl1* morphant embryos were recovered pharmacologically, by inhibiting the BMP pathway at the receptor level during the late embryonic stage. The recovery of the motility and axonal phenotype observed in this *atl1* knockdown model suggested that BMP plays a key role in *atl1*-dependent HSP (Fassier et al., 2010).

SPG4 and SPG33

SPAST (the SPG4 gene) encodes spastin, a microtubule-severing protein that belongs to the AAA (ATPase associated with various cellular activities) family of ATPase and regulates the

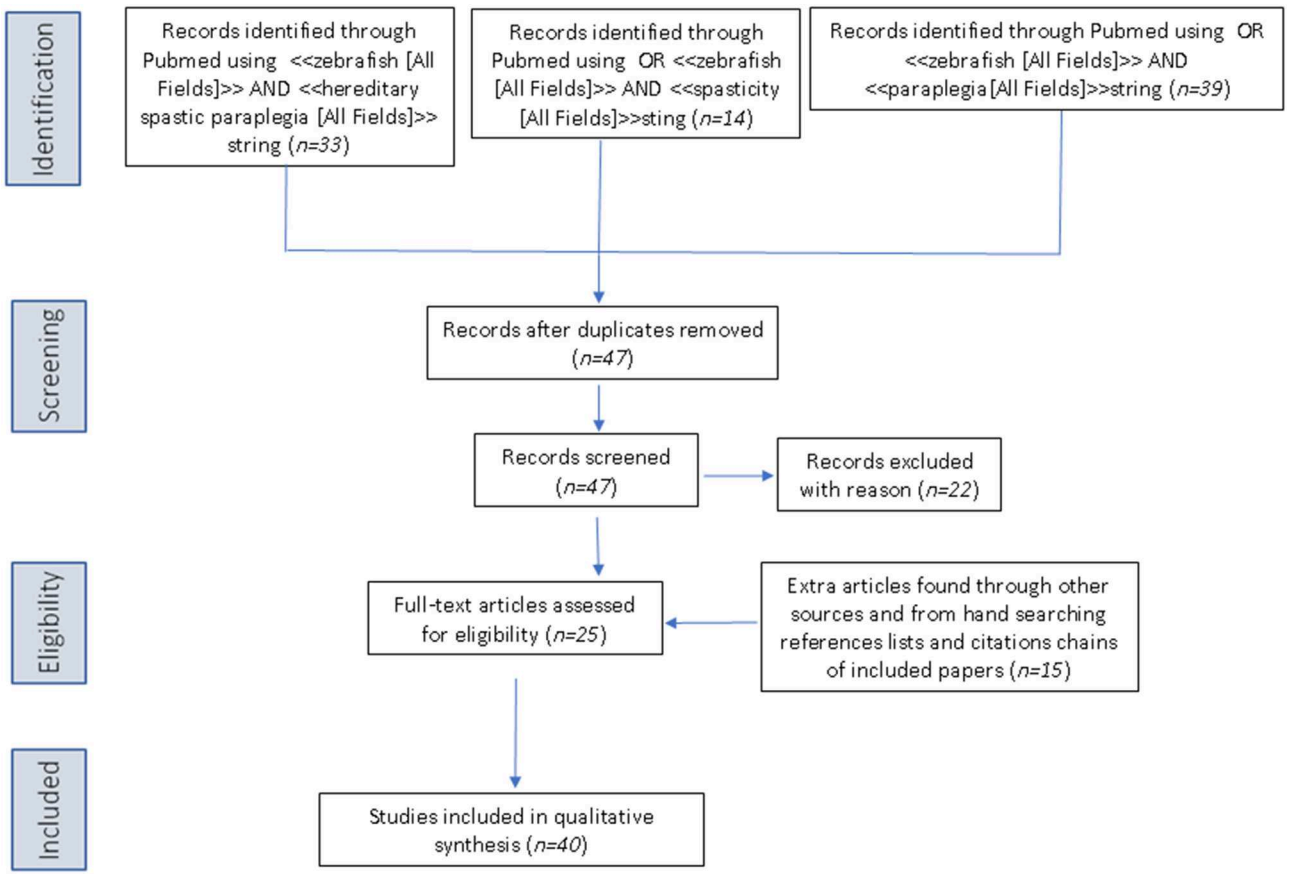

FIGURE 2 | PRISMA flow diagram for literature research.

number and mobility of microtubules (Kadnikova et al., 2019). In addition, spastin is involved in the early secretory pathway and in BMP signaling (Evans et al., 2005; Salinas et al., 2005; Connell et al., 2009; Zhao and Hedera, 2013). Haploinsufficiency is the prevalent opinion as to the mechanism of the disease, but gain-of-function toxicity of the mutant proteins is another possibility (Qiang et al., 2019).

Mutations in SPG4 are associated with 40% of cases of autosomal dominant HSP. *SPAST* is required for motor axon morphogenesis and function during embryonic development. In zebrafish, *spast* morphants displayed dramatic defects in motor axon outgrowth and were morphologically abnormal with impaired motility (**Table 1**) compared with control embryos (Wood, 2006). Moreover, *SPAST* promotes neurite outgrowth in a protrudin (*ZFYVE27*)-dependent way. In fact, *ZFYVE27* (the SPG33 gene, also termed *PROTRUDIN*) is another gene whose mutations cause autosomal dominant HSP (Hashimoto et al., 2014). Double-morphant zebrafish (i.e., with mutation of both *spast* and *protrudin*) showed impaired head and yolk sac extension with a curly tail phenotype that was more severe than in fish injected with MOs specific for single transcripts. These phenotypes were partially rescued by wild-type human *SPAST* or *PROTRUDIN* overexpression (Zhang et al., 2012). Furthermore, a pharmacological study in *spast* morphants showed partial rescue of the morphological phenotype, the microtubule defects (**Table 1**), and the high levels of oxidative stress (typical of HSP disease) through ER-modulating drugs, such as methylene blue and salubrinal, and, to a lesser extent, guanabenz, and phenazine (Julien et al., 2015). In 2018, two *spast* isoforms (DrM1 and DrM61) were identified in zebrafish. Knockdown of each of these isoforms led to different motor neuron and locomotion defects, not rescued by the selective expression of the other isoform. Indeed, the expression and the distribution of the two isoforms were found to differ in zebrafish embryos. Isoform-specific knockdown led to morphants with distinctive characteristics: MO-*DrM1* morphants displayed a curved tail, whereas MO-*DrM61* morphants showed smaller eyes and yolk tube agenesis. In both cases, the embryos failed to hatch from their chorion and at t 72 hpf the larvae showed locomotion defects and secondary motor neuron axon pathfinding defects (**Table 1**). These results were more recently confirmed in *spast* mutant zebrafish strain harboring a truncating mutation after the second ATG codon, that impedes the synthesis of both DrM1 and DrM61 spastin isoforms (**Table 1**; Jardin et al., 2018).

TABLE 1 | Phenotype description of zebrafish models for HSP studies.

Human genes	Zebrafish genes	Zebrafish modeling	Phenotype			References
			Life cycle	Behavior	Morphology	
AUTOSOMAL DOMINANT HSP GENES						
SPG3A/*ATL1*	*atl1*	Morphant		Reduction of larval motility	Increased branching of spinal motor axons	Fassier et al., 2010
		Overexpression			Inhibition of BMP signaling with complete loss of ventral structures	Fassier et al., 2010
SPG4/*SPAST*	*spast*	Morphant		Impaired motility	Dramatic defects in motor axon outgrowth, curved tail, shorter and more disordered axons with aberrant position of branchiomotor neuron cell bodies	Wood, 2006
	spast	Morphant			Disorganized microtubule networks in the spinal cord, thinner microtubules in the spinal motor neuron axon	Julien et al., 2015
	spast	DrM1 morphant	Embryos failed to hatch from their chorion	Locomotion defects with reduced swimming speed and distances covered	Curved tail	Jardin et al., 2018
	spast	DrM61 morphant	Embryos failed to hatch from their chorion	Locomotion defects with reduced swimming speed and distances covered	Smaller eyes, yolk tube agenesis	Jardin et al., 2018
	spast	DrM1 and DrM61 mutant		Reduced swimming speed	Pathfinding defects of spinal motor neurons axons	Jardin et al., 2018
SPG33/*PROTRUDIN*	*protrudin*	Double morphant (*spast* and *protrudin*) together			Impaired head and yolk sac extension, curly tail	Zhang et al., 2012
SPG10/*KIF5A*	*kif5Aa*	Mutant	Larval lethality	Hyperexcitability, diminished touch response	Sensorimotor deficits, peripheral polyneuropathy, degeneration of peripheral sensory axons, inflated swim bladder, increased lateral, and dorsal pigmentation	Campbell et al., 2014
	kif5Aa	Mutant	Death at 10 days post-fertilization	Failed to inflate swim bladder	Darker embryos with expanded melanosomes	Auer et al., 2015
SPG8/*WASHC5*	*spg8*	Morphant			Slight or severe curly tail, enlarged heart cavities, abnormal development of motor neurons and interneurons in the spinal cord with irregular branching	Valdmanis et al., 2006
	spg8	Morphant		Short shiver response to tactile stimulation	Pericardial edema, severe skeletal muscle dysfunction, curved tails, reduction of the caudal neuronal tube, complete abolition of ventral and caudal motor neurons	Clemen et al., 2010
SPG17/*BSCL2*	*seipin*	Mutant		Decrease in spontaneous swimming	No motor neurons loss or morphological abnormalities	Holtta-Vuori et al., 2013
SPG42/*SLC33A1*	*slc33a1*	Morphant			Curly tails, defective axon outgrowth from spinal cord, scarce and poorly organized motor axons	Lin et al., 2008; Mao et al., 2015
SPG80/*UBAP1*	*ubap1*	Mutant			Misshapen axon and shorter motor neuron length	Farazi Fard et al., 2019
AUTOSOMAL RECESSIVE HSP GENES						
ALS2/*ALSIN*	*als2*	Morphant		Behavioral abnormalities, swimming defects	Irregular motor neuron outgrowth in the spinal cord	Gros-Louis et al., 2008

(Continued)

TABLE 1 | Continued

Human genes	Zebrafish genes	Zebrafish modeling	Phenotype			References
			Life cycle	Behavior	Morphology	
SPG11/*KIAA1840*	*spg11*	Morphant			Abnormal axon outgrowth, enlarged heart cavity, curly tail, deformities of the fin, CNS abnormalities	Martin et al., 2012
	spg11	Morphant			Perturbation of neuronal differentiation	Southgate et al., 2010
	spg11	Morphant		Loss of motility and paralysis	Accumulation of simple gangliosides in lysosomes	Boutry et al., 2018
SPG15/ZFYVE26	*suf*	Morphant		Motor impairment	Motor axon outgrowth failure	Martin et al., 2012; Kanagaraj et al., 2014
	suf	Mutant suf$^{(-/-)}$	No phenotype	No phenotype	No phenotype	Kanagaraj et al., 2014
SPG39/*PNPLA6*	*pnpla6*	Morphant			Developmental abnormalities, fewer motor neurons, abnormal axons, curly tail, aberrant eyes, reduced optic vesicle size	Song et al., 2013
	pnpla6	Morphant			Body curvature, small head, and eyes	Hufnagel et al., 2015
SPG46/*GBA2*	*gba2*	Morphant		Locomotor phenotype	Curvy tail, axonal shortening/branching of motor neurons	Martin et al., 2013
SPG53/*VPS37A*	*vps37a*	Morphant		Striking and significant loss of motility		Zivony-Elboum et al., 2012
SPG76/*CAPN1*	*capn1a*				Abnormal branchiomotor neuron migration, disorganized axonal networks	Gan-Or et al., 2016
SPOAN/*KLC2*	*kcl2*	Overexpression morphant	High mortality		Curly-tail phenotype	Melo et al., 2015
PCYT2	*pcyt2*	Mutant *pcyt2_3*	Larval lethality			Vaz et al., 2019
	pcyt2	Mutant *pcyt2_13*			Smaller overall size and abnormal tail-fin morphology	Vaz et al., 2019
OTHER FORMS OF HSP						
ARL6IP1, PGAP1, and *USP8*	*arl6ip1, pgap1,* and *usp8*	Morphants		Reduction of larval movement	Curvy tail, abnormal branching of spinal motor neuron axons	Novarino et al., 2014
MARS	*mars*	Morphant			Too severe to be analyzed	Novarino et al., 2014
X-LINKED FORMS						
SPG1/L1CAM	*l1.1*	Morphant			Hydrocephalus, defects in axonal outgrowth, myelination abnormalities	Linneberg et al., 2019
SPG22/*MCT8*	*mct8*	Mutant *mct8*$^{(-/-)}$		Impaired locomotor activity, decreased response to external stimuli	Defects in neural circuit assembly, alteration in the expression of myelin-related genes	Zada et al., 2014, 2016
ATAXIA-SPASTIC SPECTRUM (ASS) GENES						
SCA3/*ATXN3*	*sca3*	Mutant EGFP-Ataxin 3 84Q	Shorter mean survival time	Shorter swimming distance, signs of ataxin-3 neuropathology	Decreased axonal length of motor neurons	Watchon et al., 2017
	sca3	Mutant EGFP-Ataxin 3 23Q	Shorter mean survival time			Watchon et al., 2017

(Continued)

TABLE 1 | Continued

Human genes	Zebrafish genes	Zebrafish modeling	Phenotype			References
			Life cycle	Behavior	Morphology	
ABCD1	*abcd1*	Mutant abcd1sa509	Reduced larval survival	Decrease in larval evoked response, reduced swim distance, velocity, and time spent moving in spontaneous swimming in adult	Reduction of myelination of axons, increased apoptosis in the brain	Strachan et al., 2017
EXOSC3	*exosc3*	Morphant	Premature death	Poor motility	Small brain, short curved spine and reduced expression of dorsal hindbrain progenitor and cerebellar specific markers	Wan et al., 2012
PRNP/Prp	*prp1*	Morphant	High mortality		Defective midbrain and hindbrain development	Nourizadeh-Lillabadi et al., 2010
	prp2	Morphant	High mortality		Defective midbrain and hindbrain development, aberrant morphology of the trigeminal ganglion, reduced number of peripheral neurons	Nourizadeh-Lillabadi et al., 2010
PSEN1 and *PSEN2*	*psen1, psen2*	Morphant			Shorter tail, disruption of posterior somite formation and smaller head-eye and total size, hydrocephalus	Campbell et al., 2006
	psen1, psen2	Double morphants			Embryos co-injected with Pen-2 MO and Pen-2 RNA appears morphologically normal	Campbell et al., 2006
	psen1	Morphant			Expanded hindbrain and midbrain ventricular spaces, absent yolk extension and increased yolk ball size, fewer and smaller melanocytes, decreased pigmentation, increased head angle, thinner spinal cord, smaller larva size, hydrocephalus	Nornes et al., 2008
	psen2	Morphant			Expanded hindbrain and midbrain ventricular spaces, absent yolk extension and increased yolk ball size, fewer and smaller melanocytes, decreased pigmentation, increased head angle, thinner spinal cord, smaller larva size, hydrocephalus	Nornes et al., 2008
	psen1	Morphant		Specific cognitive deficits in response behavior (reduced capacity to follow a non-aversive visual stimulus) and aversive behavior (reduced escape response)	Pericardial and brain edema, blood accumulation, aberrations in yolk extension, eye, and tail malformations	Nery et al., 2017
NPC1	*npc1*	Morphant	Premature death, before 2 dpf			Schwend et al., 2011
	npc1	Morphant	Premature death at 5 dpf			Louwette et al., 2013

(Continued)

TABLE 1 | Continued

Human genes	Zebrafish genes	Zebrafish modeling	Phenotype			References
			Life cycle	Behavior	Morphology	
	npc1	Mutant	High mortality during embryonic or juvenile stages	Ataxia symptoms in swimming at 4 dpf	Slower length growth, loss of Purkinje cells in cerebellum at 4 dpf	Lin et al., 2018
	npc1	Mutant	Early death between 8 and 12 dpf in larvae, inability to reproduce in adults	A swimming defect of balance with inability to maintain upright position in adult	Diffuse Purkinje cells, dark liver phenotype	Tseng et al., 2018

SPG10

SPG10/*KIF5A* is responsible for HSP in about 3% of families with a dominant form of the disease. *KIF5A* codes for the kinesin heavy chain of the main neuronal motor protein involved in long-distance axonal transport (Hirokawa et al., 2010). Due to a genome-wide duplication event, zebrafish possess two kinesin 5a genes, *kif5Aa* and *kif5Ab*, which have an overlapping expression that is strictly zygotic and neural specific (brain, spinal cord, and eye) (Campbell and Marlow, 2013). Mutations in *kif5Aa* (but not in *kif5Ab*) lead to larval lethality and sensorimotor deficits similar to those observed in human patients; moreover, zebrafish *kif5Aa* mutants were found to exhibit hyperexcitability and peripheral polyneuropathy as defective mitochondrial transport resulted in degeneration of peripheral sensory axons. At 6 dpf (days-post-fertilization), *kif5Aa* mutants had an inflated swim bladder, increased lateral and dorsal pigmentation, and a diminished touch response (Campbell et al., 2014). The other five kif5 zebrafish proteins were not able to rescue *kif5Aa* deficiency in mutants. Similarly, the generation of loss-of-function alleles of the anterograde motor protein *kif5Aa* resulted in darker embryos with expanded melanosomes within their melanocytes; the embryos failed to inflate the swim bladder and died at 10 dpf. Moreover mutant fish showed de-synchronization of retinal axon and tectal growth (Auer et al., 2015).

SPG8

WASHC5/SPG8 encodes strumpellin, also known as SWIP. Strumpellin is implicated in endosomal trafficking and it is a direct interactor of valosin-containing protein (VCP). VCP is involved in protein aggregation in several neurodegenerative syndromes (Hirabayashi et al., 2001) and myofibrillar myopathies (Schröder and Schoser, 2009). In zebrafish, *spg8* morphant embryos show a slight or severe curly tail phenotype and enlarged heart cavities. Furthermore, knockdown embryos display abnormal development of motor neurons and interneurons in the spinal cord; both were found to be shorter with irregular branching (Valdmanis et al., 2006). Furthermore, *spg8* morphants developed pericardial edema, due to impaired ventricular contractility, and severe skeletal muscle dysfunction (**Table 1**), displaying a short shiver response to tactile stimulation (Clemen et al., 2010). Finally, morphant embryos showed a dramatic reduction of the caudal neuronal tube with complete abolition of the ventral and caudal motor neurons (Clemen et al., 2010).

SPG17

BSCL2 encodes seipin, an endoplasmic reticulum resident protein involved in lipid metabolism; mutations affecting its N-glycosylation lead to a dominantly inherited motor neuron disease, known as SPG17 or Silver syndrome (Warner et al., 2004). In this case, a zebrafish model has been used to test the effect of the "common" mutation p.N88S in seipin (Holtta-Vuori et al., 2013). Expression of the mutant protein in zebrafish led to a motility defect without motor neuron loss or morphological abnormalities. This reduction in swimming was paralleled by decreased triglyceride content in the developing head, possibly due to disturbances in the mobilization of yolk lipids. Oleic acid supplementation restored the motility defect of seipin-N88S-expressing fish. In this way, zebrafish have proven useful in showing that impairment of lipid metabolism is a contributing factor in the pathology associated with SEIPIN-N88S mutation (Holtta-Vuori et al., 2013).

SPG42

SLC33A1 encodes the endoplasmic reticulum (ER) membrane acetyl-CoA transporter, which is responsible for carrying acetyl-carboxylase (acetyl-CoA) into the ER lumen (Kanamori et al., 1997). Knockdown of the *slc33a1* gene in zebrafish using MOs generates embryos with curved tails and defective axon outgrowth from the spinal cord with scarce and poorly organized motor axons. This phenotype can be rescued by human wild-type mRNA, but not mutant mRNA (Lin et al., 2008). Moreover, Mao et al. (2015) discovered that *slc33a1* knockdown led to motor axonopathy through upregulation of BMP signaling, a pathway that regulates axonal growth, guidance and differentiation. Motor axon defects, consisting of shortened axons with increased axon branching, could be rescued by inhibition of BMP signaling by administration of dorsomorphin (DM), a drug that inhibits BMP receptor-1 activity (Mao et al., 2015). DM also promotes the differentiation of neuron progenitor cells from human pluripotent stem cells (PSCs) (Morizane et al., 2011) and the differentiation of cardiomyocytes from mouse and human PSCs

(Hao et al., 2008; Kattman et al., 2011). Therefore, the zebrafish model of SPG42 has provided preliminary experimental support for the rationale of testing DM, with a view to proposing the drug for future trials in mammals.

SPG80

Very recently, Farazi Fard et al. (2019) identified a novel autosomal-dominant gene responsible for HSP in 10 families of diverse geographic origin. SPG80 is a juvenile-onset neurological disorder characterized by a progressive spasticity and hyperreflexia. Some affected subjects also showed cerebellar signs and mild cognitive impairment (Farazi Fard et al., 2019). All affected individuals carried heterozygous non-sense or frameshift mutations in the *UBAP1* (ubiquitin-associated protein 1) gene. *UBAP1* is a member of the UBA domain family, which includes proteins that have a role in the ubiquitin and ubiquitination pathways (Qian et al., 2001).

Seeking to unveil the effects of mutations in *UBAP1 in vivo*, Farazi Fard et al. (2019) found that microinjection of CRISPR/Cas9 and sgRNAs against *UBAP1* in the transgenic fish with fluorescently labeled motor neuron Tg(Oligo2::DsRed) resulted in misshapen axons and shorter motor neuron length compared with what was observed in controls (Farazi Fard et al., 2019). This work further reinforced the suggestion that "UBAP1 links endosomal trafficking to the ubiquitination machinery pathways that have been previously implicated in HSPs."

AUTOSOMAL RECESSIVE COMPLICATED HSP GENES

Different genes have been associated with autosomal recessive (AR) HSP, all acting through loss-of-function and dominant-negative molecular mechanisms. Such mechanisms can be easily modeled at genetic level in zebrafish. There follows a brief overview of the AR-HSP genes studied in zebrafish.

ALS2

Mutations in *ALS2*/alsin are associated with different neurodegenerative disorders, such as juvenile-onset amyotrophic or primary lateral sclerosis and AR hereditary spastic paraplegia. *ALS2* encodes for a protein (alsin) with multiple homology motifs similar to guanine-nucleotide exchange factor, indicating Rho and Rab5 activity. Members of the Rho and Rab5 family of GTPase proteins have been implicated in numerous cellular functions, the best characterized being regulation of the actin cytoskeleton (Rho) and protein trafficking through early endosomes (Rab5) (Otomo, 2003; Topp et al., 2004). *Als2* knockout mice developed rather normally and showed an only mild motor neuron phenotype (Cai, 2005; Yamanaka et al., 2006). Thus, in an attempt to mimic the disease phenotype, zebrafish *als2* morphant embryos were generated; these were found to show developmental and behavioral abnormalities (**Table 1**), which were rescued by overexpression of both full-length and novel *Als2* mouse transcripts (Gros-Louis et al., 2008). Hence, *alsin* might be implicated in motor axon pathfinding and thus be important in early development.

SPG11

Hereditary spastic paraplegia with thin corpus callosum is a complicated form of AR-HSP linked to SPG11 mutations. The *KIAA1840*/SPG11 gene encodes spatacsin (Stevanin et al., 2007), whose mutations have been linked to spastic gait disorder, variably associated with cognitive impairment, peripheral neuropathy, cerebellar ataxia, parkinsonism, and retinal degeneration (Stevanin et al., 2007). Spatacsin is preferentially expressed in human and mouse cortical neurons and it is detected within neurites and growth cones and colocalizes with synaptic markers playing a role also in intracellular cargo trafficking (Pérez-Brangulí et al., 2014).

In mice, loss of *Spg11* led to early cognitive and motor deficits, consistent with the symptoms observed in the majority of patients with mutations in the SPG11 gene (Branchu et al., 2017). Loss of spatacsin impairs the formation of membrane tubules in lysosomes and cause lysosomal lipid accumulation altering the homeostatic equilibrium between cholesterol trafficking and cytosolic calcium levels (Boutry et al., 2019b). Downregulation of *spg11* in zebrafish resulted in abnormal axon outgrowth (Martin et al., 2012) and a range of developmental defects (**Table 1**) and CNS abnormalities. In general, morphant embryos exhibited perturbation of neuronal differentiation (Southgate et al., 2010). More recently, Boutry et al. (2018) demonstrated, both in mouse and in neuronal human cells, that loss of spatacsin led to accumulation of simple gangliosides in lysosomes due to impairment of their recycling. Altered lysosomal activity has also been observed in other models of HSP (Renvoisé et al., 2014; Allison et al., 2017), suggesting that the accumulation of undigested material could be responsible for a build-up of autophagy markers and thus for neurodegeneration. Moreover, Jeyakumar et al. (1999), using an antisense MO for *spg11*, showed that morphant larvae display a motor phenotype characterized by either a loss of motility or paralysis. This motor activity reduction was rescued by treating morphant larvae with miglustat, an FDA-approved drug that inhibits glucosyl-ceramide synthase, and is known to decrease GM2 ganglioside levels in a model of Sandhoff disease (Jeyakumar et al., 1999). This work offered new therapeutic strategies for neurodegenerative diseases linked to such lysosomal dysfunction (Boutry et al., 2018).

SPG15

The *ZFYVE26*/SPG15 gene encodes spastizin; this locus was first reported to account for a rare form of spastic paraplegia, variably associated with mental retardation, hearing and visual defects, dysarthria, cerebellar signs, and distal amyotrophy, and sometimes referred to as Kjellin syndrome (Hanein et al., 2008; Goizet et al., 2009). Spastizin is a large protein (270 kDa) that localizes on the endoplasmic reticulum, on vesicles, and in the endosomal and lysosomal compartment. Spastizin plays a critical role in autophagy process and in particular in the formation and maturation of autophagosomes (Vantaggiato et al., 2019).

In cultured cells, spastizin co-localized partially with ER and endosome markers. This suggests that it may play a role in intracellular trafficking and that it is required for CNS function (Hanein et al., 2008). Clinically, SPG15 is very similar to SPG11 and recent studies have suggested interactions of the SPG15

and SPG11 proteins with the late endosomal/lysosomal adaptor protein complex AP-5 (Renvoisé et al., 2014). Functional studies in zebrafish showed that knockdown of the zebrafish SPG15 ortholog (*suf*) led to motor axon outgrowth failure and motor impairment (Martin et al., 2012). However, Kanagaraj et al. (2014) found that zygotic zebrafish $suf^{-/-}$ embryos did not show a neurological phenotype or motor axon outgrowth failure, while they confirmed, after the MO injection, the previously reported severe phenotypes (Kanagaraj et al., 2014). These authors described an uncharacterized cellular mechanism for suf/spastizin activity during secretory vesicle maturation in zebrafish oogenesis, which raised the possibility of novel avenues for HSP therapy research (Kanagaraj et al., 2014).

SPG39

Mutations in patatin-like phospholipase domain containing 6 (*PNPLA6*) have been implicated in a broad spectrum of neurodegenerative conditions including the complicated form of spastic paraplegia referred to as type 39 (SPG39). The SPG39 protein is a conservative protein found in many species ranging from yeast to mammals (Lush et al., 1998; Chang et al., 2008). Although its tissue distribution and function are well-established, its mechanism of action in the nervous system remains to be elucidated. Several animal models of *PNPLA6* mutation have been generated, including mice, fruit fly, and zebrafish. In particular, the zebrafish provided a vertebrate model able to better characterize the role of the protein in neural development. MO-induced loss of *pnpla6* in zebrafish caused developmental abnormalities (**Table 1**), which were rescued by overexpression of wild-type human *PNPLA6* mRNA (Song et al., 2013). Additionally, knockdown of *pnpla6* resulted in overactivation of BMP signaling, which can lead to impairment of axonal transport machinery and maintenance of long axons (Song et al., 2013). Hufnagel et al. (2015) identified eight mutations in the *PNPLA6* gene in six families with Oliver-McFarlane or Laurence-Moon syndrome and used zebrafish to functionally validate these mutations. They found that mutation-harboring mRNAs did not rescue the morphant phenotype, whereas wild-type human PNPLA6 mRNA did (Hufnagel et al., 2015). The discovery of these additional PNPLA6-opathies has considerable implications for the diagnostic and prognostic evaluation of patients with cerebellar or pyramidal dysfunction.

SPG46

Autosomal recessive spastic paraplegia 46 (SPG46) is another neurodegenerative disorder characterized by onset in childhood of slowly progressive spastic paraplegia and cerebellar signs. Martin et al. (2013) identified, in three distinct families, four different mutations in *GBA2*, a gene that encodes for a microsomal non-lysosomal glucosylceramidase involved in lipid metabolism. Transient loss of the zebrafish *gba2* orthologous gene led to abnormal motor behavior and axonal shortening/branching of motor neurons. These phenotypes were rescued by co-injection of the human wild-type mRNA, but not by use of the same mRNA carrying the mutation. This study unveiled a new role of ceramide metabolism in HSP pathology (Martin et al., 2013).

SPG53

As highlighted above, microtubule dynamics and vesicle trafficking play a critical role in HSP. Zivony-Elboum et al. (2012) demonstrated the involvement of *VPS37A* in an AR complicated HSP form (SPG53). *VPS37A* encodes a protein member of the endosomal sorting complex required for transport (ESCRT) system. The ESCRT system is involved in intracellular trafficking, in the maturation of multivesicular bodies, and in the sorting of ubiquitinated membrane proteins into internal luminal vesicles (Hurley, 2010). Zivony-Elboum et al. (2012) described 9 patients, from two different families, with early-onset spastic paraplegia in whom linkage analysis, followed by candidate gene sequencing, identified a homozygous mutation in *VPS37A*. Loss-of-function experiments using the MO strategy in zebrafish showed that morphant embryos presented striking and significant loss of motility compared with embryos injected with a standard control MO. Moreover, rescue experiments through co-injection of WT, but not mutated SPG53 mRNA, were able to restore the phenotype. These data suggested, and provided evidence for, the involvement of *VPS37A* in AR-HSP (Zivony-Elboum et al., 2012).

SPG76

Another AR-HSP gene, this one responsible for spastic paraplegia 76 (SPG76), is *CAPN1,* identified by performing whole-exome sequencing in nine affected individuals from three families. *CAPN1* encodes calpain 1, a protease that is widely expressed in the CNS and has roles in synaptic plasticity, synaptic restructuring, and axon maturation and maintenance (Liu et al., 2008). Gan-Or et al. (2016) generated three models of calpain 1 deficiency, studying the effects of loss of function of *CAPN1* orthologs in nematode, fruit fly and zebrafish. In zebrafish, there are two orthologs of *CAPN1* (*cpn1a* and *capn1b*) but only the MO against *capn1a* led to a phenotype, because *capn1a* is largely expressed in the brain starting at 24 hpf (hours-post-fertilization) (Lepage and Bruce, 2008). Moreover, the authors injected the *capn1a*-MO in the Tg(islet1::GFP) zebrafish line expressing the green fluorescent protein (GFP) in the motor neurons, including the branchiomotor neurons. Capn1a deficiency resulted in abnormal branchiomotor neuron migration and disorganized axonal networks in the brain, supporting a neuroprotective role of calpain 1 (Gan-Or et al., 2016). This work opened up new avenues for expanding our knowledge about the role and effects of the different calpains on neurodegeneration and neuroprotection, and thus for furthering our understanding of the *CAPN1*-associated HSP phenotypes.

SPOAN/*KLC2*

Twenty-six Caucasian individuals belonging to consanguineous families affected by a complicated form of AR spastic paraplegia, with optic atrophy and neuropathy (SPOAN syndrome) were identified in early 2000 (Macedo-Souza et al., 2009). Ten years later, Melo et al. (2015) described the SPOAN causative mutation, a small deletion in the non-coding region that causes kinesin light chain-2 (*KLC2*) overexpression. The zebrafish has proved to be an indispensable model for studying *in vivo* the effects of *klc2*

knockdown and overexpression. Loss of function was obtained using two different *klc2* MOs (a translation-blocking MO and a splice MO); the effects of both MOs were evident at 48 hpf and the phenotypes observed were rescued by injection of WT *kcl2* mRNA. Moreover, the *kcl2* overexpression was associated with phenotypes similar to those displayed by morphants (**Table 1**) described in several reports that employed zebrafish to study other forms of HSP (Melo et al., 2015). The similar phenotypes, observed both in loss-of-function and in gain-of-function experiments, supported the idea that *kcl2* is an essential gene for motor neuron function and development (Melo et al., 2015).

PCYT2

Very recently, Vaz et al. generated two distinct *pcyt2* knockout zebrafish lines, one targeting exon 3 *(pcyt2_03)* and the other targeting the final exon 13 *(pcyt2_13)* (Vaz et al., 2019). The gene *PCYT2* encodes phosphoethanolamine cytidylyltransferase, an enzyme in the phosphatidylethanolamine synthesis via, one of the most abundant membrane lipids presents in the brain (Nakashima et al., 1997). *Pcyt2*$^{-/-}$ mice are embryonically lethal (Fullerton et al., 2007). In zebrafish, the survival analysis at both 5 days and 6 weeks, showed that the Complete abrogation of *pcyt2* (*pcyt2_03 line)* in zebrafish showed high mortality whereas *pcyt2_13* strain with some residual protein function revealed a higher survival compared to *pcyt2_03* line. Moreover, at 6 weeks of age, the *pcyt2_13* line showed smaller size and abnormal tail-fin morphology compared with the WT. This model highlighted that alterations in lipid metabolism may lead to complex HSP (Martin et al., 2013; Vaz et al., 2019).

OTHER FORMS OF HSP

In 2014, Novarino et al. performed whole-exome sequencing in combination with network analysis in 55 families displaying AR-HSP and identified several previously unknown putative HSP genes. To establish the role of these disease genes in HSP, they studied their expression profiles, considering multiple human tissues, and then functionally validated many mutated genes by performing knockdown experiments in zebrafish, and generating fish models of *ARL6IPI*, *PGAP1*, *USP8*, and *MARS* deficiency by means of the MO strategy. Morphant larvae were evaluated for mortality, body axis defects, and altered motor neuron morphology, and were submitted to evoked and spontaneous swimming behavior analysis (**Table 1**; Novarino et al., 2014). Unfortunately, the *mars* morphants were too severe to be analyzed, whereas the phenotypes associated with the other genes were similar to those previously reported for other HSP candidate genes. The mutations and genes involved link HSP to cellular transport, nucleotide metabolism and synapse and axon development. Overall, this work led to the construction of a "HSPome" interaction map that may help guide future studies (Novarino et al., 2014).

X-Linked Forms

Allan-Herndon-Dudley syndrome (AHDS), a rare disorder of brain development with neuromuscular involvement, is characterized by a combination of severe intellectual disability, spastic paraplegia, and disturbed thyroid hormone (TH) parameters (Bohan and Azizi, 2004). The AHDS locus was identified on chromosome X, and this condition occurs exclusively in young males. Bohan and Azizi (2004) suggested that AHDS was the fourth locus for X-linked spastic paraplegia, and proposed the term "SPG22" for the locus Xq21 that encompasses the AHDS region (Bohan and Azizi, 2004). AHDS is caused by mutations in *MCT8*, a gene that encodes a TH transporter. Since knockout mice were found to lack the neurological defects present in AHDS patients (Di Cosmo et al., 2010, 2013), Zada et al. (2016) created a *mct8* zebrafish mutant (*mct8*$^{-/-}$) using a zinc-finger nuclease strategy. Zebrafish mutants showed neurological and behavioral alterations reminiscent of those seen in the human disease. Using several experimental approaches, the authors found abnormalities in the expression of myelin-related genes, defects in neural circuit assembly, a reduction of locomotor activity, and a decreased response to external stimuli. They suggested that these impaired neurological phenotypes and behaviors could be conserved between zebrafish and AHDS patients. In addition, the fact that treatment with TH analogs was able to recover a portion of the neurological phenotypes seems to pave the way for the use of zebrafish for large-scale testing of possible therapeutic treatments for AHDS pathology (Zada et al., 2014). Two years later, analysis of a mutant *mct8*$^{-/-}$ zebrafish line focused on hypermyelination in the CNS of the mutant larvae, and showed a reduction in the number of oligodendrocytes in the brain and spinal cord, and an increase in the number of Schwann cells in the trunk (Zada et al., 2016). In addition, the authors evaluated the therapeutic effect of putative drugs, and it emerged that TH analogs and clemastine were able to partially restore hypomyelination in *mct8*$^{-/-}$ mutants. Furthermore, the expression of mct8 was specifically targeted in the endothelial cells of the vascular system, with the outcome of a complete rescue of hypomyelinaton in *mct8*$^{-/-}$ embryos before the maturation of the BBB. These data open the possibility of acting pharmacologically and genetically on hypomyelination in AHDS patients (Zada et al., 2016).

Jouet et al. showed that mutation in the *L1CAM* gene cause SPG1 and MASA syndrome characterized by corpus callosum aplasia, mental retardation, spasticity in the upper and lower limbs, and hydrocephalus (L1 syndrome) (Jouet et al., 1994; Fransen et al., 1995). Yu et al. revealed that *l1.1*, the ortholog of mammalian *L1CAM*, contributes to spinal cord regeneration in adult zebrafish (Chen et al., 2016). Recently, it has been shown that knockdown experiments of *l1.1* lead to hydrocephalus, defects in axonal outgrowth, and myelination abnormalities (Linneberg et al., 2019). These phenotypes have been previously associated with the L1 syndrome.

Another gene X-linked associated with spastic paraplegia is *PLP1* (SPG2) that encodes a primary constituent of myelin in the central nervous system. Few data are available on *plp1* in zebrafish (Brösamle, 2010) and no morphant investigations have been published.

THE ATAXIA-SPASTICITY SPECTRUM GENES

The novel ASS classification proposed by Synofzik and Schüle (2017) considers 69 genes whose mutations are associated with both ataxia and spasticity. Among these genes, only 12 were previously classified as HSP (SPG) genes and 17 as SCA/SCAR genes (Synofzik and Schüle, 2017). Some SCA/SCAR genes included in the ASS classification, as well as other ASS genes not previously classified as HSP or HA genes have been modeled in zebrafish and hence they will here be described. Pathological polyQ expansion in the coding region of the *ATXN1* gene causes spinocerebellar ataxia type 1 (SCA1) (Klement et al., 1999). Two genes, designated *atxn1a* and *atxn1b*, were identified in zebrafish as homologs of human *ATXN1*. The products of *atxn1a* and *atxn1b* were expressed preferentially in the cerebellum, which is the main site of SCA1 disease (Carlson et al., 2009).

A similar study investigated the expression of *ataxin3*, the ortholog of *ATXN3* whose polyQ pathological expansion causes Machado-Joseph disease (MJD), also known as spinocerebellar ataxia type 3 (MJD/SCA3) (Matos et al., 2019). Recently, Watchon et al. created, as a model of SCA3 l, two transgenic zebrafish lines, expressing enhancer green fluorescence plasmid (EGFP). These lines were called EGFP-Ataxin 3-23Q and EGFP-Ataxin 3-84Q (Watchon et al., 2017). The two mutants showed a significantly shorter mean survival time, depending on the length of the polyQ expansion. The axonal length of motor neurons in 48 hpf larvae expressing EGFP-Ataxin 3-84Q was found to be decreased compared with what was observed in non-transgenic and EGFP-Ataxin 3-23Q-expressing larvae. The EGFP-Ataxin 3-84Q zebrafish also showed a significantly shorter swimming distance at 6 days and at 12 months of age compared with the other two groups, even when the human ataxin-3 protein was limited to motor neurons using a mir218-enhancer-Kal4 driver line (Watchon et al., 2017). The transgenic zebrafish also developed signs of ataxin-3 neuropathology. A neuritic beading-staining pattern (positive for ataxin-3 and polyQ), as previously observed in the medullary white matter of patients with MJD, was observed in the medulla of the EGFP-Ataxin 3-84Q zebrafish (Watchon et al., 2017). Interestingly, immunoblotting on protein lysate of transgenic zebrafish lines revealed the presence of ataxin 3-positive cleavage fragments as reported in MJD patient samples. Testing inhibitor compounds on these zebrafish lines, created as animal models of MJD, revealed that calpeptin, a calpain inhibitor, might represent a possible treatment, as it prevented the formation of the proteolytic cleavage products (Watchon et al., 2017).

Adrenoleukodystrophy (ADL) is another X-linked neurodegenerative disease. Caused by mutations in the *ABCD1* gene (Strachan et al., 2017), it affects the myelin of central and peripheral nervous systems. Mutations in *ABCD1* cause a spectrum of phenotypes ranging from cerebral forms of infantile adrenoleukodystrophy to adenomyeloneuropathy mimicking HSP. Zebrafish models of ADL were created by Strachan et al. (2017) through transcription activator-like effector nucleases in exon 1 of *abcd1* (*abcd1*^{zc90}) and these authors also characterized a mutant model from the Zebrafish Mutation Project with a point mutation in *abcd1* exon 9 (*abcd1*^{sa509}) (Strachan et al., 2017). The *abcd1*^{sa509} mutant showed increased levels of very long chain fatty acids in 7-8 dpf larvae, reduced myelinization of axons in 5 dpf larvae, and increased apoptosis in the brain at 72 hpf, not observed in *abcd1*^{zc90} mutants (Strachan et al., 2017). The *abcd1*^{sa509} 6 dpf mutants also showed reduced larval survival and a motor behavior deficit (**Table 1**) also seen in adults (Strachan et al., 2017).

In another study, Wan et al. (2012) used a zebrafish morphant to functionally examine the effects of mutations in exosome component 3 (*EXOSC3*), a gene associated with pontocerebellar hypoplasia 1 (PCH1) and distal hereditary motor neuronopathy, both of which resemble HSP. EXOSC3 is a component of the RNA exosome complex, and mutations in the relative gene were found in 13 families with signs of PCH1 (Wan et al., 2012). The *exosc3* knockdown model showed a severe phenotype at 3 dpf (**Table 1**; Wan et al., 2012). Other zebrafish gene orthologs in addition to those referred to in the group of ASS etiologies, including *prp1/2*, have also been studied and the main results are summarized in **Table 1**.

Among others, it is important to highlight *npc1*, the ortholog of the Niemann-Pick disease type C1 gene (*NPC1*). Mutations in this gene are responsible for 95% of cases of Niemann-Pick disease, a rare AR lysosomal storage disorder (Torres et al., 2017) with heterogeneous symptoms that include jaundice, hepatosplenomegaly, ataxia, spasticity, and intellectual decline leading to dementia (Schwend et al., 2011; Louwette et al., 2013; Lin et al., 2018; Tseng et al., 2018). The transmembrane protein NPC1 is implicated in the retrograde transport of cholesterol and glycolipids from lysosomes, and mutated NPC1 causes an accumulation of these substances in lysosomes, leading to onset of variable neurological manifestations (Lin et al., 2018; Tseng et al., 2018). The first studies of this gene in zebrafish were conducted using MOs, but morphants were characterized by premature death, before 2 dpf (Schwend et al., 2011) or at around 5 dpf when higher doses of MO were used (Louwette et al., 2013). The *npc1*-knockdown zebrafish showed developmental defects as reported in **Table 1** (Schwend et al., 2011; Louwette et al., 2013). More recently, *npc1*$^{-/-}$ zebrafish models were created using CRISPR/Cas9 technology (Lin et al., 2018; Tseng et al., 2018). Lin et al. observed that most *npc1*$^{-/-}$ zebrafish with truncated Npc1 protein died during the embryonic or juvenile stages, and the few survivors showed slower length growth compared with the wild type; however, none survived after 8 dpf (Lin et al., 2018). At 4 dpf, survivors expressed ataxia symptoms in swimming that corresponded to a loss of Purkinje cells in the cerebellum (Lin et al., 2018). Concurrently, two other lines of *npc1* null mutants were created by Tseng et al. (2018). They observed similar results with massive early death between 8 and 12 dpf and a maximum lifetime of 6 dpf (Tseng et al., 2018). In this case, adult *npc1* mutants showed a swimming defect of balance with inability to maintain the upright position, likely due to a CNS defect more clearly

observed in the Purkinje cells (Tseng et al., 2018). In addition, Tseng et al. observed a dark liver phenotype and inability to reproduce; they also found increased LysoTracker staining in neuromasts from 3 dpf null *npc1* mutants, a parameter that might be used as an *in vivo* screen for therapeutic drugs (Tseng et al., 2018).

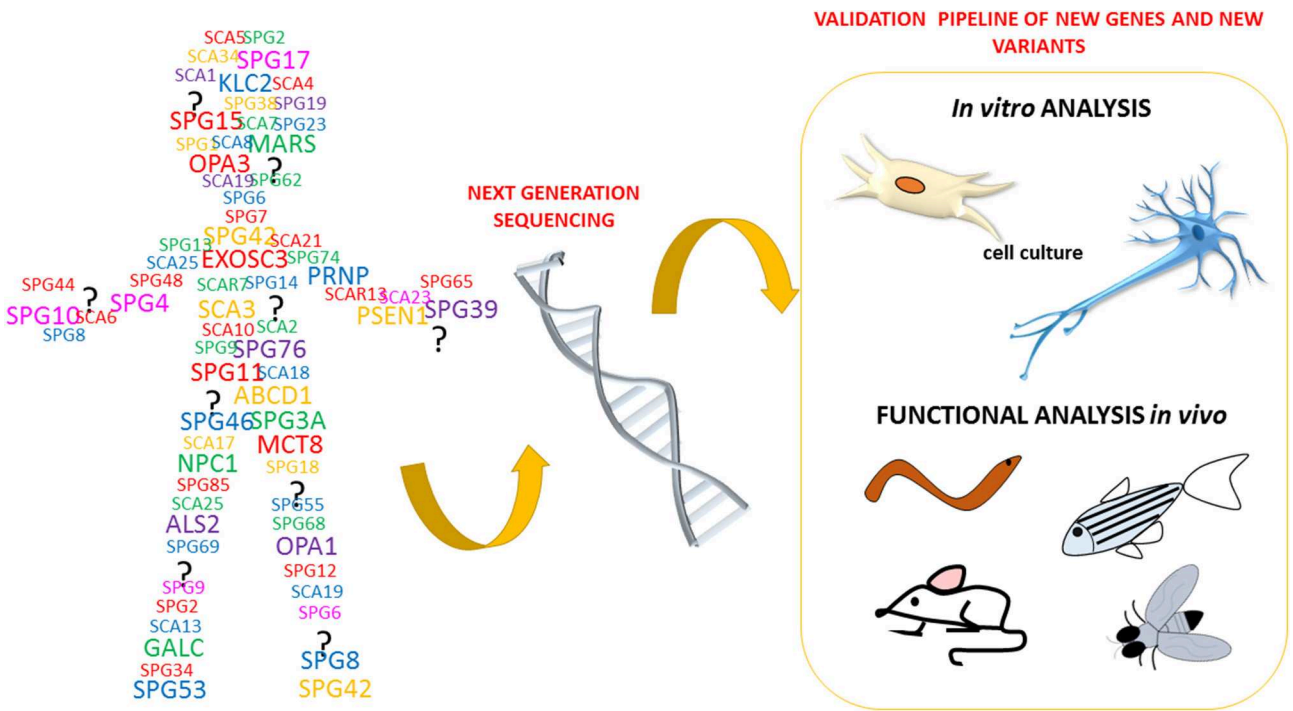

FIGURE 3 | HSP phenotype identification and specificity assessment.

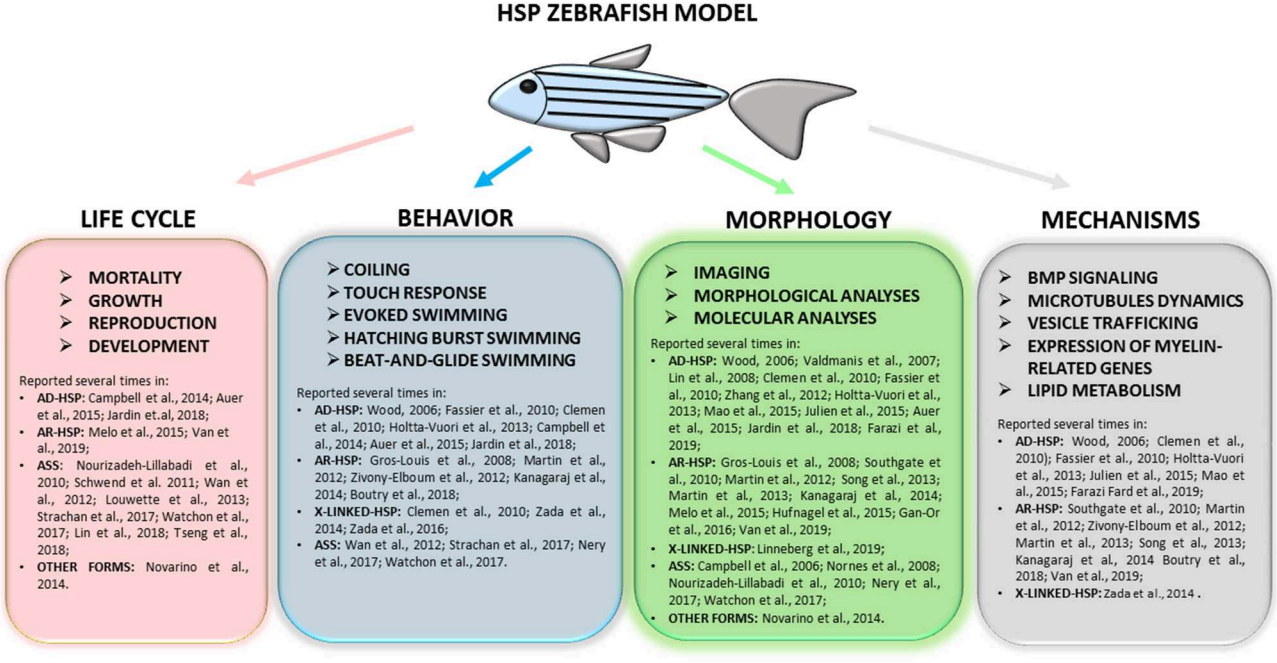

FIGURE 4 | Full overview on the wide range of tests applied to research complicated HSP phenotypes in zebrafish and of molecular mechanisms recurrent in different models. Refer to the literature mentioned in the text for specific protocols.

CONCLUSIONS AND FUTURE APPLICATIONS

The recent technological advances in gene sequencing that allow the analysis of entire genomes of patients affected by neurodegenerative disorders, such as HSP and spastic ataxias (ASS) (**Figure 3**), have brought rapid developments in terms of the identification of novel genes and potentially pathogenic variants. This, in turn, has created a pressing need for functional characterization of these new variants and genes. To date, it clearly emerged that HSP, HA, ASS, and other neurological disorders are part of a continuum of overlapping clinical conditions. For instance, the clinical overlap of HSP with HA or intellectual/ developmental disability is not new and so it is the overlap with the mechanisms involved in more common neurological conditions including amyotrophic lateral sclerosis, multiple sclerosis, Parkinson disease, and dementias (Patten et al., 2014; Parodi et al., 2017; Boutry et al., 2019b; Shribman et al., 2019). Since HSP and ASS are a group of disorders characterized by high genetic diversity, researchers have widely exploited the zebrafish as an *in vivo* model system of these pathologies.

In this review, we have highlighted some of the key features that make the zebrafish a compelling organism for modeling complicated forms of HSP and ASS. Zebrafish has been used to study molecular and functional aspects of HSP and ASS *in vivo*, as well as to functionally validate new mutations identified in patients. Even though the main publications in this field focus on loss-of function experiments performed using the MO strategy, research has now started to exploit the possibility of creating stable mutant lines to be used to better identify the mechanisms of complicated forms of HSP, and as a tool for drug screening. Taken together, these approaches have resulted in the development of gene-specific of HSP and ASS zebrafish models.

This literature review highlights several common phenotypes among the different disease models thus far described: almost all showed locomotor impairment, motor neuron defects, and body malformations. However, these phenotypes can also be relevant to other forms of neurodegeneration impacting on upper and lower motor neurons and long neuronal tracts. As outlined in **Figure 3**, our review shows that certain zebrafish phenotypes are common traits in the complicated forms of HSP but also that there is not yet a straightforward readout correlating functional studies with mutations in HSP and ASS genes (**Table 1**). Obviously, zebrafish cannot be expected to fully replicate complex human disorders. Thus far, efforts to identify HSP traits in zebrafish models have involved the use a wide range of tests (behavioral, life cycle, and morphological) (**Figure 4**), but there is a great variability between studies, due to the intrinsic limits of the tests chosen, and also because, in many cases, the analyses, being based on operator choice, are biased. Standardization of the processes used to characterize zebrafish phenotypes would certainly help to better define ones corresponding to neurodegenerative diseases in humans, including HSP and related conditions, and would clearly improve the validity of this model system and likely facilitate its use in drug screening.

AUTHOR CONTRIBUTIONS

FS, VN, and MM: conceptualization. VN and MM: methodology. GF, SM, and VN: investigation. GF and VN: resources and writing original draft preparation. FS, MM, AO, AD, FG, and VN: writing review and editing. SM: visualization. FS and MM: supervision and funding acquisition. VN: project administration.

FUNDING

Funding from RC Conto Capitale MITONEXT and MIT-OMICS, and the Italian Ministry of Health-Ricerca Finalizzata RF-2016-02361610 (to FS), and the E-RARE-3 Joint Transnational Call grant Preparing therapies for autosomal recessive ataxias (PREPARE) (MoH; project 3398 to FS) are acknowledged. MM was the recipient of the Starting Grant SG-2018-12367839 from the Italian Ministry of Health.

ACKNOWLEDGMENTS

We thank Catherine J. Wrenn for her expert editorial assistance.

REFERENCES

Allison, R., Edgar, J. R., Pearson, G., Rizo, T., Newton, T., Günther, S., et al. (2017). Defects in ER–endosome contacts impact lysosome function in hereditary spastic paraplegia. *J. Cell Biol.* 216, 1337–1355. doi: 10.1083/jcb.201609033

Auer, T. O., Xiao, T., Bercier, V., Gebhardt, C., Duroure, K., Concordet, J., et al. (2015). Deletion of a kinesin I motor unmasks a mechanism of homeostatic branching control by neurotrophin-3. *Elife* 4:e05061. doi: 10.7554/eLife.05061

Babin, P. J., Goizet, C., and Raldúa, D. (2014). Zebrafish models of human motor neuron diseases: Advantages and limitations. *Prog. Neurobiol.* 118, 36–58. doi: 10.1016/j.pneurobio.2014.03.001

Basnet, R. M., Zizioli, D., Taweedet, S., Finazzi, D., and Memo, M. (2019). Zebrafish larvae as a behavioral model in neuropharmacology. *Biomedicines* 7:23. doi: 10.3390/biomedicines7010023

Bellofatto, M., De Michele, G., Iovino, A., Filla, A., and Santorelli, F. M. (2019). Management of hereditary spastic paraplegia: a systematic review of the literature. *Front. Neurol.* 10:3. doi: 10.3389/fneur.2019.00003

Bohan, T. P., and Azizi, P. (2004). Allan-herndon-dudley syndrome: should the locus for this hereditary spastic paraplegia be designated SPG 22? *Arch. Neurol.* 61, 1470–1; author reply 1471. doi: 10.1001/archneur.61.9.1470-c

Boutry, M., Branchu, J., Lustremant, C., Pujol, C., Pernelle, J., Matusiak, R., et al. (2018). Inhibition of lysosome membrane recycling causes accumulation of gangliosides that contribute to neurodegeneration. *Cell Rep.* 23, 3813–3826. doi: 10.1016/j.celrep.2018.05.098

Boutry, M., Morais, S., and Stevanin, G. (2019a). Update on the genetics of spastic paraplegias. *Curr. Neurol. Neurosci. Rep.* 19:18. doi: 10.1007/s11910-019-0930-2

Boutry, M., Pierga, A., Matusiak, R., Branchu, J., Houllegatte, M., Ibrahim, Y., et al. (2019b). Loss of spatacsin impairs cholesterol trafficking and calcium homeostasis. *Commun Biol.* 2:380. doi: 10.1038/s42003-019-0615-z

Branchu, J., Boutry, M., Sourd, L., Depp, M., Leone, C., Corriger, A., et al. (2017). Loss of spatacsin function alters lysosomal lipid clearance leading to upper and lower motor neuron degeneration. *Neurobiol. Dis.* 102, 21–37. doi: 10.1016/j.nbd.2017.02.007

Brösamle, C. (2010). The myelin proteolipid DMα in fishes. *Neuron Glia Biol.* 6, 109–112. doi: 10.1017/S1740925X09000131

Cai, H. (2005). Loss of ALS2 function is insufficient to trigger motor neuron degeneration in knock-out mice but predisposes neurons to oxidative stress. *J. Neurosci.* 25, 7567–7574. doi: 10.1523/JNEUROSCI.1645-05.2005

Campbell, P. D., and Marlow, F. L. (2013). Temporal and tissue specific gene expression patterns of the zebrafish kinesin-1 heavy chain family, kif5s, during development. *Gene Expr. Patterns* 13, 271–279. doi: 10.1016/j.gep.2013.05.002

Campbell, P. D., Shen, K., Sapio, M. R., Glenn, T. D., Talbot, W. S., and Marlow, F. L. (2014). Unique function of kinesin Kif5A in localization of mitochondria in axons. *J. Neurosci.* 34, 14717–14732. doi: 10.1523/JNEUROSCI.2770-14.2014

Campbell, W. A., Yang, H., Zetterberg, H., Baulac, S., Sears, J. A., Liu, T., et al. (2006). Zebrafish lacking Alzheimer presenilin enhancer 2 (Pen-2) demonstrate excessive p53-dependent apoptosis and neuronal loss. *J. Neurochem.* 96, 1423–1440. doi: 10.1111/j.1471-4159.2006.03648.x

Carlson, K. M., Melcher, L., Lai, S., Zoghbi, H. Y., Clark, H. B., and Orr, H. T. (2009). Characterization of the zebrafish atxn1/axh gene family. *J. Neurogenet.* 23, 313–323. doi: 10.1080/01677060802399976

Chang, P.-A., Sun, Q., Ni, X.-M., Qv, F.-Q., Wu, Y.-J., and Song, F.-Z. (2008). Molecular cloning and expression analysis of cDNA ends of chicken neuropathy target esterase. *Chem. Biol. Interact.* 172, 54–62. doi: 10.1016/j.cbi.2007.11.014

Chen, T., Yu, Y., Hu, C., and Schachner, M. (2016). L1.2, the zebrafish paralog of L1.1 and ortholog of the mammalian cell adhesion molecule L1 contributes to spinal cord regeneration in adult zebrafish. *Restor. Neurol. Neurosci.* 34, 325–335. doi: 10.3233/RNN-150602

Clemen, C. S., Tangavelou, K., Strucksberg, K. H., Just, S., Gaertner, L., Regus-Leidig, H., et al. (2010). Strumpellin is a novel valosin-containing protein binding partner linking hereditary spastic paraplegia to protein aggregation diseases. *Brain* 133, 2920–2941. doi: 10.1093/brain/awq222

Connell, J. W., Lindon, C., Luzio, J. P., and Reid, E. (2009). Spastin couples microtubule severing to membrane traffic in completion of cytokinesis and secretion. *Traffic* 10, 42–56. doi: 10.1111/j.1600-0854.2008.00847.x

Dahlem, T. J., Hoshijima, K., Jurynec, M. J., Gunther, D., Starker, C. G., Locke, A. S., et al. (2012). Simple methods for generating and detecting locus-specific mutations induced with TALENs in the zebrafish genome. *PLoS Genet.* 8:e1002861. doi: 10.1371/journal.pgen.1002861

D'Amore, A., Tessa, A., Casali, C., Dotti, M. T., Filla, A., Silvestri, G., et al. (2018). Next generation molecular diagnosis of hereditary spastic paraplegias: an Italian cross-sectional study. *Front. Neurol.* 9:981. doi: 10.3389/fneur.2018.00981

Di Cosmo, C., Liao, X.-H., Dumitrescu, A. M., Philp, N. J., Weiss, R. E., and Refetoff, S. (2010). Mice deficient in MCT8 reveal a mechanism regulating thyroid hormone secretion. *J. Clin. Invest.* 120, 3377–3388. doi: 10.1172/JCI42113

Di Cosmo, C., Liao, X.-H., Ye, H., Ferrara, A. M., Weiss, R. E., Refetoff, S., et al. (2013). Mct8-deficient mice have increased energy expenditure and reduced fat mass that is abrogated by normalization of serum T 3 levels. *Endocrinology* 154, 4885–4895. doi: 10.1210/en.2013-1150

Elert-Dobkowska, E., Stepniak, I., Krysa, W., Ziora-Jakutowicz, K., Rakowicz, M., Sobanska, A., et al. (2019). Next-generation sequencing study reveals the broader variant spectrum of hereditary spastic paraplegia and related phenotypes. *Neurogenetics*, 27–38. doi: 10.1007/s10048-019-00565-6

Evans, K. J., Gomes, E. R., Reisenweber, S. M., Gundersen, G. G., and Lauring, B. P. (2005). Linking axonal degeneration to microtubule remodeling by Spastin-mediated microtubule severing. *J. Cell Biol.* 168, 599–606. doi: 10.1083/jcb.200409058

Farazi Fard, M. A., Rebelo, A. P., Buglo, E., Nemati, H., Dastsooz, H., Gehweiler, I., et al. (2019). Truncating mutations in UBAP1 cause hereditary spastic paraplegia. *Am. J. Hum. Genet.* 104, 767–773. doi: 10.1016/j.ajhg.2019.03.001

Fassier, C., Hutt, J. A., Scholpp, S., Lumsden, A., Giros, B., Nothias, F., et al. (2010). Zebrafish atlastin controls motility and spinal motor axon architecture via inhibition of the BMP pathway. *Nat. Neurosci.* 13, 1380–1387. doi: 10.1038/nn.2662

Fransen, E., Lemmon, V., Van Camp, G., Vits, L., Coucke, P., and Willems, P. J. (1995). CRASH syndrome: clinical spectrum of corpus callosum hypoplasia, retardation, adducted thumbs, spastic paraparesis and hydrocephalus due to mutations in one single gene, L1. *Eur. J. Hum. Genet.* 3, 273–284. doi: 10.1159/000472311

Fullerton, M. D., Hakimuddin, F., and Bakovic, M. (2007). Developmental and metabolic effects of disruption of the mouse CTP:phosphoethanolamine cytidylyltransferase gene (Pcyt2). *Mol. Cell. Biol.* 27, 3327–3336. doi: 10.1128/MCB.01527-06

Fusco, C., Frattini, D., Farnetti, E., Nicoli, D., Casali, B., Fiorentino, F., et al. (2010). Hereditary spastic paraplegia and axonal motor neuropathy caused by a novel SPG3A *de novo* mutation. *Brain Dev.* 32, 592–594. doi: 10.1016/j.braindev.2009.08.003

Galatolo, D., Tessa, A., Filla, A., and Santorelli, F. M. (2018). Clinical application of next generation sequencing in hereditary spinocerebellar ataxia: increasing the diagnostic yield and broadening the ataxia-spasticity spectrum. A retrospective analysis. *Neurogenetics* 19, 1–8. doi: 10.1007/s10048-017-0532-6

Gan-Or, Z., Bouslam, N., Birouk, N., Lissouba, A., Chambers, D. B., Vérièpe, J., et al. (2016). Mutations in CAPN1 cause autosomal-recessive hereditary spastic paraplegia. *Am. J. Hum. Genet.* 98, 1038–1046. doi: 10.1016/j.ajhg.2016.04.002

Goizet, C., Boukhris, A., Maltete, D., Guyant-Marechal, L., Truchetto, J., Mundwiller, E., et al. (2009). SPG15 is the second most common cause of hereditary spastic paraplegia with thin corpus callosum. *Neurology* 73, 1111–1119. doi: 10.1212/WNL.0b013e3181bacf59

Gros-Louis, F., Kriz, J., Kabashi, E., McDearmid, J., Millecamps, S., Urushitani, M., et al. (2008). Als2 mRNA splicing variants detected in KO mice rescue severe motor dysfunction phenotype in Als2 knock-down zebrafish. *Hum. Mol. Genet.* 17, 2691–2702. doi: 10.1093/hmg/ddn171

Hanein, S., Martin, E., Boukhris, A., Byrne, P., Goizet, C., Hamri, A., et al. (2008). Identification of the SPG15 gene, encoding spastizin, as a frequent cause of complicated autosomal-recessive spastic paraplegia, including kjellin syndrome. *Am. J. Hum. Genet.* 82, 992–1002. doi: 10.1016/j.ajhg.2008.03.004

Hao, J., Daleo, M. A., Murphy, C. K., Yu, P. B., Ho, J. N., Hu, J., et al. (2008). Dorsomorphin, a selective small molecule inhibitor of BMP signaling, promotes cardiomyogenesis in embryonic stem cells. *PLoS ONE* 3:e2904. doi: 10.1371/journal.pone.0002904

Harding, A. E. (1983). Classification of the hereditary ataxias and paraplegias. *Lancet* 321, 1151–1155. doi: 10.1016/S0140-6736(83)92879-9

Hashimoto, Y., Shirane, M., Matsuzaki, F., Saita, S., Ohnishi, T., and Nakayama, K. I. (2014). Protrudin regulates endoplasmic reticulum morphology and function associated with the pathogenesis of hereditary spastic paraplegia. *J. Biol. Chem.* 289, 12946–12961. doi: 10.1074/jbc.M113.528687

Hensiek, A., Kirker, S., and Reid, E. (2015). Diagnosis, investigation and management of hereditary spastic paraplegias in the era of next-generation sequencing. *J. Neurol.* 262, 1601–1612. doi: 10.1007/s00415-014-7598-y

Hirabayashi, M., Inoue, K., Tanaka, K., Nakadate, K., Ohsawa, Y., Kamei, Y., et al. (2001). VCP/p97 in abnormal protein aggregates, cytoplasmic vacuoles, and cell death, phenotypes relevant to neurodegeneration. *Cell Death Differ.* 8, 977–984. doi: 10.1038/sj.cdd.4400907

Hirokawa, N., Niwa, S., and Tanaka, Y. (2010). Molecular motors in neurons: transport mechanisms and roles in brain function, development, and disease. *Neuron* 68, 610–638. doi: 10.1016/j.neuron.2010.09.039

Holtta-Vuori, M., Salo, V. T., Ohsaki, Y., Suster, M. L., and Ikonen, E. (2013). Alleviation of seipinopathy-related ER stress by triglyceride storage. *Hum. Mol. Genet.* 22, 1157–1166. doi: 10.1093/hmg/dds523

Hufnagel, R. B., Arno, G., Hein, N. D., Hersheson, J., Prasad, M., Anderson, Y., et al. (2015). Neuropathy target esterase impairments cause Oliver-McFarlane and Laurence-Moon syndromes. *J. Med. Genet.* 52, 85–94. doi: 10.1136/jmedgenet-2014-102856

Hurley, J. H. (2010). The ESCRT complexes. *Crit. Rev. Biochem. Mol. Biol.* 45, 463–487. doi: 10.3109/10409238.2010.502516

Hwang, W. Y., Fu, Y., Reyon, D., Maeder, M. L., Tsai, S. Q., Sander, J. D., et al. (2013). Efficient *in vivo* genome editing using RNA-guided nucleases HHS public access author manuscript. *Nat. Biotechnol.* 31, 227–229. doi: 10.1038/nbt.2501

Jardin, N., Giudicelli, F., Ten Martín, D., Vitrac, A., De Gois, S., Allison, R., et al. (2018). BMP- and neuropilin 1-mediated motor axon navigation relies on spastin alternative translation. *Development* 145:dev162701. doi: 10.1242/dev.162701

Jeyakumar, M., Butters, T. D., Cortina-Borja, M., Hunnam, V., Proia, R. L., Perry, V. H., et al. (1999). Delayed symptom onset and increased life expectancy in Sandhoff disease mice treated with N-butyldeoxynojirimycin.

Proc. Natl. Acad. Sci. U.S.A. 96, 6388–6393. doi: 10.1073/pnas.96.11.6388

Jouet, M., Rosenthal, A., Armstrong, G., MacFarlane, J., Stevenson, R., Paterson, J., et al. (1994). X–linked spastic paraplegia (SPG1), MASA syndrome and X–linked hydrocephalus result from mutations in the L1 gene. *Nat. Genet.* 7, 402–407. doi: 10.1038/ng0794-402

Julien, C., Lissouba, A., Madabattula, S., Fardghassemi, Y., Rosenfelt, C., Androschuk, A., et al. (2015). Conserved pharmacological rescue of hereditary spastic paraplegia-related phenotypes across model organisms. *Hum. Mol. Genet.* 25, 1088–1099. doi: 10.1093/hmg/ddv632

Kadnikova, V. A., Rudenskaya, G. E., Stepanova, A. A., Sermyagina, I. G., and Ryzhkova, O. P. (2019). Mutational spectrum of spast (Spg4) and Atl1 (Spg3a) genes in Russian patients with hereditary spastic paraplegia. *Sci. Rep.* 9:14412. doi: 10.1038/s41598-019-50911-9

Kanagaraj, P., Gautier-Stein, A., Riedel, D., Schomburg, C., Cerdà, J., Vollack, N., et al. (2014). Souffle/spastizin controls secretory vesicle maturation during zebrafish oogenesis. *PLoS Genet.* 10:e1004449. doi: 10.1371/journal.pgen.1004449

Kanamori, A., Nakayama, J., Fukuda, M. N., Stallcup, W. B., Sasaki, K., Fukuda, M., et al. (1997). Expression cloning and characterization of a cDNA encoding a novel membrane protein required for the formation of O-acetylated ganglioside: a putative acetyl-CoA transporter. *Proc. Natl. Acad. Sci. U.S.A.* 94, 2897–2902. doi: 10.1073/pnas.94.7.2897

Kattman, S. J., Witty, A. D., Gagliardi, M., Dubois, N. C., Niapour, M., Hotta, A., et al. (2011). Stage-specific optimization of activin/nodal and BMP signaling promotes cardiac differentiation of mouse and human pluripotent stem cell lines. *Cell Stem Cell* 8, 228–240. doi: 10.1016/j.stem.2010.12.008

Klebe, S., Stevanin, G., and Depienne, C. (2015). Clinical and genetic heterogeneity in hereditary spastic paraplegias: From SPG1 to SPG72 and still counting. *Rev. Neurol.* 171, 505–530. doi: 10.1016/j.neurol.2015.02.017

Klement, I. A., Zoghbi, H. Y., and Orr, H. T. (1999). Pathogenesis of polyglutamine-induced disease: a model for SCA1. *Mol. Genet. Metab.* 66, 172–178. doi: 10.1006/mgme.1999.2801

Lepage, S. E., and Bruce, A. E. E. (2008). Characterization and comparative expression of zebrafish calpain system genes during early development. *Dev. Dyn.* 237, 819–829. doi: 10.1002/dvdy.21459

Lin, P., Li, J., Liu, Q., Mao, F., Li, J., Qiu, R., et al. (2008). A missense mutation in SLC33A1, which encodes the Acetyl-CoA transporter, causes autosomal-dominant spastic paraplegia (SPG42). *Am. J. Hum. Genet.* 83, 752–759. doi: 10.1016/j.ajhg.2008.11.003

Lin, Y., Cai, X., Wang, G., Ouyang, G., and Cao, H. (2018). Model construction of Niemann-Pick type C disease in zebrafish. *Biol. Chem.* 399, 903–910. doi: 10.1515/hsz-2018-0118

Linneberg, C., Toft, C. L. F., Kjaer-Sorensen, K., and Laursen, L. S. (2019). L1cam-mediated developmental processes of the nervous system are differentially regulated by proteolytic processing. *Sci. Rep.* 9:3716. doi: 10.1038/s41598-019-39884-x

Liu, J., Liu, M. C., and Wang, K. K. W. (2008). Calpain in the CNS: from synaptic function to neurotoxicity. *Sci. Signal.* 1:re1. doi: 10.1126/stke.114re1

Lo Giudice, T., Lombardi, F., Santorelli, F. M., Kawarai, T., and Orlacchio, A. (2014). Hereditary spastic paraplegia: clinical-genetic characteristics and evolving molecular mechanisms. *Exp. Neurol.* 261, 518–539. doi: 10.1016/j.expneurol.2014.06.011

Louwette, S., Régal, L., Wittevrongel, C., Thys, C., Vandeweeghde, G., Decuyper, E., et al. (2013). NPC1 defect results in abnormal platelet formation and function: studies in Niemann–Pick disease type C1 patients and zebrafish. *Hum. Mol. Genet.* 22, 61–73. doi: 10.1093/hmg/dds401

Lush, M. J., LI, Y., Read, D. J., Willis, A. C., and Glynn, P. (1998). Neuropathy target esterase and a homologous Drosophila neurodegeneration-associated mutant protein contain a novel domain conserved from bacteria to man. *Biochem. J.* 332, 1–4. doi: 10.1042/bj3320001

Macedo-Souza, L. I., Kok, F., Santos, S., Licinio, L., Lezirovitz, K., Cavaçana, N., et al. (2009). Spastic paraplegia, optic atrophy, and neuropathy: new observations, locus refinement, and exclusion of candidate genes. *Ann. Hum. Genet.* 73, 382–387. doi: 10.1111/j.1469-1809.2009.00507.x

Mao, F., Li, Z., Zhao, B., Lin, P., Liu, P., Zhai, M., et al. (2015). Identification and functional analysis of a SLC33A1: c.339T>G (p.Ser113Arg) variant in the original SPG42 family. *Hum. Mutat.* 36, 240–249. doi: 10.1002/humu.22732

Martin, E., Schüle, R., Smets, K., Rastetter, A., Boukhris, A., Loureiro, J. L., et al. (2013). Loss of function of glucocerebrosidase GBA2 is responsible for motor neuron defects in hereditary spastic paraplegia. *Am. J. Hum. Genet.* 92, 238–244. doi: 10.1016/j.ajhg.2012.11.021

Martin, E., Yanicostas, C., Rastetter, A., Naini, S. M. A., Maouedj, A., Kabashi, E., et al. (2012). Spatacsin and spastizin act in the same pathway required for proper spinal motor neuron axon outgrowth in zebrafish. *Neurobiol. Dis.* 48, 299–308. doi: 10.1016/j.nbd.2012.07.003

Matos, C. A., de Almeida, L. P., and Nóbrega, C. (2019). Machado-Joseph disease/spinocerebellar ataxia type 3: lessons from disease pathogenesis and clues into therapy. *J. Neurochem.* 148, 8–28. doi: 10.1111/jnc.14541

Melo, U. S., Macedo-Souza, L. I., Figueiredo, T., Muotri, A. R., Gleeson, J. G., Coux, G., et al. (2015). Overexpression of KLC2 due to a homozygous deletion in the non-coding region causes SPOAN syndrome. *Hum. Mol. Genet.* 24, 6877–6885. doi: 10.1093/hmg/ddv388

Morizane, A., Doi, D., Kikuchi, T., Nishimura, K., and Takahashi, J. (2011). Small-molecule inhibitors of bone morphogenic protein and activin/nodal signals promote highly efficient neural induction from human pluripotent stem cells. *J. Neurosci. Res.* 89, 117–126. doi: 10.1002/jnr.22547

Nakashima, A., Hosaka, K., and Nikawa, J. (1997). Cloning of a human cDNA for CTP-phosphoethanolamine cytidylyltransferase by complementation *in vivo* of a yeast mutant. *J. Biol. Chem.* 272, 9567–9572. doi: 10.1074/jbc.272.14.9567

Nasevicius, A., and Ekker, S. C. (2000). Effective targeted gene "knockdown" in zebrafish. *Nat. Genet.* 26, 216–220. doi: 10.1038/79951

Nery, L. R., Silva, N. E., Fonseca, R., and Vianna, M. R. M. (2017). Presenilin-1 targeted morpholino induces cognitive deficits, increased brain Aβ1–42 and decreased synaptic marker PSD-95 in zebrafish larvae. *Neurochem. Res.* 42, 2959–2967. doi: 10.1007/s11064-017-2327-4

Nornes, S., Newman, M., Verdile, G., Wells, S., Stoick-Cooper, C. L., Tucker, B., et al. (2008). Interference with splicing of Presenilin transcripts has potent dominant negative effects on Presenilin activity. *Hum. Mol. Genet.* 17, 402–412. doi: 10.1093/hmg/ddm317

Nourizadeh-Lillabadi, R., Seilø Torgersen, J., Vestrheim, O., König, M., Aleström, P., and Syed, M. (2010). Early embryonic gene expression profiling of zebrafish prion protein (Prp2) morphants. *PLoS ONE* 5:e13573. doi: 10.1371/journal.pone.0013573

Novarino, G., Novarino, G., Fenstermaker, A. G., Zaki, M. S., Hofree, M., Silhavy, J. L., et al. (2014). Exome sequencig links cortospinal motor neuron disease to common neurodegenerative didorders. *Science* 506, 506–511. doi: 10.1126/science.1247363

Orger, M. B., and de Polavieja, G. G. (2017). Zebrafish behavior : opportunities and challenges. *Annu. Rev. Neurosci.* 40, 125–147. doi: 10.1146/annurev-neuro-071714-033857

Orso, G., Pendin, D., Liu, S., Tosetto, J., Moss, T. J., Faust, J. E., et al. (2009). Homotypic fusion of ER membranes requires the dynamin-like GTPase atlastin. *Nature* 460, 978–983. doi: 10.1038/nature08280

Otomo, A. (2003). ALS2, a novel guanine nucleotide exchange factor for the small GTPase Rab5, is implicated in endosomal dynamics. *Hum. Mol. Genet.* 12, 1671–1687. doi: 10.1093/hmg/ddg184

Parodi, L., Fenu, S., Stevanin, G., and Durr, A. (2017). Hereditary spastic paraplegia: more than an upper motor neuron disease. *Rev. Neurol.* 173, 352–360. doi: 10.1016/j.neurol.2017.03.034

Patten, S. A., Armstrong, G. A. B., Lissouba, A., Kabashi, E., Parker, J. A., and Drapeau, P. (2014). Fishing for causes and cures of motor neuron disorders. *Dis. Model. Mech.* 7, 799–809. doi: 10.1242/dmm.015719

Peng, F., Sun, Y., Quan, C., Wang, J., and Wu, J. (2019). Two novel homozygous mutations of CAPN1 in Chinese patients with hereditary spastic paraplegia and literatures review. *Orphanet. J. Rare Dis.* 14:83. doi: 10.1186/s13023-019-1053-1

Pérez-Brangulí, F., Mishra, H. K., Prots, I., Havlicek, S., Kohl, Z., Saul, D., et al. (2014). Dysfunction of spatacsin leads to axonal pathology in SPG11-linked hereditary spastic paraplegia. *Hum. Mol. Genet.* 23, 4859–4874. doi: 10.1093/hmg/ddu200

Qian, J., Zhang, X. H., Yang, J. B., Wang, J. R., Zhang, B. C., and Tang, K., L. G. (2001). Cloning and expression analysis of a novel gene, UBAP1, possibly involved in ubiquitin pathway. *Acta Biochim. Biophys. Sin.* 33, 147–152.

Qiang, L., Piermarini, E., Muralidharan, H., Yu, W., Leo, L., Hennessy, L. E., et al. (2019). Hereditary spastic paraplegia: gain-of-function mechanisms

revealed by new transgenic mouse. *Hum Mol Genet*. 28,1136–1152. doi: 10.1093/hmg/ddy419

Renvoisé, B., Chang, J., Singh, R., Yonekawa, S., FitzGibbon, E. J., Mankodi, A., et al. (2014). Lysosomal abnormalities in hereditary spastic paraplegia types SPG15 and SPG11. *Ann. Clin. Transl. Neurol.* 1, 379–389. doi: 10.1002/acn3.64

Ruano, L., Melo, C., Silva, M. C., and Coutinho, P. (2014). The global epidemiology of hereditary ataxia and spastic paraplegia: a systematic review of prevalence studies. *Neuroepidemiology* 42, 174–183. doi: 10.1159/000358801

Salinas, S., Carazo-Salas, R. E., Proukakis, C., Cooper, J. M., Weston, A. E., Schiavo, G., et al. (2005). Human spastin has multiple microtubule-related functions. *J. Neurochem.* 95, 1411–1420. doi: 10.1111/j.1471-4159.2005.03472.x

Salinas, S., Proukakis, C., Crosby, A., and Warner, T. T. (2008). Hereditary spastic paraplegia: clinical features and pathogenetic mechanisms. *Lancet Neurol.* 7, 1127–1138. doi: 10.1016/S1474-4422(08)70258-8

Scarano, V., Mancini, P., Criscuolo, C., De Michele, G., Rinaldi, C., Tucci, T., et al. (2005). The R495W mutation in SPG3A causes spastic paraplegia associated with axonal neuropathy. *J. Neurol.* 252, 901–903. doi: 10.1007/s00415-005-0768-1

Schröder, R., and Schoser, B. (2009). Myofibrillar myopathies: a clinical and myopathological guide. *Brain Pathol.* 19, 483–492. doi: 10.1111/j.1750-3639.2009.00289.x

Schwend, T., Loucks, E. J., Snyder, D., and Ahlgren, S. C. (2011). Requirement of Npc1 and availability of cholesterol for early embryonic cell movements in zebrafish. *J. Lipid Res.* 52, 1328–1344. doi: 10.1194/jlr.M012377

Shribman, S., Reid, E., Crosby, A. H., Houlden, H., and Warner, T. T. (2019). Hereditary spastic paraplegia: from diagnosis to emerging therapeutic approaches. *Lancet Neurol.* 18, 1136–1146. doi: 10.1016/S1474-4422(19)30235-2

Song, Y., Wang, M., Mao, F., Shao, M., Zhao, B., Song, Z., et al. (2013). Knockdown of Pnpla6 protein results in motor neuron defects in zebrafish. *Dis. Model. Mech.* 6, 404–413. doi: 10.1242/dmm.009688

Southgate, L., Dafou, D., Hoyle, J., Li, N., Kinning, E., Critchley, P., et al. (2010). Novel SPG11 mutations in Asian kindreds and disruption of spatacsin function in the zebrafish. *Neurogenetics* 11, 379–389. doi: 10.1007/s10048-010-0243-8

Stevanin, G., Santorelli, F. M., Azzedine, H., Coutinho, P., Chomilier, J., Denora, P. S., et al. (2007). Mutations in SPG11, encoding spatacsin, are a major cause of spastic paraplegia with thin corpus callosum. *Nat. Genet.* 39, 366–372. doi: 10.1038/ng1980

Strachan, L. R., Stevenson, T. J., Freshner, B., Keefe, M. D., Miranda Bowles, D., and Bonkowsky, J. L. (2017). A zebrafish model of X-linked adrenoleukodystrophy recapitulates key disease features and demonstrates a developmental requirement for abcd1 in oligodendrocyte patterning and myelination. *Hum. Mol. Genet.* 26, 3600–3614. doi: 10.1093/hmg/ddx249

Synofzik, M., and Schüle, R. (2017). Overcoming the divide between ataxias and spastic paraplegias: shared phenotypes, genes, and pathways. *Mov. Disord.* 32, 332–345. doi: 10.1002/mds.26944

Topp, J. D., Gray, N. W., Gerard, R. D., and Horazdovsky, B. F. (2004). Alsin Is a Rab5 and Rac1 guanine nucleotide exchange factor. *J. Biol. Chem.* 279, 24612–24623. doi: 10.1074/jbc.M313504200

Torres, S., Balboa, E., Zanlungo, S., Enrich, C., Garcia-Ruiz, C., and Fernandez-Checa, J. C. (2017). Lysosomal and mitochondrial liaisons in Niemann-Pick disease. *Front. Physiol.* 8:982. doi: 10.3389/fphys.2017.00982

Tseng, W.-C., Loeb, H. E., Pei, W., Tsai-Morris, C.-H., Xu, L., Cluzeau, C. V., et al. (2018). Modeling Niemann-Pick disease type C1 in zebrafish: a robust platform for *in vivo* screening of candidate therapeutic compounds. *Dis. Model. Mech.* 11:dmm034165. doi: 10.1242/dmm.034165

Valdmanis, P. N., Meijer, I. A., Reynolds, A., Lei, A., MacLeod, P., Schlesinger, D., et al. (2006). Mutations in the KIAA0196 gene at the SPG8 locus cause hereditary spastic paraplegia. *Am. J. Hum. Genet.* 80, 152–161. doi: 10.1086/510782

Vantaggiato, C., Panzeri, E., Castelli, M., Citterio, A., Arnoldi, A., Santorelli, F. M., et al. (2019). ZFYVE26/SPASTIZIN and SPG11/SPATACSIN mutations in hereditary spastic paraplegia types AR-SPG15 and AR-SPG11 have different effects on autophagy and endocytosis. *Autophagy* 15, 34–57. doi: 10.1080/15548627.2018.1507438

Vaz, F. M., McDermott, J. H., Alders, M., Wortmann, S. B., Kölker, S., Pras-Raves, M. L., et al. (2019). Mutations in PCYT2 disrupt etherlipid biosynthesis and cause a complex hereditary spastic paraplegia. *Brain* 142, 3382–3397. doi: 10.1093/brain/awz291

Wan, J., Yourshaw, M., Mamsa, H., Rudnik-Schöneborn, S., Menezes, M. P., Hong, J. E., et al. (2012). Mutations in the RNA exosome component gene EXOSC3 cause pontocerebellar hypoplasia and spinal motor neuron degeneration. *Nat. Genet.* 44, 704–708. doi: 10.1038/ng.2254

Warner, T., Patel, H., Proukakis, C., Reed, J., McKie, L., Wills, A., et al. (2004). A clinical, genetic and candidate gene study of Silver syndrome, a complicated form of hereditary spastic paraplegia. *J. Neurol.* 251, 1068–74. doi: 10.1007/s00415-004-0401-8

Watchon, M., Yuan, K. C., Mackovski, N., Svahn, A. J., Cole, N. J., Goldsbury, C., et al. (2017). Calpain inhibition is protective in Machado–Joseph disease zebrafish due to induction of autophagy. *J. Neurosci.* 37, 7782–7794. doi: 10.1523/JNEUROSCI.1142-17.2017

Wood, J. D. (2006). The microtubule-severing protein Spastin is essential for axon outgrowth in the zebrafish embryo. *Hum. Mol. Genet.* 15, 2763–2771. doi: 10.1093/hmg/ddl212

Yamanaka, K., Miller, T. M., McAlonis-Downes, M., Chun, S. J., and Cleveland, D. W. (2006). Progressive spinal axonal degeneration and slowness in ALS2-deficient mice. *Ann. Neurol.* 60, 95–104. doi: 10.1002/ana.20888

Zada, D., Tovin, A., Lerer-Goldshtein, T., and Appelbaum, L. (2016). Pharmacological treatment and BBB-targeted genetic therapy for MCT8-dependent hypomyelination in zebrafish. *Dis. Model. Mech.* 9, 1339–1348. doi: 10.1242/dmm.027227

Zada, D., Tovin, A., Lerer-Goldshtein, T., Vatine, G. D., and Appelbaum, L. (2014). Altered behavioral performance and live imaging of circuit-specific neural deficiencies in a zebrafish model for psychomotor retardation. *PLoS Genet.* 10:e1004615. doi: 10.1371/journal.pgen.1004615

Zhang, C., Li, D., Ma, Y., Yan, J., Yang, B., Li, P., et al. (2012). Role of spastin and protrudin in neurite outgrowth. *J. Cell. Biochem.* 113, 2296–2307. doi: 10.1002/jcb.24100

Zhao, J., and Hedera, P. (2013). Hereditary spastic paraplegia-causing mutations in atlastin-1 interfere with BMPRII trafficking. *Mol. Cell. Neurosci.* 52, 87–96. doi: 10.1016/j.mcn.2012.10.005

Zhao, X., Alvarado, D., Rainier, S., Lemons, R., Hedera, P., Weber, C. H., et al. (2001). Mutations in a newly identified GTPase gene cause autosomal dominant hereditary spastic paraplegia. *Nat. Genet.* 29, 326–331. doi: 10.1038/ng758

Zhu, P.-P. (2006). SPG3A protein atlastin-1 is enriched in growth cones and promotes axon elongation during neuronal development. *Hum. Mol. Genet.* 15, 1343–1353. doi: 10.1093/hmg/ddl054

Zhu, P.-P., Patterson, A., Lavoie, B., Stadler, J., Shoeb, M., Patel, R., et al. (2003). Cellular localization, oligomerization, and membrane association of the hereditary spastic paraplegia 3A (SPG3A) protein atlastin. *J. Biol. Chem.* 278, 49063–49071. doi: 10.1074/jbc.M306702200

Zivony-Elboum, Y., Westbroek, W., Kfir, N., Savitzki, D., Shoval, Y., Bloom, A., et al. (2012). A founder mutation in Vps37A causes autosomal recessive complex hereditary spastic paraparesis. *J. Med. Genet.* 49, 462–472. doi: 10.1136/jmedgenet-2012-100742

Conflict of Interest: The authors declare that the research was conducted in the absence of any commercial or financial relationships that could be construed as a potential conflict of interest.

frontiers in Neuroscience

ORIGINAL RESEARCH
published: 21 February 2020
doi: 10.3389/fnins.2020.00111

Efficacy of a Combined Treatment of Botulinum Toxin and Intensive Physiotherapy in Hereditary Spastic Paraplegia

Gabriella Paparella[1], Marinela Vavla[1,2], Lisa Bernardi[1], Giulia Girardi[1], Cristina Stefan[1] and Andrea Martinuzzi[1,2]*

[1] *Acquired Neuropsychological Disease Rehabilitation Unit, Scientific Institute, IRCCS Eugenio Medea, Pieve di Soligo, Italy,*
[2] *Severe Developmental Disabilities Unit, Scientific Institute, IRCCS Eugenio Medea, Conegliano, Italy*

Introduction: The Hereditary Spastic Paraplegia (HSP) is a heterogeneous group of neurodegenerative disorders characterized by progressive spasticity and lower limbs (LL) weakness. There is no treatment to cure or halt the disease, except for symptomatic therapy. The use of botulinum toxin type A (BoNT-A) is one of the primary treatment for focal spasticity. Physiotherapy (PT) can help in maintaining residual functioning. We performed a retrospective study to evaluate the effect of the combined BoNT-A and intensive PT in patients with HSP.

Methods: Eighteen adult patients (50% females) with clinical diagnosis of HSP were recruited. Eleven patients had a genetic diagnosis of SPG4, 5, 7, 8, 11, 72. Patients were all autonomously deambulant or needed support. BoNT-A was injected in 36 LL in different spastic muscles under electromyographic guidance and followed by intensive PT sessions. Outcome measures included disease severity, motor functional measures, perceived pain self-report and quality of life. Assessments occurred at baseline, 1 and 3 months after BoNT-A injection.

Results: Most inoculated muscles were hamstrings, rectus femoris and gastrocnemius. We observed an improvement in muscle tone, in the gait velocity and distance length. Spastic Paraplegia Rating Scale was significantly reduced after treatment, in addition to improving pain and quality of life. These results were riconfirmed in 3 months time.

Conclusion: Our study indicates that combined treatment of BoNT-A and PT can lead to improvement of spasticity and quality of life in patients with HSP.

Keywords: hereditary spastic paraplegia, spasticity, lower limbs, botulinum toxin A, physiotherapy

OPEN ACCESS

Edited by:
Mark P Burns,
Georgetown University, United States

Reviewed by:
Federica Vellante,
Università degli Studi G. d'Annunzio Chieti e Pescara, Italy
Jonas Alex Morales Saute,
Federal University of Rio Grande do Sul, Brazil

****Correspondence:***
Gabriella Paparella
gabriella.paparella@lanostrafamiglia.it

Specialty section:
This article was submitted to Neurodegeneration, a section of the journal Frontiers in Neuroscience

Received: *05 August 2019*
Accepted: *28 January 2020*
Published: *21 February 2020*

Citation:
Paparella G, Vavla M, Bernardi L, Girardi G, Stefan C and Martinuzzi A (2020) Efficacy of a Combined Treatment of Botulinum Toxin and Intensive Physiotherapy in Hereditary Spastic Paraplegia. Front. Neurosci. 14:111. doi: 10.3389/fnins.2020.00111

INTRODUCTION

The Hereditary Spastic Paraplegia (HSP) or Strumpell-Lorrain syndrome comprises a heterogeneous group of neurodegenerative disorders caused by axonal retrograde degeneration of the long corticospinal tracts (Fink, 2014; Lo Giudice et al., 2014; Klebe et al., 2015; de Souza et al., 2017). HSP presents with progressive spasticity and weakness of the lower limbs (LL), reduced

vibration sense, hyperactive deep tendon reflexes and inconstant urinary urgency (Fink, 2014; Lo Giudice et al., 2014; Klebe et al., 2015; de Souza et al., 2017).

The HSP prevalence is difficult to estimate due to different data present in literature. According to a recent epidemiological survey, the world-wide prevalence of HSP is 1.8 – 5.5: 10^5, with variability depending on the geographical area considered (Ruano et al., 2014). The age of onset is variable, ranging from early childhood to the eighth decade (Fink, 2014; Lo Giudice et al., 2014; Klebe et al., 2015). Currently, more than 85 genomic loci and 79 mutated genes associated with HSP have been identified, highlighting the extreme heterogeneity in the mode of transmission and in the role of encoded proteins (Parodi et al., 2018). The prognosis and the severity of the clinical picture in HSP varies between families and, to a lesser extent, within the same family, although life expectancy is normal. When the disease occurs in early childhood, the symptoms may not progress significantly for several years and decades; on the contrary, the late-onset HSPs might be associated with a more insidious worsening pattern (Harding, 1993). Finally, it has been reported that, while in the pure forms patients rarely resort to using the wheelchair but frequently walk with aids, in the complex forms the functional disability depends on the extent and severity of extra-motor involvement (Lo Giudice et al., 2014).

The LL spasticity, often accompanied by muscle weakness, is the key clinical sign of HSP that affects a wide group of muscles such as the hamstrings, quadriceps, adductors, gastrocnemius and soleus. In particular, the weakness primarily concerns the iliopsoas, hamstring muscles, and tibialis anterior (Fink, 2014). Typically, there is a strong discrepancy between the severity of spasticity, often present at disease onset, and the weakness which might be subtler and appear at a late stage of disease (McDermott et al., 2000). There is no specific treatment for HSP to prevent or reduce the gait impairment and disability progression. Current therapies are symptomatic and aim to prevent complications such as multiple LL muscle contractures, pain and fractures, and also aim to improve patients' quality of life (de Souza et al., 2017).

Physiotherapy (PT) is generally recommended to improve articulation, maintain and increase LL strength, prevent muscle atrophy, delay or prevent contractures or deformities, improve cardiovascular endurance and mobility in spastic patients (Fink, 2013). Even though frequently prescribed and performed, little experience has been reported in regard to the PT in HSP patients.

The selective chemodenervation via intramuscular injection of botulinum toxin type A (BoNT-A) is widely used in the treatment of focal spasticity in patients with stroke, multiple sclerosis, spinal cord injuries and various neurological disorders (Dunne et al., 1995; Keren et al., 2000; Ward, 2008). There have been several reports on the use of botulinum toxin in HSP patients but with discrepancy of the various clinical protocols (Rousseaux et al., 2007; Hecht et al., 2008; Geva-Dayan et al., 2010; de Niet et al., 2015; Riccardo et al., 2016; Servelhere et al., 2018). Previous studies demonstrate the effectiveness of toxin injection at the level of triceps sural and/or of the adductors muscles as beneficial in reducing the spasticity and increasing the walking speed (Rousseaux et al., 2007; Hecht et al., 2008; de Niet et al., 2015). However, functional improvements have been found only in a limited number of patients with a clinical diagnosis of HSP. The motor and non-motor effects of BoNT-A were described in 33 patients with definite HSP diagnosis (Servelhere et al., 2018), reporting improvement in terms of adductors tone reduction and perceived fatigue. The muscles more frequently inoculated were: triceps sural and adductors. The muscles more inoculated were: triceps sural and adductors. Toxin infiltration was performed with only palpation as a guide and this could limit the accuracy and effectiveness of the treatment. Most of the other studies (Hecht et al., 2008; de Niet et al., 2015; Riccardo et al., 2016) evaluated the functional effects of botulinum toxin associated with PT treatment in patients with HSP. However, none of these studies disclosed the PT rehabilitation program to which patients were subjected.

The objective of this study was to investigate the effects of a combined treatment of BoNT-A injection and subsequent intensive PT in the management of spasticity in adult HSP patients. This experience could provide an indication for a rehabilitation protocol in these patients.

MATERIALS AND METHODS

Design

This was a retrospective observational cohort study, as classified by the Institutional Review Board (IRB). The study scheme is represented in **Figure 1**.

Participants

A total of 18 patients with clinical diagnosis of HSP treated with BoNT-A injections were recruited at the "Eugenio Medea" Scientific Institute in Pieve di Soligo (Treviso, Italy) from 2013 until 2018. Our study has been approved by the Institutional Ethics Committee of "Eugenio Medea" Research Institute (# 63/09CE) and was conducted in accordance to the ethical standards of the Declaration of Helsinki (World Medical Association, 1964). All participants were informed about the experimental nature of the study and signed an informed consent for participation. During treatment patients had not been subjected to any other form of PT in addition to the program scheduled in the study protocol. The inclusion criteria were: clinical diagnosis of HSP, confirmed or ongoing genetic investigation, aged 18 years and older, ambulant patients with or without walking aid. Moreover, the recruited patients had been referred to our institute for LL BoNT-A injection. Exclusion criteria included any orthopedic injury that could eventually limit their ability to mobilize and/or any clinical condition that could affect their motor skills.

Intervention

BoNT-A Injection

All patients received intramuscular injection of BoNT-A under electromyographic guidance. Three forms of BoNT-A were used: Xeomin (Merz), Dysport (Ipsen) and Botox (Allergan). The dose of botulinum toxin was determined after careful evaluation of each patient's weight, degree of spasticity, number and type of

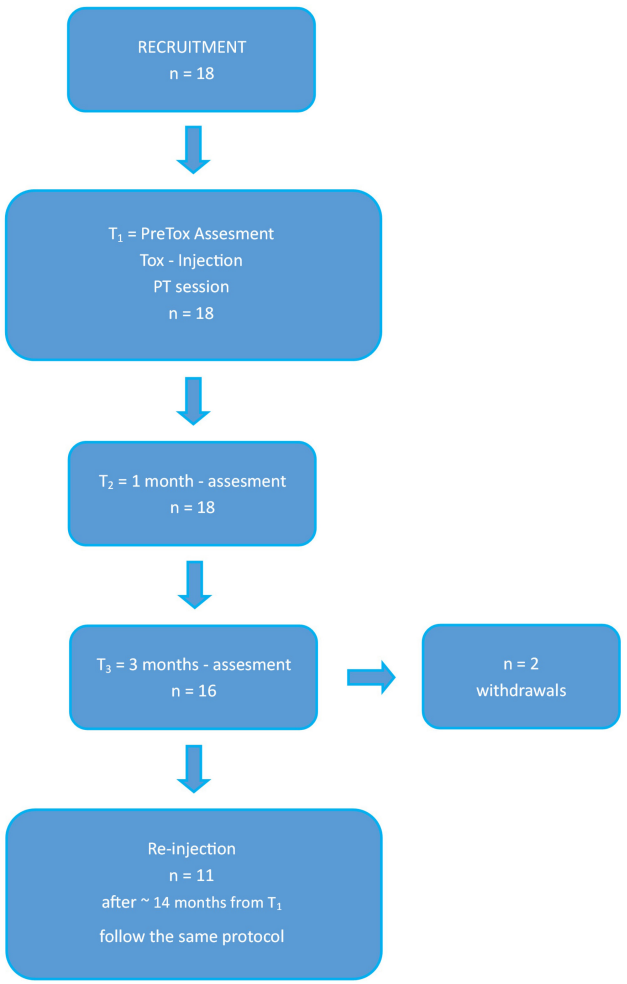

FIGURE 1 | Study scheme. Working flowchart used for this study. Tox, toxin, PT, physiotherapy, T1, assessment at baseline; T2, assessment at 1 month; T3, assessment at 3 months.

target muscles injected. The injections were repeated twice with a minimum inter-injection interval of 3 months in 11 of the 18 enrolled patients.

PT Protocol

After the focal chemodenervation, the patients underwent intensive PT, according to their functionality, impairments and goals. The intervention was an individualized inpatient rehabilitation program consisting in 2 h PT daily for overall 10 sessions. The focus of the PT program was to improve physical abilities, in particular postural control, balance abilities and gait pattern that would subsequently prevent falls, inactivity, reduce the fatigue in walking in order to maintain the independence.

The PT protocol followed some key points given below:

(1) Stretching and mobilizing in order to lengthen the inoculated muscles;
(2) Postural control and trunk stability with activation of deep trunk musculature and paravertebral musculature;
(3) Foot core training;
(4) Stimulation of anticipatory postural adjustments in order to reduce compensations or fixation, following an appropriate orientation of LL;
(5) Strengthening focused on LL (in particular of antagonist muscles) and trunk muscles. The muscle strengthening should be specific, without the use of rewards on motor control. The weak muscles are usually represented from hip extensor and abductors, knee extensor and ankle dorsal flexors, that are important even in the antigravity postural control;
(6) Gait training to improve gait pattern and reduce the risk of falls;
(7) Cardiovascular activity that includes cycle ergometer, treadmill and gait trainer. This improves muscular endurance and strength, helps integrating learned patterns and prevents the weakness of not activated muscles.

Outcome Measures

Assessments occurred at baseline (T1), one (T2), and 3 months (T3) after BoNT-A injection. Patients were assessed according to a specific clinical protocol executed by the same physiotherapist.

The assessment consisted in the following measures:

- Spastic Paraplegia Rating Scale (SPRS, Schüle et al., 2006), which has been approved as a valid measure of disease severity in HSP. It has a maximum score of 52 (maximum severity) and a minimum of 0 (normal).
- Walking Handicap Scale (WHS, Perry et al., 1995) which evaluates the level of functional walking ability at home and in the community. This scale ranges from 1 (physiological walker) to 6 (community walker).
- The Modified Ashworth Scale (MAS, Bohannon and Smith, 1987) used to measure the spasticity. The MAS measures resistance during the passive stretch of a joint. This scale ranges from 0 (normal tone) to 4 (rigidity of the joint).
- The 10 Meter Walking Test (10MWT, Rossier and Wade, 2001) and 2 Minute Walking Test (2MWT, Bohannon et al., 2015) used to measure the deambulation skills. These scales measure velocity and resistance of gait. We consider only comfortable gait as a normal speed gait.
- Timed UP and Go test (TUG, Podsiadlo and Richardson, 1991) assesses functional mobility, walking ability, balance and risk of falls.
- The Visual Analogical Scale (VAS, Hayes and Patterson, 1921) and Numeric Rating Scale (NRS, Williamson and Hoggart, 2005) which assess the perceived quality of life and pain respectively. Both scales range from 0 (no pain/none satisfaction in quality of life) to 10 (severe pain/full satisfaction in quality of life).

Statistical Analysis

Linear mixed models were used to study the relationship between the results of each test (i.e., 10MWT, 2MWT, TUG, WHS, VAS, NRS, SPRS) at the three time points (fixed effect), considering the subject as a random effect. The "lme4" R package was used to fit the aforementioned models (Bates et al., 2015). *Post hoc* tests were used to pairwise compare the values between time

points (i.e., T1 vs. T2, T1 vs. T3, and T2 vs. T3), based on *t*-Student distribution with degrees of freedom (df) computed by the Kenward-Rogers method using the "emmeans" R package (Lenth, 2019).

Similarly, in order to study the MAS values that were measured on an ordinal scale, we adopted a cumulative link mixed model that handles the ordered nature of the data. The time points (T1, T2, and T3) and the LL (right or left) were considered as fixed effects, while the subject was incorporated in each model as random effect. The "ordinal" R package was used to fit these models (Christensen, 2019). *Post hoc* tests were used to pairwise compare the MAS values between time points (i.e., T1 vs. T2, T1 vs. T3, and T2 vs. T3), based on asymptotic approximation using the "emmeans" R package (Lenth, 2019). Results of the *post hoc* tests were computed considering the average over the right and left MAS values of each muscle. Correction of the *post hoc* tests for multiple comparisons was performed with Benjamini-Hochberg (false discovery rate) procedure. Adjusted $P < 0.05$ was considered significant. Analyses were done in R (version 3.6.0).

RESULTS

Patients

According to defined inclusion criteria we recruited 18 patients with mean age of 53.9 ± 12.2 years, disease duration of 9.5 ± 5.3 years and age at onset of 44.4 ± 13.01 years. There were nine females. All patients included in the study were able to walk with (n = 6) or without (n = 12) walking aids on a level surface. Defined molecular diagnosis of HSP was reached in eleven patients: SPG4 was the most frequent genotype (27.8%); the remaining study population had SPG8, 5, 7, 11, 72 diagnosis. Seven patients did not have a defined molecular diagnosis at the time of examination, but they showed either a recessive (n = 3) or dominant (n = 4) inheritance pattern. The demographic and clinical data of these subjects are presented in **Table 1**.

TABLE 1 | Demographic and clinical data of patients included in this study.

Variable	Patients n = 18
Gender *M/F*	9/9
	Mean ± SD (Range)
Age, years	53.9 ± 12.2 (30.7–75.2)
Age at onset, years	44.4 ± 13.0 (26–70)
Disease duration, years	9.5 ± 5.3 (2.5–22.2)
Genotype	***n (%)***
SPG4	5 (27.8)
SPG5	1 (5.55)
SPG7	1 (5.55)
SPG8	2 (11.1)
SPG11	1 (5.55)
SPG72	1 (5.55)
Molecular diagnosis ongoing	7 (38.9)
Deambulation	***n (%)***
Independent	12 (66.7)
With a cane	3 (16.6)
With a walker	2 (11.1)
With crutches	1 (5.6)

M, male; F, female; SD, standard deviation; SPG, spastic paraplegia gene.

TABLE 2 | Evolution of Modified Ashworth scores in time.

Muscle	N	Mean ± SD (Min-Max)		
		T1	T2	T3
Rectus femoris	28	1.6 ± 0.7 (1–3)	1.1 ± 0.8 (0–2)	0.6 ± 0.5 (0–2)
Hamstring	28	1.3 ± 0.7 (0–3)	0.9 ± 0.9 (0–3)	1 ± 0.8 (0–2)
Adductors	8	2 ± 0.5 (1–3)	1.4 ± 0.9 (0–3)	0.9 ± 0.6 (0–2)
Gastrocnemius	13	1.7 ± 0.9 (1–3)	0.8 ± 0.8 (0–3)	1.33 ± 1.1 (0–3)
Soleus	5	1.8 ± 1 (1–3)	1 ± 1.4 (0–3)	1 ± 1.2 (0–3)

T1, assessment at baseline; T2, assessment at 1 month; T3, assessment at 3 months.

Intervention and Evaluations

All patients included in the study were given intramuscular injections of BoNT-A and afterward underwent the intensive PT sessions, completing the proposed treatment. BoNT-A was injected in 36 LL (18 right LL, 18 left LL), for a total of 85 muscles. Most inoculated muscles were hamstrings (n = 28), rectus femoris (n = 28), gastrocnemius (n = 13) and adductors (n = 8). None of the patients enrolled had side effects after treatment. All patients have been evaluated according to the clinical protocol. Only two patients have not been assessed 3 months after BoNT-A injection (T3) for missed appointments.

Variations of Modified Ashworth Scale in Time

Table 2 presents variation of spasticity in time for the muscles injected. As shown in **Table 3**, MAS values were significantly reduced from T1 to T2 for rectus femoris (z = −4.086, adjusted P = 0.0004) and hamstring (z = −2.787, adjusted P = 0.0166) with rectus femoris MAS values decreasing further from T2 and T3 (z = −3.242, adjusted P = 0.0071) (see **Figures 2**, **3**). Finally, treatment also resulted in a significant reduction in gastrocnemius spasticity from T1 to T2 (z = −112.825, adjusted P = 0.0166).

Variations of Functional Scales in Time

Table 4 presents evolutions of other evaluation scales in time. First of all, treatment resulted in a significant improvement in the 10MWT (see **Figure 4**). We observed a significant variation from T1 to T3 for the values of all scales, specifically a reduction for 10MWT (t = −4.034, df = 30, adjusted P = 0.0012), TUG (t = −2.477, df = 30, adjusted P = 0.0364), and an increase

TABLE 3 | Results of the *post hoc* comparisons of the Modified Ashworth scores between time points.

Muscle	First injection		
	T1 vs. T2	T1 vs. T3	T2 vs. T3
Rectus Femoris	**0.0004**	**<0.0001**	**0.0071**
Hamstring	**0.0166**	**0.0447**	0.9058
Adductors	0.0561	**0.0166**	0.0956
Gastrocnemius	**0.0166**	0.0818	0.1211
Soleus	0.1631	0.1916	0.8556

Data are adjusted P-values with Benjamini-Hochberg correction. Numbers in bold: adjusted $P < 0.05$. T1, assessment at baseline; T2, assessment at 1 month; T3, assessment at 3 months.

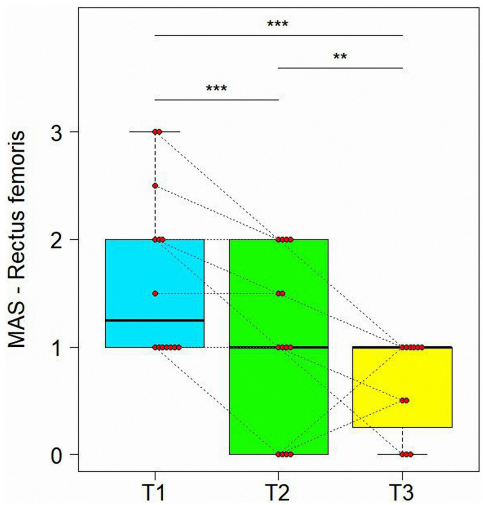

FIGURE 2 | Variations of Modified Ashworth scores (MAS) in time for Rectus Femoris. Data are represented by boxplots at three time point: before the treatment (T1), after 1 month (T2) and after 3 months (T3) from the treatment. At each time, individual values of patients are also shown as red points. Values of the same subject at different times are connected by a line. Significant differences between times are represented with asterisks: **$0.001 < P < 0.01$, ***$P < 0.001$.

for 2MWT ($t = 4.116$, $df = 30$, adjusted $P = 0.0012$) and WHS ($t = 3.185$, $df = 27$, adjusted $P = 0.0084$) (**Table 5**). Similar significant variations were found also between T1 and T2 for 10MWT ($t = -5.136$, $df = 30$, adjusted $P = 0.0002$) and 2MWT ($t = 3.277$, $df = 30$, adjusted $P = 0.0080$).

Variations of VAS and NRS Scores in Time

As reported in **Table 5**, there was a significant reduction from T1 to T3 for VAS ($t = 3.36$, $df = 19$, adjusted $P = 0.0084$) and NRS ($t = -5.500$, $df = 24$, adjusted $P = 0.0002$) scores. We also found a significant improvement from T1 to T2 for NRS ($t = -4.170$, $df = 24$, adjusted $P = 0.0012$) (see **Figure 5**).

Variations of SPRS Scores in Time

The main result of BoTN-A injections and intensive PT was a reduction of disease severity, highlighted by evolution of SPRS in time (see **Figure 6**). In fact, we demonstrate a significant

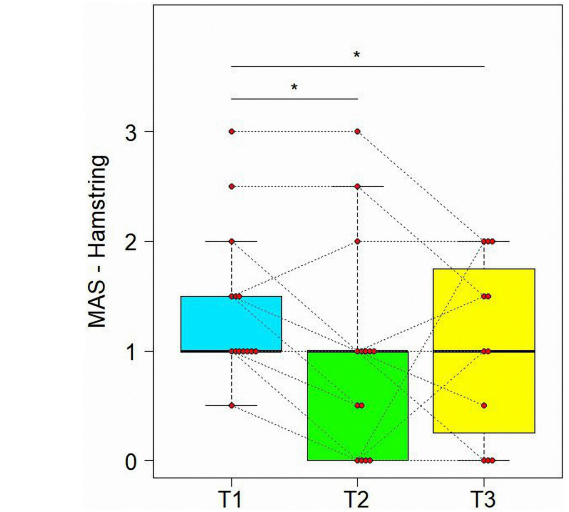

FIGURE 3 | Variations of Modified Ashworth scores (MAS) in time for Hamstring. Data are represented by boxplots at three time points: before the treatment (T1), after 1 month (T2) and after 3 months (T3) from the treatment. At each time, individual values of patients are also shown as red points. Values of the same subject at different times are connected by a line. Significant differences between times are represented with asterisks: *$0.01 < P < 0.05$.

reduction from T1 to T3 for SPRS score ($t = -4.677$, $df = 30$, adjusted $P = 0.0004$). Similar significant improvement was found also between T1 and T2 ($t = -3.008$, $df = 30$, adjusted $P = 0.0111$), as shown in **Table 5**.

Re-injection

Of the initial group ($n = 18$), eleven patients underwent a second combined treatment of BoTN-A and intensive PT, after 1.2 ± 0.4 years from the first one. As the first injection, most injected muscles were rectus femoris ($n = 16$), hamstring ($n = 12$), and gastrocnemius ($n = 8$). All these patients were subjected a second standardized clinical evaluation, which highlighted results comparable to those obtained at first injection. In particular, as shown in **Table 6**, the same muscles showed lower MAS values at T2 than T1, but they were not significantly different between T2 and T3. Analogous results were also observed for NRS scale, that had significantly lower values only at T3 with respect to both T1 ($t = -3.836$, $df = 16$, adjusted $P = 0.0075$) and T2 ($t = -2.542$, $df = 16$, adjusted $P = 0.0450$). By contrast, TUG values were no longer statistically different between the three time points, as shown in **Table 7**.

DISCUSSION

The aim of this study was to evaluate the effects of a combined treatment of BoTN-A followed by intensive PT in HSP patients with preserved walking ability. Our study showed significant functional improvement in all the outcome measures used, which was maintained for at least 3 months.

Although previous studies concerning BoTN-A treatment in HSP patients focused on distal musculature (gastrocnemius

TABLE 4 | Evolution of other evaluation scales in time.

Scale	T1			T2			T3		
	n	Median	Range (min-max)	n	Median	Range (min-max)	n	Median	Range (min-max)
10MWT *(s)*	18	9	4.5–35.8	18	7.1	3.1–24.7	14	7	4.4–27.6
2MWT *(m)*	18	78.5	22–179	18	99.5	29.5–184	14	99.5	27.5–190.7
TUG *(s)*	18	14.3	6.5–55	18	12.5	6.5–51	14	11.9	5.2–49.5
WHS *(1–6)*	16	5	2–5	16	5	2–6	13	5	3–6
VAS *(0–10)*	12	4	2–8	12	4	0–8	10	4	0–6
NRS *(0–10)*	18	5	1–8	18	3.5	0–6	14	3	0–6
SPRS *(0–52)*	18	17	7–36	18	17	6–35	14	15.5	6–34

10MWT, 10 Meter Walk Test; 2MWT, 2 Minute Walk Test; TUG, Timed Up and Go; WHS, Walking Handicap Scale; VAS, Visual Analogical Scale; NRS, Numeric Rating Scale; SPRS, Spastic Paraplegia Rating Scale; T1, assessment at baseline; T2, assessment at 1 month; T3, assessment at 3 months.

and soleus) or adductors, we decided to perform the BoTN-A treatment especially on hamstrings, rectus femoris, and, to a lesser extent, on gastrocnemius and adductors. Our choice was based on studies carried out in HSP patients with gait analysis: the spasticity of rectus femoris is often cause of an excessive antiversion of the pelvis on the sagittal plane and an excessive flexion of the hip during gait cycle (Piccinini et al., 2011). The Gait analysis highlighted hamstrings and rectus femoris co-contraction. This can reduce gait stability and patients may adopt expensive compensatory strategies at knee (e.g., hyperextension) and trunk (e.g., forward lean). Our study identified a short and medium-term improvement in rectus femoris and hamstrings spasticity. In accordance to previous studies, the reduction of the MAS was relatively modest. Nevertheless, HSP patients exhibit dynamic hypertonus during gait and perhaps it would be more appropriate to evaluate muscle spasticity with Gait Analysis.

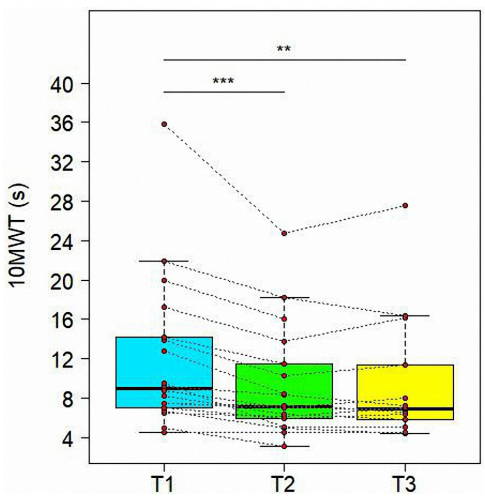

FIGURE 4 | Variations of 10 Meter Walk Test (10MWT) in time. Data are represented by boxplots at three time points: before the treatment (T1), after 1 month (T2) and after 3 months (T3) from the treatment. At each time, individual values of patients are also shown as red points. Values of the same subject at different times are connected by a line. Significant differences between times are represented with asterisks: **$0.001 < P < 0.01$, ***$P < 0.001$.

From a functional point of view, the treatment proposed in this study gave rise to a significant increase in the comfortable gait velocity as evaluated with the 10MWT. These results are in agreement with several previous studies that considered the same outcome measure for evaluating the efficacy of the BoNT-A (Rousseaux et al., 2007; de Niet et al., 2015). Secondly, the combination of BoNT-A and the intensive PT has led to an increase of the distance walked in 2MWT and in exercise resistance. Indeed, the injection of some specific muscles (rectus femoris, hamstring and gastrocnemius), leads to a reduction in spasticity and less compensatory strategies implemented by patients during the walk, improvement of biomechanics and reduced energy consumption.

Thirdly, a significant improvement was obtained with the TUG test, in particular at 3 months after the BoNT-A injection. This result highlights the effectiveness of the combined treatment of BoNT-A and intensive PT in terms of better stability and increased capacity for selective muscle control. de Niet et al. (2015) previously administered this outcome measure, but in contrast they registered no post-treatment improvement. This discrepancy of results could be attributed to the difference in muscles treated (only plantar flexors) and also could be due to the differences in the PT program that consisted in independently

TABLE 5 | Results of the *post hoc* comparisons of the evaluation scales between time points.

Scale	First injection		
	T1 vs. T2	T1 vs. T3	T2 vs. T3
10MWT	**0.0002**	**0.0012**	0.5335
2MWT	**0.0080**	**0.0012**	0.2907
TUG	0.1408	**0.0364**	0.3731
WHS	0.1408	**0.0084**	0.1616
VAS	0.2472	**0.0084**	0.0949
NRS	**0.0012**	**0.0002**	0.1616
SPRS	**0.0111**	**0.0004**	0.0984

Data are adjusted P-values with Benjamini-Hochberg correction. Numbers in bold: adjusted $P < 0.05$. 10MWT, 10 Meter Walk Test; 2MWT, 2 Minute Walk Test; TUG, Timed Up and Go; WHS, Walking Handicap Scale; VAS, Visual Analogical Scale; NRS, Numeric Rating Scale; SPRS, Spastic Paraplegia Rating Scale; T1, assessment at baseline; T2, assessment at 1 month; T3, assessment at 3 months.

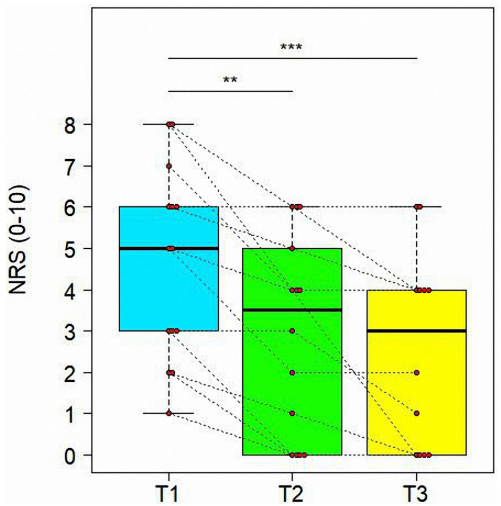

FIGURE 5 | Variations of Numeric Rating Scale (NRS) in time. Data are represented by boxplots at three time points: before the treatment (T1), after 1 month (T2) and after 3 months (T3) from the treatment. At each time, individual values of patients are also shown as red points. Values of the same subject at different times are connected by a line. Significant differences between times are represented with asterisks: $^{**}0.001 < P < 0.01$, $^{***}P < 0.001$.

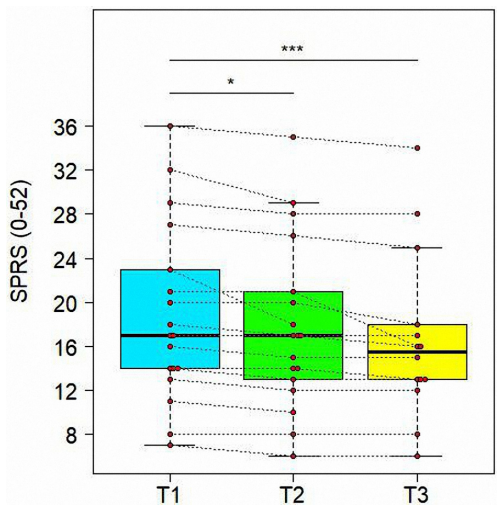

FIGURE 6 | Variations of Spastic Paraplegia Rating Scale (SPRS) in time. Data are represented by boxplots at three time points: before the treatment (T1), after 1 month (T2) and after 3 months (T3) from the treatment. At each time, individual values of patients are also shown as red points. Values of the same subject at different times are connected by a line. Significant differences between times are represented with asterisks: $^{*}0.01 < P < 0.05$, $^{***}P < 0.001$.

performed single stretching exercise (de Niet et al., 2015). It is plausible that the lack of a specific PT program may have reduced the selective control capacity of patients.

Finally, a further functional improvement, was recorded in the WHS scale. In most cases, there has been a short-term

TABLE 6 | Results of the *post hoc* comparisons of the Modified Ashworth scores between time points at the second injection.

Muscle	Second injection		
	T1 vs. T2	**T1 vs. T3**	**T2 vs. T3**
Rectus Femoris	**0.0131**	**0.0131**	0.9885
Hamstring	**0.0303**	**0.0131**	0.3094
Adductors	NA	NA	NA
Gastrocnemius	**0.0303**	**0.0271**	0.0748
Soleus	NA	NA	NA

Data are adjusted P-values with Benjamini-Hochberg correction. Numbers in bold: adjusted $P < 0.05$. NA = Not Available due to limited sample size. T1, assessment at baseline; T2, assessment at 1 month; T3, assessment at 3 months.

TABLE 7 | Results of the *post hoc* comparisons of the other evaluation scales between time points at second injection.

Scale	Second injection		
	T1 vs. T2	**T1 vs. T3**	**T2 vs. T3**
10MWT	**0.0241**	**0.0258**	0.9673
2MWT	**0.0248**	0.2841	0.2890
TUG	0.0682	0.2841	0.4935
WHS	0.2890	**0.0159**	0.1000
VAS	**0.0071**	**0.0035**	0.4935
NRS	0.3094	**0.0075**	0.0450
SPRS	**0.0130**	**0.0035**	0.4062

Data are adjusted P-values with Benjamini-Hochberg correction. Numbers in bold: adjusted $P < 0.05$. 10MWT, 10 Meter Walk Test; 2MWT, 2 Minute Walk Test; TUG, Timed Up and Go; WHS, Walking Handicap Scale; VAS, Visual Analogical Scale; NRS, Numeric Rating Scale; SPRS, Spastic Paraplegia Rating Scale; T1, assessment at baseline; T2, assessment at 1 month; T3, assessment at 3 months.

improvement in the quality of the walking in the social sphere. This scale is less sensitive to variations because it is a coarse scale that includes only 6 functional categories. The treatment proposed in this study was demonstrated to be effective in terms of quality of life, with a significant improvement at 3 months. Our study also showed a significant improvement of the pain perceived by patients. Only one previous study has investigated the effectiveness of BoNT-A in HSP in terms of pain reduction, but showed no significant improvements (Servelhere et al., 2018). However, the same study did not combine the chemodenervation with PT and this may have mitigated the effects of the treatment. In our study, pain and the quality of life perceived by patients, improved significantly 3 months after treatment. We hypothesize that the intensive.

PT we proposed after the injection has conducted to a gradual training of the muscle chains and a progressive modification of the motor pattern. This has determined a reduction of pain and stiffness perceived either in static or dynamic posture in the medium-long term.

One of the major contributions of our study concerns the use of SPRS as an outcome measure of disease severity in HSP. The significant improvement on SPRS scores recorded

both at 1 month, and especially at 3 months, highlights the effectiveness of the proposed intervention in terms of modifying disease severity. This could be also an indicator of an improved quality of life.

Another fundamental contribution of this study concerns the design of a combined protocol of BoNT-A injection with a specific PT programme that contributes to improvement of postural control, balance abilities and gait pattern. Use of BoNT-A combined with PT shows interesting results after the second chemodenervation, suggesting this formula as an appropriate therapy for an incurable disease. Finally, the intervention proposed in our study showed an excellent tolerability for all the patients since no adverse events were reported.

A limitation of this study is the small patient sample, as well the genetic and clinical heterogeneity of our cohort. In addition, there was no specific BoNT-A injection protocol, since the target muscles, botulinum type and administration of doses were left to the evaluating physicians. It was also a retrospective study with no control group.

Therefore, it is essential that future studies include larger cohorts of participants and a randomized controlled design. The combined treatment protocol of BoNT-A injection and PT could be compared to control groups such as intensive PT or BoNT-A only. In addition, it could be of interest to investigate the different treatment outcomes and protocols in various SPG types and distinct clinical phenotypes.

Future studies could systematically implement the use of more detailed techniques such as gait analysis that provides biomechanical measurement of the gait cycle. Although the MAS is the most widely used tool for assessing muscle tone, it is not very sensitive. For that reason, spasticity could be assessed more accurately also by the Tardieu Scale due to its better sensibility in differentiating the contractures from spasticity (Patrick and Ada, 2006). Moreover, the inclusion of an objective outcome measure such as the energy cost of walking, measured by cycle ergometry, could add strength to the results and provide a more rigorous rationale to explain the functional perceived improvement.

The results of this study highlight that a combined treatment of BoNT-A and intensive PT improves function for people with HSP. Larger randomized controlled trials are needed to confirm the results obtained with this retrospective study and to possibly validate the effectiveness of this approach. These results could provide meaningful treatment options for the care of HSP patients.

DATA AVAILABILITY STATEMENT

All datasets generated for this study are available on request.

ETHICS STATEMENT

The studies involving human participants were reviewed and approved by the Institutional Ethics Committee of "Eugenio Medea" Research Institute (# 63/09CE) and were conducted in accordance to the ethical standards of the Declaration of Helsinki (World Medical Association, 1964). The patients/participants provided their written informed consent to participate in this study.

AUTHOR CONTRIBUTIONS

GP and LB collected and analyzed the data, and prepared the manuscript. GP, GG, and CS evaluated the patients and provided the data. GP and MV provided the design of the study. AM provided the design of the study, supervision and manuscript revision. All authors revised the manuscript for important intellectual content, provided approval for publication, and agreed to be accountable for all aspects of the work.

FUNDING

The author AM received funding from the Italian Ministry of Health (RC2019).

ACKNOWLEDGMENTS

We are very grateful to patients who took part in this study. We thank the statistical support of Riccardo Pascuzzo.

REFERENCES

Bates, D., Maechler, M., Bolker, B., and Walker, S. (2015). Fitting linear mixed-effects models using lme4. *J. Stat. Softw.* 67, 1–48.

Bohannon, R. W., and Smith, M. B. (1987). Interrater reliability of a modified Ashworth scale of muscle spasticity. *Phys. Ther.* 67, 206–207. doi: 10.1093/ptj/67.2.206

Bohannon, R. W., Wang, Y. C., and Gershon, R. C. (2015). Two-minute walk test performance by adults 18 to 85 years: normative values, reliability, and responsiveness. *Arch. Phys. Med. Rehabil.* 96, 472–477. doi: 10.1016/j.apmr.2014.10.006

Christensen, R. H. B. (2019). *ordinal - Regression Models for Ordinal Data. R Package Version 2019.4-25*. Available at: http://www.cran.r-project.org/package=ordinal/

de Niet, M., de Bot, S. T., van de Warrenburg, B. P. C., Weerdesteyn, V., and Geurts, A. C. (2015). Functional effects of botulinum toxin type-A treatment and subsequent stretching of spastic calf muscles: a study in patients with hereditary spastic paraplegia. *J. Rehabil. Med.* 47, 147–153. doi: 10.2340/16501977-1909

de Souza, P. V. S., de Rezende Pinto, W. B. V., de Rezende Batistella, G. N., Bortholin, T., and Oliveira, A. S. B. (2017). Hereditary spastic paraplegia: clinical and genetic hallmarks. *Cerebellum* 16, 525–551. doi: 10.1007/s12311-016-0803-z

Dunne, J. W., Heye, N., and Dunne, S. L. (1995). Treatment of chronic limb spasticity with botulinum toxin A. *J. Neurol. Neurosurg. Psychiatry* 58, 232–235. doi: 10.1136/jnnp.58.2.232

Fink, J. K. (2013). Hereditary spastic paraplegia: clinico-pathologic features and emerging molecular mechanisms. *Acta Neuropathol.* 126, 307–328. doi: 10.1007/s00401-013-1115-8

Fink, J. K. (2014). Hereditary spastic paraplegia: clinical principles and genetic advances. *Semin. Neurol.* 34, 293–305. doi: 10.1055/s-0034-1386767

Geva-Dayan, K., Domenievitz, D., Zahalka, R., and Fattal-Valevski, A. (2010). Botulinum toxin injections for pediatric patients with hereditary spastic

paraparesis. *J. Child Neurol.* 25, 969–975. doi: 10.1177/0883073809356037

Harding, A. E. (1993). Hereditary spastic paraplegias. *Semin. Neurol.* 13, 333–336. doi: 10.1055/s-2008-1041143

Hayes, M. H. S., and Patterson, D. G. (1921). Experimental development of the graphic rating method. *Psychol. Bull.* 18, 98–99.

Hecht, M. J., Stolze, H., Auf Dem Brinke, M., Giess, R., Treig, T., Winterholler, M., et al. (2008). Botulinum neurotoxin type A injections reduce spasticity in mild to moderate hereditary spastic paraplegia— Report of 19 cases. *Mov. Disord.* 23, 228–233. doi: 10.1002/mds.21809

Keren, O., Shinberg, F., Catz, A., and Giladi, N. (2000). Botulin toxin for spasticity in spinal cord damage by treating the motor endplate. *Harefuah* 138, 204–208.

Klebe, S., Stevanin, G., and Depienne, C. (2015). Clinical and genetic heterogeneity in hereditary spastic paraplegias: from SPG1 to SPG72 and still counting. *Rev. Neurol.* 171, 505–530. doi: 10.1016/j.neurol.2015.02.017

Lenth, R. (2019). *emmeans: Estimated Marginal Means, aka Least-Squares Means. R Package Version 1.3.5*. Available at: https://CRAN.R-project.org/package=emmeans

Lo Giudice, T., Lombardi, F., Santorelli, F. M., Kawarai, T., and Orlacchio, A. (2014). Hereditary spastic paraplegia: clinical-genetic characteristics and evolving molecular mechanisms. *Exp. Neurol.* 261, 518–539. doi: 10.1016/j.expneurol.2014.06.011

McDermott, C. J., White, K., Bushby, K., and Shaw, P. J. (2000). Hereditary spastic paraparesis: a review of new developments. *J. Neurol. Neurosurg. Psychiatry* 69, 150–160. doi: 10.1136/jnnp.69.2.150

Parodi, L., Coarelli, G., Stevanin, G., Brice, A., and Durr, A. (2018). Hereditary ataxias and paraparesias: clinical and genetic update. *Curr. Opin. Neurol.* 31, 462–471. doi: 10.1097/WCO.0000000000000585

Patrick, E., and Ada, L. (2006). The tardieu scale differentiates contracture from spasticity whereas the ashworth scale is confounded by It. *Clin. Rehabil.* 20, 173–182. doi: 10.1191/0269215506cr922oa

Perry, J., Garrett, M., Gronley, J. K., and Mulroy, S. J. (1995). Classification of walking handicap in the stroke population. *Stroke* 26, 982–989. doi: 10.1161/01.str.26.6.982

Piccinini, L., Cimolin, V., D'Angelo, M. G., Turconi, A. C., Crivellini, M., and Galli, M. (2011). 3D gait analysis in patients with hereditary spastic paraparesis and spastic diplegia: a kinematic, kinetic and EMG comparison. *Eur. J. Paediatr. Neurol.* 15, 138–145. doi: 10.1016/j.ejpn.2010.07.009

Podsiadlo, D., and Richardson, S. (1991). The timed "Up & Go": a test of basic functional mobility for frail elderly persons. *J. Am. Geriatr. Soc.* 39, 142–148. doi: 10.1111/j.1532-5415.1991.tb01616.x

Riccardo, M., Angela, L., Angela, D., Vita, P., Giulio, L., and Pietroq, F. (2016). Combined treatment Fkt-botulinum toxin type A (Btx-A) in patients with strumpell-lorrain disease. *Curr. Pharm. Des.* 22, 758–763. doi: 10.2174/1381612822666151204001830

Rossier, P., and Wade, D. T. (2001). Validity and reliability comparison of 4 mobility measures in patients presenting with neurologic impairment. *Arch. Phys. Med. Rehabil.* 82, 9–13. doi: 10.1053/apmr.2001.9396

Rousseaux, M., Launay, M. J., Kozlowski, O., and Daveluy, W. (2007). Botulinum toxin injection in patients with hereditary spastic paraparesis. *Eur. J. Neurol.* 14, 206–212. doi: 10.1111/j.1468-1331.2006.01617.x

Ruano, L., Melo, C., Silva, M. C., and Coutinho, P. (2014). The global epidemiology of hereditary ataxia and spastic paraplegia: a systematic review of prevalence studies. *Neuroepidemiology* 42, 174–183. doi: 10.1159/000358801

Schüle, R., Holland-Letz, T., Klimpe, S., Kassubek, J., Klopstock, T., Mall, V., et al. (2006). The spastic paraplegia rating scale (SPRS): a reliable and valid measure of disease severity. *Neurology* 67, 430–434. doi: 10.1212/01.wnl.0000228242.53336.90

Servelhere, K. R., Faber, I., Martinez, A., Nickel, R., Moro, A., Germiniani, F. M. B., et al. (2018). Botulinum toxin for hereditary spastic paraplegia: effects on motor and non-motor manifestations. *Arq. Neuropsiquiatr.* 76, 183–188. doi: 10.1590/0004-282x20180013

Ward, A. B. (2008). Spasticity treatment with botulinum toxins. *J. Neural Transm.* 115, 607–616. doi: 10.1007/s00702-007-0833-2

Williamson, A., and Hoggart, B. (2005). Pain: a review of three commonly used pain rating scales. *J. Clin. Nurs.* 14, 798–804. doi: 10.1111/j.1365-2702.2005.01121.x

World Medical Association (1964). WMA's declaration of helsinki serves as guide to physicians. *JAMA* 189, 33–34. doi: 10.1001/jama.1964.03070130073046

Conflict of Interest: The authors declare that the research was conducted in the absence of any commercial or financial relationships that could be construed as a potential conflict of interest.

frontiers in Neuroscience

REVIEW
published: 28 February 2020
doi: 10.3389/fnins.2020.00074

Lipids in the Physiopathology of Hereditary Spastic Paraplegias

Frédéric Darios[1,2,3,4]*, *Fanny Mochel*[1,2,3,4,5] *and Giovanni Stevanin*[1,2,3,4,6]

[1] Sorbonne Université, Paris, France, [2] Inserm, U1127, Paris, France, [3] CNRS, UMR 7225, Paris, France, [4] Institut du Cerveau et de la Moelle Epinière, Paris, France, [5] National Reference Center for Neurometabolic Diseases, Pitié-Salpêtrière University Hospital, Assistance Publique-Hôpitaux de Paris, Paris, France, [6] Equipe de Neurogénétique, Ecole Pratique des Hautes Etudes, PSL Research University, Paris, France

Hereditary spastic paraplegias (HSP) are a group of neurodegenerative diseases sharing spasticity in lower limbs as common symptom. There is a large clinical variability in the presentation of patients, partly underlined by the large genetic heterogeneity, with more than 60 genes responsible for HSP. Despite this large heterogeneity, the proteins with known function are supposed to be involved in a limited number of cellular compartments such as shaping of the endoplasmic reticulum or endolysosomal function. Yet, it is difficult to understand why alteration of such different cellular compartments can lead to degeneration of the axons of cortical motor neurons. A common feature that has emerged over the last decade is the alteration of lipid metabolism in this group of pathologies. This was first revealed by the identification of mutations in genes encoding proteins that have or are supposed to have enzymatic activities on lipid substrates. However, it also appears that mutations in genes affecting endoplasmic reticulum, mitochondria, or endolysosome function can lead to changes in lipid distribution or metabolism. The aim of this review is to discuss the role of lipid metabolism alterations in the physiopathology of HSP, to evaluate how such alterations contribute to neurodegenerative phenotypes, and to understand how this knowledge can help develop therapeutic strategy for HSP.

Keywords: phospholipids, sphingolipids, fatty acids, cholesterol, metabolism, myelin, lysosome

OPEN ACCESS

Edited by:
Patrícia Maciel,
University of Minho, Portugal

Reviewed by:
Javier Fernández-Ruiz,
Complutense University of Madrid, Spain
Jürgen Winkler,
University of Erlangen-Nuremberg, Germany

***Correspondence:**
Frédéric Darios
frederic.darios@upmc.fr

Specialty section:
This article was submitted to Neurodegeneration, a section of the journal Frontiers in Neuroscience

Received: *30 September 2019*
Accepted: *20 January 2020*
Published: *28 February 2020*

Citation:
Darios F, Mochel F and Stevanin G (2020) Lipids in the Physiopathology of Hereditary Spastic Paraplegias. Front. Neurosci. 14:74. doi: 10.3389/fnins.2020.00074

INTRODUCTION

Hereditary spastic paraplegias (HSP) are a group of rare neurodegenerative diseases characterized by weakness of lower limbs and spasticity (Harding, 1983). These symptoms are due to the degeneration of the long axons of the neurons from the motor cortex. Since the longest axons seemed to be more sensitive to neurodegeneration, it was proposed that altered intracellular trafficking could underlie the physiopathology of HSP (Soderblom and Blackstone, 2006). HSP are clinically heterogeneous, and complex forms of HSP are associated with various other neurological symptoms such as cognitive impairment or ataxia, due to degeneration of other neuronal populations. This clinical heterogeneity is partly underlined by the genetic heterogeneity of this group of diseases. Indeed, in the last decade, the emergence of new genetic tools allowed the identification of many genes responsible for HSP (Boutry et al., 2019a). Among the recently identified genes, many encode enzymes that are directly implicated in the metabolism of lipids. Since brain is mainly composed of lipids, identification of such lipid-related pathways opens

new perspectives to evaluate the physiopathology of HSP. Importantly, beside the identification of genes encoding lipid-modifying enzymes, mutations in genes responsible for HSP and coding proteins involved in membrane trafficking can also alter lipid homeostasis in some subcellular compartments. The formation of myelin, the most prominent lipidic structure in the brain, also appears to play a critical role in the maintenance of axon in several forms of HSP. Therefore, it becomes evident that lipids are of critical importance for the physiopathology of almost all HSP. In this review, we propose in a first part an overview of the various metabolic pathways that are altered by mutations in genes responsible for HSP and HSP-related disorders such as leukodystrophies presenting with spasticity. In a second part, we examine the consequences of altered lipid metabolism on cellular functions to highlight various physiopathological pathways that could be altered in the different forms of HSP.

ALTERATIONS OF LIPID METABOLISM DUE TO HSP-CAUSING MUTATIONS

The emergence of next-generation sequencing in the last decade allowed the identification of many genes responsible for HSP. Among all the newly identified genes, a quarter of them are encoding enzymes that are directly involved in the metabolism of lipids (**Table 1**). It appears that all the main classes of lipids could be implicated in the physiopathology of HSP.

Cholesterol

Cholesterol is a lipid highly enriched in the brain, as this organ contains about 20% of total body cholesterol (Dietschy and Turley, 2004). Most of the brain cholesterol enters in the composition of myelin, but cholesterol is also found in the membranes of glial and neuronal cells where it is actively trafficked.

Cholesterol Hydroxylation

The identification of mutations in cytochrome P450-7B1 (*CYP7B1*) in SPG5 patients (Tsaousidou et al., 2008) was the first indication that lipid metabolism could play a role in the physiopathology of HSP. SPG5 patients often present with pure HSP, but some of them may present with complicated forms of HSP and mild white matter abnormalities (Goizet et al., 2009; Marelli et al., 2018). *CYP7B1* encodes a cytochrome P450 7α-hydroxylase responsible for the degradation of oxysterols. Consequently, loss of CYP7B1 leads to the accumulation of oxysterols such as 25-hydroxycholesterol, 26-hydroxycholesterol, 27-hydroxysterol, and 3β-hydroxy-5-cholestenoic acid (3β-CA) in serum and cerebrospinal fluid of SPG5 patients (Schüle et al., 2010; Theofilopoulos et al., 2014; Marelli et al., 2018). 3β-CA was demonstrated to exert toxic effects on rodent oculomotor neurons *in vitro* and zebrafish motor neurons *in vivo via* activation of liver X receptors (LXRs) (Theofilopoulos et al., 2014). In addition, an *in vitro* study using NSC-34 cell line and neurons derived from human induced pluripotent stem (iPS) cells showed that oxysterols and 3β-CA had a cytotoxic activity. In that study, 25-OHC and 27-OHC were harmful at concentrations comparable to levels measured in serum of SPG5 patients (Schöls et al., 2017). However, in both studies, the toxicity observed required levels of oxysterols that were much higher than the levels detected in the cerebrospinal fluid of SPG5 patients. The cytotoxic action of oxysterols are mainly due to their incorporation into the natural lipid bilayer, where they can change the interaction between molecules (Mitomo et al., 2009) and thus alter membrane properties. In both studies investigating the toxic accumulation of CYP7B1 substrates, oxysterols added to the medium likely partitioned between medium and membranes, and their real concentration in membranes were not analyzed. Furthermore, the concentration of oxysterols that need to be reached in the membranes to induce a deleterious effect are not known, and further investigations are required to evaluate the mechanisms underlying neurodegeneration in SPG5 patients. Based on the hypothesis that oxysterols are neurotoxic, two concomitant therapeutic trials were conducted in SPG5 patients with decreased plasma oxysterols as the primary outcome measure (Schöls et al., 2017; Marelli et al., 2018). In both short-term phase II trials, atorvastatin significantly decreased plasma 27-OHC (Schöls et al., 2017; Marelli et al., 2018). Furthermore, treatment with chenodeoxycholic acid (CDCA) restored bile acids profile in SPG5 patients (Marelli et al., 2018). However, the clinical benefit of such metabolic intervention remains to be established and surrogate markers are needed due to the very slowly progressive course and the rarity of this disease. Another clinical trial levels using monoclonal antibodies that inhibit proprotein convertase subtilisin-kexin type 9 (PCSK9) to reduce cholesterol levels has recently been initiated (Chen, 2019). It will monitor levels of 27-OHC as a primary outcome.

Another HSP related to defective cholesterol hydroxylation is cerebrotendinous xanthomatosis (CTX) due to *CYP27A1* mutations, which encodes the mitochondrial cytochrome P450 enzyme sterol 27-hydroxylase. Deficiency in this enzyme interferes with sterol intermediates in the alternative bile acid pathway. More specifically, CTX is associated with reduced synthesis of 27-OHC and CDCA, as well as the shunting of sterol intermediates into the microsomal pathway for cholic acid formation (Salen et al., 1991). CTX is also characterized by high production of cholestanol, which accumulates in various tissues, as well as increased levels of bile alcohols in urine (Berginer et al., 1984). Evidence that cholestanol may be neurotoxic is supported by the finding of cholestanol deposition and apoptosis in neuronal cells in the cerebellum of rats fed a 1% cholestanol diet (Inoue et al., 1999). As the influx of 27-OHC may be involved in brain cholesterol homeostasis, the lack of 27-OHC may also impact cholesterol synthesis in the brain (Mignarri et al., 2016). About 60% of CTX patients (Wong et al., 2018) present with a complex form of HSP that includes systemic (infantile cholestasis, juvenile-onset cataracts, Achilles tendon xanthomas, chronic diarrhea, and osteoporosis) and/or neuropsychiatric symptoms (learning disability and/or autism spectrum disorder, cerebellar ataxia, peripheral neuropathy, parkinsonism, dementia, and psychiatric disturbances) (Nie et al., 2014). Importantly, there is a critical therapeutic window in most CTX patients before the onset of disabling neuropsychiatric symptoms (Yahalom et al., 2013). CDCA remains the treatment of choice in CTX

TABLE 1 | Genes responsible for HSP encoding enzymes of the metabolism of lipids.

Gene	Protein name	Function
Cholesterol		
CYP7B1 (*SPG5*)	Cytochrome P450-7B1	Degradation of oxysterols
CYP27A1 (CTX)	Cytochrome p450-7A1	Degradation of oxysterols
Phospholipids		
EPT1/Selenoi	Ethanolaminephospho-transferase 1	Phosphatidylethanolamine synthesis, plasmalogens synthesis
SERAC1	SERAC1	Phosphatidylglycerol remodeling
PNPLA6/NTE (SPG39)	Patatin-like phospholipase domain containing 6/Neuropathy target esterase	Phospholipase A2
PLA2G6	Group VI phospholipase A2, iPLA2b	Phospholipase A2, release of docosahexaenoic acid from phospholipids
DDHD1 (SPG28)	DDHD1	Phospholipase A1, hydrolysis of PI, PA, PS
DDHD2 (SPG54)	DDHD2	Phospholipase A1, hydrolysis of PA; TAG lipase
CYP2U1 (SPG49/56)	CYP2U1	Cytochrome P450, hydroxylation of fatty acids, oxidation of N-arachidonoylserotonin
Glycosphingolipids		
B4GALNT1 (SPG26)	β-1,4-N-acetyl-galactosaminyltransferase	Synthesis of complex gangliosides
GBA2 (SPG46)	β-Glucosidase 2	Non-lysosomal glucosylceramidase
FA2H (SPG35)	Fatty acid-2 hydroxylase	Formation of 2-hydroxy fatty acids incorporated into galactosylceramide
SLC33A1 (SPG42)	Acetyl-coA transporter 1	O-acetylation of complex gangliosides GD3 and GT3?
GALC (Krabbe)	Galactosylcerebrosidase	Degradation of galactosylceramide
ARSA (MLD)	Arylsulfatase A	Degradation of sulfatides
Fatty acids		
ABCD1 (X-ALD)	Adrenoleukodystrophy protein (ADLP)	VLCFA import into peroxisomes
ELOVL1	Fatty acid Elongase 1	Elongation of fatty acids
ELOVL4	Fatty acid Elongase 4	Elongation of fatty acids
ALDH3A2 (SLS)	Aldehyde Dehydrogenase 3 Family Member A2	Aldehyde Dehydrogenase

PI: phosphatidylinositol, PA: phosphatidic acid; PS: phosphatidylserine; TAG: triacylglycerols.

as it down-regulates CYP27A1, restores the imbalance between CDCA and cholic acid, and is the only drug that has shown beneficial effects on neurological symptoms so far (Nie et al., 2014; Salen and Steiner, 2017). Several studies have emphasized that the response to treatment strongly depends on when CDCA is initiated (Amador et al., 2018; Duell et al., 2018; Stelten et al., 2019). In a cohort of 56 Dutch CTX patients treated by CDCA with a median follow-up time of 8 years, neurological symptoms, assessed by the modified Rankin Scale and Expanded Disability Status Scale (EDSS) scores, disappeared in all patients who were diagnosed before the age of 24 and treated since (Stelten et al., 2019). Furthermore, treatment prevented the development of new neurological symptoms during the follow-up period (Stelten et al., 2019).

Alteration of Cholesterol Synthesis or Trafficking in HSP

Oxysterols are present at very low levels compared to cholesterol (Wnętrzak et al., 2017), and alterations of cholesterol synthesis or trafficking are induced by the loss of function of several genes responsible for HSP.

For example, loss of function of Erlin1 and Erlin2, mutated in SPG62 and SPG18, respectively, are responsible for early onset autosomal recessive HSP associated with cognitive impairment (Alazami et al., 2011; Novarino et al., 2014). Autosomal dominant mutations in *Erlin2*, associated with SPG37, are also implicated in less severe forms of motor neuron diseases (Rydning et al., 2018; Stevanin et al., 2019). Erlin1 and Erlin2 form a heteromultimeric complex of ∼2 MDa (Pearce et al., 2009). This complex is localized in the lumen of the ER and is anchored to cholesterol-rich lipid domains by the N-terminus of the proteins (Browman, 2006). Downregulation of Erlin1 and 2 was shown to activate the sterol regulatory element binding protein (SREBP) transcription factors, leading to upregulation of their target genes. This increased cholesterol content in cells and cells containing cytoplasmic lipid inclusions stained with Oil Red O (Huber et al., 2013). However, the relevance of this function for the physiopathology of HSP has not been evaluated yet.

Loss of spatacsin, due to mutations in *SPG11*, is responsible for a complicated form of HSP where spasticity is often associated with cognitive impairment and lower motor neuron degeneration. White matter anomalies may be detected on brain MRI (Hehr et al., 2007; Stevanin et al., 2007, 2008). Spatacsin is implicated in the autophagic lysosome reformation, a mechanism allowing the formation of tubules in autolysosomes at the end of the autophagy process in order to recycle lysosome membrane (Chang et al., 2014). Recently, it was shown that the formation of tubules on lysosomes mediated by spatacsin allows the recycling of cholesterol from lysosomes. Loss of spatacsin led to an accumulation of

cholesterol in lysosomes and decreased cholesterol content in plasma membrane (Boutry et al., 2019b), which could affect membrane properties and function. This highlights that impaired cholesterol trafficking and not only cholesterol overload in lysosomes could contribute to the pathology. However, the contribution of this mechanism to neuronal death is still not known.

Alteration of Phospholipid Synthesis and Degradation in Some HSP Entities

Phospholipids are the main components of cellular membranes. They are composed of a glycerol backbone to which two fatty acids are attached as esters. The third alcohol group of the glycerol is attached to a phosphoric acid that can associate various hydrophilic moieties, determining the nature of the phospholipid (phosphatidyl-choline, phosphatidyl inositol, etc.) (**Figure 1**). Several enzymes implicated in the metabolism of phospholipids have been associated with HSP or related disorders.

Altered Synthesis of Phospholipids

Mutations in *EPT1/SELENOI* have been found in patients presenting an early onset complicated HSP with white matter abnormalities detected on brain MRI (Ahmed et al., 2017; Horibata et al., 2018). EPT1 is an ethanolamine transferase implicated in the synthesis of phosphatidylethanolamine (PE), the second most abundant phospholipid in membranes. Analysis of a patient's fibroblasts as well as *EPT1* knockout Hela cells showed decreased PE biosynthesis, as well as an imbalance in plasmalogens (increased plasmanyl-phosphatidylcholine and decreased plasmenyl-phosphatidylethanolamine) (Horibata et al., 2018). Of note, plasmenyl-phosphatidylethanolamine represents more than 50% of ethanolamine glycerophospholipids in the brain (Braverman and Moser, 2012), which highlights why the loss of EPT1 activity may lead to such severe brain dysfunction.

Mutations in *SERAC1* were known to cause the autosomal recessive MEGDEL syndrome, characterized by infantile onset symptoms including feeding problem, liver failure, deafness, dystonia, encephalopathy, spasticity, and Leigh-like syndrome (Wortmann et al., 2012). Recently, mutations in *SERAC1* were found in a family presenting juvenile onset complicated HSP (Roeben et al., 2018). SERAC1 is a phospholipid remodeling enzyme that converts phosphatidylglycerol 34:1 (PG34:1) into phosphatidylglycerol 36:1 (PG36:1). Families presenting with an HSP phenotype had a milder change in the PG34:1/PG36:1 ratio compared to patients with MEGDEL syndrome (Roeben et al., 2018), suggesting phenotype–genotype correlation.

Mutations in *PGAP1* have been identified in one family of complex HSP (SPG67) (Novarino et al., 2014), but also in cases of intellectual disability and encephalopathy (Murakami et al., 2014). *PGAP1* encodes an ER protein that promotes the deacylation of inositol in the glycosylphosphatidylinositol (GPI)-anchored proteins (Tanaka et al., 2004). During their synthesis, GPI-anchored proteins are localized in the lumen of the ER. The remodeling of GPI anchor by PGAP1 is required for the sorting of GPI-anchored proteins to ER exit sites, allowing their export out of the ER (Fujita et al., 2011).

Degradation of Glycerophospholipids

Several enzymes with phospholipase activity have been associated with HSP. Mutations in the genes encoding two calcium-independent phospholipases, NTE/PNPLA6 and PLA2G6, are responsible for a variety of neurodegenerative disorders. Mutations in neuropathy target esterase (*NTE/PNPLA6*) are responsible for autosomal recessive HSP (SPG39) (Rainier et al., 2008), but also other neurological syndromes combining ataxia, spasticity, retinal degeneration, and/or hypogonadism (Synofzik et al., 2014). PLA2G6 associated neurodegeneration is a group of heterogeneous neurodegenerative disorders, including infantile neuroaxonal dystrophy, neurodegeneration with brain iron accumulation, parkinsonism, and HSP. Both enzymes hydrolyze the sn-2 acyl chain of phospholipids. NTE/PNPLA6 seems to have a privileged affinity for phosphatidylcholine, as its levels were increased in the brain of *nestin-cre:NTEfl/fl* mice (Read et al., 2009). The product of *PLA2G6* mediates the release of docosahexaenoic acid from brain phospholipids (Green et al., 2008), suggesting that different actions of phospholipases can contribute to the physiopathology of HSP.

Another group of phospholipases associated with the physiopathology of HSP are DDHD containing enzymes DDHD1 and DDHD2 (Schuurs-Hoeijmakers et al., 2012; Tesson et al., 2012). Mutations in *DDHD1* are responsible for pure or complex HSP (SPG28), sometimes associated with brain iron accumulation (Dard et al., 2017). *DDHD2* is mutated in SGP54, which is usually characterized by very early onset spastic paraplegia, intellectual disability, and white matter abnormalities (Schuurs-Hoeijmakers et al., 2012), but adult onset forms have been reported for both DDHD1 and DDHD2 (Doi et al., 2015; Dard et al., 2017). As a unique finding in DDHD2, proton magnetic resonance spectroscopy revealed an abnormal lipid peak in the basal ganglia and thalamus area (Schuurs-Hoeijmakers et al., 2012). *In vitro* experiments proposed that DDHD1 and DDHD2 have a phosphatidic acid-preferring phospholipase A1 action, hydrolyzing the sn-1 acyl chain (Higgs et al., 1998; Inoue et al., 2012). These results were challenged by lipidomic analysis of knockout mouse models for these two genes. Knockout of *Ddhd2* led to accumulation of triacylglycerol, and recombinant DDHD2 was revealed to have a triacylglycerol-lipase activity (Inloes et al., 2014). Recently, lipidomic analysis of the brain of *Ddhd1* knockout mice showed that phosphatidylinositol and phosphatidylserine are the main physiological substrates of DDHD1 (Inloes et al., 2018). It is conceivable that DDHD1 and DDHD2 have different substrates depending on the cell type that is investigated.

Metabolism of Phospholipid and Cellular Signaling

The metabolism of phospholipids can contribute to signaling pathways by modifying various lipid species. One of the most studied lipid signaling pathway relies on the phosphorylation state of phosphoinositides (Wang et al., 2019). Interestingly, loss

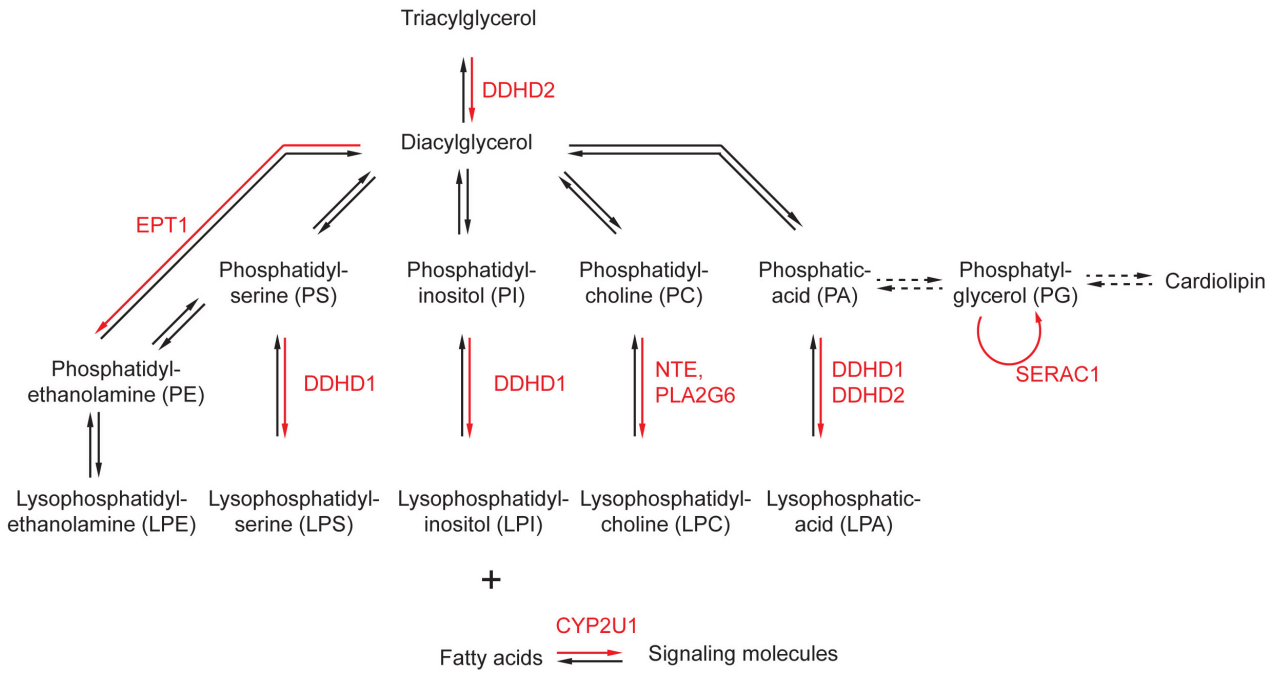

FIGURE 1 | Alteration of phospholipid metabolism by genes implicated in the physiopathology of HSP. The main metabolic pathways affecting phospholipids and phospholipid-related molecules are represented. The enzymes affected by mutations in genes responsible for HSP are highlighted in red. Dashed arrows represent conversion requiring more than one enzymatic reaction.

of Ddhd1 in mice led to striking remodeling of phosphoinositides in the brain (Inloes et al., 2018). Furthermore, spastizin (*ZFYVE26*) mutated in SPG15 (Hanein et al., 2008) has a FYVE domain that mediates interaction with phosphatidylinositol-3-phosphate (PI3P). The ability of the spastizin FYVE domain to bind PI3P is required for addressing protein to lysosomes (Chang et al., 2014), even if the content of PI3P in this subcellular compartment is poorly characterized. Deletion of the FYVE domain or point mutation abolishing the interaction with PI3P impaired the localization of spastizin to lysosomes (Chang et al., 2014). Loss of phosphatidylinositol 4-kinase 2alpha activity in mouse caused neurological symptoms resembling HSP (Simons et al., 2009). In this mouse model, the authors revealed neurodegeneration that was associated to accumulation of lipofuscin-like material, similar to the observation made in *Spg15* knockout mice (Khundadze et al., 2013). Although mutations in phosphatidylinositol 4-kinase 2 alpha have not been identified in HSP patients so far, this illustrates the role of signaling phosphoinositides in the physiopathology of HSP.

It is important to note that the phospholipases A1 or A2 may release lysosphospholipids such as lysophosphatidic acid or lysophosphatidyl-inositol and some of them play an important a role in cellular signaling (Yung et al., 2015). The phospholipases A2 hydrolyze phospholipids in the sn-2 position, releasing a fatty acid that is often unsaturated. Such fatty acid can be hydroxylated by the cytochrome P450 *CYP2U1* that is mutated in the early onset form of complex HSP SPG49 (HUGO) or SPG56 (OMIM) (Chuang et al., 2004; Tesson et al., 2012). Oxidation of unsaturated fatty acids can produce a variety of signaling molecules, but their identities and roles are still to be uncovered. The role of such signaling molecules in the physiopathology of HSP has not been investigated so far, and it may open new avenues to identify targets of therapeutic interest for these diseases.

Alteration of Sphingolipid Metabolism in HSP

Sphingolipids are a group of lipids derived from the sphingosine backbone. They are synthesized in the ER and the Golgi apparatus, and are degraded by lysosomes (**Figure 2**). Alteration of both biosynthetic and degradative pathways of sphingolipids have been associated with HSP phenotype.

Sphingolipid Biosynthesis

Loss-of-function mutations in fatty acid-2-hydroxylase (FA2H) are responsible for the complex form of autosomal recessive HSP (SPG35) (Edvardson et al., 2008) and allelic neurological disorders. A recent study showed that patients with nonsense or missense mutations presented a rather homogeneous phenotype, with a spastic tetraparesis frequently associated with cognitive deficits. Symptoms onset is in early childhood and all patients presented white matter abnormalities on brain MRI (Rattay et al., 2019). FA2H is the enzyme responsible for the formation of 2-hydroxy-fatty acids (Alderson et al., 2004) that are frequently incorporated as N-acyl chain in galactosylceramide (Bowen and Radin, 1968). In mouse models, the loss of function of Fa2h

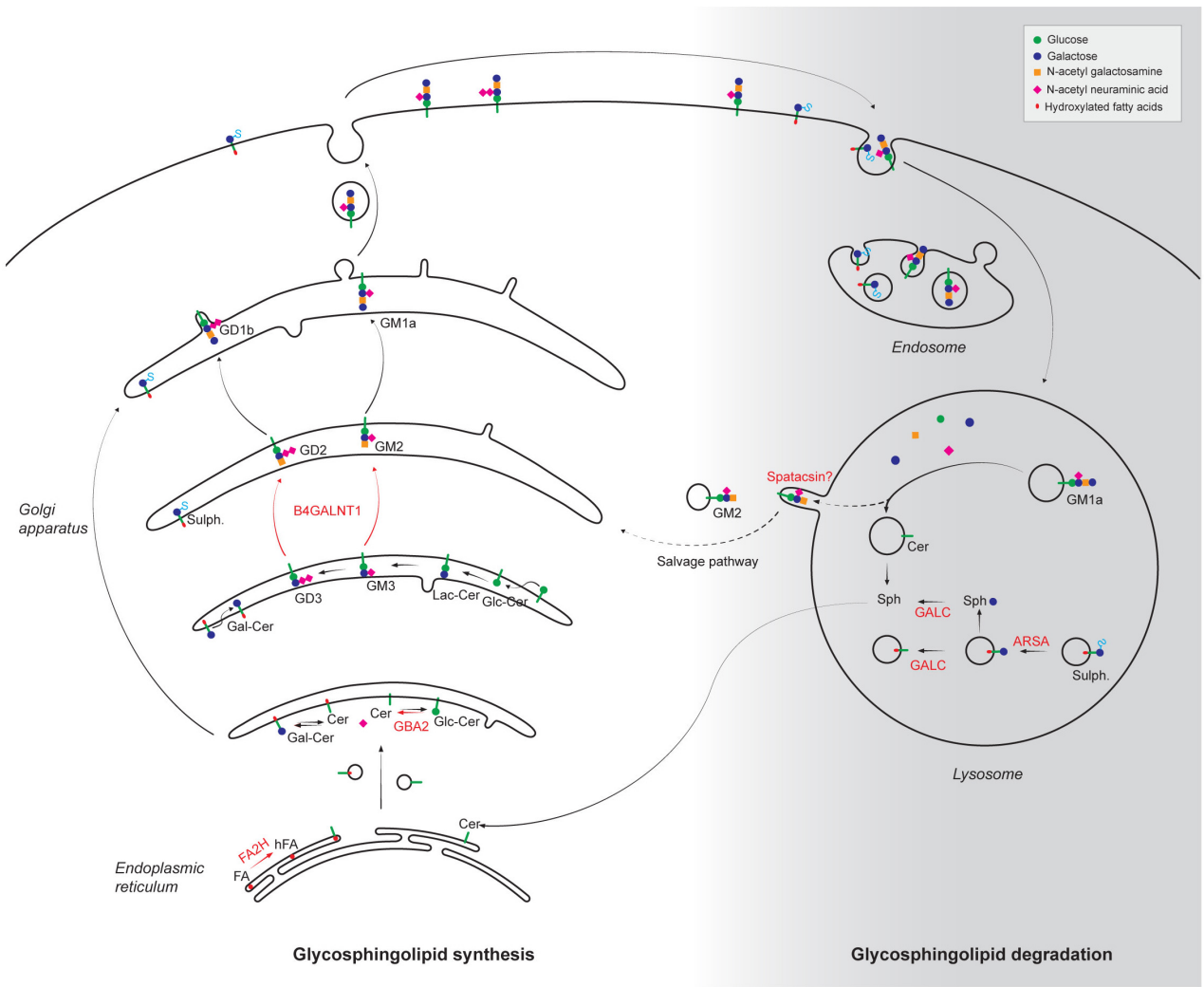

FIGURE 2 | Alteration of synthesis and degradation pathways of glycosphingolipids in the physiopathology of HSP. The different steps of glycosphingolipid biosynthesis occur in the endoplasmic reticulum and the Golgi apparatus by progressive addition of the molecules indicated in the top right panel. Following internalization by endocytosis, plasma membrane glycosphinglipids are progressively degraded in lysosome into basic building blocks. The products of HSP-mutated genes that are implicated in the metabolism of glycosphingolipids are highlighted in red. FA, fatty acids; hFA, hydroxylated fatty acids; Cer, Ceramide; Gal-Cer, Galatosyl-ceramide; Glc-Cer, Glucosyl-ceramide; Lac-Cer, Lactosyl-ceramide; Sulf: Sulfatides; Sph, Sphingosine; FA2H, fatty acid-2-hydroxylase; GBA2, β-glucosidase 2; B4GALNT1, β-1,4-N-acetyl-galactosaminyltransferase; GALC, Galactosyl-cerebrosidase; ARSA, Arylsulfatase A. It has been proposed that some gangliosides could be recycled from the lysosomes using a salvage pathway. Whether spatacsin could be implicated in such pathway is still unclear.

was associated with the absence of sphingolipids containing 2-hydroxylated fatty acids and increased non-hydroxylated galactosylceramide (Zoller et al., 2008).

Gangliosides are synthesized in the ER. These glycosphingolipids are highly enriched at the plasma membranes of neurons and glial cells, notably complex gangliosides such as GM1 and GD1. These molecules serve as coreceptors for many factors. *B4GALNT1* is mutated in SPG26 that is characterized by complex HSP frequently associated with intellectual disability (Boukhris et al., 2013). *B4GALNT1* encodes β-1,4-N-acetyl-galactosaminyl transferase 1 or GM2/GD2 synthase that converts GM3 into GM2 and GD3 into GD2. Accordingly, analysis in fibroblasts of SPG26 patients showed a lack of GM2 associated with increased levels of its precursor GM3 (Harlalka et al., 2013). Knockout of the GM2 synthase in mouse leads to a progressive demyelination and axonal loss that lead to motor dysfunction (Sheikh et al., 1999; Chiavegatto et al., 2000), similar to the symptoms observed in patients.

Other forms of HSP are putatively linked to sphingolipid metabolism, although the roles of the mutated gene products are still elusive. Deficiency in carnitine palmitoyltransferase 1C (CPT1C) accounts for SPG73 and has been associated with sphingolipid metabolism (Rinaldi et al., 2015). This enzyme belongs to a family mediating the trans-esterification of palmitoyl-coA and carnitine, to allow the formation of a molecule that can be transported through membranes, in contrast

to palmitoyl-CoA. While CPT1A and CPT1B are enriched in mitochondria and allow the transport of acyl-CoA into mitochondria to undergo β-oxidation, CPT1C is localized in the ER and its carnitine palmitoyl transferase activity is low compared to CPT1A and CPT1B (Casals et al., 2016). In contrast, a lipidomic analysis in the brain of fasted *Cpt1c* knockout mice showed lower levels of ceramide and sphingosine (Carrasco et al., 2012). The molecular mechanisms leading to this change in sphingolipid metabolism are however unknown.

A missense mutation in *SLC33A1* (p. S113R) has been observed in a large family of patients presenting with an autosomal dominant spastic paraplegia (SPG42) (Lin et al., 2008). *SLC33A1* encodes the acetyl-CoA transporter 1 (AT-1) localized in the ER, which has been proposed to play a key role in the acetylation of proteins but also of gangliosides such as O-Ac-GD3 or O-Ac-GT3 (Kanamori et al., 1997). The p. S113R mutant is supposed to disrupt the second transmembrane domain of the protein, thus blocking its function (Lin et al., 2008). A knock-in mouse model expressing the p.S113R mutant at the heterozygous state presents impaired locomotion at the age of 12 months (Liu et al., 2017). This phenotype is associated with a demyelination and alteration of ER and mitochondria in the cell body of neurons. However, whether the synthesis of O-Ac-GD3 or O-Ac-GT3 was decreased in this mouse model has not been investigated. Acetyl-coA has also been associated with fatty acid metabolism (Yoshii et al., 2015), but it has not been investigated whether fatty acid metabolism is impaired in SPG42 patients or in the Spg42 mouse model.

Sphingolipid Degradation

Krabbe disease and metachromatic leukodystrophy are two autosomal recessive diseases due to impaired lysosomal degradation of sphingolipids. Both are progressive diseases, usually characterized by spasticity, often related to brain white matter lesions detected on brain MRI—peripheral neuropathy and cognitive impairment (Orsini et al., 2000; Gomez-Ospina, 2006). Krabbe disease is caused by loss of function of galactosylcerebrosidase (GALC) (Rafi et al., 1995). GALC degrades galactosylceramide, the major sphingolipid of myelin, as well as other sphingolipids containing galactose such as psychosine (D-galactosylsphingosine). In the absence of a functional GALC, galactosylceramide can be degraded by GM1 ganglioside β-galactosidase (Kobayashi et al., 1985) and thus do not accumulate in cells of Krabbe disease patients. In contrast, psychosine cannot be metabolized by GM1 ganglioside β-galactosidase and thus accumulates in the brain of Krabbe patients (Svennerholm et al., 1980). In the Twitcher mouse, a natural model of Krabbe disease, a biochemical analysis revealed decreased levels of galactosylceramide and sulfatides at early stages, as well as strong accumulation of psychosine (Igisu et al., 1983; Igisu and Suzuki, 1984). Metachromatic leukodystrophy is due to a deficiency in arylsulfatase A (Gomez-Ospina, 2006). This enzyme mediates the degradation of a class of glycosphingolipids, sulfatides (Mehl and Jatzkewitz, 1968). Consequently, metachromatic leukodystrophy patients present high levels of sulfatides in many tissues, including the brain, and they excrete high levels of sulfatides in urines (Gomez-Ospina, 2006). A mouse model deficient in arylsulfatase presents with early onset accumulation of sulfatides in lysosomes of neurons and oligodendrocytes (Wittke et al., 2004). In both Krabbe disease and metachromatic leukodystrophy, allogenic hematopoietic stem cell transplantation (HSCT) can stabilize/slow-down cerebral demyelinating lesions for pre- or early-symptomatic juvenile or adult patients (van Rappard et al., 2016; Laule et al., 2018).

Krabbe disease and metachromatic leukodystrophy belong to the group of lysosomal storage disorders. However, accumulation of some glycosphingolipids in lysosomes has also been observed in SPG11 models of HSP (Boutry et al., 2018) that is not classically considered as a lysosomal storage disorder. Accumulation of gangliosides in SPG11 was likely not due to impaired function of ganglioside-degrading enzymes, suggesting that the accumulation of gangliosides has another cause. SPG11 is due to the loss of function of spatacsin, a protein that has been implicated in the autophagic lysosome reformation, a mechanism allowing formation of tubule in autolysosomes at the end of the autophagy process to recycle lysosome membrane (Chang et al., 2014). It has been proposed that inhibition of the tubulation in absence of spatacsin could lead to accumulation of gangliosides in lysosomes, which could contribute to the motor dysfunction observed in the mouse model (Branchu et al., 2017; Boutry et al., 2018). Some SPG11 patients are diagnosed as cases of amyotrophic lateral sclerosis or Charcot-Marie tooth disease (Orlacchio et al., 2010; Montecchiani et al., 2016). Of note, the levels of several glycosphingolipids, including gangliosides, were upregulated in the spinal cord of ALS patients, suggesting that they could participate to neurodegeneration in this disease as well (Dodge et al., 2015). SPG11 patients also frequently present parkinsonian features (Anheim et al., 2009). It is interesting to note that the main risk factor identified so far for Parkinson's disease is the heterozygous loss of *GBA1* (Aharon-Peretz et al., 2004). This gene encodes lysosomal glucosylceramidase, which is a lysosomal enzyme implicated in the degradation of glycosphingolipids downstream the degradation of gangliosides.

Mutations in *GBA1* have not been found in HSP patients, but loss of its paralog *GBA2* is responsible for spastic ataxia with cognitive impairment (SPG46) (Hammer et al., 2013; Martin et al., 2013). GBA2 is a non-lysosomal glucosylceramidase, hydrolyzing glucosylceramide into glucose and ceramide. Most mutations impair the enzymatic function of GBA2 and can thus be considered from an enzymatic perspective as null mutants (Sultana et al., 2015). *Gba2* knockout mice exhibit gait abnormalities (Woeste et al., 2019) and fertility impairment due to abnormal sperm morphology (Raju et al., 2015). This is consistent with male infertility reported in SPG46 patients (Martin et al., 2013). Lipidomic analysis in Sertoli cells confirmed that loss of GBA2 promotes accumulation of glucosylceramide (Raju et al., 2015). In cerebellum, no difference was observed in the total levels of glucosylceramide between control and *Gba2* knockout mice. However, levels of the gangliosides GM1a, GT1b, GD1b, and GM3 were slightly increased in the cerebellum of *Gba2* knockout mice compared to wild-type mice (Woeste et al., 2019). Yet, the link between accumulation of glucosylceramide and neurodegeneration is not known. It was proposed that

accumulation of glucosylceramide could alter the membrane fluidity, which could lead to increased actin polymerization (Raju et al., 2015).

Alteration of Fatty Acid Metabolism in Syndromes Presenting Spasticity

Several rare neurodegenerative diseases presenting spasticity are implicated in the metabolism of fatty acids. Fatty acids are building blocks for other lipids such as phospholipids, ceramide, cholesterol esters, and thus change in fatty acid metabolism can have an impact on many classes of lipids as illustrated below.

X-linked adrenoleukodystrophy (X-ALD) is an X-linked syndrome caused by mutations in the *ABCD1* gene that codes for the adrenoleukodystrophy protein (ALDP) (Mosser et al., 1993). First, symptoms may occur from childhood to adulthood, leading to progressive demyelination of the central and peripheral nervous system. The earlier the illness begins, the more severe it will be and childhood forms of X-ALD are characterized by a devastating cerebral demyelination, leading to rapid cognitive and motor decline, vegetative state within a few months, and premature death. The clinical spectrum in males with X-ALD ranges from childhood cerebral ALD (CALD: onset 5–12 years, 35–40% of affected males) to slowly progressive spastic paraplegia in adulthood (adrenomyeloneuropathy: onset 20–30 years, 60% of affected males) (Kemp et al., 2012). Approximately 20% of males with adrenomyeloneuropathy will also develop CALD later in life with the same poor prognosis as in children. The only available therapy for CALD is allogenic HSCT (Raymond et al., 2019; Waldhüter et al., 2019). If performed in patients with minimal brain lesions and no/minor clinical symptoms, it may arrest the progression of demyelinating lesions. To overcome the limitations of allogeneic transplantation (lack of donor, graft versus host reaction, high mortality rate), autologous transplantation of HSC corrected *ex vivo* with a lentiviral vector expressing the *ABCD1* gene is currently under clinical trial in children with CALD with very encouraging results (Eichler et al., 2017). Women carriers of *ABCD1* mutations may develop milder forms of the disease, usually with spastic paraplegia, and sometimes peripheral neuropathy, in adulthood (Huffnagel et al., 2019). However, it is increasingly recognized that *ABCD1*-mutated women develop a wide spectrum of neurological diseases with age (Engelen et al., 2014). All male patients present elevated plasma levels of very long chain fatty acids (VLCFA) but they may be normal in female carriers. The accumulation of VLCFA is also detected in lipid molecules or proteins complexing fatty acids. The myelin of X-ALD patients showed a strong enrichment in VLCFA complexed in cholesterol esters and sphingomyelin (Brown et al., 1983), an increased proportion of proteolipid protein (PLP) complexed to monounsaturated VLCFA (Bizzozero et al., 1991), and increased amount of VLCFA in glycerophospholipids (Theda et al., 1992). VLCFA accumulation is also associated with clinically significant microglial activation (Eichler et al., 2008). These observations highlight the variety of effects that can result from the accumulation of VLCFA. This accumulation in X-ALD patients is the consequence of the impaired β-oxidation of VLCFA by peroxisomes. The *ABCD1* product, ALDP, is a membrane transporter of the ATP-binding cassette family of proteins and is localized in peroxisomes (Watkins et al., 1995). It was shown that ALDP can transport the VLCFA from the cytosol across the peroxisome membrane, allowing their β-oxidation (van Roermund et al., 2008). VLCFA accumulation in X-ALD patients is the consequence of the absence of functional ALDP protein.

VLCFA can be obtained from food, but they can also be synthesized in the ER by elongases that are enzymes allowing the elongation of fatty acids (Jakobsson et al., 2006). Heterozygous mutations in the gene encoding the elongase ELOVL4 was associated with autosomal dominant juvenile macular degeneration (Zhang et al., 2001), or spinocerebellar ataxia SCA34 (Ozaki et al., 2015). However, recessive mutations in *ELOVL4* were found in patients presenting ichthyosis, seizures, mental retardation, and spastic paraplegia (Aldahmesh et al., 2011). Deficiency in ELOVL4 in mice led to perinatal death and was associated with a reduction in VLCFA (Cameron et al., 2007), as well as decreased levels of ceramide with omega-hydroxy VLCFA (Li et al., 2007). Recently, a dominant mutation in *ELOVL1* was found in two pediatric patients presenting ichthyosis, spasticity, mild hypomyelination detected on brain MRI, and dysmorphic features (Kutkowska-Kaźmierczak et al., 2018). Expression of the pathogenic variant in cell lines reduced the production of VLCFA (Kutkowska-Kaźmierczak et al., 2018). Analysis of patient cells also revealed a moderate decrease in the levels of ceramide with fatty acids longer than 24 carbons (Mueller et al., 2019). Consistently, knockout of *Elovl1* in mice resulted in decreased levels of ceramide with VLCFA (Sassa et al., 2013). The X-ALD and elongase-linked syndromes highlight the importance of the balance between synthesis and degradation of VLCFA for proper brain function. The interplay between the two cellular function was also demonstrated by the beneficial action of downregulating ELOVL1 in fibroblasts of X-ALD patients (Ofman et al., 2010).

Sjogren Larsson syndrome (SLS) is an autosomal recessive disorder characterized by ichthyosis, spastic paraplegia, and intellectual disability (Sjogren and Larsson, 1957). This syndrome results from the accumulation of fatty aldehydes (Rizzo and Craft, 1991). Consistently, mutations in *ALDH3A2* that encodes a fatty aldehyde dehydrogenase were identified as responsible for SLS (Laurenzi et al., 1996). It was demonstrated that fibroblasts of SLS patients are more sensitive to cell death induced by fatty aldehydes (James and Zoeller, 1997). This effect could be due to reactions between accumulating fatty aldehydes and proteins or lipids such as phosphatidylethanolamine that would disrupt their biochemical functions (James and Zoeller, 1997).

Mutations in genes encoding enzymes involved in the metabolism of various lipid molecules highlight the role of lipids in the physiopathology of HSP. It is important to note that both synthesis and degradation of most classes of lipids are responsible for diseases with overlapping presentation. This highlights the importance of lipid homeostasis for the normal function of polarized cells like neurons or oligodendrocytes. However, it is not clear how the change in lipid metabolism can lead to axon loss or neurodegeneration. Some functional links have been

established from the study of other forms of HSP, as discussed in the next part of this review.

FUNCTIONAL CONSEQUENCES OF THE ALTERATION OF LIPID METABOLISM

Lipids being major membrane constituents, alteration of their metabolism is likely to alter various membrane-related functions. We will see that alterations of lipid metabolism can affect various cellular functions (**Table 2**), which could contribute to neurodegeneration. However, it has also emerged in the last few years that mutations in genes affecting various subcellular compartments can secondarily lead to alteration of lipid metabolism, reinforcing its implication in the physiopathology of HSP.

Lipid Droplets

Lipid droplets (LD) are storage organelles that are formed by a core of neutral lipids surrounded by a monolayer of phospholipids. The main lipids stored in LDs are triacylglycerols (TAG) and esterified cholesterol. LDs formation occurs in the membrane of the ER. They are dynamic organelles, playing a key role in lipid metabolism and energy homeostasis (Olzmann and Carvalho, 2019).

Consistent with the formation of LD in the ER membrane, several proteins implicated in the morphogenesis of the ER network have been associated with LD biogenesis or have been shown to modify their dynamics. When overexpressed, atlastin and REEP1 are localized at the rim of LD, and the coexpression of both proteins increases the size of LD (Klemm et al., 2013). Similarly, M1 spastin, but not M87 spastin, was colocalized with LD, and overexpression of the M1 spastin isoform increased the size of LD in HeLa cells, as well as in *Drosophila* fat body, muscle, and nerve tissues (Papadopoulos et al., 2015). Conversely, downregulation of spastin in *Drosophila* or *Caenorhabditis elegans* decreased the number of LD and TAG levels (Papadopoulos et al., 2015). Atlastin loss of function in *C. elegans* or *Drosophila* reduced LD size and TAG levels (Klemm et al., 2013). *Reep1* knockout mice also presented with a lipoatrophy, associated with reduced levels of serum cholesterol and TAG. The number of LD was also reduced in neurons of *Reep1* knockout mice (Renvoisé et al., 2016). Since atlastin-1, spastin, and Reep1 are ER-shaping proteins (Park et al., 2010), these studies nicely show a correlation between ER morphology and accumulation of LD. CPT1C, an atlastin binding protein, has not been shown to alter ER morphology, but its knockout in mouse also decreased the number and size of LD (Rinaldi et al., 2015). It is noteworthy that SPG3 (atlastin-1), SPG4 (spastin), SPG31 (REEP1), and SPG73 (CPT1C) are rather pure forms of HSP. Yet, it is not known whether the alteration of ER morphology or the alteration of LD metabolism is responsible for patients' phenotype. Recently, it was proposed that M1 spastin promotes the docking of LD to peroxisomes, allowing the transfer of fatty acids from LD to peroxisomes. Expression of a mutant spastin prevented this transfer and led to accumulation of peroxided lipids, which could contribute to cell death (Chang et al., 2019).

Spartin and seipin, which are mutated in the complex forms of HSP SPG20 and SPG17, respectively, were also found in contact with LD (Szymanski et al., 2007; Eastman et al., 2009). Spartin interacts with the E3 ubiquitin ligases AIP4 and AIP5 (Edwards et al., 2009), and it was proposed to promote the ubiquitylation of lipid droplet proteins (Hooper et al., 2010). Downregulation of spartin leads to increased LD number and size (Eastman et al., 2009). Seipin is also implicated in the regulation of ER-LD contact and loss of seipin function impaired the formation of LD in fibroblasts (Szymanski et al., 2007; Salo et al., 2016). However, SPG17 is due to gain-of-function mutation in the *BSCL2* gene, altering glycosylation sites of the protein, and the consequences of these mutations on LD metabolism have not yet been investigated.

Another complex form of HSP associated with the accumulation of LD is SPG54. LD accumulated prominently in neurons when the main brain TAG lipase, DDHD2, is knocked out (Inloes et al., 2014). The loss of Ddhd2 in mice was also responsible for motor and cognitive impairment. In this mouse model, LD accumulated in neurons, including axons and dendrites (Inloes et al., 2014). It was proposed that accumulation of LD in neuronal processes can lead to swellings and disturb intraneuronal trafficking, which could contribute to neurodegeneration. *Ddhd2* knockdown in *Drosophila* reduced the number of active zones at synaptic terminals (Schuurs-Hoeijmakers et al., 2012). LD may thus disrupt trafficking of proteins and lipids required for synapse assembly (Pennetta and Welte, 2018).

Interestingly, these studies suggest that mutations leading to reduced LD are associated with rather pure forms of HSP. In contrast, other forms of HSP that were associated with accumulation of LD are rather complex HSP. However, it is not clear whether the severity of the phenotype is only due to alteration of LD. Indeed, LD are in interaction with other subcellular compartments such as mitochondria or lysosomes that can also be affected and could contribute to the physiopathology of HSP.

Mitochondria Dysfunction

Mitochondria play a key role in lipid metabolism, as they can degrade lipids through β-oxidation, or contribute to synthesis of TAG (Benador et al., 2019). It is interesting to note that loss of DDHD2 or spartin that are associated with accumulation of LD also leads to mitochondrial dysfunction (Joshi and Bakowska, 2011; Maruyama et al., 2018). Yet, neurons are not known to utilize lipids as an energy source for mitochondria, raising the question of other possible roles of lipids in the regulation of mitochondrial function. Alternatively, motor neuron dysfunction could also result from altered energy supply from glial cells that use lipids as energetic substrates.

DDHD1 and DDHD2 were initially described as phosphatidic acid (PA)-preferring phospholipases A1 (Higgs et al., 1998; Inoue et al., 2012). The content of PA in outer mitochondrial membrane can regulate the dynamics of mitochondria fusion and fission (Kameoka et al., 2018). Knockdown of *DDHD1* or

TABLE 2 | Genes responsible for HSP encoding proteins modifying cellular lipid metabolism.

Gene	Protein name	Function
Lipid droplets (LD)		
ATL (*SPG3*)	Atlastin	Regulation of LD size
SPAST (SPG4)	Spastin	Regulation of LD size and number
REEP1 (SPG31)	REEP1	Regulation of LD size
CPT1C (SPG73)	Carnitine palmitoyl transferase 1C	Regulation of LD size and number
Spartin (SPG20)	Spartin	Regulation of LD size and number
DDHD2 (SPG54)	DDHD2	Triacylglycerol lipase, hydrolysis of LD
Mitochondrial function		
DDHD1 (SPG28)	DDHD1	Mitochondria fusion/fission, ROS production, ATP synthesis
DDHD2 (SPG54)	DDHD2	Mitochondria fusion/fission, ROS production, ATP synthesis, regulate levels of cardiolipins
SERAC1	SERAC1	Altered levels of cardiolipins, altered function of the respiratory chain
Spartin (SPG20)	Spartin	Regulation of mitochondrial membrane potential
ABCD1 (X-ALD)	Adrenoleukodystrophy protein (ADLP)	Mitochondrial depolarization, ROS production
Lysosome function		
GALC (Krabbe)	Galactosylcerebrosidase	Accumulation of psychosine
ARSA (MLD)	Arylsulfatase A	Accumulation of sulfatides
ATP13A2 (SPG78)	P5-type ATPase	Regulates lysosomal degradative activity, accumulation of membranes in lysosomes
AP5Z1 (SPG48)	Subunit ζ of adapter complex 5	Accumulation of membranes in lysosomes
SPG11	Spatacsin	Regulation of autophagic lysosome recovery, accumulation of gangliosides in lysosomes
ZFYVE26 (SPG15)	Spastizin	Regulation of autophagic lysosome recovery, accumulation of membranes in lysosomes
SERAC1	SERAC1	Reduced levels of bis-monoacylglycerol-phosphate in lysosomes
Synaptic function		
PLA2G6	Group VI phospholipase A2, iPLA2b	Alteration of synaptic structure
PNPLA6/NTE (SPG39)	Patatin-like phospholipase domain containing 6/Neuropathy target esterase	Reduction of the activity of the secretory pathway
BSCL2 (SPG17)	Seipin (N88S variant: altered glycosylation of seipin)	Decreased number of docked synaptic vesicles in sypases
Myelin/axon maintenance		
PLP1 (SPG2)	Proteolipid protein	Constituent of myelin, required for long term axon maintenance
MAG (SPG75)	Myelin associated glycoprotein	Constituent of myelin, binds to gangliosides present in axon membrane, required for long term axon maintenance
GJC2 (SPG44)	Connexin 47	Gap junction protein, required for glial coupling in white matter
FA2H (SPG35)	Fatty acid-2 hydroxylase	Decreased levels of galactosylceramide, required for long-term axon maintenance
GALC (Krabbe)	Galactosylcerebrosidase	Defective myelin formation and later on demyelination; psychosine-induced toxicity of oligodendrocytes
ARSA (MLD)	Arylsulfatase A	Demyelination

DDHD2 in some cells types, but not all of them, promoted elongation of mitochondria, probably by enhancing their fusion (Baba et al., 2014). The equilibrium between fusion and fission of mitochondria is required to clear damaged mitochondria (Twig et al., 2008). Loss of DDHD2 in mouse embryonic fibroblasts increased mitochondrial membrane potential and reduced ATP production and O_2 consumption. These mitochondrial dysfunction were associated with production of reactive oxygen species (Maruyama et al., 2018). Similar to loss of DDHD2, lymphoblasts of SPG28 patients devoid of DDHD1 also presented higher ROS production and lower ATP production compared to control cells (Tesson et al., 2012). Excessive fusion observed in the absence of DDHD1 or DDHD2 could explain the accumulation of dysfunctional mitochondria and thus impaired ATP production, which could contribute to neurodegeneration.

Importantly, the alteration of mitochondrial function in *DDHD2* knockout fibroblasts was not associated with the accumulation of LD or increased levels of TAG, but it was associated with decreased levels of cardiolipin, a mitochondria-specific lipid class (Maruyama et al., 2018). Cardiolipin can regulate the fusion of mitochondria and the formation of mitochondrial respiratory supercomplexes (Mileykovskaya and Dowhan, 2014; Kameoka et al., 2018). In fibroblasts of patients with *SERAC1* mutations (MEGDEL syndrome), the levels of

cardiolipin were increased compared to controls. This was associated with a dysfunction of the mitochondrial respiratory chain (Wortmann et al., 2012). It has not been investigated whether mitochondrial function was altered in fibroblasts of HSP patients with *SERAC1* mutations. Spartin, implicated in SPG20, was also shown to interact with cardiolipins and was present on the outer mitochondrial membrane. Downregulation of spartin decreased mitochondrial membrane potential (Joshi and Bakowska, 2011), but it is not clear whether this effect is caused by a change in the levels of mitochondria lipid composition.

In vitro experiments showed that exposition to VLCFA induced death of astrocytes and oligodendrocytes (Hein et al., 2008). VLCFA exposition deregulated intracellular calcium homeostasis in neurons, astrocytes, and oligodendrocytes, but the latter were the most affected cell type (Hein et al., 2008). VLCFA exposition induced mitochondrial depolarization and reactive oxygen species production (Hein et al., 2008), which could contribute to oligodendrocyte death. Consistently, astrocytes derived from *Abcd1* knockout mice exhibited impaired energy metabolism and increased ROS production when exposed to supraphysiological concentration of VLCFA (Kruska et al., 2015).

Change in mitochondrial function was also observed in fibroblasts and lymphoblasts from SPG49/56 patients. In the absence of functional CYP21U, the oxygen consumption was reduced and was associated with increased oxidative stress (Tesson et al., 2012). The subcellular localization of CYP2U1 is still not clear. This cytochrome was proposed to metabolize arachidonic acid into 19- and 20-HETE (Chuang et al., 2004), or to oxidize the endocannabinoid N-arachidonoylserotonin to downregulate its action (Siller et al., 2014). However, it is not known whether these molecules can regulate mitochondrial function directly or whether this is mediated by other metabolites, not yet identified, of this cytochrome P450.

Lysosomal Dysfunction

The clearest link between alteration of lysosome function and spasticity is provided by Krabbe and metachromatic leukodystrophy patients. Indeed, these two pathologies belong to the group of lysosomal storage disorders. Both diseases result from the loss of activity of a lysosomal enzyme leading to abnormal accumulation of substrates: psychosine (Krabbe) and sulfatides (Metachromatic leukodystrophy). Why such accumulation of substrates leads to spasticity is not clear.

Several other forms of HSP have also been proposed to be associated with impaired lysosomal function. Mutations of *ATP13A2* were found in families with complex hereditary spastic paraplegia (SPG78) (Estrada-Cuzcano et al., 2017). ATP13A2 is a P5ATPase that is mainly localized in the membrane of lysosomes (Ramirez et al., 2006), and dysfunction of this protein was shown to be responsible for impaired lysosomal degradation (Dehay et al., 2012). Consistently, homozygous mutations in fibroblasts of SPG78 patients increased the number of lysosomes and impaired lysosomal degradative activity, and electron microscopy analysis revealed that lysosomes accumulated abnormal material consisting of whirls and stacks of membranes (Estrada-Cuzcano et al., 2017). This was reminiscent of neuronal ceroid lipofuscinosis, also found in patients mutated in this gene (Bras et al., 2012). Similar accumulation of lysosomal membranes was also observed in fibroblasts of SPG48 patients with loss-of-function mutation in the ζ subunit of the AP-5 complex (Hirst et al., 2015). Electron microscopy analysis of fibroblasts of SPG15 patients and neurons of *Spg15* knockout mice showed the accumulation of zebra or fingerprint bodies (Khundadze et al., 2013; Renvoisé et al., 2014), which are lysosomes with accumulation of membranes similar to those found in some lysosomal storage disorders (Parkinson-Lawrence et al., 2010). Analysis of SPG11 patient fibroblasts, in contrast, did not reveal accumulation of lamellar structures by electron microscopy. However, in brains of *Spg15*, *Spg11*, and *Spg48* knockout mice, ultrastructural analysis showed the presence of electron dense deposits that looked like lipofuscin (Khundadze et al., 2013, 2019; Varga et al., 2015; Branchu et al., 2017). In all three models, the presence of these deposits was proposed to result from the accumulation of autolysosomes or impaired autophagic clearance. In the case of *Spg11* knockout mice, the lysosomal deposits were shown to contain lipids, and a lipidomic analysis revealed that the lysosomes accumulated simple gangliosides (Boutry et al., 2018). Whether gangliosides accumulate upon loss of function of spastizin or AP-5ζ is not known. Likewise, it is not clear why gangliosides accumulate in absence of spatacsin, the product of *SPG11*. It was proposed that such accumulation could be a consequence of impaired lysosomal membrane recycling (Boutry et al., 2018), but other mechanisms could contribute to this accumulation. For example, the levels of bis-monoacylglycerol-phosphate (BMP), which facilitates the degradation of GM2 ganglioside (Anheuser et al., 2015), were reduced in fibroblasts of patients with *SERAC1* mutations compared to controls (Wortmann et al., 2012). Importantly, mutations in *SPG11*, *SPG15*, *SPG48*, *ATP13A2*, and *SERAC1* have been associated with parkinsonism in some patients (Ramirez et al., 2006; Anheim et al., 2009; Schicks et al., 2011; Hirst et al., 2016; Ma et al., 2018). The clinical overlap between these patients, as well as the similarities observed in the lysosomal dysfunction suggest that these HSP entities may share some physiopathological pathways, although some differences may exist between them (Vantaggiato et al., 2019). Accumulation of membrane structures in lysosomes has also been observed in cells derived from *Spg4* or *Spg31* knockout mice. These defects resulted from impaired ER-mediated endosomal tubule fission (Allison et al., 2017). Yet, it is not clear whether these lysosomal structures share similarities in composition with the lysosomes accumulating membranes observed in fibroblasts of SPG11, SPG15, SPG48, or ATP13A2-deficient patients.

In SPG11 models, decreased gangliosides synthesis prevented neuronal death *in vitro* and improved the motor phenotype in a zebrafish model, suggesting that accumulation of gangliosides could contribute to neurodegeneration (Boutry et al., 2018). These results were notably obtained using miglustat, a non-specific inhibitor of glucosylceramide synthase that is used in the treatment of Gaucher disease. However, miglustat poorly crosses the blood–brain barrier and is not efficient for symptoms of neuropathic Gaucher Disease (Schiffmann et al., 2008). Furthermore, in a mouse model of Sandhoff disease, miglustat

increased the levels of brain glycosphingolipids (Ashe et al., 2011), questioning its efficacy in the central nervous system. Decreasing ganglioside synthesis is thus of therapeutic interest for SPG11 patients, but it is still unsure whether miglustat is a good therapeutic option for these patients. Further studies are thus required to validate this therapeutic strategy. If such a therapy was efficient in SPG11, it would be worth validating whether a similar strategy could also be efficient in other forms of HSP presenting alteration of lysosomal function and a phenotypic presentation overlapping with SPG11 patients. Besides synthesis of gangliosides, other studies have shown a beneficial effect of clinically used GSK3 blocker tideglusib on the neurodevelopmental phenotype observed in SPG11 models (Mishra et al., 2016; Pérez-Brangulí et al., 2019). However, it is not known yet whether such a treatment would affect the metabolism of gangliosides or act on a different pathway. It has also not been evaluated whether restoration of normal development in SPG11 could prevent neurodegeneration that occurs later in life of SPG11 patients.

Alteration of Synaptic Function

Neuropathological investigations on autopsic cases of HSP have proposed a "dying back" mechanism of axonal degeneration (DeLuca et al., 2004). Such mechanisms would be compatible with a primary alteration of synaptic function. Exocytosis and endocytosis of synaptic vesicles have been thought to be mainly mediated by proteins, but it has emerged that lipid composition of membranes and lipid mediators also play a key role in these processes (Darios et al., 2007; Mochel, 2018). It is therefore tempting to speculate that alteration of lipid metabolism observed in some HSP would impair synaptic function and underlie some symptoms of the disease. For example, the product of *PLA2G6*, the calcium-independent phospholipase A2 β (iPLA2β), is localized in axon terminals and dendritic spines of neurons (Ong et al., 2005) where it releases polyunsaturated fatty acids (PUFAs) from brain phospholipids (Green et al., 2008). Accordingly, brains of *Pla2g6* knockout mice present alteration of some PUFAs (Beck et al., 2011). Ultrastructural analyses of the posterior horn in this model showed the presence of loose presynaptic membranes containing synaptic vesicles (Beck et al., 2011). This insufficient membrane remodeling was proposed to contribute to the generation of axonal spheroids (Beck et al., 2011). Synaptic dysfunction could also underlie early behavioral symptoms in these mice, before the onset of neurodegeneration. Similarly, deficiency in NTE, another phospholipase associated with HSP, is associated with increased levels of phosphatidylcholine in brain—as described in the first part of the review—and a 20% decrease of protein secretion (Read et al., 2009). Alteration of the secretory pathway could affect synaptic vesicles and contribute to neuronal dysfunction long before neurodegeneration. Yet, iPLA2β and NTE have different lipid targets and may act by different mechanisms to regulate synaptic function. DDHD2, which was proposed to have a PLA1 action, also leads to synaptic defects in a drosophila model (Schuurs-Hoeijmakers et al., 2012). It would be interesting to further analyze how the loss of function of these enzymes contributes to synaptic dysfunction and underlie some early symptoms of HSP.

Alteration of synaptic function has also been observed upon expression of N88S seipin mutant in neurons, which decreased the number of synaptic vesicles docked to the plasma membrane. This alteration decreased the amplitude of evoked postsynaptic response (Wei et al., 2014). Yet, the link between the function of seipin in LD and the alteration of synaptic vesicles docking is unknown. Similarly, loss of spastin or atlastin, which regulates LD formation as illustrated above, affects synaptic functions (Trotta et al., 2004; De Gregorio et al., 2017). Whether this is related to the change in ER morphology due to loss of spastin or atlastin, or to the action of these proteins on LD remains to be established.

Importance of Myelin for Axon Maintenance

The most prominent lipid component of the brain is myelin that surrounds axons and promotes fast propagation of membrane depolarization. Most, if not all, forms of complex HSP are associated with white matter abnormalities detected on brain MRI. On the other hand, most, if not all, forms of leukodystrophies can present with spastic paraplegia such as Krabbe disease and metachromatic leukodystrophy. Likewise, it becomes increasingly difficult to make a distinction between HSP and leukodystrophy genes as illustrated by FA2H (Kruer et al., 2010).

Mutations in proteolipid protein gene (*PLP1*), *GJC2*, and *MAG* are responsible for a variety of phenotype ranging from hereditary spastic paraplegias (SPG2, SPG44, and SPG75, respectively) to neurodevelopmental disorders including Pelizaeus-Merzbacher disease, a hypomyelinating disorder of the central nervous system (Saugier-Veber et al., 1994; Orthmann-Murphy et al., 2009; Novarino et al., 2014; Lossos et al., 2015). The proteins encoded by these genes are essential for the maintenance of the myelin and axon integrity. Furthermore, loss of PLP1 in an oligodendrocyte cell line led to decreased levels of ethanolamine plasmalogen (Wood et al., 2011), highlighting the link between lipid metabolism and myelin maintenance. *PLP1* encodes two proteins, PLP and DM20, that are essential constituents of myelin. An autopsic case of SPG2 showed widespread white matter pallor in the central nervous system. Demyelination was associated with loss of axons and remaining fibers contained spheroids (Suzuki et al., 2011). Similarly, *Plp1* knockout mice assembled compact myelin sheaths, but subsequently showed progressive degeneration of axons (Griffiths, 1998), suggesting that maintenance of myelin is required to sustain neuronal function. This was confirmed by the specific deletion of *Plp1* in oligodendroglial lineage, demonstrating that PLP is essential in oligodendrocytes to sustain axonal function and prevent axonal degeneration (Lüders et al., 2017). Loss of PLP was shown to alter fast axonal transport, leading to accumulation of membranous organelles and formation of axonal swellings (Edgar et al., 2004).

Similarly to loss of Plp, *Mag* knockout mice did not show impaired myelination, but when they became older than

8 months, they presented alteration of the maintenance of axon-myelin units, resulting in both axon and myelin degeneration (Fruttiger et al., 1995). MAG is expressed on the myelin membrane wrap that is directly apposed to the membrane of neurons, and it binds to receptors on axons (Schnaar and Lopez, 2009). Among the putative receptors on axon membranes, GD1a and GT1b were identified as potent MAG receptors (Yang et al., 1996). *B4galnt1* knockout mice, which are deficient in a key enzyme for ganglioside extension, lack GD1a and GT1b and present progressive axon degeneration (Sheikh et al., 1999; Chiavegatto et al., 2000). Expression of B4GALNT1 specifically in neurons in the *B4galnt1*$^{-/-}$ mice prevented axon degeneration, suggesting that neuronal gangliosides are critical to maintain axon integrity (Yao et al., 2014). Interestingly, comparison of *Mag*, *B4galnt1*, and double knockout mice in the same genetic background showed similar axon degeneration, suggesting that oligodendroglial MAG binding to neuronal gangliosides contributes to maintain axon function (Pan et al., 2005).

Beside mutations affecting proteins that are myelin constituents, other mutations affect the lipid composition of myelin. Myelin is highly enriched in sphingolipids containing 2-hydroxylated fatty acids that require the FA2H enzyme for their synthesis, as illustrated in the first section of the review. The absence of FA2H in mouse did not prevent the formation of myelin sheaths. However, as mice were aging, axon and myelin sheath degeneration was observed (Zoller et al., 2008). Similar to the observations made in mice devoid of PLP or MAG, this suggests that axon degeneration is a consequence of impaired support provided by myelin. Specific deletion of FA2H in Schwann cells and oligodendrocytes showed demyelination similar to that observed in a constitutive *Fa2h* knockout mouse model (Potter et al., 2011). However, these mice did not show impaired cognitive function as observed in constitutive knockout, suggesting that FA2H could also have important function outside myelinating cells (Potter et al., 2011). Levels of 2-hydroxygalactosylceramide are also strongly reduced in the *Aldh3a2* knockout mouse model of Sjorgren–Larsson syndrome, due to inactivation of FA2H (Kanetake et al., 2019). Consistent with the *Fa2h* knockout, the formation of myelin was not impaired in *Aldh3a2* knockout mice (Kanetake et al., 2019).

As already discussed, X-ALD patients present progressive demyelination. In these patients and in a mouse model of the disease, the composition of myelin is altered (Brown et al., 1983; Bizzozero et al., 1991; Theda et al., 1992; Hama et al., 2018), but it is still not known whether this change in lipid composition contributes to demyelination. Patients affected by Krabbe disease or metachromatic leukodystrophy also present a strong demyelination, although the molecular mechanism underlying this phenomenon is still unclear. Loss of arylsulfatase A activity both in metachromatic leukodystrophy patients and in a mouse model of the disease leads to a strong accumulation of sulfatides, a class of lipids enriched in myelin. Yet, the mouse model of this disease did not present any gross white matter defect (Hess et al., 1996). In Krabbe disease, defective myelin formation as well as demyelination at a late disease stage have been observed in the natural Twitcher mouse model of the disease (Takahashi and Suzuki, 1984; Inamura et al., 2018). The alterations were proposed to result from impaired differentiation and survival of oligodendrocytes, due to accumulation of psychosine (Inamura et al., 2018).

Abnormal white matter has been detected on brain MRI in many HSP subtypes. Therefore, the loss of support provided by myelin to maintain axon function could contribute to the physiopathology in many forms of HSP. However, the mechanism of myelin loss in many forms of HSP is not known, and it will be important to determine whether loss of myelin is the primary defect or whether it is secondary or concomitant to axon degeneration.

CONCLUSION

HSP can be due to various mutations in genes encoding proteins involved in lipid metabolism, affecting most classes of lipids (sterols, fatty acids, phospholipids, and sphingolipids). This review of the literature highlights that alteration of both synthesis and degradation of the various classes of lipids can lead to HSP or HSP-related disorders, highlighting the importance of lipid homeostasis for the brain physiology. Based on current knowledge, the products of some genes can be connected within metabolic pathways, but many gaps exist between these products. Since the genetic cause is still unknown in about 50% of HSP patients, the identification of new causative genes may help to fill this gap. However, the identification of genes responsible for diseases has become challenging, as the main genes have likely been identified. Combination of genomic with lipidomic analysis could help us to uncover new genes and complete the map of genes responsible for HSP that are implicated in lipid metabolism.

As illustrated here, various steps of the metabolism of lipid molecules can be affected, leading to alteration in various subcellular compartments. Alteration of mitochondrial functions, oxidative stress or impairment of axonal transport can occur in some forms of HSP associated with alteration of lipid metabolism. Yet, the link between alteration of lipid metabolism and neurodegeneration is still unclear in most forms of HSP. Indeed, many studies have been performed in cell lines or cells derived from patients to demonstrate which lipid class was primarily affected. As shown by the investigation of myelin–axon interaction, studies modulating lipid metabolism in animal models, or at least cultured neuronal models, are now required to evaluate the role of lipids in neurodegeneration in HSP. This kind of study will be critical to develop therapeutic strategies. Indeed, metabolic processes, including lipid metabolism, are in theory druggable and understanding the role of lipids in neurodegeneration could help to identify therapeutic targets.

AUTHOR CONTRIBUTIONS

All authors listed have made a substantial, direct and intellectual contribution to the work, and approved it for publication.

FUNDING

This work was supported by the "Investissements d'avenir" program grants (ANR-10-IAIHU-06) and (ANR-11-INBS-0011) and received funding from the European Union's Horizon 2020 Research and Innovation Programme under grant agreement No. 779257-SOLVE-RD (to GS), the GIS-Maladies Rares Foundation (to GS), the E-Rare program (Neurolipid and Prepare consortia, to GS), and the European Research Council (European Research Council Starting [grant No. 311149] to FD).

ACKNOWLEDGMENTS

The authors thank B. Gurchenkov for his help with illustrations.

REFERENCES

Aharon-Peretz, J., Rosenbaum, H., and Gershoni-Baruch, R. (2004). Mutations in the glucocerebrosidase gene and Parkinson's disease in ashkenazi jews. *N. Engl. J. Med.* 351, 1972–1977. doi: 10.1056/NEJMoa033277

Ahmed, M. Y., Al-Khayat, A., Al-Murshedi, F., Al-Futaisi, A., Chioza, B. A., Pedro Fernandez-Murray, J., et al. (2017). A mutation of *EPT1 (SELENOI)* underlies a new disorder of Kennedy pathway phospholipid biosynthesis. *Brain* 140, 547–554. doi: 10.1093/brain/aww318

Alazami, A. M., Adly, N., Al Dhalaan, H., and Alkuraya, F. S. (2011). A nullimorphic ERLIN2 mutation defines a complicated hereditary spastic paraplegia locus (SPG18) *Neurogenetics* 12, 333–336. doi: 10.1007/s10048-011-02918

Aldahmesh, M. A., Mohamed, J. Y., Alkuraya, H. S., Verma, I. C., Puri, R. D., Alaiya, A. A., et al. (2011). Recessive mutations in ELOVL4 cause ichthyosis, intellectual disability, and spastic quadriplegia. *Am. J. Hum. Genet.* 89, 745–750. doi: 10.1016/j.ajhg.2011.10.011

Alderson, N. L., Rembiesa, B. M., Walla, M. D., Bielawska, A., Bielawski, J., and Hama, H. (2004). The human *FA2H* gene encodes a fatty acid 2-hydroxylase. *J. Biol. Chem.* 279, 48562–48568. doi: 10.1074/jbc.M406649200

Allison, R., Edgar, J. R., Pearson, G., Rizo, T., Newton, T., Günther, S., et al. (2017). Defects in ER–endosome contacts impact lysosome function in hereditary spastic paraplegia. *J. Cell Biol.* 216, 1337–1355. doi: 10.1083/jcb.201609033

Amador, M. D. M., Masingue, M., Debs, R., Lamari, F., Perlbarg, V., Roze, E., et al. (2018). Treatment with chenodeoxycholic acid in cerebrotendinous xanthomatosis: clinical, neurophysiological, and quantitative brain structural outcomes. *J. Inherit. Metab. Dis.* 41, 799–807. doi: 10.1007/s10545-018-01627

Anheim, M., Lagier-Tourenne, C., Stevanin, G., Fleury, M., Durr, A., Namer, I. J., et al. (2009). SPG11 spastic paraplegia. A new cause of juvenile parkinsonism. *J. Neurol.* 256, 104–108. doi: 10.1007/s00415-009-0083-3

Anheuser, S., Breiden, B., Schwarzmann, G., and Sandhoff, K. (2015). Membrane lipids regulate ganglioside GM2 catabolism and GM2 activator protein activity. *J. Lipid Res.* 56, 1747–1761. doi: 10.1194/jlr.M061036

Ashe, K. M., Bangari, D., Li, L., Cabrera-Salazar, M. A., Bercury, S. D., Nietupski, J. B., et al. (2011). Iminosugar-based inhibitors of glucosylceramide synthase increase brain glycosphingolipids and survival in a mouse model of sandhoff disease. *PLoS ONE* 6:e21758. doi: 10.1371/journal.pone.0021758

Baba, T., Kashiwagi, Y., Arimitsu, N., Kogure, T., Edo, A., Maruyama, T., et al. (2014). Phosphatidic acid (PA)-preferring phospholipase A1 regulates mitochondrial dynamics. *J. Biol. Chem.* 289, 11497–11511. doi: 10.1074/jbc.M113.531921

Beck, G., Sugiura, Y., Shinzawa, K., Kato, S., Setou, M., Tsujimoto, Y., et al. (2011). Neuroaxonal dystrophy in calcium-independent phospholipase A2 deficiency results from insufficient remodeling and degeneration of mitochondrial and presynaptic membranes. *J. Neurosci.* 31, 11411–11420. doi: 10.1523/JNEUROSCI.0345-11.2011

Benador, I. Y., Veliova, M., Liesa, M., and Shirihai, O. S. (2019). Mitochondria bound to lipid droplets: where mitochondrial dynamics regulate lipid storage and utilization. *Cell Metab.* 29, 827–835. doi: 10.1016/j.cmet.2019.02.011

Berginer, V. M., Salen, G., and Shefer, S. (1984). Long-term treatment of cerebrotendinous xanthomatosis with chenodeoxycholic acid. *N. Engl. J. Med.* 311, 1649–1652. doi: 10.1056/NEJM198412273112601

Bizzozero, O. A., Zuñiga, G., and Lees, M. B. (1991). Fatty acid composition of human myelin proteolipid protein in peroxisomal disorders. *J. Neurochem.* 56, 872–878. doi: 10.1111/j.1471-4159.1991.tb02003.x

Boukhris, A., Schule, R., Loureiro, J. L., Lourenço, C. M., Mundwiller, E., Gonzalez, M. A., et al. (2013). Alteration of ganglioside biosynthesis responsible for complex hereditary spastic paraplegia. *Am. J. Hum. Genet.* 93, 118–123. doi: 10.1016/j.ajhg.2013.05.006

Boutry, M., Branchu, J., Lustremant, C., Pujol, C., Pernelle, J., Matusiak, R., et al. (2018). Inhibition of lysosome membrane recycling causes accumulation of gangliosides that contribute to neurodegeneration. *Cell Rep.* 23, 3813–3826. doi: 10.1016/j.celrep.2018.05.098

Boutry, M., Morais, S., and Stevanin, G. (2019a). Update on the genetics of spastic paraplegias. *Curr. Neurol. Neurosci. Rep.* 19:18. doi: 10.1007/s11910-019-09302

Boutry, M., Pierga, A., Matusiak, R., Branchu, J., Houllegatte, M., Ibrahim, Y., et al. (2019b). Loss of spatacsin impairs cholesterol trafficking and calcium homeostasis. *Commun. Biol.* 2:380. doi: 10.1038/s42003-019-0615-z

Bowen, D. M., and Radin, N. S. (1968). Hydroxy fatty acid metabolism in brain. *Adv. Lipid Res.* 6, 255–272. doi: 10.1016/b978-1-4831-9942-9.50013-9

Branchu, J., Boutry, M., Sourd, L., Depp, M., Leone, C., Corriger, A., et al. (2017). Loss of spatacsin function alters lysosomal lipid clearance leading to upper and lower motor neuron degeneration. *Neurobiol. Dis.* 102, 21–37. doi: 10.1016/j.nbd.2017.02.007

Bras, J., Verloes, A., Schneider, S. A., Mole, S. E., and Guerreiro, R. J. (2012). Mutation of the parkinsonism gene ATP13A2 causes neuronal ceroid-lipofuscinosis. *Hum. Mol. Genet.* 21, 2646–2650. doi: 10.1093/hmg/dds089

Braverman, N. E., and Moser, A. B. (2012). Functions of plasmalogen lipids in health and disease. *Biochim. Biophys. Acta BBA – Mol. Basis Dis.* 1822, 1442–1452. doi: 10.1016/j.bbadis.2012.05.008

Browman, D. T. (2006). Erlin-1 and erlin-2 are novel members of the prohibitin family of proteins that define lipid-raft-like domains of the ER. *J. Cell Sci.* 119, 3149–3160. doi: 10.1242/jcs.03060

Brown, F. R., Chen, W. W., Kirschner, D. A., Frayer, K. L., Powers, J. M., Moser, A. B., et al. (1983). Myelin membrane from adrenoleukodystrophy brain white matter? Biochemical properties. *J. Neurochem.* 41, 341–348. doi: 10.1111/j.1471-4159.1983.tb04748.x

Cameron, D. J., Tong, Z., Yang, Z., Kaminoh, J., Kamiyah, S., Chen, H., et al. (2007). Essential role of Elovl4 in very long chain fatty acid synthesis, skin permeability barrier function, and neonatal survival. *Int. J. Biol. Sci.* 3, 111–119. doi: 10.7150/ijbs.3.111

Carrasco, P., Sahún, I., McDonald, J., Ramírez, S., Jacas, J., Gratacós, E., et al. (2012). Ceramide levels regulated by carnitine palmitoyltransferase 1c control dendritic spine maturation and cognition. *J. Biol. Chem.* 287, 21224–21232. doi: 10.1074/jbc.M111.337493

Casals, N., Zammit, V., Herrero, L., Fadó, R., Rodríguez-Rodríguez, R., and Serra, D. (2016). Carnitine palmitoyltransferase 1C: from cognition to cancer. *Prog. Lipid Res.* 61, 134–148. doi: 10.1016/j.plipres.2015.11.004

Chang, C.-L., Weigel, A. V., Ioannou, M. S., Pasolli, H. A., Xu, C. S., Peale, D. R., et al. (2019). Spastin tethers lipid droplets to peroxisomes and directs fatty acid trafficking through ESCRT-III. *J. Cell Biol.* 218, 2583–2599. doi: 10.1083/jcb.201902061

Chang, J., Lee, S., and Blackstone, C. (2014). Spastic paraplegia proteins spastizin and spatacsin mediate autophagic lysosome reformation. *J. Clin. Invest.* 124, 5249–5262. doi: 10.1172/JCI77598

Chen, W.-J. (2019). *PCSK9 Inhibitor Treatment for Patients With Hereditary Spastic Paraplegia Type 5*. Available at: https://clinicaltrials.gov/ct2/show/NCT04101643.

Chiavegatto, S., Sun, J., Nelson, R. J., and Schnaar, R. L. (2000). A functional role for complex gangliosides: motor deficits in GM2/GD2 synthase knockout mice. *Exp. Neurol.* 166, 227–234. doi: 10.1006/exnr.2000.7504

Chuang, S. S., Helvig, C., Taimi, M., Ramshaw, H. A., Collop, A. H., Amad, M., et al. (2004). CYP2U1, a novel human thymus- and brain-specific cytochrome P450, Catalyzes ω- and (ω-1)-Hydroxylation of Fatty Acids. *J. Biol. Chem.* 279, 6305–6314. doi: 10.1074/jbc.M311830200

Dard, R., Meyniel, C., Touitou, V., Stevanin, G., Lamari, F., Durr, A., et al. (2017). Mutations in DDHD1, encoding a phospholipase A1, is a novel cause of retinopathy and neurodegeneration with brain iron accumulation. *Eur. J. Med. Genet.* 60, 639–642. doi: 10.1016/j.ejmg.2017.08.015

Darios, F., Connell, E., and Davletov, B. (2007). Phospholipases and fatty acid signalling in exocytosis: phospholipases and fatty acid signalling in exocytosis. *J. Physiol.* 585, 699–704. doi: 10.1113/jphysiol.2007.136812

De Gregorio, C., Delgado, R., Ibacache, A., Sierralta, J., and Couve, A. (2017). *Drosophila* Atlastin in motor neurons is required for locomotion and presynaptic function. *J. Cell Sci.* 130, 3507–3516. doi: 10.1242/jcs.201657

Dehay, B., Ramirez, A., Martinez-Vicente, M., Perier, C., Canron, M.-H., Doudnikoff, E., et al. (2012). Loss of P-type ATPase ATP13A2/PARK9 function induces general lysosomal deficiency and leads to Parkinson disease neurodegeneration. *Proc. Natl. Acad. Sci. U.S.A.* 109, 9611–9616. doi: 10.1073/pnas.1112368109

DeLuca, G. C., Ebers, G. C., and Esiri, M. M. (2004). The extent of axonal loss in the long tracts in hereditary spastic paraplegia. *Neuropathol. Appl. Neurobiol.* 30, 576–584. doi: 10.1111/j.1365-2990.2004.00587.x

Dietschy, J. M., and Turley, S. D. (2004). Thematic review series: brain lipids. Cholesterol metabolism in the central nervous system during early development and in the mature animal. *J. Lipid Res.* 45, 1375–1397. doi: 10.1194/jlr.R400004-JLR200

Dodge, J. C., Treleaven, C. M., Pacheco, J., Cooper, S., Bao, C., Abraham, M., et al. (2015). Glycosphingolipids are modulators of disease pathogenesis in amyotrophic lateral sclerosis. *Proc. Natl. Acad. Sci. U.S.A.* 112, 8100–8105. doi: 10.1073/pnas.1508767112

Doi, H., Ushiyama, M., Baba, T., Tani, K., Shiina, M., Ogata, K., et al. (2015). Late-onset spastic ataxia phenotype in a patient with a homozygous DDHD2 mutation. *Sci. Rep.* 4:7132. doi: 10.1038/srep07132

Duell, P. B., Salen, G., Eichler, F. S., DeBarber, A. E., Connor, S. L., Casaday, L., et al. (2018). Diagnosis, treatment, and clinical outcomes in 43 cases with cerebrotendinous xanthomatosis. *J. Clin. Lipidol.* 12, 1169–1178. doi: 10.1016/j.jacl.2018.06.008

Eastman, S. W., Yassaee, M., and Bieniasz, P. D. (2009). A role for ubiquitin ligases and Spartin/SPG20 in lipid droplet turnover. *J. Cell Biol.* 184, 881–894. doi: 10.1083/jcb.200808041

Edgar, J. M., McLaughlin, M., Yool, D., Zhang, S.-C., Fowler, J. H., Montague, P., et al. (2004). Oligodendroglial modulation of fast axonal transport in a mouse model of hereditary spastic paraplegia. *J. Cell Biol.* 166, 121–131. doi: 10.1083/jcb.200312012

Edvardson, S., Hama, H., Shaag, A., Gomori, J. M., Berger, I., Soffer, D., et al. (2008). Mutations in the fatty acid 2-hydroxylase gene are associated with leukodystrophy with spastic paraparesis and dystonia. *Am. J. Hum. Genet.* 83, 643–648. doi: 10.1016/j.ajhg.2008.10.010

Edwards, T. L., Clowes, V. E., Tsang, H. T. H., Connell, J. W., Sanderson, C. M., Luzio, J. P., et al. (2009). Endogenous spartin (SPG20) is recruited to endosomes and lipid droplets and interacts with the ubiquitin E3 ligases AIP4 and AIP5. *Biochem. J.* 423, 31–39. doi: 10.1042/BJ20082398

Eichler, F., Duncan, C., Musolino, P. L., Orchard, P. J., De Oliveira, S., Thrasher, A. J., et al. (2017). Hematopoietic stem-cell gene therapy for cerebral adrenoleukodystrophy. *N. Engl. J. Med.* 377, 1630–1638. doi: 10.1056/NEJMoa1700554

Eichler, F. S., Ren, J.-Q., Cossoy, M., Rietsch, A. M., Nagpal, S., Moser, A. B., et al. (2008). Is microglial apoptosis an early pathogenic change in cerebral X-linked adrenoleukodystrophy? *Ann. Neurol.* 63, 729–742. doi: 10.1002/ana.21391

Engelen, M., Barbier, M., Dijkstra, I. M. E., Schür, R., de Bie, R. M. A., Verhamme, C., et al. (2014). X-linked adrenoleukodystrophy in women: a cross-sectional cohort study. *Brain* 137, 693–706. doi: 10.1093/brain/awt361

Estrada-Cuzcano, A., Martin, S., Chamova, T., Synofzik, M., Timmann, D., Holemans, T., et al. (2017). Loss-of-function mutations in the ATP13A2/PARK9 gene cause complicated hereditary spastic paraplegia (SPG78). *Brain* 140, 287–305. doi: 10.1093/brain/aww307

Fruttiger, M., Montag, D., Schachner, M., and Martini, R. (1995). Crucial role for the myelin-associated glycoprotein in the maintenance of axon-myelin integrity. *Eur. J. Neurosci.* 7, 511–515. doi: 10.1111/j.1460-9568.1995.tb00347.x

Fujita, M., Watanabe, R., Jaensch, N., Romanova-Michaelides, M., Satoh, T., Kato, M., et al. (2011). Sorting of GPI-anchored proteins into ER exit sites by p24 proteins is dependent on remodeled GPI. *J. Cell Biol.* 194, 61–75. doi: 10.1083/jcb.201012074

Goizet, C., Boukhris, A., Durr, A., Beetz, C., Truchetto, J., Tesson, C., et al. (2009). CYP7B1 mutations in pure and complex forms of hereditary spastic paraplegia type 5. *Brain* 132, 1589–1600. doi: 10.1093/brain/awp073

Gomez-Ospina, N. (2006). "Arylsulfatase a deficiency," in *GeneReviews®* , eds M. P. Adam, H. H. Ardinger, R. A. Pagon, S. E. Wallace, L. J. Bean, K. Stephens, et al. (Seattle, WA: University of Washington, Seattle).

Green, J. T., Orr, S. K., and Bazinet, R. P. (2008). The emerging role of group VI calcium-independent phospholipase A2 in releasing docosahexaenoic acid from brain phospholipids: Fig. 1. *J. Lipid Res.* 49, 939–944. doi: 10.1194/jlr.R700017-JLR200

Griffiths, I. (1998). Axonal swellings and degeneration in mice lacking the major proteolipid of myelin. *Science* 280, 1610–1613. doi: 10.1126/science.280.5369.1610

Hama, K., Fujiwara, Y., Morita, M., Yamazaki, F., Nakashima, Y., Takei, S., et al. (2018). Profiling and imaging of phospholipids in brains of *Abcd1*-deficient mice. *Lipids* 53, 85–102. doi: 10.1002/lipd.12022

Hammer, M. B., Eleuch-Fayache, G., Schottlaender, L. V., Nehdi, H., Gibbs, J. R., Arepalli, S. K., et al. (2013). Mutations in GBA2 cause autosomal-recessive cerebellar ataxia with spasticity. *Am. J. Hum. Genet.* 92, 245–251. doi: 10.1016/j.ajhg.2012.12.012

Hanein, S., Martin, E., Boukhris, A., Byrne, P., Goizet, C., Hamri, A., et al. (2008). Identification of the SPG15 gene, encoding spastizin, as a frequent cause of complicated autosomal-recessive spastic paraplegia, including kjellin syndrome. *Am. J. Hum. Genet.* 82, 992–1002. doi: 10.1016/j.ajhg.2008.03.004

Harding, A. E. (1983). Classification of the hereditary ataxias and paraplegias. *Lancet Lond. Engl.* 1, 1151–1155. doi: 10.1016/s0140-6736(83)928799

Harlalka, G. V., Lehman, A., Chioza, B., Baple, E. L., Maroofian, R., Cross, H., et al. (2013). Mutations in B4GALNT1 (GM2 synthase) underlie a new disorder of ganglioside biosynthesis. *Brain* 136, 3618–3624. doi: 10.1093/brain/awt270

Hehr, U., Bauer, P., Winner, B., Schule, R., Olmez, A., Koehler, W., et al. (2007). Long-term course and mutational spectrum of spatacsin-linked spastic paraplegia. *Ann. Neurol.* 62, 656–665. doi: 10.1002/ana.21310

Hein, S., Schonfeld, P., Kahlert, S., and Reiser, G. (2008). Toxic effects of X-linked adrenoleukodystrophy-associated, very long chain fatty acids on glial cells and neurons from rat hippocampus in culture. *Hum. Mol. Genet.* 17, 1750–1761. doi: 10.1093/hmg/ddn066

Hess, B., Saftig, P., Hartmann, D., Coenen, R., Lullmann-Rauch, R., Goebel, H. H., et al. (1996). Phenotype of arylsulfatase A-deficient mice: relationship to human metachromatic leukodystrophy. *Proc. Natl. Acad. Sci. U.S.A.* 93, 14821–14826. doi: 10.1073/pnas.93.25.14821

Higgs, H. N., Han, M. H., Johnson, G. E., and Glomset, J. A. (1998). Cloning of a phosphatidic acid-preferring phospholipase A1 from bovine testis. *J. Biol. Chem.* 273, 5468–5477. doi: 10.1074/jbc.273.10.5468

Hirst, J., Edgar, J. R., Esteves, T., Darios, F., Madeo, M., Chang, J., et al. (2015). Loss of AP-5 results in accumulation of aberrant endolysosomes: defining a new type of lysosomal storage disease. *Hum. Mol. Genet.* 24, 4984–4996. doi: 10.1093/hmg/ddv220

Hirst, J., Madeo, M., Smets, K., Edgar, J. R., Schols, L., Li, J., et al. (2016). Complicated spastic paraplegia in patients with *AP5Z1* mutations (SPG48). *Neurol. Genet.* 2:e98. doi: 10.1212/NXG.0000000000000098

Hooper, C., Puttamadappa, S. S., Loring, Z., Shekhtman, A., and Bakowska, J. C. (2010). Spartin activates atrophin-1-interacting protein 4 (AIP4) E3 ubiquitin ligase and promotes ubiquitination of adipophilin on lipid droplets. *BMC Biol.* 8:72. doi: 10.1186/1741-7007-872

Horibata, Y., Elpeleg, O., Eran, A., Hirabayashi, Y., Savitzki, D., Tal, G., et al. (2018). EPT1 (selenoprotein I) is critical for the neural development and maintenance of plasmalogen in humans. *J. Lipid Res.* 59, 1015–1026. doi: 10.1194/jlr.P081620

Huber, M. D., Vesely, P. W., Datta, K., and Gerace, L. (2013). Erlins restrict SREBP activation in the ER and regulate cellular cholesterol homeostasis. *J. Cell Biol.* 203, 427–436. doi: 10.1083/jcb.201305076

Huffnagel, I. C., Dijkgraaf, M. G. W., Janssens, G. E., van Weeghel, M., van Geel, B. M., Poll-The, B. T., et al. (2019). Disease progression in women with

X-linked adrenoleukodystrophy is slow. *Orphanet J. Rare Dis.* 14:30. doi: 10.1186/s13023-019-10086

Igisu, H., Shimomura, K., Kishimoto, Y., and Suzuki, K. (1983). Lipids of developing brain of twitcher mouse. An authentic murine model of human Krabbe disease. *Brain J. Neurol.* 106(Pt 2), 405–417. doi: 10.1093/brain/106.2.405

Igisu, H., and Suzuki, K. (1984). Progressive accumulation of toxic metabolite in a genetic leukodystrophy. *Science* 224, 753–755. doi: 10.1126/science.6719111

Inamura, N., Kito, M., Go, S., Kishi, S., Hosokawa, M., Asai, K., et al. (2018). Developmental defects and aberrant accumulation of endogenous psychosine in oligodendrocytes in a murine model of Krabbe disease. *Neurobiol. Dis.* 120, 51–62. doi: 10.1016/j.nbd.2018.08.023

Inloes, J. M., Hsu, K.-L., Dix, M. M., Viader, A., Masuda, K., Takei, T., et al. (2014). The hereditary spastic paraplegia-related enzyme DDHD2 is a principal brain triglyceride lipase. *Proc. Natl. Acad. Sci. U.S.A.* 111, 14924–14929. doi: 10.1073/pnas.1413706111

Inloes, J. M., Jing, H., and Cravatt, B. F. (2018). The spastic paraplegia-associated phospholipase DDHD1 is a primary brain phosphatidylinositol lipase. *Biochemistry* 57, 5759–5767. doi: 10.1021/acs.biochem.8b00810

Inoue, H., Baba, T., Sato, S., Ohtsuki, R., Takemori, A., Watanabe, T., et al. (2012). Roles of SAM and DDHD domains in mammalian intracellular phospholipase A1 KIAA0725p. *Biochim. Biophys. Acta BBA – Mol. Cell Res.* 1823, 930–939. doi: 10.1016/j.bbamcr.2012.02.002

Inoue, K., Kubota, S., and Seyama, Y. (1999). Cholestanol induces apoptosis of cerebellar neuronal cells. *Biochem. Biophys. Res. Commun.* 256, 198–203. doi: 10.1006/bbrc.1998.9497

Jakobsson, A., Westerberg, R., and Jacobsson, A. (2006). Fatty acid elongases in mammals: their regulation and roles in metabolism. *Prog. Lipid Res.* 45, 237–249. doi: 10.1016/j.plipres.2006.01.004

James, P. F., and Zoeller, R. A. (1997). Isolation of animal cell mutants defective in long-chain fatty aldehyde dehydrogenase: sensitivity to fatty aldehydes and schiff's base modification of phospholipids: implications for sjögren-larsson syndrome. *J. Biol. Chem.* 272, 23532–23539. doi: 10.1074/jbc.272.38.23532

Joshi, D. C., and Bakowska, J. C. (2011). SPG20 protein spartin associates with cardiolipin via its plant-related senescence domain and regulates mitochondrial Ca2+ homeostasis. *PLoS ONE* 6:e19290. doi: 10.1371/journal.pone.0019290

Kameoka, S., Adachi, Y., Okamoto, K., Iijima, M., and Sesaki, H. (2018). Phosphatidic acid and cardiolipin coordinate mitochondrial dynamics. *Trends Cell Biol.* 28, 67–76. doi: 10.1016/j.tcb.2017.08.011

Kanamori, A., Nakayama, J., Fukuda, M. N., Stallcup, W. B., Sasaki, K., Fukuda, M., et al. (1997). Expression cloning and characterization of a cDNA encoding a novel membrane protein required for the formation of O-acetylated ganglioside: a putative acetyl-CoA transporter. *Proc. Natl. Acad. Sci. U.S.A.* 94, 2897–2902. doi: 10.1073/pnas.94.7.2897

Kanetake, T., Sassa, T., Nojiri, K., Sawai, M., Hattori, S., Miyakawa, T., et al. (2019). Neural symptoms in a gene knockout mouse model of Sjögren-Larsson syndrome are associated with a decrease in 2-hydroxygalactosylceramide. *FASEB J.* 33, 928–941. doi: 10.1096/fj.201800291R

Kemp, S., Berger, J., and Aubourg, P. (2012). X-linked adrenoleukodystrophy: clinical, metabolic, genetic and pathophysiological aspects. *Biochim. Biophys. Acta BBA – Mol. Basis Dis.* 1822, 1465–1474. doi: 10.1016/j.bbadis.2012.03.012

Khundadze, M., Kollmann, K., Koch, N., Biskup, C., Nietzsche, S., Zimmer, G., et al. (2013). A hereditary spastic paraplegia mouse model supports a role of ZFYVE26/SPASTIZIN for the endolysosomal system. *PLoS Genet.* 9:e1003988. doi: 10.1371/journal.pgen.1003988

Khundadze, M., Ribaudo, F., Hussain, A., Rosentreter, J., Nietzsche, S., Thelen, M., et al. (2019). A mouse model for SPG48 reveals a block of autophagic flux upon disruption of adaptor protein complex five. *Neurobiol. Dis.* 127, 419–431. doi: 10.1016/j.nbd.2019.03.026

Klemm, R. W., Norton, J. P., Cole, R. A., Li, C. S., Park, S. H., Crane, M. M., et al. (2013). A conserved role for atlastin GTPases in regulating lipid droplet size. *Cell Rep.* 3, 1465–1475. doi: 10.1016/j.celrep.2013.04.015

Kobayashi, T., Shinnoh, N., Goto, I., and Kuroiwa, Y. (1985). Hydrolysis of galactosylceramide is catalyzed by two genetically distinct acid beta-galactosidases. *J. Biol. Chem.* 260, 14982–14987.

Kruer, M. C., Paisán-Ruiz, C., Boddaert, N., Yoon, M. Y., Hama, H., Gregory, A., et al. (2010). Defective FA2H leads to a novel form of neurodegeneration with brain iron accumulation (NBIA). *Ann. Neurol.* 68, 611–618. doi: 10.1002/ana.22122

Kruska, N., Schönfeld, P., Pujol, A., and Reiser, G. (2015). Astrocytes and mitochondria from adrenoleukodystrophy protein (ABCD1)-deficient mice reveal that the adrenoleukodystrophy-associated very long-chain fatty acids target several cellular energy-dependent functions. *Biochim. Biophys. Acta BBA – Mol. Basis Dis.* 1852, 925–936. doi: 10.1016/j.bbadis.2015.01.005

Kutkowska-Kaźmierczak, A., Rydzanicz, M., Chlebowski, A., Kłosowska-Kosicka, K., Mika, A., Gruchota, J., et al. (2018). Dominant ELOVL1 mutation causes neurological disorder with ichthyotic keratoderma, spasticity, hypomyelination and dysmorphic features. *J. Med. Genet.* 55, 408–414. doi: 10.1136/jmedgenet-2017-105172

Laule, C., Vavasour, I. M., Shahinfard, E., Mädler, B., Zhang, J., Li, D. K. B., et al. (2018). Hematopoietic stem cell transplantation in late-onset krabbe disease: no evidence of worsening demyelination and axonal loss 4 years post-allograft. *J. Neuroimaging* 28, 252–255. doi: 10.1111/jon.12502

Laurenzi, V. D., Rogers, G. R., Hamrock, D. J., Marekov, L. N., Steinert, P. M., Compton, J. G., et al. (1996). Sjögren–Larsson syndrome is caused by mutations in the fatty aldehyde dehydrogenase gene. *Nat. Genet.* 12, 52–57. doi: 10.1038/ng0196-52

Li, W., Sandhoff, R., Kono, M., Zerfas, P., Hoffmann, V., Ding, B. C.-H., et al. (2007). Depletion of ceramides with very long chain fatty acids causes defective skin permeability barrier function, and neonatal lethality in ELOVL4 deficient mice. *Int. J. Biol. Sci.* 3, 120–128. doi: 10.7150/ijbs.3.120

Lin, P., Li, J., Liu, Q., Mao, F., Li, J., Qiu, R., et al. (2008). A missense mutation in slc33a1, which encodes the Acetyl-CoA transporter, causes autosomal-dominant spastic paraplegia (SPG42). *Am. J. Hum. Genet.* 83, 752–759. doi: 10.1016/j.ajhg.2008.11.003

Liu, P., Jiang, B., Ma, J., Lin, P., Zhang, Y., Shao, C., et al. (2017). S113R mutation in SLC33A1 leads to neurodegeneration and augmented BMP signaling in a mouse model. *Dis. Model. Mech.* 10, 53–62. doi: 10.1242/dmm.026880

Lossos, A., Elazar, N., Lerer, I., Schueler-Furman, O., Fellig, Y., Glick, B., et al. (2015). Myelin-associated glycoprotein gene mutation causes Pelizaeus-Merzbacher disease-like disorder. *Brain* 138, 2521–2536. doi: 10.1093/brain/awv204

Lüders, K. A., Patzig, J., Simons, M., Nave, K.-A., and Werner, H. B. (2017). Genetic dissection of oligodendroglial and neuronal *Plp1* function in a novel mouse model of spastic paraplegia type 2. *Glia* 65, 1762–1776. doi: 10.1002/glia.23193

Ma, J., Wang, L., Yang, Y.-M., Mao, C.-H., and Wan, X.-H. (2018). Novel SERAC1 mutations in a Chinese patient presenting with parkinsonism and dystonia. *Neurol. Sci.* 39, 967–969. doi: 10.1007/s10072-018-3247-z

Marelli, C., Lamari, F., Rainteau, D., Lafourcade, A., Banneau, G., Humbert, L., et al. (2018). Plasma oxysterols: biomarkers for diagnosis and treatment in spastic paraplegia type 5. *Brain* 141, 72–84. doi: 10.1093/brain/awx297

Martin, E., Schüle, R., Smets, K., Rastetter, A., Boukhris, A., Loureiro, J. L., et al. (2013). Loss of function of glucocerebrosidase GBA2 is responsible for motor neuron defects in hereditary spastic paraplegia. *Am. J. Hum. Genet.* 92, 238–244. doi: 10.1016/j.ajhg.2012.11.021

Maruyama, T., Baba, T., Maemoto, Y., Hara-Miyauchi, C., Hasegawa-Ogawa, M., Okano, H. J., et al. (2018). Loss of DDHD2, whose mutation causes spastic paraplegia, promotes reactive oxygen species generation and apoptosis. *Cell Death Dis.* 9:797. doi: 10.1038/s41419-018-0815-3

Mehl, E., and Jatzkewitz, H. (1968). Cerebroside 3-sulfate as a physiological substrate of arylsulfatase A. *Biochim. Biophys. Acta BBA – Enzymol.* 151, 619–627. doi: 10.1016/0005-2744(68)90008-9

Mignarri, A., Magni, A., Del Puppo, M., Gallus, G. N., Björkhem, I., Federico, A., et al. (2016). Evaluation of cholesterol metabolism in cerebrotendinous xanthomatosis. *J. Inherit. Metab. Dis.* 39, 75–83. doi: 10.1007/s10545-015-98731

Mileykovskaya, E., and Dowhan, W. (2014). Cardiolipin-dependent formation of mitochondrial respiratory supercomplexes. *Chem. Phys. Lipids* 179, 42–48. doi: 10.1016/j.chemphyslip.2013.10.012

Mishra, H. K., Prots, I., Havlicek, S., Kohl, Z., Perez-Branguli, F., Boerstler, T., et al. (2016). GSK3ß-dependent dysregulation of neurodevelopment in SPG11-patient induced pluripotent stem cell model: neurodevelopmental defects in motor neuron disease. *Ann. Neurol.* 79, 826–840. doi: 10.1002/ana.24633

Mitomo, H., Chen, W.-H., and Regen, S. L. (2009). Oxysterol-induced rearrangement of the liquid-ordered phase: a possible link to Alzheimer's disease? *J. Am. Chem. Soc.* 131, 12354–12357. doi: 10.1021/ja904308y

Mochel, F. (2018). Lipids and synaptic functions. *J. Inherit. Metab. Dis.* 41, 1117–1122. doi: 10.1007/s10545-018-02041

Montecchiani, C., Pedace, L., Lo Giudice, T., Casella, A., Mearini, M., Gaudiello, F., et al. (2016). ALS5/SPG11/*KIAA1840* mutations cause autosomal recessive axonal Charcot–Marie–Tooth disease. *Brain* 139, 73–85. doi: 10.1093/brain/awv320

Mosser, J., Douar, A.-M., Sarde, C.-O., Kioschis, P., Feil, R., Moser, H., et al. (1993). Putative X-linked adrenoleukodystrophy gene shares unexpected homology with ABC transporters. *Nature* 361, 726–730. doi: 10.1038/361726a0

Mueller, N., Sassa, T., Morales-Gonzalez, S., Schneider, J., Salchow, D. J., Seelow, D., et al. (2019). De novo mutation in *ELOVL1* causes ichthyosis, *acanthosis nigricans*, hypomyelination, spastic paraplegia, high frequency deafness and optic atrophy. *J. Med. Genet.* 56, 164–175. doi: 10.1136/jmedgenet-2018-105711

Murakami, Y., Tawamie, H., Maeda, Y., Büttner, C., Buchert, R., Radwan, F., et al. (2014). Null mutation in PGAP1 impairing gpi-anchor maturation in patients with intellectual disability and encephalopathy. *PLoS Genet.* 10:e1004320. doi: 10.1371/journal.pgen.1004320

Nie, S., Chen, G., Cao, X., and Zhang, Y. (2014). Cerebrotendinous xanthomatosis: a comprehensive review of pathogenesis, clinical manifestations, diagnosis, and management. *Orphanet J. Rare Dis.* 9:179. doi: 10.1186/s13023-014-01794

Novarino, G., Fenstermaker, A. G., Zaki, M. S., Hofree, M., Silhavy, J. L., Heiberg, A. D., et al. (2014). Exome sequencing links corticospinal motor neuron disease to common neurodegenerative disorders. *Science* 343, 506–511. doi: 10.1126/science.1247363

Ofman, R., Dijkstra, I. M. E., van Roermund, C. W. T., Burger, N., Turkenburg, M., van Cruchten, A., et al. (2010). The role of ELOVL1 in very long-chain fatty acid homeostasis and X-linked adrenoleukodystrophy. *EMBO Mol. Med.* 2, 90–97. doi: 10.1002/emmm.201000061

Olzmann, J. A., and Carvalho, P. (2019). Dynamics and functions of lipid droplets. *Nat. Rev. Mol. Cell Biol.* 20, 137–155. doi: 10.1038/s41580-018-0085-z

Ong, W.-Y., Yeo, J.-F., Ling, S.-F., and Farooqui, A. A. (2005). Distribution of calcium-independent phospholipase A2 (iPLA2) in monkey brain. *J. Neurocytol.* 34, 447–458. doi: 10.1007/s11068-006-87304

Orlacchio, A., Babalini, C., Borreca, A., Patrono, C., Massa, R., Basaran, S., et al. (2010). SPATACSIN mutations cause autosomal recessive juvenile amyotrophic lateral sclerosis. *Brain* 133, 591–598. doi: 10.1093/brain/awp325

Orsini, J. J., Escolar, M. L., Wasserstein, M. P., and Caggana, M. (2000). "Krabbe disease," in *GeneReviews®* , eds M. P. Adam, H. H. Ardinger, R. A. Pagon, S. E. Wallace, L. J. Bean, K. Stephens, et al. (Seattle, WA: University of Washington, Seattle).

Orthmann-Murphy, J. L., Salsano, E., Abrams, C. K., Bizzi, A., Uziel, G., Freidin, M. M., et al. (2009). Hereditary spastic paraplegia is a novel phenotype for GJA12/GJC2 mutations. *Brain* 132, 426–438. doi: 10.1093/brain/awn328

Ozaki, K., Doi, H., Mitsui, J., Sato, N., Iikuni, Y., Majima, T., et al. (2015). A novel mutation in ELOVL4 leading to spinocerebellar ataxia (SCA) with the hot cross bun sign but lacking erythrokeratodermia: a broadened spectrum of SCA34. *JAMA Neurol.* 72, 797–805. doi: 10.1001/jamaneurol.2015.0610

Pan, B., Fromholt, S. E., Hess, E. J., Crawford, T. O., Griffin, J. W., Sheikh, K. A., et al. (2005). Myelin-associated glycoprotein and complementary axonal ligands, gangliosides, mediate axon stability in the CNS and PNS: neuropathology and behavioral deficits in single- and double-null mice. *Exp. Neurol.* 195, 208–217. doi: 10.1016/j.expneurol.2005.04.017

Papadopoulos, C., Orso, G., Mancuso, G., Herholz, M., Gumeni, S., Tadepalle, N., et al. (2015). Spastin binds to lipid droplets and affects lipid metabolism. *PLoS Genet.* 11:e1005149. doi: 10.1371/journal.pgen.1005149

Park, S. H., Zhu, P.-P., Parker, R. L., and Blackstone, C. (2010). Hereditary spastic paraplegia proteins REEP1, spastin, and atlastin-1 coordinate microtubule interactions with the tubular ER network. *J. Clin. Invest.* 120, 1097–1110. doi: 10.1172/JCI40979

Parkinson-Lawrence, E. J., Shandala, T., Prodoehl, M., Plew, R., Borlace, G. N., and Brooks, D. A. (2010). Lysosomal storage disease: revealing lysosomal function and physiology. *Physiology* 25, 102–115. doi: 10.1152/physiol.00041.2009

Pearce, M. M. P., Wormer, D. B., Wilkens, S., and Wojcikiewicz, R. J. H. (2009). An endoplasmic reticulum (ER) membrane complex composed of SPFH1 and SPFH2 mediates the er-associated degradation of inositol 1,4,5-trisphosphate receptors. *J. Biol. Chem.* 284, 10433–10445. doi: 10.1074/jbc.M809801200

Pennetta, G., and Welte, M. A. (2018). Emerging links between lipid droplets and motor neuron diseases. *Dev. Cell* 45, 427–432. doi: 10.1016/j.devcel.2018.05.002

Pérez-Brangulí, F., Buchsbaum, I. Y., Pozner, T., Regensburger, M., Fan, W., Schray, A., et al. (2019). Human SPG11 cerebral organoids reveal cortical neurogenesis impairment. *Hum. Mol. Genet.* 28, 961–971. doi: 10.1093/hmg/ddy397

Potter, K. A., Kern, M. J., Fullbright, G., Bielawski, J., Scherer, S. S., Yum, S. W., et al. (2011). Central nervous system dysfunction in a mouse model of Fa2h deficiency. *Glia* 59, 1009–1021. doi: 10.1002/glia.21172

Rafi, M. A., Luzi, P., Chen, Y. Q., and Wenger, D. A. (1995). A large deletion together with a point mutation in the GALC gene is a common mutant allele in patients with infantile Krabbe disease. *Hum. Mol. Genet.* 4, 1285–1289. doi: 10.1093/hmg/4.8.1285

Rainier, S., Bui, M., Mark, E., Thomas, D., Tokarz, D., Ming, L., et al. (2008). Neuropathy target esterase gene mutations cause motor neuron disease. *Am. J. Hum. Genet.* 82, 780–785. doi: 10.1016/j.ajhg.2007.12.018

Raju, D., Schonauer, S., Hamzeh, H., Flynn, K. C., Bradke, F., vom Dorp, K., et al. (2015). Accumulation of glucosylceramide in the absence of the beta-glucosidase GBA2 alters cytoskeletal dynamics. *PLoS Genet.* 11:e1005063. doi: 10.1371/journal.pgen.1005063

Ramirez, A., Heimbach, A., Gründemann, J., Stiller, B., Hampshire, D., Cid, L. P., et al. (2006). Hereditary parkinsonism with dementia is caused by mutations in ATP13A2, encoding a lysosomal type 5 P-type ATPase. *Nat. Genet.* 38, 1184–1191. doi: 10.1038/ng1884

Rattay, T. W., Lindig, T., Baets, J., Smets, K., Deconinck, T., Söhn, A. S., et al. (2019). FAHN/SPG35: a narrow phenotypic spectrum across disease classifications. *Brain* 142, 1561–1572. doi: 10.1093/brain/awz102

Raymond, G. V., Aubourg, P., Paker, A., Escolar, M., Fischer, A., Blanche, S., et al. (2019). Survival and functional outcomes in boys with cerebral adrenoleukodystrophy with and without hematopoietic stem cell transplantation. *Biol. Blood Marrow Transplant.* 25, 538–548. doi: 10.1016/j.bbmt.2018.09.036

Read, D. J., Li, Y., Chao, M. V., Cavanagh, J. B., and Glynn, P. (2009). Neuropathy target esterase is required for adult vertebrate axon maintenance. *J. Neurosci.* 29, 11594–11600. doi: 10.1523/JNEUROSCI.3007-09.2009

Renvoisé, B., Chang, J., Singh, R., Yonekawa, S., FitzGibbon, E. J., Mankodi, A., et al. (2014). Lysosomal abnormalities in hereditary spastic paraplegia types SPG15 and SPG11. *Ann. Clin. Transl. Neurol.* 1, 379–389. doi: 10.1002/acn3.64

Renvoisé, B., Malone, B., Falgairolle, M., Munasinghe, J., Stadler, J., Sibilla, C., et al. (2016). *Reep1* null mice reveal a converging role for hereditary spastic paraplegia proteins in lipid droplet regulation. *Hum. Mol. Genet.* 25, 5111–5125. doi: 10.1093/hmg/ddw315

Rinaldi, C., Schmidt, T., Situ, A. J., Johnson, J. O., Lee, P. R., Chen, K., et al. (2015). Mutation in *CPT1C* Associated With Pure Autosomal Dominant Spastic Paraplegia. *JAMA Neurol.* 72:561. doi: 10.1001/jamaneurol.2014.4769

Rizzo, W. B., and Craft, D. A. (1991). Sjögren-Larsson syndrome. Deficient activity of the fatty aldehyde dehydrogenase component of fatty alcohol:NAD+ oxidoreductase in cultured fibroblasts. *J. Clin. Invest.* 88, 1643–1648. doi: 10.1172/JCI115478

Roeben, B., Schüle, R., Ruf, S., Bender, B., Alhaddad, B., Benkert, T., et al. (2018). SERAC1 deficiency causes complicated HSP: evidence from a novel splice mutation in a large family. *J. Med. Genet.* 55, 39–47. doi: 10.1136/jmedgenet-2017-104622

Rydning, S. L., Dudesek, A., Rimmele, F., Funke, C., Krüger, S., Biskup, S., et al. (2018). A novel heterozygous variant in *ERLIN2* causes autosomal dominant pure hereditary spastic paraplegia. *Eur. J. Neurol.* 25, 943-e71. doi: 10.1111/ene.13625

Salen, G., Shefer, S., and Berginer, V. (1991). Biochemical abnormalities in cerebrotendinous xanthomatosis. *Dev. Neurosci.* 13, 363–370. doi: 10.1159/000112186

Salen, G., and Steiner, R. D. (2017). Epidemiology, diagnosis, and treatment of cerebrotendinous xanthomatosis (CTX). *J. Inherit. Metab. Dis.* 40, 771–781. doi: 10.1007/s10545-017-00938

Salo, V. T., Belevich, I., Li, S., Karhinen, L., Vihinen, H., Vigouroux, C., et al. (2016). Seipin regulates ER–lipid droplet contacts and cargo delivery. *EMBO J.* 35, 2699–2716. doi: 10.15252/embj.201695170

Sassa, T., Ohno, Y., Suzuki, S., Nomura, T., Nishioka, C., Kashiwagi, T., et al. (2013). Impaired epidermal permeability barrier in mice lacking Elovl1, the gene responsible for very-long-chain fatty acid production. *Mol. Cell. Biol.* 33, 2787–2796. doi: 10.1128/mcb.00192-13

Saugier-Veber, P., Munnich, A., Bonneau, D., Rozet, J.-M., Le Merrer, M., Gil, R., et al. (1994). X–linked spastic paraplegia and Pelizaeus–Merzbacher disease are allelic disorders at the proteolipid protein locus. *Nat. Genet.* 6, 257–262. doi: 10.1038/ng0394-257

Schicks, J., Synofzik, M., Pétursson, H., Huttenlocher, J., Reimold, M., Schöls, L., et al. (2011). Atypical juvenile parkinsonism in a consanguineous *SPG15* family: letters to the editor. *Mov. Disord.* 26, 565–566. doi: 10.1002/mds.23472

Schiffmann, R., FitzGibbon, E. J., Harris, C., DeVile, C., Davies, E. H., Abel, L., et al. (2008). Randomized, controlled trial of miglustat in Gaucher's disease type 3. *Ann. Neurol.* 64, 514–522. doi: 10.1002/ana.21491

Schnaar, R. L., and Lopez, P. H. H. (2009). Myelin-associated glycoprotein and its axonal receptors. *J. Neurosci. Res.* 87, 3267–3276. doi: 10.1002/jnr.21992

Schöls, L., Rattay, T. W., Martus, P., Meisner, C., Baets, J., Fischer, I., et al. (2017). Hereditary spastic paraplegia type 5: natural history, biomarkers and a randomized controlled trial. *Brain* 140, 3112–3127. doi: 10.1093/brain/awx273

Schüle, R., Siddique, T., Deng, H.-X., Yang, Y., Donkervoort, S., Hansson, M., et al. (2010). Marked accumulation of 27-hydroxycholesterol in SPG5 patients with hereditary spastic paresis. *J. Lipid Res.* 51, 819–823. doi: 10.1194/jlr.M002543

Schuurs-Hoeijmakers, J. H. M., Geraghty, M. T., Kamsteeg, E.-J., Ben-Salem, S., de Bot, S. T., Nijhof, B., et al. (2012). Mutations in DDHD2, encoding an intracellular phospholipase A1, cause a recessive form of complex hereditary spastic paraplegia. *Am. J. Hum. Genet.* 91, 1073–1081. doi: 10.1016/j.ajhg.2012.10.017

Sheikh, K. A., Sun, J., Liu, Y., Kawai, H., Crawford, T. O., Proia, R. L., et al. (1999). Mice lacking complex gangliosides develop Wallerian degeneration and myelination defects. *Proc. Natl. Acad. Sci. U.S.A.* 96, 7532–7537. doi: 10.1073/pnas.96.13.7532

Siller, M., Goyal, S., Yoshimoto, F. K., Xiao, Y., Wei, S., and Guengerich, F. P. (2014). Oxidation of endogenous *N*-arachidonoylserotonin by human cytochrome P450 2U1. *J. Biol. Chem.* 289, 10476–10487. doi: 10.1074/jbc.M114.550004

Simons, J. P., Al-Shawi, R., Minogue, S., Waugh, M. G., Wiedemann, C., Evangelou, S., et al. (2009). Loss of phosphatidylinositol 4-kinase 2α activity causes late onset degeneration of spinal cord axons. *Proc. Natl. Acad. Sci. U.S.A.* 106, 11535–11539. doi: 10.1073/pnas.0903011106

Sjogren, T., and Larsson, T. (1957). Oligophrenia in combination with congenital ichthyosis and spastic disorders; a clinical and genetic study. *Acta Psychiatr. Neurol. Scand. Suppl.* 113, 1–112.

Soderblom, C., and Blackstone, C. (2006). Traffic accidents: molecular genetic insights into the pathogenesis of the hereditary spastic paraplegias. *Pharmacol. Ther.* 109, 42–56. doi: 10.1016/j.pharmthera.2005.06.001

Stelten, B. M. L., Huidekoper, H. H., van de Warrenburg, B. P. C., Brilstra, E. H., Hollak, C. E. M., Haak, H. R., et al. (2019). Long-term treatment effect in cerebrotendinous xanthomatosis depends on age at treatment start. *Neurology* 92, e83–e95. doi: 10.1212/WNL.0000000000006731

Stevanin, G., Azzedine, H., Denora, P., Boukhris, A., Tazir, M., Lossos, A., et al. (2008). Mutations in SPG11 are frequent in autosomal recessive spastic paraplegia with thin corpus callosum, cognitive decline and lower motor neuron degeneration. *Brain* 131, 772–784. doi: 10.1093/brain/awm293

Stevanin, G., Rastetter, A., Esteves, T., Hanein, S., Depienne, C., Brice, A., et al. (2019). Dominant negative heterozygous mutation in Erlin2 prevents degradation of IP3 receptors and is responsible for hereditary spastic paraplegia 37. *Eur. J. Hum. Genet.* 1174–1813. doi: 10.1038/s41431-019-04942

Stevanin, G., Santorelli, F. M., Azzedine, H., Coutinho, P., Chomilier, J., Denora, P. S., et al. (2007). Mutations in SPG11, encoding spatacsin, are a major cause of spastic paraplegia with thin corpus callosum. *Nat. Genet.* 39, 366–372. doi: 10.1038/ng1980

Sultana, S., Reichbauer, J., Schüle, R., Mochel, F., Synofzik, M., and van der Spoel, A. C. (2015). Lack of enzyme activity in GBA2 mutants associated with hereditary spastic paraplegia/cerebellar ataxia (SPG46). *Biochem. Biophys. Res. Commun.* 465, 35–40. doi: 10.1016/j.bbrc.2015.07.112

Suzuki, S. O., Iwaki, T., Arakawa, K., Furuya, H., Fujii, N., and Iwaki, A. (2011). An autopsy case of adult-onset hereditary spastic paraplegia type 2 with a novel mutation in exon 7 of the proteolipid protein 1 gene. *Acta Neuropathol. (Berl.)* 122, 775–781. doi: 10.1007/s00401-011-0916-x

Svennerholm, L., Vanier, M. T., and Månsson, J. E. (1980). Krabbe disease: a galactosylsphingosine (psychosine) lipidosis. *J. Lipid Res.* 21, 53–64.

Synofzik, M., Hufnagel, R. B., and Züchner, S. (2014). "PNPLA6-related disorders," in *GeneReviews®* , eds M. P. Adam, H. H. Ardinger, R. A. Pagon, S. E. Wallace, L. J. Bean, K. Stephens, et al. (Seattle, WA: University of Washington, Seattle).

Szymanski, K. M., Binns, D., Bartz, R., Grishin, N. V., Li, W.-P., Agarwal, A. K., et al. (2007). The lipodystrophy protein seipin is found at endoplasmic reticulum lipid droplet junctions and is important for droplet morphology. *Proc. Natl. Acad. Sci. U.S.A.* 104, 20890–20895. doi: 10.1073/pnas.0704154104

Takahashi, H., and Suzuki, K. (1984). Demyelination in the spinal cord of murine globoid cell leukodystrophy (the twitcher mouse). *Acta Neuropathol. (Berl.)* 62, 298–308. doi: 10.1007/BF00687612

Tanaka, S., Maeda, Y., Tashima, Y., and Kinoshita, T. (2004). Inositol deacylation of glycosylphosphatidylinositol-anchored proteins is mediated by mammalian PGAP1 and yeast Bst1p. *J. Biol. Chem.* 279, 14256–14263. doi: 10.1074/jbc.M313755200

Tesson, C., Nawara, M., Salih, M. A. M., Rossignol, R., Zaki, M. S., Al Balwi, M., et al. (2012). Alteration of fatty-acid-metabolizing enzymes affects mitochondrial form and function in hereditary spastic paraplegia. *Am. J. Hum. Genet.* 91, 1051–1064. doi: 10.1016/j.ajhg.2012.11.001

Theda, C., Moser, A. B., Powers, J. M., and Moser, H. W. (1992). Phospholipids in X-linked adrenoleukodystrophy white matter: fatty acid abnormalities before the onset of demyelination. *J. Neurol. Sci.* 110, 195–204. doi: 10.1016/0022-510X(92)90028-J

Theofilopoulos, S., Griffiths, W. J., Crick, P. J., Yang, S., Meljon, A., Ogundare, M., et al. (2014). Cholestenoic acids regulate motor neuron survival via liver X receptors. *J. Clin. Invest.* 124, 4829–4842. doi: 10.1172/JCI68506

Trotta, N., Orso, G., Rossetto, M. G., Daga, A., and Broadie, K. (2004). The Hereditary Spastic Paraplegia Gene, Spastin, Regulates Microtubule Stability To Modulate Synaptic Structure And Function. *Curr. Biol.* 14, 1135–1147. doi: 10.1016/j.cub.2004.06.058

Tsaousidou, M. K., Ouahchi, K., Warner, T. T., Yang, Y., Simpson, M. A., Laing, N. G., et al. (2008). Sequence alterations within CYP7B1 implicate defective cholesterol homeostasis in motor-neuron degeneration. *Am. J. Hum. Genet.* 82, 510–515. doi: 10.1016/j.ajhg.2007.10.001

Twig, G., Elorza, A., Molina, A. J. A., Mohamed, H., Wikstrom, J. D., Walzer, G., et al. (2008). Fission and selective fusion govern mitochondrial segregation and elimination by autophagy. *EMBO J.* 27, 433–446. doi: 10.1038/sj.emboj.7601963

van Rappard, D. F., Boelens, J. J., van Egmond, M. E., Kuball, J., van Hasselt, P. M., Oostrom, K. J., et al. (2016). Efficacy of hematopoietic cell transplantation in metachromatic leukodystrophy: the Dutch experience. *Blood* 127, 3098–3101. doi: 10.1182/blood-2016-03-708479

van Roermund, C. W. T., Visser, W. F., IJlst, L., van Cruchten, A., Boek, M., Kulik, W., et al. (2008). The human peroxisomal ABC half transporter ALDP functions as a homodimer and accepts acyl-CoA esters. *FASEB J.* 22, 4201–4208. doi: 10.1096/fj.08-110866

Vantaggiato, C., Panzeri, E., Castelli, M., Citterio, A., Arnoldi, A., Santorelli, F. M., et al. (2019). ZFYVE26/SPASTIZIN and SPG11/SPATACSIN mutations in hereditary spastic paraplegia types AR-SPG15 and AR-SPG11 have different effects on autophagy and endocytosis. *Autophagy* 15, 34–57. doi: 10.1080/15548627.2018.1507438

Varga, R.-E., Khundadze, M., Damme, M., Nietzsche, S., Hoffmann, B., Stauber, T., et al. (2015). In vivo evidence for lysosome depletion and impaired autophagic clearance in hereditary spastic paraplegia type SPG11. *PLoS Genet.* 11:e1005454. doi: 10.1371/journal.pgen.1005454

Waldhüter, N., Köhler, W., Hemmati, P. G., Jehn, C., Peceny, R., Vuong, G. L., et al. (2019). Allogeneic hematopoietic stem cell transplantation with myeloablative conditioning for adult cerebral X-linked adrenoleukodystrophy. *J. Inherit. Metab. Dis.* 42, 313–324. doi: 10.1002/jimd.12044

Wang, H., Lo, W.-T., and Haucke, V. (2019). Phosphoinositide switches in endocytosis and in the endolysosomal system. *Curr. Opin. Cell Biol.* 59, 50–57. doi: 10.1016/j.ceb.2019.03.011

Watkins, P. A., Gould, S. J., Smith, M. A., Braiterman, L. T., Wei, H. M., Kok, F., et al. (1995). Altered expression of ALDP in X-linked adrenoleukodystrophy. *Am. J. Hum. Genet.* 57, 292–301.

Wei, S., Soh, S. L.-Y., Xia, J., Ong, W.-Y., Pang, Z. P., and Han, W. (2014). Motor neuropathy-associated mutation impairs Seipin functions in neurotransmission. *J. Neurochem.* 129, 328–338. doi: 10.1111/jnc.12638

Wittke, D., Hartmann, D., Gieselmann, V., and Lüllmann-Rauch, R. (2004). Lysosomal sulfatide storage in the brain of arylsulfatase A-deficient mice: cellular alterations and topographic distribution. *Acta Neuropathol. (Berl.)* 108, 261–271. doi: 10.1007/s00401-004-08836

Wnętrzak, A., Makyła-Juzak, K., Filiczkowska, A., Kulig, W., and Dynarowicz-Łątka, P. (2017). Oxysterols versus cholesterol in model neuronal membrane. I. The case of 7-ketocholesterol, the langmuir monolayer study. *J. Membr. Biol.* 250, 553–564. doi: 10.1007/s00232-017-99848

Woeste, M. A., Stern, S., Raju, D. N., Grahn, E., Dittmann, D., Gutbrod, K., et al. (2019). Species-specific differences in nonlysosomal glucosylceramidase GBA2 function underlie locomotor dysfunction arising from loss-of-function mutations. *J. Biol. Chem.* 294, 3853–3871. doi: 10.1074/jbc.RA118.006311

Wong, J. C., Walsh, K., Hayden, D., and Eichler, F. S. (2018). Natural history of neurological abnormalities in cerebrotendinous xanthomatosis. *J. Inherit. Metab. Dis.* 41, 647–656. doi: 10.1007/s10545-018-01529

Wood, P. L., Smith, T., Pelzer, L., and Goodenowe, D. B. (2011). Targeted metabolomic analyses of cellular models of pelizaeus-merzbacher disease reveal plasmalogen and myo-inositol solute carrier dysfunction. *Lipids Health Dis.* 10:102. doi: 10.1186/1476-511X-10102

Wortmann, S. B., Vaz, F. M., Gardeitchik, T., Vissers, L. E. L. M., Renkema, G. H., Schuurs-Hoeijmakers, J. H. M., et al. (2012). Mutations in the phospholipid remodeling gene SERAC1 impair mitochondrial function and intracellular cholesterol trafficking and cause dystonia and deafness. *Nat. Genet.* 44, 797–802. doi: 10.1038/ng.2325

Yahalom, G., Tsabari, R., Molshatzki, N., Ephraty, L., Cohen, H., and Hassin-Baer, S. (2013). Neurological outcome in cerebrotendinous xanthomatosis treated with chenodeoxycholic acid: early versus late diagnosis. *Clin. Neuropharmacol.* 36, 78–83. doi: 10.1097/WNF.0b013e318288076a

Yang, L. J., Zeller, C. B., Shaper, N. L., Kiso, M., Hasegawa, A., Shapiro, R. E., et al. (1996). Gangliosides are neuronal ligands for myelin-associated glycoprotein. *Proc. Natl. Acad. Sci. U.S.A.* 93, 814–818. doi: 10.1073/pnas.93.2.814

Yao, D., McGonigal, R., Barrie, J. A., Cappell, J., Cunningham, M. E., Meehan, G. R., et al. (2014). Neuronal expression of GalNAc transferase is sufficient to prevent the age-related neurodegenerative phenotype of complex ganglioside-deficient mice. *J. Neurosci.* 34, 880–891. doi: 10.1523/JNEUROSCI.3996-13.2014

Yoshii, Y., Furukawa, T., Saga, T., and Fujibayashi, Y. (2015). Acetate/acetyl-CoA metabolism associated with cancer fatty acid synthesis: overview and application. *Cancer Lett.* 356, 211–216. doi: 10.1016/j.canlet.2014.02.019

Yung, Y. C., Stoddard, N. C., Mirendil, H., and Chun, J. (2015). Lysophosphatidic acid signaling in the nervous system. *Neuron* 85, 669–682. doi: 10.1016/j.neuron.2015.01.009

Zhang, K., Kniazeva, M., Han, M., Li, W., Yu, Z., Yang, Z., et al. (2001). A 5-bp deletion in ELOVL4 is associated with two related forms of autosomal dominant macular dystrophy. *Nat. Genet.* 27, 89–93. doi: 10.1038/83817

Zoller, I., Meixner, M., Hartmann, D., Bussow, H., Meyer, R., Gieselmann, V., et al. (2008). Absence of 2-hydroxylated sphingolipids is compatible with normal neural development but causes late-onset axon and myelin sheath degeneration. *J. Neurosci.* 28, 9741–9754. doi: 10.1523/JNEUROSCI.0458-08.2008

Conflict of Interest: The authors declare that the research was conducted in the absence of any commercial or financial relationships that could be construed as a potential conflict of interest.

frontiers in Neuroscience

ORIGINAL RESEARCH
published: 04 June 2020
doi: 10.3389/fnins.2020.00325

Multimodal MRI Longitudinal Assessment of White and Gray Matter in Different SPG Types of Hereditary Spastic Paraparesis

Domenico Montanaro[1], M. Vavla[2], F. Frijia[3], G. Aghakhanyan[4], A. Baratto[5], A. Coi[6], C. Stefan[7], G. Girardi[7], G. Paparella[7], S. De Cori[1], P. Totaro[1], F. Lombardo[1], G. Piccoli[5] and Andrea Martinuzzi[2]*

[1] U.O.C. Risonanza Magnetica Specialistica e Neuroradiologia, Fondazione CNR/Regione Toscana G. Monasterio, Pisa, Italy, [2] Severe Developmental Disabilities Unit, Scientific Institute, IRCCS Eugenio Medea, Conegliano, Italy, [3] U.O.C Bioengineering and Clinical Technology, Fondazione CNR/Regione Toscana G. Monasterio, Pisa, Italy, [4] Department of Translational Research on New Technologies in Medicine and Surgery, Regional Center of Nuclear Medicine, University of Pisa, Pisa, Italy, [5] Department of Radiology S. Maria dei Battuti Hospital – Conegliano, ULSS2-Marca Trevigiana, Conegliano, Italy, [6] Institute of Clinical Physiology, National Research Council, Pisa, Italy, [7] Acquired Neuropsychological Disease Rehabilitation Unit, Scientific Institute, IRCCS Eugenio Medea, Pieve di Soligo, Italy

OPEN ACCESS

Edited by:
Arumugam R. Jayakumar, Miami VA Healthcare System, United States

Reviewed by:
Gianluca Serafini, San Martino Hospital (IRCCS), Italy
Kannappan Sriramajayam, University of Miami Health System, United States
Ravindran Caspa Gokulan, University of Miami Health System, United States

***Correspondence:**
Domenico Montanaro
domont@ftgm.it

Specialty section:
This article was submitted to Neurodegeneration, a section of the journal Frontiers in Neuroscience

Received: *22 October 2019*
Accepted: *19 March 2020*
Published: *04 June 2020*

Citation:
Montanaro D, Vavla M, Frijia F, Aghakhanyan G, Baratto A, Coi A, Stefan C, Girardi G, Paparella G, De Cori S, Totaro P, Lombardo F, Piccoli G and Martinuzzi A (2020) Multimodal MRI Longitudinal Assessment of White and Gray Matter in Different SPG Types of Hereditary Spastic Paraparesis. Front. Neurosci. 14:325. doi: 10.3389/fnins.2020.00325

Hereditary spastic paraplegias (HSP) are a group of genetically and clinically heterogeneous neurologic disorders. Hereby we describe a relatively large group of patients (pts) affected by HSP studied at baseline (31 pts) and at follow-up (mean period 28.9 ± 8.4 months; 23 pts) with multimodal advanced MRI: high-resolution T1 images for voxel-based morphometry (VBM) analysis, magnetic resonance spectroscopy (MRS), and diffusion tensor imaging (DTI). An age-matched healthy control (HC) group underwent the same neuroimaging protocol in a time schedule matched with the HSP patients. At baseline, VBM showed gray matter (GM) reduction in HSP in the right pre-frontal cortex and bilaterally in the thalami. MRS at baseline depicted in HSP patients compared to the HC group reduction of NAA/Cr ratio in the right pre-frontal region, increase of Cho/Cr ratio in the right pre-central regions, and increase of mI/Cr ratio on the left pre-central area. At cross-sectional follow-up analysis and longitudinal evaluation, no VBM and MRS statistically significant results were obtained. Tract-based spatial statistics (TBSS) analysis showed widespread DTI brain white matter (WM) alterations in patients compared to HC at baseline, which are characterized by reduction of fractional anisotropy (FA) and increase of mean diffusivity (MD), axial diffusivity (AD), and radial diffusivity, as confirmed on cross-analysis of the follow-up dataset. A longitudinal analysis with TBSS in HSP patients did not show significant variations, while upon applying region-based analysis we found increased FA and decreased MD and AD in specific brain WM fiber complex during follow-up. The changes were not correlated with the clinical presentation (pure *vs* complicated HSP), motor function, and motility indexes or history of specific treatments (botulinum toxin). In conclusion, the cross-sectional analysis of the multiparametric MRI data in our HSP patients confirmed the non-prominent involvement of the cortex in the primary motor regions but rather of other more associative areas. On the contrary, DTI demonstrated

a widespread involvement of the brain WM, including the primary motor regions, which was confirmed at follow-up. The longitudinal analysis revealed an apparent inversion of tendency when considering the expected evolution of a neurodegenerative process: we detected an increase of FA and a decrease of MD and AD. These time-related modifications may suggest a repair attempt by the residual central WM fibers, which requires confirmation with a larger group of patients and with a longer time interval.

Keywords: HSP, hereditary spastic paraplegia, MRS – 1H nuclear magnetic resonance spectra, VBM, voxel-based morphometry, DTI (diffusion tensor imaging), longitudinal analyze

INTRODUCTION

Hereditary spastic paraplegias (HSP) are a group of genetically and clinically heterogeneous neurologic disorders, also known as Strümpell–Lorrain disease (Faber et al., 2017), the authors who first described the clinical (Strümpell, 1880) and the neuropathological traits (Nayrac et al., 1953) of this disease.

The hinge points of HSP are progressive lower extremity spasticity with weakness and degeneration of the long axonal fibers of the cortico-spinal tract (CST) and the posterior cords (Fink and Hedera, 1999).

HSP is an inherited disease and the presence of a family history or consanguinity addresses toward a hereditary condition. Its absence, however, once other possible etiologies have been ruled out, should not dissuade the clinician from pursuing the search for a possible diagnosis of HSP (Faber et al., 2017).

Neuropathological reports on HSP are rare as the lifespan of these patients tends not to be shortened and they rarely die in hospital (Bisharat-Kernizan et al., 2018). Consequently, the pathological features first described in detail in 1952 (Schwarz, 1952) and subsequently categorized in 1974 (Behan and Maia, 1974) remain substantially the same at the moment. The common findings are represented by bilateral degeneration of the crossed CSTs with involvement of the uncrossed tracts, loss of Betz cells and spinal motor neurons, symmetrical degeneration of the gracile and cuneate fasciculi, mostly visible at thoracic level and increasing toward cervical regions up to the bulbar nuclei, and bilateral loss of fibers in the spinocerebellar tracts. No macroscopic lipid degeneration products and only occasional atrophy of the basal ganglia are reported (Erichsen et al., 2009). These postmortem studies suggest the degeneration of the distal ends of the longest motor and sensory axons as a possible pathogenetic mechanism. It is possibly due to a generalized failure of cells to maintain the vitality of terminal axons of more than a certain length, rather than a specific impairment of a particular neuronal system as observed in other neurodegenerative conditions, such as amyotrophic lateral sclerosis (ALS). Pathology descriptions suggest that the degeneration begins at the distal end of the axons and progresses toward the cell body, strengthening the hypothesis of a *dying back* axonopathy (Deluca et al., 2004). However, recent clinical and paraclinical studies revealed a wide involvement of the brain structures in HSP, including cerebellum, basal ganglia, and white matter (WM) of multiple brain regions, therefore suggesting how the simple *dying back* pathology is an incomplete unifying model (Aghakhanyan et al., 2014).

Classically, HSPs are subdivided on the basis of phenotypes into pure forms (pHSP), referring to the dominance of pyramidal signs, and complicated forms (cHSP), in which pyramidal findings are associated with dysfunction depending on other neurological systems, such as ataxia, parkinsonism, and cognitive impairment, or with systemic involvement, such as cataract, ichthyosis, etc. (Harding, 1983; Fink and Hedera, 1999). However, pure forms not rarely can show deficits typically seen in complicated forms, such as cognitive impairment (Jacinto-Scudeiro et al., 2019), and others seen in acquired motor neuron degeneration, like ALS (Denora et al., 2016), portraying the picture of a mosaicism of HSP phenotypes.

HSP have perhaps the inheritance patterns with the most striking heterogeneity among the neurogenetic diseases. The large genetic HSP heterogeneity is represented by over 85 spastic gait (SPG) disease loci and 79 known causative SPG identified genes (Parodi et al., 2018a; Coarelli et al., 2019). SPG4 type is the most frequent autosomal dominant subtype (Burguez et al., 2017). Genetic investigations have contributed to link HSP-related genes to other disorders, such as ALS and Alzheimer's and Parkinson's diseases (Novarino et al., 2014; Denora et al., 2016), or with genes previously associated with early-onset Charcot–Marie–Tooth disease and complicated encephalopathy (Parodi et al., 2018a; Olivieri et al., 2019). The identification of a number of casual genes and the determination of their products' dysfunction is helping to better understand common elements underlying the cellular process involved in the disease (Boutry et al., 2019).

Diagnosing HSP is a difficult task due to the high degree of genetic heterogeneity and the wide spectrum of clinical features that may confound HSP with other neurological diseases, particularly in patients without a positive family history (Cui et al., 2018). In this widely heterogeneous clinical and genetic landscape, magnetic resonance imaging (MRI) of the brain is fundamental as it allows to exclude other diseases such as acquired myelopathies, primary progressive multiple sclerosis, vitamin B12 deficiency, copper deficiency, spinal cord tumors or malformations, and degenerative disorders of the spine. Conventional MRI of the brain is usually normal in pHSP, and non-specific findings are present in cHSP (cortical atrophy and subcortical and periventricular WM alterations; Kassubek et al., 2006). Thin corpus callosum (TCC), brain iron accumulation, and cerebellar hypoplasia/atrophy are findings associated in HSP with intellectual disability or cognitive involvements. TCC is frequent in SPG11 and SPG15, even if it can be occasionally present in other

forms, collectively labeled as "HSPs with TCC subgroup" (Abdel Aleem, 2017).

In the last decades, among all the neuroimaging field, the so-called advanced MRI techniques have been widely applied as useful tools in HSP. These include voxel-based morphometry (VBM) and diffusion tensor imaging (DTI) (Graça et al., 2019) that demonstrated *in vivo* structural abnormalities correlated with disease mechanisms and progression (Faber et al., 2018). Their specific added benefits consist in the possibility to perform automated and unbiased whole-brain analyses and to localize *in vivo* the distribution of neural damage not otherwise visually evaluable (França et al., 2012).

Magnetic resonance spectroscopy (MRS) is another MRI advanced technique that enables the biochemical characterization of disease-related cerebral abnormalities, identifying either specific metabolites or variations of the most frequently reported brain macromolecules (Dreha-Kulaczewski et al., 2006; Schneider-Gold et al., 2017), among which reduction of Choline (Cho) and N-Acetyl Aspartate (NAA) were described in SPG4 patients compared to age-matched healthy controls (HC) in frontal WM and motor cortex, with a trend of an increase of myo-inositol, indicating neuro/axonal dysfunction and astroglia-mediated repair attempt (Erichsen et al., 2009).

DTI is applied to characterize the *in vivo* microstructural organization of the WM. The common DTI indices are fractional anisotropy (FA), sensitive to microstructural changes and associated with the presence of oriented structures in tissues, and mean diffusivity (MD), which is proportional to the overall presence of obstacles to diffusion. Other indices, such as axial diffusivity (AD) and radial diffusivity (RD), are elements useful to differentiate axonal injury and demyelination (Aghakhanyan et al., 2014).

Longitudinal changes occurring over time in the brains of HSP patients are still unclear: for example, disease progression seems to differ between the various HSP forms because little or no progression is described in some (SPG3), while a clear worsening is documented in others (SPG4) even within a few years (Schneider-Gold et al., 2017). Defining the extent and the longitudinal progression of brain involvement is fundamental in neurodegenerative diseases for understanding the pathophysiology, assessing prognosis, and thus improving care and monitoring experimental treatments in therapeutic trials. In this context, MRI has provided several biomarker candidates that may be offered as probes for the investigation of the natural disease progression and the effectiveness of therapeutic approaches (Menke et al., 2018). In particular, several types of advanced MRI techniques have been proposed as objective measures of dysfunctions in various motor neuron diseases, such as in ALS (Senda et al., 2011; Keil et al., 2012; Kwan et al., 2012). The same methodologies were proposed for the study on HSP, aimed to cross-sectional observations, while available longitudinal studies are poor and mostly technically limited (de Albuquerque et al., 2017).

This study was designed to reproduce literature data on the role of a multimodal advanced MRI approach (DTI, VBM, and MRS) in defining disease-specific alterations in HSP. Following the same group of HSP patients and HC over time and with the identical MRI methodology, we aimed also to evaluate longitudinal brain changes in HSP, possibly identifying specific anatomic involvement and types of brain modifications, in one of the relatively larger group of HSP patients ever reported.

MATERIALS AND METHODS

Patients

Thirty-one patients affected by HSP (age 43.5 ± 12 mean ± SD) attended at the Medea Scientific Institute in Conegliano (TV), Italy, and 36 HCs matched by age and gender (age 43.65 ± 10, mean ± SD) were recruited from 2009 to 2017. All the HSP patients underwent molecular genetic studies. Disease severity measures were assessed with various clinical tests, including the Spastic Paraplegia Rating Scale (SPRS) (Schüle et al., 2006) that was the only clinical measure used for correlation with the MRI variables.

Imaging Protocol

All the subjects were included in the protocol on the basis of the common criteria for a MRI study. They were examined with a 1.5 Tesla equipment (Philips Achieva 2.5 XR, Royal Philips Healthcare, Eindhoven, NL) at baseline (T_0) and at follow-up (T_1).

Depending on the quality of the single acquisitions in the presence of movement artifacts, datasets were discarded. From the initial group of subjects, 23 patients and a corresponding 23 age-matched HC group, after the basal MRI examination (T_0), underwent MRI follow-up (T_1) adopting the same standard and advanced sequences. The mean interval between the two examinations was 28.9 ± 8.4 months, corresponding to 2.40 ± 0.70 years. MRI data were analyzed cross-sectionally (at T_0 and at T_1) and longitudinally (T_0 *vs* T_1).

The study was approved by the Institutional Ethics Committee of the IRCCS "Eugenio Medea" Research Institute (# 63/09CE) and was conducted in accordance to the ethical standards of the Declaration of Helsinki (1964). All the adult participants and parents or legal tutors provided written informed consent prior to inclusion in the study. All the related documents were collected and stored by the clinical investigators of the center (MV and AM) according to the Institutional Ethic Committee guidance.

The MRI examinations included a standard protocol in order to exclude other pathologies (T2, proton density, and T1-weighted images). Sequences dedicated to the present study were obtained as follows:

T1-weighted 3D isotropic images with 1 mm voxel size (turbo-FFE, TR/TE 7.1/3.2, acquisition matrix 260 × 232, turbo FE factor 232, NSA 1);

Single-voxel H1-MR spectroscopy (MRS) localized in WM/gray matter (GM) of the bilateral pre-central (for primary motor functions) and in pre-frontal regions (for associative motor functions), for a total of four samplings for each study (PRESS sequence: TR 2000 ms, TE 35 ms, voxel size 15 × 15 × 15 mm);

DTI acquisition with single-shot FLAIR EPI-Echo Planar Image on axial plane (TR 10000 ms, TE 69 ms; IR 2400 ms; EPI

factor 55; acquisition matrix 104 × 102; *b*-value 0–1000 s/mm^2; 102 contiguous slices), voxel size 2 × 2 × 2 mm; 32 different gradient directions.

Voxel-Based Morphometry

VBM evaluations were performed with FSL-VBM (Douaud et al., 2009), an optimized VBM protocol (Good et al., 2001) carried out with FSL tools (Smith et al., 2004). First, the structural images were brain-extracted and cortical and deep GM was segmented before being registered to the 2-mm MNI 152 standard space using non-linear registration (Andersson et al., 2007a,b). The resulting images were averaged and flipped along the x-axis to create a left–right symmetric, study-specific GM template. Then, all the native GM images were non-linearly registered to this study-specific template and "modulated" to correct for local expansion (or contraction) due to the non-linear component of the spatial transformation. During the modulation step, each voxel of every registered GM image was multiplied by the Jacobian of the warp field (Good et al., 2001). This defines the direction (larger or smaller) and the amount of modulation. The modulated GM images were then smoothened with an isotropic Gaussian kernel with a sigma of 3 mm.

Magnetic Resonance Spectroscopy

The major brain metabolites detectable with H-MRS were analyzed: N-acetyl aspartate (NAA, processing at 2 ppm, marker for axonal density), choline (Cho, 3.2 ppm, index of membrane turnover), creatine-phosphocreatine complex (Cr, index of cell/axonal energy metabolism), and myo-inositol (mI, 3.5 ppm, index of glial activity). To define a peaks' table for each metabolite, data were processed with *Spectro View Software* (Philips Healthcare, NL), measuring peaks and areas under the curves as ratio referred to the Cr, which was considered as normative inter-subject units (Han and Ma, 2010).

Diffusion Tensor Imaging

Whole-brain DTI analyses were performed using tract-based spatial statistics (TBSS) in FSL version 4.1.1 (Smith et al., 2004), the Oxford Centre for Functional MRI of the Brain (FMRIB)[1] software library. First, raw diffusion data were corrected for motion artifacts and eddy current distortions with an automated procedure; then, the brain was extracted using the brain extraction tool (Smith, 2002). The FMRIB's diffusion toolbox (Behrens et al., 2003) was used to fit the diffusion tensor and compute the diagonal elements (eigenvalues λ1, λ2, and λ3) for each brain voxel, from which the derived metrics FA, MD, AD, and RD matrix were calculated for each subject. Voxelwise statistical analysis of these matrices was carried out with TBSS (Smith et al., 2006), part of FSL. All subjects' FA data aligned into a common space (1 × 1 × 1 mm FMRIB58_FA standard space was used as target images), applying the non-linear registration tool FNIRT (Andersson et al., 2007a,b). Next, the mean FA image was created and thinned (threshold FA value of 0.3) to create a mean FA skeleton which represents the center of all tracts common to the group. Finally, all subjects' spatially normalized FA, AD, RD, and MD data were projected onto the skeleton and the resulting data were analyzed into voxelwise cross-subject statistics. Individual skeleton images were submitted to a general linear model (GLM) analysis with appropriate design matrices and linear contrasts defined for the group comparisons.

A DTI region-based analysis (ROI) was applied using atlas-based predefined brain regions on the basis of the JHU White Matter Tractography and Harvard–Oxford Cortical Structural Atlas (part of FSL) (Mori et al., 2005). The ROIs were projected on the FA, MD, RD, and AD maps, and the mean values of each of the DTI indices were extracted using fsl meant tool (part of FSL).

Statistical Analysis

To assess gray and white matter decline at baseline and over the time, different comparisons between groups were performed: (1) comparison between HSP patients and HC group, (2) difference between pure and complicated form, (3) comparison between the SPG4 patients and the HC group, (4) SPG4 compared with other SPG forms, and (5) analysis of longitudinal changes from baseline and follow-up. Correlation with SPRS scale and treatment with botulinum toxin were tested within the HSP group.

For the VBM analysis, a design matrix for a GLM was constructed in FSL to compare the GM differences between two groups accounting for age as a nuisance covariate. Threshold-free cluster enhancement (TFCE)-based analysis was applied with 5000 permutations (Bullmore et al., 1999; Hayasaka and Nichols, 2004), which is an optimized method to detect clusters without having to define clusters in a binary way (Smith and Nichols, 2009). Family-wise error rate (FWE) was controlled and FWE-corrected *p*-values less than 0.05 were accepted.

The MRS data were analyzed in each investigated area (pre-central and pre-frontal, right and left) with Student's *t*-test or the non-parametric unpaired Wilcoxon test for continuous variables, evaluating differences in concentration of metabolite mean values with a confidence interval of 95% (CI95). In all analyses, a two-sided $p < 0.05$ was considered as statistically significant. Statistical analyses were performed using STATA software (StataCorp. Stata Statistical Software: Release 13, StataCorp LP, College Station, TX, United States, 2013).

DTI-based voxelwise statistics were carried out using the program Randomize, part of FSL, which uses Monte Carlo permutation testing to generate *n* number of random permutations for non-parametric statistics (Nichols and Holmes, 2002). With this approach, voxelwise differences among groups applying two-sample *t*-tests were assessed. We used the thresholded mean FA skeleton (mean value of 0.3), setting the number of permutations to 5000 with TFCE option and the significance threshold at $p = 0.05$ corrected for multiple comparisons to control FWE. The data were analyzed accounting for age as a nuisance covariate.

In order to implement a longitudinal design matrix for statistical analysis for VBM and TBSS, we subtracted each time-point 0 image from the time-point 1 image. All subsequent whole-brain statistical analyses (the same applied at the baseline study) were performed on these different images.

The GLM randomized test was applied also using SPRS indices as a covariate for correlations between imaging measures (VBM and DTI maps).

[1] http://www.fmrib.ox.ac.uk/fsl

RESULTS

All the HSP patients were molecularly defined with confirmed mutations in the SPG loci, except for one patient who, at the time of this study, had not yet been molecularly characterized but whose clinical history and presentation were strongly suggestive of a pHSP; so he was included in the list, as other authors suggest (Faber et al., 2017). The SPG types of all HSP patients are reported in **Table 1**. Their distribution reflects that described in most studies conducted on Western Europe population (Bisharat-Kernizan et al., 2018).

On the basis of the clinical presentation, HSP patients were subdivided into pure (16 patients, 52%) or complicated forms (15 patients, 48%).

The phenotypical characteristics of the patients were represented by lower limbs (LL) clonus (seven patients, 23%), LL dyskinesias (one patient, 3%), muscle hypo-atrophy (five patients, 16%), hypo-pallesthesia (12 patients, 39%), cerebellar involvement (seven patients, 23%), dystonic tremor (one patient 3%), nystagmus (two patients, 6%), urinary urgency (two patients, 6%), and axonal neuropathy (one patient, 3%). The neuropsychological profiles were characterized by deficits in spared tests as follows: in five patients (16%) deficits of verbal fluency, in 11 patients (35%) deficits of memory, and in 10 patients (32%) deficits of attention, praxia, and visuo-spatial perception.

At visual inspection and qualitative assessment, MRI showed on standard morphological images normal aspects in almost a third of all tested patients. Alterations in deep supratentorial WM, diffuse or focal brain atrophy, and the "ear of the lynx" sign were detected in some cases, with percentage matched with our previous report (Martinuzzi et al., 2016): WM alterations in 32%, corpus callosum atrophy in 16%, "ears of lynx" sign in 19%, and visually evaluable cortical and/or cerebellar atrophy in 40%.

TABLE 1 | Demographic and clinical data of HSP patients and healthy control group.

	HSP patients ***N*** **= 31**	**Healthy controls** ***N*** **= 36**
Gender	16 F, 15 M	26 F, 10 M
Disease onset (years)	27 ± 17	
Age at first MRI (years)	43.5 ± 12	43.65 ± 10
Age at follow-up MRI (years)	44 ± 12.8	47.8 ± 7.4
Disease duration at first MRI (years)	14 ± 13	
Disease duration at follow up MRI (years)	18 ± 13	
SPastic Gate gene		
SPG4	40% (12)	
SPG5	13% (4)	
SPG30	10% (3)	
SPG3	10% (3)	
SPG8	6% (2)	
SPG11	6% (2)	
SPG7	3% (1)	
SPG72	3% (1)	
SPG10	3% (1)	
SPG31	3% (1)	
SPG not defined	3% (1)	

Advanced MRI Results

At Baseline

VBM analysis performed with whole-brain volumetric method at the baseline revealed a volumetric loss in HSP patients compared to the HC group (number of subjects in each group = 31) in the right pre-frontal cortex and bilaterally in both thalami ($p < 0.05$, FWE corrected) (**Figure 1**). No statistical correlation was found stratifying by clinical presentation (pure *vs* complicated forms), disease severity measure (SPRS), history of specific treatments (chemodenervation using botulinum toxin or antispasticity drugs), and disease duration.

Statistical differences were detected in MRS spectra (**Table 2**): HSP patients showed increased mI/Cr ratio in the left pre-central area, lower NAA/Cr in HSP than HC in the right pre-frontal area, and higher Cho/Cr in HSP than HC in the right pre-central region. Comparing SPG4 patients and HC, higher levels of NAA in the left pre-frontal of HC than of SPG4 were detected. Comparing the various SPG subtypes within HSP patients, mI/Cr in non-SPG4 types were significantly higher than in SPG4 patients in the left pre-central area and in the right pre-frontal region.

An analysis of DTI data with TBSS revealed significant differences bilaterally in widespread brain regions ($p < 0.05$, FWE corrected, 28 HSPs – three were excluded for poor quality of images – and 36 HCs): CST, cingulum, corpus callosum, inferior fronto-occipital fasciculi, inferior longitudinal fasciculi, and superior longitudinal fasciculi. In particular, we observed patients with reduced FA (including parts of the brainstem) and increased MD and AD (not involving brainstem) and RD (involving the brainstem) (**Figure 2**). No area with increased FA and decreased MD was detected.

In a subgroup analysis comparing only SPG4 (10 subjects, two were excluded for technical reasons) and healthy subjects (36 subjects), the patients showed reduction of FA and increase of MD and RD in widespread regions; AD was also increased, but only on the right side of the corpus callosum, corona radiate, and semioval center. There were no differences between SPG4 (10 subjects) and the other SPG forms (18 subjects) in any of the DTI measurements. In HSP patients, no statistical correlation was found between DTI indices and SPRS and between patients with and without history of treatments with botulinum toxin.

Follow-up and Longitudinal Analysis

On cross-sectional analysis at follow-up and at the longitudinal analysis, VBM comparing residual 23 HC and 23 patients did not reveal any statistically significant variation. Similarly, MRS at follow-up cross-sectional analysis and at longitudinal comparisons did not show any significant change (41 samples for pre-central areas – 17 HC and 24 patients and 33 for pre-frontal region – 13 HC and 20 patients).

Comparing at follow-up the DTI results in HSP patients (valid for analysis 19 patients) with those in HCs (18 subjects), we confirmed the presence of significantly reduced FA values (with the sparing of the brainstem) and higher MD and RD

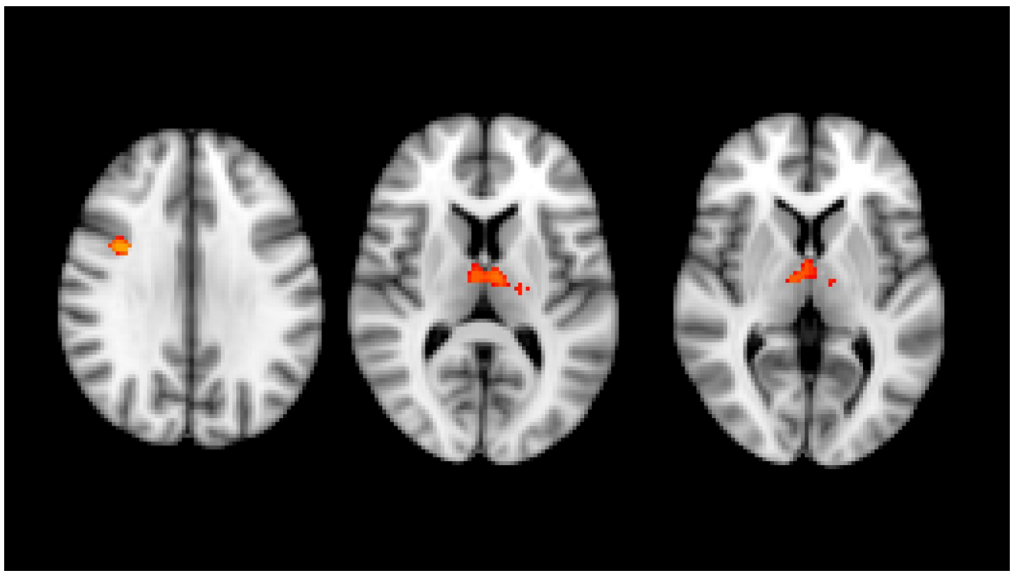

FIGURE 1 | Results of whole brain voxel-based morphometry analyses superimposed on the T1-weighted structural MRI images in the standard MNI space. T-statistics of the clusters with significant changes in between-group VBM analysis at baseline. Red-yellow clusters show gray matter volumetric reduction in HSP patients compared with healthy control group (right prefrontal cortex and both thalami).

TABLE 2 | Metabolite ratios on MRS samplings of HSP patients and control group at baseline.

	R pre-central			L pre-central			R pre-frontal			L pre-frontal		
	Patients (*n* = 31)	**Control (*n* = 31)**	***p*-value**	**Patients (*n* = 31)**	**Control (*n* = 31)**	***p*-value**	**Patients (*n* = 16)**	**Control (*n* = 14)**	***p*-value**	**Patients (*n* = 16)**	**Control (*n* = 14)**	***p*-value**
NAA/Cr	1.72 ± 0.21	1.74 ± 0.18	ns	1.75 ± 0.16	1.81 ± 0.15	ns	**1.70 ± 0.16**	**1.84 ± 0.20**	**0.040**	1.95 ± 0.29	2.09 ± 0.21	ns
Cho/Cr	**0.77 ± 0.13**	**0.70 ± 0.11**	**0.032**	0.75 ± 0.14	0.77 ± 0.12	ns	0.74 ± 0.11	0.75 ± 0.15	ns	0.73 ± 0.11	0.78 ± 0.13	ns
myo-Ins/Cr	0.61 ± 0.24	0.56 ± 0.08	ns	**0.64 ± 0.12**	**0.57 ± 0.09**	**0.018**	0.66 ± 0.14	0.61 ± 0.12	ns	0.64 ± 0.16	0.62 ± 0.08	ns

NAA, N-acetyl-aspartate; Cr, creatine; Cho, choline; myo-Ins, myo-inositol; ns, not significant. Bold characters represent values with $p < 0.05$.

($p < 0.05$, FEW-corrected); no statistically significant differences were detected for AD.

The longitudinal analysis (T_0 *vs* T_1) by whole-based voxelwise paired TBSS did not detect for all the DTI indices any significant differences in the patient group (19 subjects). No statistical correlation was found in the HSP longitudinal data with SPRS and history of specific treatments (chemodenervation with botulinum toxin).

Region-based analysis in the same group of HSP patients identified statistically significant differences as reported in **Table 3**: at T_1, the FA values increased (left superior longitudinal fasciculus $p < 0.05$, right pre-central gyrus $p < 0.02$, left pre-central gyrus $p < 0.03$, right post-central gyrus $p < 0.04$, left post-central gyrus $p < 0.02$); decreased values were detected for MD (left CST $p < 0.03$, forceps major $p < 0.01$, forceps minor $p < 0.03$, left superior longitudinal fasciculus $p < 0.03$, right pre-central gyrus $p < 0.02$, left pre-central gyrus $p < 0.02$, right post-central gyrus $p < 0.04$, left post-central gyrus $p < 0.009$) and RD (left CST $p < 0.02$, right cingulum $p < 0.03$, left cingulum $p < 0.02$, forceps major $p < 0.02$, forceps minor $p < 0.03$, left inferior fronto occipital $p < 0.04$, left superior longitudinal fasciculus $p < 0.02$, right pre-central gyrus $p < 0.01$, left pre-central gyrus $p < 0.02$, right post-central gyrus $p < 0.03$, left post-central gyrus $p < 0.006$); conversely, the AD values varied without a constant tendency (at T_1 increased with respect to T_0 in the left superior longitudinal fasciculus $p < 0.05$ and left post-central gyrus $p < 0.02$; at T_1 decreased with respect to T_0 in left $p < 0.03$ and right $p < 0.02$ pre-central gyri and right post-central gyrus $p < 0.04$).

A longitudinal clinical evaluation with SPRS in the entire cohort of our patients did not reveal any significant modification; also, upon evaluating SPG4 and non-SPG4, we did not depict variations.

The longitudinal evaluation of the HCs (18 subjects) did not show any modification in DTI indices, both applying the whole-based voxelwise paired TBSS analysis and the region-based analysis.

DISCUSSION

In this study, we explored cerebral changes in a relatively large group of molecularly characterized HSP patients by applying advanced MRI methods: voxel-based morphometry, to assess

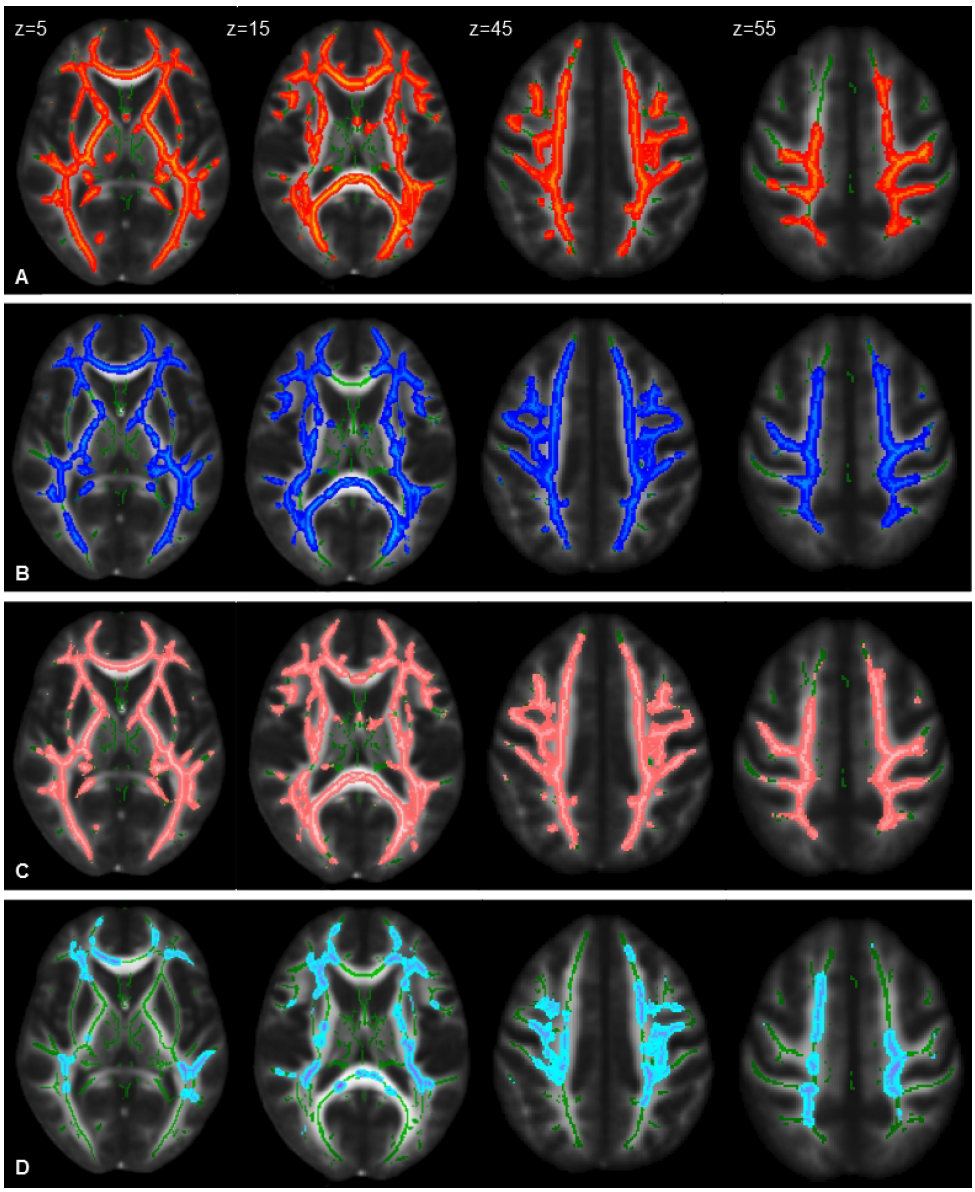

FIGURE 2 | Statistical maps of DTI indexes ($P < 0.05$, FWE corrected) in HSP patients compared with healthy control group at the baseline represented on the FMRIB58_FA_1mm template. Images correspond to the same z-axis coordinates (in millimeters), reported on the left top of images on the first raw; green lines represent the mean white matter skeleton of all participants. Referred to HSP patients: **(A)** red-yellow, areas of decreased FA; **(B)** blue-light blue, areas of increased MD; **(C)** pink-light pink, areas of increased RD; **(D)** cold-light blue areas of increased AD.

cortical and deep GM; MRS to sample correlated metabolic changes in pre-central and pre-frontal regions; and diffusion tensor imaging with multiple diffusivity indices to evaluate WM microstructural alterations. The most relevant data is a variation of DTI values at longitudinal analysis, suggestive of an improvement of the WM organization.

Our data obtained with both VBM and MRS revealed scattered brain modifications in HSP patients compared to HCs but did not show macroscopic primary motor cortex modifications to be possibly correlated to the neurodegenerative process underlying HSP.

VBM identified a reduction of the brain volume in the right pre-frontal cortex and bilaterally in the thalami. MRS revealed in patients decreased NAA/Cr in pre-frontal regions, an expression of neuronal/axonal pauperization or hypo-functionality, but not in the primary pre-central motor regions. The ratio mI/Cr, probably related to a complex gliotic and astrogliotic reaction, was increased in the pre-central regions. No variation was detected on the longitudinal analysis both for VBM and MRS possibly because of the reduced number of subjects (from 31 HSPs and 36 HCs to 23 HSPs and 23 HCs) and the poor quality of some

TABLE 3 | DTI mean values in HSP patients at baseline (T_0) and at follow-up (T_1) and statistical results in longitudinal comparison (p-values of differences T_0 *vs* T_1).

Fiber bundles	Groups	FA (mean ± SD)	MD (mean ± SD)*	RD (mean ± SD)*	AD (mean ± SD)*
L corticospinal tract	HSP T_0	0.496 ± 0.028	0.687 ± 0.028	0.472 ± 0.035	1.117 ± 0.032
	HSP T_1	0.508 ± 0.028	0.678 ± 0.030	0.460 ± 0.031	1.122 ± 0.036
	p-value	ns	**0.03**	**0.02**	ns
L cingulum	HSP T_0	0.467 ± 0.036	0.719 ± 0.030	0.517 ± 0.039	1.122 ± 0.030
	HSP T_1	0.481 ± 0.035	0.712 ± 0.046	0.504 ± 0.039	1.080 ± 0.104
	p-value	ns	ns	**0.02**	ns
R cingulum	HSP T_0	0.407 ± 0.039	0.723 ± 0.026	0.552 ± 0.037	1.065 ± 0.032
	HSP T_1	0.428 ± 0.052	0.718 ± 0.042	0.537 ± 0.037	1.128 ± 0.080
	p-value	ns	ns	**0.03**	ns
Corpus callosum with forceps major	HSP T_0	0.496 ± 0.028	0.834 ± 0.046	0.575 ± 0.046	1.352 ± 0.061
	HSP T_1	0.505 ± 0.027	0.822 ± 0.048	0.561 ± 0.045	1.343 ± 0.071
	p-value	ns	**0.01**	**0.02**	ns
Corpus callosum with forceps minor	HSP T_0	0.413 ± 0.029	0.787 ± 0.054	0.595 ± 0.057	1.172 ± 0.052
	HSP T_1	0.425 ± 0.023	0.775 ± 0.051	0.579 ± 0.047	1.168 ± 0.066
	p-value	ns	**0.03**	**0.03**	ns
L inferior fronto-occipital longitudinal fasciculus	HSP T_0	0.424 ± 0.031	0.799 ± 0.043	0.599 ± 0.050	1.198 ± 0.038
	HSP T_1	0.435 ± 0.023	0.792 ± 0.040	0.588 ± 0.042	1.191 ± 0.053
	p-value	ns	ns	**0.04**	ns
L superior longitudinal fasciculus	HSP T_0	0.389 ± 0.023	0.738 ± 0.040	0.579 ± 0.041	1.056 ± 0.044
	HSP T_1	0.397 ± 0.023	0.729 ± 0.042	0.558 ± 0.042	1.061 ± 0.058
	p-value	**0.05**	**0.03**	**0.02**	**0.05**
L pre-central gyrus	HSP T_0	0.163 ± 0.013	0.488 ± 0.029	0.426 ± 0.030	0.612 ± 0.028
	HSP T_1	0.176 ± 0.022	0.471 ± 0.012	0.406 ± 0.014	0.584 ± 0.022
	p-value	**0.03**	**0.02**	**0.02**	**0.03**
R pre-central gyrus	HSP T_0	0.154 ± 0.010	0.476 ± 0.024	0.416 ± 0.025	0.595 ± 0.023
	HSP T_1	0.167 ± 0.022	0.459 ± 0.012	0.396 ± 0.015	0.601 ± 0.023
	p-value	**0.02**	**0.02**	**0.01**	**0.02**
L post-central gyrus	HSP T_0	0.133 ± 0.010	0.407 ± 0.026	0.355 ± 0.026	0.509 ± 0.027
	HSP T_1	0.143 ± 0.015	0.391 ± 0.009	0.337 ± 0.011	0.510 ± 0.015
	p-value	**0.02**	**0.009**	**0.006**	**0.02**
R post-central gyrus	HSP T_0	0.136 ± 0.008	0.413 ± 0.023	0.360 ± 0.023	0.519 ± 0.023
	HSP T_1	0.145 ± 0.014	0.400 ± 0.010	0.345 ± 0.011	0.497 ± 0.015
	p-value	**0.04**	**0.04**	**0.03**	**0.04**

*White matter tracts labeled according to probabilistic JHU White-Matter Tractography Atlas. L, left; R, right. * × 10^{-3} mm^2/s. NS, not significant. Bold characters indicate values with $p < 0.05$.*

MRS samplings. As an example, of a total of 184 MRS samplings expected for all the subjects at follow-up, only 53 samplings in pre-central regions and 42 in pre-frontal areas were acceptable for analysis.

The cross-sectional analysis of DTI data at baseline and at follow-up identified in HSP patients a widespread impoverishment of the WM microstructure, involving also the primary motor regions, similarly to the previous literature reports. Interestingly, in this study we observed a significant inversion of DTI trends on longitudinal analysis in HSP patients, with an increase in FA and decrease in MD in multiple cerebral WM regions. Such changes paradigmatically can be an expression of a structural improvement that is fascinating and intriguing, but complicated to discuss.

The major feature in HSPs is an axonal degeneration, which is maximal at the terminal portions of the longest descending and ascending tracts as confirmed by modern neuroimaging studies (Graça et al., 2019). The extension of the neurodegenerative process to the cerebral WM is mainly produced by a *dying back* degeneration (Deluca et al., 2004; Hourani et al., 2009). Biochemical studies, supported by clinical and neuroimaging observations, pointed out that *dying back* degeneration cannot be the only pathophysiologic mechanism as in HSP there is a widespread brain and spinal involvement that extends well beyond the primary motor and sensory areas (Erichsen et al., 2009; Aghakhanyan et al., 2014; Graça et al., 2019; List et al., 2019). The wide variability in the clinical presentation of patients with HSP itself and the variability in genetic background suggest that damage is not restricted to the CST in most SPG forms.

In this heterogeneity, MRI demonstrated to be an efficient neuroimaging technique in revealing meaningful changes in HSP. In our patients, standard MRI did not reveal many alterations and those that are considered indicative of HSP are very few, as reported in literature (Ortega and Rosemberg, 2019). Conversely, the so-called advanced MRI assesses the CNS quantitatively and proves to be an exquisite sensitivity tool for subtle anatomical abnormalities higher than the pure visual analyses.

Among the advanced MRI techniques, VBM aims to identify local differences of brain tissue by analyzing groups of 3D MRI datasets. It can include cortex and deep GM and can be assessed with different techniques. In this study, we applied VBM methods and identified in HSP patients at baseline a significant volume reduction in the right pre-frontal cortex and bilaterally in the thalamus in HSP patients at baseline, while no alteration was detected in the GM of the primary motor areas. This finding supports the idea that the main target of HSP pathological mechanism is not directly the primary motor cortex as other advanced MRI and neuropathological studies already reported (Kassubek et al., 2006; Denora et al., 2016; Parodi et al., 2018b; Coarelli et al., 2019; Graça et al., 2019).

The variations that we observed in the pre-frontal cortex and in the thalami from a pathophysiological perspective can be considered as involvement of associative motor areas, but it is well known that the same areas are also involved in the connections of the wide extra-motor world. Okubo and colleagues reported a SPECT study in HSP and demonstrated both at cross-sectional and at longitudinal analysis a decreased perfusion in various cerebral areas. Specifically, they found decreased perfusion in the lateral frontal cortex and in the thalamus at long-term follow-up that correlated with clinical cognitive deterioration (Okubo et al., 2000). The investigation of possible correlation between thalami reduction and cognitive involvement in HSP was subsequently pursued also with advanced MRI techniques (França et al., 2007; França et al., 2012; Faber et al., 2018). It has been frequently stressed that the deterioration of cognitive functions is not exclusive of complicated HSPs but can be observed also in the so-called pure forms (Balconi and Bortolotti, 2013; Agosta et al., 2015; Martinuzzi et al., 2016; Menke et al., 2018; Jacinto-Scudeiro et al., 2019). Systematic studies investigating cognitive performances in SPG4 reported dysfunctions in 41 to 96% of HSP patients, depending on the test and the domain investigated (Rezende et al., 2015), and an abnormal fMRI connectivity between the middle frontal and the orbitofrontal gyri (Liao et al., 2018).

In this study, we did not detect significant longitudinal changes by VBM but we cannot exclude that such negative result is due to limits intrinsic to the methodology and to the small size of our cohort. For the latter reason, we are planning to expand our study to a larger HSP group and to apply more detailed methods of GM analysis, such as the cortical thickness analysis, similar to previous studies in ALS (Kwan et al., 2012) and to a recent one on HSP (Faber et al., 2018) showing interesting preliminary data.

Our MRS data confirm that HSP is a disease not primarily affecting the neurons of the primary motor regions. NA-acetylcholine is synthesized from choline and can be reduced in many neurological diseases, including neurodegenerative conditions such as Alzheimer's disease, as it is an index of concentration and/or functionality of neurons. The NAA/Cr ratio in our study is reduced in the pre-frontal areas, but not in the pre-central motor regions. This finding is confirmed also by comparing the genetically homogeneous group of SPG4 patients to normal subjects. At baseline, the only MRS variation involving the pre-central regions is an increase of mI/Cr ratio observed in patients. The same finding is the only difference identified at baseline in non-SPG4 patients compared to SPG4. Myo-inositol is considered as an index of membrane activity, referred not only to neurons/axons but also to oligodendrocytes, expressing possibly reparative attempts. Even if our group of patients includes various SPG types, the statistical variation of mI/Cr at baseline probably expresses a slow evolution of the HSP pathology.

Other MRS studies reported a stable level of Cho in HSP when compared to the normal subjects or eventually a reduction, reflecting an impairment of membrane turnover and/or prevailing cell loss. On the contrary, our study describes an increase of Cho/Cr ratio in patients compared to HC in the pre-central region in absence of an evident reactive/inflammatory brain activity that usually is expressed in MRS as increase of Cho. Our MRS data reflect the extreme inhomogeneity of the reports in literature on HSP. The heterogeneity in terms of SPG forms considered, localization of the sampled regions, the influence of the clinical extramotor involvement, in particular in the cognitive dominion, are the main limits in studies with MRS. Only Erichsen and colleagues analyzed a homogeneous group of SPG (eight SPG4 patients), placing the MRS boxes of sampling in areas similar to ours (left frontal white matter and pre-central gyrus). The results are at variance with ours: they found a reduction of the Cho/Cr in the pre-central cortex, in contrast to our study; decreased NAA/Cr in the frontal regions, similar to our study, but also in the motor cortex, where we did not find any change; and increased mI/Cr in patients, but without statistical significance, while our increased mI/Cr values are statistically significant. The conclusion is that the complexity of these results must be considered with caution given the many potentially confounding variables, the relatively small size of the observed changes, the variability also seen in the controls, and the heterogeneity and small number of patients studied. To overcome at least some of these problems, cooperative multicentric studies pooling data from various centers are recommendable once the technical aspects of the procedure are agreed upon and harmonized. A possible solution, which however entails a very expensive acquisition time, could be the application of techniques of absolute MRS quantification, as reported over 10 years ago in a single report on only one HSP patient (Dreha-Kulaczewski et al., 2006).

From the complexity and heterogeneity of our VBM and MRS data, the constantly emerging element is the apparent absence of a direct involvement of the primary motor cortex in HSP patients, in agreement with similar neuroimaging and neuropathologic reports. Conversely, our DTI data indicate an intense alteration of brain WM that includes also the primary motor cortex. As reported in literature, DTI indexes are characterized by decreased FA and quite anatomically corresponding increased MD, with a variable but often corresponding increase of RD and AD that is to be globally considered as an expression of WM reduction in fiber density and homogeneity in spatial orientation, with myelin degradation over axonal degeneration (França et al., 2012; Garaci et al., 2014; Schneider-Gold et al., 2017).

Our VBM and MRS data at baseline highlight another element: a possible widespread brain involvement in HSP

patients not focused on the primary motor areas. This is strongly confirmed by DTI. These results lead to include HSP among the non-regional or neural system specific pathologies; that is intriguing, but not surprising given what has been shown in other neurodegenerative pictures, such as in Parkinson's and Alzheimer's disease and in ALS (Senda et al., 2011; Agosta et al., 2012; Menke et al., 2018).

The paradigm of FA reduction and MD increase is usually correlated to a reduced axonal density, referred to as a decrease in the number of fibers and/or in the thickness of their myelin sheaths, that causes a disarrangement in the spatial orientation of the fibers with an increase of the extracellular spaces (Werring et al., 1999; Rosas et al., 2006), as sustained by findings from a comparative study between DTI and gross pathological features (Mottershead et al., 2003). The novel data from our study are the significant time-related changes moving on longitudinal analysis of DTI indices in the opposite direction to what we would expect from a progressing disease: FA increased and MD decreased in widespread areas. Such DTI changes were never reported before; rather, some authors underlined the absence of regions with significant FA increase in HSP (França et al., 2012).

We should take into account the small number of patients completing the follow-up, but we should also consider that the comparison with the controls sampled with the same methodology and after the same time interval strengthens the significance of the results. Interference by technical problems is avoided by this approach, given the data stability seen in our cohort of HC in whom no DTI variation was detected. The WM DTI changes in our patients involved scattered cerebral regions, such as the superior longitudinal fasciculus and pre-central and post-central WM, and they could be considered as improvement in terms of functionality. This is supported by the decrease of RD, while AD showed an alternating time effect.

Understanding the pathophysiological mechanisms of these DTI variations is not easy and requires further targeted investigations. On the basis of the classical interpretations of DTI indexes, we could speculate that we observed an increase of homogeneity of WM fibers and a reduction of free spaces between the fibers themselves, that could represent a reorganization attempt of the residual fibers at the microscopic level. These findings have no clinical correlation as we didn't observe any longitudinal variation of SPRS data.

While studies with advanced MRI on longitudinal progression are common in other neurodegenerative diseases, such as ALS (Agosta et al., 2009a,b; de Albuquerque et al., 2017; Menke et al., 2018), they are rare in HSP (Garaci et al., 2014) or conducted in very small sample sizes: Dreha-Kulaczewski and colleagues (Dreha-Kulaczewski et al., 2006) described a single patient with HSP-TCC studied with MRS and DTI with a 5-year follow-up, showing variations in the frontal WM, thalamus, and pyramidal motor system. Most of the studies that recruited a larger patient cohort was designed to implement only one or two MRI techniques (França et al., 2007) or presented intergroup comparison with controls scanned only at baseline or only at follow-up. To date we are not aware of any other study that scanned patients and controls in parallel over time.

None of the metrics reported in previous studies based on DTI or on WM volumes displays any correlation with disease duration in HSP (Faber et al., 2018), suggesting that the clinical indicators are either moving at a different pace or are not sensitive enough to detect the finer variations that DTI can identify (Fink, 2013; Faber et al., 2018). Clinical scales, albeit useful and validated, often display coarse sensibility and possibly ceiling/floor effects. HSPs are very slowly and not uniformly progressive disorders and this, as their rarity, greatly limits the ability to conduct randomized controlled trials in a reasonable time frame (6–24 months). In a cohort of 116 HSP patients, the analysis of the progression revealed in the subjects with slower course a less severe outcome, which was not explained by age at onset or genotypes (Parodi et al., 2018b). In another study on SPG7 patients, a rapid progression was detected in the first stage of the disease, after which the patients reached a plateau (Coarelli et al., 2019). Other authors reported a progression of symptoms during follow-up only in 58.3% cases, while 41.7% showed no motor worsening (Ortega and Rosemberg, 2019). Disease-ameliorating processes promoting the recovery of damaged axons or functional compensation through neuroplasticity could contribute to slow down the rate of neurodegeneration. A neuropathological study on HSP patients can be illuminating in the interpretation of our DTI data: Parodi and colleagues (Parodi et al., 2018b) described the high density of very small fibers with thin myelin in the brain and the spinal cord of HSP patients, interpreted as evidence of regeneration attempts within the CST. In this respect, the potential role of advanced MRI as a biomarker for HSP is still to be supported (Graça et al., 2019).

At the longitudinal analysis we found no correlation between our DTI data and treatment history (physiotherapy, chemodenervation, and anti-spasticity medications) unlike what is highlighted in other reports on chemodenervation with botulin toxin, in which improvement of DTI indexes correlated with clinical conditions (Xi et al., 2018).

Prognostic data for individual SPG types are also scarce and do not help to clarify our DTI data as the median disease duration until loss of independent walking is estimated in 22 years (Shribman et al., 2019), leading to consider our follow-up interval (about 30 months) as too short to be able to evaluate consistent variations in clinical and para-clinical parameters. Still our results allow us to confirm that the DTI technique might offer a more sensitive way to monitor and document changes over time.

Some studies report an atypical increase of FA values in the absence of appreciable clinical improvement in neurodegenerative diseases, such as Huntington's disease (Douaud et al., 2009) and in chronic secondary neurodegenerative evolution related to Wallerian degeneration (Pierpaoli et al., 2001). The interpretation offered in these reports is the possible loss of crossing fibers that can induce an apparent prevalence of co-oriented fibers, technically leading to an increase in FA. These reports suggested the application of modern DTI analysis of WM, such as fixel-based techniques, disentangling crossing from non-crossing fibers

(Raffelt et al., 2017), or deconvolution model (Dell'Acqua and Tournier, 2019). With these modern techniques, it is possible to quantify fiber density and fiber bundle cross-section in order to obtain a more complete WM structural morphometry, combining information from both within-voxel microscopic fiber density and macroscopic fiber bundle cross-section (Raffelt et al., 2017; Genc et al., 2018). These techniques are really promising, but the FA increase in the longitudinal analysis that we observed displays a fundamental difference with respect to a possible effect due to the reduced crossing fibers: while in the reports on Huntington's disease and Wallerian degeneration the increased FA corresponded to an increase of the MD values, that express the enlargement of the inter-axonal spaces due to degenerative processes, in our study, the increased FA is associated to a parallel decrease of MD. For this, it is possible to sustain that our results reveal a quite different scenario.

Our study presents several limits, the main of which are the mixed types of SPG forms and the low number of patients, even considering the rarity of the disease and the difficulty in recruiting patients. The variability in clinical presentation, onset of the symptoms, and progression of the disease would be taken into account when analyzing MRI data, that need to extend the number of participants of each single type of genetical and phenotypical form. This could be relevant in particular for MRS and VBM analysis that hardly depend on the sampled population.

Another limit is the analysis of our DTI data themselves: on longitudinal analysis, the whole-based voxelwise paired TBSS analysis did not show significant differences in the patients' DTI indexes, while our statistical results are based on anatomic regional selection. Whole-based voxelwise paired TBSS analysis has high spatial resolution, but probably the small size of our sample gave insufficient statistical power. Voxelwise analysis itself is not exempt from limitations, depending on the possible residual misregistration when warping the diffusion images into a common standard space: the method described in this paper depends heavily on having reliable normalization in patients who can present diffuse or sectional brain atrophy that can influence the final results. The voxel-by-voxel comparison is only possible if voxels can be assumed to represent exactly the same anatomic region in every subject and the normalization process does not introduce or remove bugs (Schwartzman et al., 2005). For these reasons, we added to the analysis a ROI approach that allowed us to obtain specific DTI values from limited brain districts with high sensitivity. But, this approach too is an averaging measure of multiple voxels, so we cannot exclude a partial volume averaging effect in the application of a general atlas that uses automated templates. The most important risk is to include structures that are a mixture of gray and white matter. Therefore, future studies should include single portions of bundles or anatomic district divided in sub-segments, free from averaging volume effect, as previously manually attempted (Martinuzzi et al., 2016).

Our results require confirmation on larger and genetically homogeneous cohorts; therefore, we agree with the proposal of Parodi and colleagues on the importance of creating networking study groups to focus on the neuroimaging approach to HSP (Parodi et al., 2018b). This could help in overcoming genetic, clinical, and technical limits and in identifying sensible and specific biomarkers, needed to proceed with therapeutic trials.

DATA AVAILABILITY STATEMENT

The datasets generated for this study are available on request to the corresponding author.

ETHICS STATEMENT

The studies involving human participants were reviewed and approved by Institutional Ethics Committee of the IRCCS "Eugenio Medea" Research Institute (#63/09CE). Written informed consent to participate in this study was provided by the participants' legal guardian/next of kin.

AUTHOR CONTRIBUTIONS

DM, MV, and AM: design and plan of the study, collection of the clinical data, discussion, interpretation, and description of the results. FF and GA: image analysis of the advanced MRI and interpretation of the data, discussion, interpretation, and description of the results. CS, GG, and GPa: collection of the clinical data. AB and GPi: acquisition of the MRI exams. AC: statistical analysis of the data. SD, PT, and FL: critical revision of the results and discussion. The manuscript was written and edited by all the authors.

ACKNOWLEDGMENTS

Here, we want to thank Professor Giuseppe Rossi, epidemiologist of the Institute of Clinical Physiology-CNR in Pisa, Italy, who died of a terrible disease, from whose brilliant idea this work was born.

REFERENCES

Abdel Aleem, A. K. (2017). "Hereditary spastic paraplegias. Clinical spectrum and growing list of genes," in the Neurodegenerative Diseases, ebook ed. SMGroup, ND-17-02.

Aghakhanyan, G., Martinuzzi, A., Frijia, F., Vavla, M., Hlavata, H., Baratto, A., et al. (2014). Brain white matter involvement in hereditary spastic paraplegias: analysis with multiple diffusion tensor indices. *AJNR* 35, 1533–1538. doi: 10.3174/ajnr.A3897

Agosta, F., Gorno-Tempini, M. L., Pagani, E., Sala, S., Caputo, D., Perini, M., et al. (2009a). Longitudinal assessment of grey matter contraction in amyotrophic lateral sclerosis: a tensor based morphometry study. *Amyotrophic Lateral Sclerosis* 10, 168–174. doi: 10.1080/17482960802603841

Agosta, F., Rocca, M. A., Valsasina, P., Sala, S., Caputo, D., Perini, M., et al. (2009b). A longitudinal diffusion tensor MRI study of the cervical cord and brain in amyotrophic lateral sclerosis patients. *J. Neurol. Neurosurg. Psychiatry* 80, 53–55. doi: 10.1136/jnnp.2008.154252

Agosta, F., Scarlato, M., Spinelli, E. G., Canu, E., Benedetti, S., Bassi, M. T., et al. (2015). Hereditary spastic paraplegia: beyond clinical phenotypes toward a unified pattern of central nervous system damage. *Radiology* 276, 207–218. doi: 10.1148/radiol.14141715

Agosta, F., Valsasina, P., Riva, N., Copetti, M., Messina, M. J., Prelle, A., et al. (2012). The cortical signature of amyotrophic lateral sclerosis. *PLoS One* 7:e42816. doi: 10.1371/journal.pone.0042816

Andersson, J. L. R., Jenkinson, M., and Smith, S. (2007a). *Non-Linear Optimisation. FMRIB Technical Report TR07JA1*. Available online at: https://www.fmrib.ox.ac.uk/analysis/techrep

Andersson, J. L. R., Jenkinson, M., and Smith, S. (2007b). *Non-Linear Registration, aka Spatial Normalisation FMRIB Technical Report TR07JA2.* Available online at: https://www.fmrib.ox.ac.uk/analysis/techrep

Balconi, M., and Bortolotti, A. (2013). Conscious and unconscious face recognition is improved by high-frequency RTMS on pre-motor cortex. *Conscious Cogn.* 22, 771–778. doi: 10.1016/j.concog.2013.04.013

Behan, W. M., and Maia, M. (1974). Strümpell's familial spastic paraplegia: genetics and neuropathology. *J. Neurol. Neurosurg. Psychiatry* 37, 8–20. doi: 10.1136/jnnp.37.1.8

Behrens, T. E. J., Woolrich, M. W., Jenkinson, M., Johansen-Berg, H., Nunes, R. G., Clare, S., et al. (2003). Characterization and Propagation of Uncertainty in Diffusion-Weighted MR Imaging. *Magn. Reson. Med.* 50, 1077–1088. doi: 10.1002/mrm.10609

Bisharat-Kernizan, J., Watson, C., and Margetis, K. (2018). What the future holds for the challenging hereditary spastic paraplegia? *Clin. Trials Degen. Dis. Par.* 3, 95–100.

Boutry, M., Morais, S., and Stevanin, G. (2019). Update on the genetics of spastic paraplegias. *Curr. Neurol. Neurosci. Rep.* 19:18. doi: 10.1007/s11910-019-0930-932

Bullmore, E. T., Suckling, J., Overmeyer, S., Rabe-Hesketh, S., Taylor, E., and Brammer, M. J. (1999). Global, voxel, and cluster tests, by theory and permutation, for a difference between two groups of structural MR images of the brain. *IEEE Trans. Med. Imaging* 18, 32–42. doi: 10.1109/42.750253

Burguez, D., Polese-Bonatto, M., Jacinto Scudeiro, L. A., Björkhem, I., Schöls, L., Bannach, L., et al. (2017). Clinical and molecular characterization of hereditary spastic paraplegias: a next-generation sequencing panel approach. *J. Neurol. Sci.* 383, 18–25. doi: 10.1016/j.jns.2017.10.010

Coarelli, G., Schule, R., van de Warrenburg, B. P. C., De Jonghe, P., Ewenczyk, C., Martinuzzi, A., et al. (2019). Loss of paraplegin drives spasticity rather than Ataxia in a cohort of 241 patients with SPG7. *Neurology* 92, e2679–e2690. doi: 10.1212/WNL.0000000000007606

Cui, F., Sun, L., Qiao, J., Xiong, J., Zhao, Y., Li, J., et al. (2018). Hereditary and idiopathic spastic paraparesis: preliminary findings of a single center experience. *Neurol. Res.* 40, 1088–1093. doi: 10.1080/01616412.2018.1522412

de Albuquerque, M., Branco, L. M., Rezende, T. J., de Andrade, H. M., Nucci, A., and Cavalcante França, M. (2017). Longitudinal evaluation of cerebral and spinal cord damage in amyotrophic lateral sclerosis. *Neuroimage Clin.* 14, 269–276. doi: 10.1016/j.nicl.2017.01.024

Dell'Acqua, F., and Tournier, J. D. (2019). Modelling white matter with spherical deconvolution: how and why? *NMR Biomed.* 32:e3945. doi: 10.1002/nbm.3945

Deluca, G. C., Ebers, G. C., and Esiri, M. M. (2004). The extent of axonal loss in the long tracts in hereditary spastic paraplegia. *Neuropathol. Appl. Neurobiol.* 30, 576–584. doi: 10.1111/j.1365-2990.2004.00587.x

Denora, P. S., Smets, K., Zolfanelli, F., Ceuterick-de Groote, C., Casali, C., Deconinck, T., et al. (2016). Motor neuron degeneration in spastic paraplegia 11 mimics amyotrophic lateral sclerosis lesions. *Brain* 139(Pt 6), 1723–1734. doi: 10.1093/brain/aww061

Douaud, G., Behrens, T. E., Poupon, C., Cointepas, Y., Jbabdi, S., Gaura, V., et al. (2009). In vivo evidence for the selective subcortical degeneration in Huntington's disease. *Neuroimage* 46, 958–966. doi: 10.1016/j.neuroimage.2009.03.044

Dreha-Kulaczewski, S., Dechent, P., Helms, G., Frahm, J., Gärtner, J., and Brockmann, K. (2006). Cerebral metabolic and structural alterations in hereditary spastic paraplegia with thin corpus callosum assessed by MRS and DTI. *Neuroradiology* 48, 893–898. doi: 10.1007/s00234-006-0148-142

Erichsen, A. K., Server, A., Landrø, N. I., Sandvik, L., and Tallaksen, C. M. E. (2009). Proton magnetic resonance spectroscopy and cognition in patients with spastin mutations. *J. Neurol. Sci.* 277, 124–129. doi: 10.1016/j.jns.2008.10.030

Faber, I., Martinez, A. R. M., de Rezende, T. J. R., Martins, C. R. Jr., Martins, M. P., Lourenço, C. M., et al. (2018). SPG11 mutations cause widespread white matter and basal ganglia abnormalities, but restricted cortical damage. *Neuroimage Clin.* 19, 848–857. doi: 10.1016/j.nicl.2018.05.031

Faber, I., Pereira, E. R., Martinez, A. R. M., França, M. C., and Ghizoni Teive, H. A. (2017). Hereditary spastic Paraplegia from 1880 to 2017: an historical review. *Arq. Neuropsiquiatr.* 75, 813–818. doi: 10.1590/0004-282X20170160

Fink, J. K. (2013). Hereditary spastic paraplegia: clinico-pathologic features and emerging molecular mechanisms. *Acta Neuropathol.* 126, 307–328. doi: 10.1007/s00401-013-1115-1118

Fink, J. K., and Hedera, P. (1999). Hereditary spastic paraplegia: genetic heterogeneity and genotype-phenotype correlation. *Semin. Neurol.* 19, 301–309. doi: 10.1055/s-2008-1040846

França, M. C., D'Abreu, A., Maurer-Morelli, C. V., Seccolin, R., Appenzeller, S., Alessio, A., et al. (2007). Prospective neuroimaging study in hereditary spastic paraplegia with thin corpus callosum. *Mov. Disord.* 22, 1556–1562. doi: 10.1002/mds.21480

França, M. C., Yasuda, C. L., Pereira, F. R. S., D'Abreu, A., Lopes-Ramos, C. M., Rosa, M. V., et al. (2012). White and grey matter abnormalities in patients with SPG11 mutations. *J. Neurol. Neurosurg. Psychiatry* 83, 828–833. doi: 10.1136/jnnp-2011-300129

Garaci, F., Toschi, N., Lanzafame, S., Meschini, A., Bertini, E., Simonetti, G., et al. (2014). Diffusion tensor imaging in SPG11- and SPG4-linked hereditary spastic paraplegia. *Int. J. Neurosci.* 124, 261–270. doi: 10.3109/00207454.2013.836705

Genc, S., Smith, R. E., Malpas, C. B., Anderson, V., Nicholson, J. M., Efron, D., et al. (2018). Development of white matter fibre density and morphology over childhood: a longitudinal fixel-based analysis. *Neuroimage* 183, 666–676. doi: 10.1016/j.neuroimage.2018.08.043

Good, C. D., Johnsrude, I. S., Ashburner, J., Henson, R. N., Friston, K. J., and Frackowiak, R. S. (2001). A voxel-based morphometric study of ageing in 465 normal adult human brains. *Neuroimage* 14(1 Pt 1), 21–36. doi: 10.1006/nimg.2001.0786

Graça, F. F., de Rezende, T. J. R., Vasconcellos, L. R. V., Pedroso, J. L., Barsottini, O. G. P., and França, M. C. (2019). Neuroimaging in hereditary spastic paraplegias: current use and future perspectives. *Front. Neurol.* 9:1117. doi: 10.3389/fneur.2018.01117

Han, J., and Ma, L. (2010). Study of the features of proton MR spectroscopy ((1)H-MRS) on amyotrophic lateral sclerosis. *JMRI* 31, 305–308. doi: 10.1002/jmri.22053

Harding, A. E. (1983). Classification of the hereditary ataxias and paraplegias. *Lancet* 1, 1151–1155. doi: 10.1016/s0140-6736(83)92879-92879

Hayasaka, S., and Nichols, T. E. (2004). Combining voxel intensity and cluster extent with permutation test framework. *Neuroimage* 23, 54–63. doi: 10.1016/j.neuroimage.2004.04.035

Hourani, R., El-Hajj, T., Barada, W. H., Hourani, M., and Yamout, B. I. (2009). MR imaging findings in autosomal recessive hereditary spastic paraplegia. *AJNR* 30, 936–940. doi: 10.3174/ajnr.A1483

Jacinto-Scudeiro, L. A., Dariva Machado, G., Ayres, A., Burguêz, D., Polese-Bonato, M., González-Salazar, C., et al. (2019). Are cognitive changes in hereditary spastic paraplegias restricted to complicated forms? *Front. Neurol.* 10:508. doi: 10.3389/fneur.2019.00508

Kassubek, J., Sperfeld, A. D., Baumgartner, A., Huppertz, H. J., Riecker, A., and Juengling, F. D. (2006). Brain atrophy in pure and complicated hereditary spastic paraparesis: a quantitative 3D MRI study. *Eur. J. Neurol.* 13, 880–886. doi: 10.1111/j.1468-1331.2006.01380.x

Keil, C., Prell, T., Peschel, T., Hartung, V., Dengler, R., and Grosskreutz, J. (2012). Longitudinal diffusion tensor imaging in amyotrophic lateral sclerosis. *BMC Neurosci.* 13:141. doi: 10.1186/1471-2202-13-141

Kwan, J. Y., Meoded, A., Danielian, L. E., Wu, T., and Floeter, M. K. (2012). Structural imaging differences and longitudinal changes in primary lateral sclerosis and amyotrophic lateral sclerosis. *Neuroimage Clin.* 2, 151–160. doi: 10.1016/j.nicl.2012.12.003

Liao, X., Huang, M., Xing, W., Wu, X., Liao, W., Wang, X., et al. (2018). Resting State FMRI studies in SPG4-linked hereditary spastic paraplegia. *J. Neurol. Sci.* 384, 1–6. doi: 10.1016/j.jns.2017.10.048

List, J., Kohl, Z., Winkler, J., Marxreiter, F., Doerfler, A., and Schmidt, M. A. (2019). Ascending axonal degeneration of the corticospinal tract in pure hereditary spastic paraplegia: a cross-sectional DTI study. *Brain Sci.* 9:268. doi: 10.3390/brainsci9100268

Martinuzzi, A., Montanaro, D., Vavla, M., Paparella, G., Bonanni, P., Musumeci, O., et al. (2016). Clinical and paraclinical indicators of motor system impairment in hereditary spastic paraplegia: a pilot study. *PLoS One* 11:e0153283. doi: 10.1371/journal.pone.0153283

Menke, R. A. L., Proudfoot, M., Talbot, K., and Turner, M. R. (2018). The Two-Year progression of structural and functional cerebral MRI in amyotrophic lateral sclerosis. *Neuroimage Clin.* 17, 953–961. doi: 10.1016/j.nicl.2017.12.025

Mori, S., Wakana, S., van Zijl, P. C. M., and Nagae-Poetscher, L. M. (2005). *MRI Atlas of Human White Matter - 1st Edition*. Amsterdem: Elsevier Science.

Mottershead, J. P., Schmierer, K., Clemence, M., Thornton, J. S., Scaravilli, F., Barker, G. J., et al. (2003). High Field MRI correlates of myelin content and axonal density in multiple sclerosis–a post-mortem study of the spinal cord. *J. Neurol.* 250, 1293–1301. doi: 10.1007/s00415-003-0192-3

Nayrac, P., Fontan, M., Warot, P., and Lorrain, A. (1953). Pierre Marie's hereditary cerebellar ataxia; familial observation. *L'echo Medical Du Nord* 24, 279–284.

Nichols, T. E., and Holmes, A. P. (2002). Nonparametric permutation tests for functional neuroimaging: a primer with examples. *Hum. Brain Mapp.* 15, 1–25. doi: 10.1002/hbm.1058

Novarino, G., Fenstermaker, A. G., Zaki, M. S., Hofree, M., Silhavy, J. L., Heiberg, A. D., et al. (2014). Exome sequencing links corticospinal motor neuron disease to common neurodegenerative disorders. *Science* 343, 506–511. doi: 10.1126/science.1247363

Okubo, S., Ueda, M., Kamiya, T., Mizumura, S., Terashi, A., and Katayama, Y. (2000). Neurological and neuroradiological progression in hereditary spastic paraplegia with a thin corpus callosum. *Acta Neurol. Scand.* 102, 196–199. doi: 10.1034/j.1600-0404.2000.102003196.x

Olivieri, G., Pro, S., Diodato, D., Di Capua, M., Longo, D., Martinelli, D., et al. (2019). Corticospinal tract damage in HHH syndrome: a metabolic cause of hereditary spastic paraplegia. *Orphanet J. Rare Dis.* 14:208. doi: 10.1186/s13023-019-1181-1187

Ortega, R. P. M., and Rosemberg, S. (2019). Hereditary spastic paraplegia: a clinical and epidemiological study of a brazilian pediatric population. *Arq. Neuropsiquiatr.* 77, 10–18. doi: 10.1590/0004-282X20180153

Parodi, L., Coarelli, G., Stevanin, G., Brice, A., and Durr, A. (2018a). Hereditary ataxias and paraparesias: clinical and genetic update. *Curr. Opin. Neurol.* 31, 462–471. doi: 10.1097/WCO.0000000000000585

Parodi, L., Fenu, S., Barbier, M., Banneau, G., Duyckaerts, C., Tezenas du Montcel, S., et al. (2018b). Spastic paraplegia due to SPAST mutations is modified by the underlying mutation and sex. *Brain* 141, 3331–3342. doi: 10.1093/brain/awy285

Pierpaoli, C., Barnett, A., Pajevic, S., Chen, R., Penix, L. R., Virta, A., et al. (2001). Water diffusion changes in wallerian degeneration and their dependence on white matter architecture. *Neuroimage* 13(6 Pt 1), 1174–1185. doi: 10.1006/nimg.2001.0765

Raffelt, D. A., Tournier, J.-D., Smith, R. E., Vaughan, D. N., Jackson, G., Ridgway, G. R., et al. (2017). Investigating white matter fibre density and morphology using fixel-based analysis. *Neuroimage* 144(Pt A), 58–73. doi: 10.1016/j.neuroimage.2016.09.029

Rezende, T. J. R., de Albuquerque, M., Lamas, G. M., Martinez, A. R. M., Campos, B. M., Casseb, R. F., et al. (2015). Multimodal MRI-based study in patients with SPG4 mutations. *PLoS One* 10:e0117666. doi: 10.1371/journal.pone.0117666

Rosas, H. D., Tuch, D. S., Hevelone, N. D., Zaleta, A. K., Vangel, M., Hersch, S. M., et al. (2006). Diffusion tensor imaging in presymptomatic and early Huntington's disease: selective white matter pathology and its relationship to clinical measures. *Mov. Disord.* 21, 1317–1325. doi: 10.1002/mds.20979

Schneider-Gold, C., Dekomien, G., Regensburger, M., Schneider, R., Trampe, N., Krogias, C., et al. (2017). Monozygotic twins with a new compound heterozygous spg11 mutation and different disease expression. *J. Neurol. Sci.* 381, 265–268. doi: 10.1016/j.jns.2017.09.005

Schüle, R., Holland-Letz, T., Klimpe, S., Kassubek, J., Klopstock, T., Mall, T. V., et al. (2006). The spastic paraplegia rating scale (SPRS): a reliable and valid measure of disease severity. *Neurology* 67, 430–434. doi: 10.1212/01.wnl.0000228242.53336.90

Schwartzman, A., Dougherty, R. F., and Taylor, J. E. (2005). Cross-subject comparison of principal diffusion direction maps. *Magn. Reson. Med.* 53, 1423–1431. doi: 10.1002/mrm.20503

Schwarz, G. A. (1952). Hereditary (Familial) spastic paraplegia. *A.M.A. Arch. Neurol. Psychiatry* 68, 655–662.

Senda, J., Kato, S., Kaga, T., Ito, M., Atsuta, N., Nakamura, T., et al. (2011). Progressive and widespread brain damage in ALS: MRI voxel-based morphometry and diffusion tensor imaging study. *Amyotrophic Lateral Sclerosis* 12, 59–69. doi: 10.3109/17482968.2010.517850

Shribman, S., Reid, E., Crosby, A. H., Houlden, H., and Warner, T. T. (2019). Hereditary spastic paraplegia: from diagnosis to emerging therapeutic approaches. *Lancet Neurol.* 18, doi: 10.1016/S1474-4422(19)30235-30232

Smith, S. M. (2002). Fast robust automated brain extraction. *Hum. Brain Mapp.* 17, 143–155. doi: 10.1002/hbm.10062

Smith, S. M., Jenkinson, M., Johansen-Berg, H., Rueckert, D., Nichols, T. E., Mackay, C. E., et al. (2006). Tract-based spatial statistics: voxelwise analysis of multi-subject diffusion data. *Neuroimage* 31, 1487–1505. doi: 10.1016/j.neuroimage.2006.02.024

Smith, S. M., Jenkinson, M., Woolrich, M. W., Beckmann, C. F., Behrens, T. E. J., Johansen-Berg, H., et al. (2004). Advances in functional and structural mr image analysis and implementation as FSL. *Neuroimage* 23(Suppl. 1), S208–S219. doi: 10.1016/j.neuroimage.2004.07.051

Smith, S. M., and Nichols, T. E. (2009). Threshold-free cluster enhancement: addressing problems of smoothing, threshold dependence and localisation in cluster inference. *NeuroImage* 44, 83–98. doi: 10.1016/j.neuroimage.2008.03.061

Strümpell, A. (1880). Beiträge zur Pathologie des Rückenmarks. *Archiv für Psychiatrie und Nervenkrankheiten* 10, 676–717. doi: 10.1007/BF02224539

Werring, D. J., Clark, C. A., Barker, G. J., Thompson, A. J., and Miller, D. H. (1999). Diffusion tensor imaging of lesions and normal-appearing white matter in multiple sclerosis. *Neurology* 52, 1626–1632. doi: 10.1212/wnl.52.8.1626

Xi, S. D., Zhu, Y. L., Chen, C., Liu, H. Q., Wang, W. W., and Li, F. (2018). The plasticity of the corticospinal tract in children with obstetric brachial plexus palsy after botulinum toxin a treatment. *J. Neurol. Sci.* 394, 19–25. doi: 10.1016/j.jns.2018.08.025

Conflict of Interest: The authors declare that the research was conducted in the absence of any commercial or financial relationships that could be construed as a potential conflict of interest.

frontiers in Neuroscience

ORIGINAL RESEARCH
published: 10 August 2020
doi: 10.3389/fnins.2020.00816

Endoplasmic Reticulum Lumenal Indicators in *Drosophila* Reveal Effects of HSP-Related Mutations on Endoplasmic Reticulum Calcium Dynamics

Megan K. Oliva[1], Juan José Pérez-Moreno[1], Jillian O'Shaughnessy[1], Trevor J. Wardill[2] and Cahir J. O'Kane[1]**

[1] Department of Genetics, University of Cambridge, Cambridge, United Kingdom, [2] College of Biological Sciences, University of Minnesota, Minneapolis, MN, United States

OPEN ACCESS

Edited by:
Xin Qi,
Case Western Reserve University, United States

Reviewed by:
Antonio Orlacchio, Santa Lucia Foundation (IRCCS), Italy
Brandon K. Harvey, National Institute on Drug Abuse (NIDA), United States

***Correspondence:**
Megan K. Oliva
megan.k.oliva@gmail.com
Cahir J. O'Kane
c.okane@gen.cam.ac.uk

Specialty section:
This article was submitted to Neurodegeneration, a section of the journal Frontiers in Neuroscience

Received: *18 February 2020*
Accepted: *10 July 2020*
Published: *10 August 2020*

Citation:
Oliva MK, Pérez-Moreno JJ, O'Shaughnessy J, Wardill TJ and O'Kane CJ (2020) Endoplasmic Reticulum Lumenal Indicators in Drosophila Reveal Effects of HSP-Related Mutations on Endoplasmic Reticulum Calcium Dynamics. Front. Neurosci. 14:816. doi: 10.3389/fnins.2020.00816

Genes for endoplasmic reticulum (ER)-shaping proteins are among the most commonly mutated in hereditary spastic paraplegia (HSP). Mutation of these genes in model organisms can lead to disruption of the ER network. To investigate how the physiological roles of the ER might be affected by such disruption, we developed tools to interrogate its Ca^{2+} signaling function. We generated GAL4-driven Ca^{2+} sensors targeted to the ER lumen, to record ER Ca^{2+} fluxes in identified *Drosophila* neurons. Using *GAL4* lines specific for Type Ib or Type Is larval motor neurons, we compared the responses of different lumenal indicators to electrical stimulation, in axons and presynaptic terminals. The most effective sensor, ER-GCaMP6-210, had a Ca^{2+} affinity close to the expected ER lumenal concentration. Repetitive nerve stimulation generally showed a transient increase of lumenal Ca^{2+} in both the axon and presynaptic terminals. Mutants lacking neuronal reticulon and REEP proteins, homologs of human HSP proteins, showed a larger ER lumenal evoked response compared to wild type; we propose mechanisms by which this phenotype could lead to neuronal dysfunction or degeneration. Our lines are useful additions to a *Drosophila* Ca^{2+} imaging toolkit, to explore the physiological roles of ER, and its pathophysiological roles in HSP and in axon degeneration more broadly.

Keywords: hereditary spastic paraplegia, endoplasmic reticulum, calcium imaging, *Drosophila*, neurodegeneration

INTRODUCTION

Hereditary spastic paraplegia (HSP) is a genetically heterogeneous disorder, with over 80 loci and 60 genes identified. It also shows phenotypic heterogeneity in manifestations such as age of onset and the presence of other symptoms (Blackstone, 2018). Despite this heterogeneity, there is evidence for some common mechanisms of cellular pathophysiology. The endoplasmic reticulum (ER) is implicated in these mechanisms, with HSP mutations affecting ER proteins

with a variety of roles including lipid metabolism, ER membrane-contact-site function, and ER architecture (Blackstone, 2018). Gene products that shape the tubular ER network are among the most commonly mutated in HSP, and mutation of these genes in model organisms leads to physical disruption of the ER network (O'Sullivan et al., 2012; Fowler and O'Sullivan, 2016; Summerville et al., 2016; Yalçın et al., 2017; Lindhout et al., 2019). These studies point to the importance of a continuous and connected tubular ER network throughout axons and presynaptic terminals and suggest disruption to this network as a common thread in HSP pathogenesis. Although changes in synaptic structure and function are found in these mutants (Summerville et al., 2016; Li et al., 2017; Lindhout et al., 2019), the direct physiological consequences of altered ER architecture remain elusive. It is imperative to understand the roles of ER architecture and the consequences of disrupting it, to understand how this might result in a neurodegenerative cascade.

We therefore need tools to study the physiological functions of axonal and presynaptic ER that depend on its architecture. Recently, de Juan-Sanz et al. (2017) developed sensitive genetically encoded calcium indicators (GECIs) targeted to the ER lumen, to examine the role of the ER in Ca^{2+} handling and signaling in synaptic activity in mammalian cultured neurons. In parallel to our work, Handler et al. (2019) used one of these sensors (ER-GCaMP6-210) to detect Ca^{2+} release from the ER in mushroom body Kenyon cells. Here we have expressed this probe and two others with higher Ca^{2+} affinities under GAL4 control in *Drosophila* motor neurons. We show ER-GCaMP6-210 as the most effective reporter of the three by consistently producing the largest changes in fluorescent intensity and characterize its localization and its reporting of stimulation-frequency-dependent ER Ca^{2+} fluxes in axon and presynaptic terminals. We then use it to show perturbation of Ca^{2+} handling in *Drosophila* in which ER organization is disrupted by loss of HSP-related ER-modeling proteins.

TABLE 1 | Stocks and plasmids used in this work.

***Drosophila* stock genotype**	**RRID**	**Source/References**
y w; +; 17xUASTattB-ER-GCaMP6-210(attP86Fb)	–	This paper
y w; +; 17xUASTattB-CEPIA3-ER(attP86Fb)	–	This paper
y w; +; 17xUASTattB-CEPIA4-ER(attP86Fb)	–	This paper
w^{1118}*; +; UAS-tdTomato:Sec61β(attP2)*	BDSC_64747	Summerville et al., 2016
w; UAS-Sturkopf:GFP; + (Formerly UAS-CG9186:GFP)	–	(Thiel et al., 2013) Yalçın et al., 2017
w; +; UAS-jRCaMP1b(VK00005)	BDSC_63793	Dana et al., 2016
w; Rtnl1^{-} *ReepA*$^{-}$ *ReepB*$^{-}$*/CyO; +*	BDSC_77904	Yalçın et al., 2017
w; ReepA^{+} *; +* (WT control)	–	Yalçın et al., 2017
w^{1118}*; +; Dpr-GMR94G06-GAL4(attP2)*	BDSC_40701	Pfeiffer et al., 2008; Perez-Moreno and O'Kane, 2019
w^{1118}*; +; FMR-GMR27E09-GAL4(attP2)*	BDSC_49227	Pfeiffer et al., 2008; Perez-Moreno and O'Kane, 2019
Plasmid		
ER-GCaMP6-210	Addgene_86919	Tim Ryan (de Juan-Sanz et al., 2017)
pCMV CEPIA3mt	Addgene_58219	Masamitsu Iino (Suzuki et al., 2014)
pCMV CEPIA4mt	Addgene_58220	Masamitsu Iino (Suzuki et al., 2014)
p17xUASTattB	–	This paper
p17xUASTattB-ER-GCaMP6-210	–	This paper
p17xUASTattB-CEPIA3-ER	–	This paper
p17xUASTattB-CEPIA4-ER	–	This paper

MATERIALS AND METHODS

Gene Constructs

The *pUASTattB* vector (Bischof et al., 2007) was previously modified to include *attR* sites and the *ccdB* gene to make it compatible with the Gateway cloning system (Invitrogen) (Moreau et al., 2014). We further modified this vector, increasing the number of GAL4-binding sites from 5 to 17, to generate *p17xUASTattB*, and increase GAL4-dependent gene expression (**Supplementary Datasheet 2**). To generate *p17xUASTattB-ER-GCaMP6-210*, we PCR-amplified a fragment encoding GCaMP210-KDEL fused to a calreticulin signal peptide, from Addgene plasmid *ER-GCaMP6-210* (de Juan-Sanz et al., 2017) (**Table 1**), while adding *attB1* and *attB2* sites to its 5' and 3' ends to enable it to integrate into *p17xUASTattB* using the Gateway cloning system (**Supplementary Datasheet 2**). To generate *p17xUASTattB-CEPIA3-ER* and *p17xUASTattB-CEPIA4-ER*, we PCR-amplified the CEPIA coding region from Addgene plasmids *pCMV CEPIA3mt* and *pCMV CEPIA4mt* (Suzuki et al., 2014) (**Table 1**), while adding *attB1* and a BiP signal sequence to the 5' end, and HDEL and *attB2* to the 3' end [BiP and HDEL ER-targeting as in Summerville et al. (2016)], and then integrating it into *p17xUASTattB* (**Supplementary Datasheet 2**).

Drosophila Genetics

p17xUASTattB-ER-GCaMP6-210, *p17xUASTattB-CEPIA3-ER*, and *p17xUASTattB-CEPIA4-ER* were injected into *Drosophila* embryos and integrated at landing site *attP86Fb* (Bischof et al., 2007) using phiC31 integrase-mediated integration, by the University of Cambridge Genetics Department injection service. Other fly stocks used can be found in **Table 1**.

Histology

Third instar larvae were dissected in ice-cold Ca^{2+}-free HL3 solution (Stewart et al., 1994). HL3 was then replaced with PBS and larvae fixed for 10 min in PBS with 4% formaldehyde. Fixed preparations were mounted in Vectashield (Vector Laboratories), and images were collected using EZ-C1 acquisition software (Nikon) on a Nikon Eclipse C1si confocal microscope (Nikon Instruments, United Kingdom). Images were captured using a 40×/1.3 NA oil objective.

Live Imaging

Third instar larvae were dissected in ice-cold Schneider's insect medium (Sigma). Before imaging, Schneider's medium was

replaced with HL3 containing (in mM) 70 NaCl, 5 KCl, 0.5 $MgCl_2$, 10 $NaHCO_3$, 115 sucrose, 5 trehalose, 5 HEPES, 1 $CaCl_2$ and 7 L-glutamic acid, pH ∼7.2 ± 0.05. The ER lumenal response to electrical stimulation was sensitive to Mg^{2+}, with only very small or no responses elicited in HL3 containing 20 mM $MgCl_2$, which was used for fixed samples; a low-Mg^{2+} HL3 solution (0.5 mM $MgCl_2$) gave much more reliable responses.

Segmental nerves were cut with dissection scissors and then drawn by suction into a heat-polished glass pipette, ∼10 μm internal diameter (Macleod et al., 2002), which was connected to a stimulator and train generator [DS2A-MK.II Constant Voltage Stimulator and DG2A Train/Delay Generator (Digitimer, Welwyn Garden City, United Kingdom)] to deliver supra-threshold electrical pulses (∼5 V). Larval neuromuscular junction (LMJ) responses were recorded in abdominal segments A4-A6. After 10 s of baseline image acquisition, 400-μs impulses were delivered for 2 s at a range of frequencies. The interval between different stimulation frequencies was ∼60 s, or until ER lumen fluorescence returned to baseline levels (whichever was longer).

Wide-field Ca^{2+} imaging was performed on an upright Zeiss Axiskop2 microscope with Optosplit II (Cairn) using a 40× NA 1.0 water-immersion objective (W Plan-Apochromat 40×/1.0 DIC M27), a 2× C-Mount Fixed Focal Length Lens Extender (Cairn, Faversham, United Kingdom) and an Andor EMCCD camera (Model iXon Ultra 897_BV, 512 × 512 pixels, Andor Technology, Belfast, United Kingdom) at 10 frames per second, 100 ms exposure, and EM gain level 100. Imaging data were acquired using Micro-Manager (Edelstein et al., 2014) and saved as multi-layer tif files before analysis using ImageJ Fiji[1] (Schindelin et al., 2012).

Image Analysis and Figure Preparation

Confocal microscopy images of fixed samples were collected using EZ-C1 acquisition software on a Nikon Eclipse C1si confocal microscope. Images were analyzed and processed using ImageJ Fiji[2] (Schindelin et al., 2012). Wide-field live images were opened in ImageJ Fiji, and channels were individually bleach-corrected (simple ratio, background intensity = 0). Fluorescent intensity time courses were obtained for an ROI (region of interest) traced around the entire NMJ, or axon segment, in each frame in a given data set using Time Series Analyzer V3 plugin, averaging the fluorescence in the ROI. The time courses were saved as txt files and fed into R scripts written by the authors to obtain the resting fluorescence data (averaged 30 frames before stimulus) and the $\Delta F/F$ data (**Supplementary Datasheet 3**). Graphs were generated using GraphPad Prism 8. Figures were made using Adobe Illustrator.

Statistical Analysis

Data were analyzed in GraphPad Prism, using 2-way ANOVA, unpaired two-tailed Student's *t*-tests; graphs show mean ± SEM or Mann–Whitney U tests (for data not normally distributed); graphs show median with interquartile range. Pearson's correlation was used to examine relationships between datasets. Sample sizes are reported in figures.

[1] https://fiji.sc

[2] See footnote 1.

RESULTS

The ER Lumenal Ca^{2+} Evoked Response Is More Delayed and Sustained Compared to the Cytoplasmic Response

To monitor Ca^{2+} flux in the ER lumen, we generated transgenic flies that encoded ER-GCaMP6-210 (de Juan-Sanz et al., 2017), a GCaMP6 sensor fused to a signal peptide and ER retention signal, with a Ca^{2+} affinity optimized for the relatively high [Ca^{2+}] in ER lumen. ER-GCaMP6-210 localization in presynaptic terminals largely overlapped with the ER marker tdTomato:Sec61β (**Figure 1A**), being more restricted than cytoplasmic jRCaMP1b (**Figure 1B**; see comparison to ER marker Sturkopf:GFP, previously known as CG9186:GFP), consistent with localization to the ER lumen. To test the response of the sensor to neuronal activation we electrically stimulated the nerve. The cytoplasmic Ca^{2+} response quickly reached a peak in the first couple of seconds following stimulation, and decayed back to resting levels over several seconds. In contrast, the ER-GCaMP6-210 lumenal response increased more slowly, reaching a peak five or more seconds following stimulation, with a slow return to resting levels, in some cases over minutes (**Figures 2A,B** and **Supplementary Video 1**), in keeping with the slower dynamics reported previously for these constructs (de Juan-Sanz et al., 2017). Cytoplasmically, jRCaMP1b and GCaMP6f have similar kinetics in neurons as reported previously, with just a slightly slower half decay time (0.6 s) for jRCaMP1b (Dana et al., 2016), compared to GCaMP6f (0.4 s) (Chen et al., 2013) at 10 Hz. In around 10% of nerves, usually at higher stimulation frequencies, we alternatively (or sometimes additionally) observed small, sharp decreases in ER lumenal fluorescence immediately following stimulation. This decrease was followed by a quick return to baseline fluorescence or by a slow increase in fluorescence as described above. This short-term decrease in fluorescence was observed more frequently in the axon than at the NMJ. There did not appear to be anything notably different in the cytoplasmic flux in these instances, compared to when the ER flux showed only an increase in fluorescence (**Figure 2A** and **Supplementary Datasheet 1**). Together, these data suggest a slower and somewhat less predictable ER Ca^{2+} flux, compared to the cytoplasmic flux in axons and NMJs of motor neurons.

ER Lumenal Sensor With Affinity Closest to Predicted ER Lumenal [Ca^{2+}] Shows the Strongest Response

Since the high surface/volume ratio of the small ER tubules of axons might potentially make them more susceptible than other ER regions to leakage of Ca^{2+} to the cytosol, we generated transgenic flies carrying two additional ER lumenal sensors with higher Ca^{2+} affinities. The highest affinity sensor, CEPIA3-ER (K_d = 11 μM), showed very

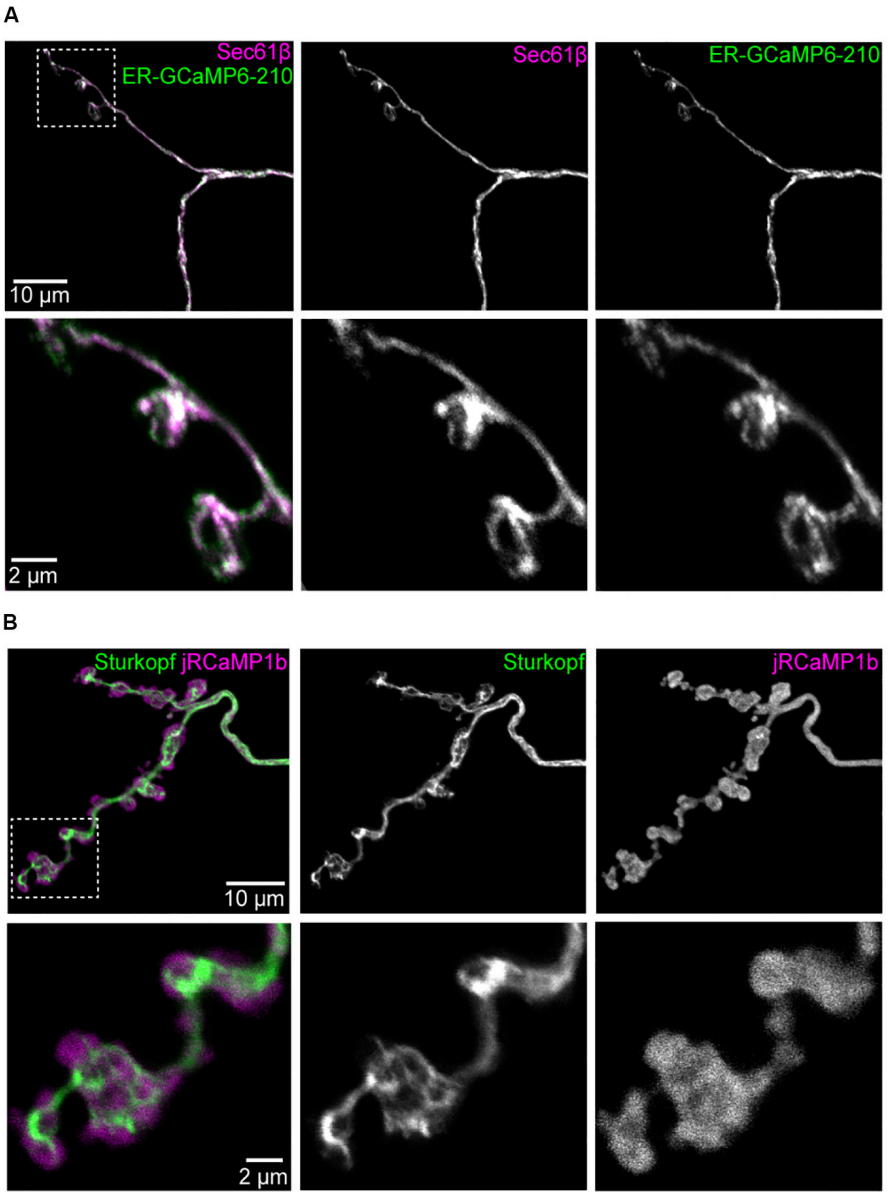

FIGURE 1 | The ER lumenal sensor ER-GCaMP6-210 has an overlapping distribution with ER at the neuromuscular junction. Panels show markers in Ib boutons at muscle 1 NMJ, segment A2, expressed using *Dpr-GMR94G06-GAL4*; all images are maximum intensity projections of confocal stacks. **(A)** Overlap of ER-GCaMP6-210 and ER membrane marker tdTomato:Sec61β. **(B)** jRCaMP1b is more broadly distributed than ER membrane marker Sturkopf:GFP. Magnified views of each inset are in respective lower rows.

small or no responses at multiple NMJs of seven larval preparations, even when a robust cytoplasmic response was elicited (not shown); CEPIA4-ER (K_d = 59 μM) usually showed a small response at most frequencies. ER-GCaMP6-210 (K_d = 210 μM) produced the most consistent response, and the magnitude of its response increased with increasing stimulation frequency (**Figures 2B–D**). As sensors with a K_d that approximates the surrounding [Ca^{2+}] are best suited as reporters, this is consistent with the estimated resting neuronal ER lumenal [Ca^{2+}] of 150–200 μM reported previously (de Juan-Sanz et al., 2017).

The Axonal Cytoplasmic Evoked Response Is Smaller Compared to NMJ Response, Whereas the ER Lumenal Evoked Response Is Consistent Across Locations

As we were interested to see if we could observe Ca^{2+} signals along the length of the axon, we used *FMR-GMR27E09-GAL4* to record in the two Type Is motor neurons per hemisegment where it drives expression: RP2 and RP5, which together innervate several NMJs (Perez-Moreno and O'Kane, 2019). We compared

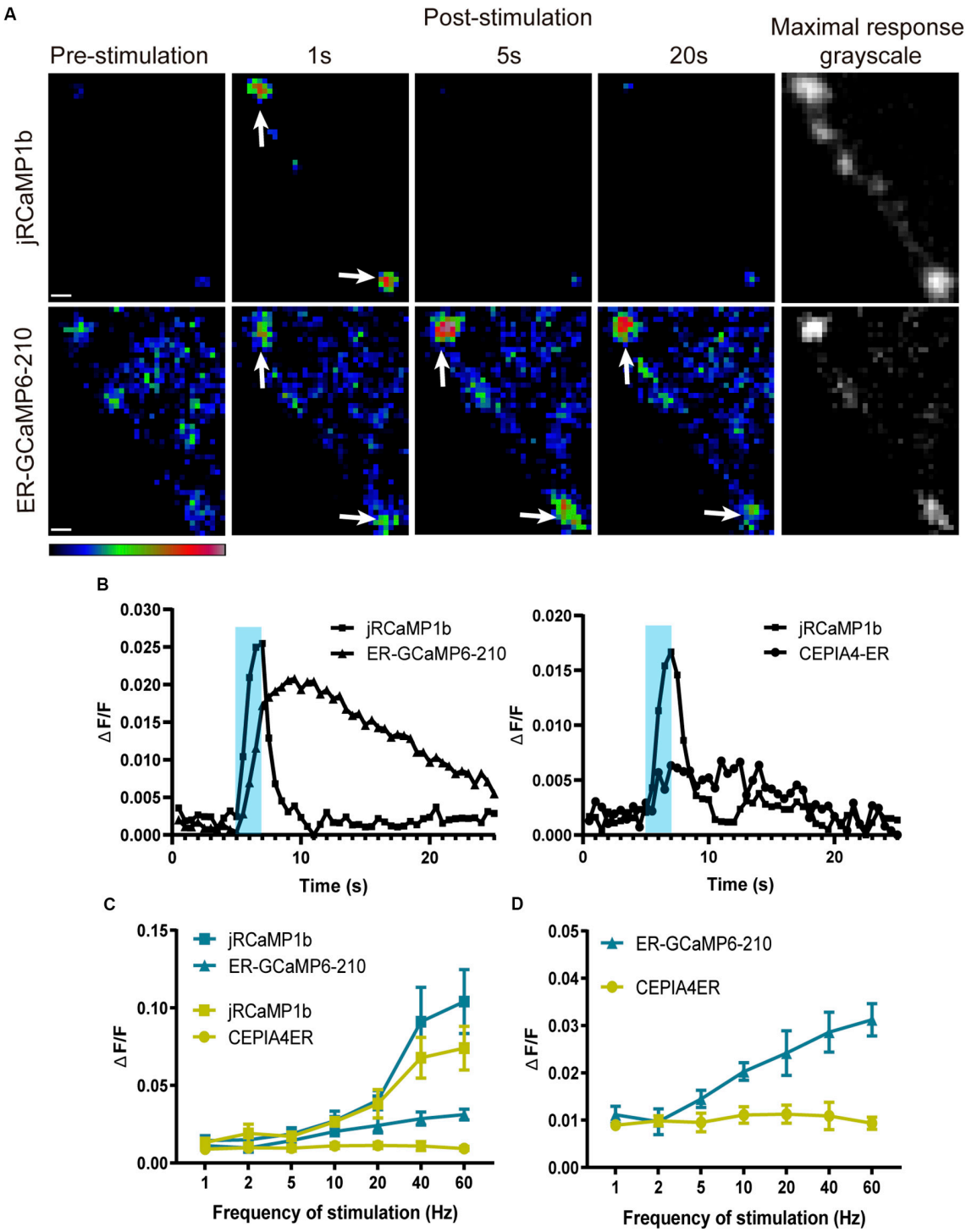

FIGURE 2 | ER lumenal Ca^{2+} responses to electrical stimulation at the NMJ, visualized using ER-GCaMP6-210, were delayed and more sustained compared to cytoplasmic responses. **(A)** Representative pseudocolor images of responses to 40 Hz stimulation, with maximal responses shown in grayscale (**right panels**) to show position of synapse. Panels show responses of jRCaMP1b (**top row**) and ER-GCaMP6-210 (**bottom row**) at muscle 6/7, expressed in the same RP5 Type Is motor neuron using *FMR-GMR27E09-GAL4*. Arrows show examples of boutons. Pseudocolor bar shows low to high relative intensity; scale bar, 2 μm. **(B)** Representative responses to 20 Hz stimulation of ER-GCaMP6-210 and CEPIA4-ER with corresponding jRCaMP1b response at muscle 6/7, expressed in RP5 Type Is motor neuron using *FMR-GMR27E09-GAL4*. Shading represents the stimulation period. **(C)** Average fold-change in peak fluorescence at different stimulation frequencies, of ER-GCaMP6-210 and CEPIA4-ER, compared with jRCaMP1b at muscle 6/7, expressed in the same RP5 Type Is motor neuron using *FMR-GMR27E09-GAL4* (ER-GCaMP6-210, $N = 5$; CEPIA4-ER, $N = 6$). **(D)** Comparison of ER lumenal sensors only, replotted from **(C)** with the *y*-axis expanded.

several axonal and NMJ locations within a muscle hemisegment (**Supplementary Datasheet 1**). Motor neuron RP2 (also known as ISN-Is) innervates dorsal muscles, and we recorded from its NMJ boutons at muscle 1, and from two axonal locations: the "entry" point at which the axon starts to cross the muscles as it emerges from the ventral nerve cord, and more laterally as it passes over muscle 4. Motor neuron RP5 (also known as ISN b/d) innervates ventral muscles, and we recorded from its NMJ at muscle 6/7, and from one axonal location, the "entry" point, as defined for motor neuron RP2 (**Supplementary Datasheet 1** and **Supplementary Video 2**). *Dpr-GMR94G06-GAL4* drives expression in the aCC Type Ib motor neuron (also known as MN1-Ib), which innervates muscle 1 (Perez-Moreno and O'Kane, 2019). The responses of both cytosolic and lumenal sensors at the aCC muscle 1 NMJ boutons were comparable to those in RP2 at the same muscle (**Figures 3A,B**), suggesting a comparable action potential response between the two neuronal types. Fluorescence of the sensors driven by *Dpr-GMR94G06-GAL4* in the axons of the Type Ib aCC neuron was too dim to obtain reliable evoked responses, which may be due to a relatively small diameter of its axon, and hence relatively low amounts of sensors at this subcellular location.

The evoked cytoplasmic NMJ and axonal Ca^{2+} responses were both comparable between the two Type Is motor neurons, although axonal responses were consistently smaller than NMJ responses whereas ER lumenal evoked responses were consistent across all NMJ and axonal locations (**Figure 3C**). This did not appear to be due to alterations in ER volume as resting fluorescence was consistent across locations (**Supplementary Datasheet 1**). Both cytoplasmic and ER lumenal responses reached peak fluorescence on similar timescales across locations (**Figure 3D**), suggesting that the observed responses were due to Ca^{2+} flux across the plasma membrane, and not a propagation of Ca^{2+} down the axon. The ER lumenal response appeared in general not to be influenced by the cytoplasmic response; most locations showed no correlation of peak $\Delta F/F$ between ER lumen and cytosol, apart from RP2 axon at entry point (**Figures 3E,F** and **Table 2**). This suggests a more complex transfer of Ca^{2+} within and between intracellular compartments, than simply a flow of Ca^{2+} from cytosol to ER lumen.

Rtnl1^{-} *ReepA*$^{-}$ *ReepB*$^{-}$ Mutants Display an Increased ER Lumenal Evoked Response Compared to Wild Type (WT)

Rtnl1^{-} *ReepA*$^{-}$ *ReepB*$^{-}$ mutant larvae have a disrupted axonal ER network, with larger and fewer tubules, and occasional fragmentation (Yalçın et al., 2017). To test whether these ER changes had functional consequences, we used *Dpr-GMR94G06-GAL4* to examine the cytoplasmic and ER lumen evoked responses at muscle 1 NMJ in these mutants. Mutant NMJs showed an increased evoked response compared to WT in the ER lumen, but not in the cytoplasm (**Figures 4A,B**). There was no significant difference in lumen resting fluorescence between mutant and WT (**Figure 4C**).

There was no correlation between cytoplasmic and ER lumenal evoked responses in either mutant or WT at 40 Hz (**Supplementary Datasheet 1**), supporting the finding in **Figure 3** of a more complex intracellular transfer of calcium. It has been reported that ER lumen $[Ca^{2+}]$ affects presynaptic cytoplasmic Ca^{2+} flux (de Juan-Sanz et al., 2017); however, we found no correlation here between resting ER fluorescence and peak cytoplasmic fluorescence, in either WT or mutant stimulated at 40 Hz (**Supplementary Datasheet 1**). The time-to-peak in the cytoplasm or ER lumen was not significantly different between mutant and WT at 40 Hz (**Supplementary Datasheet 1**). The time for decay to half-maximal in the cytoplasm was also not significantly different between mutant and WT at 40 Hz (**Supplementary Datasheet 1**). This parameter was not measured in the ER lumen due to the slow temporal dynamics of this flux.

These data suggest a significant increase in ER lumenal evoked responses in *Rtnl1*$^{-}$ *ReepA*$^{-}$ *ReepB*$^{-}$ mutants compared to WT, with no change in ER lumenal resting fluorescence levels, no corresponding change in the cytoplasmic evoked response, and no change in the temporal dynamics of the response.

DISCUSSION

Direct measurement of ER lumenal Ca^{2+} dynamics is essential for reporting on the physiological and pathophysiological responses of the ER network. An ER lumenal *UAS-GECI*, ER-GCaMP6-210, provided the most robust responses in *Drosophila* motor neurons (**Figure 2**), in keeping with results in mammalian hippocampal neurons (de Juan-Sanz et al., 2017). Handler et al. (2019) also expressed this sensor in transgenic flies using a 10× UAS vector, and used these to detect Ca^{2+} release from the ER in mushroom body Kenyon cells. Our work provides a more detailed characterization of the responses of this sensor to a range of stimulation frequencies, as well as providing an additional 17xUAS vector that we predict allows higher expression of the sensor.

In mutant *Drosophila* lacking various ER-shaping HSP protein homologs, we previously found decreased ER levels compared to WT, or occasional discontinuity of the ER network (Yalçın et al., 2017). As sustained discontinuity could potentially disrupt long-range ER communication along the axon, we wanted to investigate if we could record Ca^{2+} fluxes in WT axons. We analyzed both cytoplasmic and ER lumenal Ca^{2+} fluxes, at three axonal recording positions across two neurons. The amplitude of the ER lumenal evoked response was similar in axons and at the NMJ; however, cytoplasmic evoked responses were smaller in axons compared to the NMJ. Even though Ca^{2+} would be fluxing across the ER membrane in response to stimulation, it appears that the two signals do not influence each other in most cases (**Figure 3**).

While we observe Ca^{2+} signals along the length of motor axons, we do not find any indication of propagation via a Ca^{2+} wave. Propagation speeds for Ca^{2+} waves in dendrites have been measured at 60–90 μm/s (Nakamura et al., 2002), with a rapid lumenal Ca^{2+} diffusion through dendritic ER at ∼30 μm/s (Choi et al., 2006). Here we find no evidence for any spatial differences in the time to peak fluorescence

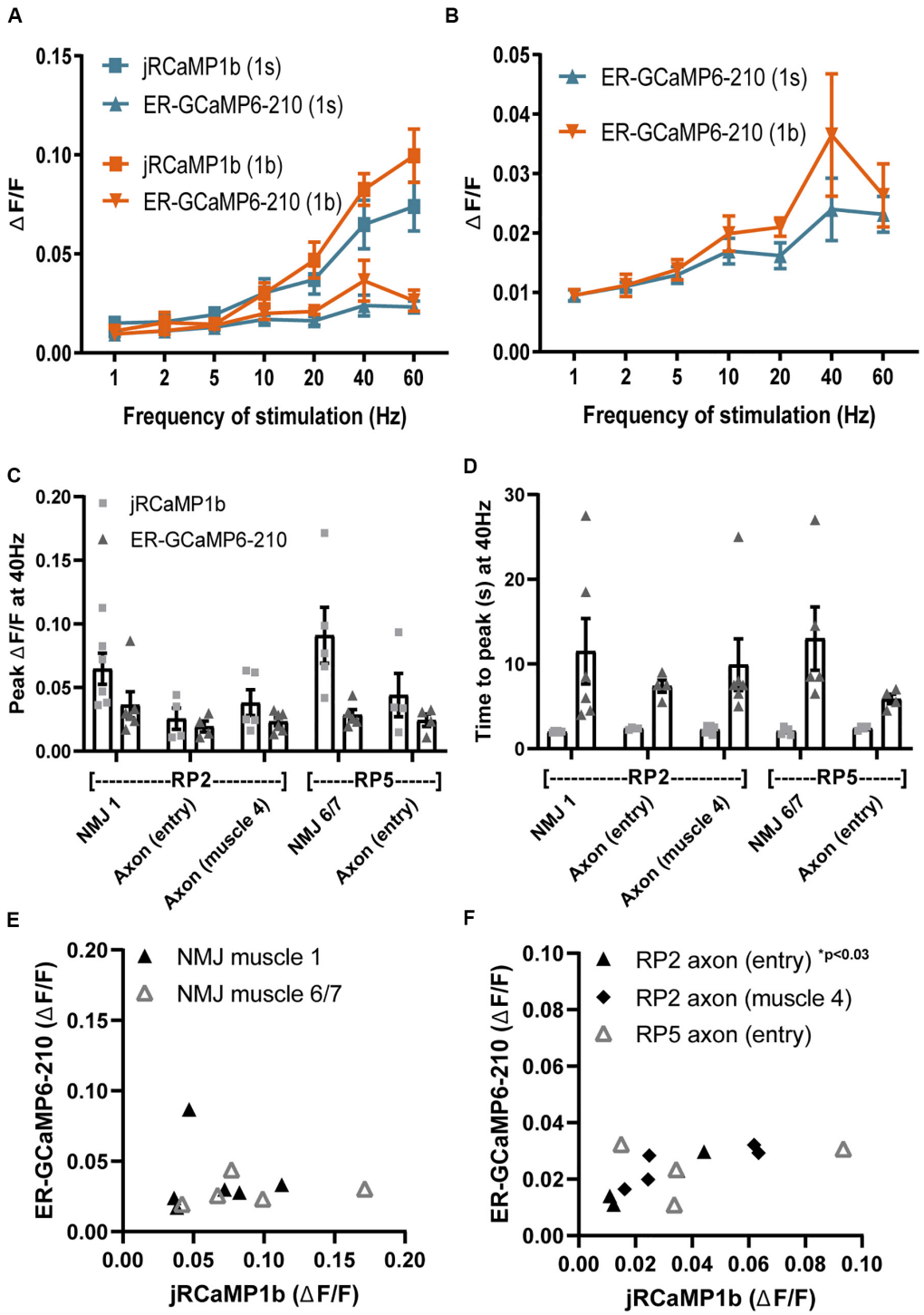

FIGURE 3 | Comparisons of ER lumenal and cytoplasmic Ca^{2+} responses across axons and NMJs of Type Ib and Is motor neurons. **(A)** Evoked responses of lumenal ER-GCAMP6-210 and cytoplasmic jRCaMP1b to a range of stimulation frequencies, in Type Ib boutons of the aCC neuron at the muscle 1 NMJ, expressed using *Dpr-GMR94G06-GAL4* ($N = 6$), or in Type Is boutons at the muscle 1 NMJ of the RP2 neuron expressed using *FMR-GMR27E09-GAL4* ($N = 6$). **(B)** Comparison of ER lumen sensor data only, from **(A)** but with *y*-axis expanded. **(C)** Lumen and cytoplasmic Ca^{2+} fluxes at different positions of Type Is neurons RP2 and RP5 (**Supplementary Datasheet 1**), with sensors expressed using *FMR-GMR27E09-GAL4*. **(D)** The time to peak $\Delta F/F$, for both lumen and cytoplasmic responses, was similar across all axon and NMJ positions. **(E,F)** Peak amplitudes (from **C**) of individual ER lumen and cytoplasm responses were plotted for the NMJ **(E)** and axonal **(F)** compartments of RP2 and RP5. A positive correlation was found only for RP2 axon entry but not for other locations (**Table 2**). One outlier in RP2 axon (muscle 4) jRCaMP1b was excluded from graphs **(C)** and **(F)** (value 0.29), but included in analysis in **(F)**.

TABLE 2 | Correlation analysis of peak $\Delta F/F$ between ER lumen and cytosol in NMJ and axons using Pearson's correlation coefficient.

FMR-GMR27E09 neuronal location	*r*	*p*	*N* (larvae)
RP2 NMJ muscle 1	0.10	0.85	6
RP5 NMJ muscle 6/7	0.21	0.73	5
RP2 axon (entry)	0.98	0.02*	4
RP2 axon (muscle 4)	0.50	0.32	6
RP5 axon (entry)	0.23	0.77	4

*$P < 0.05$.

between different axon positions and the NMJ, both for ER lumen and cytoplasmic evoked responses (**Figure 3**); in a typical video frame width of 100 μm (e.g., **Supplementary Datasheet 1**) we should easily detect propagation at these speeds with our frame rate of 10 Hz. The instantaneous spread of Ca^{2+} responses that we observe is more consistent with them being a consequence of the action potentials generated by stimulation, which propagate so fast that we cannot resolve their spread using our optical recording. Detection of Ca^{2+} waves that propagate along the ER membrane or through the lumen would probably require recording of ER Ca^{2+} fluxes in the absence of action potentials.

Although the cytoplasmic evoked responses of *Rtnl1*$^{-}$ *ReepA*$^{-}$ *ReepB*$^{-}$ mutants were normal, the ER lumenal evoked responses were significantly larger than WT (**Figure 4**). This did not appear to be due to increased resting ER lumenal [Ca^{2+}] since resting fluorescence levels showed no significant difference between genotypes, for either ER or cytoplasmic sensors.

In the simplest interpretation, the presynaptic ER lumen appears to take up more Ca^{2+} on stimulation in the *Rtnl1*$^{-}$ *ReepA*$^{-}$ *ReepB*$^{-}$ mutant compared to WT. Since cytoplasmic Ca^{2+} responses are unaffected in mutants, increased cytosolic Ca^{2+} cannot be an explanation for the increased ER response in mutants, implying that the increased ER response is due to intrinsic changes in Ca^{2+}-handling properties of the mutant ER, consistent with the roles of reticulon and REEP proteins in directly shaping ER architecture. The change in shape and composition of the ER tubules may change their flexibility (Georgiades et al., 2017) and effectiveness of ER tubule contraction (Holcman et al., 2018), hence a decrease in active flow, thereby slowing the redistribution, and presenting as a transient increase in ER lumenal Ca^{2+}. However, as ER tubules have a larger diameter in mutant ER (Yalçın et al., 2017), this would work against this theory, as the larger tubules should enable active flow (Holcman et al., 2018). Alternatively, expression of ER Ca^{2+} proteins may be affected, such as the ER Ca^{2+} release channel RyR, highly expressed at axonal boutons (Sharp et al., 1993). If its expression levels were decreased, or its distribution altered, this could account for the lack of Ca^{2+} able to escape the lumen and explain the transient increase in Ca^{2+} uptake observed on stimulation. Increased uptake of Ca^{2+} by mutant ER does not lead to decreased cytoplasmic [Ca^{2+}]; however, we might not detect very local reductions in [Ca^{2+}] close to the ER, if masked by excess cytoplasmic fluorescence away from its immediate vicinity. Increasing bath [Ca^{2+}] can

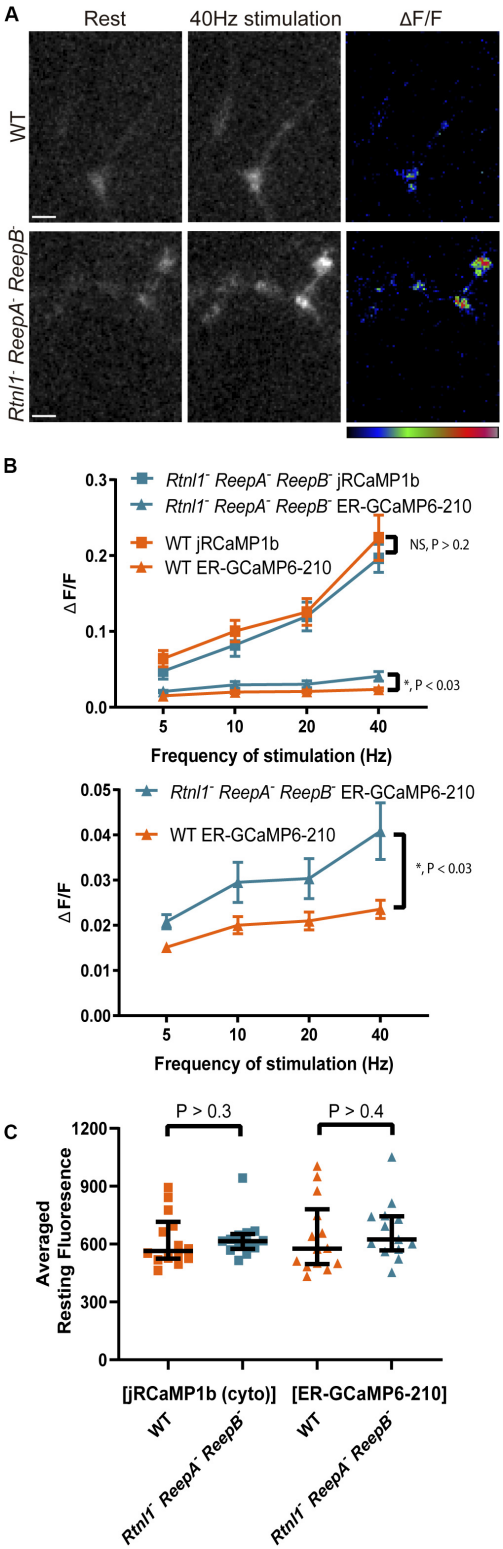

FIGURE 4 | ER lumenal, but not cytoplasmic, responses were significantly increased in *Rtnl1*$^{-}$ *ReepA*$^{-}$ *ReepB*$^{-}$ mutant Type Ib boutons compared to *WT*, with no difference in resting fluorescence intensity. **(A)** Lumenal ER-GCaMP6-210 expressed in aCC using *Dpr-GMR94G06-GAL4* showed a

(Continued)

FIGURE 4 | Continued
larger evoked response in Type Ib NMJs at muscle 1 in mutants, compared to *WT*; 40 Hz stimulation panel shows the maximum response of the given GECI following stimulation. GECIs were co-expressed in the same neuron. Pseudocolor bar (for $\Delta F/F$ panels) shows low to high $\Delta F/F$; scale bar, 5 μm. **(B)** There was no significant difference between mutant (N = 13 larvae) and WT (N = 14 larvae) in cytoplasmic responses (jRCaMP1b) at these boutons stimulated over a range of frequencies, but there was a significant increase in the ER lumenal response (2-way ANOVA). The lower graph shows the ER lumenal response only, with the y-axis expanded. **(C)** There was no significant effect of the triple mutant on the resting fluorescence intensity (from the 40 Hz recording) of either sensor (Mann–Whitney U test).

rescue transmitter release phenotypes in *atl* and *Rtnl1* mutants (Summerville et al., 2016); reducing bath [Ca^{2+}] in our setup might reveal cytoplasmic dysfunction not apparent at higher bath [Ca^{2+}].

Could the increased ER lumenal Ca^{2+} responses in mutants have any effects on cell physiology, if there is no corresponding increase in [Ca^{2+}] in the cytoplasm, where many Ca^{2+} effectors reside? There are Ca^{2+} effectors in the ER lumen such as calreticulin (Opas et al., 1991), although the protein-folding chaperone role of calreticulin is more likely to place its main function in rough rather than smooth ER. However, altered lumenal Ca^{2+} responses could also affect physiology of organelles that obtain Ca^{2+} from the ER, including mitochondria and endo/lysosomal organelles (Raffaello et al., 2016). These effects could endure well beyond the original train of action potentials, due to the slow kinetics of Ca^{2+} uptake and release by the ER, with lumenal [Ca^{2+}] not always returning to baseline during our recordings. Furthermore, aberrant ER Ca^{2+} handling has been postulated as a trigger for neurodegeneration, so what we are observing may well reflect deleterious changes in cellular health (Stutzmann and Mattson, 2011; Ureshino et al., 2019). In support of our findings, mutation or knockdown of genes with a role in ER shaping, including *atl*, *Rtnl1,* and *VAP*, also affect aspects of presynaptic function including neurotransmitter release and synaptic vesicle density, and the cytoplasmic presynaptic Ca^{2+} response (Summerville et al., 2016; De Gregorio et al., 2017; Lindhout et al., 2019). Given the number of HSP genes whose products localize to ER (Montenegro et al., 2012; Blackstone, 2018) and could therefore affect Ca^{2+} dynamics, altered Ca^{2+} handling in axons or axonal terminals could potentially be a contributory factor to HSP pathology. Taken together, these data strongly suggest a role for ER in modulating presynaptic function and highlight the importance of having an intact, functional ER network.

CONCLUSION

In conclusion, we have demonstrated the use of ER lumenally targeted GECIs for use in *Drosophila*, successfully recording fluxes at both the NMJ and the axon. We have demonstrated the utility of these sensors in identifying functional differences between WT and *Rtnl1*$^{-}$ *ReepA*$^{-}$ *ReepB*$^{-}$ mutant flies, whose axonal ER network it is known to be affected. We anticipate these will be useful additions to a *Drosophila* Ca^{2+} imaging toolkit in the future, to further our understanding of HSP and neurodegeneration more broadly.

DATA AVAILABILITY STATEMENT

This article contains previously unpublished data. Underpinning data are available on: https://www.repository.cam.ac.uk/, DOI link: doi: 10.17863/CAM.55394.

AUTHOR CONTRIBUTIONS

MO performed all the cloning and Ca^{2+} imaging experiments. MO and CO'K designed the experiments. JP-M performed the confocal imaging acquisition. JO'S performed the preliminary experiments and contributed to the data analysis. TW provided the initial training and support for Ca^{2+} imaging experiments and assisted in the experimental design. The manuscript was written by MO and CO'K with comments and edits by JP-M, TW, and JO'S. All authors contributed to the article and approved the submitted version.

FUNDING

This work was supported by grants BB/L021706 from the UK Biotechnology and Biological Sciences Research Council and MR/S011226 from the UK Medical Research Council to CO'K. MO was supported by a Newton International Fellowship (NF150362) from The Royal Society and a Marie Skłodowska-Curie Fellowship (701397) from the European Commission. JP-M was supported by a Marie Skłodowska-Curie Fellowship (745007) from the European Commission. TW was supported by a David Phillips Fellowship from the Biotechnology and Biological Sciences Research Council (BBSRC) (BB/L024667/1) and later by the College of Biological Sciences, University of Minnesota.

ACKNOWLEDGMENTS

We thank the Department of Genetics Fly Facility, University of Cambridge, for providing the *Drosophila* microinjection service, Timothy Ryan for providing the FCK(1.3)GW-ER-GCaMP6-210 plasmid, and Bloomington *Drosophila* Stock Centre for the stocks. This manuscript has been released as a pre-print at bioRxiv (Oliva et al., 2020).

SUPPLEMENTARY MATERIAL

The Supplementary Material for this article can be found online at: https://www.frontiersin.org/articles/10.3389/fnins.2020.00816/full#supplementary-material

REFERENCES

Bischof, J., Maeda, R. K., Hediger, M., Karch, F., and Basler, K. (2007). An optimized transgenesis system for *Drosophila* using germ-line-specific phiC31 integrases. *Proc. Natl. Acad. Sci. U.S.A.* 104, 3312–3317. doi: 10.1073/pnas.0611511104

Blackstone, C. (2018). Converging cellular themes for the hereditary spastic paraplegias. *Curr. Opin. Neurobiol.* 51, 139–146. doi: 10.1016/j.conb.2018.04.025

Chen, T. W., Wardill, T. J., Sun, Y., Pulver, S. R., Renninger, S. L., Baohan, A., et al. (2013). Ultrasensitive fluorescent proteins for imaging neuronal activity. *Nature* 499, 295–300. doi: 10.1038/nature12354

Choi, Y. M., Kim, S. H., Chung, S., Uhm, D. Y., and Park, M. K. (2006). Regional interaction of endoplasmic reticulum Ca2+ signals between soma and dendrites through rapid luminal Ca2+ diffusion. *J. Neurosci.* 26, 12127–12136. doi: 10.1523/JNEUROSCI.3158-06.2006

Dana, H., Mohar, B., Sun, Y., Narayan, S., Gordus, A., Hasseman, J. P., et al. (2016). Sensitive red protein calcium indicators for imaging neural activity. *eLife* 5:e12727 doi: 10.7554/eLife.12727

De Gregorio, C., Delgado, R., Ibacache, A., Sierralta, J., and Couve, A. (2017). *Drosophila* Atlastin in motor neurons is required for locomotion and presynaptic function. *J. Cell Sci.* 130, 3507–3516. doi: 10.1242/jcs.201657

de Juan-Sanz, J., Holt, G. T., Schreiter, E. R., de Juan, F., Kim, D. S., and Ryan, T. A. (2017). Axonal endoplasmic reticulum Ca(2+) content controls release probability in CNS nerve terminals. *Neuron* 93, 867–881. doi: 10.1016/j.neuron.2017.01.010

Edelstein, A. D., Tsuchida, M. A., Amodaj, N., Pinkard, H., Vale, R. D., and Stuurman, N. (2014). Advanced methods of microscope control using muManager software. *J. Biol. Methods* 1, e10–e20. doi: 10.14440/jbm.2014.36

Fowler, P. C., and O'Sullivan, N. C. (2016). ER-shaping proteins are required for ER and mitochondrial network organization in motor neurons. *Hum. Mol. Genet.* 25, 2827–2837. doi: 10.1093/hmg/ddw139

Georgiades, P., Allan, V. J., Wright, G. D., Woodman, P. G., Udommai, P., Chung, M. A., et al. (2017). The flexibility and dynamics of the tubules in the endoplasmic reticulum. *Sci. Rep.* 7, 16474–16484. doi: 10.1038/s41598-017-16570-4

Handler, A., Graham, T. G. W., Cohn, R., Morantte, I., Siliciano, A. F., Zeng, J., et al. (2019). Distinct dopamine receptor pathways underlie the temporal sensitivity of associative learning. *Cell* 178, 60–75.e19. doi: 10.1016/j.cell.2019.05.040

Holcman, D., Parutto, P., Chambers, J. E., Fantham, M., Young, L. J., Marciniak, S. J., et al. (2018). Single particle trajectories reveal active endoplasmic reticulum luminal flow. *Nat. Cell Biol.* 20, 1118–1125. doi: 10.1038/s41556-018-0192-2

Li, J., Yan, B., Si, H., Peng, X., Zhang, S. L., and Hu, J. (2017). Atlastin regulates store-operated calcium entry for nerve growth factor-induced neurite outgrowth. *Sci. Rep.* 7–16, 43490. doi: 10.1038/srep43490

Lindhout, F. W., Cao, Y., Kevenaar, J. T., Bodzeta, A., Stucchi, R., Boumpoutsari, M. M., et al. (2019). VAP-SCRN1 interaction regulates dynamic endoplasmic reticulum remodeling and presynaptic function. *EMBO J.* 38, e101345. doi: 10.15252/embj.2018101345

Macleod, G. T., Hegstrom-Wojtowicz, M., Charlton, M. P., and Atwood, H. L. (2002). Fast calcium signals in *Drosophila* motor neuron terminals. *J. Neurophysiol.* 88, 2659–2663. doi: 10.1152/jn.00515.2002

Montenegro, G., Rebelo, A. P., Connell, J., Allison, R., Babalini, C., D'Aloia, M., et al. (2012). Mutations in the ER-shaping protein reticulon 2 cause the axon-degenerative disorder hereditary spastic paraplegia type 12. *J. Clin. Invest.* 122, 538–544. doi: 10.1172/JCI60560

Moreau, K., Fleming, A., Imarisio, S., Lopez Ramirez, A., Mercer, J. L., Jimenez-Sanchez, M., et al. (2014). PICALM modulates autophagy activity and tau accumulation. *Nat. Commun.* 5-24:4998. doi: 10.1038/ncomms5998

Nakamura, T., Lasser-Ross, N., Nakamura, K., and Ross, W. N. (2002). Spatial segregation and interaction of calcium signalling mechanisms in rat hippocampal CA1 pyramidal neurons. *J. Physiol.* 543, 465–480. doi: 10.1113/jphysiol.2002.020362

Oliva, M. K., Pérez-Moreno, J. J., O'Shaughnessy, J., Wardill, T. J., and O'Kane, C. J. (2020). Endoplasmic reticulum (ER) lumenal indicators in *Drosophila* reveal effects of HSP-related mutations on ER calcium dynamics. *bioRxiv* [Preprint]. doi: 10.1101/2020.02.20.957696

Opas, M., Dziak, E., Fliegel, L., and Michalak, M. (1991). Regulation of expression and intracellular distribution of calreticulin, a major calcium binding protein of nonmuscle cells. *J. Cell Physiol.* 149, 160–171. doi: 10.1002/jcp.1041490120

O'Sullivan, N. C., Jahn, T. R., Reid, E., and O'Kane, C. J. (2012). Reticulon-like-1, the *Drosophila* orthologue of the hereditary spastic paraplegia gene reticulon 2, is required for organization of endoplasmic reticulum and of distal motor axons. *Hum. Mol. Genet.* 21, 3356–3365. doi: 10.1093/hmg/dds167

Perez-Moreno, J. J., and O'Kane, C. J. (2019). GAL4 drivers specific for type Ib and type Is motor neurons in *Drosophila*. *G3* 9, 453–462. doi: 10.1534/g3.118.200809

Pfeiffer, B. D., Jenett, A., Hammonds, A. S., Ngo, T. T., Misra, S., Murphy, C., et al. (2008). Tools for neuroanatomy and neurogenetics in *Drosophila*. *Proc. Natl. Acad. Sci. U.S.A.* 105, 9715–9720. doi: 10.1073/pnas.0803697105

Raffaello, A., Mammucari, C., Gherardi, G., and Rizzuto, R. (2016). Calcium at the center of cell signaling: interplay between endoplasmic reticulum, mitochondria, and lysosomes. *Trends Biochem. Sci.* 41, 1035–1049. doi: 10.1016/j.tibs.2016.09.001

Schindelin, J., Arganda-Carreras, I., Frise, E., Kaynig, V., Longair, M., Pietzsch, T., et al. (2012). Fiji: an open-source platform for biological-image analysis. *Nat. Methods* 9, 676–682. doi: 10.1038/nmeth.2019

Sharp, A. H., McPherson, P. S., Dawson, T. M., Aoki, C., Campbell, K. P., and Snyder, S. H. (1993). Differential immunohistochemical localization of inositol 1,4,5-trisphosphate- and ryanodine-sensitive Ca2+ release channels in rat brain. *J. Neurosci.* 13, 3051–3063. doi: 10.1523/jneurosci.13-07-03051.1993

Stewart, B. A., Atwood, H. L., Renger, J. J., Wang, J., and Wu, C. F. (1994). Improved stability of *Drosophila* larval neuromuscular preparations in haemolymph-like physiological solutions. *J. Comp. Physiol. A* 175, 179–191. doi: 10.1007/bf00215114

Stutzmann, G. E., and Mattson, M. P. (2011). Endoplasmic reticulum Ca(2+) handling in excitable cells in health and disease. *Pharmacol. Rev.* 63, 700–727. doi: 10.1124/pr.110.003814

Summerville, J. B., Faust, J. F., Fan, E., Pendin, D., Daga, A., Formella, J., et al. (2016). The effects of ER morphology on synaptic structure and function in *Drosophila melanogaster*. *J. Cell Sci.* 129, 1635–1648. doi: 10.1242/jcs.184929

Suzuki, J., Kanemaru, K., Ishii, K., Ohkura, M., Okubo, Y., and Iino, M. (2014). Imaging intraorganellar Ca2+ at subcellular resolution using CEPIA. *Nat. Commun.* 5:4153. doi: 10.1038/ncomms5153

Thiel, K., Heier, C., Haberl, V., Thul, P. J., Oberer, M., Lass, A., et al. (2013). The evolutionarily conserved protein CG9186 is associated with lipid droplets, required for their positioning and for fat storage. *J. Cell Sci.* 126, 2198–2212. doi: 10.1242/jcs.120493

Ureshino, R. P., Erustes, A. G., Bassani, T. B., Wachilewski, P., Guarache, G. C., Nascimento, A. C., et al. (2019). The interplay between Ca(2+) signaling pathways and neurodegeneration. *Int. J. Mol. Sci.* 20:6004. doi: 10.3390/ijms20236004

Yalçın, B., Zhao, L., Stofanko, M., O'Sullivan, N. C., Kang, Z. H., Roost, A., et al. (2017). Modeling of axonal endoplasmic reticulum network by spastic paraplegia proteins. *eLife* 6:e23882. doi: 10.7554/eLife.23882

Conflict of Interest: The authors declare that the research was conducted in the absence of any commercial or financial relationships that could be construed as a potential conflict of interest.

The reviewer BH declares that the endorsement is based on his professional opinion and it is not an endorsement by the US government.

frontiers in Neuroscience

BRIEF RESEARCH REPORT
published: 04 September 2020
doi: 10.3389/fnins.2020.00912

Suppression of *spastin* Mutant Phenotypes by *Pak3* Loss Implicates a Role for Reactive Glia in AD-HSP

*Emily F. Ozdowski, Jill S. Wentzell, Stefanie M. Engert, Helena Abbott and Nina T. Sherwood**

Department of Biology, Duke University, Durham, NC, United States

Neurodegenerative mechanisms due to mutations in *spastin* currently center on neuronal defects, primarily in microtubule and endomembrane regulation. Spastin loss in *Drosophila* larvae compromises neuronal microtubule distribution, alters synaptic bouton morphology, and weakens synaptic transmission at glutamatergic neuromuscular junction (NMJ) synapses. Pak3, a p21-activated kinase that promotes actin polymerization and filopodial projections, is required for these *spastin* mutant defects; animals lacking both genes have normal NMJs. Here we show that Pak3 is expressed in central and peripheral glial populations, and reduction of Pak3 specifically in subperineurial glial cells is sufficient to suppress the phenotypes associated with *spastin* loss. Subperineurial glia in the periphery ensheathe motor neuron axons and have been shown to extend actin-based projections that regulate synaptic terminals during normal NMJ development. We find that these subperineurial glial projections are Pak3-dependent and nearly twice as frequent in *spastin* mutants, while in *Pak3, spastin* double mutants, neither glial projections nor synaptic defects are observed. Spastin deficiency thus increases Pak3-dependent subperineurial glia activity, which is in turn required for neuronal defects. Our results demonstrate a central role for Pak3-mediated, altered glial behavior in the neuronal defects due to *spastin* loss, and suggest that a similar reactive glia-mediated mechanism may underlie human AD-HSP pathogenesis.

Keywords: Spastin, Pak3, Autosomal Dominant Hereditary Spastic Paraplegia, p21-activated kinase, subperineurial glia, microtubule severing proteins, reactive glia

OPEN ACCESS

Edited by:
Cahir Joseph O'Kane, University of Cambridge, United Kingdom

Reviewed by:
Yong Qing Zhang, Chinese Academy of Sciences (CAS), China
J. Troy Littleton, Massachusetts Institute of Technology, United States
Mihaela Serpe, National Institutes of Health (NIH), United States

***Correspondence:**
Nina T. Sherwood
nina.sherwood@duke.edu

Specialty section:
This article was submitted to Neurodegeneration, a section of the journal Frontiers in Neuroscience

Received: *31 March 2020*
Accepted: *06 August 2020*
Published: *04 September 2020*

Citation:
Ozdowski EF, Wentzell JS, Engert SM, Abbott H and Sherwood NT (2020) Suppression of spastin Mutant Phenotypes by Pak3 Loss Implicates a Role for Reactive Glia in AD-HSP. Front. Neurosci. 14:912. doi: 10.3389/fnins.2020.00912

INTRODUCTION

The identification of human *SPAST* as the most common gene mutated in Autosomal-Dominant Hereditary Spastic Paraplegia two decades ago was a major advance, enabling multiple model systems to be leveraged toward understanding the requirement for Spastin in nervous system function (Hazan et al., 1999). Spastin likely serves to coordinately regulate the microtubule cytoskeleton and membrane components (reviewed in Lumb et al., 2012), and although clear consensus is still in progress, several working hypotheses have emerged for its neuronal roles. Potential processes include neural stem cell proliferation (Jeong et al., 2019), remodeling the endoplasmic reticulum and other endomembrane components (e.g., Park et al., 2010; Allison et al., 2019), lipid droplet function (Papadopoulos et al., 2015; Chang et al., 2019), axon regeneration

(Stone et al., 2012), axon outgrowth (Wood et al., 2006), axon transport (Tarrade et al., 2006; Kasher et al., 2009), and synaptic morphology and transmission (Sherwood et al., 2004; Trotta et al., 2004).

Drosophila spastin was identified in a forward screen for genes involved in nervous system development (Sherwood et al., 2004). Just as *SPAST* mutations impair the longest axons of the central nervous system in humans, diminishing patient mobility, homozygous deletion of *Drosophila spastin* (the $spastin^{5.75}$ allele) impairs mobility in adult flies, with the distal-most limbs also appearing the weakest. These adult flies are rarely viable, and although homozygous null larvae appear healthy, electrophysiological analysis of the larval neuromuscular junction (NMJ), a well-established model for vertebrate glutamatergic central synapses (Collins and DiAntonio, 2007), reveals reduced synaptic transmission due to defects at the presynaptic terminal (Sherwood et al., 2004; Ozdowski et al., 2011). This functional weakening is accompanied by distinctive changes in presynaptic arbor morphology. In contrast to wild type NMJs, $spastin^{5.75}$ larvae have more highly branched axon terminal arbors, with smaller and more numerous synaptic boutons that often form bunched, rather than linear, arrays. Subcellularly, the normally continuous microtubule cytoskeleton appears sparse or undetectable in mutant terminal boutons, suggesting that Spastin's microtubule severing activity is required for the generation and/or penetration of microtubules into distal sites. Consistent with this model, recent *in vitro* studies have shown that Spastin promotes stabilization and subsequent growth of severed microtubules, in addition to its well-established severing activity (Vemu et al., 2018; Kuo et al., 2019). These subcellular, morphological, and functional phenotypes in *spastin* mutants are all significantly rescued by low-level, neuron-specific expression of fly – or human – wild type Spastin, demonstrating that Spastin function is well-conserved between flies and humans, and is required within neurons (Sherwood et al., 2004; Du et al., 2010).

To understand the molecular and cellular mechanisms underlying the consequences of *spastin* loss, we executed a forward genetic screen for modifiers of *spastin* mutant phenotypes and identified *Pak3*, a member of the p21-activated serine/threonine kinase family (Ozdowski et al., 2011). Pak proteins are conserved from amoebae to humans, and typically activated downstream of Rac and Cdc42 small GTPase signaling, leading to alterations in the actin cytoskeleton and phosphorylation of a wide range of other protein targets (reviewed in Kumar et al., 2017; Semenova and Chernoff, 2017). The Paks are particularly well-studied because of their demonstrated roles inducing cell motility, invasion, and metastasis in several cancers, as well as contributing to cardiac and neurological disorders. Humans have six PAK genes (PAK 1–6), segregated into two structurally distinct groups. The group I PAKs, characterized by highly conserved autoinhibitory (AID) and kinase domains, form inactive dimers that depend upon Rac or Cdc42 binding for relief of autoinhibition and subsequent kinase activity. The group II PAKs lack an AID and do not require RhoGTPase binding for kinase activity. Of the proteins encoded by the three *Drosophila* Pak genes, *Pak*, *mushroom bodies tiny* (*mbt*), and *Pak3*, Pak is orthologous to the group I vertebrate Paks, mbt falls clearly into the group II subfamily, and Pak3, while less similar than Pak, is also considered a group I Pak due to its clear AID and ∼60% amino acid identity in the kinase domain (Mentzel and Raabe, 2005). Both overexpression and knockdown of *Drosophila Pak3* in various cell lines alters actin distribution and cell motility (Mentzel and Raabe, 2005; Asano et al., 2009; Ribeiro et al., 2014). *In vivo*, Pak3 is important in dorsal closure (Bahri et al., 2010), epidermal wound healing (Baek et al., 2012), podosome invasion during myoblast fusion (Duan et al., 2012), and border cell migration during oogenesis (Felix et al., 2015), all processes that require rearrangements of the actin cytoskeleton and changes in cell motility downstream of Rac signaling.

At the larval NMJ, ubiquitous, genetic loss of *Pak3* does not significantly affect synapse form or function; however, *Pak3* reduction in a *spastin* deficient background dramatically rescues the defects that characterize *spastin* mutants at this stage (Ozdowski et al., 2011). NMJ synapses in *Pak3*, *spastin* double mutants exhibit near-wild type morphology, with large and linearly-arrayed synaptic boutons. Subcellularly, continuity of the microtubule cytoskeleton within boutons is restored, and functionally, synaptic strength is indistinguishable from wild type levels. Absence of *Pak3* thus renders these neurons resistant to *spastin* loss.

Given this striking rescue, we sought to understand how the presence of Pak3 confers *spastin* mutant phenotypes. We examined the Pak3 expression pattern and used tissue-specific knockdown to determine the cells in which it acts when *spastin* is lost. Surprisingly, *Pak3* is not required in the motor neurons where Spastin functions, but rather, in the peripheral glia that ensheathe them. These glia provide essential support to the motor neurons, including extending filopodial projections that regulate the neuronal bouton arbor during development (Fuentes-Medel et al., 2009; Brink et al., 2012). We find that Pak3 promotes glial projections at the NMJ. Furthermore, in *spastin* mutants these glial projections are more numerous, while reduction of glial Pak3 suppresses both the projections and *spastin* mutant bouton morphology. Together, these data support a model in which *spastin* loss leads to increased Pak3-mediated glial activity, changing glial behavior such that they become toxic, rather than supportive, to synaptic terminals. Increasing evidence of a central role for reactive glial behavior in the progression of several major neurodegenerative diseases (Liddelow and Barres, 2017) makes these results particularly intriguing, as it suggests that pathogenesis in AD-HSP may be similarly mediated by reactive, toxic changes in a normally supportive subpopulation of glia.

MATERIALS AND METHODS

Drosophila Stocks and Sources

Stocks and crosses were maintained on standard molasses-based food (Archon Scientific), except for experiments using the *flower* (*fwe*) loss of function alleles, fwe^{DB56} and fwe^{DB25} (gift of H. Bellen), which were raised on yeasted grape juice plates to facilitate recovery of the desired genotypes. All larvae and adults assayed were from crosses kept at 25°C. Unless

otherwise specified, controls were w^{1118} flies, the common genetic background for transgenic strains; their NMJs are indistinguishable from wild type flies so are also referred to here as "wild type." Driver lines were *repo-GAL4* (gift of M. Freeman), *gliotactin (gli)-GAL4* (gift of V. Auld), *e22c-Gal4 spaghetti-squash (sqh)-GAL4* (gift of D. Kiehart), *breathless* (*btl*)*-GAL4* (gift of M. Metzstein), and $elav^{C155}$*-GAL4*, *Mef2-GAL4*, *Mhc-GAL4*, and *nSyb-GAL4* (all from the Bloomington Drosophila Stock Center, BDSC). *Pak3* alleles were *PBac{RB}*$Pak3^{e00329}$, *P{XP}*$Pak3^{d02472}$ (abbreviated $Pak3^{d}$ in **Figures 3**, **4**; BDSC), *GAL4* insertion line *P{GawB}*$Pak3^{NP4472}$ (Kyoto Drosophila Genomics and Genetic Resources Center), and RNAi lines $Pak3^{NIG.14895R-2}$ (National Institute of Genetics, NIG-FLY), $Pak3^{GL00287}$ (*P{TRiP.GL00287}attB*, BDSC), and $Pak3^{v39844}$ (P*{GD8481}v39844*, Vienna Drosophila Resource Center). Generation of the deletion allele *Df(3R)Pak3* (abbreviated $Pak3^{Df}$ in **Figures 3**, **4**), was previously described (Ozdowski et al., 2011). *UAS-Pak3::GFP* constructs (gift of B. Baum) were injected into *Drosophila* embryos and two lines established: one insertion on chromosome II, *UAS-*$Pak3^{50}$*::GFP*, and one on chromosome III, *UAS-*$Pak3^{32}$*::GFP*. Tissue-specific expression of *UAS-*$Pak3^{50}$*::GFP* rescues *Pak3* mutant adult lethality, consistent with the transgene producing functional Pak3 protein (E.F.O., unpublished results). *UAS-*$Pak3^{32}$*::GFP* was used for *Pak3* overexpression in glia. Tissue-specific GFP was expressed using *UAS-mCD8::GFP* or *UAS-nls::GFP* flies (BDSC).

Immunofluorescence

Wandering third-instar larvae were dissected in room temperature Phosphate Buffered Saline (PBS, Invitrogen) or HL3 Ringer's medium without Ca^{2+} for < 20 min., or when quantifying glial projections, in HL3 Ringer's containing 1.5 mM Ca^{2+} for <10 min. prior to fixation. Filets were then fixed in 4% paraformaldehyde (Electron Microscopy Sciences) for 30 min., washed in PBS with 0.2% Triton X-100 (PBST), and blocked in PBST with 5% normal goat serum, 0.01% bovine serum albumin, and 0.01% sodium azide for up to 2 h at room temperature. Filets were incubated overnight at 4°C in primary antibody diluted in block. Primary antibodies used were mouse polyclonal αPak3 (gift of S. Bahri, 1:250), rabbit αHRP (Jackson, 1:100), mouse αDLG (4F3 supernatant, Developmental Studies Hybridoma Bank [DSHB], 1:100), rat αElav (7E8A10, DSHB, 1:100), mouse αSlit (C555.6D, DSHB, 1:50), and mouse (mAb 3E6) or rabbit αGFP (Invitrogen, 1:300). Filets were then washed in PBST and incubated with the species-appropriate Alexa Fluor 488 or 568 secondary antibodies (Invitrogen) diluted 1:300 in block, for 2 h at room temperature or overnight at 4°C. After further washing, filets were mounted in Vectashield (Vector Laboratories) or ProLong Antifade (ThermoFisher).

Synaptic Bouton and Glial Quantification and Imaging

Slide-mounted filets were scored with the experimenter blinded to larval genotypes, using an inverted fluorescence compound microscope (Zeiss Axiophot with a 63X, 1.2NA oil immersion objective or Zeiss Axio Imager with a 100X, 1.4NA oil immersion objective). Representative confocal images were obtained using a Zeiss 880 Airyscan confocal microscope and 63X, 1.2NA oil immersion or a 20X, 0.8NA dry objective. Images were false-colored magenta in Adobe Photoshop to aid visualization by color blind readers. Abdominal muscle 4 was identified for each hemisegment and type 1b synaptic bouton numbers were recorded. Type 1b bouton identity was confirmed by double staining with anti-DLG whenever possible (in all larvae for which anti-GFP immunostaining was not needed); otherwise, they were distinguished from type 1s boutons based on size and branch morphology. Terminal boutons, a measurement of synaptic arbor branching, were defined as any synaptic bouton with only one connection. This included all termini along the arbor and at the distal tips, regardless of size. Subperineurial glial projections were visualized using anti-GFP to visualize *gliotactin-GAL4*-driven expression of *UAS-mCD8::GFP*. Glial morphology at each main axon branch was characterized as (1) blunt, ending at synaptic boutons, (2) broad lamellipodia extending over synaptic boutons, (3) long, thin filopodia (gliopods) extending over synaptic boutons, away from the axon, or to neighboring axons, or (4) rounded structures (gliobulbs) that resemble boutons. Numbers of gliopods and gliobulbs were combined as a measure of glial projections. Glial and bouton counts from individual hemisegments were averaged for each larva and all values plotted as bee-swarm superplots using GraphPad Prism (Lord et al., 2020). Statistical significance of larval means was determined by two-tailed Student's t-test in Microsoft Excel (**Figure 2** and **Supplementary Figure S1**) or one-way ANOVA with Sidak's *post hoc* test for multiple comparisons in GraphPad Prism (**Figures 3**, **4**). P-values are denoted as ns for $p > 0.05$, * for $0.01 < p \leq 0.05$, ** for $0.001 < p \leq 0.01$, and *** for $p \leq 0.001$.

RESULTS

Pak3 Is Expressed in Larval Glia

To begin to identify the specific cells in which *Pak3* loss prevents *spastin* mutant defects, we used a polyclonal antibody directed against the *Drosophila* Pak3 protein (kind gift of Sami Bahri; Bahri et al., 2010) to determine its endogenous expression pattern in larvae. Anti-Pak3 staining in wild type controls was strongly detected in the ventral nerve cord (VNC, analogous to the spinal cord of vertebrates) in a dashed pattern characteristic of midline glial cells (**Figure 1A**, arrow). Immunofluorescence was also seen in a thin layer on the surface of the larval brain, and along axonal projections emanating from the brain and ventral nerve cord (**Figure 1A**, arrowheads). The strength of the antibody signal correlated with predicted protein expression levels consistent with RNA disruption in different *Pak3* alleles, supporting the specificity of the antibody for Pak3 (compare **Figures 1A–C**).

Pak3 expression was also assessed using a *Pak3* promoter and GFP reporter system. The *Pak3* promoter-*GAL4* transgenic line $Pak3^{NP4472}$, in which the GAL4 gene is inserted 160 bp upstream of the *Pak3* translational start site, was crossed to UAS-membrane GFP flies (*UAS-mCD8::GFP*; Lee and Luo, 1999). Larval progeny displayed strong GFP expression in cells that, similar to those revealed by the anti-Pak3 antibody, were

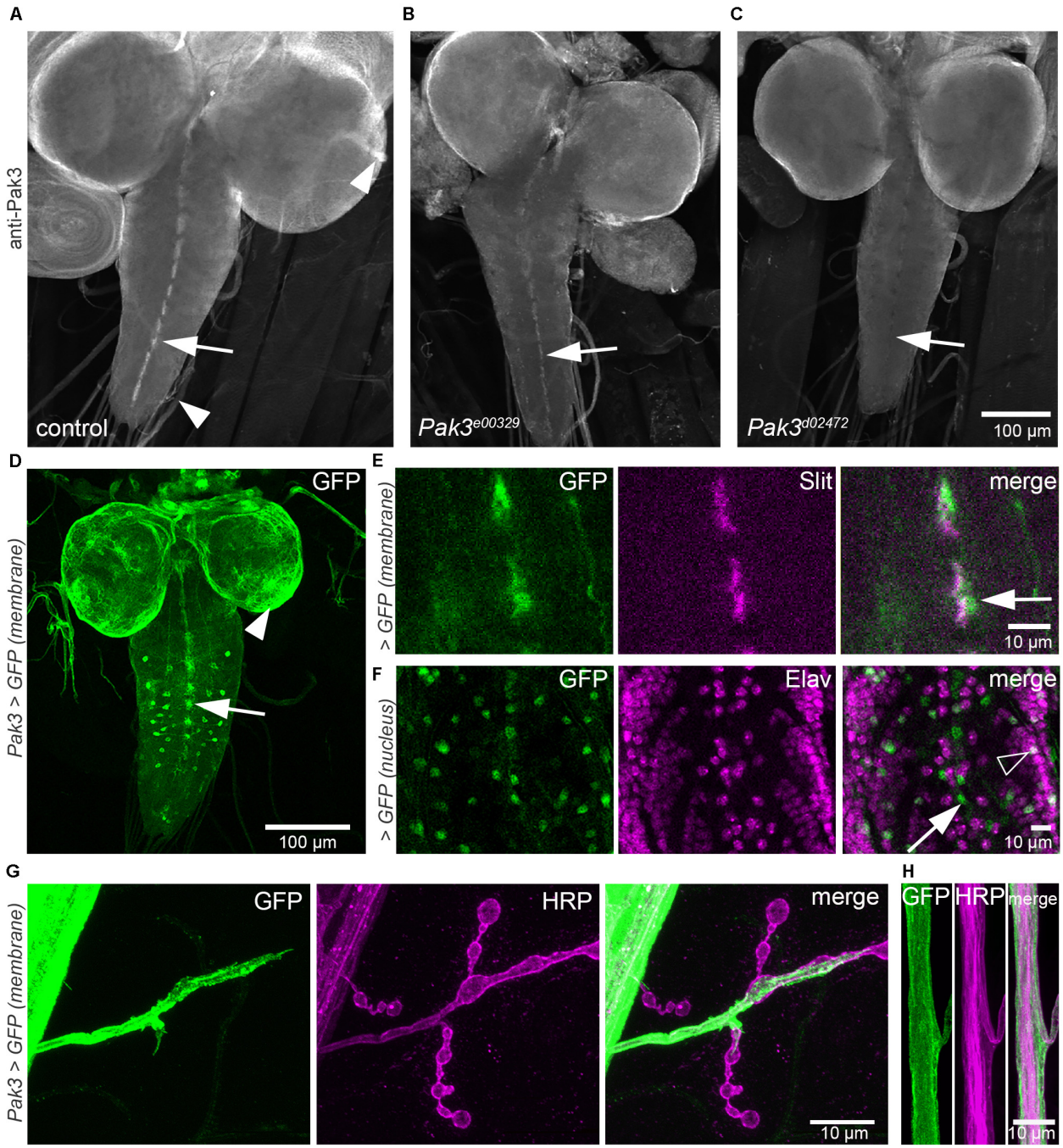

FIGURE 1 | Pak3 is expressed in larval glia. **(A–C)** An anti-Pak3 polyclonal antibody reveals immunostaining consistent with glial cell expression: in larval ventral nerve cord (VNC) midline cells (**A**, arrow), along axonal projections emanating from the brain and VNC (**A**, arrowheads), and on the surface of the CNS. Expression is reduced in *Pak3*^{e00329} mutants **(B)** and almost undetectable in *Pak3*^{d02472} mutants **(C)**, consistent with the severity of RNA disruption in these alleles and thus supporting antibody specificity. **(D)** A second method of observing Pak3 expression using the *GAL4-UAS* reporter system, *Pak3-GAL4*^{NP4472} > *UAS-mcD8::GFP*, shows similar membrane GFP expression patterns (midline cells, arrow; surface cells, arrowhead), with additional cells visible in the VNC. **(E)** Midline membrane GFP expression (green) overlaps with anti-Slit (magenta; arrow), a marker for midline glia from embryonic through larval stages (Oliva et al., 2016). **(F)** Expression of nuclear-localized GFP (green) in animals with *Pak3-GAL4*^{NP4472} > *UAS-nls::GFP* confirms that the midline cells are anti-Elav-negative, indicating non-neuronal identity (arrow), but other GFP-positive cells in the VNC are neuronal (open arrowhead). **(G,H)** Along motor axons and at neuromuscular junction (NMJ) synapses, strong membrane GFP expression (green) extends beyond regions staining with the neuronal marker HRP (magenta), appearing to wrap the axons as well as project over proximal synaptic boutons, consistent with Pak3 expression in peripheral glia.

arrayed in a dashed pattern characteristic of VNC midline glia (**Figure 1D**, arrow). Consistent with this identity, GFP-expressing cells at the midline colocalized with immunostaining for Slit, a protein secreted by midline glia (**Figure 1E**, arrow). They also failed to colocalize with anti-Elav, confirming their non-neuronal identity (**Figure 1F**, arrow). Also consistent with the anti-Pak3 antibody results, robust GFP signal was observed in glia covering the brain surface (**Figure 1D**, arrowhead) and ensheathing the motor axons between the ventral nerve cord and the periphery (**Figures 1G,H**). $Pak3^{NP4472}$-driven GFP expression also revealed several other GFP-positive tissues that were not observed using the Pak3 polyclonal antibody, likely due to signal amplification conferred by both the GAL4-UAS system and immunostaining. These included a subset of Elav-positive neurons in the VNC (**Figure 1F**, open arrowhead), sensory neuron glia, and several tissues outside of the nervous system, particularly the trachea, oenocytes and salivary glands (data not shown). GFP expression was not detected in the larval body wall muscles, although Pak3 plays a significant role in myoblast fusion during embryonic stages (Duan et al., 2012). The expression pattern of the *Pak3* promoter-*GAL4* line thus corroborated the Pak3 antibody staining results, revealing surface, midline, and peripheral glia as major sites of Pak3 expression at this stage, but also suggested Pak3 functions in other cell types including neurons and trachea.

Glial Knockdown of Pak3 Rescues the *spastin* Mutant Phenotype

Given that loss of *Pak3* in the whole animal rescues the synaptic phenotype of *spastin* mutants, we next narrowed *Pak3* knockdown to specific tissues and looked for the same rescuing effect. Using tissue-specific GAL4 expression to drive RNAi targeting *Pak3* in a *spastin* null background ($spastin^{5.75}$; Sherwood et al., 2004), we assayed type Ib glutamatergic synaptic boutons on muscle 4 of each larval hemisegment, as the neuronal arbors on this muscle are relatively simple, easily observed, and representative of the NMJ arbors across body wall muscles. Bouton and branching frequencies, measured primarily by terminal bouton number, were quantified for each genotype (**Figure 2**); increases in both at the larval NMJ are *spastin* loss of function hallmarks. $spastin^{5.75}$ mutants had typically small and clustered boutons, averaging over twice as many terminal boutons as compared to w^{1118} controls (**Figures 2A,B,J**; $p = 4.6 \times 10^{-4}$). Separate experiments in which the total number of boutons was scored instead of just the terminals yielded equivalent results (**Supplementary Figure S1**, w^{1118} vs. *spas*; $p = 1.7 \times 10^{-4}$). To identify an effective *Pak3* RNAi line, we used *e22c-GAL4*, *spaghetti squash-GAL4* (*e22c,sqh-GAL4*; Franke et al., 2005) to drive ubiquitous expression of candidate RNAi transgenes in the $spastin^{5.75}$ background, with the expectation that effective *Pak3* knockdown should recapitulate the suppression of *spastin* mutant phenotypes observed with genetic loss of *Pak3*. Of the publicly available lines we tested, $Pak3^{NIG.14895R-2}$ (henceforth referred to as "$Pak3^{RNAi}$" *or* "*Pak3[RNAi]*") was the most effective. In the absence of a GAL4 driver it did not significantly affect the *spastin* mutation (**Figures 2C,J**; $p = 2.3 \times 10^{-4}$ compared to controls; **Supplementary Figure 1**, $Pak3^{RNAi}$ vs. $Pak3^{RNAi}$, *spas*; $p = 1.3 \times 10^{-3}$). When ubiquitously expressed, however, $Pak3^{RNAi}$ in the $spastin^{5.75}$ null background resulted in larger and more linearly arrayed (less branched) boutons resembling wild type rather than $spastin^{5.75}$ mutants (compare **Figure 2D** to the wild type control in **Figure 2A** versus $spastin^{5.75}$ in **Figures 2B,C**). Terminal bouton number in $spastin^{5.75}$ mutants also decreased to wild type levels, although due to difficulties obtaining healthy *e22c,sqh; spas* paired controls (i.e., animals with the *e22c,sqh-GAL4* driver and *spastin* mutation but no $Pak3^{RNAi}$), this change did not reach statistical significance (**Figure 2J**; $p = 0.13$ for *e22c,sqh; spas* vs. *e22c,sqh* > $Pak3^{RNAi}$, *spas*). However, comparison of *e22c,sqh* > $Pak3^{RNAi}$, *spas* larvae to *e22c,sqh* > $Pak3^{RNAi}$ controls (ubiquitously expressing $Pak3^{RNAi}$ in a wild type, rather than *spastin* mutant background) showed no difference in bouton number, providing further support that ubiquitous expression of this $Pak3^{RNAi}$ transgene potently suppresses the effects of *spastin* mutation (**Supplementary Figure S1**, $p = 0.67$).

We then compared the consequence of *Pak3* reduction using the pan-neuronal driver *nSyb-GAL4* (Jenett et al., 2012), the glial driver *repo-GAL4* (Sepp et al., 2001), the muscle drivers *Mef2-GAL4* and *Mhc-GAL4*, and the tracheal driver *btl-GAL4* (Shiga et al., 1996), as all of these cell types have been implicated in regulating *Drosophila* NMJ synapses and show evidence of Pak3 expression as discussed above. *nSyb-GAL4*-, *Mef2-GAL4*-, and *Mhc-GAL4*-mediated $Pak3^{RNAi}$ expression all failed to alleviate $spastin^{5.75}$, excluding neurons ($p = 0.90$) and muscles ($p = 0.28$ and 0.79 for *Mef2* and *Mhc*, respectively), as sites of Pak3's deleterious effects (**Figures 2E,H,J**; *Mhc-GAL4* data not shown, $n = 3$ and 4 larvae for control and experimental groups). *Spastin* mutant synapses were rescued only with glial-specific reduction of *Pak3* using *repo-GAL4*, which drives expression in all glia except for those at the midline (**Figures 2F,J**; $p = 1.9 \times 10^{-3}$ for *repo-GAL4, spas* vs. *repo-GAL4* > $Pak3^{RNAi}$, *spas*). *Repo-GAL4*-mediated *Pak3* knockdown restored synapse morphology of $spastin^{5.75}$ mutants to wild type (**Figure 2F**), comparable to ubiquitous (*e22c,sqh-GAL4*-driven) knockdown (**Figure 2D**) or genetic loss of *Pak3* (Ozdowski et al., 2011). Parallel experiments showed no significant difference in bouton number between glial *Pak3* knockdown in wild type versus *spastin* mutant backgrounds, further supporting a requirement for glial Pak3 in the *spastin* mutant phenotype (**Supplementary Figure S1**, $p = 0.07$). Simultaneous expression of two independently generated *Pak3* RNAi transgenes ($Pak3^{GL0028}$ and $Pak3^{v39844}$) with *repo-GAL4* also suppressed the $spastin^{5.75}$ phenotype (**Supplementary Figure S2**, $Pak3^{GL0028}$,$Pak3^{v39844}$, *spas* controls vs. *repo-GAL4* > $Pak3^{GL0028}$,$Pak3^{v39844}$, *spas*; $p = 1.3 \times 10^{-3}$), and had no effect when expressed using the neuron-specific *elav-GAL4* driver (**Supplementary Figure S2**, $Pak3^{GL0028}$,$Pak3^{v39844}$, *UAS-Dcr2, spas* controls vs. $elav^{C155}$-*GAL4* > $Pak3^{GL0028}$,$Pak3^{v39844}$, *UAS-Dcr2, spas*; $p = 0.32$), supporting that these results are specific to Pak3 reduction and not due to RNAi off-target interactions. We were unable to draw

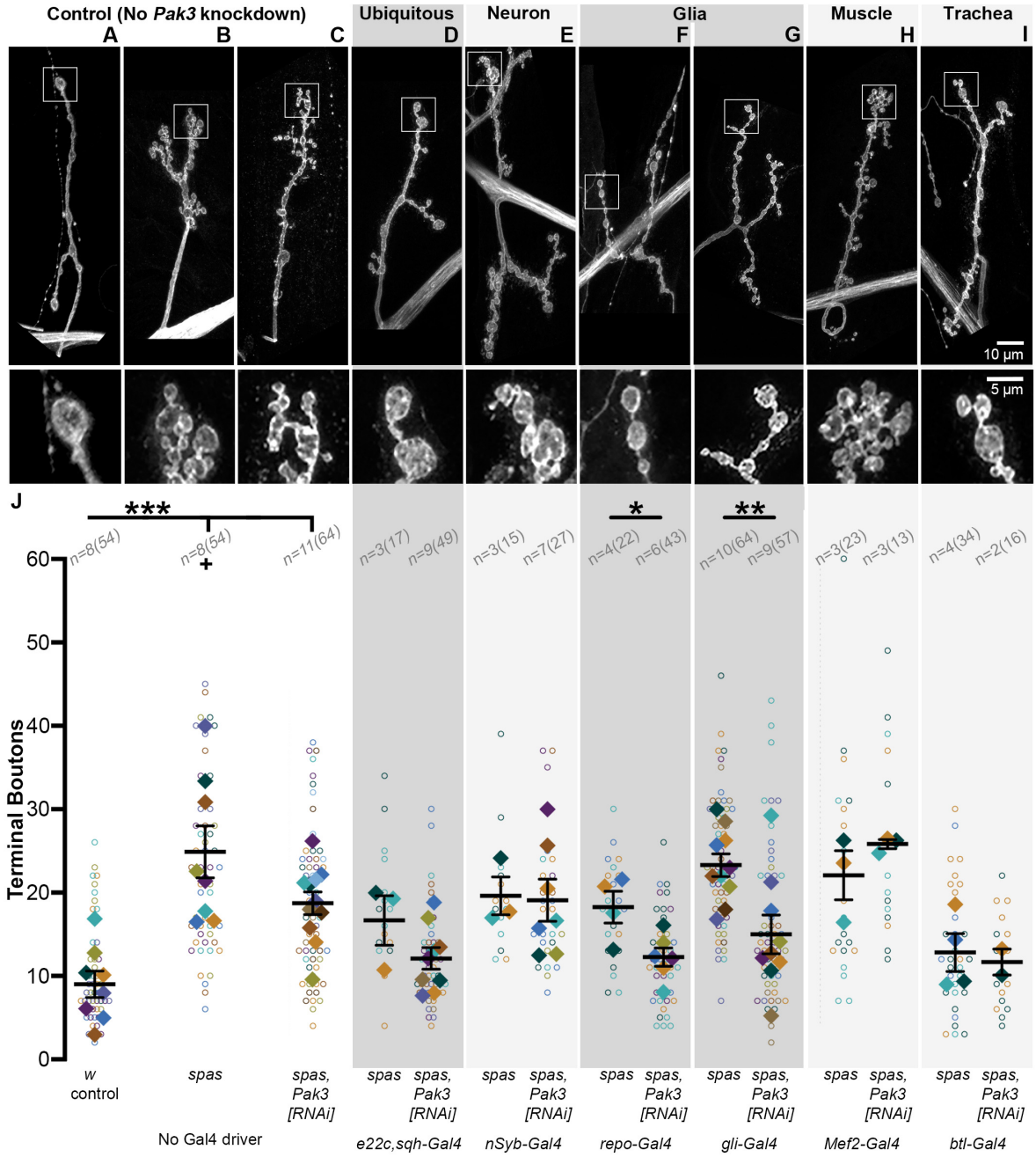

FIGURE 2 | Glial, and specifically subperineurial glial, knockdown of *Pak3* rescues *spastin* synaptic defects. **(A–I)** Anti-HRP staining shows neuronal morphology at the NMJ. The area within the box is magnified below. **(A–C)** are genetic background controls in which $Pak3^{RNAi}$ is not expressed via GAL4 activation (**A** wild type; **B,C**: $spastin^{5.75}$ mutant); **(D–I)** are representative arbors from $spastin^{5.75}$ mutants in which $Pak3^{RNAi}$ is expressed in the specified tissues. **(A)** Wild type synaptic boutons are arrayed linearly with few branches, while **(B)** $spastin^{5.75}$ loss of function mutants have highly branched arbors with many small, bunched boutons. **(C)** In the absence of a *GAL4* driver, the $Pak3^{RNAi}$ transgene has little effect on $spastin^{5.75}$ morphology; terminal boutons remain significantly increased compared to wild type. **(D)** Ubiquitous expression of $Pak3^{RNAi}$ in the $spastin^{5.75}$ background yields terminal boutons more similar in size, arrangement, and number to wild type. **(E)** $Pak3^{RNAi}$ expression in neurons does not rescue the *spastin* mutant phenotype, but **(F,G)** *Pak3* knockdown in all except midline glia with *repo-GAL4* **(F)**, or in subperineurial glia with *gliotactin-GAL4* **(G)**, significantly rescues $spastin^{5.75}$. **(H,I)** Knockdown of *Pak3* in muscle **(H)** or trachea **(I)** show no difference in morphology from their $spastin^{5.75}$ controls. **(J)** Synaptic morphologies are quantified by measuring the number of terminal boutons at each muscle 4 in a larva. In this and subsequent graphs, each open circle represents the quantity scored at an individual muscle; solid diamonds are the average of these counts for each larva, grouped by color; bars represent larval mean ± SEM; n(N) = number of larvae (number of muscles scored). "+" denotes two data points (y = 65 and 77) that fall outside of the *y*-axis range. The number of terminal boutons is statistically reduced compared to its driver-specific $spastin^{5.75}$ control only when $Pak3^{RNAi}$ is expressed in glia or subperineurial glia. When compared to the $spastin^{5.75}$ control, $Pak3^{RNAi}$ alleviates the *spastin* mutant phenotype if expressed ubiquitously, in all glia, or in subperineurial glia ($p = 0.02$). Statistical significance is calculated by Student's *t*-test; asterisks signify $p \leq 0.001$ (***), $0.001 < p \leq 0.01$ (**), or $0.01 < p \leq 0.05$ (*).

any conclusions regarding a role for trachea using this tissue-specific knockdown approach since the *btl-GAL4* transgene alone with $spastin^{5.75}$ had near-wild type morphology (**Figures 2I,J**). Regardless, together with the Pak3 expression pattern, these data substantiate glia as the major cell type in which Pak3 acts to cause neuronal defects when *spastin* is lost.

Pak3 Acts in the Subperineurial Glia

The *Drosophila* nervous system includes multiple glial cell types, each with distinct functions that bear striking molecular and behavioral parallels to vertebrate glial subtypes (reviewed in Freeman, 2015; Yildirim et al., 2019). Motor axons projecting from the larval VNC to the NMJ are ensheathed by three layers of glia. The outermost, perineurial glial (PG) layer, and middle, subperineurial glia (SPG) layer, effectively shield the axons from their surroundings, just as they do in the CNS where, as the "surface glia" (at least some of which express Pak3, see **Figure 1**), they form the blood-brain-barrier. The innermost layer, the wrapping glia, directly contact individual axons and mediate their homeostasis. All three layers ensheathe the motor axons along their lengths, typically ending at or near the first synaptic bouton at the NMJ. Beyond this point, the perineurial and subperineurial, but not wrapping, glial layers extend dynamic, actin-based processes that interact with synaptic arbors at the NMJ (Fuentes-Medel et al., 2009; Brink et al., 2012). We found that expression of $Pak3^{RNAi}$ using the subperineurial-specific glia driver *gliotactin (gli)-GAL4* (Sepp et al., 2000) rescued the *spastin* mutant phenotype as effectively as *repo-GAL4* or *e22c,sqh-GAL4*, reducing terminal bouton number by 35% and restoring wild type morphology (**Figures 2G,J**; $p = 5.7 \times 10^{-3}$ for *gli-GAL4, spas* vs. *gli-GAL4 > $Pak3^{RNAi}$, spas*). Subperineurial glia can therefore account for the majority of $spastin^{5.75}$ rescue conferred by *Pak3* loss, supporting the idea that neuronal damage due to *spastin* loss requires Pak3 in the SPG.

SPG Projections Depend on Pak3 and Are Enhanced in *spastin* Mutants

How might Pak3 in subperineurial glia damage neuronal synapses? One possibility is that deleterious effects are mediated by the SPG projections that interact with the synaptic arbor. Given that Pak3 promotes actin polymerization and that these glial projections are actin-rich (Brink et al., 2012), we predicted that neurotoxic Pak3 in *spastin* mutants would be reflected in enhanced numbers of these glial projections. We used *gli-GAL4* driven-expression of *UAS-mCD8::GFP* to visualize SPG membranes (**Figures 3A–D**, green) and anti-HRP immunostaining to label neurons (magenta) in (**Figure 3A**) wild type, (**Figure 3B**) $Pak3^{Df}/Pak3^{d02472}$ mutant, (**Figure 3C**) $spastin^{5.75}$ mutant, or (**Figure 3D**) the $Pak3^{Df}/Pak3^{d02472}$, $spastin^{5.75}$ double mutant backgrounds. These animals were dissected in physiological levels of Ca^{2+} since glial projections are highly Ca^{2+}-sensitive (Brink et al., 2012). Gliopods (long, thin projections) and gliobulbs (rounded, resembling a bouton) were scored separately, but no genotype-dependent changes were observed between the two morphologies so they were combined. In the control background ("*gli > GFP* control" in **Figure 3A**), we observed on average 10 terminal boutons (**Figure 3F**) and a single SPG projection (**Figure 3G**) per muscle 4. Glial projections in $Pak3^{Df}/Pak3^{d02472}$ loss of function animals were rarer, averaging only one projection for every 5 muscles scored (**Figures 3B,G**; $p = 0.017$ compared to controls). This demonstrated that Pak3 is generally required for the formation of SPG projections (**Figure 3G**), but that these projections are not required for normal synaptic bouton arbors, which were no different from controls (**Figure 3F**, $p = 0.97$). In contrast, $spastin^{5.75}$ mutants had twice as many projections compared to controls (**Figures 3C,G**; $p = 0.011$), consistent with increased Pak3-mediated glial activity when *spastin* is lost, and correlating with the increase in average terminal bouton numbers (**Figures 3C,F**; $p = 8.0 \times 10^{-3}$). Animals deficient for both *spastin* and *Pak3* had near-wild type bouton numbers as expected (**Figures 3D,F**; $p = 0.87$), and similar to the *Pak3* mutant alone, glial projections were virtually absent (**Figures 3D,G**; $p > 0.99$). Thus, SPG projections depend on Pak3, are enhanced in *spastin* mutants, which have aberrant synaptic arbors, and are sparse in *Pak3, spastin* double mutants, which have normal synaptic arbors.

Given that Pak3 in SPG is necessary for *spastin* mutant synapses, we asked whether overexpression of *Pak3* in wild type SPG is sufficient to elicit synaptic defects characteristic of *spastin* loss. *Pak3* was overexpressed in GFP-labeled SPG using *gli-GAL4* to drive expression of *UAS-Pak3* and *UAS-mCD8::GFP* in an otherwise wild type background. *UAS-Pak3* induces actin-rich projections in the synaptic bouton arbor when overexpressed in neurons (Ozdowski et al., 2011) and rescues adult lethality in *Pak3* loss of function animals (E.F.O. unpublished results). *Pak3* overexpression in SPG induced small boutons like those seen in *spastin* mutants (**Figure 3E**), but did not significantly increase terminal bouton number (**Figure 3F**, $p = 0.21$ compared to controls) or alter glial projections (**Figures 3E,G**; $p > 0.99$). Closer examination of the relationship between terminal bouton and glial projection numbers at individual muscles confirmed an absence of synapse-specific correlation between neuronal boutons and glial projections in wild type as well as *spastin* loss of function animals (Pearson's correlation coefficient $r_{wildtype} = -0.06$ and $r_{spastin} = -0.2$), despite their strong association on average. While this could suggest that SPG projections are simply an epiphenomenon, their intimate association with the NMJ and role in sculpting synaptic arbors (Fuentes-Medel et al., 2009) argue for their functional relevance in this context.

Pak3-Mediated Toxicity Shows Specificity to *spastin* Loss

The striking efficacy of *Pak3* removal in suppressing defects due to *spastin* loss suggested that Pak3-mediated changes in glial behavior might be a common mechanism underlying neuronal dysfunction. To test this possibility, we investigated genetic mutants in *flower* (*fwe*), which like *spastin* mutants, exhibit small, highly branched, supernumerary boutons (**Figure 4**; Yao et al., 2009, 2017). Mutants bearing these morphological hallmarks are thought to be functionally related, most likely in aspects of endosomal cycling (Dickman et al., 2006), and we reasoned that

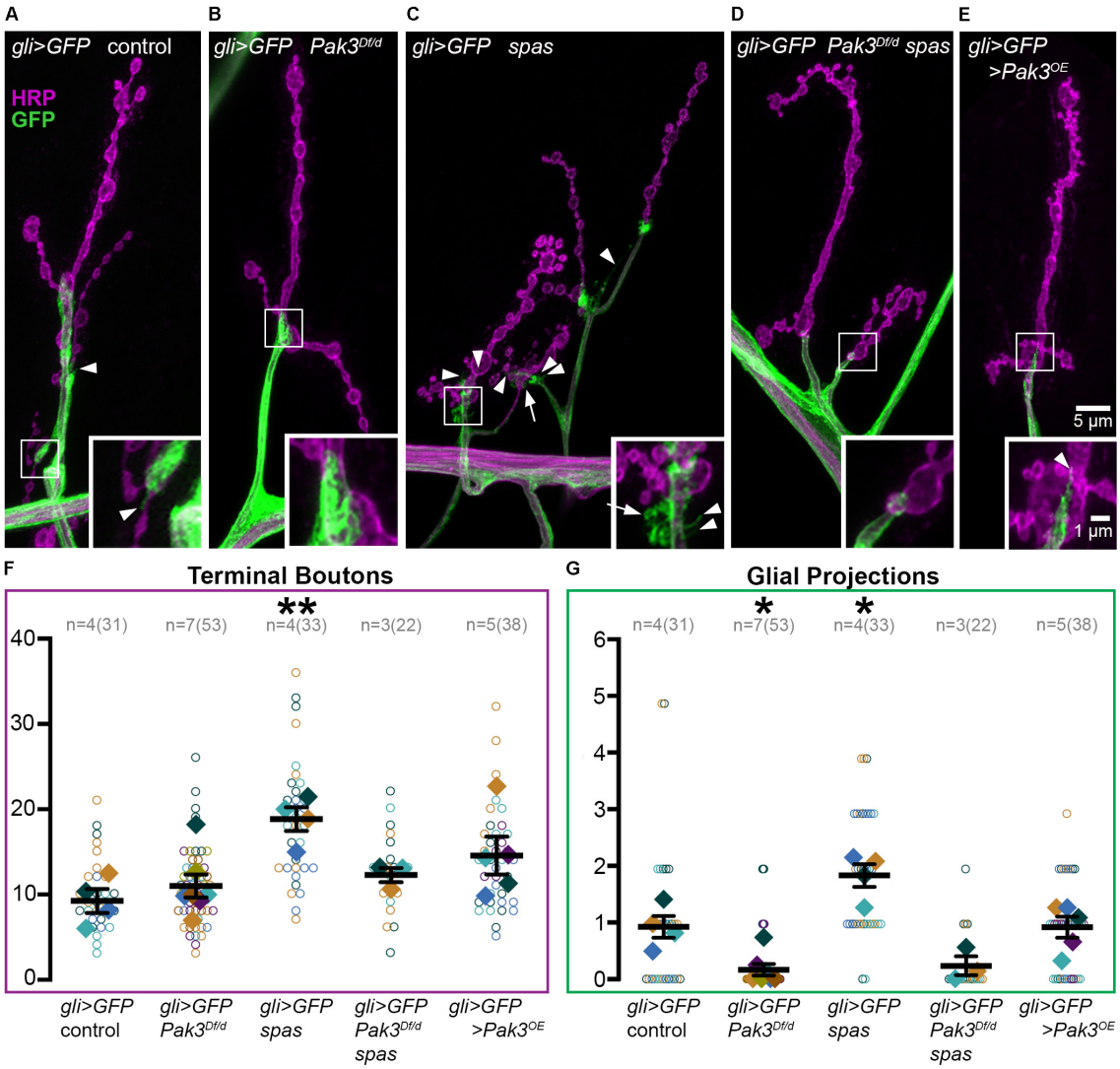

FIGURE 3 | Subperineurial glia projections depend on Pak3 and are doubled in *spastin* mutants. **(A–E)** Anti-HRP shows neuronal morphology in magenta, anti-GFP shows glial morphology in green. **(A)** *gli-GAL4, UAS-mCD8::GFP* (*gli > GFP*) controls have linearly arrayed synaptic boutons and average one glial projection (arrowhead) per muscle 4. **(B)** *Pak3* loss of function mutants, *gli > GFP*; $Pak3^{Df}/Pak3^{d02472}$ (abbreviated "$Pak3^{Df/d}$") have similarly arrayed bouton arbors but very few glial projections. **(C)** $spastin^{5.75}$ loss of function, *gli > GFP*; *spas*, causes extra glial projections in addition to extra terminal boutons. These projections include thin glial filopodia (arrowheads) and round glial projections (arrows). **(D)** Consistent with these extra glial projections requiring Pak3 function, *gli > GFP*; $Pak3^{Df}$, *spas*/$Pak3^{d02472}$, *spas* double mutants display few glial projections, and have wild type bouton arbors. **(E)** Overexpression of *Pak3* in subperineurial glia does not affect glial projections or terminal bouton numbers compared to controls, although small, clustered terminal boutons are observed. **(F,G)** Graphs of individual (open circles) and averaged (solid diamonds) values per larva for terminal boutons **(F)** and glial projections **(G)** are shown for each of the genotypes in **(A–E)**. Significant differences relative to gli > GFP controls are calculated by one-way ANOVA followed by Sidak's multiple comparisons test. *P*-values are denoted as * for $0.01 < p \leq 0.05$, and ** for $0.001 < p \leq 0.01$.

functionally related proteins are more likely to have conserved regulatory mechanisms. We compared the NMJs of trans-heterozygous loss of function mutants in *fwe* (fwe^{DB56}/fwe^{DB25}) with and without *Pak3* loss of function, and found no rescue of terminal bouton number or overall morphology of *fwe* mutants with *Pak3* loss (compare **Figures 4C,D**; $p = 0.96$). Loss of *Pak3* in SPG thus does not act as a non-specific suppressor of synaptic defects; rather, its rescuing role is specific, at least in part, to the sequelae of *spastin* loss.

DISCUSSION

Through an unbiased, forward genetic screen for modifiers of Spastin activity, we previously showed that the actin regulator Pak3 is required for the manifestation of morphological and functional synaptic defects due to *spastin* loss (Ozdowski et al., 2011). Here, we have determined that Pak3 functions in larval subperineurial glia cells, where it promotes projections that extend into the NMJ synaptic arbor. The SPG projections are

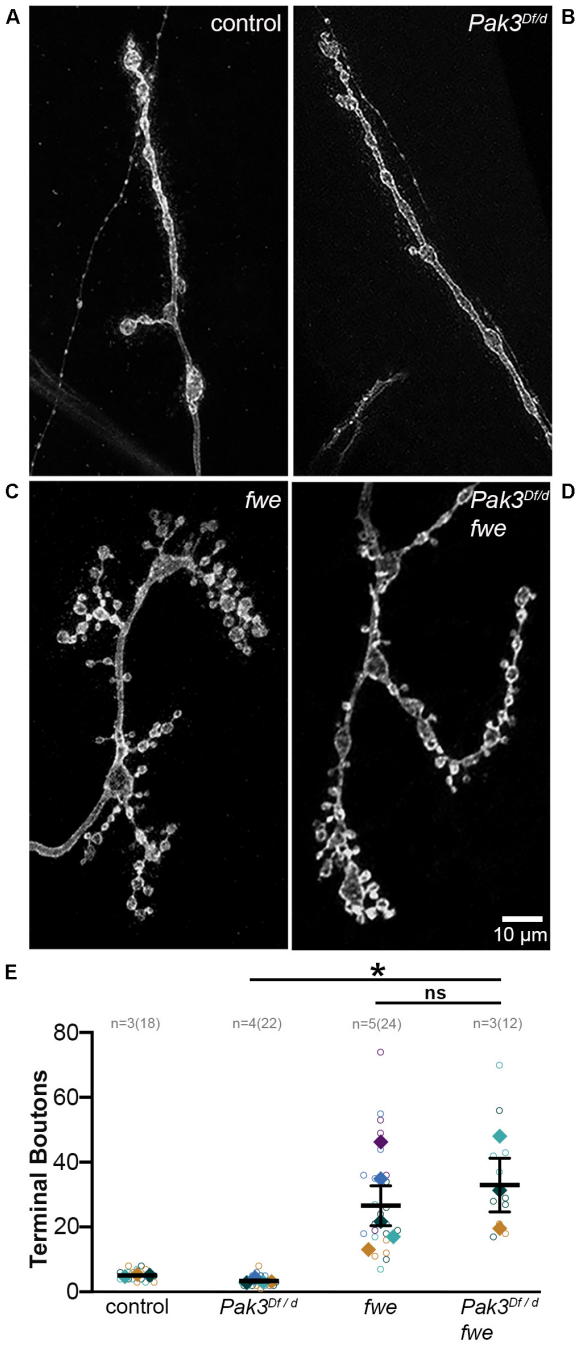

FIGURE 4 | *Pak3* loss of function does not rescue all supernumerary bouton mutants. **(A–D)** Anti-HRP staining shows neuronal morphology at the NMJ. **(A)** Wild type synaptic boutons are arrayed linearly with only a few branches and **(B)** *Pak3* loss of function mutants, $Pak3^{Df}/Pak3^{d02472}$, show no differences from wild type. **(C)** Loss of function mutations in *flower* (fwe^{DB56}/fwe^{DB25}) result in extreme branching of the neuronal arbor and small bouton size, similar to *spastin* mutant morphology. **(D)** Loss of *Pak3* function does not rescue the supernumerary bouton phenotype in *fwe* mutants, indicating that *Pak3* loss is not a generalized mechanism to reduce extra synaptic branching. **(E)** Individual terminal bouton numbers (open circles) and larval averages (solid diamonds) are shown for each of the genotypes in **(A–D)**. Significant differences are calculated by one-way ANOVA and Sidak's multiple comparisons test. * denotes $0.01 < p \leq 0.05$.

highly dependent on Pak3, whether in wild type animals, where these glia serve supportive roles in synaptic development (e.g., Fuentes-Medel et al., 2009, 2012), or in *spastin* mutants, where the projections are twice as frequent and synapses are defective.

The ability of *Pak3* loss to suppress *spastin* mutant defects suggests that Pak3-dependent glial projections are a critical aspect of SPG toxicity when *spastin* is lost. Excess glial projections could, for example, reflect phagocytic behavior gone awry, given that wild type projections positively regulate synaptic arbor morphology through this mechanism (Fuentes-Medel et al., 2009). Indeed, these phagocytic engulfment events, mediated by the Draper receptor, have been shown to play both neuroprotective and neurodegenerative roles in the CNS, depending on context (reviewed in Logan, 2017; Hilu-Dadia and Kurant, 2019). Whether SPG projections in *spastin* mutants have analogous functions remains to be determined, however, particularly given the lack of correlation we observed between synaptic bouton and SPG morphologies at individual NMJs in both wild type and mutant animals. Even with rapid dissection, it is possible that our fixed preparations fail to accurately capture the distribution of these dynamic glial structures and their precise relationship to associated synaptic boutons. Additionally, glial projections may represent only a subset of Pak3-mediated changes within SPG cells contributing to the *spastin* mutant phenotype. Finally, while Pak3 in SPG is required for the *spastin* mutant phenotype, other cell types may also be involved. We do not yet know whether *spastin* loss affects perineurial glia behavior, for example, or the underlying muscle or adjacent trachea, all of which have been shown to interact with the presynaptic arbor (Fuentes-Medel et al., 2009; Brink et al., 2012; Chen et al., 2019).

In addition to defining the contribution of these additional cell types, future experiments will be important to determine whether Pak3 is altered in response to *spastin* loss within the same SPG cells, or if changes in Pak3 are induced cell non-autonomously. Our earlier results used tissue-specific rescue to demonstrate that *spastin* is primarily required in neurons (Sherwood et al., 2004; Du et al., 2010), and expression studies in mouse and human also support this neuron-specific requirement (Ma et al., 2006). If so, this argues for a model in which *spastin*-deficient neurons send a signal that leads to Pak3 upregulation in SPG, and subsequent deleterious effects on synaptic boutons. Given that our neuron-specific rescue of the *spastin* phenotype was incomplete, however, we cannot rule out roles for Spastin in other cells (Sherwood et al., 2004). *Spastin* RNAi has been ineffective in our hands, and neither antibodies nor promoter-*GAL4* lines have convincingly revealed its endogenous expression pattern in *Drosophila*. However, Spastin expression has been shown via Western blots in normal human primary cerebellar astrocytes, glioblastoma cells, and rodent reactive astrocytes, consistent with possible roles in non-neuronal cell types and specifically glia (Ma et al., 2006; Draberova et al., 2011; Havlicek et al., 2014).

Although they remain the "support cells" of the nervous system, the idea that glia can also induce neuronal toxicity, particularly in the context of other defects, is increasingly evident. In flies, the requirement for Pak3 to elicit neuronal dysfunction during *spastin* loss bears striking parallels to the glial-derived,

prodegenerative signaling molecule Eiger (the mammalian TNF-α ortholog; Keller et al., 2011). Neither protein is required for normal synapse development; rather, it is their glial deployment in mutant contexts (Pak3 in *spastin* mutants, Eiger in *ankyrin* mutants), that promotes neuronal dysfunction. Our inability to generate excess glial projections or significantly alter bouton number by overexpressing *Pak3* in wild type animals supports, additionally, that activation of these glial pathways is only damaging to neurons in specific mutant contexts. Conversely, as seen with the *fwe* experiment, absence of these proteins does not serve as a generalized mechanism by which even potentially related synaptic defects can be rescued.

Dramatic changes in glial morphology and behavior, from non-reactive to reactive states, are also observed in mammalian nervous systems in response to damage (reviewed in Liddelow and Barres, 2017). Ischemic versus inflammatory insults induce distinct forms of reactive astrocytes; while ischemic damage leads to "A2" reactive astrocytes that support repair and survival, neuroinflammatory insults induce "A1" reactive astrocytes that are toxic to synapses. These A1 reactive astrocytes are now thought to play causal roles in the progression of several neurodegenerative diseases including ALS, Alzheimer's, Parkinson's, and Huntington's. Our results suggest that AD-HSP is also a candidate for this list, and that putative reactive glial behavior could be mediated by excess Pak activity. *Drosophila* Pak3 bears considerable amino acid identity and functional correspondence to the vertebrate group 1 Paks (Mentzel and Raabe, 2005), which are extensively studied for their roles in several cancers and actively targeted in drug development (reviewed in Rane and Minden, 2019). Should evidence for a Pak-mediated reactive glial mechanism be revealed in AD-HSP, the group I Paks will be promising targets for therapeutic intervention.

DATA AVAILABILITY STATEMENT

The raw data supporting the conclusions of this article will be made available by the authors, without undue reservation, to any qualified researcher.

AUTHOR CONTRIBUTIONS

EO and NS contributed to the conception and experimental design. JW, SE, and HA generated and characterized genetic tools, including the efficacy of GAL4 drivers and RNAi lines, and obtained pilot data on bouton and glial phenotypes. EO performed dissections and immunofluorescence with anti-Pak3, -Slit, -Elav, and -GFP, and quantified adult eclosion rates, boutons for the *fwe* mutant experiment, and glial projections. EO, NS, and HA performed genetic crosses, larval dissections, immunofluorescence, acquired confocal images, and performed statistics on numeric data for the tissue-specific RNAi experiments. NS wrote the first draft of the manuscript. EO compiled the figures and figure legends and contributed to manuscript revision. All authors read and approved the written work.

FUNDING

This work was enabled by generous funding from the Shepard Broad Foundation, Raquelle de la Rocha, and the GT-Hele Fund. Publication costs were supported by the Duke University Libraries' Compact for Open Access Publishing Equity (COPE) Fund to remove cost barriers in making Duke research open.

ACKNOWLEDGMENTS

We are grateful to Buzz Baum, Sami Bahri, Marc Freeman, Vanessa Auld, Hugo Bellen, Mark Metzstein, and Donald Fox for generously sharing reagents and fly stocks, as well as to Nicole Fox, Jaeda Coutinho-Budd, and Eric Monson for helpful discussions. We thank former lab members, particularly Charlene Chen, Caitlin Cristante, and Daniel Ren for their assistance with the *fwe* mutant experiments. Additional stocks were obtained from the Bloomington Drosophila Stock Center (NIH P40OD018537), National Institute of Genetics (NIG-FLY, Japan), Kyoto Drosophila Genomics and Genetics Resources (DGGR, Kyoto Institute of Technology), and the Vienna Drosophila Resource Center (VDRC, www.vdrc.at). Monoclonal antibodies were obtained from the Developmental Studies Hybridoma Bank, created by the NICHD of the NIH and maintained at The University of Iowa, Department of Biology. Duke's Light Microscopy Core Facility, the D. Sherwood lab, and E. Spana provided valuable microscopy support.

SUPPLEMENTARY MATERIAL

The Supplementary Material for this article can be found online at: https://www.frontiersin.org/articles/10.3389/fnins.2020.00912/full#supplementary-material

FIGURE S1 | Ubiquitous or glial-specific $Pak3^{RNAi}$ expression in wild type versus *spastin* mutant backgrounds suppresses the effects of *spastin* mutation. From left to right: Loss of *spastin* in Controls induces a nearly twofold increase in total bouton number (left two genotypes), and this effect is not altered by the presence of the $Pak3^{RNAi}$ transgene (next two genotypes). Ubiquitous $Pak3^{RNAi}$ expression makes larval synapses resistant to *spastin* removal, as bouton numbers in wild type (left; *e,sqh > Pak3[RNAi]*) and *spastin* mutant (right; *e,sqh > Pak3[RNAi],spas*) backgrounds are not significantly different. Neither neuron- nor muscle-specific $Pak3^{RNAi}$ expression suppress supernumerary boutons in *spastin* mutants. These results are consistent with those of **Figure 2**. The effects of tracheal $Pak3^{RNAi}$ expression are inconclusive, as the *btl-GAL4* driver alone may suppress the *spastin* mutant phenotype independent of *Pak3* (see **Figure 2**). Statistical significance is determined by Student's *t*-test. *P*-values are denoted as ns for $p > 0.05$, * for $0.01 < p \leq 0.05$, ** for $0.001 < p \leq 0.01$, and *** for $p \leq 0.001$.

FIGURE S2 | Expression of two different *Pak3* RNAi transgenes, and use of a different pan-neuronal driver, independently support alleviation the *spastin* mutant phenotype by glial, and not neuronal, *Pak3* knockdown. Simultaneous pan-neuronal expression of the $Pak3^{GL0028}$ and $Pak3^{v39844}$ RNAi transgenes ("*Pak3[2xRNAi]*") does not alleviate supernumerary boutons of *spastin* mutants ($p = 0.32$ compared to paired control). The neuronal driver used in these experiments is $elav^{C155}$*-GAL4* rather than *nsyb-GAL4*; *Dcr2* was also expressed to increase RNAi efficacy. In contrast, pan-glial expression of these *Pak3* RNAi transgenes has the same effect as $Pak3^{NIG.14895R-2}$ RNAi expression (from **Figure 2** and **Supplementary Figure S1**), reducing terminal bouton number in *spastin* mutants to wild type levels ($p = 1.3 \times 10^{-3}$; Student's *t*-test).

REFERENCES

Allison, R., Edgar, J. R., and Reid, E. (2019). Spastin MIT domain disease-associated mutations disrupt lysosomal function. *Front. Neurosci.* 13:1179. doi: 10.3389/fnins.2019.01179

Asano, Y., Jimenez-Dalmaroni, A., Liverpool, T. B., Marchetti, M. C., Giomi, L., Kiger, A., et al. (2009). Pak3 inhibits local actin filament formation to regulate global cell polarity. *HFSP J.* 3, 194–203. doi: 10.2976/1.3100548

Baek, S. H., Cho, H. W., Kwon, Y. C., Lee, J. H., Kim, M. J., Lee, H., et al. (2012). Requirement for Pak3 in Rac1-induced organization of actin and myosin during *Drosophila* larval wound healing. *FEBS Lett.* 586, 772–777. doi: 10.1016/j.febslet.2012.01.061

Bahri, S., Wang, S., Conder, R., Choy, J., Vlachos, S., Dong, K., et al. (2010). The leading edge during dorsal closure as a model for epithelial plasticity: pak is required for recruitment of the Scribble complex and septate junction formation. *Development* 137, 2023–2032. doi: 10.1242/dev.045088

Brink, D. L., Gilbert, M., Xie, X., Petley-Ragan, L., and Auld, V. J. (2012). Glial processes at the *Drosophila* larval neuromuscular junction match synaptic growth. *PLoS One* 7:e37876. doi: 10.1371/journal.pone.0037876

Chang, C. L., Weigel, A. V., Ioannou, M. S., Pasolli, H. A., Xu, C. S., Peale, D. R., et al. (2019). Spastin tethers lipid droplets to peroxisomes and directs fatty acid trafficking through ESCRT-III. *J. Cell. Biol.* 218, 2583–2599. doi: 10.1083/jcb.201902061

Chen, P. Y., Tsai, Y. W., Cheng, Y. J., Giangrande, A., and Chien, C. T. (2019). Glial response to hypoxia in mutants of NPAS1/3 homolog Trachealess through Wg signaling to modulate synaptic bouton organization. *PLoS Genet.* 15:e1007980. doi: 10.1371/journal.pgen.1007980

Collins, C. A., and DiAntonio, A. (2007). Synaptic development: insights from *Drosophila*. *Curr. Opin. Neurobiol.* 17, 35–42. doi: 10.1016/j.conb.2007.01.001

Dickman, D. K., Lu, Z., Meinertzhagen, I. A., and Schwarz, T. L. (2006). Altered synaptic development and active zone spacing in endocytosis mutants. *Curr. Biol.* 16, 591–598. doi: 10.1016/j.cub.2006.02.058

Draberova, E., Vinopal, S., Morfini, G., Liu, P. S., Sladkova, V., Sulimenko, T., et al. (2011). Microtubule-severing ATPase spastin in glioblastoma: increased expression in human glioblastoma cell lines and inverse roles in cell motility and proliferation. *J. Neuropathol. Exp. Neurol.* 70, 811–826. doi: 10.1097/NEN.0b013e31822c256d

Du, F., Ozdowski, E. F., Kotowski, I. K., Marchuk, D. A., and Sherwood, N. T. (2010). Functional conservation of human Spastin in a *Drosophila* model of autosomal dominant-hereditary spastic paraplegia. *Hum. Mol. Genet.* 19, 1883–1896. doi: 10.1093/hmg/ddq064

Duan, R., Jin, P., Luo, F., Zhang, G., Anderson, N., and Chen, E. H. (2012). Group I PAKs function downstream of Rac to promote podosome invasion during myoblast fusion in vivo. *J. Cell. Biol.* 199, 169–185. doi: 10.1083/jcb.201204065

Felix, M., Chayengia, M., Ghosh, R., Sharma, A., and Prasad, M. (2015). Pak3 regulates apical-basal polarity in migrating border cells during *Drosophila oogenesis*. *Development* 142, 3692–3703. doi: 10.1242/dev.125682

Franke, J. D., Montague, R. A., and Kiehart, D. P. (2005). Nonmuscle myosin II generates forces that transmit tension and drive contraction in multiple tissues during dorsal closure. *Curr. Biol.* 15, 2208–2221. doi: 10.1016/j.cub.2005.11.064

Freeman, M. R. (2015). *Drosophila* central nervous system glia. *Cold Spring Harb Perspect Biol* 7:a020552. doi: 10.1101/cshperspect.a020552

Fuentes-Medel, Y., Ashley, J., Barria, R., Maloney, R., Freeman, M., and Budnik, V. (2012). Integration of a retrograde signal during synapse formation by glia-secreted TGF-beta ligand. *Curr. Biol.* 22, 1831–1838. doi: 10.1016/j.cub.2012.07.063

Fuentes-Medel, Y., Logan, M. A., Ashley, J., Ataman, B., Budnik, V., and Freeman, M. R. (2009). Glia and muscle sculpt neuromuscular arbors by engulfing destabilized synaptic boutons and shed presynaptic debris. *PLoS Biol.* 7:e1000184. doi: 10.1371/journal.pbio.1000184

Havlicek, S., Kohl, Z., Mishra, H. K., Prots, I., Eberhardt, E., Denguir, N., et al. (2014). Gene dosage-dependent rescue of HSP neurite defects in SPG4 patients' neurons. *Hum. Mol. Genet.* 23, 2527–2541. doi: 10.1093/hmg/ddt644

Hazan, J., Fonknechten, N., Mavel, D., Paternotte, C., Samson, D., Artiguenave, F., et al. (1999). Spastin, a new AAA protein, is altered in the most frequent form of autosomal dominant spastic paraplegia. *Nat. Genet.* 23, 296–303. doi: 10.1038/15472

Hilu-Dadia, R., and Kurant, E. (2019). Glial phagocytosis in developing and mature *Drosophila* CNS: tight regulation for a healthy brain. *Curr. Opin. Immunol.* 62, 62–68. doi: 10.1016/j.coi.2019.11.010

Jenett, A., Rubin, G. M., Ngo, T. T., Shepherd, D., Murphy, C., Dionne, H., et al. (2012). A GAL4-driver line resource for *Drosophila* neurobiology. *Cell. Rep.* 2, 991–1001. doi: 10.1016/j.celrep.2012.09.011

Jeong, B., Kim, T. H., Kim, D. S., Shin, W. H., Lee, J. R., Kim, N. S., et al. (2019). Spastin contributes to neural development through the regulation of microtubule dynamics in the primary cilia of neural stem cells. *Neuroscience* 411, 76–85. doi: 10.1016/j.neuroscience.2019.05.024

Kasher, P. R., De Vos, K. J., Wharton, S. B., Manser, C., Bennett, E. J., Bingley, M., et al. (2009). Direct evidence for axonal transport defects in a novel mouse model of mutant spastin-induced hereditary spastic paraplegia (HSP) and human HSP patients. *J. Neurochem.* 110, 34–44. doi: 10.1111/j.1471-4159.2009.06104.x

Keller, L. C., Cheng, L., Locke, C. J., Muller, M., Fetter, R. D., and Davis, G. W. (2011). Glial-derived prodegenerative signaling in the *Drosophila* neuromuscular system. *Neuron* 72, 760–775. doi: 10.1016/j.neuron.2011.09.031

Kumar, R., Sanawar, R., Li, X., and Li, F. (2017). Structure, biochemistry, and biology of PAK kinases. *Gene* 605, 20–31. doi: 10.1016/j.gene.2016.12.014

Kuo, Y. W., Trottier, O., Mahamdeh, M., and Howard, J. (2019). Spastin is a dual-function enzyme that severs microtubules and promotes their regrowth to increase the number and mass of microtubules. *Proc. Natl. Acad. Sci. U.S.A.* 116, 5533–5541. doi: 10.1073/pnas.1818824116

Lee, T., and Luo, L. (1999). Mosaic analysis with a repressible cell marker for studies of gene function in neuronal morphogenesis. *Neuron* 22, 451–461. doi: 10.1016/s0896-6273(00)80701-1

Liddelow, S. A., and Barres, B. A. (2017). Reactive astrocytes: production, function, and therapeutic potential. *Immunity* 46, 957–967. doi: 10.1016/j.immuni.2017.06.006

Logan, M. A. (2017). Glial contributions to neuronal health and disease: new insights from *Drosophila*. *Curr. Opin. Neurobiol.* 47, 162–167. doi: 10.1016/j.conb.2017.10.008

Lord, S. J., Velle, K. B., Mullins, R. D., and Fritz-Laylin, L. K. (2020). SuperPlots: communicating reproducibility and variability in cell biology. *J. Cell. Biol.* 219:e202001064. doi: 10.1083/jcb.202001064

Lumb, J. H., Connell, J. W., Allison, R., and Reid, E. (2012). The AAA ATPase spastin links microtubule severing to membrane modelling. *Biochim. Biophys. Acta* 1823, 192–197. doi: 10.1016/j.bbamcr.2011.08.010

Ma, D. L., Chia, S. C., Tang, Y. C., Chang, M. L., Probst, A., Burgunder, J. M., et al. (2006). Spastin in the human and mouse central nervous system with special reference to its expression in the hippocampus of mouse pilocarpine model of status epilepticus and temporal lobe epilepsy. *Neurochem. Int.* 49, 651–664. doi: 10.1016/j.neuint.2006.05.008

Mentzel, B., and Raabe, T. (2005). Phylogenetic and structural analysis of the *Drosophila melanogaster* p21-activated kinase DmPAK3. *Gene* 349, 25–33. doi: 10.1016/j.gene.2004.12.030

Oliva, C., Soldano, A., Mora, N., De Geest, N., Claeys, A., Erfurth, M. L., et al. (2016). Regulation of *Drosophila* brain wiring by neuropil interactions via a slit-robo-RPTP signaling complex. *Dev. Cell.* 39, 267–278. doi: 10.1016/j.devcel.2016.09.028

Ozdowski, E. F., Gayle, S., Bao, H., Zhang, B., and Sherwood, N. T. (2011). Loss of *Drosophila melanogaster* p21-activated kinase 3 suppresses defects in synapse structure and function caused by spastin mutations. *Genetics* 189, 123–135. doi: 10.1534/genetics.111.130831

Papadopoulos, C., Orso, G., Mancuso, G., Herholz, M., Gumeni, S., Tadepalle, N., et al. (2015). Spastin binds to lipid droplets and affects lipid metabolism. *PLoS Genet.* 11:e1005149. doi: 10.1371/journal.pgen.1005149

Park, S. H., Zhu, P. P., Parker, R. L., and Blackstone, C. (2010). Hereditary spastic paraplegia proteins REEP1, spastin, and atlastin-1 coordinate microtubule interactions with the tubular ER network. *J. Clin. Invest.* 120, 1097–1110. doi: 10.1172/JCI40979

Rane, C. K., and Minden, A. (2019). P21 activated kinase signaling in cancer. *Semin. Cancer Biol.* 54, 40–49. doi: 10.1016/j.semcancer.2018.01.006

Ribeiro, S. A., D'Ambrosio, M. V., and Vale, R. D. (2014). Induction of focal adhesions and motility in *Drosophila* S2 cells. *Mol. Biol. Cell.* 25, 3861–3869. doi: 10.1091/mbc.E14-04-0863

Semenova, G., and Chernoff, J. (2017). Targeting PAK1. *Biochem. Soc. Trans.* 45, 79–88. doi: 10.1042/BST20160134

Sepp, K. J., Schulte, J., and Auld, V. J. (2000). Developmental dynamics of peripheral glia in *Drosophila melanogaster*. *Glia* 30, 122–133. doi: 10.1002/(sici)1098-1136(200004)30:2<122::aid-glia2>3.0.co;2-b

Sepp, K. J., Schulte, J., and Auld, V. J. (2001). Peripheral glia direct axon guidance across the CNS/PNS transition zone. *Dev. Biol.* 238, 47–63. doi: 10.1006/dbio.2001.0411

Sherwood, N. T., Sun, Q., Xue, M., Zhang, B., and Zinn, K. (2004). *Drosophila* spastin regulates synaptic microtubule networks and is required for normal motor function. *PLoS Biol.* 2:e429. doi: 10.1371/journal.pbio.0020429

Shiga, Y., Tanaka-Matakatsu, M., and Hayashi, S. (1996). A nuclear GFP / beta-galactosidase fusion protein as a marker for morphogenesis in living *Drosophila*. *Dev. Growth Diff.* 38, 99–106. doi: 10.1046/j.1440-169x.1996.00012.x

Stone, M. C., Rao, K., Gheres, K. W., Kim, S., Tao, J., La Rochelle, C., et al. (2012). Normal spastin gene dosage is specifically required for axon regeneration. *Cell. Rep.* 2, 1340–1350. doi: 10.1016/j.celrep.2012.09.032

Tarrade, A., Fassier, C., Courageot, S., Charvin, D., Vitte, J., Peris, L., et al. (2006). A mutation of spastin is responsible for swellings and impairment of transport in a region of axon characterized by changes in microtubule composition. *Hum. Mol. Genet.* 15, 3544–3558. doi: 10.1093/hmg/ddl431

Trotta, N., Orso, G., Rossetto, M. G., Daga, A., and Broadie, K. (2004). The hereditary spastic paraplegia gene, spastin, regulates microtubule stability to modulate synaptic structure and function. *Curr. Biol.* 14, 1135–1147. doi: 10.1016/j.cub.2004.06.058

Vemu, A., Szczesna, E., Zehr, E. A., Spector, J. O., Grigorieff, N., Deaconescu, A. M., et al. (2018). Severing enzymes amplify microtubule arrays through lattice GTP-tubulin incorporation. *Science* 361:eaau1504. doi: 10.1126/science.aau1504

Wood, J. D., Landers, J. A., Bingley, M., McDermott, C. J., Thomas-McArthur, V., Gleadall, L. J., et al. (2006). The microtubule-severing protein Spastin is essential for axon outgrowth in the zebrafish embryo. *Hum. Mol. Genet.* 15, 2763–2771. doi: 10.1093/hmg/ddl212

Yao, C. K., Lin, Y. Q., Ly, C. V., Ohyama, T., Haueter, C. M., Moiseenkova-Bell, V. Y., et al. (2009). A synaptic vesicle-associated Ca2+ channel promotes endocytosis and couples exocytosis to endocytosis. *Cell* 138, 947–960. doi: 10.1016/j.cell.2009.06.033

Yao, C. K., Liu, Y. T., Lee, I. C., Wang, Y. T., and Wu, P. Y. (2017). A Ca2+ channel differentially regulates Clathrin-mediated and activity-dependent bulk endocytosis. *PLoS Biol.* 15:e2000931. doi: 10.1371/journal.pbio.2000931

Yildirim, K., Petri, J., Kottmeier, R., and Klambt, C. (2019). *Drosophila* glia: few cell types and many conserved functions. *Glia* 67, 5–26. doi: 10.1002/glia.23459

Conflict of Interest: The authors declare that the research was conducted in the absence of any commercial or financial relationships that could be construed as a potential conflict of interest.

frontiers in Neuroscience

ORIGINAL RESEARCH
published: 15 October 2020
doi: 10.3389/fnins.2020.547746

In vivo Analysis of CRISPR/Cas9 Induced Atlastin Pathological Mutations in *Drosophila*

Aldo Montagna[1†], Nicola Vajente[2,3†], Diana Pendin[2,3] and Andrea Daga[1*]*

[1] *Laboratory of Molecular Biology, Scientific Institute IRCCS E. Medea, Lecco, Italy,* [2] *Neuroscience Institute, Italian National Research Council, Padua, Italy,* [3] *Department of Biomedical Sciences, University of Padua, Padua, Italy*

The endoplasmic reticulum (ER) is a highly dynamic network whose shape is thought to be actively regulated by membrane resident proteins. Mutation of several such morphology regulators cause the neurological disorder Hereditary Sp astic Paraplegia (HSP), suggesting a critical role of ER shape maintenance in neuronal activity and function. Human Atlastin-1 mutations are responsible for SPG3A, the earliest onset and one of the more severe forms of dominant HSP. Atlastin has been initially identified in *Drosophila* as the GTPase responsible for the homotypic fusion of ER membrane. The majority of SPG3A-linked Atlastin-1 mutations map to the GTPase domain, potentially interfering with atlastin GTPase activity, and to the three-helix-bundle (3HB) domain, a region critical for homo-oligomerization. Here we have examined the *in vivo* effects of four pathogenetic missense mutations (two mapping to the GTPase domain and two to the 3HB domain) using two complementary approaches: CRISPR/Cas9 editing to introduce such variants in the endogenous atlastin gene and transgenesis to generate lines overexpressing atlastin carrying the same pathogenic variants. We found that all pathological mutations examined reduce atlastin activity *in vivo* although to different degrees of severity. Moreover, overexpression of the pathogenic variants in a wild type atlastin background does not give rise to the loss of function phenotypes expected for dominant negative mutations. These results indicate that the four pathological mutations investigated act through a loss of function mechanism.

Keywords: atlastin, mutation, CRISPR/Cas9, hereditary spastic paraplegia, endoplasmic reticulum, Golgi

OPEN ACCESS

Edited by:
Craig Blackstone, National Institute of Neurological Disorders and Stroke (NINDS), United States

Reviewed by:
Junjie Hu, Institute of Biophysics (CAS), China
Niamh C. O'Sullivan, University College Dublin, Ireland

***Correspondence:**
Andrea Daga
andrea.daga@gmail.com
Diana Pendin
diana.pendin@unipd.it;
diana.pendin@gmail.com

† These authors have contributed equally to this work

Specialty section:
This article was submitted to Neurodegeneration, a section of the journal Frontiers in Neuroscience

Received: *31 March 2020*
Accepted: *09 September 2020*
Published: *15 October 2020*

Citation:
Montagna A, Vajente N, Pendin D and Daga A (2020) In vivo Analysis of CRISPR/Cas9 Induced Atlastin Pathological Mutations in Drosophila. Front. Neurosci. 14:547746. doi: 10.3389/fnins.2020.547746

INTRODUCTION

Atlastin-1 is one of a three-member family of dynamin-like GTPases present in vertebrate genomes, however, single homologs of atlastin are present also in invertebrates, yeast and plants (Hu and Rapoport, 2016). The atlastins are membrane proteins, embedded in the endoplasmic reticulum (ER) bilayer, whose main function is to mediate ER homotypic membrane fusion, a process crucial for proper ER morphogenesis and maintenance (Hu and Rapoport, 2016). To date, however, this ability to promote fusion has been demonstrated exclusively for invertebrate atlastins (Orso et al., 2009; Anwar et al., 2012; Zhang et al., 2013; Wu et al., 2014). An involvement of atlastin in controlling Golgi morphology (Namekawa et al., 2007; Rismanchi et al., 2008; Chen et al., 2011; Behrendt et al., 2019) as well as in COPII formation (Niu et al., 2019) has also been proposed.

However, the former was based exclusively on overexpression experiments and the latter has been identified using a very specific mutation (R48A/R77A) capable of uncoupling fusion and tethering (Pendin et al., 2011; Niu et al., 2019).

Mutations in Atlastin-1 have been identified as the cause of SPG3A, an autosomal dominant form of hereditary spastic paraplegia (HSP; Zhao et al., 2001; Zhao and Liu, 2017). The HSPs are a group of clinically heterogeneous neurological disorders classified into "pure" or "complicated" on the basis of the clinical features (Blackstone, 2018; Shribman et al., 2019). The pure HSP is defined by progressive spasticity and weakness limited to the lower limbs, while the complicated HSP may include other neurological manifestations (Blackstone, 2018). Clinically, HSPs can also be classified into early onset (1st decade of life) and late onset (between the 2nd and 4th decade) type. The main pathological changes associated with HSP include the axonal degeneration of the corticospinal tracts and back column (Shribman et al., 2019). There are currently over 80 genes or genetic loci linked to HSP (Blackstone, 2018). *Atlastin-1*-linked SPG3A is the second most common type of HSP accounting for approximately 10% of the autosomal dominant forms. More than 60 different *ATL1* gene mutations have been described, mostly missense mutations but also a limited number of small deletions, small insertions, splice site mutations, and whole exon deletions (Blackstone, 2018). Nevertheless, the genotype-phenotype correlation remains utterly unclear (Zhao and Liu, 2017).

Because of atlastins role in ER morphogenesis, the simplest explanation for the axonal degeneration associated with *SPG3A*-HSP would be the reduced ability of Atlastin-1/SPG3A disease variants to catalyze ER membrane fusion thus impairing network formation and/or maintenance. Although fascinating, the demonstration that a reduction in the membrane fusion activity of Atlastin-1 may be the reason for HSP lacks decisive experimental support. Indeed, while the fly atlastin (Orso et al., 2009) and other orthologs in more distantly related organisms (Anwar et al., 2012; Zhang et al., 2013) have been shown to produce *in vitro* the fusion of synthetic lipid bilayers, the human proteins do not display this ability. Thus, assessment of fusion has relied on reproducing a few conserved Atlastin-1 disease variants in the *Drosophila* ortholog and testing them for *in vitro* fusion (Bian et al., 2011). In addition, other pathological mutants were analyzed biochemically for their ability to hydrolyze GTP and dimerize in a nucleotide-dependent manner (Byrnes and Sondermann, 2011; O'Donnell et al., 2018). These studies, however, were unable to uncover an obvious correlation between disease-causing mutations and fusion/biochemical activity of atlastin.

It is furthermore uncertain whether ER morphology defects are the cause of *SPG3A*-HSP. The main reason for this is dual. Suitable animal models for the disease are unavailable and imaging the complex structure of the neuronal ER *in vivo* within the tissue in order to determine morphological differences between wild type and mutant ER is challenging if not impossible. In any case, further investigation is needed to determine whether *Atlastin-1/SPG3A* mutations consistently perturb ER network structure.

A functional replacement assay demonstrated that exogenously introduced *Drosophila* atlastin was capable of functionally replacing human Atlastins in HeLa cells depleted of the endogenous proteins (Faust et al., 2015). However, assessment of conserved pathological mutations in the *Drosophila* ortholog on both ER morphogenesis in HeLa cells and membrane fusion catalysis *in vitro* did not provide a deeper understanding of genotype-phenotype correlation (Ulengin et al., 2015). On the basis of these findings it has been questioned whether impaired ER membrane fusion is the exclusive driver of *SPG3A*-HSP.

To gain insight into the mechanism of *SPG3A*-HSP and verify the importance of ER morphology in disease pathophysiology, we examined the *in vivo* effects of four conserved pathological mutations introduced in the atlastin fly homolog. We took advantage of CRISPR/Cas9-mediated genome editing to introduce four different pathological mutations, including the most common R214C (R239C in humans), into the *Drosophila* atlastin gene. We reasoned that this approach would generate the closest possible system to a *SPG3A* patient where an endogenous allele is mutated.

MATERIALS AND METHODS

Drosophila Stocks and Crosses

The UAS-Datlastin-myc and UAS-BiP-sfGFP-HDEL fly lines used in this study were described previously (Orso et al., 2009; Summerville et al., 2016). The Gal4 strains used were: tubulin-Gal4, elav-Gal4, D42-Gal4, and GMR-Gal4 obtained from Bloomington *Drosophila* Stock Center. To increase protein expression, experimental crosses were performed at 28°C, except for crosses with GMR-Gal4 which were performed at 25°C. Control genotypes included promoter-Gal4/+ individuals. Fly food was prepared using NUTRI-fly-IF mixture (Genesee Scientific), according to the manufacturer instructions.

Constructs and Transgenic Lines Generation

Drosophila atlastin cDNA cloned in pCDNA3.1 in frame with a myc tag (Pendin et al., 2011) was mutagenized using Stratagene kit for site-directed mutagenesis. Primer pairs were designed as follows:

R192Q: 5′-AGTTCCTCGTCCAGGACTGGAGCTT-3′

R214C: 5′-ATTCTGAAACGATGTCTGGAGGTGT-3′

C350R: 5′-GCTCATGGAGGAGGTGCGCGGTGGAACGCG GC-3′

M383T: 5′-GCCAAGCGCAAGACGGGTGGTGAGGA GTTC-3′

Transgenic fly lines for the expression of atlastin carrying each of the mutations were generated by subcloning mutated myc-atlastin cDNA in pUAST vector. The plasmids obtained were microinjected in w^{1118} flies, thus generating transgenic lines UAS-atlastin^{R192Q}, UAS-atlastin^{R214C}, UAS-atlastin^{C350R}, and UAS-atlastin^{M383T}.

Generation of CRISPR Mutants

CRISPR mutants were generated by microinjection (performed by BestGene Inc.) of two gRNAs, a 5′gRNA and a 3′gRNA, respectively, upstream and downstream of the atlastin gene fragment in the donor construct, cloned in the pCFD vector[1], and a donor DNA template for homologous recombination into the y^2 cho^2 v^1; attP40{nos-Cas9}/CyO strain (NIG-FLY stock #CAS-0001). Each donor DNA was constructed by Gibson assembly cloning in the BSSK(+) plasmid and contained a fragment of the *atlastin* gene carrying the desired pathological mutation and two flanking homology arms approximately 800 bp in length. The *atlastin* fragment was engineered to contain a novel *Eco*RI restriction site by silent mutagenesis for screening and identification of the mutant lines. Microinjected F_0 flies were crossed *en masse* to TM3,Sb/TM6B,Tb flies (#2537, Bloomington *Drosophila* Stock Center), then F_1 males were individually crossed to TM3,Sb/TM6B,Tb females. F_2 sisters and brothers carrying TM6B balancers were crossed to obtain single lines. The presence of the correct mutation was identified by PCR followed by *Eco*RI restriction digest and confirmed by Sanger sequencing.

Primers:

For 5′gRNA: CTTCGTTGAGCACAATGCTGTCCT;

Rev 5′gRNA: AAACAGGACAGCATTGTGCTCAAC;

For 3′gRNA: CTTCGCAACTGGAAGATGATCTTG;

Rev 3′gRNA: AAACCAAGATCATCTTCCAGTTGC;

For 5′homology region: ctatagggcgaattgggtaccAAAAGGAACAAATGAATAAGTG;

Rev 5′homology region: tgcactgaggACAGCATTGTGCTCAACG;

For atlastin: acaatgctgtCCTCAGTGCAGATATACAACC;

Rev atlastin: ttggtgaagaCCTCTTCAAGATCATCTTCC;

For 3′homology region: cttgaagaggTCTTCACCAACTACCAAGC;

Rev 3′homology region: tggatcccccgggctgcaggGATGCCAAGTCAAGTTGC.

Electron Microscopy

Larval brains were fixed in 4% paraformaldehyde and 2% glutaraldehyde and embedded as previously described (Orso et al., 2009). Electron microscopy (EM) images were acquired from thin sections under a FEI Tecnai-12 electron microscope at the DeBio imaging EM Facility (University of Padova). EM images of individual neurons for the measurement of the length of ER profiles were collected from three brains for each genotype. At least 40 neurons were analyzed for each genotype. Quantitative analyses of ER profiles length were performed with ImageJ software.

Confocal Images of Larval Brains

Brains and ventral ganglia from third instar larvae expressing BiP-sfGFP-HDEL alone or together with mutated atlastin were dissected in M1 medium (30 mM HEPES, 150 mM NaCl, 5 mM KCl, 1 mM $MgCl_2$, 35 mM sucrose, 5 glucose, and pH 7.2 at RT) containing 1 mM $CaCl_2$. Motor neuron cell bodies from freshly dissected brains were imaged on a Leica TCS SP5 II confocal microscope, equipped with a HCX PL APO lambda blue 63×/1.40–0.60 Oil objective or a PlanApo 100×/1.4 Oil objective using an Argon laser line (488 nm). Confocal microscopy imaging was performed at 1024 × 1024 pixels per image, with a 200 Hz acquisition rate.

[1]http://www.crisprflydesign.org/grna-expressionvectors/

HeLa Cells Transfection and Live Imaging

HeLa cells were cultured following standard protocols in DMEM (high glucose, from Merck) supplemented with fetal bovine serum (10%), L-glutamine (2 mM), penicillin (100 U/mL), and streptomycin (100 μg/mL). For fluorescence microscopy experiments, cells were plated on 18 mm coverslips and co-transfected when at 60% confluence with vectors for the expression of ER-sfGFP-3 (Addgene, plasmid #56482) and one of atlastin (wild type or mutated) plasmids (1 μg total DNA) using TransIT-LT1 transfection reagent (Mirus Bio LLC) according to the manufacturer procedures. 24 h after transfection, coverslips were mounted on an open top chamber thermostated at 37°C, covered with an extracellular-like medium (135 mM NaCl, 5 mM KCl, 1 mM $MgCl_2$, 0.4 mM KH_2PO_4, 20 mM HEPES, 11 mM glucose, and pH 7.4 at 37°C) and imaged on a Leica TCS SP5 II confocal microscope, equipped with a HCX PL APO lambda blue 63×/1.40–0.60 Oil objective or a PlanApo 100×/1.4 Oil objective using the Argon laser line (488 nm). Confocal microscopy imaging was performed at 1024 × 1024 pixels per image, with a 200 Hz acquisition rate.

Immunohistochemistry

CRISPR-mutations third-instar larvae raised at 25°C were harvested, dissected in PBS 1×, fixed in 4% paraformaldehyde for 15 min and washed twice in PBS containing 0.3% Triton X-100 (Sigma-Aldrich). Dissected larvae were probed with anti-GM130 (Abcam, ab30637, rabbit, 1:1000) overnight at 4°C, then washed 3 times with PBS plus 0.3% Triton X-100 and incubated with Alexa Fluor 555 anti-rabbit antibody (Molecular Probes Invitrogen, 1:500). Larvae were washed 3 times with PBS and mounted on coverslips using Mowiol (Sigma-Aldrich).

HeLa cells transfected as indicated above were fixed in PBS containing 4% paraformaldehyde for 15 min, incubated with 50 mM NH_4Cl for 20 min, permeabilized with 0.1% Triton X-100 in PBS for 3 min and then blocked with 2% BSA and 0.2% gelatin for 30 min. Antibodies used were anti-GM130 (BD, #610822, mouse, 1:1000); anti-TGN46 (Abcam, ab50595, rabbit, 1:200). Alexa Fluor 555 conjugated goat anti-mouse and Alexa Fluor 647 conjugated goat anti-rabbit (Molecular Probes Invitrogen) were applied for 1 h at room temperature. Coverslips were mounted using Mowiol (Sigma-Aldrich).

All confocal images were acquired using a Leica TCS SP5 II confocal microscope, equipped with a PlanApo 100×/1.4 Oil objective, using a 543 nm laser line. Confocal microscopy imaging was performed at 1024 × 1024 pixels per image, with a 200 Hz acquisition rate.

Protein Extraction and Western Blotting

Proteins were extracted from 20 fly heads expressing wild type or mutated atlastin under the control of the GMR-Gal4 promoter or from 20 brains extracted from CRISPR-mutant larvae. Heads or brains were placed in SDS-loading buffer, homogenized with a pestle and boiled for 5 min. Homogenates were cleared by centrifugation at 10,000 *g* for 5 min. Proteins were separated by SDS-PAGE, transferred into nitrocellulose membranes (GE Healthcare, 10600001) and probed using the following antibodies: anti-atlastin (Orso et al., 2009), 1:2000; anti-ACT (beta-actin; Sigma-Aldrich, A2228, 1:2500). The intensity of the bands was determined using Uvitec Alliance software (Uvitec Cambridge).

Viability Assessment

For each CRISPR-mutation heterozygous flies were brother-sister crossed at 25°C. The offspring was collected and the number of individuals for each of the expected genotypic classes was counted. Results are expressed as the ratio of observed over expected percentage of individuals, normalized to a control experiment. At least 200 animals were counted from three independent crosses.

Statistical Analyses

Data were analyzed using Microsoft Excel or GraphPad Prism 8. Average ER length values are expressed as mean ± standard error of the mean (SEM; n = number of profiles, unless otherwise specified). Statistical analyses were performed using unpaired Student's t-test. Analyses of differences between fly populations were made using chi-square independent proportion analysis. Both tests were applied with a confidence interval of 95% ($^{*}p < 0.05$, $^{**}p < 0.01$, and $^{***}p < 0.001$).

RESULTS

While the basis for disease causation of mutations that disable atlastin GTP binding/hydrolysis activity seems to be rather evident, a large number of the variants examined shows only modest impairment of atlastin function when tested *in vitro*. To understand better the basis for atlastin-linked HSP, we took an *in vivo* approach in *Drosophila*. We selected four mutations: R192Q (corresponding to R217Q in Atlastin-1) defective in GTP hydrolysis, R214C (corresponding to R239C in Atlastin-1), C350R (corresponding to C375R in atlastin-1), and M383T (corresponding to M408T in Atlastin-1), both positioned in the 3HB region of atlastin. *In vitro* studies of these variants in atlastin-1 or Drosophila atlastin had shown very different behaviors. R192Q/R217Q is completely defective in dimerization, GTPase and fusion activities (Bian et al., 2011; Byrnes and Sondermann, 2011; Ulengin et al., 2015); R214C/R239C is essentially indistinguishable from wild type under all *in vitro* experimental paradigms (Byrnes and Sondermann, 2011; Ulengin et al., 2015), despite being the most common pathological mutation; the C350R/C375R variant has not been studied *in vitro* because it is insoluble due to protein folding or stability issues (Byrnes and Sondermann, 2011; Ulengin et al., 2015); M383T/M408T dimerization and GTPase activities have been shown to be slightly lower but comparable to wild type while its fusion activity has not been tested (Bian et al., 2011; Byrnes and Sondermann, 2011).

Transgenic lines for tissue specific expression of the selected pathogenic variants were generated to evaluate their severity in comparison to that of the wild type protein (**Supplementary Figure 1A**). *Drosophila* atlastin produces a small and rough eye when overexpressed under the control of the GMR-Gal4 driver and causes embryonic lethality upon ubiquitous overexpression with tub-Gal4 (Orso et al., 2009). Consistent with dysfunction in GTP hydrolysis, expression of UAS-atlastin^{R192Q} did not give rise to a rough eye nor did it cause lethality (**Figure 1A**). In contrast, expression of the other three variants in the fly eye resulted in a graded rough eye phenotype with UAS-atlastin^{R214C} yielding the most severe outcome and UAS-atlastin^{M383T} the mildest (**Figure 1A**). Upon ubiquitous overexpression, the R214C variant caused second/third larva stage lethality, suggesting a weak impairment of atlastin function, while overexpression of the C350R and M383T variants permitted adult eclosure indicating a more acute functional impairment of the protein. We conclude that all the pathological mutations examined reduce atlastin activity *in vivo* although to different degrees of severity.

To evaluate the impact of the overexpression of pathogenic variants of atlastin on ER morphology, we co-expressed in motor neurons the ER marker BiP-sfGFP-HDEL (Summerville et al., 2016) using the driver D42-Gal4 and examined third instar larva brains by confocal microscopy. Similar to the overexpression of wild type atlastin (Orso et al., 2009), the R214C mutant causes heavy overfusion of ER membranes with the resulting formation of large globular ER structures within the cytoplasm of neurons (**Figure 1B**). The size of these structures is progressively reduced concomitantly with the overexpression of variants that had weaker effects on eye morphology and lethality, confirming that the impact of these mutations on atlastin function *in vivo* increases along the series R214C, C350R, M383T, and R192Q (**Figure 1B**).

To further build on this result, we studied how expression of *Drosophila* atlastin pathogenic mutants affects the morphology of the ER in HeLa cells where this organelle displays a flat, network-like shape. HeLa cells were thus co-transfected with individual atlastin mutations and the ER luminal marker sfGFP-ER-3. We found that, with the expected exception of the GTPase-dead R192Q mutant, expression of equivalent levels of the other variants disrupt ER morphology as indicated by the increased presence of bright fluorescence spots, indicative of ER hyperfusion, and by the progressive expansion of ER sheets and loss of ER tubules (**Figure 2**). In addition, overexpression of Drosophila wild type atlastin in HeLa cells induces dispersion of Golgi membranes (Pendin et al., 2011) and the pathological variants here analyzed also cause Golgi dispersion although less severely and in line with the observed gravity of their ER phenotypes (**Supplementary Figure 2**). These results indicate that in HeLa cells the behavior of atlastin pathogenic variants parallels that observed *in vivo* in flies, with the R192Q mutation being essentially inactive and R214C only barely less active than wild type atlastin.

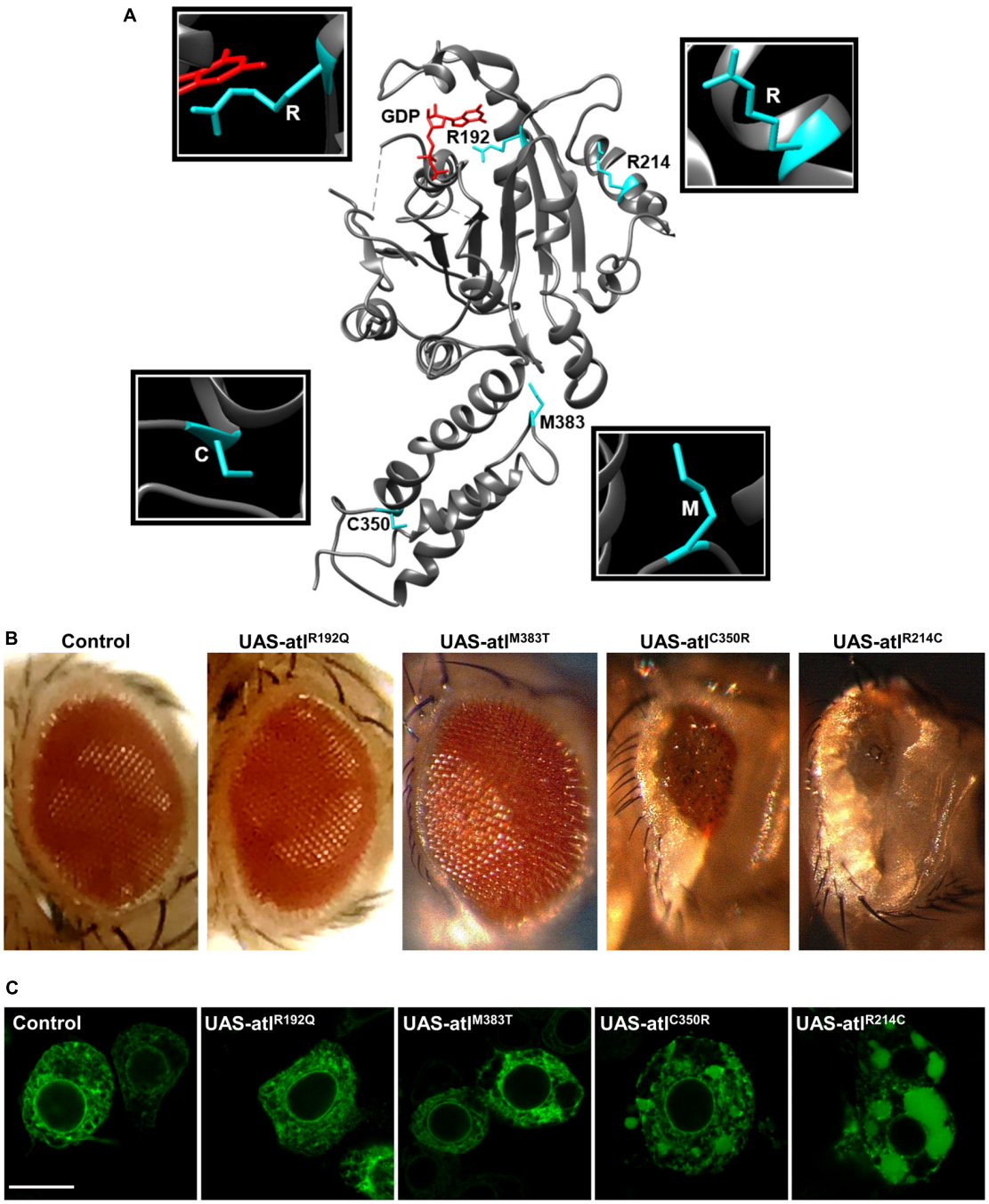

FIGURE 1 | (A) Representation of atlastin protein structure (cytosolic domain only, PDB: 3X1D); the position of the mutated residues examined is highlighted. **(B)** Expression of UAS-atlastin carrying the indicated mutations driven by the GMR-Gal4 driver. **(C)** Confocal microscopy images of third instar larva brains co-expressing atlastin carrying the indicated mutations and the ER marker BiP-sfGFP-HDEL under the control of the motor neuron driver D42-Gal4. Scalebar 10 μm.

Although the overexpression approach allows us to predict the severity of pathological mutations, it would be ideal to analyze their effects in a physiological context *in vivo*, by replacing one or two copies of the normal gene with the pathogenic variants so as to mimic the patients genetic condition. We therefore took advantage of the recently devised CRISPR/Cas9 technology to enable the introduction of the four mutant variants here studied in the endogenous *atlastin* gene. The four knock-in lines thus generated were named CRISPR-R192Q, CRISPR-R214C, CRISPR-C350R, and CRISPR-M383T. We initially established that the expression levels of mutant atlastin were comparable to those of wild type atlastin (**Supplementary Figure 1B**). On

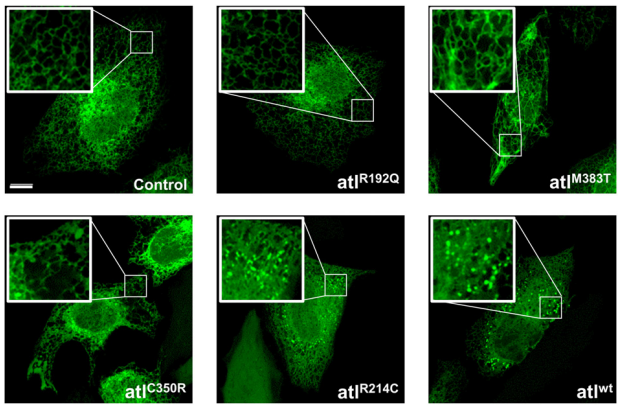

FIGURE 2 | Confocal images of HeLa cells co-expressing UAS-atlastin carrying the indicated mutations and the luminal ER marker ER-sfGFP-3. Scalebar 10 μm.

the basis of overexpression paradigms in cell culture (Rismanchi et al., 2008; Hu et al., 2009; Wang et al., 2016; Zhao et al., 2016) a dominant negative mechanism has been proposed for R217Q, a mutation that critically impacts the GTPase activity of Atlastin-1. We found that flies overexpressing UAS-atlastin^{R192Q} or flies heterozygous for CRISPR-R192Q are fully viable and do not display the lethality typically associated to atlastin loss of function, suggesting that this mutation in an *in vivo* model does not elicit a dominant negative effect. Likewise, heterozygous CRISPR-R214C, CRISPR-C350R, or CRISPR-M383T flies are viable indicating that, at least in *Drosophila*, these mutations do not function through a dominant negative mechanism.

We then evaluated for potential phenotypes flies carrying the above pathogenic variants in homozygosity. Atlastin null mutations are homozygous embryonic lethal with a small number of escapers [1% for *atl*^{2} (Lee et al., 2009)] (**Figure 3A**), and all developmental stages characteristically display a much smaller size than w^{1118} controls (**Figure 3B**). Similarly, CRISPR-R192Q homozygous mutant individuals eclosed at a very low rate (3%; **Figure 3A**), in agreement with this mutation disabling atlastin GTPase activity, and when compared to w^{1118} controls had an obviously smaller size that was, however, perceptibly bigger than *atl*^{2} null mutants (**Figure 3B**). The other homozygous pathological CRISPR mutants displayed greater eclosion rates and thus a less severe lethality as well as a progressively larger size than atlastin null and CRISPR-R192Q mutants, suggesting a partial loss of function mechanism (**Figure 3B**). It is interesting to note that both the viability and size of CRISPR pathological mutants are inversely proportional to the gravity of the mutation that, consistent with our previous observations based on overexpression, increases along the sequence CRISPR-R214C, CRISPR-C350R, CRISPR-M383T, CRISPR-R192Q (**Figures 3A,B**).

To establish whether the presence of the CRISPRed pathological mutations had a bearing on ER morphology, we expressed the ER marker BiP-sfGFP-HDEL in mutant motor neurons and performed live confocal microscopy analysis. Because *Drosophila* third instar larva neurons are very small and embedded in living tissue, it turned out to be difficult to characterize in detail ER morphology, in order to define obvious differences in network organization among neurons expressing the different CRISPR mutations by fluorescence microscopy. Nevertheless, we observed that w^{1118} controls, homozygous R214C and homozygous C350R neurons displayed indistinguishable ER morphologies while R192Q and M383T had both altered ER shape (**Figure 4A** and **Supplementary Figure 3**). For this reason, we evaluated the length of ER profiles on thin EM sections of homozygous third instar larva mutant brains. ER profile length has been considered a parameter capable of reporting accurately on the functional state of atlastin since null *atl*^{2} mutant neurons are characterized by a much shorter average ER profile length than w^{1118} control neurons, a phenotype linked to increased ER fragmentation due to the prevalence of ER membrane fission in the absence of the fusion activity mediated by atlastin (Espadas et al., 2019). Our analysis reveals that the stronger the loss of function mutation, the shorter the neuronal ER profiles (**Figures 4B,C**). Indeed, CRISPR-R192Q displayed the shortest average ER profile length while the CRISPR-R214C variant had the longest (**Figures 4B,C**). Thus, the severity of the CRISPR homozygous mutants suggests a graded loss of function effect, confirming the results obtained from the

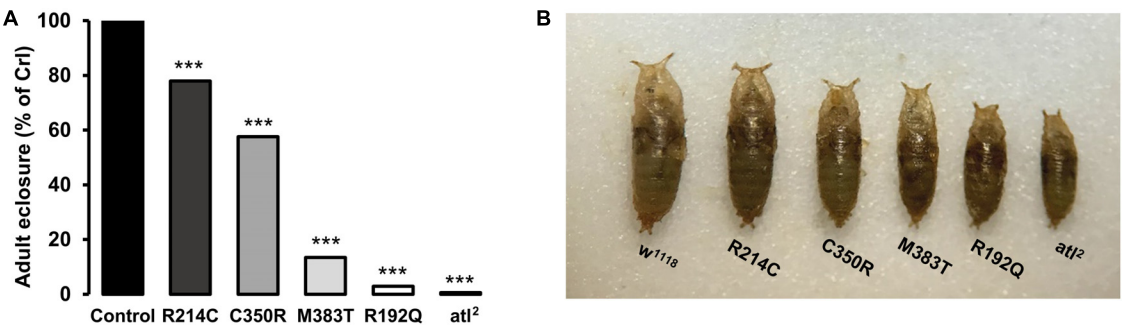

FIGURE 3 | (A) Eclosion rates of homozygous CRISPR and *atl*^{2} mutants. The rate is calculated as the ratio between observed over expected individuals, normalized to controls. **(B)** Comparison of the size of homozygous CRISPR mutants with control (w^{1118}) and *atl*^{2} mutant flies. ***$p < 0.001$.

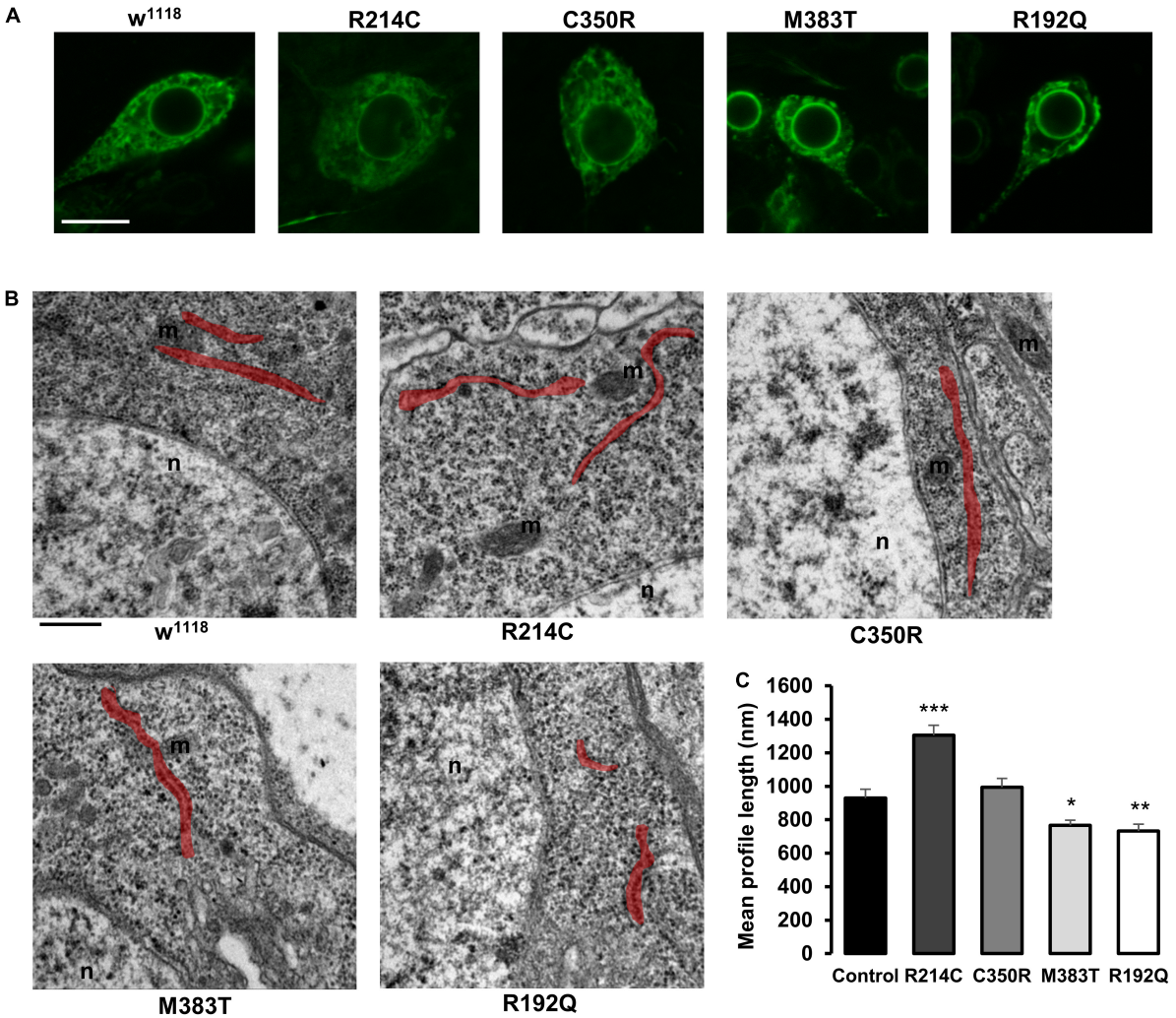

FIGURE 4 | (A) Confocal microscopy images of third instar larva brain motor neurons of CRISPR mutants expressing the ER marker BiP-sfGFP-HDEL with the driver D42-Gal4. Scalebar 10 μm **(B)** TEM images of third instar larva brains neurons of CRISPR mutants. ER profiles are highlighted in red. Scalebar 500 nm **(C)** Quantification of the mean length of ER profiles measured in TEM sections. Mean ± SEM, n ≥ 50 profiles. *$p < 0.05$, **$p < 0.01$, ***$p < 0.001$.

previous experiments. We note that average ER profile length in controls (w^{1118} stock), while consistent with previous reports (Orso et al., 2009; Espadas et al., 2019; Vajente et al., 2019), is shorter than in some mutants as if mutants had a greater baseline profile length (**Figures 4B,C**). However, because the graded effect of the mutations is solid and all lines are grown under the same environmental conditions, we hypothesize that this could be due to the potentially very different genetic background between w^{1118} controls and mutants (Chandler et al., 2013).

Several reports have suggested that expression of atlastin pathogenetic variants affects also Golgi apparatus morphology (Namekawa et al., 2007; Rismanchi et al., 2008; Chen et al., 2011; Behrendt et al., 2019). We thus investigated whether this was the case also in our knock-in CRISPR models. Immunohistochemical analysis of third instar larvae neuronal cell bodies and body wall muscles revealed that in all the mutant lines the structure and distribution of the Golgi apparatus were perturbed (**Figure 5**). When compared to w^{1118} controls, the Golgi stacks in knock-in mutants appear more abundant in the perinuclear region, where abnormally enlarged structures are occasionally present in the most severe mutants (**Figure 5**). Moreover, the number of dots corresponding to single stacks is increased in CRISPR larvae. When examined by TEM, the morphology of individual Golgi stacks looks altered, as dilated ER or Golgi cisternae are often present, as well as double- or multi-membrane autophagosomes (**Figure 6**). While in w^{1118} control flies, among 40 Golgi apparatus imaged, we found in only 17.5% of them dilated ER/Golgi cisternae and in 15% autophagosomes, mutant flies displayed more frequently these phenotypes (R192Q: 36% dilated Golgi, 19% autophagosomes; R214C: 41% dilated Golgi, 44% autophagosomes; C350R, 37% dilated Golgi, 29% autophagosomes; and M383T, 46% dilated Golgi, 19% autophagosomes).

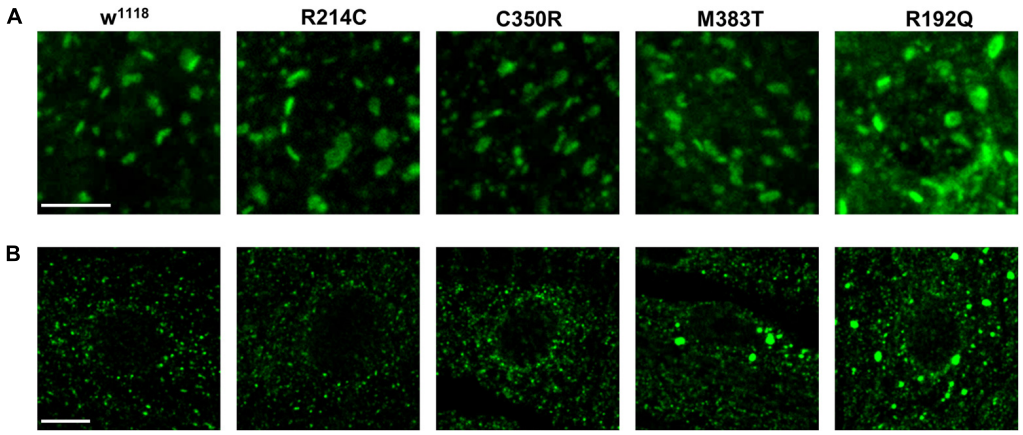

FIGURE 5 | Confocal microscopy images of third instar larva motor neuron cell bodies **(A)** and body wall muscles **(B)** of CRISPR mutants, stained with *cis*-Golgi marker GM130. Scalebars: 5 μm in **(A)** and 10 μm in **(B)**.

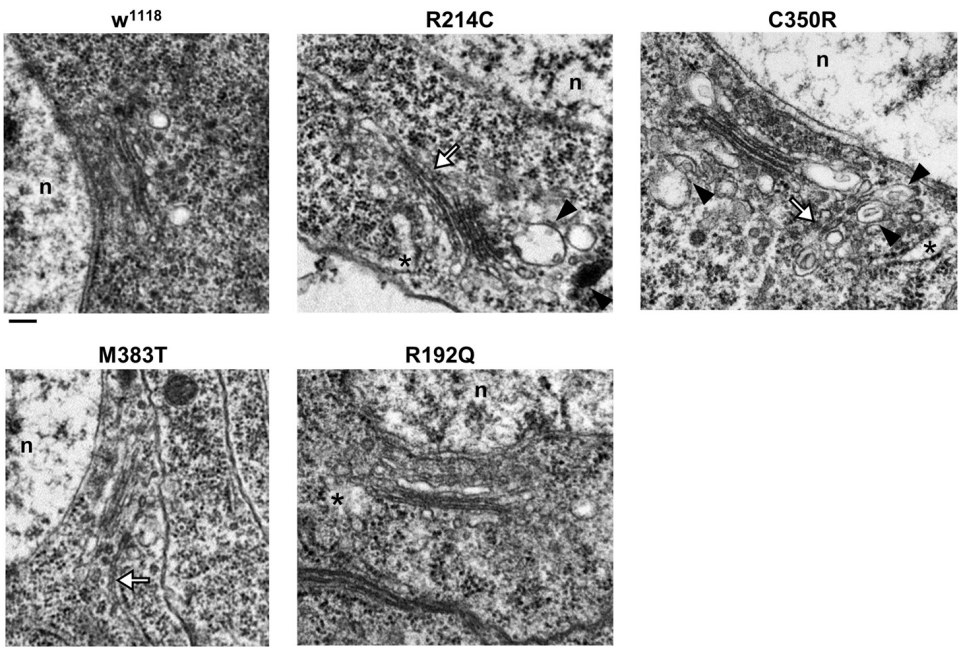

FIGURE 6 | TEM images of third instar larva brains neurons of CRISPR mutants. Asterisks indicate dilated ER profiles; arrowheads indicate autophagosomes; white arrows indicate abnormally long Golgi cisternae/connecting two adjacent stacks. Scalebar 200 nm.

DISCUSSION

Our study exploits *Drosophila* as an *in vivo* system to comprehend the role of organelle morphology in the onset of *SPG3A*-HSP disease and to model the mechanism whereby highly conserved pathological mutations cause this disease.

The morphological hallmark of the ER in atlastin null mutants is fragmentation, reported as a prominent shortening of the average length of neuronal ER profiles in EM sections. Pathological disease mutants when compared among themselves also display a progressive shortening of ER profiles that becomes more pronounced the more severe the mutation, according to the scale described in the above results. However, in all mutants the absolute value of ER profile length remains close to or greater than that of wild type ER. Irrespective of the underlying reason, this result suggests that ER morphology impairment may not be the prime driver of *SPG3A*-HSP pathology, as severe mutants die before reaching adulthood despite having an almost normal ER profile length, as measured by EM. Alternatively, it is possible that neuronal ER profile length as measured by EM is not an accurate readout for the complex morphological features of the ER. Although we have found evidence of morphological alterations within the Golgi apparatus of CRISPRed knock-in mutants, we believe that these alterations are too limited to be

linked with the lethality of the mutants since it is known that integrity of the Golgi stacks is not required for proper secretory pathway trafficking (Kondylis and Rabouille, 2009; Dunlop et al., 2017). Our data suggest that more careful, deeper investigation of the function of affected organelles will be required to understand the root of this disease.

Although SPG3A mutations include small deletions, small insertions, splice site mutations, as well as whole exon deletions, the vast majority of them is represented by missense variants (Zhao and Liu, 2017). It has been suggested that a dominant negative mechanism underlies most of disease-causing mutation (O'Donnell et al., 2018), however, evidence for this supposition is largely based upon experiments conducted in cell culture upon overexpression of these variants. To reproduce a model more closely related to the pathological condition of patients, we introduced the mutations into the *Drosophila* genome by CRISPR/Cas9 editing in addition to examining their effects under overexpression *in vivo*. Four variants, two (R192Q and R214C) mapping to the GTPase domain of atlastin and the other two localized within the 3HB region (C350R and M383T), were studied. We found that the four pathological missense mutations investigated all act through a common loss of function mechanism though they differed for the severity of the phenotypes elicited. Indeed, all mutations in homozygosity caused a decrease of the adult eclosion rate and a reduction in size of all developmental stages, both typical features of *atlastin* null mutants. The gravity of the phenotypes, however, differed increasing along the succession R214C, C350R, M383T, R192Q such that the smaller R192Q homozygous individuals eclosed the least while the bigger R214C homozygous individuals eclosed at a greater rate. Corroboration of mutation severity came also from overexpression paradigms converging to show that the loss of atlastin function was almost complete for the GTPase-deficient R192Q and progressively decreased from M383T to C350R with R214C overexpression causing phenotypes almost as severe as those induced by wild type atlastin. Interestingly, we did not find evidence supporting the prevailing theory that most atlastin mutations act through a dominant negative mechanism (O'Donnell et al., 2018; Liu et al., 2019), not only because individuals heterozygous for all mutations eclose at normal rates and have normal size but also because overexpression of the pathological variants in a wild type background, i.e., in the presence of endogenous atlastin levels, does not give rise to the loss (or partial loss) of function phenotypes expected for dominant negative mutations.

Our results underscore that there is no obvious correlation between the effects of pathological mutations *in vivo* and the biochemical activity of atlastin *in vitro*. In fact, while R192Q/R217Q is a known GTPase-deficient mutation and therefore predicted to cause loss of protein function, the GTPase activity, homodimerization ability of the R214C/R239C and M383T/M408T variants as well as the membrane fusion competence of R214C are comparable to those of wild type atlastin (Bian et al., 2011; Ulengin et al., 2015; O'Donnell et al., 2018). Yet, these variants *in vivo* cause the same, though graded, loss of function phenotypes with the mildest mutation R214C/R239C being by and large the most common variant identified in SPG3A patients (Ulengin et al., 2015; Zhao and Liu, 2017). In conclusion, all four pathological mutations here investigated, irrespective of their position within the protein and often in contrast with data on their *in vitro* activity, cause loss of atlastin function *in vivo* in flies suggesting that this is the main mechanistic road to *SPG3A*-HSP disease.

DATA AVAILABILITY STATEMENT

The raw data supporting the conclusions of this article will be made available by the authors, without undue reservation.

AUTHOR CONTRIBUTIONS

AD and DP conceived the work, wrote the manuscript, and secured funding. AM, NV, and DP performed the experiments and analyzed the results. All authors contributed to the article and approved the submitted version.

FUNDING

This work was supported by the Ministry of Education, University and Research (MIUR; fellowship to NV); Fondazione Cassa di Risparmio di Padova e Rovigo (CARIPARO Foundation, Starting Grant 2015 to DP); Fondazione Telethon (GGP19304 to DP; GGP11189 to AD); and Italian Ministry of Health (5 × 1000 and RC 2018, 2019, 2020 to AD).

ACKNOWLEDGMENTS

We thank Jessica Tosetto, Tatiana Trevisan, Giulia Misticoni, Genny Orso, and Alessia Gazziero for generating fly lines and constructs used in this study. Stocks obtained from the Bloomington *Drosophila* Stock Center (NIH P40OD018537) were used in this study. atl^2 fly line was a kind gift from S. Lee.

SUPPLEMENTARY MATERIAL

The Supplementary Material for this article can be found online at: https://www.frontiersin.org/articles/10.3389/fnins.2020.547746/full#supplementary-material

Supplementary Figure 1 | (A,B) Representative western blot **(A)** and quantification, normalized to β-actin levels **(B)**, of the amount of atlastin in heads of individuals expressing the wild type protein or carrying the indicated mutations under the control of the GMR-Gal4 driver. Note that the transgenic line expressing wild type atlastin has been selected for its lower expression levels in order to permit survival of adult flies. Protein extracts from control flies (w^{1118} strain) are loaded for comparison with endogenous atlastin levels. Mean ± SEM, $n = 3$. **(C,D)** Representative western blot **(C)** and quantification, normalized to β-actin levels **(D)**, of atlastin in brains of CRISPR homozygous mutants, compared to w^{1118} controls. Mean ± SEM, $n = 3$.

Supplementary Figure 2 | Confocal images of HeLa cells co-expressing UAS-atlastin carrying the indicated mutations and the luminal ER marker ER-sfGFP-3. Cells are immunostained with *cis*-Golgi marker GM130 and *trans*-Golgi marker TGN46. Scalebar 10 μm.

Supplementary Figure 3 | Confocal microscopy images of third instar larva ventral ganglia of CRISPR mutants expressing the ER marker BiP-sfGFP-HDEL with the driver D42-Gal4. Scalebar 10 μm. Higher magnification images are reported in **Figure 4A**.

REFERENCES

Anwar, K., Klemm, R. W., Condon, A., Severin, K. N., Zhang, M., Ghirlando, R., et al. (2012). The dynamin-like GTPase Sey1p mediates homotypic ER fusion in S. *cerevisiae*. *J. Cell Biol.* 197, 209–217. doi: 10.1083/jcb.201111115

Behrendt, L., Kurth, I., and Kaether, C. (2019). A disease causing ATLASTIN 3 mutation affects multiple endoplasmic reticulum-related pathways. *Cell. Mol. Life Sci.* 76, 1433–1445. doi: 10.1007/s00018-019-03010-x

Bian, X., Klemm, R. W., Liu, T. Y., Zhang, M., Sun, S., Sui, X., et al. (2011). Structures of the atlastin GTPase provide insight into homotypic fusion of endoplasmic reticulum membranes. *Proc. Natl. Acad. Sci. U.S.A.* 108, 3976–3981. doi: 10.1073/pnas.1101643108

Blackstone, C. (2018). Hereditary spastic paraplegia. *Handb. Clin. Neurol.* 148, 633–652. doi: 10.1016/B978-0-444-64076-5.00041-47

Byrnes, L. J., and Sondermann, H. (2011). Structural basis for the nucleotide-dependent dimerization of the large G protein atlastin-1/SPG3A. *Proc. Natl. Acad. Sci. U.S.A.* 108, 2216–2221. doi: 10.1073/pnas.1012792108

Chandler, C. H., Chari, S., and Dworkin, I. (2013). Does your gene need a background check? how genetic background impacts the analysis of mutations, genes, and evolution. *Trends Genet.* 29, 358–366. doi: 10.1016/j.tig.2013.01.009

Chen, J., Stefano, G., Brandizzi, F., and Zheng, H. (2011). Arabidopsis RHD3 mediates the generation of the tubular ER network and is required for golgi distribution and motility in plant cells. *J. Cell Sci.* 124(Pt 13), 2241–2252. doi: 10.1242/jcs.084624

Dunlop, M. H., Ernst, A. M., Schroeder, L. K., Toomre, D. K., Lavieu, G., and Rothman, J. E. (2017). Land-locked mammalian Golgi reveals cargo transport between stable cisternae. *Nat. Commun.* 8:432. doi: 10.1038/s41467-017-00570-z

Espadas, J., Pendin, D., Bocanegra, R., Escalada, A., Misticoni, G., Trevisan, T., et al. (2019). Dynamic constriction and fission of endoplasmic reticulum membranes by reticulon. *Nat. Commun.* 10:5327. doi: 10.1038/s41467-019-13327-13327

Faust, J. E., Desai, T., Verma, A., Ulengin, I., Sun, T. L., Moss, T. J., et al. (2015). The atlastin C-terminal tail is an amphipathic helix that perturbs the bilayer structure during endoplasmic reticulum homotypic fusion. *J. Biol. Chem.* 290, 4772–4783. doi: 10.1074/jbc.M114.601823

Hu, J., and Rapoport, T. A. (2016). Fusion of the endoplasmic reticulum by membrane-bound GTPases. *Semin. Cell Dev. Biol.* 60, 105–111. doi: 10.1016/j.semcdb.2016.06.001

Hu, J., Shibata, Y., Zhu, P. P., Voss, C., Rismanchi, N., Prinz, W. A., et al. (2009). A Class of Dynamin-like GTPases involved in the generation of the tubular ER network. *Cell* 138, 549–561. doi: 10.1016/j.cell.2009.05.025

Kondylis, V., and Rabouille, C. (2009). The golgi apparatus: lessons from *Drosophila*. *FEBS Lett.* 583, 3827–3838. doi: 10.1016/j.febslet.2009.09.048

Lee, M., Paik, S. K., Lee, M. J., Kim, Y. J., Kim, S., Nahm, M., et al. (2009). Drosophila Atlastin regulates the stability of muscle microtubules and is required for synapse development. *Dev. Biol.* 330, 250–262. doi: 10.1016/j.ydbio.2009.03.019

Liu, X., Guo, X., Niu, L., Li, X., Sun, F., Hu, J., et al. (2019). Atlastin-1 regulates morphology and function of endoplasmic reticulum in dendrites. *Nat. Commun.* 10, 1–15. doi: 10.1038/s41467-019-08478-8476

Namekawa, M., Muriel, M. P., Janer, A., Latouche, M., Dauphin, A., Debeir, T., et al. (2007). Mutations in the SPG3A gene encoding the GTPase atlastin interfere with vesicle trafficking in the ER/Golgi interface and Golgi morphogenesis. *Mol. Cell. Neurosci.* 35, 1–13. doi: 10.1016/j.mcn.2007.01.012

Niu, L., Ma, T., Yang, F., Yan, B., Tang, X., Yin, H., et al. (2019). Atlastin-mediated membrane tethering is critical for cargo mobility and exit from the endoplasmic reticulum. *Proc. Natl. Acad. Sci. U.S.A.* 116, 14029–14038. doi: 10.1073/pnas.1908409116

O'Donnell, J. P., Byrnes, L. J., Cooley, R. B., and Sondermann, H. (2018). A hereditary spastic paraplegia-associated atlastin variant exhibits defective allosteric coupling in the catalytic core. *J. Biol. Chem.* 293, 687–700. doi: 10.1074/jbc.RA117.000380

Orso, G., Pendin, D., Liu, S., Tosetto, J., Moss, T. J., Faust, J. E., et al. (2009). Homotypic fusion of ER membranes requires the dynamin-like GTPase Atlastin. *Nature* 460, 978–983. doi: 10.1038/nature08280

Pendin, D., Tosetto, J., Moss, T. J., Andreazza, C., Moro, S., McNew, J. A., et al. (2011). GTP-dependent packing of a three-helix bundle is required for atlastin-mediated fusion. *Proc. Natl. Acad. Sci. U.S.A.* 108, 16283–16288. doi: 10.1073/pnas.1106421108

Rismanchi, N., Soderblom, C., Stadler, J., Zhu, P. P., and Blackstone, C. (2008). Atlastin GTPases are required for Golgi apparatus and ER morphogenesis. *Hum. Mol. Genet.* 17, 1591–1604. doi: 10.1093/hmg/ddn046

Shribman, S., Reid, E., Crosby, A. H., Houlden, H., and Warner, T. T. (2019). Hereditary spastic paraplegia: from diagnosis to emerging therapeutic approaches. *Lancet Neurol.* 18, 1136–1146. doi: 10.1016/S1474-4422(19)30235-30232

Summerville, J. B., Faust, J. F., Fan, E., Pendin, D., Daga, A., Formella, J., et al. (2016). The effects of ER morphology on synaptic structure and function in Drosophila melanogaster. *J. Cell Sci.* 129, 1635–1648. doi: 10.1242/jcs.184929

Ulengin, I., Park, J. J., and Lee, T. H. (2015). ER network formation and membrane fusion by atlastin1/SPG3A disease variants. *Mol. Biol. Cell* 26, 1616–1628. doi: 10.1091/mbc.E14-10-1447

Vajente, N., Norante, R., Redolfi, N., Daga, A., Pizzo, P., and Pendin, D. (2019). Microtubules stabilization by mutant spastin affects ER morphology and Ca2+ handling. *Front. Physiol.* 10:1544. doi: 10.3389/fphys.2019.01544

Wang, S., Tukachinsky, H., Romano, F. B., and Rapoport, T. A. (2016). Cooperation of the ER-shaping proteins atlastin, lunapark, and reticulons to generate a tubular membrane network. *Elife* 5:e18605. doi: 10.7554/eLife.18605

Wu, F., Hu, X., Bian, X., Liu, X., and Hu, J. (2014). Comparison of human and *Drosophila* atlastin GTPases. *Protein Cell* 6, 139–146. doi: 10.1007/s13238-014-0118-110

Zhang, M., Wu, F., Shi, J., Zhu, Y., Zhu, Z., Gong, Q., et al. (2013). ROOT HAIR DEFECTIVE3 family of dynamin-like GTPases mediates homotypic endoplasmic reticulum fusion and is essential for *Arabidopsis* development. *Plant Physiol.* 163, 713–720. doi: 10.1104/pp.113.224501

Zhao, G., Zhu, P. P., Renvoisé, B., Maldonado-Báez, L., Park, S. H., and Blackstone, C. (2016). Mammalian knock out cells reveal prominent roles for atlastin GTPases in ER network morphology. *Exp. Cell Res.* 349, 32–44. doi: 10.1016/j.yexcr.2016.09.015

Zhao, G. H., and Liu, X. M. (2017). Clinical features and genotype-phenotype correlation analysis in patients with ATL1 mutations: a literature reanalysis. *Transl. Neurodegener.* 6:9. doi: 10.1186/s40035-017-0079-73

Zhao, X., Alvarado, D., Rainier, S., Lemons, R., Hedera, P., Weber, C. H., et al. (2001). Mutations in a newly identified GTPase gene cause autosomal dominant hereditary spastic paraplegia. *Nat. Genet.* 29, 326–331. doi: 10.1038/ng758

Conflict of Interest: The authors declare that the research was conducted in the absence of any commercial or financial relationships that could be construed as a potential conflict of interest.

Advantages of publishing in Frontiers

OPEN ACCESS
Articles are free to read for greatest visibility and readership

FAST PUBLICATION
Around 90 days from submission to decision

HIGH QUALITY PEER-REVIEW
Rigorous, collaborative, and constructive peer-review

TRANSPARENT PEER-REVIEW
Editors and reviewers acknowledged by name on published articles

Frontiers
Avenue du Tribunal-Fédéral 34
1005 Lausanne | Switzerland

Visit us: www.frontiersin.org
Contact us: frontiersin.org/about/contact

REPRODUCIBILITY OF RESEARCH
Support open data and methods to enhance research reproducibility

DIGITAL PUBLISHING
Articles designed for optimal readership across devices

FOLLOW US
@frontiersin

IMPACT METRICS
Advanced article metrics track visibility across digital media

EXTENSIVE PROMOTION
Marketing and promotion of impactful research

LOOP RESEARCH NETWORK
Our network increases your article's readership